

Online ISSN : 2395-602X

Print ISSN : 2395-6011

www.ijsrst.com



**Conference
Proceedings**

Online National Conference on Recent Advances in Chemical and Physical Sciences

[RACPS-2022]

Date : 14th December 2022

Organized By

B. S. V Education Society Wapti's

Bahirji Smarak Mahavidyalaya, Basmath Dist. Hingoli, Maharashtra, India

[NAAC Reaccredited B+ Grade]

Affiliated to S, R. T. M University, Nanded

Best College Award of 2020, S, R. T. M University, Nanded

In Collaboration with

Shiv Chatrapati College, N3, CIDCO, Aurangabad

INTERNATIONAL JOURNAL OF SCIENTIFIC RESEARCH IN SCIENCE AND TECHNOLOGY

PEER REVIEWED AND REFEREED INTERNATIONAL SCIENTIFIC RESEARCH JOURNAL

VOLUME 9, ISSUE 17 NOVEMBER-DECEMBER-2022

Scientific Journal Impact Factor : 8.014

Email : editor@ijsrst.com Website : <http://ijsrst.com>





Online National Conference on Recent Advances in Chemical and Physical Sciences (RACPS-2022)

14th December 2022

Organised by

B. S. V Education Society Wapti's Bahirji Smarak Mahavidyalaya,
Basmath Dist. Hingoli, Maharashtra, India

[NAAC Reaccredited B+ Grade]

Affiliated to S. R. T. M University, Nanded

Best College Award of 2020, S. R. T. M University, Nanded

In Collaboration with

Shiv Chatrapati College, N3, CIDCO, Aurangabad

In Association with

International Journal of Scientific Research in Science and Technology

Print ISSN: 2395-6011 Online ISSN : 2395-602X

Volume 9, Issue 17, November-December-2022

International Peer Reviewed, Open Access Journal

Published By

Technoscience Academy



(The International Open Access Publisher)

website: www.technoscienceacademy.com

Prof. Dr. Gawali P. G I/c.
Principal & Convener

Prof. Dr. Swami M.B
[Chief Organizer]

Prof. Dr. Pawar R.
P Principal & Convener

Prof. Kalyankar A.N
[Chief Organizer]

About US

Our College monogram contains in it the meaningful words “Satkarmi Rati Wadho” (Let the love for good deeds grow in us), from the great Saint Gnyaneshwara’s Pasaydan. In this permise Gnyaneshwara seeks the benedictions of the almighty God for the prosperity and happiness of the whole Universe. And to achieve this sublime goal the gooddeeds of humanrace are essential. Martyr Bahirji Shinde sacrificed his life for the liberation of the people, out of this Sentiment only. Our desideratum is to engender a sensible generation of tommorow, through the medium of education, to build a new post independent democratic India.

ऑनलाईन प्रवेश अर्ज (पदवी अभ्यासक्रम)

कला, वाणिज्य व विज्ञान
सण २०२१-२२



CONTENTS

Sr. No	Article/Paper	Page No
1	Synthesis and Estimation of Noval Heterocyclic Compounds with Its Biological Properties Manorama B. Motegaonkar	01-07
2	Evaluation of Antimicrobial Activity of 4-(Benzo[D]Thiazol-2-Yl) Phenol and Its Derivatives A. S. Mathwale, V. K. Jadhav, A. B. Chidrawar	08-12
3	Physico-Chemical Analysis of Bore well Water Sample of Tadola Village (M.S.) Dr. Kadam Dadasaheb Devidasrao	13-19
4	Synthesis and Antimicrobial Activities of New 3-(Chloromethyl)-2-(Piperazin-1-Yl) Quinolone Derivatives Rajkumar U. Pokalwar	20-27
5	Understanding the Electronic Structure of Doped TiO₂ Photoanode for Water Splitting Reactions : A Review on First Principle Studies Yogesh S. Nalwar, Harshada Barve, Rajaram S. Mane, Krishna Chaitanya Gunturu	28-36
6	Synthesis and Characterization of Some Biologically Active Transition Metal Complexes of Bidentate Ligand V. A. Shelke, S. M. Jadhav, S. G. Shankarwar	37-47
7	Green Chemistry and Useful Effects of Catalyst H. A. Tirpude	48-52
8	One Pot Efficient Synthesis of Pyranopyrazole Derivative Pande P.R., Patki A.S.	53-57
9	Oxidised Activated Carbon: Highly Efficient and Recyclable Catalyst for The Synthesis of 1, 8-Dioxooctahydroxanthene Derivatives Mantosh B. Swami, Sushil R. Mathapati	58-64
10	A Review on Synthetic Strategies of Imidazole and its Biological Activities Sandip S. Dhotre, Vidya S. Dofe, Rajendra P. Pawar	65-70
11	Synthesis and Characterization of 2-Amino-5 (Substituted Phenyl) 1,3,4-Thiadiazole Based Imines and Their Study M. B. Zade, S. N. Ibatte, J. A. Angulwar	71-76
12	Formulation and Evaluation of Nanosponge Based Topical Gel Preparation by QbD Approach Dr. Padmaja Giram, Dr. Nalwar Yogesh S., Omprakash G. Bhusnure, Dr. Sachin B. Gholve, Alok A. Kadam, Sachin kabade	77-82
13	A Facile and Expeditious Approach to Substituted 5-Arylpyrimido-Quinoline-Diones Catalyzed by Iodine Yogesh S. Nalwar	83-89

14	Microwave Assisted Synthesis of N-Acetylpyrazolines Derived from Bis-Chalones Yogesh S. Nalwar	90-92
15	Synthesis and Antimicrobial Evaluation of Some Novel 2, 4-(Substituted-Phenyl)-2, 3-Dihydro-1H-1, 5-Benzodiazepine Derivatives Kendre M. M., Vidule R. R.	93-100
16	A Kinetic Study of Solvent Effect on Hydrolysis of Aceticanhydride by Conductivity Method Suresh D. Dhage, Mahesh B. Swami	101-104
17	Oxidation of Methanol by Benzimidazolium Fluorochromate in Aqueous Acetic Acid Medium : A Kinetic Study M. H. Gagare, Mahesh B. Swami, Suresh D. Dhage	105-112
18	A Brief Review on Synthesis of Meldrum Acid Chalcone Derivatives and It's Pharmacological Studies Kuldeep T. Padhyar, Nandkishor Shirsath, Navanand B. Wadwale, Milind C. Nagare, Avinash U. Nerkar, R.S. Nirwan	113-121
19	A Short Review on The Application of Phase Transfer Catalyst (PTC) Towards the Synthesis of Heterocyclic Compounds Sindhu A. Bhosale, Akshaykumar B. Harepatil, Rajendra P. Pawar, Vidya S. Dofe, Vivekanand B. Jadhav	122-128
20	A Review on Schiff Base Ligands and Their Biologically Important Metal Complexes Nirmal R. Joshi, Saroj R. Bembalkar, Rajendra P. Pawar	129-133
21	The Numerous Pharmacological Activity of Curcuma longa : A Review Mahesh Walle, S.P. Gawali, S.S. Kamble, R.P. Pawar, R.D. Ingle	134-139
22	An Efficient and Reusable ZnS NPs Catalyst for Synthesis of α-Hydroxyphosphonates Tidke Vishwamber Angadrao	140-145
23	PEG-400 Mediated Synthesis of Pyranopyrazole Derivatives Via a Three-Component One Pot Reaction Yogesh Nalwar, Trambak Kendre, Arvind Patil, Charushila Nerkar, Santosh Chobe	146-150
24	Thienodiazepine - A Comprehensive Review of Their Synthesis and Diverse Biological Importance Vidya S. Dofe, Anant B. Kanagare, Dattatraya N. Pansare, Ravindra D. Suryawanshi, Rajendra P. Pawar	151-154
25	Green And Efficient Synthesis of Bis (Indolyl) Methanes Using Zinc Triflate Nakkalwar S. L., Kasralikar H. M., Kaminwar N. S.	155-159
26	Synthesis, Characterization and Biological Activity of New Schiff Bases Derived from Aminopyrimidine and Their Metal Complexes D. T. Sakhare	160-173
27	Synthesis of β-amino Carbonyl Compounds by Michael Reaction	174-

	Dr. Jaishri Somwanshi, Dr. M.B Swami	181
28	Silica Supported PPA : An Efficient and Recyclable Catalyst for Benzimidazoles Synthesis at Room Temperature Sushil R Mathapati, Sujit S Mathakari, Mahesh B Swami, Mantosh B Swami	182- 192
29	Study of Nickel (II) and Mercury (II) Schiff Bases Metal Complexes S. Anjanikar, S. Chandole	193- 199
30	Waste Plastic to Useful Fuel B. P. Pingle, R. D. Suryawanshi, R. P. Pawar	200- 205
31	Synthesis, Characterization and Microbial Activity of Aldimine Metal Complexes Dinkar P. Kotwal	206- 210
32	One-Pot Three Component Synthesis of Pyrimido Thiadiazolo Pyrimidine Dione Using 1-Butyl-3-Methyl Imidazolium Chloride with Their Antioxidant Activities Gopinath S Khansole, Vijay N. Bhosale	211- 218
33	An Overview of Green Synthesis & Biomedical Applications of Zinc Oxide (ZnO) Nanoparticles Jagannath S. Godse, Santosh B. Gaikwad, Ravindra Suryawanshi, Sanjay B. Ubale, Rajendra P. Pawar	219- 229
34	Study of Polymer in the presence of Drug Using Dielectric Relaxation Spectroscopy Ravikant Karale, Komal B. Kabara, Suad Alwaleedy, Saeed Mohemmed, Savita Kamble, Ashok C. Kumbharkhane, Arvind V. Sarode	230- 237
35	Dielectric Relaxation Studies of Halo butanes in The Frequency Range 10 MHz to 30 GHz Using a Time Domain Reflectometry (TDR) Technique Gubre Ashwini G., Kumbharkhane A.C	238- 244
36	Structural and Dielectric Relaxation Studies of Propionitrile-1, 4 Dioxane Mixtures Using A TDR D. G. Dongre, A. C. Kumbharkhane	245- 251
37	Water Dynamics on The Structural Properties of Amino Acid in Presence of NSAID : An Approach Through Dielectric Spectroscopy Suad Alwaleedy, Saeed Mohemmed, Ravikant Karale, Komal B. Kabara, Ashok C. Kumbharkhane, Bunty Rani Roy, Arvind V. Sarode	252- 268
38	Study of the Characteristics of the Soil of Dindori at X-Band Frequency Dr. Manisha Dhiware	269- 274
39	Chemically Deposited Copper Sulfide Thin Film for Photo Voltaics Performance R. V. Suryawanshi, M. A. Barote, R. M. Mahindrakar, G. D. Tingare	275- 281
40	Analysis of Structural Properties of Nanocrystalline Ni, Zn, Ce, Ferrites S. L. Gaikwad, A.G. Gacche, A. B. Mugutkar, S. S. Jadhav	282- 286
41	Dielectric Relaxation Study of DPG Using a TDR at 20oC Pankaj A. Chalikwar, Abdulrahman W. Pathan, K. R. Borude, G. R. Mahajan	287- 292
42	Dielectric Dispersion Study of Binary Mixtures of Polysorbate-40 with Aqueous	293-

	Solutions G T Jinklor, V S Pabboj, H N Lakhmawad, K S Kanse, Y S Joshi, D N Rander	299
43	Dielectric Relaxation Studies of Aqueous Polyvinyl Pyrrolidone Komal Kabara, Ravi Karale, Suad Alwaleedy, Savita Kamble, Ashok Kumbharkhane, Arvind Sarode	300-305
44	Dielectric Relaxation Studies of Potentised Homeopathic Medicines Mahajan G. R., Parimal Patwe, Pathan A.W., Chalikwar P.A.	306-310
45	Investigation of Solute -Solute interaction and Complex Formation in Binary Mixtures of Iso-Amyl Alcohol and Ethylenediamine at Microwave Frequency B. S. Narwade	311-316
46	Microwave Frequency Dielectric Dispersion of 1, 2-Ethenediol with Water using TDR Shamsundar S. Kadam	317-320
47	Molecular and Dielectric Study of the Binary Liquid Mixture of 2,3-Dichloroaniline and Ethylene Glycol at FDR Nemmaniwar. G. Bhupesh	321-323
48	Study of Atmospheric Aerosol Using Optical Remote Sensing: A Review Govind B. Munde, Shafiyoddin B. Sayyad, Pradeep D. Gaikwad	324-329
49	Annealing Effects on Optical and Electrical Properties of a-(Ge₂₀Se₈₀)₉₀Bi₁₀ Thin Films Deposited by Physical Thermal Evaporation Akshay Kumar	330-339
50	Comparison of Radar Backscattering Models IEM, Oh & Dubois for Synthetic Aperture Radar (SAR) Data Monika S. Khole, Dr. Sanjay K. Tupe, Dr. Shafiyoddin Sayyad	340-348
51	Molecular Interaction between Carbohydrates and Amino Acid Using Dielectric Spectroscopy Savita Kamble, Ravikant Karale, Komal B. Kabara, Suad Alwaleedy, Saeed Mohemmed, Ashok C. Kumbharkhane, Arvind V. Sarode	349-354
52	Study of Molecular Interaction in Aqueous Valine-Aceclofenac Mixture Using Dielectric Relaxation Spectroscopy (DRS) Arvind V. Sarode, Suad Alwaleedy, Saeed Mohemmed, Ravikant Karale, Komal B. Kabara, Ashok C. Kumbharkhane	355-368
53	Synthesis, Characterisation of Ni-beta Zeolite A. N. Kalyankar, S. S.Jadhav, A.L.Choudhari	369-373
54	To Analyze Intermolecular Interactions among Hydrogen Bonded Liquids by using TDR and FTIR Spectroscopy Neware S G, Pathan A W, Kumbharkhane A C, Chalikwar P A , Mahajan G R ., Shaikh Y H	374-384
55	Incorporation of Zeolites Na-A and Na-X from Condensed and Calcite Coal Fly Ash	385-392

	Dr. Kapure G.P.	
56	Synthesis, Characterization and Biological Activity of Novel Thiazole Derivatives : A Mini Review Vishnu A. Gore, Sunil U. Tekale, Rajendra P. Pawar	393- 398
57	Structural and Electrical Properties of Nickel Ferrite Nanoparticles: Influence of Mixed Fuel Approach V.K. Mande, A.R Bansode, S.R Daruwale, S.P Gadekar R.B. Borade	399- 404
58	A Comprehensive Review on Biological Activity of Flavonoids Sindhu A. Bhosale, Sandip S. Dhotre, Vidya S. Dofe, Rajendra P. Pawar	405- 411
59	Structural and Compositional Study of Al³⁺ doped Cobalt Zinc Nanoferrite Synthesized by Sol-Gel Auto Combustion Method Anil G. Gacche, Arati Chandragupta Mehere, Satish V. Gaikwad, Sopan M. Rathod	412- 419
60	Introductory Optical and Microwave Remote Sensing : A Review Rajeshwari C. Pangarkar, Dheeraj B. Raut, Archana D. Kusale, Satyawan N. Arsul, Nitin B. Gaikwad, Pssradnya R.Maheshmalkar, Sayyad Shafiyoddin	420- 426

Synthesis and Estimation of Noval Heterocyclic Compounds with Its Biological Properties

Manorama B. Motegaonkar

Assistant Professor, Department of Chemistry, Azad Mahavidyalaya AUSA, Maharashtra, India

ABSTRACT

Chalcones were synthesized by the condensation product of DHA in combination with aromatic aldehydes in presence of strong base. It was found that the synthesized chalcones were having prominent role in modern coordination chemistry. The chalcone synthesized by base catalyzed condensation of 3-acetyl-6-methyl-2H-pyran-2,4-(3H) dione (DHA) with different aromatic aldehyde. These chalcones were used for synthesis of derivatives i.e. flavones. The synthesized compounds were characterized by IR, ¹HNMR and mass spectral analysis. The derivatives were further used for the estimation of its biological properties. It was found that the derivative possesses efficient antimicrobial properties. From the study it was found that the synthesized compounds are efficient for further research work.

Keywords: Chalcone, Flavone, IR, ¹HNMR Mass Spectroscopy, Biological Properties

I. INTRODUCTION

Chalcones are the special ligand molecules that used for the synthesis of complexes with desired properties. The complexes are having variations in physical, chemical and biological properties. The existence of the α , β -unsaturated ketone moiety in chalcones is a common part found in a large number of biological active compounds [1]. Therefore, chalcone derivatives from nature or synthetic origin exhibit diverse pharmacological activities, such as antimicrobial [2], antitumor [3], anticancer [4], radical scavenger [5] and inhibitor of topoisomerase I. [6]

Flavanones are important naturally occurring organic compounds possessing a wide range of biological activities used in the treatment of various diseases [7]. Different methods are used for the synthesis of flavones, includes Allan-Robinson synthesis, synthesis from chalcones and via intramolecular Wittig reaction [8]. The most common method used involves Baker-Venkatraman arrangement. In this method 2-hydroxyacetophenone are converted to benzoyl ester, which in presence of base (pyridine / KOH) form 1,3-diketones. The diketones are further cyclised under strong acidic condition to afford the flavones [9]. In recent developments such dehydrative cyclization it includes the use of Amberlyst 15, Co(III) (sulphate)OH, FeCl₃, Br₂/CHCl₃, EtOH/HCl, clay, NaOAc/AcOH and H₂SO₄ under microwave irradiation [10]. Prenylated flavanone is a unique class of naturally occurring flavonoids characterized by the presence of a prenylated side chain in the flavonoid skeleton. It was reported that one phenolic group and certain degree of lipophilicity are required for the activity of the flavonoids. Substitution of the flavonoid ring system with

prenyl groups would increase their lipophilicity and consequently enhance their interaction with cellular membranes [11]. 4',5,7-Trihydroxy-3'-prenylflavanone has been isolated for the first time in 1989 from the chloroform extract of the stem bark of *Erythrina eriotriochoa*. The chemical and pharmaceutical industries are always under the pressure to find out environmental friendly organic reaction methodologies. Microwave irradiation is used for a variety of organic reactions due to their use in a rapid and cleaner synthesis of organic compounds [12].

Flavones are a class of flavonoid based on the backbone of 2-phenyl chromene-4-one(2-phenyl-1-benzopyrane-4-one). They are polyphenolic compound which constitute one of the most numerous & ubiquitous group of plant metabolites, flavonoids are generally present as glycosylated conjugates in fruit, vegetables & other plant products consumed in a normal diet[13].

The immediate family members of flavonoids include flavones, flavanones, flavanols, anthocyanidins and catechins. Luteolin is a flavonoids more specifically, it is thought to play an important role in the human body as an antioxidant, a free radical scavenger, an agent in the prevention of inflammation, a promoter of carbohydrate metabolism, and an immune system modulator. These characteristics of luteolin are also believed to play an important part in the prevention of cancer multiple research experiments describe luteolin as a biochemical agent that can dramatically reduce inflammation and the symptoms of septic shock [14]. Luteolin is most often found in leaves, but it is also seen in rinds, barks, clover, blossom and ragweed pollen. It has also been isolated from *salvia tomentosa*. Dietary sources include celery, green pepper, perilla and camomile tea. Flavonoids have the same basic skeleton and the key feature which distinguishes one structural type from the other is the oxidation level of the various carbon in the heterocyclic ring, chromanones and flavones are integral part of human diet have been reported to exhibit a wide range of biological effects. They also demonstrate, antibacterial, abortifacient, cytotoxic, antimicrobial, antimalarial & antihypertensive activities[15].

II. RESULT AND DISCUSSION

The chalcones of DHA were synthesized by Claisen-Schmidt condensation and characterized as good to excellent yield. The structures of all the compounds were established from IR, ¹H NMR and mass spectral analysis is mentioned above. The IR spectrum of chalcones gives a broad band for OH group at (3000-3125 cm⁻¹) sharp and strong bands were observed at 1700-1750 cm⁻¹ for lactone carbonyl group. Another sharp band was observed at 1598-1650 cm⁻¹ due to the presence of carbonyl group and carbon-carbon band of α , β -unsaturated chalcone system.

The structure of synthesized compounds were converted to the corresponding flavones (MBFI to MBFV) by oxidative cyclisation of chalcones. All these flavones did not give violet colouration with ferric chloride solution and pink colouration with conc. Sulphuric acid. The IR spectra of flavones shows absence of band in the region 3000-3100 cm⁻¹ (OH group). The ¹H NMR Spectra showed singlet at δ 6.2 – 6.8 due to COCH proton and absence of singlet in the region δ 15-16 due to proton of hydroxyl group. In conclusion, we have reported that the synthesized chalcones derivatives using DHA (3-acetyl-6-methyl-2H-pyran-2,4-(3H) dione) possessing good to moderate biological properties. These compounds will be having application in

pharmaceutical, agriculture, medical field for drug development.

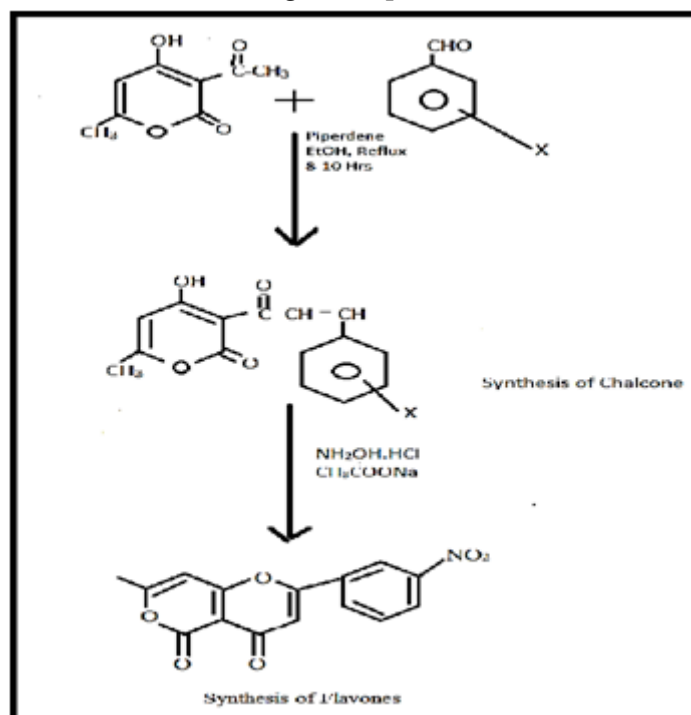


Fig. 1: Schematic representation of synthesized chalcone and Isoxazoline.

III. MATERIAL AND METHODOLOGY

Synthesis of substituted 3-Cinnamoyl-4-Hydroxy-6- Methyl-2-Pyrones (MBCI-V)

10 mmol solutions of dehydroacetic acid and the 10 mmol of aromatic aldehyde were taken and in to that 8-10 drop of piperidine was added as a catalyst. The solutions was dissolved in 30 ml of ethanol solvent, the reaction mixture was then refluxed for a reaction time of 12-15 hrs. After reaction the compounds were checked by TLC. Then the mixture were filtered, dried and recrystallized with suitable solvent i.e. chloroform.[16]

The characterizations were carried out further of synthesized compounds. Melting points were determined in open capillary and are uncorrected. IR spectra were recorded on FT-IR spectrometer using potassium bromide pellet as standard, ^1H NMR were determined on a New AVANCE-500 MHz spectrometer against TMS as internal standard. The mass analysis was also carried out using Shimadzu -machine. Purity of compounds was checked by thin layer chromatography (TLC).

General method for the synthesis of Flavones:

A solution of substituted 2-hydroxy chalcone was dissolved in DMSO (Dimethyl sulfoxide) a catalytic amount of iodine was added and the reaction mixture was refluxed for 2 to 3 hrs till the starting material had completely undergone conversion .Reaction was monitored by TLC, the reaction mixture was cooled at room temperature and sodium thiosulphate solution (10%) was added to decompose excess of iodine. The solid so

obtained was filtered and dried. The dry solid on crystallization from alcohol afforded flavone. The M.P. and Yield are listed in table. The structures of flavones were confirmed by spectral analysis (IR, ¹HNMR and mass).

Characteristic Test:

The compound does not give violet coloration with FeCl₃ solution and Wilson test was negative.

Synthesis of flavones

A solution of 1-(4-hydroxy-6-methyl-2-oxa-2H-pyran-3-yl)-3-(2-fluorophenyl)-2-propenone (0.001mol) and a crystal of iodine was added to it. The reaction mixture was refluxed for 1-2 hrs, the completion of reaction was checked by TLC. After completion of the reaction, the mixture was cooled at room temperature and diluted with water; the excess of iodine was decomposed with saturated sodium thiosulphate solution. The solid thus obtained was filtered & washed with cold water & recrystallized from ethanol to get product name. Similarly other compounds of the series were also synthesized by same procedure. The physical data of synthesized compounds are listed in table no. 1 and 2.

Spectroscopic data of synthesized Flavone derivatives (MBFI-MBFV)

MBFI : 7-methyl-2-(3-nitrophenyl) pyrano [4,3-b] pyran-4,5-dione

IR (KBr, cm⁻¹); 1650 (C=O), 1722(C=O Lactone), 2990 (C-H str. Of -CH₃)

¹HNMR (CDCl₃, δ/ ppm): 2.2 (3H, s, CH₃), 6.5 (1H, s, COCH), 6.0 (1H, s, pyran ring), 6.8 to 8.4 (4H, m, Ar-H)

Mass (m/z): (M+1) 300.

MBFII : 7-methyl-2-(3,4,5-trimethoxyphenyl) pyrano [4,3-b] pyran-4,5-dione

IR (KBr, cm⁻¹); 1648 (C=O), 1716 (C=O Lactone), 2950 (C-H str. Of -CH₃)

¹HNMR (CDCl₃, δ/ ppm): 2.0 (3H, s, CH₃), 3.8-4.2 (9H, s, 3XOCH₃), 6.2 (1H, s, COCN) 6.0 (1H, s, pyran ring), 6.4 to 8.4 (2H, m, Ar-H)

Mass (m/z): (M+1) 345.

MBFIII : 7-methyl-2-(3-methoxyphenyl) pyrano [4,3-b] pyran-4,5-dione

IR (KBr, cm⁻¹); 1658 (C=O), 1720 (C=O Lactone), 2978 (C-H str. Of -CH₃)

¹HNMR (CDCl₃, δ/ ppm): 2.3 (3H, s, CH₃), 3.9 (3H, s, OCH₃), 6.8 (1H, s, COCH), 5.9 (1H, s, pyran ring), 6.8 to 8.2 (4H, m, Ar-H)

Mass (m/z): (M+1) 283.

MBFIV : 7-methyl-2-(3,4-dimethoxyphenyl) pyrano [4,3-b] pyran-4,5-dione

IR (KBr, cm⁻¹); 1651 (C=O), 1720 (C=O Lactone), 2950 (C-H str. Of -CH₃)

¹HNMR (CDCl₃, δ/ ppm): 2.1 (3H, s, CH₃), 3.9-4.2 (6H, s, 2XOCH₃), 6.8 (1H, s, COCH), 6.0 (1H, s, pyran ring), 6.4 to 8.2 (4H, m, Ar-H)

Mass (m/z): (M+1) 315.

MBFV : 7-methyl-2-(2-florophenyl) pyrano [4,3-b] pyran-4,5-dione

IR (KBr, cm⁻¹); 1668 (C=O), 1722 (C=O Lactone), 2990 (C-H str. Of -CH₃)

¹HNMR (CDCl₃, δ/ ppm): 2.2 (3H, s, CH₃), 6.6 (1H, s, COCH), 6.0 (1H, s, pyran ring), 6.3 to 8.2 (4H, m, Ar-H)

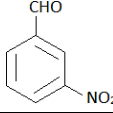
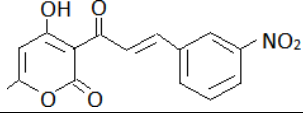
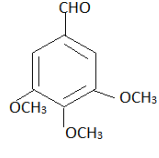
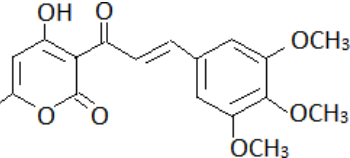
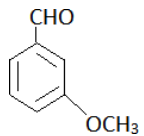
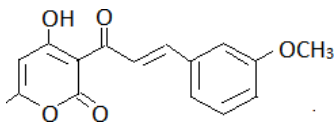
Mass (m/z): (M+1) 273.

Biological Activity

The synthesized compounds were tested in in vitro for antimicrobial activity against bacterial isolates like *S. aureus*, *E. coli* and *Salmonella Typhi* and fungi species like *Fusarium oxysporum*, *Candida albicans* and *Aspergillus flavus*. The concentrations of compounds were taken as 150 µg/ml each. The antimicrobial activity was checked by agar plate diffusion method. The concentrations used for activity was confirmed after estimating the MICs of each compound.

The solvent used for assay was dimethyl sulfoxide (DMSO) which further diluted with water. Nutrient agar and PDA (Potato Dextrose Agar) was used as the growth medium for the bacterial and fungal species respectively. DMSO was used as a negative control. The results were compared with standard drug penicillin for antimicrobial activity by measuring the zone of inhibition in mm using 150 µg/mL were mentioned in table no.3. Antimicrobial activity was measured as a diameter of zone of inhibition (mm) [17-18].

Table 1: Percentage yield and melting point of substituted 3-Cinnamoyl-4-Hydroxy-6- Methyl-2-Pyrones.

Entry	X	Product	Yield %	Melting point °C
1		MBCI 	70	190
2		MBCII 	80	198
3		MBCIII 	85	195

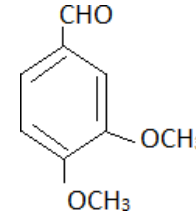
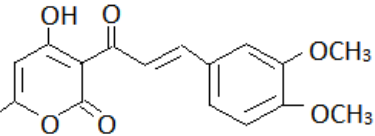
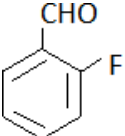
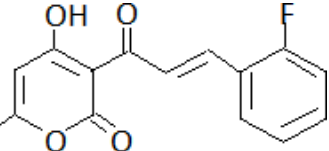
4		MBCIV		80	176
5		MBCV		84	160

Table 2 Physical data of Flavones derivation (MBFI-MBFV)

Compounds	Molecular Formula	M. P (°C)	Yield %
MBF I	C15H9O6N	210	85
MBF II	C18H16O7	250	88
MBF III	C16H12O5	212	65
MBF IV	C17H14O6	205	80
MBF V	C15H9O4F	260	79

Table 3. Antimicrobial activity of Flavones

Compound	Bacteria (Zone of Inhibition in mm)			Fungi (Zone of Inhibition in mm)		
	A	B	C	D	E	F
MBF I	14	19	21	13	16	14
MBF II	15	17	19	15	17	12
MBF III	18	15	18	18	15	18
MBF IV	19	18	18	12	18	17
MBF V	14	20	16	14	20	19
Penicillin*	11	10	12	10	12	13

*standard, A- *S. aureus* , B- *E. coli* , C- *S. Typhi* , D- *Fusarium oxysporum*, E- *Candida albicans* , F- *Aspergillusflavus*.

Acknowledgement

The authors are thankful to the director of IICT, Hyderabad and Dr. Makarand Kulkarni, Solapur University, Solapur for providing spectral analysis facilities to carry out research programme.

IV. REFERENCES

- [1]. Haripara K, Patel S, Joshi A and Paresh H, *Indian J Heterocycl Chem.*, 2004; 13:221.
- [2]. Wagner E, Becam L and Nowakowska E, *Bioorg Med Chem.*, 2004; 12:265-272.
- [3]. Ngaini Z, Siti M Haris-Fadzillah, Hasnain Hussain and Kamarulzamon Kamaruddin, *World J Chem.*, 2009; 4(1): 09-14.
- [4]. Vogel AI, *Textbook of Practical Organic Chemistry*, 4th Ed., Longman, 1981; 1371p.
- [5]. Collin C H, *Microbiological Methods*, Butter Wrths, London, 1964;92.
- [6]. Gravestock M B and Ryley J F, *Annual Reports in Medicinal Chem.*, 1984; 19:127-136.
- [7]. AFWelton, LDTobias, CFiedler-Nagy, WAnderson, WHope, KMiddelton Jr; JBHarbirne and AR Liss, New York; 1986,231.
- [8]. Havsteen. *Biochem Pharmacol* 1983;32:1141.
- [9]. A Banerji and N Goomer. *Synthesis*1980:874.
- [10]. Y Hoshino, T Oohinata and N Takeno. *Bull Chem Soc Jpn* 1986; 59:2351.
- [11]. Y LeFloch'h and M LeFeuvre. *Tetrahedron Lett* 1986; 27:2751.
- [12]. M Balogh and P Laszlo. *Organic Chemistry Using Clays*, Springer, Berlin, 1993. JChisen, IC Chisen, JS Rafelt, DJ Macquarrie and JH Clark. *Chem Commun* 1997:2203.
- [13]. Y Hoshino and N Takino. *Bull Chem Soc Jpn* 1987; 60:1919-1920.
- [14]. A Nishinaga, H Ando, K Maruyama and T Mashino. *Synthesis* 1982;839.
- [15]. PK Zubaidha, AM Hashmi and RS Bhosale. *Hetrocyclic Commun* 2005; 11:9100.
- [16]. S Garg, MPS Ishar, R Sarin, RP Gandhi. *Indian J Chem Soc* 1994;33B:1123-1128.
- [17]. JC Jung, JP Min and OS Park. *Synth Commun* 2001; 31(12):1837
- [18]. RS Verma, R. K Saini and D Kumar. *J Chem Res (S)* 1998:348-349.

Evaluation of Antimicrobial Activity of 4-(Benzo[D]Thiazol-2-Yl) Phenol and Its Derivatives

A. S. Mathwale¹, V. K. Jadhav², A. B. Chidrawar^{2*}

¹Research Center of Chemistry, Degloor College, Degloor, Dist: Nanded – 431717, Maharashtra, India

²Department of Chemistry, Vai Dhunda Maharaj Degloorkar College, Degloor, Dist: Nanded, Maharashtra, India

ABSTRACT

The synthesis of 4-(benzo[d]thiazol-2-yl)phenol(**3**) (**Scheme-1**) by reaction of 2-aminobenzenethiol(**1**) and 4-hydroxybenzaldehyde(**2**) reflux in presence of toluene as a solvent. This reaction mixture is kept for overnight, the crystals of 4-(benzo[d]thiazol-2-yl)(**3**) obtained. Filtered and dried. As well as synthesis of 4-(benzo[d]thiazol-2-yl)-2-methoxyphenol(**5**) (**Scheme-2**) by reaction of 2-aminobenzenethiol(**1**) and 4-hydroxy-3-methoxybenzaldehyde(**4**) reflux with toluene as a solvent. This reaction mixture is kept for overnight, the crystals of 4-(benzo[d]thiazol-2-yl)-2-methoxyphenol(**5**) obtained. Filtered and dried.

The structures for the synthesized compounds are assigned on the basis of IR, ¹HNMR and Mass spectral studies.

KEYWORDS: 2-amino benzenethiol, 4-hydroxybenzaldehyde, 4-(benzo[d]thiazol-2-yl), toluene, 4-hydroxy-3-methoxybenzaldehyde, 4-(benzo[d]thiazol-2-yl)-2-methoxyphenol

I. INTRODUCTION

The resistance of pathogenic bacteria and fungi to available antibiotic drugs has been posing a challenge to chemists and pharmacists. An interest in the design and development of new active antimicrobial agents can be ascribed to both the increasing emergency of bacterial resistance to antibiotic therapy and newly emerging pathogens[1,2]. Recently, the discovery of new compounds to deal with resistant bacteria and fungi has become one of the most important areas of antibacterial and antifungal research. The heterocyclic scaffold, benzothiazole is a privileged system with multiple applications. A number of 2-aminobenzothiazoles were intensively developed in the 1950s as central muscle relaxants. Riluzole(**1**) (6-trifluoromethoxy-2-benzothiazoleamine, PK-26124, RP-25279) acts as a glutamate neurotransmission agent in biochemical, electrophysiological and behavioral experiments[3]. Research has been carried out recently on benzothiazole derivatives which are found to possess diverse chemical reactivity and wide spectrum of biological activities. The benzothiazole pharmacophore unit is found in several drugs which exhibit antimicrobial[4], antitumor[5], antioxidant behaviors[6] and as an acetyl cholinesterase[7] enzyme inhibitor. It is well documented that the unique frame work of benzothiazole is found in many antagonists like Ca²⁺ channel, LTD4 and orexin receptors[8]. By bearing in mind the aforesaid pharmacological applications of benzothiazole derivatives, our

group has synthesized recently 3-(2-(benzo[d]thiazol-2-yl)phenoxy)-1-(substituted acyclic/cyclic amino)propan-1-one derivatives and found them to be potent antimicrobial agents[9]. The chemistry of organophosphorus compounds has been growing rapidly since these molecules are involved in various biological processes, such as important substrates in the drug and pro-drugs synthesis. The phosphorus molecules play a vital role in medicinal and agricultural chemistry[10]. They also offer attractive possibilities for structural, synthetic and mechanistic studies[11]. Particularly, phosphoramidates have attained a distinctive reputation in P-chemistry since they act as pro-drugs and drugs in the antiviral and antitumor therapy[12]. The cyclic phosphorus derivative, cyclophosphamide is a pro-drug and it has been used in anticancer therapy[13]. The phosphoramidates in which the phosphate group is bonded with acyclic/cyclic/aryl amines or amino acid residues could develop lipophileicity[14] and as a result enriches their bioavailability and biological potency. These groups can also modify the physicochemical properties of active benzothiazole motif. The phosphoramidate derivatives of 5-nitroquinolin-8-ol and 5-nitroindazole synthesized recently by our group showed potential antimicrobial and antioxidant activities[15] and these results encouraged us to study the synthesis of title compounds and evaluate their bioactivity.

II. EXPERIMENTAL SECTION

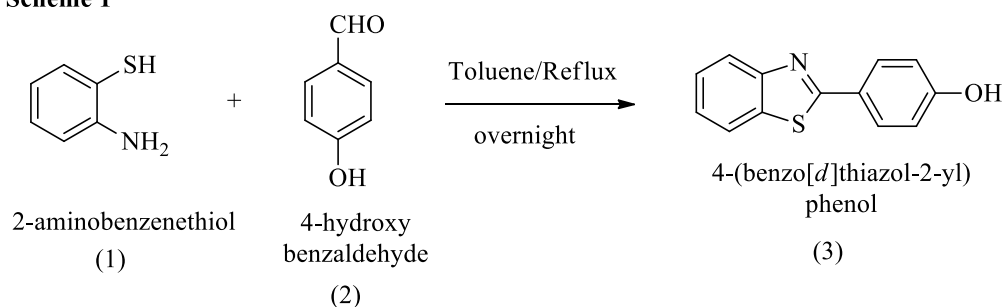
All melting points were determined in open capillary tube and were uncorrected. IR spectra were recorded with potassium bromide pellets technique, ^1H NMR spectra were recorded on AVANCE 300 MHz Spectrometer in DMSO using TMS as internal standard. Mass spectra were recorded on a FT VG-7070 H Mass Spectrometer using EI technique at 70 eV. All the reactions were monitored by thin layer chromatography.

III. MATERIAL AND METHODS

1. Synthesis of 4-(benzo[d]thiazol-2-yl)phenol :

In the present work, we report synthesis of 4-(benzo[d]thiazol-2-yl)phenol(**3**) (**Scheme-1**) by reaction of 2-amino benzenethiol(**1**) and 4-hydroxybenzaldehyde(**2**) reflux in presence of toluene as a solvent. This reaction mixture is kept for overnight, the crystals of 4-(benzo[d]thiazol-2-yl) phenol(**3**)obtained. Filtered and dried. The Purity of compound was checked by TLC. The compound observed on TLC as single spot in benzene. Structures to these compounds are assigned on the basis of elemental analysis and spectral data.

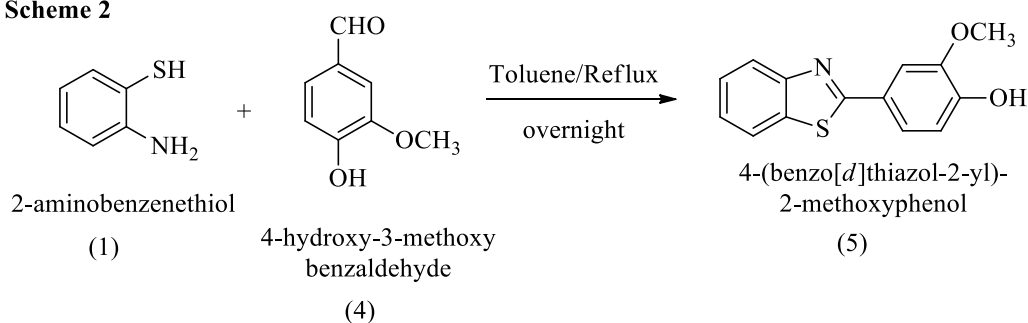
Scheme 1



2. Synthesis of 4-(benzo[d]thiazol-2-yl)-2-methoxy phenol :

In the present work, we report synthesis of 4-(benzo[d]thiazol-2-yl)-2-methoxyphenol(5) (Scheme-2) by reaction of 2-aminobenzenethiol(1) and 4-hydroxy-3-methoxybenzaldehyde(4) reflux with toluene as a solvent. This reaction mixture is kept for overnight, the crystals of 4-(benzo[d]thiazol-2-yl)-2-methoxyphenol(5) obtained. Filtered and dried. The Purity of compound was checked by TLC. The compound observed on TLC as single spot in benzene. Structures to these compounds are assigned on the basis of elemental analysis and spectral data.

Scheme 2



Chemical analysis :

1. 4-(benzo[d]thiazol-2-yl) phenol (3)

IR:(KBr/cm⁻¹) :3410 (-OH), 1621 (C=N), 1610-1590 (C=C), 780 (C-S),EI-MS: (m/z:RA%) :228 (M+1), **Elemental analysis:**C₁₃H₉NOS Calculated: (%) C, 68.70; H, 3.99; N, 6.16; O, 7.04; S, 14.11 Found (%) : C, 68.68; H, 3.95; N, 6.10; O, 7.01; S, 14.08

2. 4-(benzo[d]thiazol-2-yl)-2-methoxy phenol (5)

IR:(KBr/cm⁻¹) :3405 (-OH), 1620 (C=N), 1615-1595 (C=C), 784 (C-S),EI-MS: (m/z:RA%) :258 (M+1), **Elemental analysis:**C₁₄H₁₁NO₂S Calculated: (%) C, 65.35; H, 4.31; N, 5.44; O, 12.44; S, 12.46 Found (%) : C, 65.30; H, 4.30; N, 5.42; O, 12.42; S, 12.41

IV. RESULTS AND DISCUSSION

Substituted benzothiazoles exert adverse effects on viruses and also act on yeasts and fungi. The antiviral screening results of MBT showed significant activity against two out of three viruses tested. The antifungal effects of MBT were also tested against *Aspergillus niger* with a suspension of spore-free mycelium homogenate as inoculum, and a 33 mg L⁻¹ MBT concentration was the lower limit for 100% growth inhibition after five days of cultivation. Similar results, although obtained under other conditions, are described for the fungus *Trichophyton rubrum*. It was observed that for complete growth inhibition of *Microsporium gypseum* and *Epidermophyton floccosum*, MBT concentration had to exceed 50 mg L⁻¹. The results of a study suggested that the thiol group of MBT is essential for its toxicity, since benzothiazole (BT)

was not an active fungicide. However, in another experiment the presence of zinc destroyed the fungicidal activity of MBT, and this contradicts what was suggested above.

The antifungal activity of 4-(benzo[d]thiazol-2-yl) phenol, a significant inhibitory activity against *Aspergillus niger*, *Penicillium roqueforti*, and *Chaetomium globosum* was observed. On the other hand, 4-(benzo[d]thiazol-2-yl)-2-methoxy phenol exhibited potent inhibitory activity against *Aspergillus niger* and *Chaetomium globosum*.

V. CONCLUSION

Substituted benzothiazoles have been widely explored for industrial applications since their discovery. However, the biological activity of this class of compounds deserves further investigation. This becomes clear when microbial infections are considered. Although the research on this subject is incipient, the number of reports disclosing the effects of MBTs on pathogens of clinical interest has recently been increasing. Substituted 4-(benzo[d]thiazol-2-yl)phenols have been shown to be promising, which calls for the design of more efficient antimicrobial, anthelmintic, anti-inflammatory, and anti-allergic agents. Future studies will undoubtedly uncover unexpected properties and applications. Advances in this field will require analyses of the structure-activity relationships of MBTs, as well as the mechanisms of action of these compounds.

ACKNOWLEDGEMENTS

The authors are thankful to the Principal, Degloor College, Degloor for providing laboratory facilities and the Director, Indian Institute of Chemical Technology, Hyderabad for providing spectra.

VI. REFERENCES

- [1]. Cohen, M. L. *Nature*. 2000, 406, 762-767. doi:10.1038/35021206.
- [2]. Barrett, C. T.; Barrett, J. F. *Curr. Opin. Biotechnol.* 2003, 14, 621-626. doi:10.1016/j.copbio.2003.10.003.
- [3]. (a) Zarate, Jr, C. A.; Payne, J. L.; Quiroz, J.; Sporn, J.; Denicoff, K. K.; Luckenbaugh, D.; Charney, D. S.; Manji, H. K. *Am. J. Psychiatry*. 2004, 161, 171-174; (b) Coric, V.; Taskiran, S.; Pittenger, C.; Wasyluk, S.; Mathalon, D. H.; Valentine, G.; Saksa, J.; Wu, Y. T.; Gueorguieva, R.; Sanacora, G.; Malison, R. T.; Krystal, J. H. *Biol. Psychiatry*. 2005, 58, 424-428; (c) Mathew, S. J.; Amiel, J. M.; Coplan, J. D.; Fitterling, H. A.; Sackeim, H. A.; Gorman, J. M. *Am. J. Psychiatry*. 2005, 162, 2379- 2381.
- [4]. (a) Palmer, P. J.; Trigg, R. B.; Warrington, J. V. *J. Med. Chem.* 1971, 14, 248-251.
- [5]. (a) Hall, I. H.; Peaty, N. J.; Henry, J. R.; Easmon, J.; Heinisch, G.; Pustinger, G. *Arch. Pharm. (Weinheim)*. 1999, 332, 115-123; (b) Bénétou, V.; Besson, T.; Guillard, J.; Léonce, S.; Pfeiffer, B. *Eur. J. Med. Chem.* 1999, 34, 1053-1060; (c) Hutchinson, I.; Bradshaw, T. D.; Stevens, M. F. G.; Westwell, A. D. *Bioorg. Med. Chem. Lett.* 2003, 13, 471-474.
- [6]. (a) Ivanov, S. K.; Yuritsyn, V. S. *Neftekhimiya*. 1971, 11, 99-107; (b) Ivanov, S. K.; Yuritsyn, V. S. *Chem. Abstr.* 1971, 74, 124487m.

- [7]. Nagel, A. A.; Liston, D. R.; Jung, S.; Maher, M.; Vincent, L. A.; Chapin, D.; Chen, Y. L.; Hubbard, S.; Ives, J. L.; Jones, S. B. *J. Med. Chem.* 1995, **38**, 1084-1089.
- [8]. (a) Kashiyama, E.; Hutchinson, I.; Chua, M. S.; Stinson, S. F.; Phillips, L. R.; Kaur, G.; Sausville, E. A.; Bradshaw, T. D.; Westwell, A. D.; Stevens, M. F. G. *J. Med. Chem.* 1999, **42**, 4172-4184; (b) Lau, C. K.; Dufresne, C.; Gareau, Y.; Zamboni, R.; Labelle, M.; Young, R. N.; Metters, K. M.; Rochette, C.; Sawyer, N.; Slipetz, D. M.; Charette, L.; Jones, T.; McAuliffe, M.; McFarlane, C.; Ford-Hutchinson, A. W. *Bioorg. Med. Chem.* 1995, **5**, 1615-1620.
- [9]. Sreedhar, B.; Veera Reddy, T.; Naga Raju, C.; Padmavathi, V.; Vidya Sagar Reddy, G. *Der Pharma Chemica.* 2015, **7**, 42-47.
- [10].(a) Engel, R. *Chem. Rev.* 1977, **77**, 349-367; (b) Hiratake, J.; Oda, J. *Biosci. Biotechnol. Biochem.* 1997, **61**, 211-218; (c) Schug, K. A.; Lindner, W. *Chem. Rev.* 2005, **105**, 67-114.
- [11].(a) Hartly, R. *The Chemistry of Organophosphorous Compounds*; John Wiley and Sons: New York, USA, 1996; (b) Corbridge, D. E. C. (Ed.). *Phosphorous*; Elsevier: New York, USA, 1990. [12] (a) Congiatu, C.; McGuigan, C.; Jiang, W. G.; Davies, G.; Mason, M. D. *Nucleosides Nucleotides Nucl. Acids.* 2005, **24**, 485-489; (b) McGuigan, C.; Cahard, D.; Sheeka, H. M.; De Clercq, E.; Balzarini, J. *J. Med. Chem.* 1996, **39**, 1748-1753; (c) McGuigan, C.; Harris, S. A.; Daluge, S. M.; Gudmundsson, K. S.; McLean, E. W.; Burnette, T. C.; Marr, H.; Hazen, R.; Condreay, L. D.; Johnson, L.; De Clercq, E.; Balzarini, J. *J. Med. Chem.* 2005, **48**, 3504-3515; (d) Perrone, P.; Luoni, G. M.; Kelleher, M. R.; Daverio, F.; Angell, A.; Mulready, S.; Congiatu, C.; Rajyaguru, S.; Martin, J. A.; Le Pogam, S.; Najera, I.; Klumpp, K.; Smith, D. B.; McGuigan, C. *J. Med. Chem.* 2007, **50**, 1840-1849.
- [12].(a) Dirven, H. A. A. M.; Van Ommen, B.; Van Bladeren, P. J. *Chem. Res. Toxicol.* 1996, **9**, 351-360; (b) Niculescu-Duvaz, I.; Spooner, R.; Marais, R.; Springer, C. J. *Bioconjugate Chem.* 1998, **9**, 4-22.
- [13]. Zemlicka, J. *Biochim. Biophys. Acta.* 2002, **1587**, 276-286.
- [14]. Munichandra Reddy, S.; Subba Rao, D.; Sudhamani, H.; Gnana Kumari, P.; Naga Raju, C. *Phosphorus, Sulfur Silicon Relat. Elem.* 2015, **190**, 2005-2012.



Physico-Chemical Analysis of Bore well Water Sample of Tadola Village (M.S.)

Dr. Kadam Dadasaheb Devidasrao

Assistant Professor, Department of Chemistry, Narayanrao Waghmare College, Akhada Balapur, Dist. Hingoli-431701, Maharashtra, India

ABSTRACT

The present study is undertaken in order to find out quality of borewell water which is used for drinking purpose, cultivation of crop as well as household level in Tadola village of Maharashtra. We know that the underground water is the most important source of natural water. So the present work deals with valuation of borewell water of different place in Tadola village carried out in year 2020-2021. The physico-chemical parameters such as pH, temperature, electrical conductivity, total hardness, total alkalinity, dissolved oxygen, total dissolved solid are studied to measure quality of water.

Key words: Borewell, quality, household level, drinking water, physico-chemical analysis.

I. INTRODUCTION

We know that water is most important and most valuable natural resource available on the earth surface. Without which we cannot imagine life on the earth surface. Water is the fundamental need of all plants, animals. The chemical formula of water is H_2O . It means it is a combination of two hydrogen atoms and one oxygen atom. Near about 70% of earth surface is occupied by water. All over the world borewell water consists the largest and most important source of fresh potable water. We know that borewell water is the abundant source of drinking as well cultivation of crop in urban and rural areas in India. Due to rapid growth of population, urbanization, industrialization and irrigation affects the availability and quality of groundwater because of its over exploitation and improper waste disposal. Generally water quality of borewell changes from place to place according to the nature of soils, rocks and surfaces through which-it moves (Seth, 2014, Okora N 2017). Industrial discharges, urban activity, agriculture can affect borewell water quality (Govindarajan, 2014). Borewell water is enormous source of drinking purposes as well as for cultivation of crop used in tadola village areas. In most of the countries major diseases are caused by water because of it's poor quality.

II. METHODOLOGY

Analysis of water sample :-

The water quality parameters were P^H, electrical conductivity, total hardness, total alkalinity, temperature, dissolved oxygen, total dissolved solid. These parameters analyzed by using standard methods recommended by APHA (2005) and Trivedi and Goel (1984) for the examination of water. The values of these parameters were compared with Indian Standards (IS) Bureau of Indian Standards (BIS) and World Health Organization (WHO)

Table 1 : Water standards for ISI, BIS and WHO

Sr.No.	Parameters	IS	BIS	WHO
1	P ^H	6.5-7.5	6.5-7.5	7-8
2	Electrical conductivity (μ mho/cm)	---	---	1400
3	Total Hardness (ppm)	200-600	600	100
4	Total Alkalinity (ppm)	200-600	600	-
5	Temperature (°C)	---	---	---
6	Dissolved oxygen (mg/lit)	--	---	---
7	Total Dissolved solid (ppm)	500-2000	2000	1000

III. RESULTS AND DISCUSSION

Table 2 : Physico-chemical Analysis of Borewell water sample of Tadola Village.

Sr. No.	Parameters	S1	S2	S3	S4	S5
1	P ^H	6.75	6.76	7.2	7.0	6.2
2	Electrical conductivity (μ mho/cm)	1802	1855	1502	1432	1209
3	Total Hardness (ppm)	275	280	355	350	240
4	Total Alkalinity (ppm)	785	658	350	355	362
5	Temperature (°C)	26	28	30	29	24
6	Dissolved oxygen (mg/lit)	4.3	6.7	7.5	7.4	7.0
7	Total dissolved solids (ppm)	1342	1205	1273	1061	1103

Where,

S₁ = Kadam galli station

S₂ = Adsul galli station

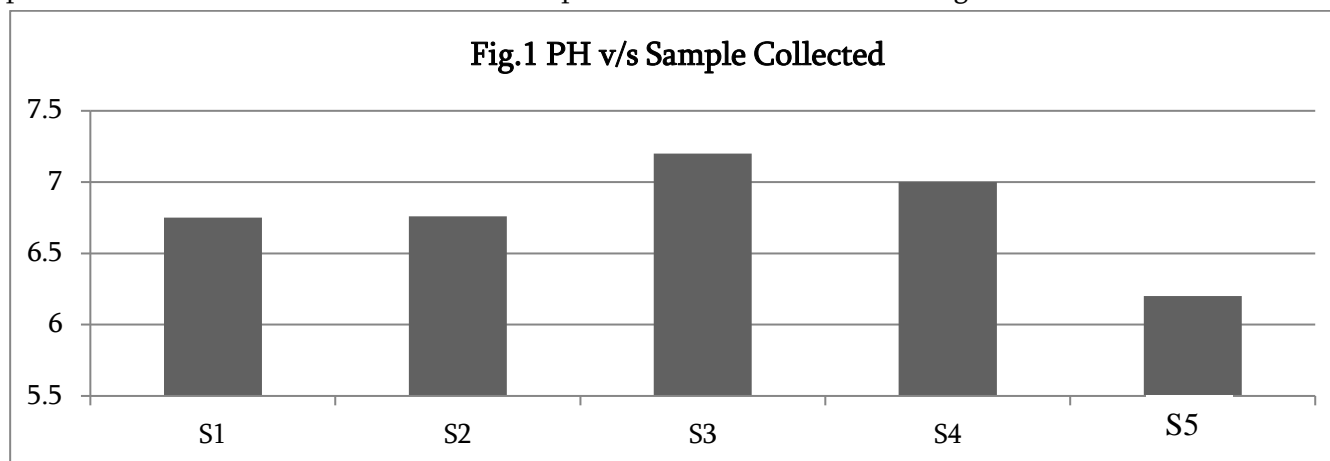
S₃ = Devi galli station.

S₄ = Maroti mandir station

S₅ = Maske galli station

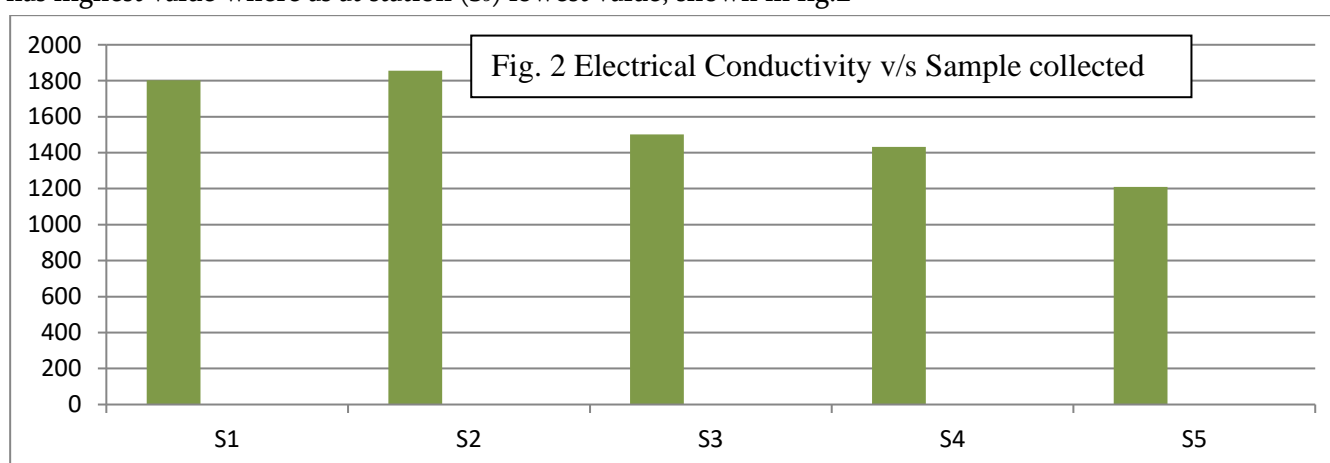
1) P^H

It is defined as hydrogen ion concentration of a solution. It is very important for aquatic life because most of the organisms are adopted to an optimum P^H range and will not stand with small change in P^H value. The P^H value of stations in the study range from 6.2 to 7.2 with a mean value 6.78 indicating slightly acidic in nature. According to Shrivastava and Patil (2002), the value of P^H below 6.5 causes corrosion in pipe and their by presence of toxic metals such as copper, zinc and cadmium. According to Indian standards (2012) the value of P^H for drinking water ranges from 6.5 to 8.5. The P^H values of sample collected at S₁, S₂, S₃ and S₄ are within permissible limits where as at S₅ is below the permissible limits as shown in fig.1



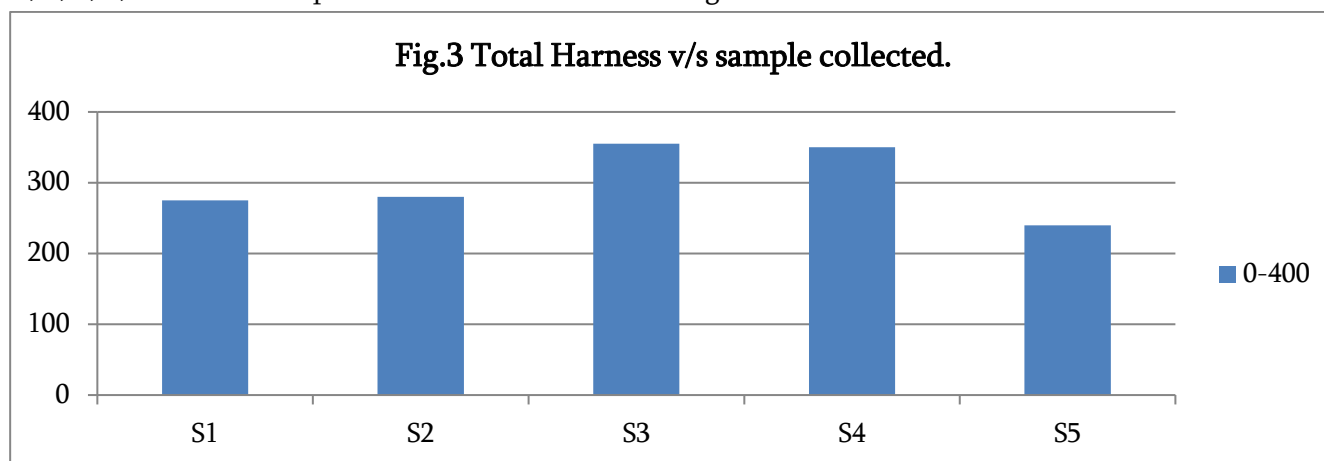
2) Electrical Conductivity :

Electrical conductivity is defined as the ability of an aqueous solution to conduct to the electric current. According to Acharya (2008) electrical conductivity is a useful for detection of purity of water. The electric conductivity depends upon the presence of free ions, temperature, nutrient status, variations in dissolved solids and mobility of water. It is observed that borewell water generally possess high electrical conductivity due to the presence of high amount of dissolved salts. It is a measure of capacity of water to conduct electric current. The electrical conductivity of water samples collected from various stations ranges from 1209 $\mu\text{mho/cm}$ to 1855 $\mu\text{mho/cm}$. the mean value of electric conductivity is 1560 $\mu\text{mho/cm}$. At station (S₂) has highest value where as at station (S₅) lowest value, shown in fig.2



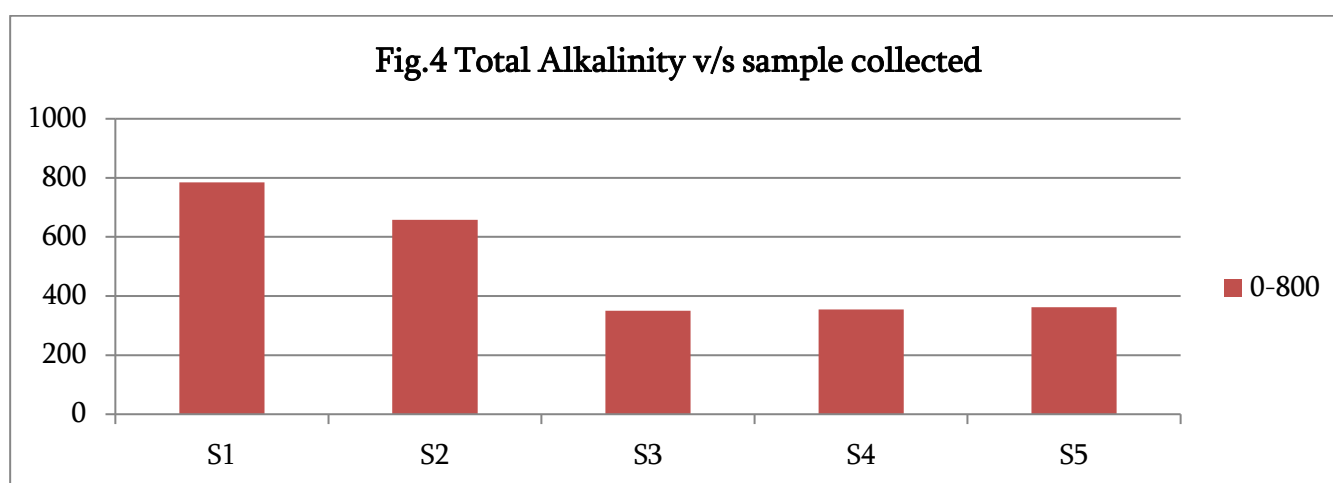
3) Total hardness :

The presence of calcium and magnesium metals constitutes the total hardness of water. The most common salts are sulphates, carbonates and fluorides of calcium and magnesium. The hardness of water is very useful in order to prevent the corrosion in the pipes by forming a thin layer of scale thereby reducing the entry of heavy metals from the pipe to the water (shrivastava, 2002). The total hardness of sample collected at S₁,S₂,S₃,S₄,&S₅ are within permissible limits as shown in fig. 3



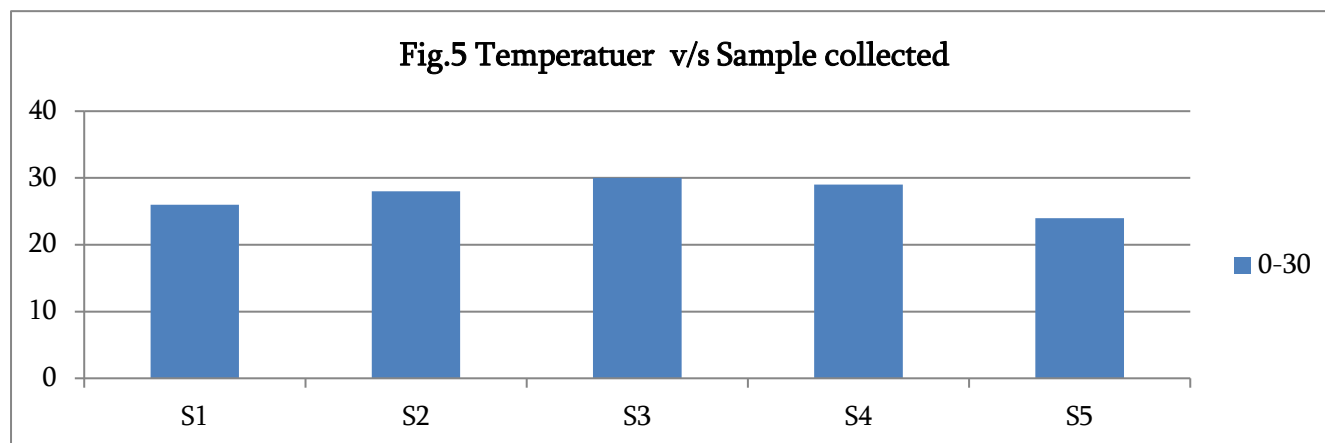
4) Total Alkalinity :-

The total alkalinity is due to the presence of minerals dissolved in water from soil. It gives information about natural salts present in water. The total alkalinity of water samples ranged between 350 ppm to 785 ppm at all the sampling stations as shown in fig. 4. The 502 ppm is the mean value of alkalinity. The alkalinity value of samples collected at S₁ and S₂ are above the Indian standard limits i.e. 200 ppm -600 ppm where as at S₃, S₄ and S₅ are within the permissible limits. The high value of alkalinity should be due to the dissolution of mineral in water from minerals rich soil. According to Sawyer et. al.(2000) the various ionic salts such as carbonates, bicarbonates, phosphates, hydroxides, organic acids, borates, silicates and in few cases ammonia or hydroxides are responsible for the alkalinity.



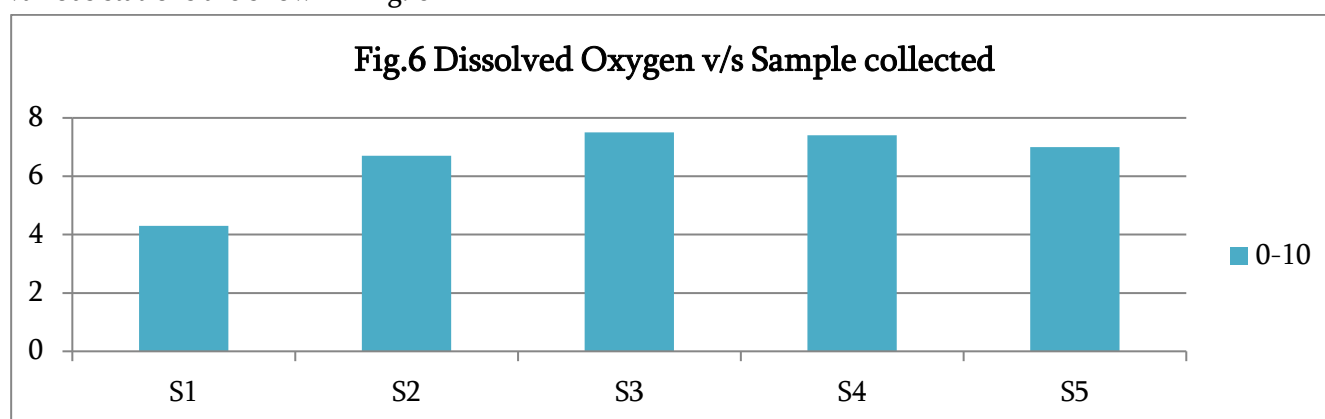
5) Temperature :-

Temperature is one of the most important physical parameter used for detection of quality of water. It affects on the aquatic organisms, vegetation and biological activity. The temperature value of samples collected ranges from 24°C to 30 °C at all the stations and which is shown in fig.5



6) Dissolved oxygen :-

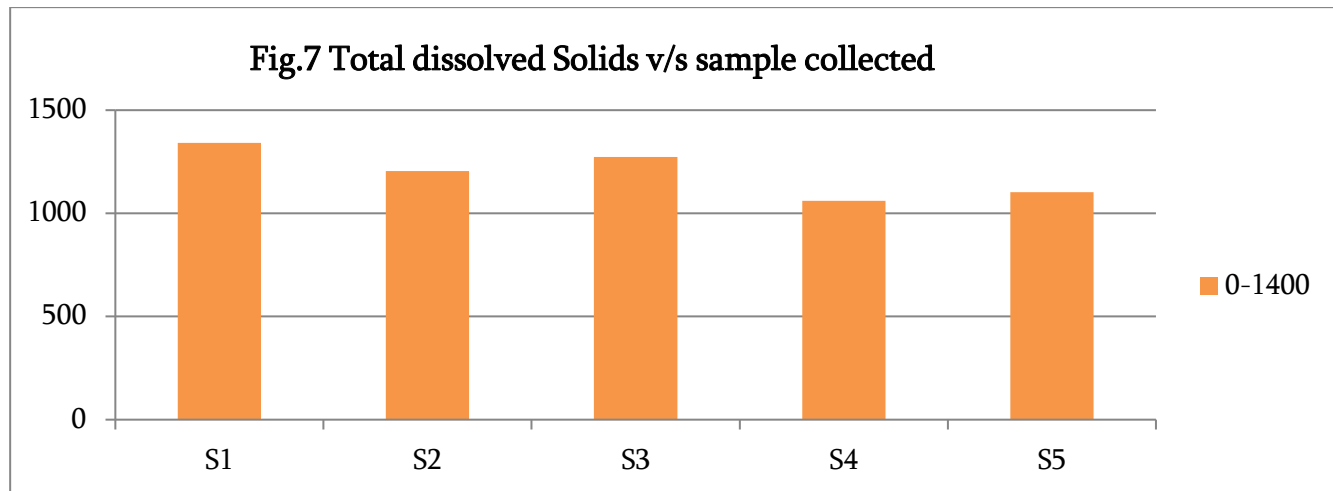
Dissolved oxygen is one of the most important parameter used in water quality assessment and biological processes preventing in the water. The degree of pollution in the water bodies can be determined with the help of dissolved oxygen. The presence of dissolved oxygen in water increases the quality of water and also acceptability. The dissolved oxygen values of water samples ranged from 4.3 mg/lit. to 7.5 mg/lit. The mean dissolved oxygen value was found to be 6.58 mg/lit. The dissolved oxygen values of samples collected at various stations are shown in fig. 6



7) Total dissolved Solids :-

The total dissolved solids mainly consists of inorganic substances which are dissolved in water. The effects of total dissolved solids on drinking water quality depends on the levels of its individual components, mineral depositions, taste, excesses hardness and corrosion are common properties of highly mineralized water. The total dissolved solids of water samples collected ranges from 1061 ppm to 1342 ppm. The mean value of total

dissolved solid was found to be 1196.8 ppm as shown in fig. 7 The total dissolved solid values of all the sampling stations are within the limits of Indian standards and safe for drinking.



IV. CONCLUSION

The present study of physico-chemical parameters is carried out during 2020-2021 of borewell water sample collected from five stations in Akhada Balapur city. During the study it was observed that the P^H values of S₁, S₂, S₃ and S₄ are normal as per IS and BIS whereas at S₅ it is below the normal level. The value of P^H at all the stations were slightly acidic in nature. The electrical conductivity value is normal as per WHO standard only at S₅ stations. The total hardness value are normal in all sampling station as per IS and BIS whereas it is above as per WHO to all the sampling stations.

It is observed that the total alkalinity at S₃, S₄ and S₅ are normal level as per IS and BIS but is above at S₁ and S₂ stations as per IS and BIS. The total dissolved solids value is within the permissible limits as per IS and BIS to all the sampling stations whereas it is high at all the sampling stations as per WHO standards.

Overall observation clears that the borewell water quality of Akhada Balapur city is recently very good. It is necessary to construct gutters to avoid percolation of dirty polluted water.

There should be pre-treatment of sewage water before disposed into the environment to minimize the contamination of avoiding health hazards.

V. REFERENCES

- [1]. Acharya GD, Hathi MV, Patel AD, Parmar Kc (2008), chemical properties of borewell water in Bhiloda Taluka Region, North Gujarat, India. E-Journal of Chemistry, 5(4): 792-796.
- [2]. Abdul Jameel A, poll.Res, 1998] 17 (2). 111-114.
- [3]. Agarwal, S., Patil, J.P.Goyal, V.C. and Singh, A.2019. Assessment of water supply-Demand Using water Evaluation and planning (WEAP) model for Ur River watershed, Madhya Pradesh, India, Journal of the Institution of Engineers (India) : series A, 100 (1) pp.21-32.

- [4]. APHA (2005) Standard methods for examination of water and waste water, American public Health Association, New York.
- [5]. Ajewole G. (2005), water an overview Nigria Institute of tool science and Technology Nigeria, 2:4-15.
- [6]. Ajay K, Charu S and Pragati S (2005) ; seasonal variation in physico-chemical and microbiological analysis of sewage water in Gwalior city, India; Indian Journal of Ecology 45 (2) : 279-282.
- [7]. Anchal R, Bhardwaj S and Meena T (2016) : surface water quality and associated aquatic insect fauna under different land-uses in solan 58 (District Solan) Himachal Pradesh; Indian Journal of Ecology 43 (1) : 58-64.
- [8]. Bansal J and Dwivedi A (2018) : Assesment of groundwater quality by using water quality index and physico-chemical parameter : review. International journal of Engineering sciences and research technology 7(2) : 170-174 .
- [9]. BIS 1991 : specification for drinking water IS: 10500:1991, Burea of Indian Standard.
- [10].Dattatraya B; Isub ali s; Gaikwad G.G. Taikar D.R., and Dhore J. (2011), physic-chmical characteristics of bore well water quality in Nagpur region (south zone), J.chem. pharm. Res; 2011 3 (2) : 922-927.
- [11].Govindarajan M, Senthilnathan T. (2014) ; Borewell water quality and its health impact analysis in an industrial area. Int.J.Curr. Microbiol.App.Sci.3 : 1028-1034
- [12].IS 10500, 1991 : Indian Standards for drinking water. 1-9.
- [13].Khadsan R and Mangesh V (2020) ; Drinking water quality analysis of some bore-well water of Chkhli Town, Maharashtra. Journal of Industrial pollution control 1(5) : 1-7
- [14].Mali V.C., Ranger K.K. Kumbhar D.A. and Lavate R.A., (2018), physico-chemical Analysis of Bore well water samples of Jath city MS, India ; Int.J.of life sciences, special issue, A10; January 2018.
- [15].Meeravali K Shik Abdul E, Mallela J (2020) ; Physico-chemical analysis of borewell Samples for drinking water quality; Indian Journal of Ecology 47 (11) : 71-74.
- [16].Trivedi RK and Goel PK (1984), Chemical and Biological methods for water pollution status. Environmental publication, karad (India).
- [17].Suresh kommu, S.S.Asadi (2019), quality assessment of bore well and Tap water in and around Hyderabad City, Int. J.or Rec. Tech. and Engi. (IJRTE), Vol.7 Issue-6C2, April 2019 : 594-598.
- [18].Shrivastava VS and Patil PR (2002) Tapti river water pollution by industrial wastes : A statistical approach. Not. Environ. Pollut.Tech.1 (3), 279-283.
- [19].Vinothkanna S, Rajee R and senthilraju K (2020) Assessing ground water quality for the suitability of irrigation of Dindigu District, Tamil Nadu; India. India Journal of Ecology 47 (1): 23-29.

Synthesis and Antimicrobial Activities of New 3-(Chloromethyl)-2-(Piperazin-1-Yl) Quinolone Derivatives

Rajkumar U. Pokalwar

Department of Chemistry, Degloor College, Degloor, Nanded-431717, Maharashtra, India

ABSTRACT

A novel and practical method was created for the synthesis of 3-(chloromethyl)-2-(piperazin-1-yl)quinoline derivatives, which were obtained from 2-chloroquinolin-3-carbaldehydes. Newly synthesised compounds were characterised by IR, ¹HNMR, and mass spectroscopy, and they were tested for their antimicrobial, antibacterial, and antifungal activities. Compounds 4a, 4b, 4c, 4d, 4e were tested against *Candida albicans*, *E. coli*, and *S. aureus* and *S. pyogenes* in comparison to common antibacterial drugs including Ampicillin, Erythromycin, Chloroamphenicol, Norfloxacin, and Ciprofloxacin.

Compounds 4a, 4b, 4c, 4d, and 4e were discovered to have effective antifungal action against *Candida albicans*, *A. niger*, and *A. niger*. Comparing *Clavatus* to common forms of Nystatin and Griseofulvin.

Keywords: 2-chloroquinoline-3-carbaldehyde, 3-(chloromethyl)-2-(piperazin-1-yl)quinoline, antibacterial, antifungal.

I. INTRODUCTION

Quinoline ring systems, in which the benzene ring is fused with the pyridine heterocyclic ring system, comprise a significant class of heterocyclic compounds. With one nitrogen atom in one benzene ring and none in the other ring or at the ring junction, quinolines are also known as benzo[b]pyridine and 1-azanaphthalene. Nitrogen-containing heterocycles have excellent and intriguing medical and pharmacological effects.¹⁻⁴ As an asthma medication, montelukast is utilised.⁵ Additionally, many different kinds of natural goods contain quinolines as their primary component.⁶⁻⁷ drugs.⁸⁻¹⁰ Many synthetic heterocyclic compounds contain and to improve their biological and therapeutic characteristics. Quinoline-ringed compounds demonstrated a range of biological, pharmacological, and chemical activities.¹¹⁻¹² e.g. anti-tuberculosis,¹³ antiplasmodial,¹⁴ antibacterial,¹⁵⁻¹⁶ antihistamine,¹⁷ antifungal,¹⁸ antimalarial,¹⁹⁻²⁰ anti-HIV,²¹ anticancer,²² anti-inflammatory,²³⁻²⁴ anti-hypertensive,²⁵ and antioxidant activities.²⁶ In addition, the use of quinolines as tyrosine kinase/PDGFR-RTK inhibitor,²⁷ inositol 5-phosphatase (SH₂),²⁸ DNA gyrase B inhibitors as *Mycobacterium tuberculosis*,²⁹ and DNA topoisomerase inhibitors,³⁰ were reported. Racemic fluoroquinolone nadifloxacin was introduced as a topical antibiotic in Japan in 1993 to treat methicillin-resistant staphylococcal infections and acne. Quinolinic acid has recently been used to research bio-organic

and bio-organometallic processes.³¹ Many pharmacologically significant synthetic compounds are designed using the skeleton of the quinoline as a crucial step.³²⁻³³

A very interesting class of organic compounds, 2-Chloroquinoline-3-carbaldehydes can be used as precursors and building blocks for the synthesis of a variety of heterocyclic systems as well as powerful antibiotics for the treatment of cancer and bacteria. The current study indicates that quinoline derivatives display antibacterial and antifungal activities, continuing our work on the synthesis, characterisation, and activity of compounds containing quinoline³⁴⁻³⁹.

II. MATERIALS AND METHODS

Using the described technique, 2-Chloroquinoline-3-carbaldehydes were produced in the lab. Methanol, sodium hydroxide, sodium borohydride, dichloromethane, and piperazine were purchased from S.D. Fine-chem. At atmospheric pressure, all physical constants were calculated in open capillaries. Using TMS as an internal standard, ¹H NMR spectra in CDCl₃, DMSO, and 400 MHz were captured on the AVANCE. On a Bruker FTIR, IR spectra were captured using KBr discs. Mass spectra were captured, displaying a molecular ion peak. TLC was used on Merck silica gel plates to determine the product purity and the rate of the reactions.

General procedure:

2-(piperazin-1-yl)quinoline-3-carbaldehyde(2a): 1.9 gm of 2-Chloroquinoline-3-carbaldehydes (10 mmol) and 4 gm of piperazine were added gradually while being stirred at room temperature in a 50 mL round-bottom flask. The reaction mixture was heated to 45°C. The progress of reaction was monitored on TLC (8:2 – Hexane: ethyl acetate). After the completion of the reaction (4 hr), the reaction mixture was poured on ice cold water, the solid obtained was filtered off and washed with water to get product 2-(piperazin-1-yl)quinoline-3-carbaldehyde, dry wt. 2.10 gm.

(2-(piperazin-1-yl)quinolin-3-yl)methanol (3a): In a 50 ml round bottom flask taken 2-(piperazin-1-yl)quinoline-3-carbaldehyde 1.95 gm (8 mmol) and 15 ml methanol was slowly added sodium borohydride (1.0 gm) under stirring at room temperature. TLC was used to track the reaction's development (8:2 – Hexane: ethyl acetate). The reaction mixture was concentrated under decreased pressure to extract residue once the reaction had finished (10 minutes). Ice cold water was then added to this residue, and the resulting solid was filtered out and rinsed with water to achieve the desired product. (2-(piperazin-1-yl)quinolin-3-yl)methanol, dried in oven at 40 °C for 5.0 hr (1.95 gm).

3-(chloromethyl)-2-(piperazin-1-yl)quinoline(4a): To the stirred solution of (2-(piperazin-1-yl)quinolin-3-yl)methanol 1.72 gm (7 mmol) in DCM (10 ml) in a 50 ml round bottom flask was added dropwise a solution of SOCl₂ (2 ml) in 5 ml DCM. After the complete addition, stirred it for 1 hr at room temperature. The reaction progress was monitored by the TLC (8:2 – Hexane: ethyl acetate), after complete conversion, distilled out the solvent under reduced pressure to get the product, dried in oven at 50 °C for 4.0 hr (1.6 gm).

Antibacterial and Antifungal activity:-

Escherichia coli (MTCC-443), *Pseudomonas aeruginosa* (MTCC-1688), *Staphylococcus aureus* (MTCC-96), and *Streptococcus pyogenes* (MTCC-442) were tested for antibacterial activity. *Candida albicans* (MTCC-227), *Aspergillus niger* (MTCC-282) and *Aspergillus clavatus* were tested for anti (MTCC-1323).

The test bacteria were grown and the medication suspension was diluted using Mueller Hinton Broth as a nutrition medium. This agar media was autoclaved at 120 °C for 30 minutes to sanitise it, then it was poured at a uniform depth of 5 mm and left to set. To achieve uniform development of the organisms, the microbial suspension (10⁵ CFU/mL) was streaked over the surface of media using a sterile cotton swab. The chemicals under test were dissolved in DMSO to produce solutions with concentrations ranging from 3.25 to 1000 g/ml. The solidified nutritional agar medium that has been treated with the appropriate microbe was deposited on sterilised filter paper discs measuring 6.25 mm in diameter. The discs had previously been soaked in a known quantity of the test substance in DMSO (fungi). Without any samples, a control disc impregnated with an equivalent amount of DMSO was also employed, but it did not result in any inhibition. The minimum bacterial inhibitory concentration (MIC) of the substance was measured using the agar streak dilution method. Ampicillin and griseofulvin were utilised as control medicines for antibacterial and antifungal activity, respectively (Hawkey and Lewis 1994). Graded amounts of the test compounds were added to a defined amount of molten sterile agar for the evaluation of antibacterial and Sabouraud dextrose agar for antifungal activity, respectively, from a stock solution of the produced compounds in DMSO. A Petri dish was filled to a depth of 4–5 mm with the medium containing the test substance, and aseptic conditions were used to allow the medium to solidify. A suspension of the respective microorganism of approximately 10⁵ CFU/mL was prepared and applied to plates with serially diluted compounds with concentrations in the range of 3.12–1000 µg/mL in DMSO and incubated at (37± 1)°C for 24 hr (bacteria) and 72 hr (fungi). Test run was triplicated; the lowest concentration of the substance that prevents the development of visible growth is considered to be the MIC value.

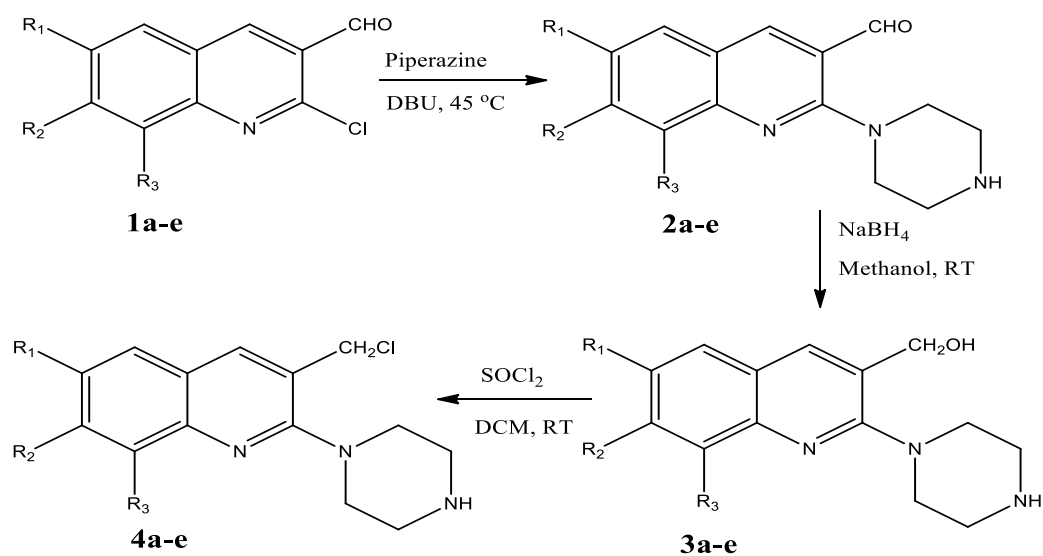
III. RESULTS AND DISCUSSION

Herein, we report a simple method for the synthesis of new 3-(chloromethyl)-2-(piperazin-1-yl)quinolone derivatives in excellent yields (**Scheme-I**). The 2-chloroquinoline-3-carbaldehyde **1a–e** when reacted with piperazine using DBU base catalyst at 45°C formed the derivatives of 2-(piperazin-1-yl)quinoline-3-carbaldehyde **2a–e** in excellent 90–95% yields (Table 1, entries 1–5). These 2-(piperazin-1-yl)quinoline-3-carbaldehyde **2a–e** derivatives on reduction with sodium borohydride in methanol at room temperature formed substituted (2-(piperazin-1-yl)quinolin-3-yl)methanol **3a–e**. These (2-(piperazin-1-yl)quinolin-3-yl)methanol react with thionyl chloride in DCM at room temperature to give the products 3-(chloromethyl)-2-(piperazin-1-yl)quinolone **4a–e** in excellent yields (88–93%) (Table-1, entries 11–15). The progress of the reaction was monitored by thin layer chromatography (8:2 - hexane: ethyl acetate solvent system). The reaction proceeded smoothly and completed in 1 hr to afford the corresponding titled compounds in very high yields (88–93%) (**Table-1, entries 11–15**). The chemical structures of all the new compounds were

confirmed by IR, ¹H NMR, mass spectroscopic data, and elemental analysis.

The antibacterial activity of the titled compounds (4a–e) was carried out against *S. pyogenes*, *P. aeruginosa*, *S. aureus* and *E. coli* using Ampicillin as the standard. MIC values were obtained by the broth dilution technique. DMSO was used as diluent. MIC values are summarized in **Table 2**. Most of the synthesized compounds displayed good antibacterial activity compared with standard drug Ampicillin with Gram +ve bacterial strains and Gram –ve strain.

The antifungal activity of the titled compounds (4a–e) was appraised against *A. niger*, *A. clavatus* and *C. albicans* using Griseofulvin as the standard drug with the broth dilution method (**Table 3**). The synthesized compounds were found to be good activity against the standard drug Griseofulvin against *A. niger*, *A. clavatus* and *C. Albicans*, strains.



Scheme-1: Synthesis of 3-(chloromethyl)-2-(piperazin-1-yl)quinoline

Table-1: Physical data of the synthesized compounds

Entry	Compound	R ₁	R ₂	R ₃	Reaction Time	Yield (%)
1	2a	H	H	H	4hr	93
2	2b	CH ₃	H	H	4hr	94
3	2c	H	H	CH ₃	4 hr	94
4	2d	H	CH ₃	H	4 hr	96
5	2e	OCH ₃	H	H	4hr	93
6	3a	H	H	H	10 min	95
7	3b	CH ₃	H	H	10 min	94
8	3c	H	H	CH ₃	10 min	94
9	3d	H	CH ₃	H	10 min	95
10	3e	OCH ₃	H	H	10 min	94

11	4a	H	H	H	60 min	91
12	4b	CH ₃	H	H	60 min	91
13	4c	H	H	CH ₃	60 min	90
14	4d	H	CH ₃	H	60 min	92
15	4e	OCH ₃	H	H	60 min	91

Table-2: Antibacterial Activity

Sr. No.	Compound	MINIMAL BACTERICIDAL CONCENTRATION			
		E.COLI MTCC 443	P.AERUGINOSA MTCC 1688	S.AUREUS MTCC 96	S.PYOGENUS MTCC 442
		MICROGRAM/ML			
1	4a	250	250	250	100
2	4b	500	250	500	250
3	4c	250	100	250	125
4	4d	100	250	500	100
5	4e	125	150	250	100

Table-3: Antifungal Activity

Sr. No.	Compound	MINIMAL FUNGICIDAL CONCENTRATION		
		C.ALBICANS MTCC 227	A.NIGER MTCC 282	A.CLAVATUS MTCC 1323
		MICROGRAM/ML		
1	4a	250	500	500
2	4b	500	500	500
3	4c	500	500	500
4	4d	500	1000	500
5	4e	500	500	500

Table-4: Standard Drugs:

MINIMAL BACTERICIDAL CONCENTRATION				
DRUG	E.COLI	P.AERUGINOSA	S.AUREUS	S.PYOGENUS
	MTCC 443	MTCC 1688	MTCC 96	MTCC 442
(MICROGRAM/ML)				
ERYTHROMYCINE	2	5	0.25	0.5
AMPICILLIN	100	100	250	100

CHLORAMPHENICOL	50	50	50	50
CIPROFLOXACIN	25	25	50	50
NORFLOXACIN	10	10	10	10

<i>MINIMAL FUNGICIDAL CONCENTRATION</i>			
DRUG	C.ALBICANS	A.NIGER	A.CLAVATUS
	MTCC 227	MTCC 282	MTCC 1323
<i>MICROGRAM/ML</i>			
NYSTATIN	100	100	100
GRESEOFULVIN	500	100	100

IV. CONCLUSION

In this study, a series of Newderivatives of 3-(chloromethyl)-2-(piperazin-1-yl)quinolone were prepared from 2-chloroquinolin-3-carbaldehydes and preliminarybiological evaluation of antimicrobial activityof the synthesized compounds showedgood antibacterialactivity with standard drug Ampicillin with Gram +vebacterial strains and Gram –vestrain. The antifungal activity of the titled compounds (4a–e) was evaluted against *A. niger*, *A. clavatus*and *C. albicans* using Griseofulvin as the standard drugwith the broth dilution method (Table 3). The synthesizedcompounds were found to be good activity with the standarddrug Griseofulvin against *A. niger*, *A. clavatus*and *C. albicans* strains.

All the reactions wereperformed under mild reaction conditionsshorter reaction time and in quantitative yields. The methodologydeveloped will be of much use tocombinatorial chemist.

Acknowledgement

Authors are thankful to the Head,Department of Chemistry, Degloorcollege,Degloor Dist. Nanded forprovidinglaboratory facilitiesand Microcare Laboratory and Tuberculosis Research Center,Surat for providing biological activities.

Spectroscopic data:-

4a) 3-(chloromethyl)-2-(piperazin-1-yl)quinoline

IR (KBr):2897 cm^{-1} (-C-H); 1613 cm^{-1} (-C=C); 748 cm^{-1} (C-Cl);

^1H NMR (CDCl_3 , δ ppm):3.41(m, 4H, CH_2);3.88(m, 6H, CH_2);3.91 (s, 2H, CH_2);7.36 (t, 1H, Ar-H); 7.58 (t, 1H, Ar-H);7.70(d, 1H, Ar-H); 7.86 (d, 1H, Ar-H); 8.13 (s, 1H, Ar-H).

ESMS: m/z 262.05(m+1)

4b) 3-(chloromethyl)-6-methyl-2-(piperazin-1-yl)quinoline

IR (KBr):2975 cm^{-1} (-C-H), 1615 cm^{-1} (-C=C), 752 cm^{-1} (-C-Cl)

^1H NMR (CDCl_3 , δ ppm):2.50(s, 3H, Ar- CH_3);3.33(m, 4H, CH_2); 3.70(m, 6H, CH_2); 3.88(s, 2H, CH_2); 7.19 (d, 1H, Ar-H); 7.26 (s, 1H, Ar-H); 7.58 (d, 1H, Ar-H); 8.03(s, 1H, Ar-H).

ESMS:m/z 276.06 (m+1)

4c) 3-(chloromethyl)-7-methyl-2-(piperazin-1-yl)quinoline**IR (KBr):** 2930 cm^{-1} (-C-H), 1608 cm^{-1} (-C=C), 748 cm^{-1} (-C-Cl) **$^1\text{H NMR}$ (CDCl_3 , δ ppm):** 2.50(s, 3H, Ar- CH_3); 3.33- 3.70 (m, 10H, CH_2); 3.92(s, 2H, CH_2); 7.21(d, 1H, Ar-H); 7.26 (s, 1H, Ar-H); 7.58 (d, 1H, Ar-H); 8.03(s, 1H, Ar-H).**ESMS:**m/z 276.06 (m+1)**4d) 3-(chloromethyl)-8-methyl-2-(piperazin-1-yl)quinoline****IR (KBr):**2919 cm^{-1} (C-H); 1594 cm^{-1} (C=C); 745 cm^{-1} (C-Cl) **$^1\text{H NMR}$ (CDCl_3 , δ ppm):** 2.50(s, 3H, Ar- CH_3); 3.33 – 3.70 (m, 10H, CH_2); 3.88(s, 2H, CH_2); 7.15 (d, 1H, Ar-H); 7.26 (s, 1H, Ar-H); 7.58 (d, 1H, Ar-H); 8.03(s, 1H, Ar-H).**ESMS:**m/z 276.02 (m+1)**4e) 3-(chloromethyl)-6-methoxy-2-(piperazin-1-yl)quinoline****IR (KBr):**2973 cm^{-1} (-C-H), 1621 cm^{-1} (-C=C), 737 cm^{-1} (-C-Cl) **$^1\text{H NMR}$ (CDCl_3 , δ ppm):** 3.30 - 3.70(s, 10H, CH_2); 3.83(s, 3H, Ar- OCH_3); 3.90(s, 2H, CH_2); 7.02 (d, 1H, Ar-H); 7.26 (s, 1H, Ar-H); 7.76 (d, 1H, Ar-H); 8.03(s, 1H, Ar-H).**ESMS:**m/z 292.02 (m+1)**V. REFERENCES**

- [1]. B. Nammalwar and R. A. Bunce, *Molecules*, 2014, 19, 204–232.
- [2]. M. J. Mphahlele and A. O. Adeloye, *Molecules*, 2013, 18, 15769–15787.
- [3]. N. H. Al-Shaalan, *Molecules*, 2007, 12, 1080–1091.
- [4]. O. Afzal, S. Bawa, S. Kumar and R. K. Tonk, *Molbank*, 2012, M748.
- [5]. J. Jaware and S. Borhade, *Indo Am. J. Pharm. Res.*, 2014, 4(5),2496–2502.
- [6]. J. P. Michael, *Nat. Prod. Rep.*, 2004, 650–668.
- [7]. J. P. Michael, *Nat. Prod. Rep.*, 2003, 476–493.
- [8]. A. A. Alhaider, M. A. Abdelkader and E. J. Lien, *J. Med. Chem.*, 1985, 28, 1394–1398.
- [9]. S. F. Campbell, J. D. Hardstone and M. J. Palmer, *J. Med. Chem.*, 1988, 31, 1031–1035.
- [10]. D. Wu, *Tetrahedron*, 2003, 59, 8649–8687.
- [11]. N. J. P. Subhashini, J. Amanaganti, L. Boddu and P. A. Nagarjuna, *J. Chem. Pharm. Res.*, 2013, 5(1), 140–147.
- [12]. W. Gao, J. Liu, Y. Jiang and Y. Li, *Beilstein J. Org. Chem.*, 2011, 7, 210–217.
- [13]. R. S. Keri and S. A. Patil, *Biomed. Pharmacother.*, 2014, 68, 1161–1175.
- [14]. S. Vandekerckhove, S. V. Herreweghe, J. Willems, B. Danneels, T. Desmet, C. de Kock, P. J. Smith, K. Chibale and M. D'hooghe, *Eur. J. Med. Chem.*, 2015, 92, 91–102.
- [15]. N. C. Desai, G. M. Kotadiya and A. R. Trivedi, *Bioorg. Med. Chem. Lett.*, 2014, 24, 3126–3130.
- [16]. R. Vlahov, J. Parushev, P. Nickel and G. Snatzke, *J. Pure Appl. Chem. Res.*, 1990, 7, 1303–1306.
- [17]. A. Srivastava, M. K. Singh and R. M. Singh, *Indian J. Chem.*, 2005, 45B, 292–296.
- [18]. S. Pramilla, S. P. Garg and S. R. Nautiyal, *Indian J. Heterocycl. Chem.*, 1998, 7, 201–204.

- [19].S. Vandekerckhove and M. D'hooghe, *Bioorg. Med. Chem.*, 2015, 23, 5098–5119.
- [20].M. A. Lyon, S. Lawrence, D. J. William and Y. A. Jackson, *J. Chem. Soc., Perkin Trans. 1*, 1999, 437–442.
- [21].N. Ahmed, K. G. Brahmabhatt, S. Sabde, D. Mitra, I. P. Singh and K. K. Bhutani, *Bioorg. Med. Chem.*, 2010, 18, 2872–2879.
- [22].V. Spano, B. Parrino, A. Carbone, A. Montalbano, Salvador, P. Brun, D. Vedaldi, P. Diana, G. Cirrincione and P. Barraja, *Eur. J. Med. Chem.*, 2015, 102, 334–351.
- [23].S. A. El-Feky, Z. K. Abd El-Samii, N. A. Osman, J. Lashine, M. A. Kamel and H. Kh. Thabet, *Bioorg. Chem.*, 2015, 58, 104–116.
- [24].M. A. Kerry, G. W. Boyd, S. P. Mackay, O. Meth-cohn and L. Platt, *J. Chem. Soc., Perkin Trans. 1*, 1999, 2315.
- [25].H. P. Heinz, H. C. Milhahn and E. Eckart, *J. Med. Chem.*, 1999, 42, 659–668.
- [26].B. Vivekanand, K. M. Raj and B. H. M. Mruthyunjayaswamy, *J. Mol. Struct.*, 2015, 1079, 214–224.
- [27].M. P. Maguire, K. R. Sheets, K. McVety, A. P. Spada and A. Zilberstein, *J. Med. Chem.*, 1994, 37, 2129–2137.
- [28].C. M. Russo, A. A. Adhikari, D. R. Wallach, S. Fernandes, N. Balch, W. G. Kerr and J. D. Chisholm, *Bioorg. Med. Chem. Lett.*, 2015, 25, 5344–5348.
- [29].B. Medapi, J. Renuka, S. Saxena, J. P. Sridevi, R. Medishetti, P. Kulkarni, P. Yogeeswari and D. Sriram, *Bioorg. Med. Chem.*, 2015, 23, 2062–2078.
- [30].J. A. Spicer, S. A. Gamage, G. J. Finlay and W. A. Denny, *J. Med. Chem.*, 1997, 42, 2383–2393.
- [31].Saito, I.; Sando, S.; Nakatani, K. *Bio Org Med Chem.* 2001, 9, 2381.
- [32].O. Meth-Cohn, B. Narine and B. A. Tarnowski, *J. Chem. Soc., Perkin Trans. 1*, 1981, 1520–1530.
- [33].Bhaduri, A. P. *Synlett* 1990, 557.
- [34].R.U.Pokalwar, R.V. Hangarge, P.V. Maske, M.S. Shingare, *Arkivoc* 2006, xi 196–204.
- [35].R.U.Pokalwar, R.V. Hangarge, B.R. Madje, M.N. Ware, M.S. Shingare, *Phosphorus, Sulfur, Silicon Relat. Elem.* 2008, 183, 1461–1470.
- [36].R.U.Pokalwar, R.V. Hangarge, A.H. Kategaonkar, M.S. Shingare, *Russian Journal of Organic Chemistry*, 2009, 45, 3, 430–433.
- [37].R.U.Pokalwar, S. A. Sadaphal, A.H. Kategaonkar, M.S. Shingare, *Green Chemistry letters and reviews* 2010, 1–6.
- [38].R.U.Pokalwar, P.V. Shinde, A.B. Chidrawar, M.S. Shingare, *Chemistry and biology interface* 2012, 2, 1, 31–37.
- [39].R.U.Pokalwar, A.B. Chidrawar, *Chemistry and biology interface* 2013, 3, 5, 339–345.

Understanding the Electronic Structure of Doped TiO₂ Photoanode for Water Splitting Reactions : A Review on First Principle Studies

Yogesh S. Nalwar¹, Harshada Barve², Rajaram S. Mane^{2*}, Krishna Chaitanya Gunturu^{3*}

¹Toshniwal Arts, Commerce & Science College, Sengaon, Hingoli, Maharashtra, India

²School of Physical Sciences, SRTM University, Nanded, Maharashtra, India

³School of Chemical Sciences, SRTM University, Nanded, Maharashtra, India

ABSTRACT

The rapid depletion of fossil fuel reserves is one of the threats to human civilization on mother earth with respect to the exponential growth rate of global energy consumption. Solar energy is the most attractive renewable replacement for fossil fuels because it is plentiful, inexhaustible, and widely distributed. Photocatalyst plays a crucial role in production of modern era fuel, Hydrogen from solar energy by means of water splitting. Recently there is rapid development in photocatalytic materials are possible with Density Functional Theory (DFT) calculation.

I. INTRODUCTION

It was estimated in year 2015 that the global energy consumption was about 17TW [1] and also projected for year 2050 in between 28 to 31TW [2,3]. This scenario has alerted us to look for alternative renewable energy solutions like photovoltaics, wind turbines, solar fuels, biomass conversion catalysts, electrification of automotive vehicles, fuel cells, storage batteries, flow batteries and any other energy conversion technology [4,5]. Amongst these, the optimal utilization of the solar energy enables us to move away from the dependency on fossil fuels owing to the fact that the energy of sunlight strikes on earth in one hour is more than the total consumption of energy in one year at global scale [6]. Of many ways to harvest solar energy, breaking chemical bonds and thereby storing energy in chemical form is prominent [5]. In photo-catalysis, the splitting of water with the help of sunlight into hydrogen and oxygen can be achieved (otherwise huge potential is required in electrochemical method) and hence became one of the promising research areas existing today to meet global energy requirements [7-9].

II. STATUS OF RESEARCH AND DEVELOPMENT IN THE SUBJECT

2.1 International Status

In the year 1972, Honda-Fujishima have published a ground breaking study on water splitting to produce hydrogen by using TiO₂ as photoanode material, provided a proof to do photo-electrochemical water splitting

[10]. The basic principle is, electrons in valence band (VB) of photoanode material will be jumped to conduction band (CB) while holes remain in VB upon irradiation to the suitable electromagnetic radiation on its surface. Then the holes will move towards the interface of anode and electrolyte to participate in water splitting and produce oxygen. At the same time, electrons move through external circuit to cathode to produce hydrogen. The free energy change in this process ($2\text{H}_2\text{O} \rightarrow 2\text{H}_2 + \text{O}_2$) amounts to 4.92 eV for four electron process i.e. each electron-hole needs 1.23 eV of potential difference to the reaction.

Since then, many research efforts have been reported not only to understand the basic mechanism of photocatalytic water splitting but also to improve the efficiency of nontoxic, low cost, stable and environmental friendly TiO_2 . The large band gap (~ 3.0 eV for rutile and ~ 3.2 eV for anatase) restricts to capture the photons beyond ultraviolet region by losing visible and long wave length near infra red region which covers more than half of the solar spectrum [11]. Doping is an effective method to tune the VB and CB and extend the absorption edge into visible region further. The doping with non-metal elements shifts VB up whereas CB will be stabilized with transition metal element dopants, in result decreasing the band gap. On the other hand co-doping with both transition metal and non-metal dopants will modify both VB and CB simultaneously [12].

The developments in terms of principles, mechanism and materials application aspects have been well documented time to time [13,14]. In a report, the mechanistic pathway of photocatalytic oxygen evolution on aqueous TiO_2 has been studied through first principle molecular dynamics to understand the reactive intermediates and also suggested that the participation of lattice oxygen in evolution of O_2 in anatase TiO_2 which is not the case in rutile counterpart [15]. The correlation between high surface area to volume ratio and photocatalytic activity has been studied with two-dimensional TiO_2 nanosheets photo and electrochemical oxidation of water along with transition metal doping effect in reducing rate limiting thermodynamic barriers and required overpotentials [16]. On the other hand, adsorption of single metal atoms of Pt, Pd, Rh and Ru on rutile TiO_2 surface has been carried out to understand the work function and surface activities of both doped and undoped anatase TiO_2 (101) surfaces [17]. Wenxian Li has reviewed recently the doping effect of several transition metals, rare earths, p-block metals and metalloids and non-metal elements as dopants and summarized the theoretical results on dopant induced variation in electronic structure, band gap and density of states of TiO_2 [18]. The prominent role of highly oxidized metal ions as dopants in photocatalytic oxygen evolution has been explored with experimental results on Mn, Fe, Co, and Ni doped various nano crystals [19]. Apart from this, the splitting of d-orbitals of doped transition metals which causes the reduction of overpotentials and facilitation of oxygen evolution has been experimentally shown in another report [20].

Similarly, many reports on main group elements as dopants in anatase TiO_2 in order to modify the VB are found. Specifically, the elements B, C, N, F and S are most widely studied as dopants to alter the VB, results shifting the band gap from UV range to visible range and improves the hole mobility at the surface [21-25]. On the other hand, the bulk vs surface doping effect of C, N and S on TiO_2 has been thoroughly dealt with both experimentally and theoretically and concluded that the surface or sub-surface doping impacts the electronic structure of TiO_2 and improves the photocatalytic activity [26].

The main disadvantage with monodoping is with respect to the partial occupation of the localized mid-gap states which may facilitate hole-electron pair recombination and thus reduce the photocatalytic activity [27]. To overcome this negative effect, the co-doping procedure is commonly adopted where transition metal ions are used for altering the CB whereas non-metal ions for VB [28-32].

2.2 National Status

Large number of research groups across India have been found active in photocatalytic water splitting research area on metal oxides, sulfides, carbon based materials, and transition metal complexes. However, outcome of the most of the works published resides mainly in hydrogen evolution reactions. S.M. Senthil Kumar et al have shown that MoS₂ nanospheres with higher defect concentration exhibited excellent hydrogen evolution activity [33]. Similarly, photoelectrocatalytic activity of MoS₂/graphene vertical heterostructures are suggested with negligible potential difference i.e. 0 eV [34]. Reduced graphene oxide-MoS₂ supported NiCo₂O₄ photocatalyst has been tested for hydrogen evolution reaction and Rhodamine B dye degradation successfully by S. Basu and co-workers [35]. On the other side, transition metal complexes and polymeric materials have also been studied by various research groups for hydrogen evolution [36-39]. Mixed metal oxides and their hetero junction photoelectrodes were also studied by both experimentally and density functional theory (DFT) for photocatalytic applications for water splitting as well as dye degradation [40-43]. The basic concepts behind improving the visible light responsive metal oxides by doping with metals, non-metals and improving the surface chemistry have been reviewed [44-45]. Apart from this, very few reports are found by research groups from CSIR-NCL, Pune and IIT, Kharagpur for photocatalytic oxygen evolution materials, namely NiCo alloy supported N-doped porous graphene and transition metal doped (Fe, Co, Cu) TiO₂ [46-47].

III. METHODOLOGY FOR DFT CALCULATIONS

As very few articles are seen with first principle DFT calculations at surface phase in contrast to the bulk phase of TiO₂, the specific objectives identified are as follows.

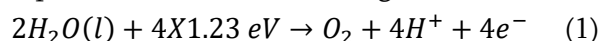
- 1) Studying the position of each dopant (metal, non-metal and metalloids) location i.e. it prefers to present on surface/sub-surface or in bulk
- 2) Understanding the interaction between H₂O and TiO₂ surface along with the reaction intermediates like -OH, -OOH and -O
- 3) Studying the effect of newly formed structural defects with doping
- 4) Studying the changes in band structure with mono and co-doping (metal and non-metal ions)
- 5) Doping of metalloids to avoid mixing of d-orbitals in the forbidden region of band gap.

All the geometries shall be fully optimized with either Vienna *Ab initio* Simulation Package (VASP) or any open source software like QUANTUM ESPRESSO using the projector augmented wave (PAW) method with the generalized gradient approximation and "Hubbard U" scheme for a better treatment of the valence electrons of metal ions. A suitable plane-wave cutoff energy shall be employed to control the fineness of this

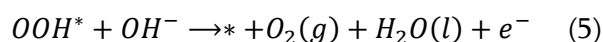
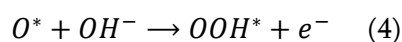
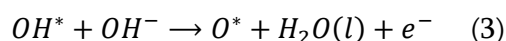
mesh. All oxygen evolution reaction steps can be investigated using fully optimized structures in which lattice vectors and ionic positions are fully relaxed until the maximum atomic forces are less than optimal value.

Using well-established structures, the catalytic activities of doped TiO₂ surfaces will be calculated by sequentially calculating the Gibbs free energies for the elementary steps based on the following mechanism.

During the electrochemical water splitting by using solar radiation, photons excite electrons in a semiconductor in which the energy level of the VB is sufficiently low to CB. This process involves with the substantial overpotential and energy losses at anode where oxygen is evolved. This reaction can be represented with the following 4 electron transfer model [equation 1].



This proposed reaction mechanism consists of four consecutive proton and electron transfer steps where HO*, O* and HOO* are found to be reaction intermediates [equations 2-5].



where * represents an active site on TiO₂ surface, (l) and (g) refer to liquid and gas phases respectively, and O*, OH* and OOH* are adsorbed intermediates.

The binding energies of the intermediates O*, OH* and OOH* on the TiO₂ surface (doped and undoped) will be obtained to know the rate limiting step in the overall reaction, on various active sites for different structures, as follows.

$$\Delta E_{OH^*} = E(OH^*) - E(*) - (E_{H_2O} - \frac{1}{2}E_{H_2}) \quad (6)$$

$$\Delta E_{OOH^*} = E(OOH^*) - E(*) - (2E_{H_2O} - \frac{2}{3}E_{H_2}) \quad (7)$$

$$\Delta E_{O^*} = E(O^*) - E(*) - (E_{H_2O} - E_{H_2}) \quad (8)$$

where E(*), E(OH*) and E(OOH*) are the ground state energies of the clean surface and surfaces adsorbed with OH*, O* and OOH* respectively. E_{H₂O} and E_{H₂} are the calculated DFT energies of H₂O and H₂ molecules in the gas phase.

Additionally, the zero-point energy and entropy corrections will be considered. From these calculations, the binding free energies like ΔE_{OH^*} , ΔE_{OOH^*} and ΔE_{O^*} could be written in terms of adsorption free energies, ΔG_{ads} , by the following equation

$$\Delta G_{ads} = \Delta E_{ads}^{DFT} + \Delta ZPE - T\Delta S \quad (9)$$

where, T is the temperature and ΔS is the entropy change.

The free energy diagram will be constructed considering the following four electron reaction paths

$$\Delta G_1 = \Delta G_{OH^*} + \mu_{e^-} - \Delta G_{OH^-} - \Delta G_* \quad (10)$$

$$\Delta G_2 = \Delta G_{O^*} + \Delta G_{H_2O} + \mu_{e^-} - \Delta G_{OH^*} - \Delta G_{OH^-} \quad (11)$$

$$\Delta G_3 = \Delta G_{OOH^*} + \mu_{e^-} - \Delta G_{O^*} - \Delta G_{OH^-} \quad (12)$$

$$\Delta G_4 = \Delta G_{O_2} + \Delta G_{H_2O} + \mu_{e^-} - \Delta G_{OOH^*} - \Delta G_{OH^-} - \Delta G_* \quad (13)$$

From the free energy diagram, an important parameter for electrocatalytic activity will be estimated that is the magnitude of the potential-determining step in four consecutive proton and electron transfer steps. This is the specific reaction step in the four-step mechanism with the largest ΔG , that is, the concluding step to become downhill in free energy as the potential increased

$$\Delta G = \max [\Delta G_1^0, \Delta G_2^0, \Delta G_3^0, \Delta G_4^0] \quad (14)$$

The theoretical overpotential at standard conditions is then given by

$$\eta = \left[\frac{G}{e} \right] - 1.23 \quad (15)$$

The lower the overpotential then superior the photocatalytic activity of doped photoanode in water splitting reaction.

The quantitative performance of doped system can be calculated by the relative position of η and absorption energy values in the volcano plot i.e. more closer to the peak confirms a better catalyst.

IV. IMPORTANCE PHOTOCATALYST IN THE CONTEXT OF CURRENT STATUS

As per discussion in the previous sections, though there exist great number of experimental results on (co) doping on TiO₂ photoanode material, the number of first principle studies of how dopants affect light absorption, carrier transport and catalytic reactions are limited. On the other hand, the reliability of results based on first principle density functional theory methods has been proven by several reports and also it has reached to prediction kind of studies as well [48]. Moreover, tuning of VB and CB in order to reduce the band gap and minimization of charge carrier recombination are successfully dealt at bulk level DFT calculations, but water splitting mechanism with respect to several dopants has not been well established with the surface of doped TiO₂. To be specific, in case of water splitting to get oxygen evolution at photoanode, several queries are still unanswered like, which parameter influence a dopant to present on surface or sub-surface of TiO₂, the interaction of H₂O and intermediates like -O, -OH, -OOH and -H are preferred to dopant or Ti center, the possibility of formation of new defects and their effect on expected band gap and mixing of dopant orbitals leads to generation of new bands are some of them. Hence, systematic studies on the gaps mentioned above are under progress with DFT calculations.

V. REFERENCES

- [1]. BP Statistical Review of World Energy. 2016. Available online: <http://www.bp.com/en/global/corporate/energy-economics/statistical-review-of-world-energy.html>
- [2]. Gerland, P., Raftery, A.E., Ševčíková, H., Li, N., Gu, D., Spoorenberg, T., Alkema, L., Fosdick, B.K., Chunn, J., Lalic, N. and Bay, G., 2014. World population stabilization unlikely this century. *Science*, 346(6206), pp.234-237.
- [3]. Jones, G.A. and Warner, K.J., 2016. The 21st century population-energy-climate nexus. *Energy Policy*, 93, pp.206-212.
- [4]. Vesborg, P.C. and Jaramillo, T.F., 2012. Addressing the terawatt challenge: scalability in the supply of

- chemical elements for renewable energy. *Rsc Advances*, 2(21), pp.7933-7947.
- [5]. Seh, Z.W., Kibsgaard, J., Dickens, C.F., Chorkendorff, I.B., Nørskov, J.K. and Jaramillo, T.F., 2017. Combining theory and experiment in electrocatalysis: Insights into materials design. *Science*, 355(6321), p.eaad4998.
- [6]. Rajeshwar, K., McConnell, R. and Licht, S., 2008. *Solar hydrogen generation. Toward a renewable energy future*. Springer: New York.
- [7]. Walter, M.G., Warren, E.L., McKone, J.R., Boettcher, S.W., Mi, Q., Santori, E.A. and Lewis, N.S., 2010. Solar water splitting cells. *Chemical reviews*, 110(11), pp.6446-6473.
- [8]. Pinaud, B.A., Benck, J.D., Seitz, L.C., Forman, A.J., Chen, Z., Deutsch, T.G., James, B.D., Baum, K.N., Baum, G.N., Ardo, S. and Wang, H., 2013. Technical and economic feasibility of centralized facilities for solar hydrogen production via photocatalysis and photoelectrochemistry. *Energy & Environmental Science*, 6(7), pp.1983-2002.
- [9]. Jafari, T., Moharreri, E., Amin, A.S., Miao, R., Song, W. and Suib, S.L., 2016. Photocatalytic water splitting—the untamed dream: a review of recent advances. *Molecules*, 21(7), p.900.
- [10]. Fujishima, A. and Honda, K., 1972. Electrochemical photolysis of water at a semiconductor electrode. *nature*, 238(5358), p.37.
- [11]. Pascual, J., Camassel, J. and Mathieu, H., 1978. Fine structure in the intrinsic absorption edge of TiO₂. *Physical Review B*, 18(10), p.5606.
- [12]. Gai, Y., Li, J., Li, S.S., Xia, J.B. and Wei, S.H., 2009. Design of narrow-gap TiO₂: a passivated codoping approach for enhanced photoelectrochemical activity. *Physical review letters*, 102(3), p.036402.
- [13]. Linsebigler, A.L., Lu, G. and Yates Jr, J.T., 1995. Photocatalysis on TiO₂ surfaces: principles, mechanisms, and selected results. *Chemical reviews*, 95(3), pp.735-758.
- [14]. Schneider, J., Matsuoka, M., Takeuchi, M., Zhang, J., Horiuchi, Y., Anpo, M. and Bahnemann, D.W., 2014. Understanding TiO₂ photocatalysis: mechanisms and materials. *Chemical reviews*, 114(19), pp.9919-9986.
- [15]. Li, Y.F. and Selloni, A., 2016. Pathway of photocatalytic oxygen evolution on aqueous TiO₂ anatase and insights into the different activities of anatase and rutile. *ACS Catalysis*, 6(7), pp.4769-4774.
- [16]. Kim, N., Turner, E.M., Kim, Y., Ida, S., Hagiwara, H., Ishihara, T. and Ertekin, E., 2017. Two-Dimensional TiO₂ Nanosheets for Photo and Electro-Chemical Oxidation of Water: Predictions of Optimal Dopant Species from First-Principles. *The Journal of Physical Chemistry C*, 121(35), pp.19201-19208.
- [17]. Jin, C., Dai, Y., Wei, W., Ma, X., Li, M. and Huang, B., 2017. Effects of single metal atom (Pt, Pd, Rh and Ru adsorption on the photocatalytic properties of anatase TiO₂. *Applied Surface Science*, 426, pp.639-646.
- [18]. Li, W., 2015. Influence of electronic structures of doped TiO₂ on their photocatalysis. *physica status solidi (RRL)-Rapid Research Letters*, 9(1), pp.10-27.
- [19]. Jang, D.M., Kwak, I.H., Kwon, E.L., Jung, C.S., Im, H.S., Park, K. and Park, J., 2015. Transition-metal doping of oxide nanocrystals for enhanced catalytic oxygen evolution. *The Journal of Physical Chemistry*

- C, 119(4), pp.1921-1927.
- [20]. Roy, N., Sohn, Y., Leung, K.T. and Pradhan, D., 2014. Engineered electronic states of transition metal doped TiO₂ nanocrystals for low overpotential oxygen evolution reaction. *The Journal of Physical Chemistry C*, 118(51), pp.29499-29506.
- [21]. Quesada-Gonzalez, M., Williamson, B.A.D., Sotelo-Vazquez, C., Kafizas, A., Boscher, N.D., Quesada-Cabrera, R., Scanlon, D.O., Carmalt, C.J. and Parkin, I.P., 2018. A Deeper Understanding of Interstitial Boron-Doped Anatase Thin Films as A Multifunctional Layer Through Theory and Experiment. *The Journal of Physical Chemistry C. The Journal of Physical Chemistry C*, 122, pp.714-726.
- [22]. Biswas, A., Chakraborty, A. and Jana, N.R., 2018. Nitrogen and Fluorine Codoped, Colloidal TiO₂ Nanoparticle: Tunable Doping, Large Red-Shifted Band Edge, Visible Light Induced Photocatalysis, and Cell Death. *ACS applied materials & interfaces*, 10(2), pp.1976-1986
- [23]. Chen, Q., Liu, M., He, K. and Li, B., 2014. Electronic Structures of S/C-Doped TiO₂Anatase (101 Surface: First-Principles Calculations. *International Journal of Photoenergy*, 2014, 816234.
- [24]. González-Torres, J.C., Poulain, E., Domínguez-Soria, V., García-Cruz, R. and Olvera-Neria, O., 2018. C-, N-, S-, and F-Doped Anatase TiO₂ (101 with Oxygen Vacancies: Photocatalysts Active in the Visible Region. *International Journal of Photoenergy*, 2018, 7506151.
- [25]. Zhao, Y., Wang, W., Li, C. and He, L., 2017. Electronic and photocatalytic properties of N/F co-doped anatase TiO₂. *RSC Advances*, 7(87), pp.55282-55287.
- [26]. Sá, J., Garlisi, C., Palmisano, G., Czapla-Masztafiak, J., Kayser, Y. and Szlachetko, J., 2018. Differences between bulk and surface electronic structure of doped TiO₂ with soft-elements (C, N and S). *Materials Chemistry and Physics*, 208, pp.281-288.
- [27]. Yang, K., Dai, Y., Huang, B. and Whangbo, M.H., 2008. On the possibility of ferromagnetism in carbon-doped anatase TiO₂. *Applied Physics Letters*, 93(13), p.132507.
- [28]. Batalović, K., Bundaleski, N., Radaković, J., Abazović, N., Mitrić, M., Silva, R.A., Savić, M., Belošević-Čavor, J., Rakočević, Z. and Rangel, C.M., 2017. Modification of N-doped TiO₂ photocatalysts using noble metals (Pt, Pd)—a combined XPS and DFT study. *Physical Chemistry Chemical Physics*, 19(10), pp.7062-7071.
- [29]. Liu, Y., Liang, W., Zhang, W., Zhang, J. and Han, P., 2013. First principle study of Cu²⁺ N, Cu and N-doped anatase TiO₂. *Solid State Communications*, 164, pp.27-31.
- [30]. Morgade, C.I. and Cabeza, G.F., 2016. Synergetic interplay between metal (Pt and nonmetal (C species in codoped TiO₂: A DFT+ U study. *Computational Materials Science*, 111, pp.513-524.
- [31]. Opoku, F., Govender, K.K., van Sittert, C.G.C.E. and Govender, P.P., 2018. Understanding the synergistic effects, optical and electronic properties of ternary Fe/C/S-doped TiO₂anatase within the DFT+ U approach. *International Journal of Quantum Chemistry*, 118(5), p.e25505.
- [32]. Zhu, H.X. and Liu, J.M., 2014. First principles calculations of electronic and optical properties of Mo and C co-doped anatase TiO₂. *Applied Physics A*, 117(2), pp.831-839.
- [33]. Kumar, S., Murugesan, S., Selvakumar, K., Karthikeyan, J., Thangamuthu, R., Murugan, P., Rajput, P., Jha, S.N., Bhattacharyya, D. and Navascues, N., 2017. Manifestation of Concealed Defects in MoS₂

- Nanospheres for Efficient and Durable Electrocatalytic Hydrogen Evolution Reaction. *ChemistrySelect*, 2(17), pp.4667-4672.
- [34].Biroju, R.K., Das, D., Sharma, R., Pal, S., Mawlong, L.P., Bhorkar, K., Giri, P.K., Singh, A.K. and Narayanan, T.N., 2017. Hydrogen Evolution Reaction Activity of Graphene–MoS₂ van der Waals Heterostructures. *ACS Energy Letters*, 2(6), pp.1355-1361.
- [35].Chakrabarty, S., Mukherjee, A. and Basu, S., 2018. RGO-MoS₂ Supported NiCo₂O₄ Catalyst toward Solar Water Splitting and Dye Degradation. *ACS Sustainable Chemistry & Engineering*, 6(4), pp.5238-5247.
- [36].Anjali, B.A., Sayyed, F.B. and Suresh, C.H., 2016. Correlation and Prediction of Redox Potentials of Hydrogen Evolution Mononuclear Cobalt Catalysts via Molecular Electrostatic Potential: A DFT Study. *The Journal of Physical Chemistry A*, 120(7), pp.1112-1119.
- [37].Rana, A., Mondal, B., Sen, P., Dey, S. and Dey, A., 2017. Activating Fe (I Porphyrins for the Hydrogen Evolution Reaction Using Second-Sphere Proton Transfer Residues. *Inorganic chemistry*, 56(4), pp.1783-1793.
- [38].Patra, B.C., Khilari, S., Manna, R.N., Mondal, S., Pradhan, D., Pradhan, A. and Bhaumik, A., 2017. A Metal-Free Covalent Organic Polymer for Electrocatalytic Hydrogen Evolution. *ACS Catalysis*, 7(9), pp.6120-6127.
- [39].Mondal, B., Sengupta, K., Rana, A., Mahammed, A., Botoshansky, M., Dey, S.G., Gross, Z. and Dey, A., 2013. Cobalt corrole catalyst for efficient hydrogen evolution reaction from H₂O under ambient conditions: reactivity, spectroscopy, and density functional theory calculations. *Inorganic chemistry*, 52(6), pp.3381-3387.
- [40].Modak, B., Modak, P. and Ghosh, S.K., 2016. Improving visible light photocatalytic activity of NaNbO₃: a DFT based investigation. *RSC Advances*, 6(93), pp.90188-90196.
- [41].Sharma, D., Upadhyay, S., Satsangi, V.R., Shrivastav, R., Waghmare, U.V. and Dass, S., 2014. Improved photoelectrochemical water splitting performance of Cu₂O/SrTiO₃ heterojunction photoelectrode. *The Journal of Physical Chemistry C*, 118(44), pp.25320-25329.
- [42].Mukherjee, A., Chakrabarty, S., Kumari, N., Su, W.N. and Basu, S., 2018. Visible-Light-Mediated Electrocatalytic Activity in Reduced Graphene Oxide-Supported Bismuth Ferrite. *ACS Omega*, 3(6), pp.5946-5957.
- [43].Sethi, Y.A., Praveen, C.S., Panmand, R.P., Ambalkar, A., Kulkarni, A.K., Gosavi, S.W., Kulkarni, M.V. and Kale, B.B., 2018. Perforated N-doped monoclinic ZnWO₄ nanorods for efficient photocatalytic hydrogen generation and RhB degradation under natural sunlight. *Catalysis Science & Technology*, 8(11), pp.2909-2919.
- [44].Martha, S., Sahoo, P.C. and Parida, K.M., 2015. An overview on visible light responsive metal oxide based photocatalysts for hydrogen energy production. *Rsc Advances*, 5(76), pp.61535-61553.
- [45].Ojha, K., Saha, S., Dagar, P. and Ganguli, A.K., 2018. Nanocatalysts for hydrogen evolution reactions. *Physical Chemistry Chemical Physics*, 20(10), pp.6777-6799.
- [46].Singh, S.K., Kumar, D., Dhavale, V.M., Pal, S. and Kurungot, S., 2016. Strategic Preparation of Efficient and Durable NiCo Alloy Supported N-Doped Porous Graphene as an Oxygen Evolution Electrocatalyst:

A Theoretical and Experimental Investigation. *Advanced Materials Interfaces*, 3(20), P.1600532

- [47]. Roy, N., Sohn, Y., Leung, K.T. and Pradhan, D., 2014. Engineered electronic states of transition metal doped TiO₂ nanocrystals for low overpotential oxygen evolution reaction. *The Journal of Physical Chemistry C*, 118(51), pp.29499-29506.
- [48]. Etacheri, V., Di Valentin, C., Schneider, J., Bahnemann, D. and Pillai, S.C., 2015. Visible-light activation of TiO₂ photocatalysts: Advances in theory and experiments. *Journal of Photochemistry and Photobiology C: Photochemistry Reviews*, 25, pp.1-29.

Synthesis and Characterization of Some Biologically Active Transition Metal Complexes of Bidentate Ligand

V.A.Shelke¹, S. M. Jadhav², S. G. Shankarwar³

¹Department of Chemistry, Indraraj Arts, Science and Commerce College, Sillod, Aurangabad – 431112, Maharashtra, India

²Department of Chemistry, Siddharth Arts, Science and Commerce College, Jafrabad Dist. Jalna -431206, Maharashtra, India

³Department of Chemistry, Dr. Babasaheb Ambedkar Marathwada University, Aurangabad, Dist- Aurangabad 431001, Maharashtra, India

ABSTRACT

The solid complexes of Mn(II), Fe(III), Ni(II) and Cu(II) have been synthesized Schiff base derived from 2-hydroxybenzohydrazide and 2-Methyl benzaldehyde. And characterized by spectral and other physicochemical techniques such as ¹H-NMR, UV-vis molar conductivity, magnetic susceptibility, thermal analysis, X-ray diffraction, FTIR, and mass spectroscopy. The analytical data of these metal complexes showed metal: ligand ratio (1:2). The physico-chemical study supports the presence of square planar geometry around Cu(II) and Ni(II) and octahedral geometry around Mn(II), and Fe(III). The IR spectral data reveal that the ligand behaves as bidentate with ON donor atom sequence towards central metal ion. The molar conductance values of metal complexes suggest their non electrolyte nature. The X-ray diffraction data suggest orthorombic crystal system for these complexes. Thermal behavior (TG/DTA) and kinetic parameters calculated by Coats-Redfern method are suggestive of more ordered activated state in complex formation. The ligand and their metal complexes were screened for antibacterial activity against *Staphylococcus aureus*, *Escherichia coli* and fungicidal activity against *Aspergillus Niger* and *Trichoderma*.

KEYWORDS: Bidentate Schiff base, Metal complexes, Thermal analysis, XRD, Antimicrobial study.

I. INTRODUCTION

Many organic compounds, heterocyclic aromatic compounds in particular like benzimidazoles, benzothiazoles are reported to possess a variety of physiological activities such as fungicidal, insecticidal, antimicrobial and anesthetic properties. Schiff bases derived from aromatic amines and aromatic aldehydes have a wide variety of applications in many fields like biological, inorganic and analytical chemistry[1-2]. The development of the field of bioinorganic chemistry has increased the interest in Schiff base complexes since it has been recognised that many of these complexes may serve as models for biologically important species [3-5]. The study of ligands involving such hydrazones is interesting as they demonstrate versatility in coordination, a tendency to yield stereochemistry of higher coordination number[6] an ability to behave as

neutral or deprotonated ligands and flexibility in assuming different conformations. Recently, several metal complexes of Schiff bases containing N, S and N, O donors have been synthesized and studied [7–9].

In the present article Mn(II), Fe(III), Ni(II), and Cu(II), complexes with Schiff base derived from 2-hydroxybenzohydrazide and 2-Methyl benzaldehyde. These have been characterized on the basis of physicochemical and spectral analysis. The antibacterial and antifungal activities of the ligand and its metal complexes were also tested. Unfortunately most schiff bases are chemically unstable and show a tendency to be involved in various equilibrium, like tautomeric interconversion hydrolysis or formation of ionised species [1, 2]

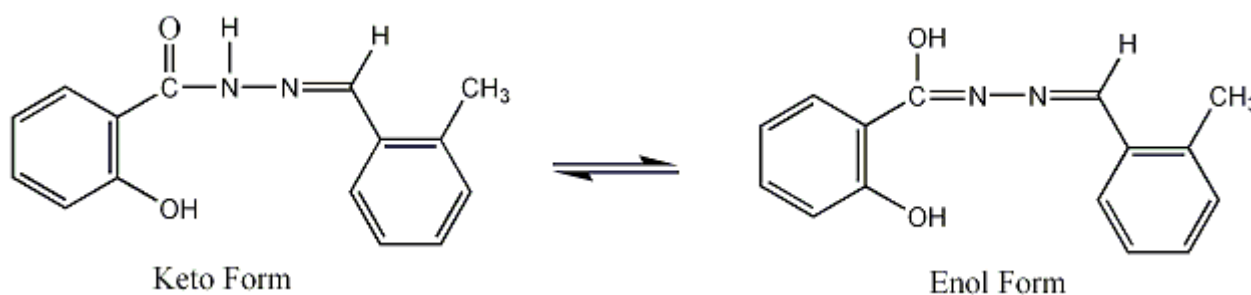


Figure 1.Keto and enol form of ligand.

II. EXPERIMENTAL

Materials

All chemicals used were of the analytical grade (AR) and of highest purity. Methyl 2-hydroxybenzoate, hydrazine and benzaldehyde were purchased from E-Merk (AR grade) and were used for synthesis of ligand. AR grade metal chlorides of S. D. Fine chemicals were used for complex preparation. Spectral grade solvents were used for spectral measurements. The carbon, hydrogen and nitrogen contents were determined on Perkin Elmer (2400) CHNS analyzer. IR spectra for ligand and metal complexes were recorded on Jasco FT-IR-4100 spectrometer using KBr pellets in the range of 4000-400 cm^{-1} . $^1\text{H-NMR}$ spectra of the ligand was measured in CDCl_3 using TMS as an internal standard. The TG/DTA analysis was recorded on Perkin Elmer TA/SDT-2960 with heating rate $10^\circ\text{C}/\text{min}$. XRD was recorded on Philips 3701 employing $\text{CuK}\alpha$ radiation ($\lambda=1.541\text{\AA}$) in the range 20° to 90° . The UV-vis spectra of the complexes were recorded on Jasco UV-530 Spectrophotometer. Magnetic susceptibility measurements were carried out on Guoy balance at room temperature using $\text{Hg}[\text{Co}(\text{SCN})_4]$ as a calibrant. Conductance was measured on Elico CM-180 conductometer using 1 mM solution in dimethyl sulphoxide.

Synthesis of Ligand

Step-I

50 mL ethanolic solution of 0.001 mol (0.168g.) of methyl salicylate was taken in round bottomed flask and to this 0.001 mol (0.108g.) of hydrazine in ethanol was added slowly under stirring. The resulting mixture was refluxed for about 4-5 h. It was naturally cooled to room temperature. After cooling, the solid residue was washed with hot ethanol and used for further study. (Yield 75%)

Step-II

Above synthesised intermediate 0.001 mol was refluxed with 0.001 mol of 2-methyl benzaldehyde in super dry ethanol for 5 h. The precipitate thus formed was filtered, dried in vacuum in presence of CaCl_2 and recrystallised in ethanol (yield: 79%).

Fig. 2

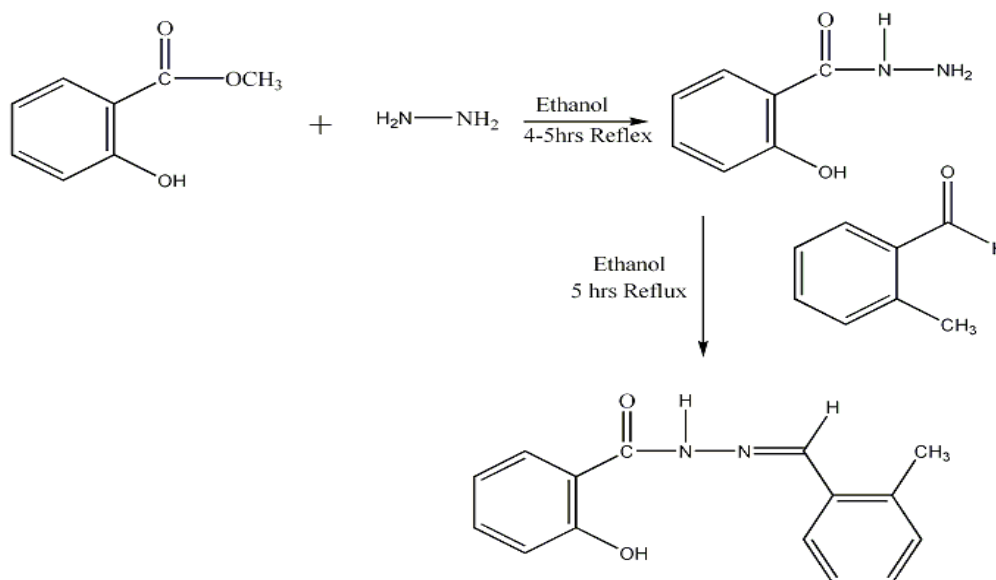


Figure 2.Synthesis of ligand.

Preparation of Complexes

To a hot solution of ligand (0.02 mol) in chloroform (25mL), methanolic solution of metal chloride (0.01 mol) was added under constant stirring. The pH of the reaction mixture was adjusted to 7.5-8.5 by adding 10 % ethanolic ammonia solution and refluxed for about 5 h. The precipitated solid metal complex was filtered and washed with hot methanol, followed by petroleum ether, ethyl acetate and dried over CaCl_2 in vacuum desiccator (yield 61%).

Fig.III. The proposed structure of the complexes

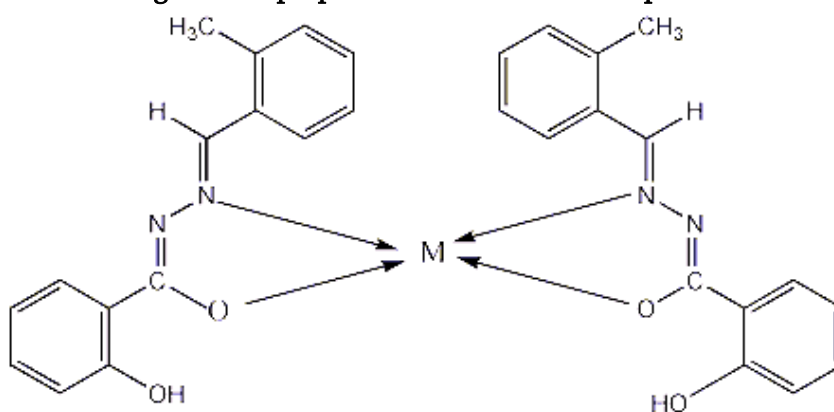


Fig.III-a

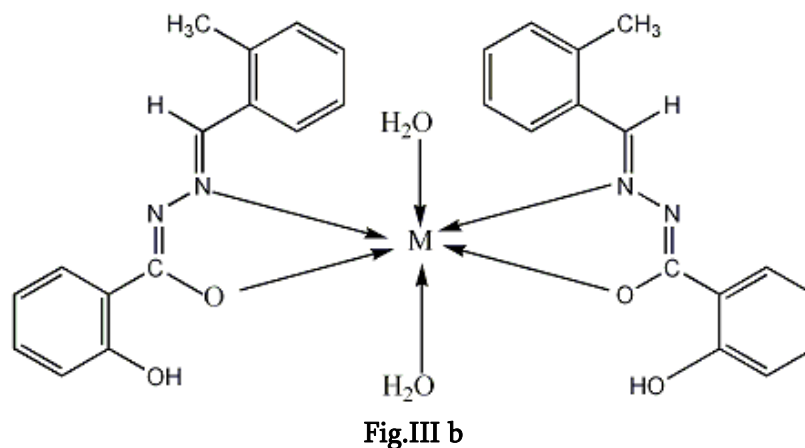


Fig.III. The proposed structure of the complexes

- a. when $M = \text{Cu(II)}$ and Fe(III)
 b. when $M = \text{Mn(II)}$ and Ni(II)

Table I. Physical characterization, analytical and molar conductance data of compounds.

Compound	F.W.	M.P./ Decom. Temp °C	Colour	Molar conductance Mho $\text{cm}^2 \text{mol}^{-1}$	%C (calcd.)	%H (calcd.)	%N (calcd.)	%M (calcd.)
H_2L	266	258	White		70.10 (70.85)	5.45 (5.54)	11.25 (11.01)	
[MnL]	544.93	>300	Yellow	4.74	63.59 (63.94)	4.95 (5.00)	9.60 (9.94)	10.01 (9.74)
[FeL]	545.84	230	Black	5.2	63.95 (63.84)	4.58 (4.99)	9.72 (9.92)	9.59 (9.89)
[NiL]	548.69	270	Brown	4.86	63.22 (63.52)	4.88 (4.97)	9.42 (9.87)	10.30 (10.36)
[CuL]	553.54	280	Pale green	17.66	62.22 (62.98)	4.88 (4.93)	9.42 (9.79)	10.38 (10.34)

III. RESULT AND DISCUSSION

All the complexes are coloured solids, air stable and are having line solubility in polar solvents DMF and DMSO. The elemental analysis show 1:2 (metal: ligand) stoichiometry for all the complexes. Micro analytical data and molar conductance values are given in Table I. The metal contents in complexes were estimated by

gravimetric analysis [10]. All the complexes show low conductance which indicates their non-electrolytic nature. The magnetic measurement studies suggest paramagnetic behavior of all these complexes

¹H-NMR spectra

¹H-NMR spectra of synthesised ligand was recorded in CDCl₃. It shows signals at 7.59 δ (s, 1H, -C-N-H), 7.08 δ (dd, 2H, Ar-H), 7.22 δ (dd, 2H, Ar-H), 7.01-7.75 δ (dd, 4H, Ar-H), 7.85 δ (s, 1H, N=C-H), 2.50 δ (s, 3H, Ar-H) and 6.10 δ (s, 1H, Ar-OH).

Mass spectra of the ligand

Mass spectra of the ligand H₂L has been recorded which show the molecular ion peak (M⁺) at m/z = 255.28 corresponding to its molecular mass.

IR spectra

The FT-IR spectrum of the free ligand shows four characteristic bands at 3240-3210, 3260, 1651 and 1615 cm⁻¹ assignable to (ν -N-H), free (-O-H) stretching phenolic moiety, amide carbonyl (-C=O) and azomethine (-C=N), stretching modes respectively. The absence of a weak broad band in 3270-3300 cm⁻¹ region, noted in the spectra of the metal complexes indicates deprotonation of bonded (-NH) group during the complexation and subsequent coordination of the oxygen of amide carbonyl to metal ion enolization[11]. The ν(C=N) band is shifted to lower frequency with respect to free ligand, indicating that the nitrogen of the azomethine group is coordinated to the metal ion, which was further confirmed by observation of the red shift in the ν(N-N) stretching frequency from 923 cm⁻¹ to 953 cm⁻¹ regions[12-14]. New bands observed in the complexes at 1621 and 1624 cm⁻¹ are attributed to the >C=N-N=C< group[13]. The spectra of metal chelates showed new bands in the 460-540 and 407-478 cm⁻¹ regions which can be assigned to ν (M-O) and (M-N) vibrations respectively[15]. The spectra of Mn(II) and Fe(III). showed a strong band at 3020-3500 cm⁻¹ region, suggesting the presence of coordinated water in these metal complexes[10]. The presence of coordinated water is further confirmed by the appearance of non-ligand band in 827-846 cm⁻¹ region[16]. The presence of coordinated water is also established and supported by TG/DTA analysis of these complexes. Hence coordination takes place via oxygen of amide and nitrogen of azomethine group of ligand molecule [17].

Electronic absorption spectra and magnetic measurements

The electronic spectra of Mn(II) complex in DMSO show bands at 12225, 16009, 27823 cm⁻¹ assignable to a ⁴T_{1g} → T_{2g}, ⁴T_{1g} → A_{2g} transition and charge transfer respectively. The electronic spectral data coupled with observed magnetic moment 5.8 B.M. suggest octahedral geometry for Mn(II) complex [18,19]. Fe(III) complex exhibits three bands at 16501, 24280 and 27871 cm⁻¹ assignable to ⁶A_{1g} → ⁴T_{1g}, ⁶A_{1g} → ⁴T_{2g} (F) transitions and charge transfer respectively. These transitions and observed magnetic moment 5.7 B.M indicate square planer geometry of the complex[20]. Ni(II) complex exhibits three bands at 12280, 16118 and 27270 cm⁻¹ assignable to ⁴T_{1g} → T_{2g}, ⁴T_{1g} → ⁴A_{2g} transitions and charge transfer respectively. These transitions and observed magnetic moment 2.6 B.M indicate octahedral geometry of the complex[17,21]. The electronic spectra of Cu(II)

complex .show bands at 12600, 17980, 23475 cm^{-1} assignable to a ${}^6A_{1g} \rightarrow {}^1T_{2g}$ transition and charge transfer respectively. The electronic spectral data coupled with observed magnetic moment 1.8 B.M. suggest square planar geometry for Cu(II) complex.[17].

Table I. Physical characterization, analytical and molar conductance data of compounds.

Compound	F.W.	M.P./ Decom. Temp °C	Colour	Molar conductance Mho $\text{cm}^2 \text{mol}^{-1}$	%C (calcd.)	%H (calcd.)	%N (calcd.)	%M (calcd.)
H ₂ L	266	258	White		70.10 (70.85)	5.45 (5.54)	11.25 (11.01)	
[MnL]	544.93	>300	Yellow	4.74	63.59 (63.94)	4.95 (5.00)	9.60 (9.94)	10.01 (9.74)
[FeL]	545.84	230	Black	5.2	63.95 (63.84)	4.58 (4.99)	9.72 (9.92)	9.59 (9.89)
[NiL]	548.69	270	Brown	4.86	63.22 (63.52)	4.88 (4.97)	9.42 (9.87)	10.30 (10.36)
[CuL]	553.54	280	Pale green	17.66	62.22 (62.98)	4.88 (4.93)	9.42 (9.79)	10.38 (10.34)

X-ray diffraction study

The X-ray diffractogram of a representative metal complex Mn(II) was scanned in the range 10-80° at wavelength 1.54 Å (Fig. 3). The diffractogram and associated data depict 2θ values for each peak, relative intensity and inter planar spacing (d-values). The diffractogram of Mn(II) complex showed fourteen reflections with maxima at 2θ (68.61°) corresponding to d value 1.35 Å. The X-ray diffraction pattern of the complex with respect to major peaks having relative intensity greater than 10 % have been indexed by using computer programme[22]. The above indexing method also yields Miller indices (hkl), unit cell parameters and volume. The unit cell of Mn(II) complex yielded values of lattice constants, a =7.55 Å, b =7.63 Å, c =8.11 Å and unit cell volume, V = 471.24 (Å)³. In concurrence with these cell parameters of Mn(II) complex, the condition a≠ b≠c and α =β =γ = 90° required for the compound to be orthorhombic lattice type. The diffractogram of Fe(III) complex shows eight reflections with maxima at 2θ =61.81 corresponding to d value 1.50Å. The observed values of lattice constants, a= 4.71Å°, b = 4.91Å°, c = 5.40Å° and α =β = 90° γ =120°. Fe(III) complex satisfies the condition a≠ b≠c and α =β = 90° γ =120° required for the compound to be monoclinic lattice type. The diffractogram of Ni(II) complex shows eight reflections with maxima at 2θ =62.38 corresponding to d value 1.43Å. The observed values of lattice constants, a= 9.70Å°, b = 9.70Å°, c = 6.63Å° and α =β = γ =.90° Ni(II) complex satisfies the condition a=b≠c and α =β =γ = 90° required for the compound to be tetragonal lattice type. The diffractogram of Cu(II) complex shows thirteen reflections with

maxima at $2\theta = 31.00$ corresponding to d value 2.88Å. The observed values of lattice constants, $a = 7.23\text{Å}$, $b = 7.48\text{Å}$, $c = 6.31\text{Å}$ and $\alpha = \beta = 90^\circ$, $\gamma = 120^\circ$ Cu(II) complex satisfies the condition $a \neq b \neq c$ and $\alpha = \beta = 90^\circ$, $\gamma = 120^\circ$ required for the compound to be monoclinic lattice type. The above values indicate that the metal complex has orthorhombic crystal system. Experimental density value of the complex was determined by using specific gravity method [23].

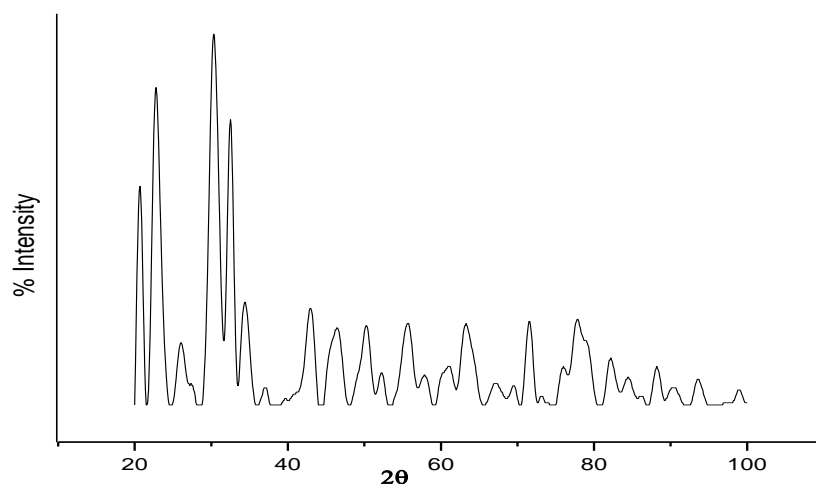


Fig. 3. X-ray diffractogram of Co(II) complex.

Thermal analysis.

The simultaneous TG/DT analysis of metal complexes was studied from ambient temperature to 1000 °C in nitrogen atmosphere using $\alpha\text{-Al}_2\text{O}_3$ as reference. The thermogram curve of Cu(II) metal complex shows mass loss 5.7 % (calcd.5.85 %) representative in the range 160-230°C. An endothermic peak in this region $\Delta T_{\text{max}} = 120^\circ\text{C}$ indicating presence of two coordinated water molecules [10]. The TG curve of Cu(II) complex, then show slow decomposition from 270°C to 480°C with mass loss 52.10% (calcd.51.20%). An exothermic peak $\Delta T_{\text{max}} = 310^\circ\text{C}$ in DTA may be attributed to the decomposition of non coordinated part of ligand. The second slow step from 510 to 790°C with mass loss of 21.20% (calcd.21.50%) corresponds to decomposition of coordinated part of ligand. A broad endotherm $\Delta T_{\text{max}} = 740^\circ\text{C}$ in DTA is observed for this. The mass of final residue 15.90 % (calcd.16.10 %) corresponds to stable CuO. All other metal complexes show similar behavior.

Kinetic calculations

The kinetic and thermodynamic parameters *viz* order of reaction (n), energy of activation (E_a), pre-exponential factor (z), entropy of activation (ΔS) and free energy change (ΔG) together with correlation coefficient (r) for non-isothermal decomposition of metal complexes have been determined by Horowitz-Metzer (HM) approximation method and Coats-Redfern integral method[24] [34]. The data is given in Table III. The results show that the value obtained by two methods is comparable. The calculated value of energy of activation of the Co(II) and Ni(II) complexes is relatively low indicating the autocatalytic effect of metal ion

on thermal decomposition of the metal complex[25,26]. The negative value of entropy of activation indicates that the activated complex is more ordered than the reactant and that the reaction is slow. The more ordered nature may be due to the polarization of bonds in activated state which might happen through charge transfer electronic transition.

Table III. The kinetic parameter of metal complexes calculated by the methods Horowitz-Metzger (HM) and Coats-Redfern (CR).

Complex	Step	n	Method	E _a (kJmol ⁻¹)	Z S ⁻¹	ΔS# JK ⁻¹ mol ⁻¹	ΔG# (kJmol ⁻¹)	Corelation coefficient (r)
Ni(II)	I	1.3	HM	12.25	3.7 × 10 ⁵	-175	50.23	0.9989
			CR	16.45	4.2 × 10 ⁴	-195	47.25	0.9990
	II	1.1	HM	21.45	3.7 × 10 ³	-161	61.47	0.9989
			CR	16.15	5.2 × 10 ⁴	-198	52.40	0.9989
Cu(II)	I	1.3	HM	24.47	6.6 × 10 ⁶	-214	41.35	0.9988
			CR	22.40	8.2 × 10 ⁴	-242	38.11	0.9995
	II	1.1	HM	11.35	8.6 × 10 ⁵	-236	40.41	0.9992
			CR	14.40	6.2 × 10 ⁴	-283	39.33	0.9995

Antimicrobial activity

The antimicrobial activity of ligand and its metal complexes were tested *in vitro* against bacteria such as *Staphylococcus aureus* and *Escherichia coli* by paper disc plate method [27]. The compounds were tested at the concentration 500 and 1000 μg cm⁻³ in DMF and compared with known antibiotics *viz* ciproflaxin (Table IV). For fungicidal activity, compounds were screened *in vitro* against *Aspergillus Niger* and *Trichoderma* by mycelia dry weight method [28] with glucose nitrate media. The compounds were tested at the concentration 250 and 500 μg cm⁻³ in DMF and compared with control (Table V). From Table 4 and 5, it is clear that the inhibition by metal chelates is higher than that of a ligand and metal salts. The results are in good agreement with previous findings with respect to comparative activity of free ligand and its complexes[17,20]. The metal chelates have higher antibacterial activity than the corresponding free ligand and control against the same microorganism under identical experimental conditions. Such enhanced activity of metal chelates is due to increased lipophilic nature of the metal ions in complexes[29]. The increase in activity with concentration is due to the effect of metal ions on the normal process.

The microbial results are presented in Tables IV and V. In case of antibacterial studies it was observed that, the ligand is moderately active towards *Stapylococcus* and less active towards *E.Coli*. Comparison of activities of the ligand and its metal chelates showed that the copper complex is approximately found to be more active than the ligand Cu(II) complex show higher activity than other metal complexes. The cobalt and manganese

complexes show the activity comparable to copper complex. However Fe(III) and Ni(II) complexes show less activity against *E.Coli* and *Stapylococcus*. The activity of these complexes follow the order Cu>Co>Mn>Ni>Fe. Investigation of antifungal activity of the ligand and its metal complexes revealed that all metal chelates are more fungi toxic than their parent ligand *Table V*. The antifungal activity of the ligand is found to enhance several times on being coordinated with metal ions. The activity of these complexes follow the order of *Aspergillus Niger* Cu> Ni >Mn>Fe and that of *Trichoderma* Cu > Ni > Mn >Fe.

As a result, metal complexes of Cu(II) and Mn(II) show good antibacterial and Cu > Ni show good antifungal activity, where as Fe(III) complexe shows comparatively less activity.

Table IV. Antibacterial activity of ligand and its metal complexes.

Test Compound	inhibition zone (mm)			
	<i>E. Coli</i>		<i>Staphylococcus</i>	
	500ppm	1000ppm	500ppm	1000ppm
<i>Ciproflaxin</i>	29	32	31	35
[C ₃₀ H ₂₈ N ₄ O ₄] (H ₂ L)	12	15	13	17
[C ₃₀ H ₂₈ N ₄ O ₄ Mn]	17	20	16	19
[C ₃₀ H ₂₈ N ₄ O ₄ Fe]	12	16	13	17
[C ₃₀ H ₂₈ N ₄ O ₄ Ni]	14	16	12	18
[C ₃₀ H ₂₈ N ₄ O ₄ Cu]	17	24	16	20

Table V. Antifungal activity of compounds yield of mycelial dry weight in mg (% inhibition)

Test Compound	<i>A.niger</i>		<i>Trichoderma</i>	
	250ppm	500ppm	250ppm	500ppm
Control	79	79	70	70
[C ₃₀ H ₂₈ N ₄ O ₄]H ₂ L	61 (22)	27 (65)	40 (42)	20 (72)
[C ₃₀ H ₂₈ N ₄ O ₄ Mn]	53 (32)	15 (81)	32 (54)	08 (87)
[C ₃₀ H ₂₈ N ₄ O ₄ Fe]	50 (36)	20 (74)	32 (54)	07 (90)
[C ₃₀ H ₂₈ N ₄ O ₄ Ni]	45 (43)	14 (82)	21 (70)	05 (93)
[C ₃₀ H ₂₈ N ₄ O ₄ Cu]	41 (48)	12 (84)	23 (68)	05 (93)

IV. CONCLUSIONS

In the light of above discussion we have proposed square-planar geometry for Cu(II) and Ni(II) complex and octahedral geometry for Mn(II) and Fe(III) complexes. On the basis of the physico-chemical and spectral data discussed above, one can assume that the ligand behave as monobasic, ON bidentate, coordinating via amide

oxygen and azomethine nitrogen as illustrated in Fig.4. The complexes are biologically active and are having enhanced antimicrobial activities compared to free ligand. Thermal study reveals thermal stability of metal complexes. The XRD study suggests monoclinic crystal system for Cu (II) and Fe(III) complex, Mn(II) complex show orthorhombic crystal structure, and Ni(III) shows tetragonal crystal structure.

V. REFERENCES

- [1]. Naik, V.M.; Sambrani, M.I.; Mallur, M.B. 2008, Synthesis, Characterization and Biological Activities of Manganese(II) Complex: Molecular Modeling of DNA Interactions, *Ind.J. of Chemistry*, 47, 1793.
- [2]. Narang, K.K.; Singh, V.P., 1997, Hydrazone as complexing agent: Synthesis, structural characterization and biological studies of some complexes, *Synth. React. Inorg. Met.-Org. Chem.*, 27, 721.
- [3]. Chowdhury, D.A.; Uddin, M.N.; Sarker, M.A.H. 2008, Metal Complexes of Schiff Bases Derived from 2-Thiophenecarboxaldehyde and Mono/Diamine as the Antibacterial Agents, *Chiang Mai J. Sci.*, 35, 483.
- [4]. Clear, M.J. *Coord. Chem. Rev.*, 1974, Transition metal complexes in cancer chemotherapy, *Chem. Rev.*, 12, 349.
- [5]. M.T.H.Tarafder, M.A.Jalil MiahR.N.Bose, M.Akbar Ali 1981, Metal complexes of some schiff bases derived from s-benzylidithiocarbamate, *J. Inorg. Nucl. Chem. Volume 43, Issue 12, , Pages 3151-3157.*
- [6]. Maurya, R.C.; Verma, R.; Singh, T. 2003, Synthesis, Magnetic, and Spectral Studies of Some Mono- and Binuclear Dioxomolybdenum(VI) Complexes with Chelating Hydrazones Derived from Acid Hydrazides and Furfural or Thiophene-2-aldehyde, *Synth. React. Inorg. Met.-Org.Chem.*, 33, 309
- [7]. Ali, M.A.; Livingstone, S. E. 1974, Metal complexes of sulphur-nitrogen chelating agents, *Coord. Chem. Rev.*, 13, 101.
- [8]. Williams, D.R. 1972, Metals, ligands, and cancer, *Chem. Rev.*, 72, 203.
- [9]. Loncle, C.; Brunel, J.M.; Vidal, N.; Dherbomez, M.; Letourneux, Y. 2004, Synthesis and antifungal activity of cholesterol-hydrazone derivatives, *Eur. J.Med.Chem.*, 39, 1067.
- [10].Kucukozel S.G.; Mazi A.; Sahin F.; Ozturk S.; Stables, J. 2003, Synthesis and biological activities of diflunisal hydrazone-hydrazones, *Eur. J. Med. Chem.*, 38, 1005.
- [11].Todeschini, R.; de Miranda, A.L.P.; da Silva, K.C.M.; Parrini, S.C., Barreiro, E.J. 1998, Synthesis and evaluation of analgesic, antiinflammatory and antiplatelet properties of new 2-pyridylarylhydrazone derivatives, *Eur. J. Med. Chem.*, 33,189.
- [12].Melnyk, P.; Leroux, V.; Sergheraert, C.; Grellier, P.; Sergheraert, C. 2006, Design, synthesis and in vitro antimalarial activity of an acylhydrazone library, *Bioorg. Med. Chem. Lett.*, 16, 31.
- [13].Lima, P.C.; Lima, L.M.; da Silva, K.C.M.; O. Le ´da, P.H.; de Miranda, A.L.P.; Fraga, C.A.M.; Barreiro, E.J. 2000, Synthesis and analgesic activity of novel N-acylarylhydrazones and isosters, derived from natural safrole, *Eur. J. Med. Chem.*, 35, 187.
- [14].V.A.ShelkeS.M.JadhavaV.R.PatharkaraS.G.ShankarwaraA.S.MundebT.K.Chondhekar, 2012, Synthesis, spectroscopic characterization and thermal studies of some rare earth metal complexes of unsymmetrical tetradentate Schiff base ligand, *Arabian Journal of Chemistry*, Volume 5, Issue 4, October, Pages 501-507
- [15].Bedia, K.K.; U. Seda, O. Elc.; Fatma, K.; Nathaly, S.; Sevim, R.; Dimoglo, A. 2006, Synthesis and

- characterization of novel hydrazide–hydrazones and the study of their structure–antituberculosis activity, *Eur. J. Med. Chem.*, 41, 1253.
- [16].Terzioglu, N.; Gu" rsoy, A. 2003, Synthesis and anticancer evaluation of some new hydrazone derivatives of 2,6-dimethylimidazo[2,1-b][1,3,4]thiadiazole-5-carbohydrazide, *Eur. J. Med. Chem.*, 38, 781.
- [17].K. Ramana Kumar , A. Raghavendra Guru Prasad, V. Srilalitha, G. Narayana Swami and L.K. Ravindranath, 2012, Synthesis and Characterization of Iron Complexes of Resacetophenone Salicyloyl Hydrazone, *Chem. Bull. "POLITEHNICA" Univ. Volume 57(71)*, 1.
- [18].Sreeja, P.B.; Sreekanth, A.; Nayar, C.R.; PrathapachandraKurup, M.R.; Usman, A.; Razak, I.A.; Chantrapomma, S.; Fun, H.K. 2003, Synthesis, spectral studies and structure of 2-hydroxyacetophenone nicotinic acid hydrazone, *J. of Molecular Structure*, .645, 221.
- [19].Salam, M.A.; Chowdhury, D. A. *Bull. Pure & Appl. Sci.* 2001, 20, 89.
- [20].Vogel, A.I.; 1975 , "A Text Book of Quantitative Inorganic Analysis," 3rd.ed., Longmans, London,. PP 540.
- [21].Baliger, R.S.; Revankar, V.K. 2006, Coordination diversity of new mononucleating hydrazone in 3d metal complexes: synthesis, characterization and structural studies, *J.Serb.Chem.Soc.*, 71, 1301.
- [22].Hueso-Urena, F.; Illan-Cabeza, N.A.; Moreno-Carretero, M.N.; Penans Chamorro, A.L., 2000, Ni(II), Cu(II), Zn(II) And Cd(II) Complexes With Dinegative N,N,Otridentate Uracil-Derived Hydrazones, *Acta Chem. Solv.*, 47, 481.
- [23].Narang, K.K.; Aggarwal, A. 1974, Salicylaldehyde salicylhydrazone complexes of some transition metal ions, *Inorg. Chim. Acta* , 9, 137.
- [24].Synthesis, characterization, antibacterial and antifungal studies of some transition and rare earth metal complexes of N-benzylidene-2-hydroxybenzohydrazide
- [25].Blout, E.R.; Fields, M.; Karplus, R. J. 1948, Absorption Spectra. VI. The Infrared Spectra of Certain Compounds Containing Conjugated Double Bonds, *Am. Chem. Soc.*, 70, 194.
- [26].Natrajan, R.; Antonysamy, K.; Thangaraja, C. 2003, Redox and antimicrobial studies of transition metal(II) tetradentate Schiff base complexes, *Transition Met. Chem.* 28, 29-36.
- [27].Munde, A.S.; Jagdale, A.N.; Jadhav, S.M.; Chondhekar, T.K. 2009, Synthesis and characterization of some transition metal complexes of unsymmetrical tetradentate Schiff base ligand, *J. of the Korean Chemical Society.*, 53, 415.
- [28].Natrajan, R.; Antonysamy, K.; Thangaraja, C. 2003, Redox and antimicrobial studies of transition metal(II) tetradentate Schiff base complexes, *Transition Met. Chem.* 28, 29.
- [29].Raman, N.; Pitchaikani Raja, Y.; Kulandaisamy, A. 2001, Synthesis and characterisation of Cu(II), Ni(II), Mn(II), Zn(II) and VO(II) Schiff base complexes derived from o-phenylenediamine and acetoacetanilide, *Proc. Indian Acad. Sci (Chem.Sci.)*, 113, 183.

Green Chemistry and Useful Effects of Catalyst

H. A. Tirpude

PG Department and Research center in Chemistry, Shivaji Mahavidyalaya, Udgir, Dist-Latur, Maharashtra,
India

ABSTRACT

The present review work focuses on the importance and economic development of green chemistry. It is a new branch in chemistry dealing with reduction of harmful and toxic chemicals in the synthesis and replacing it with ecofriendly methods. The principle of green chemistry with various benefits have been discussed to understand the basic requirement for replacement of conventional synthetic method with green chemistry synthesis. To describe it the synthetic approach for the synthesis of acetanilide has been discussed and compared.

KEYWORDS: Green Chemistry, Ecofriendly, Conventional, Acetanilide.

I. INTRODUCTION

The accelerated progress in science and technology now a days has led to economic development in world, but such economic development also cause environmental degradation which is manifested by climate change, the issue of ozone holes and accumulation of non-destructive organic pollutant in all parts of biospheres. So the present situation required the solution to balance the use of natural resources and environmental conservation. From last two decades awareness for environmental protection has increased by using the concept of "Green Chemistry". The new laws and regulations have a Aim to protect the ecosystem from harmful chemicals and develop new compounds by the approach of Green chemistry which are less dangerous to human health and the environment.

Green chemistry is new branch of chemistry involves pulling together tools and techniques that helps to chemical engineers in research related to the creation of chemical product and processes that reduce or eliminate the use of harmful chemicals as well as reducing harmful and toxic products for the development of more eco-friendly and efficient product with less wastage. Green chemistry is now going to become an essential tool in the field of synthetic chemistry.

1.1 Definition of Green Chemistry:

According to environmental protection agency, green chemistry is defined as a chemistry that designs chemical products and processes that are harmless to the environment. Chemical products should be made in such a manner that they do not remain in the environment at the end of their application and broken down into components that are harmless to environment.

1.2 History:

The term green chemistry was first given by Poul .T. Anastas in 1991 in special program launched by the US environmental Protection Agency (EPA) to implement sustainable development in chemistry ,chemical technology by industry ,academia and government. In 1995 the annual US presidential green chemistry challenge was announced. In 1996 the working party on green chemistry was created, acting within the framework of International Union of Pure and Applied Chemistry. The first book and journals on the subject of green chemistry were introduced in 1990 by the royal society of chemistry. Green chemistry includes a new approach to the synthesis, processing and application of chemical substances in such a manner to reduce scourge to health and environment like:

1. Clean Chemistry
2. Atom Economy
3. Environmentally benign chemistry.

Twelve principles of Green chemistry have been developed by Poul Anastas, speaks about the reduction of dangerous or harmful substances from the synthesis, production and application of chemical products. When designing a green chemistry process it is impossible to meet the requirements of all twelve principles of the process at the same time, but it attempts to apply as many principles during certain stages of synthesis.

1.3 Principles of Green Chemistry

- 1.3.1 **Pollution Prevention:** It is to prevent waste and to treat and clean up waste after it has been created.
- 1.3.2 **Atom Economy:** It should be designed to maximize the incorporation of all materials used in process into the final product.
- 1.3.3 **Less Hazardous Chemical Synthesis:** The synthetic method should be designed to use and generate substances that process little or no toxicity to human health and the environment.
- 1.3.4 **Designing Safer Chemicals:** Chemical product should be designed to affect their desired function while minimizing toxicity.
- 1.3.5 **Safer Solvents and Auxiliaries:** The use of auxiliary substances should be made unnecessary wherever possible.
- 1.3.6 **Design for Energy Efficiency:** energy requirements of chemical processes should be recognized at low temperature and pressure.
- 1.3.7 **Use of Renewable Feedstock's:** A raw material of feedstock should be renewable.
- 1.3.8 **Reduce Derivatives:** The unnecessary derivatization like use of blocking groups, protection, deprotection should be avoided whenever impossible.
- 1.3.9 **Catalysis:** The catalytic reagents are superior stoichiometric reagents.
- 1.3.10 **Design for Degradation:** The chemical products should be designed so that at the end of their function they breakdown into harmless degradation products and do not persist in the environment.
- 1.3.11 **Real-time analysis for Pollution Prevention:** Analytical methodologies need to be further developed to allow for real-time, in process monitoring and control prior to the formation of hazardous substances.

1.3.12 **Inherently Safer Chemistry for Accident Prevent:** The substances used in the chemical process should be chosen to minimize the potential for chemical accidents, explosion and fires. This principle can motivate chemistry at all levels like research, education and public perception.

1.4 **Benefits of Green Chemistry:**

1. Benefits for health
2. Cleaner air-less release of hazardous chemicals to air leading to less damage to lungs.
3. Cleaner water-less release of hazardous chemical wastes to water leading to cleaner drinking.
4. Increase safety for worker in chemical industry, less use of toxic materials, less potential for accident.
5. Benefits for environment
6. Plants & animals suffer less harm from toxic chemicals in environment.
7. Lower potential for global warming, ozone depletion & smog formation.
8. Economy
9. Better performance so that less product is needed to achieve the same function.

II. REVIEW LITERATURE

- 2.1 Green chemistry aims to reduce or even eliminates the production of any harmful bi-products and maximizing the desired product without compromising with the environment. The three key developments in green chemistry include use of super critical carbon di oxide as green solvent, aqueous hydrogen peroxide as an oxidizing agent and use of hydrogen in asymmetric synthesis. It also focuses on replacing traditional methods of heating with that of modern methods of heating like microwave radiations so that carbon footprint should be reduces as low as possible.
- 2.2 The work focuses to reduce the chemical wastage by applying the concept of green chemistry. Few derivative of acetanilide were synthesized by conventional method as well as by green chemistry method. In conventional method there was wastage of chemicals by the formation of acetic acid molecule but by green synthesis method the formation of byproducts was avoided and the atom economy was calculated on the basis of molecular weight of desired product and it was found to be in the range of 72 to 82% which signify the utility of green synthesis method.
- 2.3 Due to technology development the quality of life on earth became much better but harmful effect of chemistry also became pronounced main among them being the pollution of land, water and atmosphere. This is caused mainly due to the use of harmful reactants and effect of by-product of chemical industries, which are being discharge into air, rivers and the land, but by applying the concept of green chemistry these all problems can be reduced.
- 2.4 Green chemistry is a term that refers to the production of chemical products and processes that reduce the use of and production of harmful substances.
- 2.5 The green chemistry revolution provides the various numbers of challenges to those who practice chemistry in industry, education and research. It is the modern science of chemistry deals with

the application of environment friendly chemical compound in the various area of our life such as industries. The chemical industries supply us a huge variety of essential product, from plastic to pharmaceuticals, these industries has a potential to damage our environment, so green chemistry serves to promote the design and efficient use of chemicals and chemical processes.

III. EXPERIMENTATION

The synthesis of acetanilide by green chemistry has various disadvantages as there is a lot of wastage of acetic acid molecule, which can be minimized by green chemistry.

3.1 Synthesis of compounds by conventional method:

1. In a 250 ml beaker containing 125 ml of water, 4.6 ml of conc. Hydrochloric acid and 5.1 g of aniline / substituted anilines were introduced.
2. Stirred until all the anilines passes completely into solution.
3. To the resulting solution, 6.9 g (6.4ml) of redistilled acetic anhydride was added and stirred until it was dissolved.
4. Poured immediately in a solution of 3.8 g of crystalline sodium acetate in 25 ml of water.
5. Stirred vigorously and cooled in ice. Filtered the acetanilide and substituted acetanilide with suction, washed with 10 ml water, drained well and dried upon filter paper. The crude products were recrystallized from boiling water and methylated spirit.
6. Non green component: Acetic anhydride leaves one molecule of acetic acid unused.

3.2 Synthesis of compounds by green chemistry method :

1. A mixture of aniline / substituted anilines (3.3g) and zinc dust (0.16g) in acetic acid (10ml) in 100 ml round bottom flask was heated over a gentle flame using water condenser.
2. Heating was continued for about 45 min., the reaction mixture was then carefully poured in cold water (33ml) in 250ml beaker with vigorous stirring.
3. The shining crystals of product were separated slowly. After 15 min, crystals were collected by filtration. The solid crystals were washed over the Buchner funnel with water and product was dried and crystallized in boiling water.
4. Green context: Minimize waste by-products, avoids use of acetic anhydride.

IV. CONCLUSION

This review article will definitely help to understand the importance of green chemistry, which is basic requirement in today's pharmaceutical industries. The approach will help to avoid the utilization of the toxic chemicals leading to various hazards in the industry. These conventional methods can be replaced easily by the methods which utilize non toxic and environment friendly techniques for the synthesis of same.

One of such approach has been discussed for the synthesis of acetanilide. The approach will definitely help in the synthesis by keeping the environment safe.

V. REFERENCES

- [1]. Singhal M., Singh A. Khan S.P, Green Chemistry Potential for Past, Present and Future Perspectives, 2012; 3(4).
- [2]. Ahluwalia V.K, Kidwai M., New Trends In Green Chemistry, Anamaya publisher New Delhi, 2nd edition, 2007; 5-18.
- [3]. Ahluwalia V.K, Green chemistry Environmentally Benign Reactions, published by India books, 2nd EDITION, 2006; 1-10.
- [4]. Vojvodic V.Environmental Protection :Green Manufacturing in the pharmaceutical industry and cost reduction, KenInd, 2009; 58(1): 32-33.
- [5]. Anastas. P.T, Warner J.C, Green chemistry Theory and Practice, OxfordUniversity, Press, New York, 1998.
- [6]. Anastas P.T, Hovarth I.T, Innovations and Green Chemistry, Chemistry review, 2007; 107.
- [7]. Ravichandaran S., International Journal, 2010; 2(4): 2191.
- [8]. Trost B.M, Atom economy- A challenge for organic synthesis:Homogeneous catalysis leads the way, 1995; 34: 259.
- [9]. Sheldon R.A, Green solvents for sustainable organic synthesis: State of art, 2005; 7: 267.
- [10].Bharati V.B, Resonance, 2008; 1041.
- [11].Ahluwalia V.K and Kidwai M., New Trends in Green Chemistry, Anamaya Publisher, New Delhi, 2004.
- [12].Anastas P., Warner, Green Chemistry: Theory and Pracctice, Oxford University Press, Oxford, 1998.
- [13].Anastas P.T, Heine L.G, Williamson T.V, Green Chemical Synthesis and Processes, American Chemical Soceity, Washington DC, 2000.
- [14].Singhal M, Singh A, Khan S.P, Sultan E, Sachan N.K, Green chemistry potential for past present and future perspectives.
- [15].Gujral. S.S, Sheela. M.A, Khattri S., Singhla R.K. A Focus and Review on the Advancement of Green Chemsitry, Indo Global Journal of Pharmaceutical Science, 2012; 2(4): 397-408.
- [16].Redasani V.K, Kumawat V.S, Kabra R.P, Surana S.J, Application Of Green Chemistry in Organic Synthesis, International Journal of Chem Tech Research, 2010.
- [17].Singhal. M, Singh A., Khan S.P, Green Chemistry Potential for Past, Present and Future Perspectives, International Research Journal of Pharmacy, 2012; 3(4).
- [18].Ivankovic. A., Dronjic A., Review of 12 Principles of Green Chemistry in Practice, International Journal of Sustainable and Green Energy, 2017; 6(3): 39-48.
- [19].Chanshetti U., Green Chemistry: Challenges And Opportunities In Sustainable Development, International Journal of Current Research, 2014; 6.

One Pot Efficient Synthesis of Pyranopyrazole Derivative

Pande P.R.¹, Patki A.S.²

¹Department of Chemistry, Nutan Mahavidyalaya Sailu, Dist. Parbhani, Maharashtra, India

²Department of Chemistry, Shivaji Mahavidyalaya Renapur, Dist. Latur, Maharashtra, India

ABSTRACT

An multi-component reaction in PEG-400 medium in the presence of $\text{SiO}_2\text{-SnCl}_4$ has been developed for the synthesis of 1,4 dihydropyrano[2,3-c]pyrazole-5-carbonitrile. The present protocol describes synthesis of pyranopyrazole derivative starting with aromatic aldehyde, malonitrile, ethyl acetate, hydrazine hydrate under PEG-400. The present method is efficient, energy saving gives the products in good to excellent yields. $\text{SiO}_2\text{-SnCl}_4$ catalyst works effectively. The key benefit of catalyst is that it is isolated easily at the end of reaction without any dull procedure.

Keyword: $\text{SiO}_2\text{-SnCl}_4$, Multi-component reaction, PEG-400 etc

I. INTRODUCTION

Heterocyclic chemistry is of prime importance as a sub-discipline of Organic Chemistry, as millions of heterocyclic compounds are known with more being synthesized regularly.

The challenging task in chemistry is to develop practical methods, reaction media, conditions, and the use of materials based on the principles of green chemistry. The concept of "Green Chemistry" has emerged as one of the guiding principles of environmentally benign synthesis. Thus, organic chemists are switching over to the maximum use of eco-friendly and sustainable in recent years, finding creative ways to reduce environmental pollution has been the goal of many organic resources. In water, organic reactions arising from hydrophobic effect will have reduced activation energies and faster reactions. It has been focused on reducing or eliminating the use of toxic solvents to minimize damage for the human and environmental. Pyranopyrazole heterocycles have special importance in synthetic and medicinal chemistry.

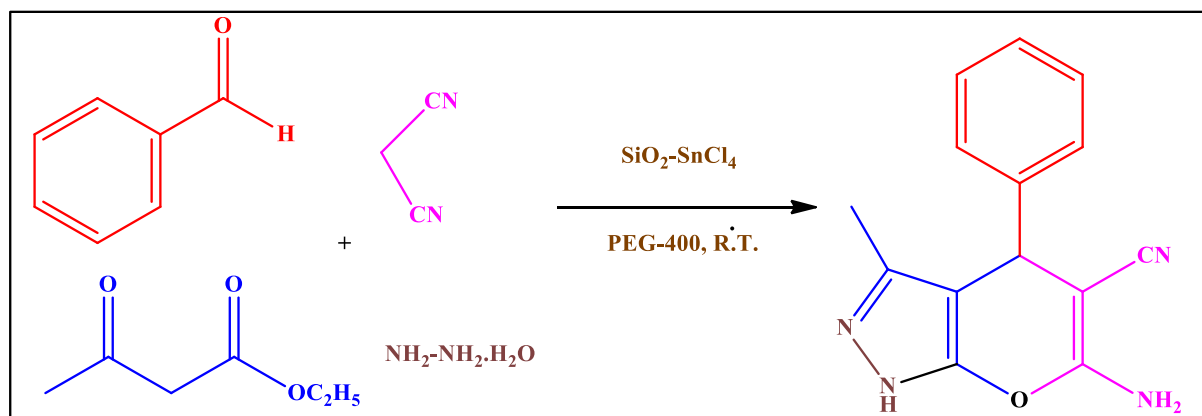
These compounds are found in synthetic products and many natural compounds that show a Wide range of biological activities [1]. It is also applicable to note that pyranopyrazole derivatives exhibit anti-inflammatory [2], antihypertensive [3], anticancer [4], antimicrobial [5], insecticidal [6], antifungal activities [7]. Multicomponent processes have recently gained considerable economic and ecological impetus as they address fundamental principles of synthetic efficiency and reaction design. Multicomponent reactions (MCRs) have been proven to be very elegant and rapid way to access complex structures in a single synthetic operation from simple building blocks and show high atom economy and high selectivity [8,9]. Therefore, choice of catalyst for green reaction is limited and has become a matter of concern for researchers nowadays. In recent times, few synthetic methods were developed for the preparation of pyranopyrazoles available in the

literature [10]. Amongst which the four components, one pot synthesis of pyranopyrazoles from ethyl acetate, malononitrile, aromatic aldehyde and hydrazine hydrate is a suitable methodology. Furthermore, a few procedures have described the one pot multicomponent synthesis of pyranopyrazoles based on catalysts such as 1,4-diazabicyclo [2.2.2] octane (DABCO) [11], cinchona alkaloid [12] and many others. The procedure had certain disadvantages such as the use of toxic catalysts, monotonous workup and poor yields.

Experimental: chemicals taken from Sigma Aldrich without further purification. Melting points of all compounds were determined on a melting point apparatus and are found to be uncorrected. IR spectra were recorded on PerkinElmer FTIR spectrophotometer. The ¹H NMR spectra were recorded on Bruker Spectrospin spectrometer (300 MHz) using TMS as an internal standard.

II. GENERAL PROCEDURE

To the aqueous mixture of hydrazine hydrate, (1 mmol) and ethyl acetoacetate (1 mmol), aromatic aldehyde (1 mmol), malononitrile (1 mmol) and SiO₂-SnCl₄ as catalyst were added in a catalytic amount at room temperature stirred for specific period till reaction is completed. The progress of reaction is confirmed by taking TLC periodically. After completion of the reaction the reaction mixture was filtered and obtained a solid crude product. The product was recrystallized by hot ethanol. The catalyst was recovered was simple filtration process which is dried under vacuum. The catalyst was recycled for further use.



Spectra of some compounds:

6-amino-4-(4-methoxy phenyl) 3-methyl-1, 4 dihydropyrano [2,3-c] pyrazole 5-carbonitrile

IR (cm⁻¹) 3490, 3254, 3110, 2838, 2170, 1632, 1498; ¹HNMR (300MHz,CDCl₃) δ 1.79 (3H,s,CH₃), 3.74 (3H,s,-OCH₃), 4.44 (1H,s,CH), 6.82 (2H,s,NH₂), 6.86-6.89 (2H,d,Ar-H), 7.05-7.09 (2H,d,Ar-H), 12.10 (1H,s,NH); ¹³C-NMR (300MHz, CDCl₃) δ 9.76, 35.46, 54.91, 57.65, 98.88, 113.70, 122.62, 126.55, 136.51, 136.46, 155.73, 158.90, 161.65 ppm; m/z 283 (M⁺,100%)

6-amino-4-(4-methyl phenyl) 3-methyl-1, 4 dihydropyrano [2,3-c] pyrazole 5-carbonitrile

IR (cm⁻¹) 3242, 3042, 2900, 2360, 1681, 1268; ¹HNMR (300MHz, CDCl₃) δ 1.83(3H,s,CH₃), 2.24 (3H,s,CH₃), 4.52(1H,s,CH), 6.92(2H,s,NH₂), 7.04-7.08 (2H,d,Ar-H), 7.10-7.12 (2H,d,Ar-H),12.10(1H,s,NH); ¹³C-NMR

(300MHz, CDCl₃) 164, 140.0, 113.8, 176.1, 27.2, 133.3, 60.4, 135.7, 129.4, 125.6, 118,14.5, 22.2 m/z 267 (M⁺,100%)

6-amino-4-(4-chloro phenyl) 3-methyl-1, 4 dihydropyrano [2,3-c] pyrazole 5-carbonitrile

IR (cm⁻¹) 3400, 3305, 3178, 2190, 1625; ¹HNMR (300MHz, CDCl₃): δ 1.91 (3H,s,CH₃), 4.63 (1H,s,CH), 6.77 (2H,s,NH₂), 7.15-7.22 (2H,d,Ar-H), 7.37-7.42 (2H,d,Ar-H), 12.14 (1H,s,NH);

¹³C-NMR (300MHz, CDCl₃) 164, 146, 113, 132, 176, 26.5, 133.4, 59.2, 126, 130, 118, 14 m/z 287 (M⁺).

6-amino-4-(2, 4-dichloro phenyl) 3-methyl-1, 4 dihydropyrano [2,3-c] pyrazole 5-carbonitrile

IR (cm⁻¹) 3482, 3250, 3118, 2189, 1642, 1590; ¹HNMR (300MHz, CDCl₃) δ1.73 (3H,s , CH₃), 4.56 (1H, s, CH),7.00 (1H, s, ArH), 7.20 (2H, s, NH₂), 7.82 (2H, d,ArH), 7.77 (2H, d, ArH), 11.89 (1H,s , NH). m/z-320(M⁺).

6-amino-4-(4-hydroxy-3-methoxy phenyl) 3-methyl-1, 4 dihydropyrano [2,3-c] pyrazole 5-carbonitrile

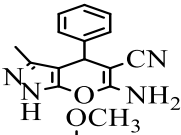
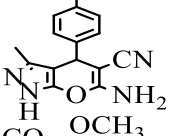
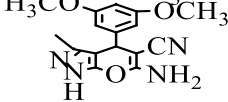
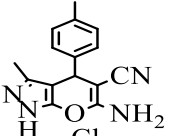
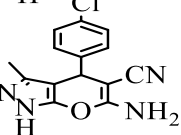
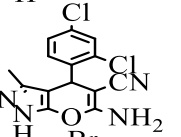
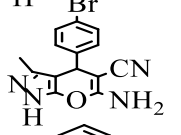
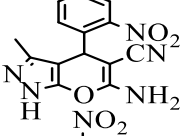
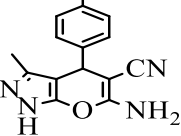
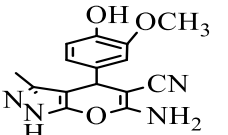
¹H NMR (300 MHz,CDCl₃): δ 1.88 (s, 3H, CH₃), 3.55 (s, 3H, OCH₃), 4.62 (s, 1H, CH), 6.48 (d, 1H, OH), 6.79 (t, 2H, CH₂), 6.77 (s, 2H, CH₂), 8.85 (s, 1H), 11.99.(s, 1H, NH); ¹³C NMR (300 MHz, CDCl₃)δ 9.9, 36, 55.8, 57.8, 98.9, 112.6,115.9, 120, 136.4, 136.8, 145.2, 147.3, 163.

Catalytic Activity:

In order to study catalytic activity of the catalyst for the synthesis of pyranopyrazole from aromatic aldehyde, malononitrile, ethyl acetate and phenyl hydrazine. We performed the synthesis of pyrano-pyrazole under optimized condition and the result is displayed in Table 1.

In the beginning of the scheme benzaldehyde, malononitrile, ethyl acetate, phenyl hydrazine reacted together undergo cyclization to give 86% of selective yield in 4 hrs (Table 1, Entry 1). Further in order to study the effect electron donating group during the cyclo-condensation process for the synthesis of pyranopyrazole. So in next attempt 4- methoxy benzaldehyde, 3,4,5- tri-methoxy benzaldehyde and 4-methyl benzaldehyde taken in separate round bottom flask is allowed to react with malonitrile, ethyl acetate and phenyl hydrazine at room temperature to yield 82%, 84%, 80% of pyranopyrazole derivative in 4.5hr., 4 hr., 5hrs. Respectively (Entry 2,3,4). So this result confirmed the presence of electron releasing group on benzaldehyde retard the rate of reaction with decrease in yield. Moving on, the same steps of reaction is carried with 4-chlorobenzaldehyde, 2,4-dichlorobenzaldehyde, 4-bromobenzaldehyde in a separate container with malononitrile, ethyl acetate and phenyl hydrazine to produce 88%, 92% and 93% of yield in 4, 3 and 3 hrs respectively (Entry 5, 6 and 7). Soon after effect of electron withdrawing group is studied with 2-nitrobenzaldehyde and 4-nitrobenzaldehyde in a separate flask of reaction with following same state of reaction as described above and very surprising output was obtained with 98% and 96% of yield within very short of time 2.5 hr. for both the reaction (Entry 8 and 9). These results clearly indicates that electron withdrawing group increases rate of reaction with increase in yield with reduction in the time required for proceeding the reaction

Table1- Synthesis of different substituted pyrano-pyrazole derivative by using SiO₂-SnCl₄ under optimized reaction.

Entry	Product	Time (hr.)	Yield (%) ^x
1		4	86
2		4.5	82
3		4	84
4		5	80
5		4	88
6		3	92
7		3	93
8		2.5	98
9		1.5	92
10		3	76

a) All reaction performed with equimolar reactant (1mmol) and with 10 mol % of catalyst.

b) x Refers to an isolated yield

III. RESULT AND DISCUSSION

In summary, a green, effective and environmentally friendly approach was considered for the synthesis pyranopyrazole. pyranopyrazole derivatives was synthesized by four component condensation reaction of various aromatic aldehydes, malononitrile, ethyl acetate and phenyl hydrazine under PEG-400 as a solvent at R.T. Considerable advantages of the presented investigation are reasonably high yield, cleaner reaction profile, short reaction time, simple work up procedure, recycle and reusability of $\text{SiO}_2\text{-SnCl}_4$. The whole reaction situation made close agreement with the green chemistry disciplines. The isolation and purification of catalyst at the end of reaction was also easy. The referred catalyst also produces surprising result of good to excellent yield of pyranopyrazole within short of time.

IV. REFERENCES

- [1]. D.S. Fischer, G.M. Allan, C. Bubert, N. Vicker, A. Smith, H.J. Tutill, A. Purohit, L. Wood, G. Packham, *J. of Med. Chem.*, **48**, 5749 (2005).
- [2]. M. E. A. Zaki, H. A. Soliman, O. A. Hiekal, A. E. Z, *Zeitschrift, Naturforschung*, **61**, 1(2006).
- [3]. V.K. Ahluwalia, A. Dahiya, V.K. Garg, *Cheminform*, **36**, 88 (1997).
- [4]. J. L Wang., D. Liu, Z. J. Zhang, S. Shan, X. Han, S. M. Srinivasula, C. M. Croce, E. S. Alnemri, Z. Huang, *Proc. of the Nat. Acad. of Sci.*, **97**, 7124 (2000).
- [5]. T. N. Bansode, R. M. Ansari, Y. K. Gawale, **4**, 1141(2011).
- [6]. Z. H. Ismail, G. M. Aly, M. S. El-Degwi, H. I. Heiba, M. M. Ghorab, *Egypt. J. of Biotechn.*, **13**, 73 (2003).
- [7]. M. Beerappa, K. Shivashankar, *Synth. Communi.*, **48**, 146 (2018).
- [8]. A. Alizadeh, F. Mobahedi, A. Esmaili, *Tetrahedron Lett.*, **47**, 4469 (2006).
- [9]. M. Umkeherer, C. Kalinski, J. Kolb, C. Burdack, *Tetrahedron Lett.*, **47**, 2391(2006).
- [10]. D. Enders, A. Grossmann, B. Gieraths, M. Duzdemir, C. Merkens, *Org. Lett.*, **14**, 4254 (2012).
- [11]. A. Keyume, Z. Esmayil, L. Wang, F. Jun, *Tetrahedron*, **70**, 3976 (2014).
- [12]. S. Gogoi, C. G. Zhao, *Tetra. Lett.*, **50**, 2252 (2009).

Oxidised Activated Carbon: Highly Efficient and Recyclable Catalyst for The Synthesis of 1, 8-Dioxooctahydroxanthene Derivatives

Mantosh B. Swami¹, Sushil R. Mathapati^{2*}

¹Department of Chemistry, Mahatma Basweshwar Mahavidyalay, Latur, Maharashtra, India

²Department of Chemistry, Madhavrao Patil College Murum, Maharashtra, India

ABSTRACT

Oxidised-AC has been found to be an effective heterogeneous catalyst for synthesis of series 1,8-dioxooctahydroxanthene derivatives from condensation followed by cyclization of 5,5-dimethyl 1,3-cyclohexanedione and substituted aldehydes. The heterogeneous catalyst was prepared and characterized by using various advanced analytical techniques and employed in present reaction. The catalyst could be easily separated by simple filtration and reused further up to six cycles without loss of catalytic activity. Key advantage of this method is high yield, short reaction time, low cost, simple and easy work-up procedure.

Keywords: Oxidised AC, Highly efficient, Recyclable Catalyst, 5, 5-dimethyl 1, 3-cyclohexanedione, 1, 8-dioxooctahydroxanthene derivatives.

I. INTRODUCTION

MCR involves three or more starting material reacts to form a product, it consist almost essential atoms from reactants. These are more convenient and useful over traditional multistep sequential assembly of target molecule. In multicomponent reactions, target molecule is prepared in convergent one step in one pot by simply mixing of starting materials. MCRs were performed via simple experimental procedure without need of any special condition. Multi-component reactions have emerged as highly efficient protocol in modern synthetic organic chemistry due to creation of various new bonds in one pot reaction[1]. These types of reactions have been studied widely in organic synthesis, primarily due to their ability to generate complex molecular functionality from simple starting materials via one-pot reactions[2]. This has considerable advantages because it saves precious time and drastically reduces effort.

Xanthene derivative possesses variety of applications in biological and pharmaceutical field; derivatives of xanthenes are reported as anti-inflammatory [3], antibacterial [4], antiviral[5], anti-tumor [6], antiproliferative [7-8], anticancer [9-10], anti-oxidant [11], antiplasmodial[12], also acts as trypanothione reductase inhibitor[13], selective estrogen receptor modulator[14]. In addition, these compounds were used as pH sensitive fluorescent materials for visualization of biomolecules[15], luminescent sensors[16], xanthene dyes fluorescence based probes for optical imaging applications[17]. These are also used as antagonists for paralyzing action of zoxazolamine[18]. Xanthenediones possesses similar special structural units constituting

many natural products and being used as versatile synthons because of inherent reactivity of their inbuilt pyran ring. In the recent year, there is enormous interest in the synthesis of this class of fused heterocyclic compounds, due to its number of applications increased in the field of medicinal chemistry and material science.

There are a number of methods for the preparation of the xanthenes have been reported, these includes synthesis by cyclization of polycyclic aryltriflate esters[19], cyclo-condensation of 2-hydroxyl aromatic aldehyde with 2-tetralone[20], and trapping of benzynes by phenols[21] as well as reaction of aryloxy magnesium halides with triethyl orthoformate[22]. Synthesis of 1, 8-dioxooctahydroxanthenes has been worked out by using variety of catalyst and solvent system.

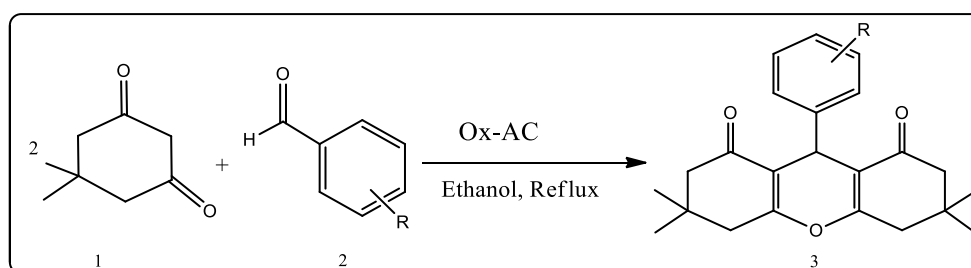
The classical method for synthesis of 1, 8-dioxooctahydroxanthenes involves cyclization between dimedone and various substituted benzaldehyde in presence of different catalysts. However, many of these methods suffer from one or more disadvantages, such as longer reaction time, hazardous and expensive solvent, harsh reaction conditions, expensive chemicals, tedious work up, recovery of catalyst and poor yield. Therefore, there is a need to develop an efficient method for one-pot synthesis of 1, 8-dioxo- octahydroxanthene derivatives.

In present protocol, we have reported one pot efficient synthesis of 1,8-dioxooctahydroxanthene derivatives from dimedone and Substituted benzaldehyde in presence of catalytic amount of freshly prepared Oxidised AC.

II. EXPERIMENTAL:

General procedure for synthesis of 1,8-dioxooctahydroxanthene using Ox-AC catalyst:

A mixture of substituted aldehyde (1mmol), 5, 5-dimethyl-1, 3-cyclohexanedione (2 mmol) and add Ox-AC(10 wt %) then the resultant mixture was refluxed for two hour and progress of reaction was monitored by TLC. After completion, the catalyst was separated by using external magnet without filtration and solvent evaporated. Crude product was further purified by recrystallization in hot ethanol to get pure xanthenes derivatives.



3,3,6,6-tetramethyl-9-(4-chloro-phenyl)-1,8-dioxooctahydroxanthene:

IR (KBr, in cm^{-1}): 3032, 2964, 2954, 1677, 1662, 1468, 1362, 1199, 1168, 1004, 852. ^1H NMR(CDCl_3 , in δ ppm): 7.18 - 7.25 (dd, 4H), 4.72 (s, 1H), 2.18 (q, 4H), 2.46 (s, 4H), 1.12 (s, 6H), 0.98 (s, 6H); ^{13}C NMR (CDCl_3 , in δ ppm): 191.10, 157.18, 137.44, 126.78, 124.54, 122.98, 110.04, 45.46, 35.62, 26.96, 26.23, 24.04, 22.06 MS (m/z):385.2 (M + 1)

3,3,6,6-tetramethyl-9-(4-hydroxy-3-methoxy-phenyl)-1,8-dioxooctahydroxanthene:

IR (KBr, in cm^{-1}): 3414, 3025, 2957, 1668, 1625, 1516, 1433, 1358, 1279, 1228, 1198, 1136, 1027, 625, 574. ^1H NMR(CDCl_3 , in δ ppm): 7.03 (s, 1H), 6.74 (d, 1H), 6.57 (dd, 1H), 5.48 (bs, 1H), 4.67 (s, 1H), 3.87 (s, 3H), 2.47 (s, 4H), 2.22 (q, 4H), 1.02 (s, 12H); ^{13}C NMR (CDCl_3 , in δ ppm): 196.5, 162.2, 145.9, 144.2, 136.5, 120.2, 115.8, 113.8, 112.3, 55.4, 50.5, 40.5, 32.4, 31.4, 29.3, 27.4; MS (m/z): 419.40

3,3,6,6-Tetramethyl-9-(4-nitrophenyl)-1,8-dioxo-octahydroxanthene

IR (KBr, in cm^{-1}): 3022, 2928, 1686, 1655, 1530, 1368, 1188, 1033, 855, 756, 633, 513. ^1H NMR(CDCl_3 , in δ ppm): 8.11 (d, 2H), 7.38 (d, 2H), 4.85 (s, 1H), 2.88 (s, 4H), 2.33 (s, 4H), 1.14 (s, 6H), 0.98 (s, 6H); ^{13}C NMR (CDCl_3 , in δ ppm): 197.20, 164.82, 148.64, 133.10, 131.42, 128.32, 126.80, 115.72, 114.40, 51.82, 43.90, 43.62, 30.10, 29.51, 27.61, 27.4; MS (m/z): 395 [M^+].

3,3,6,6-Tetramethyl-9-(4-methoxy-phenyl)-1,8-dioxooctahydro-xanthene:

IR (KBr, in cm^{-1}): 3058, 2959, 2877, 1664, 1627, 1512, 1463, 1358, 1261, 1194, 1109, 1032, 844, 564. ^1H NMR (CDCl_3 , in δ ppm): 7.22 (d, 2H), 6.77 (d, 2H), 4.68 (s, 1H), 3.74 (s, 3H), 2.46 (s, 4H), 2.19 (q, 4H), 1.08 (s, 6H), 0.99 (s, 6H); ^{13}C NMR (CDCl_3 , in δ ppm): 196.72, 162.00, 157.86, 136.52, 129.42, 115.80, 113.52, 55.22, 50.80, 40.92, 32.30, 30.83, 29.22, 27.40 MS (m/z): 381.20

III. RESULT AND DISCUSSION**Catalytic Activity:**

Ox-AC as heterogeneous catalyst utilized for conversion of dimedone and substituted benzaldehyde to 1,8-dioxooctahydroxanthenes. The reaction condition was optimized and their outcomes summarized in table II-1. First attempt was carried out in absence of catalyst and solvent to check the reactivity of component. Still no conversion observed upto 42 hours stirring. Further reaction was performed at 100°C without addition of catalyst and solvent, to determine effect of temperature on reaction; no isolated product was obtained (Table -1, entry 2). Next experiment was carried out in ethanol as solvent without catalyst at reflux temperature for prolonged time gave lower yield (entry 3).

Table-1: Optimization of reaction condition for the synthesis of 1, 8-dioxooctahydro- xanthenes using Ox-AC.

Entry	Catalyst	Cat. Amount	Solvent	Temp. (°C)	Time(h)	Yield (%)
1	-	-	-	RT	48	0
2	-	-	-	100	24	<10
3	-	-	Ethanol	Reflux	24	50
4	Ox-AC	10 wt %	-	100	10	65
5	Ox-AC	10 wt %	Acetonitrile	Reflux	5	70
6	Ox-AC	10 wt %	Toulene	Reflux	5	65

7	Ox-AC	10 wt %	THF	Reflux	2	72
8	Ox-AC	5 wt %	Ethanol	Reflux	2	80
9	Ox-AC	10 wt %	Ethanol	Reflux	2	94
10	Ox-AC	20 wt %	Ethanol	Reflux	2	95

Later on the reaction was carried out in presence Ox-AC under solvent free condition at 100°C to know the efficiency of catalyst; product was obtained with moderate yield (Table-1, entry 4). We observed that the catalyst in absence of solvent unable to produce efficient yield, so the same reaction was continued in ethanol at reflux temperature to get 95% yield of xanthenes (entry 5). In order to understand the effect of solvent on yield of reaction, number of solvent were screened for selected reaction. The model reaction was tried in presence of Ox-AC in acetonitrile at reflux temperature gives moderate yield (Table 1, entry 5). While the reaction becomes slower in tetrahydrofuran with 72% yield. Further, next reaction were conducted in toluene, it results into lowest yield and requires more time (Table-1, entry 6). Screening test of solvent reveals, reaction performed in nonpolar solvent gives lower yield, while in polar solvent enhances rate as well as yield of product. Finally, ethanol was found to be better solvent for conversion of dimedone and substituted aldehyde into 1,8-dioxooctahydroxanthene upto 95% yield. Subsequently, we tested different amount of catalyst under reflux temperature in ethanol, 10wt% of catalyst shows efficient yield (Table-1, entry 9). Moreover, we tried same reaction with reduction of catalytic amount upto 5 wt%; the reaction becomes sluggish with quite low yield (Table-1, entry 9). However, on increasing catalytic amount upto 20 wt%, yield obtained was same as of 10 and 20 wt% catalytic amount respectively. Consequently 10 wt% catalytic amount and ethanol was selected as optimized condition for the reaction.

In earlier table, we have optimized reaction conditions and selected Ox-AC catalyst for synthesis of xanthene derivatives

Moreover, aromatic aldehyde bearing electron withdrawing group such as -NO₂, -Cl, reacts smoothly with efficient yield of xanthenes (Table-2, Entry 8-11). Among the all substituted benzaldehydes, p-nitrobenzaldehyde reacts more faster with high yield (Table II-3, entry 9). To examine scope and applicability of present methodology, wide range of substituted aldehydes with electron donating and withdrawing groups was condensed with dimedone under optimized reaction condition. Monitoring of all reactions and their completion was confirmed by thin layer chromatography, time taken and yield of product was summarized in Table -2. The dimedone and substituted aldehydes undergoes cyclization in presence of little quantity of catalyst for short reaction time and gives efficient yield. Table-2, entry 1, clearly gives an idea about reactivity of aryl aldehyde with dimedone in presence of catalyst to give xanthenes. Entry 2, reveals that the decrease in reactivity due to presence of electron donating group on aryl aldehyde. Fairly similar results were observed in case hydroxy and methoxy substituted benzaldehydes (Table -2, entry 3 & 4).

Table-2: Synthesis of different substituted 1,8-Dioxooctahydro xanthene derivatives using Ox-AC in optimized reaction condition.

Entry	Aldehyde	Time (hr)	Product code	Yield (%)
1	Benzaldehyde	2	II-3a	94
2	4-Methylbenzaldehyde	2	II-3b	90
3	4-Hydroxybenzaldehyde	2	II-3c	93
4	4-Methoxybenzaldehyde	2	II-3d	92
5	4-Chlorobenzaldehyde	2	II-3e	94
6	4-Hydroxy-3-Methoxybenzaldehyde	2	II-3f	92
7	4-Flurobenzaldehyde	2	II-3g	92
8	3-Nitrobenzaldehyde	2	II-3h	95
9	4-Nitrobenzaldehyde	2	II-3i	96
10	3-Chlorobenzaldehyde	2	II-3j	94
11	4-Formylbenzaldehyde	2	II-3k	94

IV. CONCLUSIONS

In Conclusion, Ox-AC was utilized as heterogeneous catalyst for the conversion of aryl aldehyde and dione to xanthene derivatives. The catalyst was prepared and characterized successfully with help of various spectroscopic techniques which showed oxidation of Activated Carbon leads to COOH functionality. The catalyst proved itself as highly efficient and economically viable catalyst for synthesis of 1,8-dioxooctahydroxanthene derivatives. The experimental procedure is not only advantageous from the environmental point of view but also offers high yield and reaction rate. In addition, catalyst could be recycled up to six cycles without affecting yield of product. The key advantages of this method are simplicity of operation, easy work up, recyclability of catalyst, high yields with maximum purification, short reaction time.

Acknowledgements:

I am thankful to Principal, Mahtama Basweshwar Mahavidyalay, Latur and Dr. Sudhakar Patil, Maharashtra Udaygiri Mahavidyalay, Udgir, for providing research facilities. I am grateful to Dr. Arvind Jadhav, CNMS Jain University Bangalore, for their support.

V. REFERENCES

- [1]. I. Nakamura, Y. Yamamoto, Transition Metal Catalysed Reactions in Heterocyclic Synthesis, Chem. Rev., 104, 2127 (2004). <https://doi.org/10.1021/cr020095i>

- [2]. F. Mohadpour, Porous Silica Encapsuled and Magnetically Recoverable, Rh NPs: A highly Efficient, stable and Green Catalytic transfer hydrogenation with "Slow release" of Stoichiometric hydrazine in water, *Trends in green chem.*, 3, 1 (2017). <https://doi.org/10.1039/C7GC00986K>
- [3]. H. N. Hafez, M. I. Hegab, I. S. Ahmed-Farag, A. B. A. El-Gazzar, A Facile Regioselective Synthesis of Novel Spirothioxanthene and Spiro-xanthene-9,2-[1,3,4]thiadiazole derivatives as Potential Analgesic and Antiinflammatory agents, *Bioorg. Med.Chem.Lett*, 18, 4538 (2008). <https://doi.org/10.1016/j.bmcl.2008.07.042>
- [4]. J. Araujo, C. Fernandes, M. Pinto and M. E. Titrain, Chiral Derivatives of Xanthenes with Antimicrobial Activity 24, 314(2019). <https://doi.org/10.3390/molecules24020314>
- [5]. B. Baghernejad, M. Fiuzat, One Pot Synthesis of Xanthene Derivatives as Potential antiviral and anti-inflammatory Agent using Nano-SnO₂ as efficient Catalyst, *Appl. Chem. Res.* 15, 46 (2021). <https://doi.org/10.1001/1.20083815.2021.15.2.4.5>
- [6]. S-J. Tao, S-H. Guan, W. Wang, Z-Q. Lu, G-T. Chen, N. Sha, Q-X. Yue, X. Liu and D-A. Guo, Cytotoxic Polyprenylated Xanthenes from the Resin of *Garcinia hanburyi*, *J. Nat. Prod.*, 72, 117 (2009). <https://doi.org/10.1021/np800460b>
- [7]. N. Mulakyala, P. V. N. S. Murthy, D. Rambabu, M. Aeluri, R. Adepu, G. Krishna, C. M. Reddy, K. Prasad, M. Chaitanya, C. S. Kumar, M. Basaveswara, M. Pal, Catalysis by Molecular Iodine: A Rapid Synthesis of 1,8-Dioxo-octahydroxanthene and there evaluation as Potential Anticancer Agents, *Bioorganic and Medicinal Chemistry Letters*, 22, 2186 (2012). <https://doi.org/10.1016/j.bmcl.2012.01.126>
- [8]. M. V. Lembege, S. Moreau, S. Larrouture, D. Montaudon, J. Robert and A. Nuhrich, Synthesis and Antiproliferative Activity Aryl and heteroaryl-hydrazone derived from Xanthone Carbaldehydes, *Eur. J. Med. Chem.*, 43, 1336 (2008). <https://doi.org/10.1016/j.ejmech.2007.09.003>
- [9]. M. S. Kumar, J. Singh, S. K. Manna, S. Maji, R. Konwar and G. Panda, Diversity Oriented Synthesis of Chromene-Xanthene hybrids as Anti-breast Cancer Agents, *Bioorg. Med. Chem. Lett.*, 28, 778 (2018). <https://doi.org/10.1016/j.bmcl.2017.12.065>
- [10]. A. K. Bhattacharya, K. C. Rana, M. Mujahid, I. Sehar A. K. Saxena, Synthesis and invitro study of 14-Aryl-14-H- dibenzo[a,j] xanthenes as Cytotoxic agents. *Bioorg. Med. Chem. Lett.*, 19, 5590 (2009). <https://doi.org/10.1016/j.bmcl.2009.08.033>
- [11]. A-E. Hay, M-C. Aumond, S. Mallet, V. Dumontet, M. Litaudon, D. Rondeau and P. Richomme, Antioxidant Xanthenes from *Garcinia Vieillardii*, *J. Nat. Prod.*, 67, 707 (2004). <https://doi.org/10.1021/np0304971>
- [12]. F. Zelefack, D. Guilet, N. Fabre, C. Bayet, S. Chevalley, S. Ngouela, B. N. Lenta, A. Valentin, E. Tsamo, M-G. D-Franca, Cytotoxic Antiplasmodial Xanthenes from *Pentadesma butyracea*, *J. Nat. Prod.*, 72, 954 (2009). <https://doi.org/10.1021/np8005953>
- [13]. K. Chibale, M. Visser, D. V. Schalkwyk, A. Saravanamuthu, P. J. Smith and A. Fairlamb, Exploring the Potential of Xanthene derivatives as Trypanothione Reductase inhibitor and Chloroquine Potentiating agents, *Tetrahedron*, 59, 2289 (2003). [https://doi.org/10.1016/S0040-4020\(03\)00240-0](https://doi.org/10.1016/S0040-4020(03)00240-0)

- [14]. J. F. Callan, A. P. de Silva & D. C. Magri, Luminescent sensors and Switches in the Early 21st Century, *Tetrahedron*, 61, 8551 (2005). <https://doi.org/10.1016/j.tet.2005.05.043>
- [15]. R. Singla, K. B. Gupta, S. Upadhyay, M. Dhiman and V. Jaitak, Design Synthesis and Biological evaluation of Indole-xanthenedione hybrid as selective Estrogen receptor modulators, *Bioorg. Med. Chem.* 26, 266 (2018). <https://doi.org/10.1016/j.bmc.2017.11.040>
- [16]. C. G. Knight, T. Stephens, Xanthene dye labelled Phosphatidylethanolamine as probe of interfacial PH Studies in Phospholipid vesicles, *Biochem. J.*, 258, 683 (1989). <https://doi.org/10.1042/bj2580683>
- [17]. S. A. Hilderbrand & R. Weissleder, One pot Synthesis of New Symmetric and asymmetric Xanthene dyes, *Tetrahedron Lett.*, 48, 4383 (2007). <https://doi.org/10.1016/j.tetlet.2007.04.088>
- [18]. G. S-Ruf, H-T Hieu & J-P Poupelin, The effect of dibenzoxanthenes on the paralyzing action of zoxazolamine, *Naturwiss.*, 62, 584 (1975). <https://doi.org/10.1007/BF01166986>
- [19]. J-Q. Wang & R. G. Harvey, Synthesis of Polycyclic Xanthenes and furans via Palladium- Catalyzed cyclization of Polycyclic aryl triflate esters, *Tetrahedron*, 58, 5927 (2002). [https://doi.org/10.1016/S0040-4020\(02\)00534-3](https://doi.org/10.1016/S0040-4020(02)00534-3)
- [20]. A. Jha, J. Beal, Convenient Synthesis of 12 H-benzo[a] Xanthenes from 2-tetralone, *Tetrahedron Lett.*, 45, 8999 (2004). <https://doi.org/10.1016/j.tetlet.2004.10.046>
- [21]. D. W. Knight, P. B. Little, The First Efficient method for the intramolecular trapping of Benzynes by Phenols : A New Approach to Xanthenes, *J. Chem. Soc.*, 4, 1771 (2001). <https://doi.org/10.1039/B103834F>
- [22]. G. Casiraghi, G. Casnati, M. Comia, Regiospecific reactions of Phenol salts: Reaction pathways of alkyl phenoxy magnesiumhalide with Triethylorthoformate, *Tetrahedron Lett.*, 14, 679 (1973). [https://doi.org/10.1016/S0040-4039\(00\)72432-4](https://doi.org/10.1016/S0040-4039(00)72432-4)

A Review on Synthetic Strategies of Imidazole and its Biological Activities

Sandip S. Dhotre¹, Vidya S. Dofe², Rajendra P. Pawar^{1*}

¹Department Of chemistry, Shivchhatrapati College, Aurangabad-431003.²

¹Department of Chemistry, Deogiri college, Aurangabad-431005.

Corresponding Author: dhotresandip2011@gmail.com

ABSTRACT

Imidazoles derivatives are widely used in pharmacological drugs and have occupied a unique position in heterocyclic chemistry; its derivatives have attracted researcher to synthesize new derivatives by various methods and catalyst for its versatile properties in chemistry and pharmacology. This created interest in researchers to synthesize variety of imidazole derivatives and analyse for their biological activities. Imidazole is nitrogen-containing heterocyclic ring and its derivative possesses biological and pharmaceutical importance such as antibacterial¹, Antimicrobial², anti-inflammatory³, anti-fungal⁴, anticancer⁵, anti-depressant⁶, anti-viral⁷ and anti-tubercular⁷. This paper aims to review the different types of imidazole derivatives which having biological activity.

I. INTRODUCTION

Imidazole is a five-member heterocyclic aromatic compound with two nitrogen atoms present at 1, 3-position. Both Nitrogen atoms are sp² hybridized. The natural products like histamine, histidine, and nucleic acid are the important constituent of imidazole ring. Imidazole susceptible to nucleophilic and electrophilic attack. Imidazole generally colorless or pale yellow solid and it has amine like order. It is soluble in water and other polar solvents. Imidazole has melting point 88.9°C and it has boiling point 267.8°C. Imidazole has molecular formula C₃H₄N₂. The high beneficial properties of the imidazole containing drugs have encouraged the medicinal chemists to prepare a large number of new therapeutic molecules. Imidazole drugs have wide spectrum of applications in pharmaceutical, medicinal, photosensitizes and biological processes.

The Some imidazole derivatives show activity against *Mycobacterium tuberculosis*. Imidazole derivatives are pharmacologically and physiologically active and it is used in the treatment of various diseases. Imidazoles are important constituents and they are found in a large number of natural products and clinically active drug molecules. Synthetic imidazoles are present in many fungicides, anti-fungal, antiprotozoal and anti-hypertensive medications. Due to their significance, it has become a suitable target for the synthetic and clinical. There are different techniques that have been used for assembling and modifying the imidazole ring with different functional groups. The basic site in imidazole nucleus is N-3.

STRUCTURAL CHARACTERISTICS

The imidazole is a planar, five member heteroaromatic compounds with 3C and 2N atom in 1 and 3 positions. It was present in two equivalent tautomeric forms because the hydrogen atom can be located on either of the two nitrogen atom (Figure-1).

Imidazole is a highly polar compound, as evidenced by a calculated dipole of 3.61D, and is completely soluble in water. The compound is classified as aromatic due to the presence of a sextet of π -electrons, consisting of a pair of electrons from the protonated nitrogen atom and one from each of the remaining four atoms of the ring (figure-2).

Imidazole can function as both acid and base; hence it is amphoteric in nature (figure-3). As an acid, the pKa of

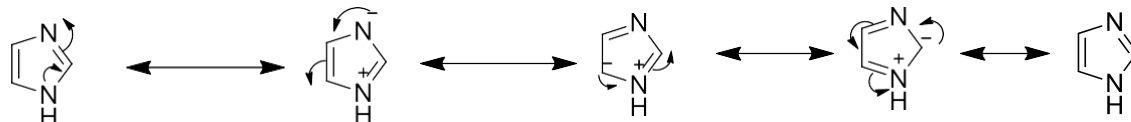


Figure-2

imidazole is 14.5, making imidazole less acidic than carboxylic acids, phenols and imides, but slightly more acidic than alcohols. The acidic proton is located on N-

1. As a base, the pKa of the conjugated acid is approximately 7, making it is approximately sixty times more basic than pyridine. The resonance interactions help to explain these properties, which increase the basicity of the 3-nitrogen atom³.

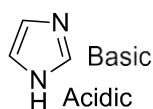


Figure-3

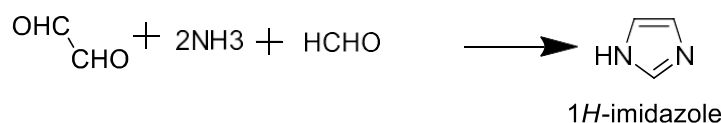
SYNTHESIS OF IMIDAZOLE AND ITS DERIVATIVES

Scheme I

Imidazole was first synthesized by Heinrich Debus in 1858, but various imidazole derivatives had been discovered as early as the 1840. The synthesis used glyoxal and formaldehyde in ammonia to form imidazole (Figure 4). Although various imidazole derivatives had been discovered earlier in the 1840. It has high boiling point 267.8°C than all other 5- membered heterocyclic compounds due to the inter- molecular H-bonding (figure-4), where there is linear association of molecule.

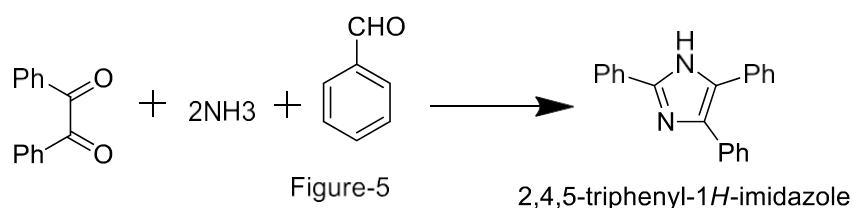
Now-a-days several methods are available for the synthesis of imidazole and its derivatives, some of these are given below in Schemes 1 and 2 .

Scheme II Figure-4



RE-Diszewski Synthesis

The synthesis denotes condensing a dicarbonyl compoundsuch as glyoxal, a keto aldehyde or a diketones with analdehyde in the presence of ammonia, with benzaldehyde and two molecules of ammonia react to yield 2,4,5-triphenyl-1H-imidazole(figure-9)^{8,9}.



SCHEME-III**WallachSynthesis**

When N,N-dimethyloxamide is treated with PCl_5 a chlorine containing compound is obtained which on reduction with HI acid Gives N-alkyl imidazole (figure-10) ^{10,11}

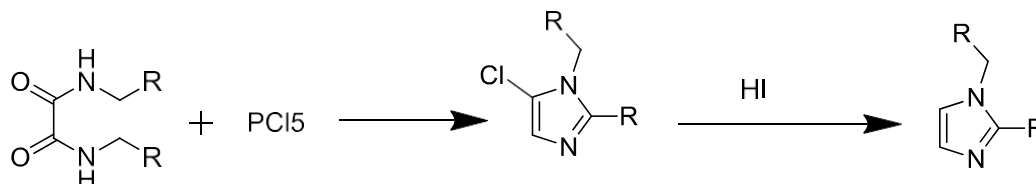


Figure-6

Biological Activity:

1) Anti-fungal and anti-bacterial activity¹²:

Ramya v et al synthesized a series of novel 5- (nitro/bromo)-styryl-2-benzimidazole derivatives and tested for the antibacterial and anti-fungal activity. This was comparable with Ciprofloxacin. ⁹

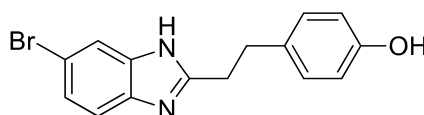


Figure-7

Namita gupta et al synthesized N-substituted imidazole derivatives and the synthesized compounds are evaluated for in vitro antimicrobial activity against *Staphylococcus aureus*, *Bacillus subtilis* (Gram positive); *Escherichia coli*, *Pseudomonas aeruginosa* (Gram negative) and *Candida albicans* and *Aspergillus niger*. All compounds showed moderate to good activity¹⁰

2) Anti-inflammatory and analgesic activities ¹²:

Kavitha C.S et al synthesized a series of 2- methylaminobenzimidazole derivatives and the synthesized compounds were screened for analgesic and anti-inflammatory activities. This compound (compound : shows analgesic and anti-inflammatory activity, Nimesulide used as standard drug ¹¹.

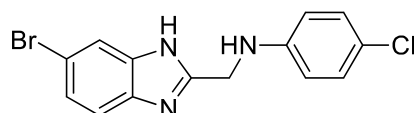


Figure-8

1) Anti-cancer activity ¹³:

Yusuf Ozkay et al synthesized many novel imidazole-(Benz)azole and imidazole epiperazine derivatives and synthesized compounds are tested for anticancer activity. All compounds showed good activity. Cisplatin was used as reference drug .

The substituted imidazoles show good antibacterial activity against gram negative bacterial strains Klebsiella

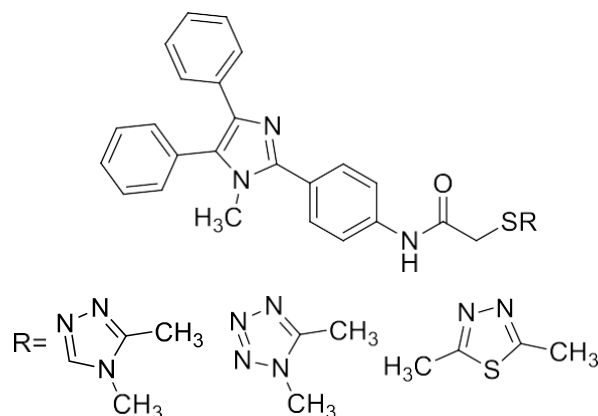
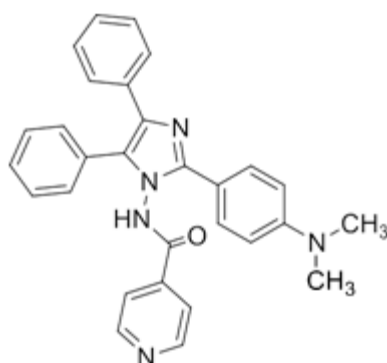


Figure-9

pneumoniae and Escherichia coli. The imidazole derivatives possess significant cytotoxic activity against Ehrlich's Ascites Carcinoma (EAC) cell lines and Dalton's Lymphoma Ascites (DLA) cell lines. Compound (Figure-10) showed the best anti cancer activity with CTC₅₀ value of 98.56 and 31.25 µg mL⁻¹ against DLA and 1 EAC cell line



3) Anti-depressant activities:

Farzin Hadizadeh et al synthesized moclobemide analogues by replacing moclobemide phenyl ring with substituted imidazole and studied for the antidepressant activity using forced swimming test. All the analogues showed moderate to good activity.

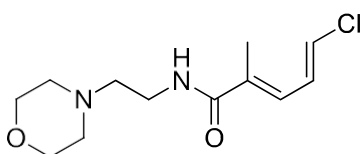


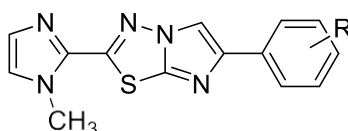
Figure-11

4) Anti-tubercular:

Harun M. Patel et.al synthesized imidazole [2, 1-b] [1, 2, 3] thiadiazole derivatives and evaluated for in-vitro antitubercular against *M. tuberculosis* strain H37Rv by using the MABA method. All the synthesized compounds (A-J) exhibited an interesting activity profile against the tested mycobacterial strain.

R= 3-nitro, 4-nitro, 4-chloro, 4-fluoro, H, 4-nitro, 4-methyl, 3-methyl, 2,4-dichloro, 2,4-dihydro

Figure-12



5) Antileishmanial activity:

A series of *N,N'*-disubstituted ethylenediamine and imidazolidine derivatives have been synthesized and their in vitro biological activities against *Leishmania* species have been evaluated. Of the nine synthesized compounds, five displayed a good activity in both *L. amazonensis* and *L. major* promastigotes. The compounds 1,2-Bis (p-

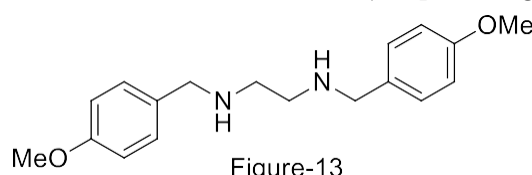


Figure-13

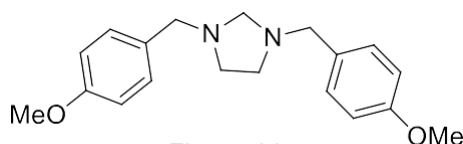


Figure-14

methoxybenzyl) ethylenediamine (Figure-12) and 1,3-Bis (p-methoxybenzyl)imidazolidines (Figure 14) showed the best activity on intracellular amastigotes, with IC values of 50 2.0 and 9.4 $\mu\text{g mL}^{-1}$, respectively²⁰.

6) Anti viral activity:

Chronic infection with the Hepatitis C Virus (HCV) is a major cause for developing cirrhosis and hepatocellular carcinoma. A series of novel compounds, 5-alkynyl-1-beta-D-ribofuranosylimidazole-4-carboxamides have been synthesized and identified as broad-spectrum antiviral agents. 5-Ethynyl-1-beta-D-ribofuranosylimidazole-4-carboxamide (EICAR) (Figure-15), the most potent congener of the group, showed antiviral potency about 10- to 100- fold superior than that of ribavirin, (Figure-16). EICAR is an 12 antiviral drug for the treatment of pox-

Figure-15

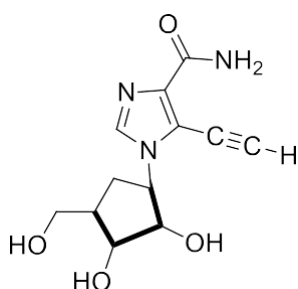
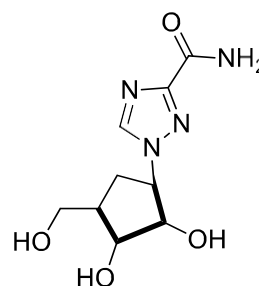


Figure-16



toga-, arena-, reo-, orthomyxo and paramyxovirus infections.

CONCLUSION:

The present review study showed that imidazole derivatives signify an interesting class of compounds possessing a wide spectrum of biological activities. On the basis of various literature survey imidazole derivatives show various activity against antimicrobial, anti-inflammatory, analgesic, antitubercular, anticancer, Antileishmanial activity, antiviral, etc. The possible improvements in the activity can be further achieved by slight modifications in the substituents on the basic imidazole nucleus. Having structural similarity with histidine imidazole compound can bind with protein molecules with ease compared to the some other heterocyclic moieties. Thus imidazole offers better pharmacodynamic characteristics. Furthermore, some imidazole drugs, at high concentrations, could exert direct inhibitory effects on membranes, without interference with sterols and sterol esters. Various recent new drugs developments in imidazole derivatives show better effect and less toxicity. Series of compounds can be synthesized by using same approach and further characterized and evaluated for desire pharmacological activity with high potency and low toxicity. Moreover the possible improvements in the activity can be achieved by slight modifications in the substituent on the imidazole nucleus. This has been noticed so far, that modifications on imidazole moiety displayed important biological activities. It will be exciting to observe that these modifications can be utilized as potent therapeutic agents in future.

References:

- 1) Siwach A. and Verma P. K., *Siwach and Verma BMC Chemistry*, 2021, 15:12.
- 2) Bathula C., MK R., Kumar A. K., Hemraj Yadav H., Sivalingam R., Shinde S., Shrestha N. K, Mahadevan K.M., Reddy V., Mohammedi A., *J. Mater Res. Technol.* 2020, 9(3):6900–6908.
- 3) Burungale S.D. and. Bhitre M. J, Burungale and Bhitre, *IJPSR*, 2013; Vol. 4(10): 4051-4057.
- 4) Altundag F.D., Saglik B.N, Cevik U.A., Isikdag I., Ozkay Y. & Gencer H.K., *Phosphorus, Sulfur, And Silicon And The Related Elements*, 2019,194,9,887-894.
- 5) Zhang, M., Ding, Y., Qin, HX. *et al. Mol Divers*, 2020, 24, 1177–1184.
- 6) Kumar P., Kapoor B., Gupta R., Gupta M., *Think India Journal*, 2019, 22,37.
- 7) Reddy R.B., Malleswari K, Sreenivasulu G., Naga Sai G., Rakesh J., *IJRAR O*, 2022,9, 4.
- 8) Anushul C, Ashu S and Anil K S., *Der pharma chemica*, , 2012, 4, 116-140.
- 9) Bhatnagar A, Sharma P. K, Kumar N, *International Journal of Pharma TechResearch*, 2011, 3, 268-282.
- 10) Deepak C., Janmajoy B., Niraj S., Nomi S., *World journal of pharmaceuticalsciences*, 3, 2015, 1668-1681.
- 11) Purnima M, Wakode S. R., Avneet K., *International journal of pharmaceuticalscience and research*, 2016, 1, 12-16.
- 12) Renjima K.M, Resmy M., Divya C., *Int. J. Pharm. Sci. Rev. Res.*, 2020 ,62(1), 15,88-93.
- 13) Kumari S., Sharma P.K., Kumar N., *Der Chemica Sinica*, 2010, 1 (3): 36-47.

Synthesis and Characterization of 2-Amino-5 (Substituted Phenyl) 1,3,4-Thiadiazole Based Imines and Their Study

M. B. Zade¹, S. N. Ibatte*², J. A. Angulwar²

¹Department of Chemistry, Azad Mahavidyalaya, Ausa, Dist-Latur-413520, Maharashtra, India

²Department of Chemistry, Dayanand Science College, Latur- 413512, Maharashtra, India

ABSTRACT

2-amino-5(substituted phenyl)1,3,4- thiadiazole is a heterocyclic nucleus plays important role in coordination chemistry. Using this nucleus the novel ligands 3-sub.benzylidene-4(5-sub.aryl-[1, 3, 4] thiadiazole-2-ylimino) pentan-2-one were synthesized by knoevenagel condensation. The derived heterocyclic nucleus condensed with substituted aromatic/heterocyclic aldehyde and acetoacetone. Synthesized ligands were characterized by 1H NMR, IR and Mass spectroscopy.

Keywords: Thiadiazole, Ligand, Synthesis, Characterization.

I. INTRODUCTION

The imines containing substituted 2-amino-5(substituted phenyl)1,3,4- thiadiazole moiety have wide range of applications such as anticonvulsant activity¹⁻², anticancer agents³, antifungal and antibacterial⁴ activity screened by various researchers. Imines of heterocyclic ligands have vital role in coordination chemistry due to presence of one or more hetero atoms in it. The ligands of substituted 1,3,4-thiadiazole have potential sites for metal complexation. Wide range of imines based on 1,3,4-thiadiazole were synthesized by extending with some active organic molecules and synthesized their metal complexes with transition metals as well as with rare earth metals.

With this interest study of new imines synthesis is carryout. The novel imines were synthesized by condensation of functionalized aromatic and heterocyclic aldehydes, acetoacetone and substituted 1,3,4-thiadiazole. Synthesized ligands were screened by electron absorption spectroscopy for elucidation of structures.

II. EXPERIMENTAL

The commercially purchased all reagents and solvents of analytical grade were used without any purification. 2-amino-5(substituted phenyl)1,3,4- thiadiazole was prepared⁵⁻⁷ in laboratory by alkanoylation of thiosemicarbazide followed by dehydration. The reaction progress was screened by thin layer chromatography (TLC). Molecular structure of derived moiety is as shown in figure 1.

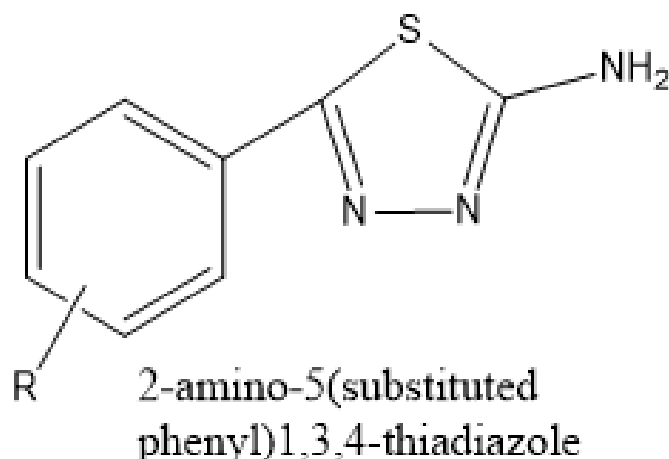


Figure 1 Preparation of novel Schiff base 3-sub. benzylidene-4(5-sub. aryl- [1, 3, 4] thiadiazole-2-ylimino) pentan-2-one:

A round bottom flask charged with substituted aromatic aldehyde, acetoacetone (10mmol) each and along with 10 mole % solid supported Morpholine in methanol (20ml) are refluxed at 70 °C by for 3 hours. The progress of reaction was monitored by using pet ether and ethyl acetate system (7:3 v/v). After that 2-amino-5-(substituted aryl) thiadiazole (10mmol) added and continued refluxing for 1 hour. The progress of reaction was monitored by benzene, acetone system (7:3 v/v). The reaction mixture was poured on flaks of ice. The obtained solid yellow precipitate of expected ligand was filtered, dried and recrystallized in methanol.

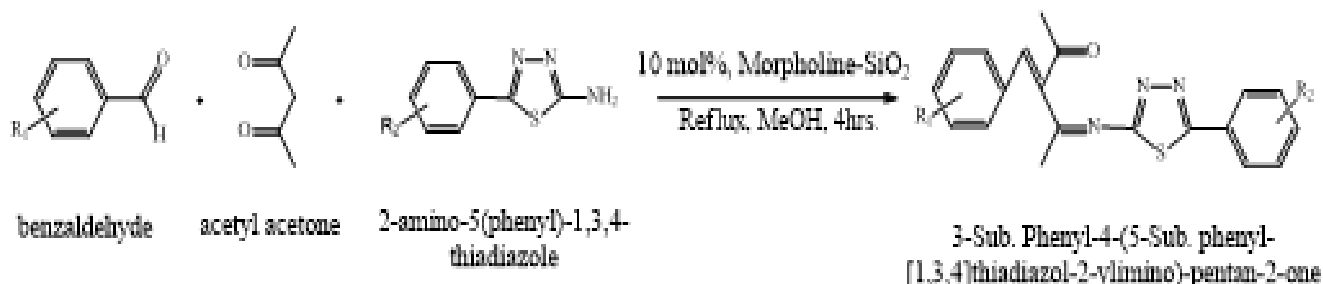


Figure-2

Obtained ligands were characterized by various analytical techniques. The melting point was recorded on Cotech digital melting point apparatus. Elemental C, H, N, and S analysis was carried out on a Fison EA1108 analyzer. The Infrared (FTIR) spectra were recorded by using FITR 8300 shimadzu spectrometer by using CsI disk in the frequency range of 4000 to 400cm⁻¹. The ¹H NMR spectra were recorded on Brunner 400 MHz spectrometer using CDCl₃ as a solvent and TMS as internal standard. Mass spectra were recorded by mass wiff (turbo spray) spectrometer.

III. RESULT AND DISCUSSION

For purity and structural elucidation synthesized ligand were screened by physical and electron absorption techniques. Synthesized ligands and their physical characterizations are shown in Table-1.

Table-1 Melting Points, Elemental Analytical data (%) and m/z values of ligands.

Compounds	Symbol	Physical appearance	M.P. (°C)	Elements (%)					m/z
				C	H	N	O	S	
C ₁₉ H ₁₇ N ₃ O ₂ S	L ₁	Yellow	107	63.70	5.05	12.38	9.43	9.45	351
C ₂₁ H ₁₈ N ₃ OSF	L ₂	Yellow	145	65.37	4.94	11.44	4.35	8.73	379
C ₂₂ H ₂₁ N ₃ O ₂ S	L ₃	Buff	136	66.47	5.58	11.07	8.43	8.45	391
C ₂₁ H ₁₈ N ₄ O ₃ S	L ₄	Yellow	138	60.90	4.60	14.20	12.17	8.13	406
C ₂₁ H ₁₉ N ₃ O ₂ S	L ₅	Yellow	132	66.20	5.29	11.02	12.59	8.41	381
C ₂₁ H ₁₈ N ₃ OSCl	L ₆	Yellow	142	63.85	4.85	10.63	8.10	8.11	395
C ₂₂ H ₂₁ N ₃ OS	L ₇	Buff	139	70.46	5.91	11.20	8.53	8.55	375
C ₂₂ H ₂₁ N ₃ O ₃ S	L ₈	Buff	144	64.92	5.45	10.32	15.72	7.88	407

The infrared spectrum data used to assign the formation of imines. The stretching bands obtained at 1693-1708 assigned characteristic¹¹ of $\nu(\text{C}=\text{O})$ and at 1606-1660 for $\nu(\text{C}=\text{N})$ for L₁-L₈. (Table-2)

The ¹H NMR spectra of ligands L₁-L₈ gave additional information of imine formation. Spectra of L₁ shown in figure-3, sharp peaks obtained are similar to the literature data. ¹H NMR (400 M Hz, CDCl₃) δ 1.79 (S, 3H, N=C-CH₃), 2.10 (S, 3H, O=C-CH₃), 5.30 (S, 1H, HC=C), 2.41 (S, 3H, Ar-CH₃), 6.20-7.80 (M, 8H, Ar-H).

TABLE-2 KEY INFRARED DATA OF LIGANDS

Compounds	Frequency (cm ⁻¹)			
	$\nu(\text{C}=\text{O})$	$\nu(\text{C}=\text{N})$	$\nu(\text{C}-\text{S}-\text{C})$	$\nu(\text{N}-\text{N})$
C ₁₉ H ₁₇ N ₃ O ₂ S	1708	1633	634	1020
C ₂₁ H ₁₈ N ₃ OSF	1693	1620	632	1018
C ₂₂ H ₂₁ N ₃ O ₂ S	1693	1606	634	1031
C ₂₁ H ₁₈ N ₄ O ₃ S	1726	1662	603	1012
C ₂₁ H ₁₉ N ₃ O ₂ S	1704	1635	634	1062
C ₂₁ H ₁₈ N ₃ OSCl	1707	1660	632	1012
C ₂₂ H ₂₁ N ₃ OS	1707	1656	634	1022
C ₂₂ H ₂₁ N ₃ O ₃ S	1691	1633	634	1033

A1

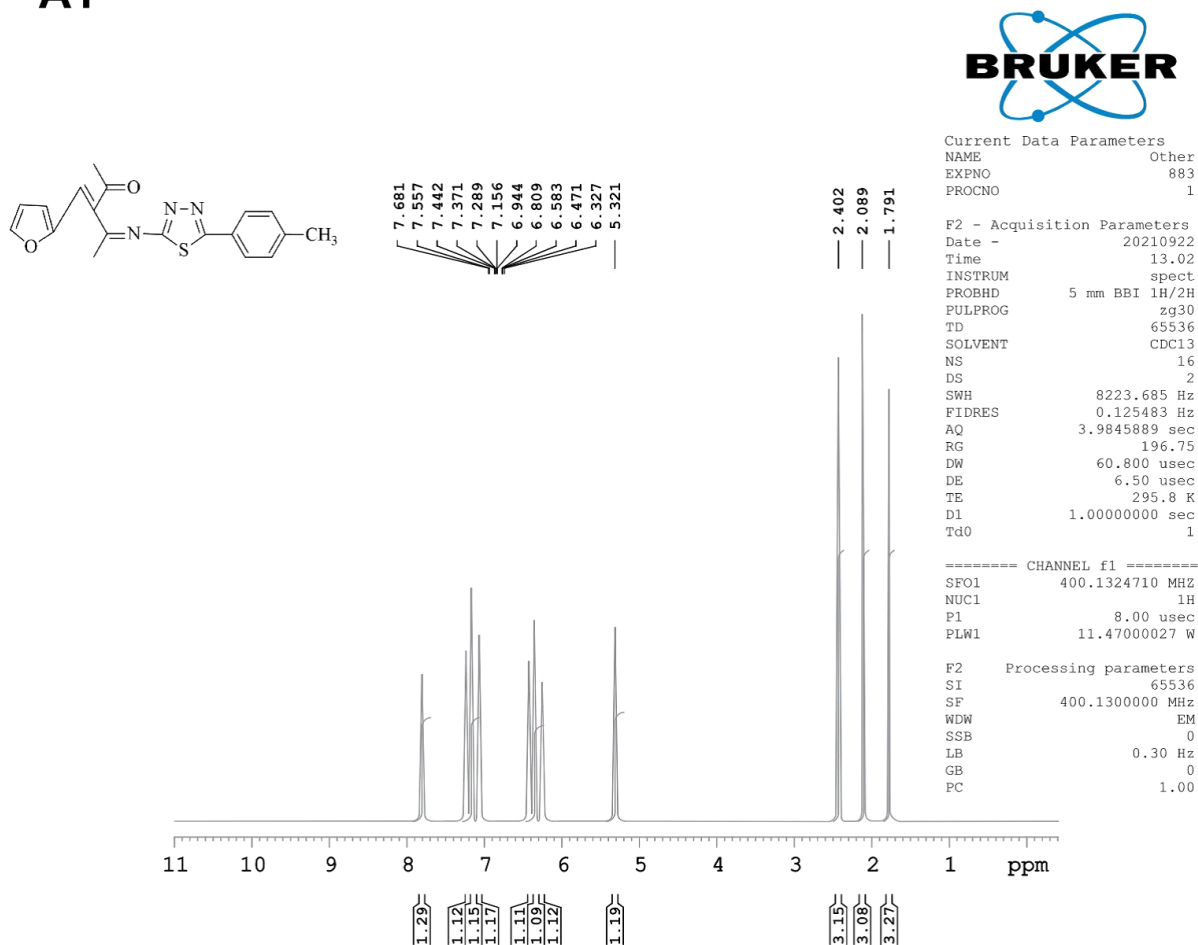


Figure-3

Synthesized ligands also screened by mass spectroscopic analysis. Mass spectra reveals confirmation of molecular structure. For ligand Li m/z is 351, spectra obtained at same mass is shown in figure-4. Furthermore spectra obtained of loss in mass with respect to temperature.

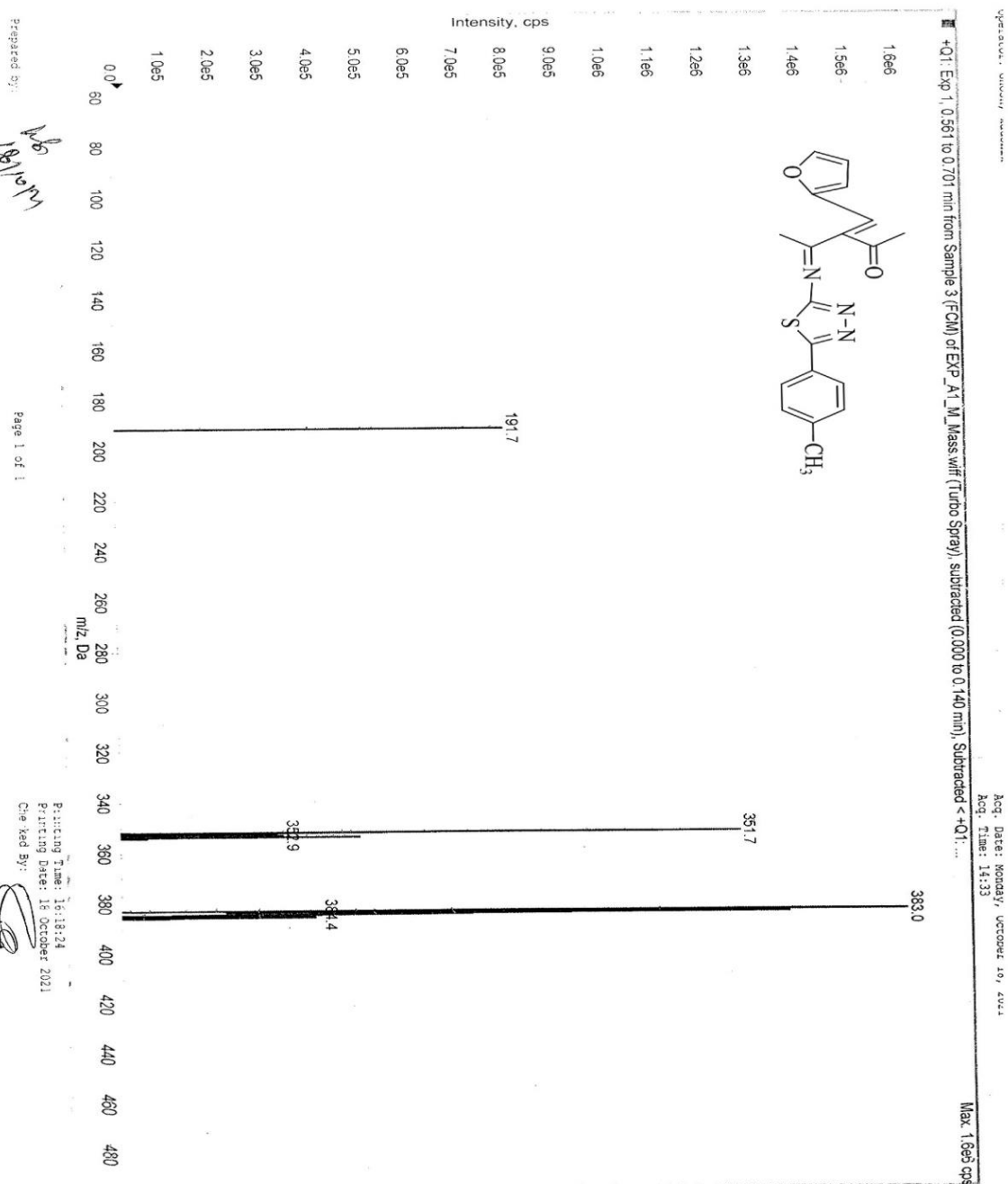


Figure-4

IV. CONCLUSION

All synthesized ligands matches with their physical and electron absorption spectroscopic data. L₁-L₈ tridentate ligands are confirmed on their analytical data. Synthesized ligands were three coordinated, analyzed by various analytical techniques.

V. REFERENCES

- [1]. Kikkeri P., Kikkeri N. Mohana and Lingappa Mallesha, *organic Chemistry International*, 1-8 (2013).
- [2]. Christopher B. Chapleo, and et. al., *J. Med. Chem.*, 29, 2273-2280(1986).
- [3]. Choubey et.al. *J. Adv. Sci, Res.*, 12(4), 154-164(2021).
- [4]. Yip Foo Win, Emad Yousif, Sie Tion Ha and Ahemed Majeed, *Asian j. Chem.*, 8, 25 (2013).
- [5]. Omprakash Sharma, Pankaj Sharma et. al. *Asian Pac. J. Health Sci.*,5(3), 325-330(2018)
- [6]. Tatiana S. Kokovina, Svyatoslav Y. Gadmsky, Alexei A. Terentiev and Nataliya A. Sanina, *Molecules*, 26, 3-6(2021).
- [7]. Bhawna Sharma, Anita Varma, Sunil Prajapati and Upendra Kumar Sharma, *Int. J. Medc. Chem.*,1-6(2013).
- [8]. Yip Foo Win, Emad Yousif, Sie Tion Ha and Ahemed Majeed, *Asian j. Chem.*, 8, 25 (2013).
- [9]. Sharma M.C., Shahu N. K., and Kohli D. V. j. *Nanomater Biostruct.*, 4, 361-367 (2009).
- [10]. Maliyappa M. Rangappa, Jathi Keshavayya, Panchanga Murali Krishna and K. Rajesh, *Inorg .Chem.Commun.*, 127(2021).
- [11]. Natrajan Raman and Narayanaperumal Pravin, *Europ. J. Medici. Chem.*, 80, 57-70 (2014).
- [12]. Davood Habibi, Mahmoud Nasrollahzadeh, Hesam Sahebekhtiari and Richard Vernon Parish, *Tetrahedron*, 69, 3082-3087 (2013).
- [13]. Manju, P. Joshi and D. Kumar, *Russ. J. Coordi. Chem.*, 40, 445-459 (2014).
- [14]. Qin Zhang, Jian Bin Zhang, Ling-Hua Cao, Yang-Ping Li and Duo-Zhi Wang, *J. Chines Chemic. Soci.*, 57, 992-997 (2010).
- [15]. J. Joseph, A. Suman and Nisha Balkrishnan, *Appli.Organometalic Chem.*, 1-9(2016).
- [16]. V. Nirai Mathi, A. Jerad Suresh and S. Chitra Bala, *Int. J. Pharmacy & Pharmace.Sci.*, 4, 651- 654(2012).
- [17]. Reshma Satyanarayana and Boja Poojary, *J.Chin. Chem.Soci.*, 1-19(2020).
- [18]. Clark J. H. and Macquarrie D. *J. Chem. Soc. Rev.*, 303(1996).
- [19]. Emam, E. A. *ARPNJ. Sci. Technol.*, 3, 356 (2013).
- [20]. Corma, A. *Chem. Rev.*,95, 559(1995).

Formulation and Evaluation of Nanosponge Based Topical Gel Preparation by QbD Approach

Dr. Padmaja Giram^{*1}, Dr. Nalwar Yogesh S.^{*2}, Omprakash G. Bhusnure³, Dr. Sachin B. Gholve³, Alok A. Kadam³, Sachin kabade³

¹Department of Pharmacology, Channabasweshwar Pharmacy College (Degree), Latur-413 512, Maharashtra, India

²Department of Chemistry, Toshniwal Arts, Commerce & Science College Tq. Sengaon Dist. Hingoli, 431542, Maharashtra, India

³Department of Pharmaceutical Quality Assurance, Channabasweshwar Pharmacy College (Degree), Latur-413 512, Maharashtra, India

ABSTRACT

Nanosponge is a modern category of material and is made up of tiny particles with a narrow cavity of few nanometers. These narrow cavities can be filled with various types of substances. These tiny particles are having a capability due to which it is able to carry both hydrophilic and lipophilic drug substance and can increase the stability of poorly water-soluble drug substance or molecules. Boswelliaserrata loaded nanosponges was developed and optimized using systematic Quality by Design approach. Firstly, the quality target product profile (QTPP) of nanosponge formulation was defined and critical quality attributes (CQAs) and critical material attributes (CMAs) were screened through risk assessment studies based on fish bone diagram. 32 full factorial Box-Behnken design using Design Expert software (version 9.0) was employed to optimize the selected CMAs. Concentration of polymer (X1), Stirring Speed (X2) and Stirring time (X3) were selected as independent CMAs. Particle size (Y1), entrapment efficiency (Y2), % Practical yield (Y3) was evaluated as dependant CQAs. Optimized formulation was then evaluated for FTIR, DSC, XRD, Particle size analysis, Zeta potential, SEM. Formulation was also found stable at different storage condition.

Keywords: Boswelliaserrata, nanosponge, colloidal carrier, Box-Behnken design. Materials and Methods

I. INTRODUCTION

1.1 Rheumatoid Arthritis

Rheumatoid arthritis (RA) is a disease of unknown origin characterized by inflammatory changes of the synovial tissue of joints, cartilage, and bone and, less frequently, extra-articular sites. In recent years, it has become evident that RA arises based on genetic and epigenetic components. The environment must also play an important role, such as cigarette smoke, dust exposure, and especially the microbiome that also represents an internal environment (Brown et al., 2020). Rheumatoid arthritis (RA) is a chronic polyarticular inflammatory arthritis that involves not only small joints of the hands and feet but also medium and large

joints. It is associated with excessive disability, mortality, and morbidity. RA is a complex inflammatory and autoimmune disease with systemic involvement and symptoms (Smolen et al., 2018).

The innate immune system and components of the adaptive immune system interact significantly. Autoantibodies, including rheumatoid factors (RF) and antibodies against post-translationally modified proteins (AMPA, which includes antibodies against various modifications including citrullination (ACPA), carbamylation (aCarP), and acetylation (AAPA)), as well as the migration of T and B lymphocytes into the synovium, are a result of abnormalities in the cellular and humoral immune response. Additionally, the tissue sites affected suffer a strong activation of the innate immune system with highly activated monocyte/macrophage system cells (Derksen et al., 2017).

The histopathological and clinical characteristics of RA are the result of different phenomena: joint discomfort, swelling, and progressive breakdown of cartilage and bone are all signs of inflammation, as are systemic manifestations brought on by inflammatory cytokines and arachidonic acid metabolites. Synovial hyperplasia is a hallmark of RA and the main contributor to the formation of an invasive pannus. The observation of T cell accumulation in the synovium has generated the hypothesis of a T cell-dependent inflammatory reaction to an unknown antigen. (Otero & Goldring, 2007) This assumption is supported by data derived from animal models, observations about disease remission in patients with AIDS, and the improvement after treatment with co-stimulation modulators. In RA, the synovial lining generally comprises 1–3 cell layers and becomes remarkably thickened. This is due to an invasion of macrophage-like cells and the proliferation of resident synovial fibroblasts (figure no 1.1). The degree of synovial hyperplasia correlates with the severity of cartilage

List of Chemical

Boswellia Serrata extract, Ethylcellulose, Dichloromethane, PVA, Carbopol 934, Ethanol, Methyl Paraben, Propylene glycol, Triethanolamin, Distilled Water, Acetone, Phosphate buffer 7.4 pH

II. MATERIAL AND METHOD

Method of preparation of nanosponges:

i. Emulsion solvent diffusion method:

In this method, two phases are used in a different proportion of organic and aqueous (ethyl cellulose and poly vinyl alcohol). The dispersed phase has ethyl cellulose and drug gets dissolved in dichloromethane (20ml) and a definite amount of polyvinyl alcohol added to 100 ml of aqueous continuous phase. Then, the mixture is stirred properly at 1000 rpm for 2hr. The nanosponges were collected by the process of filtration by using Whatman filter paper (0.45 μm) and kept for drying in an oven at 40°C for 24hr. Nanosponges are dried and restored in desiccators and residual solvent removed.

ii. Preparation of *Boswellia Serrata* loaded nanosponge

Boswellia Serrata loaded nanosponges were prepared by emulsion solvent diffusion method figure no 6.3. Polyvinyl alcohol dissolved in distilled water at 80°C for 30 min is used as aqueous phase. The drug and polymer dissolved in dichloromethane (cross-linking agent) is used as organic phase. Organic phase is subjected to sonication for 10 min in order to increase the solubility of drug in polymer solution. The organic phase is slowly added to aqueous phase to avoid foaming by using fine syringe with a size range of 0.001. This was performed on a Remi magnetic stirrer at 1000 rpm for 3 hrs. The formed solid powder was collected by using membrane filter (pore size 0.45 µm) and dried in oven for 30 min at 40°C for the removal of residual solvent. The product was then packed and stored in airtight vials for characterization (Harsha et al., 2021)

Figure no.1: Emulsion solvent method of nanosponge

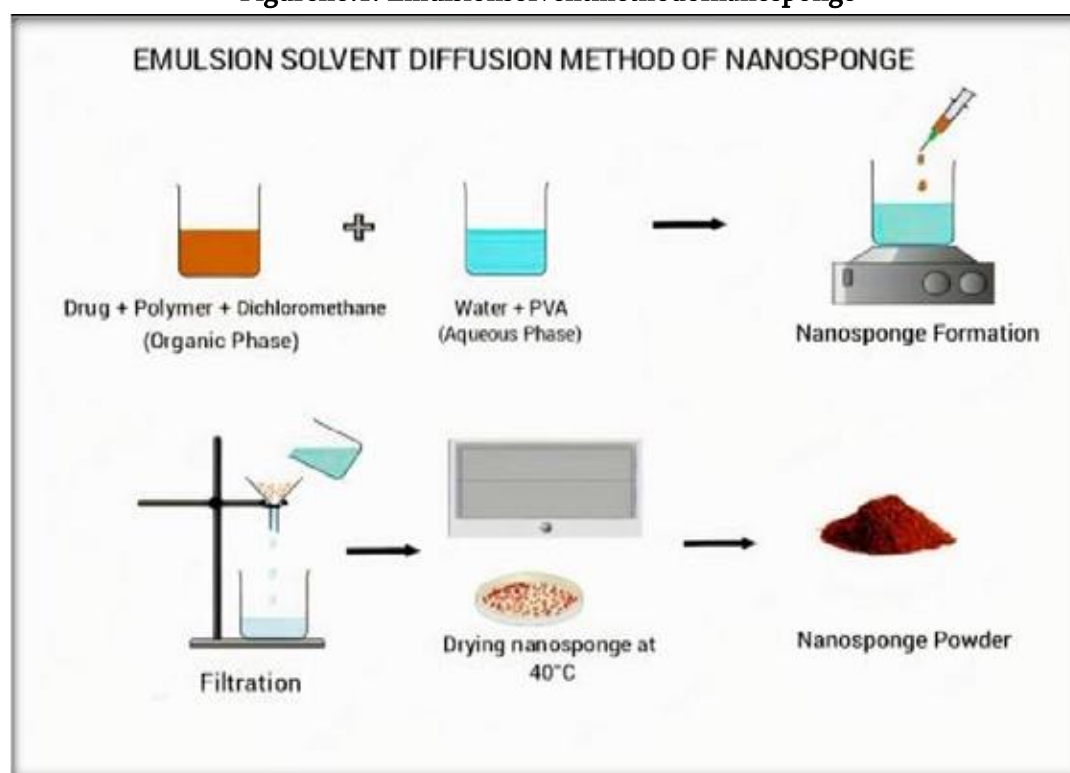


Table no.1.: Design Variables

Srno.	Independent Variables	Levels		
		Low (-1)	Medium(0)	High(+1)
1	Polymer(X1)	100	200	300
2	Stirring Speed RPM(X2)	800	1000	1200
3	Stirring Time Hrs(X3)	1	2	3
Sr no.	Dependent variables	Goal		
1	Particle size(Y1)	Minimum		
2	% Entrapment efficiency(Y2)	Maximum		
3	% Practical yield(Y3)	Maximum		

Tableno.2.:NanospongeExperimentsbyBox-BehnkenDesign

Stdrun	Sr.no	Polymer(X1)(mg)	Stirring rate RPM(X2)	Stirringtime(Hrs) (X3)
8	1	300	1000	3
13	2	200	1000	2
14	3	200	1000	2
5	4	100	1000	1
16	5	200	1000	2

iii. Preformulation studies:**I. UltravioletVisible(UV-Visible)Spectroscopy-**

The standard solutions of Boswellia Serrata were separately scanned in 200 to 400 nm range using methanol as blank. Maximum absorbance wavelengths were determined. The overlay spectrum of drug was plotted which is shown in Figure no. Dilutions were prepared and their absorbance was recorded at obtained wavelength and calibration curve was plotted (Pushpalatha D et al., 2021).

II. Fourier Transform Infra-Red (FT-IR) spectroscopy-

Boswellia Serrata, Ethyl cellulose, drug and polymer FT-IR spectra were recorded over 4000 to 400 cm⁻¹ range by Perkin Elmer UATR (Mehta et al., 2016)

iv. Evaluation and Characterization of BSNS:**1. Entrapment Efficiency (%):**

10 mg from the prepared drug loaded nanospheres by emulsion solvent diffusion method using suitable polymer were suspended in 10 ml of methanol and were subjected for ultracentrifugation for 40 minutes. The percentage of incorporated Boswellia Serrata was determined spectrophotometrically at 249 nm. After centrifugation of the aqueous suspension, amount of free drug was detected in the supernatant and the amount of incorporated drug was determined as a result of the initial drug minus the free drug. The drug entrapment efficiency (EE) of Boswellia Serrata nanospheres was determined using the formula (Harsha et al., 2021; Pushpalatha D et al., 2021).

% Entrapment efficiency

= $\frac{\text{Total drug content} - \text{Drug weight in aqueous phase}}{\text{Total drug content}} \times 100$

Total drug content

2. Practical yield(%):

For calculating production yield, the theoretical mass was calculated initially by taking the mass of solid ingredients added. Prepared nanosponge formulation was accurately weighed and the weight was recorded. The production yield of the nanosponges was then determined using the following equation (Rodrigues et al., 2022)

Practical mass of nanosponges

$$\% \text{Practical Yield} = \frac{\text{Theoretical mass (polymer + drug)}}{\text{Practical mass of nanosponges}} \times 100$$

3. SEM studies:

Nanosponges can be easily visualized by scanning electron microscopy (SEM). SEM is a powerful microscope that uses electrons to form an image. It allows for imaging of samples at magnifications which cannot be achieved using traditional microscope. Typical SEM can reach magnifications of more than 30,000X; whereas modern light microscopes can achieve a magnification of ~1,000X. The resulting pictures it forms are in black and white as SEM doesn't use light to create images (Ghose et al., 2020).

4. Size distribution studies:

Particle size of the nanosponge can be determined by dynamic light scattering (DLS). It can be determined by measuring the random changes in the intensity of light which are scattered from a sample. Small particles in the sample undergo random thermal motion called Brownian motion. Light from the laser source illuminates the sample in the cell. The scattered light signal is collected with one of two detectors, either at a 90-degree (right angle) or 173-degree (back angle) scattering angle. The obtained optical signal shows random changes due to random changing position of the particles (Rodrigues et al., 2022).

5. Zeta potential:

Zeta potential of the formulation was measured by Zetasizer. Electrophoretic light scattering method was utilized for zeta potential measurement. A dip cell with a pair of parallel Pd electrodes was used to provide electrical trigger on charged particles. The signals were collected at 24.9 °C and the data were analyzed using Zetasizer Software (Rodrigues et al., 2022).

v. Evaluation of Nanosponge based gel

- Determination of pH:** The pH of Boswellia Serrata nanosponge loaded gel formulation was determined by using digital pH meter. One gram of gel was dispersed in 100ml of distilled water and stored for two hours at constant temperature. The measurement of pH was done in triplicate and average values were calculated (Patel et al., 2012).
- Drug content:** Boswellia Serrata content in nanosponge gel was measured by dissolving 1000mg of gel in 10ml solvent (methanol) by sonication. The solution was passed through the Whatman filter paper no. 42 and filtered. Absorbance was measured after suitable dilution at 249nm in UV - 1800 spectrophotometer (Deepa Gariya, Yamini Chandola, Ankita Negi et al., 2018; Patel et al., 2012).

3. **Homogeneity:** It was determined by visual inspection for the appearance of gel and presence of any aggregates.
4. **Spreadability:** By measuring the spreading diameter of 0.5g of gel between 20 x 20 cm glass plates after 1 min, spreadability of the formulated gel was determined. The mass of the upper plate was standardized at 500g (Deepa Gariya, Yamini Chandola, Ankita Negi et al., 2018).

$$S = m \times l / t$$

Where, S = Spreadability; m = weight applied to the upper glass slide; l = length of the glass slide; t = time taken in seconds.
5. **Determination of viscosity:** Viscosity of prepared gel was determined by Brookfield DV II viscometer which contains a piston electromagnetic sensor and thermometer that provides viscosity and temperature readings respectively. The Spin-dle no 6 used for viscosity measurement at 10 rpm the results were displayed on the screen of Brookfield DVII. Determination was done in triplicates and the average was calculated (Patel et al., 2012).
6. **In vitro drug diffusion studies:**
 Nanogels were permeated through an artificial cellophane membrane. 0.5 gm of nanogel was placed in the donor compartment. The receptor medium consists of pH 7.4 phosphate buffer. The temperature was maintained at 37 ± 0.5 °C to simulate the human skin condition during the experiment. 5 ml of sample was withdrawn at 0.5, 1, 2, 6, and 12 hrs and replaced with fresh receptor solution. Collected samples were spectrophotometrically analyzed at 249 nm. The drug release amount was calculated.
7. **Stability study**
 Optimized topical gel was assessed for stability test for 30 days by exposing the sample at room temperature (25 ± 2 °C) and accelerated condition (40 ± 2 °C, 75% RH) in Stability chamber, after 30 days stability of the gel is evaluated for drug content, pH, viscosity (Pate et al., 20

III. CONCLUSION

Ethylcellulose nanosponges were prepared and screened as a carrier for topical delivery of BS. Characteristics of prepared nanosponges were influenced by different independent variables such as polymer concentration, the stirring speed, and the stirring time. Merit of prepared nanosponge-based gel such as release retardation for a more extended period, lack of significant irritation, and greater compatibility could help to reduce the dosing frequency and might cause the formulation to occupy the market in nearby future. However, further clinical studies are warranted to establish the efficacy and safety of these formulations on *In vivo* animal study and on human skin.

A Facile and Expeditious Approach to Substituted 5-Arylpyrimido-Quinoline-Diones Catalyzed by Iodine

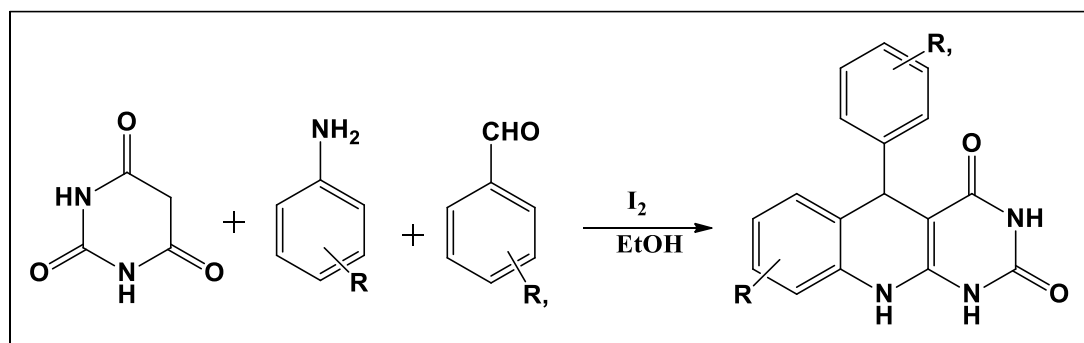
Yogesh S. Nalwar

Department of Chemistry, Toshniwal A.C.S. College, Sengaon-431542, Maharashtra, India

ABSTRACT

A facile and expeditious method for the synthesis of substituted 5-arylpyrimido-quinoline-diones using a three-component reaction involving substituted aldehydes, aromatic amines and barbituric acid catalyzed by as low as 10 mol % I₂ has been demonstrated. This synthetic system features simple operation and mild reaction conditions, and displays a broad functional group tolerance furnishing good to excellent yields.

Key words: Substituted aldehydes, aromatic amines, barbituric acid and Iodine catalysis 5-arylpyrimido-quinoline-diones.



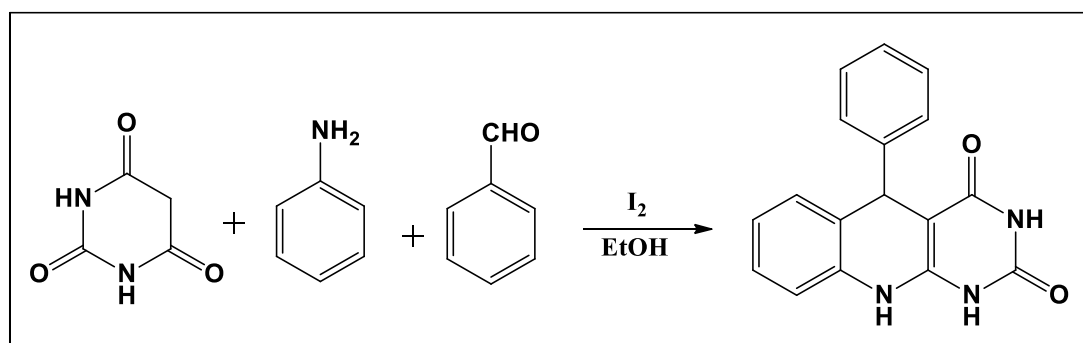
I. INTRODUCTION

Recent advances in the application of organocatalysts in organic reactions have provided a green approach for the efficient synthesis of a wide range of molecules.¹ Also, applications of organocatalysts in organic transformations due to their unique characteristics, has been enormously considered.² Utilizing organic catalysts instead of inorganic Lewis and protic acids have some advantages, including the possibility of application of acid-sensitive substrates in reactions and the fact that substrates bearing basic functional groups or electron-donating substituents that are prone to capture the acidic catalysts do not affect the reaction results.³ One of the most important classes of small molecule organocatalysts are amino acids, which are widely used as catalysts in organic reactions in recent years.⁴ Molecular iodine has shown considerable catalytic efficiency in different reactions.⁵ Molecular iodine, has also been used as a catalyst in different multicomponent reactions (MCRs), and the studies have shown that this catalyst efficiently promoted these protocols.⁶⁻⁸ In multicomponent approaches, complex products and biologically active molecules are synthesized from readily available starting materials in a single step process. From this point of view, MCRs

have emerged as green and powerful tools inorganic synthesis and drug discovery.^{9,10} Also, in MCRs, by selecting the different starting materials, a new class of compounds can be synthesized which may show interesting properties.¹¹ Organocatalyst-catalyzed MCRs and the use of environmentally benign solvents and reagents are particularly attractive, because they incorporate many of the green chemistry principles. Quinoline derivatives are common in nature, and many of the derivatives exhibit various biological activities, such as antimalarial, antitumor, anthelmintic, antibacterial, antiasthmatic, and antiplatelet.¹² Due to these useful pharmacophoric properties, they have been extensively studied.¹³ In the view point of synthetic chemistry, MCRs are known as an important strategy to extend the structural diversity of quinolines.¹⁴ In this regard, the development of new multicomponent protocols for the synthesis of new quinoline-incorporating heterocycles have attracted considerable interest in recent years.¹⁵ Moreover, pyrimido[4,5-b]quinoline derivatives are of great interest because of their biological activities, including antimalarial effects, antibacterial properties, analgesic and antitumor activities.¹⁶ They are also attractive for the synthesis of electroluminescent materials, because they exhibit high fluorescence activity.¹⁷ It is noteworthy that, pyrimido[4,5-b]quinolines can be synthesized using MCRs from a pyrimidine starting material.¹⁸ Researchers have shown that azapodophyllotoxins, as dihydropyrimidine analogues of pyrimido[4,5-b]quinolines, exert antitumor activities by inhibition of DNA topoisomerase II enzyme. This category of compounds have for the first time been synthesized by Takeya et al. in a three step process.¹⁹ In the subsequent studies, this class of compounds has been synthesized using a MCR between aldehydes, anilines, and tetronic acid.^{7,8,20} Aknin et al. have used barbituric acid instead of tetronic acid to synthesis 5-arylpyrimido[4,5-b]quinoline-2,4-(1H,3H)-dione derivatives.²¹ However, this method is much less efficient for the synthesis of 5-arylpyrimido[4,5-b]quinoline-2,4-(1H,3H,5H,10H)-dione derivatives. In the current study, we would like to report a green and efficient combinatorial approach for one-pot and regioselective synthesis of 5-arylpyrimido[4,5-b]quinoline-2,4-(1H,3H,5H,10H)-diones using the reaction of anilines, aldehydes and barbituric acids. This MCR was accomplished in refluxing in the presence of iodine.

II. PRESENT WORK

There are several improved protocols for substituted 5-arylpyrimido-quinoline-diones reaction, including transition metal Lewis acid catalysis, solid phase synthesis and activation with certain additives, ionic liquids, heterogeneous catalysis, microwave irradiation and grinding techniques. All of the above improved procedures for the three component substituted 5-arylpyrimido-quinoline-diones reaction *mainly* utilize barbituric acid as one of the substrate. The literature survey has revealed that there is a limited number of substituted 5-arylpyrimido-quinoline-diones reaction variations, which utilizes barbituric acid to afford substituted 5-arylpyrimido-quinoline-diones fused heterocycles. Owing to the importance of fused pyrimidine ring in natural products and drug chemistry, herein we wish to report one-pot three component condensation of barbituric acid, aldehyde and aromatic anilines using *iodine* as an efficient catalyst. (Scheme 1).



(Scheme-1)

III. RESULTS AND DISCUSSION

Synthesis of 5-aryl-pyrimido[4,5-b]quinoline-diones

To obtain optimised conditions for the designed protocol based on the reaction of aniline, benzaldehyde, and barbituric acid as model substrates, we checked different catalysts, solvents and temperatures and the results of this study are depicted in Table 1.

It was found that when the reaction was carried out in the absence of catalyst, no product was observed, even after 24 h (Table 1, entry 1). To obtain the desired product, we tested the reaction using different Brønsted and Lewis acids (Table 1, entries 2 & 3). As shown in Table 1, the use of these catalysts led to no desired product being obtained, even after 24 h. Thus, iodine as the best catalyst was tested for this reaction. In the presence of 10 mol% of iodine, product was isolated in 85% yield after only 4h. Performing the reaction in the presence of iodine at r.t. resulted in the production of product in lower yield (Table 1, entry 10).

Table 1 Optimization of the three-component coupling reaction between benzaldehyde, anilines, and barbituric acids

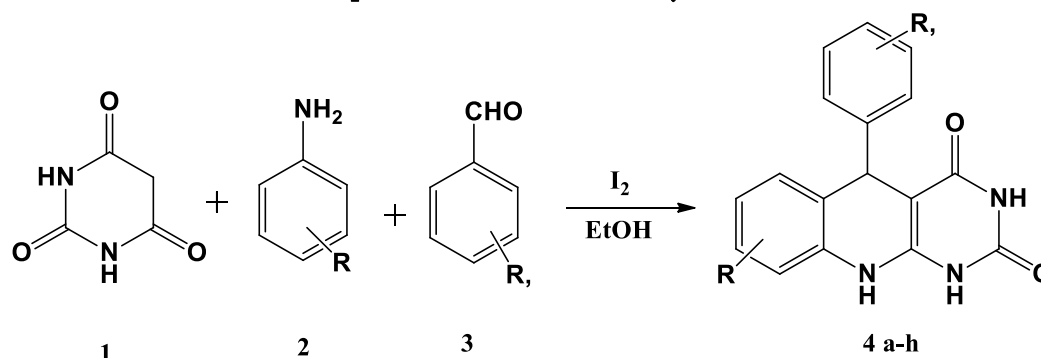
Entry	Catalyst (mol %)	solvent	Temp (°C)	Time (h)	Yield of product (%)
1	-----	EtOH	Reflux	24	0
2	CF ₃ COOH	EtOH	Reflux	24	0
3	PTSA	EtOH	Reflux	24	0
4	β-Cyclodextrin	H ₂ O	Reflux	24	0
5	Iodine (20)	EtOH	Reflux	4	86
6	Iodine (15)	EtOH	Reflux	4	86
7	Iodine (10)	EtOH	Reflux	4	85
8	Iodine (10)	CH ₂ Cl ₂	Reflux	8	57
9	Iodine (10)	CH ₃ CN	Reflux	7	59
10	Iodine (10)	EtOH	r.t.	9	55
11	Iodine (5)	EtOH	Reflux	5	82

Subsequently, the effect of solvent was examined and MeOH, CH₂Cl₂ and CH₃CN showed no superiority to EtOH as solvents. We also investigated the amount of iodine required for this reaction and it was observed that with decreasing the amount of catalyst, the yield decreased. It observed that further decrease of the catalyst loading to 5 mol% has no obvious influence on the reaction yield (Table 1, entry 11). Thus, 10 mol% of iodine is sufficient to catalyze this reaction. Under the optimized reaction conditions a series of 5-arylpyrimido[4,5-b]quinoline-2,4(1H,3H,5H,10H)-dione derivatives were synthesized and the results are summarized in Table 2.

As is clearly shown in Table 2, this multicomponent approach can be used for both aromatic aldehydes with electron-withdrawing and electron-donating groups. Similarly, heterocyclic aldehydes can be applied under optimized conditions. Furthermore, a wide range of aromatic amines were used successfully in this reaction with excellent results.

Accordingly, we have been able to prepare a library of 5-arylpyrimido[4,5-b]quinoline-2,4(1H,3H,5H,10H)-diones using barbituric acids, aromatic aldehydes, and anilines under green conditions. In this protocol, the products were separated from the reaction mixture by simple filtration, as they are not soluble in ethanol. Consequently, after completion of the reactions, by simple filtration and washing with water and ethanol, the pure products can be obtained

Table 2 The products of the three-component reactions of anilines, aldehydes and barbituric acids in the presence of iodine as catalyst.



Entry	Product	R	R ₁	Reaction Time (min)	Yield ^a (%)
1	4a	H	C ₆ H ₅	4	85
2	4b	H	4-CH ₃ O-C ₆ H ₄	5	84
3	4c	H	4-Cl-C ₆ H ₄	4	79
4	4d	H	3-NO ₂ -C ₆ H ₄	4	81
5	4e	CH ₃	C ₆ H ₅	4	83
6	4f	CH ₃	4-CH ₃ O-C ₆ H ₄	5	83
7	4g	CH ₃	4-Cl-C ₆ H ₄	4	82
8	4h	CH ₃	3-NO ₂ -C ₆ H ₄	5	85

IV. CONCLUSIONS

In summary, we have developed a convenient, green and efficient procedure for the regioselective synthesis of 5-aryl-pyrimido[4,5-b]quinoline-dione derivatives using the three-component coupling reaction of aromatic amines, aldehydes, and barbituric acids. A variety of these compounds were produced in a single step by use of different starting materials with good to excellent yields. Therefore, a new category of biologically active compounds for applications in medicinal chemistry were synthesized. While iodine, as an environmentally friendly catalyst, can efficiently catalyze these MCRs in aqueous media.

V. EXPERIMENTAL SECTION

Chemicals were purchased from Merck and Aldrich chemical companies. All the chemicals and solvents were used as received without purification. Melting points were determined in open capillary tubes in Barnstead Electrothermal 9100 BZ circulating oil melting point apparatus. The reaction monitoring was accomplished by TLC on silica gel PolyGram SILG/UV254 plates.

General procedure for the synthesis of 5-aryl-pyrimido[4,5-b]-quinoline-dione derivatives

In a conical flask (10 mL), a mixture of aromatic amine compound (1 mmol), barbituric acid (1 mmol), aldehyde (1 mmol), and Iodine (10 mol%) in refluxing EtOH (10 mL) was stirred for the time indicated in Table-2. After completion of the reaction, as confirmed by TLC, the reaction mixture was cooled to r.t. The precipitate was collected by filtration and washed with H₂O (10 mL) and EtOH (5 mL) to afford the pure product (Table 2).

VI. REFERENCES

- [1]. E. M. McGarrigle, E. L. Myers, O. Illa, M. A. Shaw, S. L. Riches and V. K. Aggarwal, *Chem. Rev.*, 2007, 107, 5841; M. Bartók, *Chem. Rev.*, 2010, 110, 1663; H. Huang, K. Zhu, W. Wu, Z. Jin and J. Ye, *Chem. Commun.*, 2012, 48, 461; H. S. Rho, S. H. Oh, J. W. Lee, J. Y. Lee, J. Chin and C. E. Song, *Chem. Commun.*, 2008, 1208; N. Tada, K. Hattori, T. Nobuta, T. Miura and A. Itoh, *Green Chem.*, 2011, 13, 1669.
- [2]. S. L. Jain, A. Modak and A. Bhaumik, *Green Chem.*, 2011, 13, 586; X. Liu, L. Lin and X. Feng, *Acc. Chem. Res.*, 2011, 44, 574; Y. Wei and M. Shi, *Acc. Chem. Res.*, 2010, 43, 1005; N. Takano and Y. Kohari, *Chem. Commun.*, 2010, 46, 4827; F. M. Gautier, S. Jones and S. J. Martin, *Org. Biomol. Chem.*, 2009, 7, 229; Y. Wei, G. N. Sastry and H. Zipse, *J. Am. Chem. Soc.*, 2008, 130, 3473.
- [3]. A. Khalafi-Nezhad, A. Parhami, A. Zare, A. R. MoosaviZare, A. Hasaninejad and F. Panahi, *Synthesis*, 2008, 617; A. J. Pearson and S. Panda, *Org. Lett.*, 2011, 13, 5548; T. K. Sen, S. C. Sau, A. Mukherjee, A. Modak, S. K. Mandal and D. Koley, *Chem. Commun.*, 2011, 47, 1172; D. Kühbeck, G. Saidulu, K. R. Reddy and D. D. Díaz, *Green Chem.*, 2012, 14, 378.
- [4]. D. Ma and Q. Cai, *Acc. Chem. Res.*, 2008, 41, 1450; J. E. Imbriglio, M. M. Vasbinder and S. J. Miller, *Org. Lett.*, 2003, 5, 3741; D. B. Ramachary and C. F. Barbas III, *Org. Lett.*, 2005, 7, 1577; H. Yang and M. W. Wong, *J. Org. Chem.*, 2011, 76, 7399; A. Córdova, H. Sundén, M. Engqvist, I. Ibrahim and J. Casas, *J. Am.*

- Chem. Soc., 2004, 126, 8914; A. Córdova, W. Zou, I. Ibrahim, E. Reyes, M. Engqvist and W.-W. Liao, Chem. Commun., 2005, 3586; D. B. Ramachary and M. Kishor, Org. Biomol. Chem., 2008, 6, 4176; P. Li and H. Yamamoto, Chem. Commun., 2009, 5412.
- [5]. N. Kumaragurubaran, K. Juhl, W. Zhuang, A. Bøgevig and K. A. Jørgensen, J. Am. Chem. Soc., 2002, 124, 6254; S. Chandrasekhar, C. Narsihmulu, N. R. Reddy and S. S. Sultana, Chem. Commun., 2004, 2450; H. Liu, L. Peng, T. Zhang and Y. Li, New J. Chem., 2003, 27, 1159; N. N. Karade, S. V. Gampawar, V. S. Shinde and W. N. Jadhav, Chin. J. Chem., 2007, 25, 1686; A. S. Lee, K.-W. Tsao, Y.-T. Chang and S.-F. Chu, Tetrahedron Lett., 2007, 48, 6790; G. Chen, Y. Wang, H. He, S. Gao, X. Yang and X. Hao, Heterocycles, 2006, 68, 2327; D. Kundu, A. Majee and A. Hajra, Chin. J. Chem., 2008, 26, 1545; N. S. Chowdari, D. B. Ramachary and C. F. Barbas III, Synlett, 2003, 1906; M. S. Rasalkar, M. K. Potdar, S. S. Mohile and M. M. Salunkhe, J. Mol. Catal. A: Chem., 2005, 235, 267; H. Ikishima, Y. Sekiguchi, Y. Ichikawa and H. Kotsuki, Tetrahedron Lett., 2006, 62, 311; A. Paraskar and A. Sudali, Tetrahedron, 2006, 62, 5756.
- [6]. A. Kumar, M. K. Gupta and M. Kumar, Green Chem., 2012, 14, 290; H. Jiang, R. Mai, H. Cao, Q. Zhu and X. Liu, Org. Biomol. Chem., 2009, 7, 4943; S. M. Rajesh, B. D. Bala, S. Perumal and J. C. Menéndez, Green Chem., 2011, 13, 3248; S. Guo and Y. Yuan, Chin. J. Chem., 2010, 28, 818; J. Pandey, N. Anand and R. P. Tripathi, Tetrahedron, 2009, 65, 9350; C. Mukhopadhyay, P. K. Tapaswi and R. J. Butcher, Tetrahedron Lett., 2010, 51, 1797; S.-B. Guo, S.-X. Wang and J.-T. Li, Synth. Commun., 2007, 37, 2111.
- [7]. C. Shi, J. Wang, H. Chen and D. Shi, J. Comb. Chem., 2010, 12, 430.
- [8]. Y. Li, H. Chen, C. Shi, D. Shi and S. Ji, J. Comb. Chem., 2010, 12, 231.
- [9]. M. Gonzalez-Lopez and J. T. Shaw, Chem. Rev., 2009, 109, 164; A. Dömling, Chem. Rev., 2006, 106, 17; V. Nair, C. Rajesh, A. U. Vinod, S. Bindu, A. R. Sreekanth, J. S. Mathen and L. Balagopal, Acc. Chem. Res., 2003, 36, 899; V. Nair, R. S. Menon, A. T. Biju and K. G. Abhilash, Chem. Soc. Rev., 2012, 41, 1050; V. Cerulli, L. Banfi, A. Basso, V. Rocca and R. Riva, Org. Biomol. Chem., 2012, 10, 1255; A. Kalafi-Nezhad and F. Panahi, Synthesis, 2011, 984.
- [10]. J. Yu, F. Shi and L.-Z. Gong, Acc. Chem. Res., 2011, 44, 1156; A. Shaabani, A. Sarvary, S. Ghasemi, A. HosseinRezayan, R. Ghadarian and S. W. Ng, Green Chem., 2011, 13, 582; A. Kumar and S. Sharma, Green Chem., 2011, 13, 2017; J.-N. Tan, M. Li and Y. Gu, Green Chem., 2010, 12, 908; V. Estévez, M. Villacampa and J. C. Menéndez, Chem. Soc. Rev., 2010, 39, 4402.
- [11]. I. Monfardini, J.-W. Huang, B. Beck, J. F. Cellitti, M. Pellicchia and A. Dömling, J. Med. Chem., 2011, 54, 890; O. N. Burchak, L. Mugherli, M. Ostuni, J. J. Lacapère and M. Y. Balakirev, J. Am. Chem. Soc., 2011, 133, 10058.
- [12]. R. Daoud, J. Desneves, L. W. Deady, L. Tilley, R. J. Scheper, P. Gros and E. Georges, Biochemistry, 2000, 39, 6094; T. Suzuki, N. Fukazawa, K. San-nohe, W. Sato, O. Yano and T. Tsuruo, J. Med. Chem., 1997, 40, 2047; R. Klingenstein, P. Melnyk, S. R. Leliveld, A. Ryckebusch and C. Korth, J. Med. Chem., 2006, 49, 5300; C.-C. Peng, J. L. Cape, T. Rushmore, G. J. Crouch and J. P. Jones, J. Med. Chem., 2008, 51, 8000; A. Lilienkampf, J. Mao, B. Wan, Y. Wang, S. G. Franzblau and A. P. Kozikowski, J. Med. Chem., 2009, 52, 2109; V. K. Zishiri, M. C. Joshi, R. Hunter, K. Chibale, P. J. Smith, R. L. Summers, R. E. Martin and T. J. Egan, J. Med. Chem., 2011, 54, 6956.
- [13]. H. V. Mierde, N. Ledoux, B. Allaert, P. V. D. Voort, R. Drozdak, D. D. Vos and F. Verpoort, New J. Chem., 2007, 31, 1572; T. G. Back and J. E. Wulff, Chem. Commun., 2002, 1710; S. Rousseaux, B. Liégault and K.

- Fagnou, *Chem. Sci.*, 2012, 3, 244; H. Huang, H. Jiang, K. Chen and H. Liu, *J. Org. Chem.*, 2009, 74, 5476; D. S. Bose and R. K. Kumar, *Heterocycles*, 2006, 68, 549; X.-S. Wang, M.-M. Zhang, Z.-S. Zeng, D.-Q. Shi, S.-J. Tu, X.-Y. Wei and Z.-M. Zong, *Chem. Lett.*, 2005, 34, 1316; M. Hatano and K. Mikami, *J. Am. Chem. Soc.*, 2003, 125, 4704; C. S. Yi, S. Y. Yun and I. A. Guzei, *J. Am. Chem. Soc.*, 2005, 127, 5782.
- [14]. S.-J. Tu, B. Jiang, R.-H. Jia, J.-Y. Zhang, Y. Zhang, C.-S. Yao and F. Shi, *Org. Biomol. Chem.*, 2006, 4, 3664; R. A. Batey and D. A. Powell, *Chem. Commun.*, 2001, 2362; X.-S. Wang, J. Zhou, M.-Y. Yin, K. Yang and S.-J. Tu, *J. Comb. Chem.*, 2010, 12, 266; J. Akbari, A. Heydari, H. R. Kalhor and S. A. Kohan, *J. Comb. Chem.*, 2010, 12, 137.
- [15]. S. Tu, C. Li, G. Li, L. Cao, Q. Shao, D. Zhou, B. Jiang, J. Zhou and M. Xia, *J. Comb. Chem.*, 2007, 9, 1144; C. Che, J. Xiang, G.-X. Wang, R. Fathi, J.-M. Quan and Z. Yang, *J. Comb. Chem.*, 2007, 9, 982; K. Kobayashi, S. Fujita, S. Fukamachi and H. Konishi, *Synthesis*, 2009, 3378; S. Kobayashi and S. Nagayama, *J. Am. Chem. Soc.*, 1996, 118, 8977.
- [16]. A. B. A. El-Gazzar, H. N. Hafez and G. A. M. Nawwar, *Eur. J. Med. Chem.*, 2009, 44, 1427; H. I. Ali, N. Ashidab and T. Nagamatsu, *Bioorg. Med. Chem.*, 2008, 16, 922; H. I. Ali, K. Tomita, E. Akaho, M. Kunishima, Y. Kawashima, T. Yamagishi and H. Ikeya, *Eur. J. Med. Chem.*, 2008, 43, 1376; H. I. Ali, K. Tomita, E. Akaho, H. Kambara, S. Miura, H. Hayakawa, N. Ashida, Y. Kawashima, T. Yamagishi, H. Ikeya, F. Yoneda and T. Nagamatsu, *Bioorg. Med. Chem.*, 2007, 15, 242; A. A. Joshi and C. L. Viswanathan, *Bioorg. Med. Chem. Lett.*, 2006, 16, 2613; Y. L. Chen, K. C. Fang, J. Y. Sheu, S. L. Hsu and C. C. Tzeng, *J. Med. Chem.*, 2001, 44, 2374.
- [17]. Z. He, G. Milburn, A. Danel, A. Puchala, P. Tomasik and D. Rasala, *J. Mater. Chem.*, 1997, 7, 2323; Y. T. Tao, C. H. Chuen, C. W. Ko and J. W. Peng, *Chem. Mater.*, 2002, 14, 4256; C. H. Chuen and Y. T. Tao, *Appl. Phys. Lett.*, 2002, 81, 4499; C. W. Ko and Y. T. Tao, *Appl. Phys. Lett.*, 2001, 79, 4234.
- [18]. Y. Chena, S. Wub, S. Tub, F. Shib and C. Lib, *J. Heterocycl. Chem.*, 2008, 45, 1243; D.-Q. Shi, L.-H. Niu, H. Yao and H. Jiang, *J. Heterocycl. Chem.*, 2009, 46, 237; J. Quiroga, A. Hormaza, B. Insuasty, A. J. Ortíz, A. Sánchez and M. Nogueras, *J. Heterocycl. Chem.*, 1998, 35, 231; J. Quiroga, J. Trilleras, B. Insuasty, R. Abonía, M. Nogueras and J. Cobo, *Tetrahedron Lett.*, 2008, 49, 2689; J. Quiroga, J. Trilleras, B. Insuasty, R. Abonía, M. Nogueras, A. Marchal and J. Cobo, *Tetrahedron Lett.*, 2010, 51, 1107; X.-S. Wang, Q. Li, J.-R. Wu and M.-M. Zhang, *Synth. Commun.*, 2009, 39, 3069; N. G. Kozlov and L. I. Basalaeva, *Russ. J. Org. Chem.*, 2007, 43, 432.
- [19]. Y. Hitosuyanagi, M. Kobayashi, H. Morita, H. Itokawa and K. Takeya, *Tetrahedron Lett.*, 1999, 40, 9107.
- [20]. C. Tratrat, S. Giorgi-Renault and H.-P. Husson, *Org. Lett.*, 2002, 4, 3187; R. Labruère, P. Helissey, S. Desbène-Finck and S. Giorgi-Renault, *J. Org. Chem.*, 2008,

Microwave Assisted Synthesis of N-Acetylpyrazolines Derived from Bis-Chalones

Yogesh S. Nalwar

Department of Chemistry, Toshniwal A.C.S. College, Sengaon-431542, Maharashtra, India

ABSTRACT

In the present communication, reported the easy, convenient route for the synthesis of N-acetyl pyrazolines from α,β -unsaturated ketone (bis-chalcones). The reaction was done in ethanol solvent through microwave irradiation. The reaction time, yield and purity of synthesized compounds were notable advantages of present method. All synthesized compounds were confirmed on the basis of IR, ^1H NMR, ^{13}C NMR and CHN analysis.

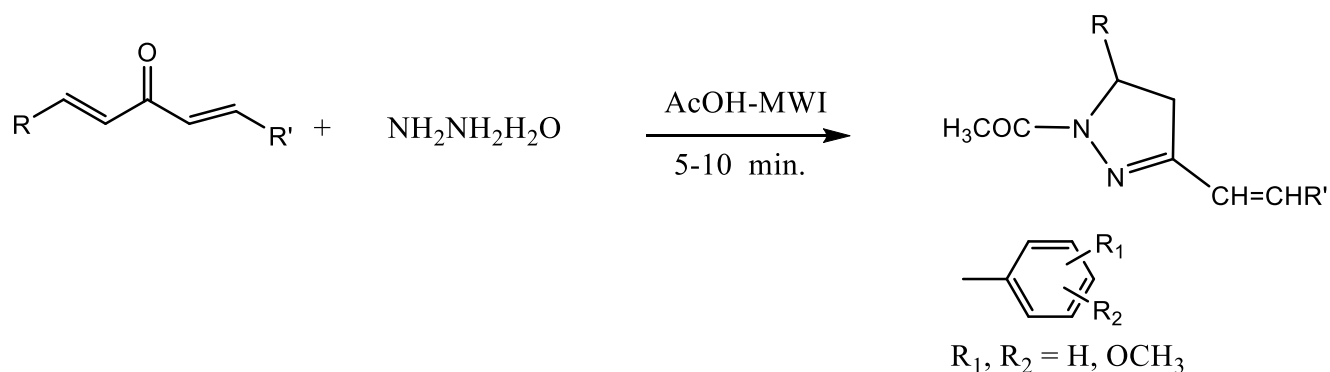
I. INTRODUCTION

Amongst five-membered heterocycles, Nitrogen containing heterocyclic compounds represents a wide range of pharmacological applications and pronounced biological properties [1-8]. Pyrazolines are useful synthons in organic chemistry and also important in the development of theory in heterocyclic chemistry [9-10]. A classical synthesis of these compounds involves the condensation of α,β -unsaturated carbonyl compounds with hydrazines [11]. The three component one step synthesis has great current interest towards development of novel synthetic organic compounds. One of the three component one step reaction involve, synthesis of *N-acetyl pyrazolines* in which α,β -unsaturated ketone reacts with hydrazine hydrate in presence of acetic acid under microwave irradiation.

II. MATERIAL AND METHODS

Chemical and Instrumentation

All chemicals, solvents and reagents used in the present study were of analytical grade purchased from Sigma, SD Fine, or Spectrochem. Melting points were determined in an open capillary tube and are uncorrected. The reactions were carried out in ethanol solvent (10 mL:10 mL, v/v) using 200. Purification of the compounds was indicated using TLC (mixture of ethyl acetate and hexane, 0.20 mL:0.20 mL, vv). IR spectra were recorded in KBr pellets on a Perkin-Elmer FT-IR Shimadzu spectrometer. ^1H and ^{13}C NMR spectra were obtained in DMSO- d_6 on Avance 300 MHz spectrometer using TMS as an internal standard. The mass spectra were recorded on EI-Shimadzu-GC-MS spectrometer.



Scheme 1: Synthesis of N-acetyl pyrazolines derived from bis-chalcones

General Procedure for synthesis of N-acetylpyrazolines derived from bis-chalcones: In 50 mL round bottom flask, a mixture of α,β -unsaturated ketones (0.01 mol), hydrazines hydrate (0.01 mmol) and acetic acid (0.01 mmol) was dissolved in ethanol (20 mL) by warming. The resulting reaction solution were irradiated under microwave irradiation for 5-10 min. The progress of reaction was indicated by TLC. After completion of reaction the precipitate formed was filtered through simple büchner funnel under vacuum pressure and crystallized from ethanol to yield 2-pyrazolines (Scheme 1).

3a. 1-(5-(4-methoxyphenyl)-3-(4-methoxystyryl)-4,5-dihydro-1H-pyrazol-1-yl)ethan-1-one:

Yield: 75%, m.p. 203-205 °C. IR (KBr): 1635 (C=O), 1588 (C=N) cm^{-1} . $^1\text{H NMR}$ (300 MHz, $\text{DMSO-}d_6$) δ 3.70 (s, 6H, two OCH₃), δ 3.21 (dd, $J = 5.0, 17.8$ HZ, 1H, HA), δ 3.65 (dd, $J = 12.0, 17.8$ HZ, 1H, HB), δ 5.57 (dd, $J = 5.1, 12.1$ HZ, 1H, HX), δ 6.74 (d, $J = 16.2$ HZ, 1H, H α), δ 7.17 (d, $J = 16.2$ HZ, 1H, H β), δ 7.29-7.74 (m, 4H, Ar-H), δ 4.32 (s, 1H, COCH₃). m/z 350 (100%).

3b. 1-(5-(3,4-dimethoxyphenyl)-3-(3,4-dimethoxystyryl)-4,5-dihydro-1H-pyrazol-1-yl)ethan-1-one.

Yield: 78%, m.p. 184-187 °C. IR (KBr): 1632 (C=O), 1580 (C=N) cm^{-1} . $^1\text{H NMR}$ (300 MHz, $\text{DMSO-}d_6$) δ 3.70 (s, 6H, four OCH₃), δ 3.24 (dd, $J = 5.0, 17.8$ HZ, 1H, HA), δ 3.69 (dd, $J = 12.0, 17.8$ HZ, 1H, HB), δ 5.57 (dd, $J = 5.1, 12.1$ HZ, 1H, HX), δ 6.78 (d, $J = 16.2$ HZ, 1H, H α), δ 7.13 (d, $J = 16.2$ HZ, 1H, H β), δ 7.24-7.54 (m, 4H, Ar-H), δ 4.35 (s, 1H, COCH₃). m/z 410 (100%).

III. CONCLUSION

In summary, present communication reported the synthesis of *N-acetyl pyrazolines* derivatives starting from α,β -unsaturated ketone in ethanol under MWI. The advantage of methods has notable advantages which includes clean reaction procedure, easy isolation of products, short reaction time and no need of special apparatus device.

IV. REFERENCES

[1]. Girisha, K. S.; Kalluraya, B.; Narayana, V.; Padmashree, P. Eur. J. Med.Chem. 2010, 45, 4640. [CrossRef]

- [2]. Banday, A. H.; Mir, B. P.; Lone, I. H.; Suri, K. A.; Sampathkumar, H. M. *Stroid* 2010, 75, 805. [CrossRef]
- [3]. Kaplancikli, Z. A.; Turan-Zitouni, G.; Ozdemir, A.; Can, O. D.; Chevallet, P. *Eur. J. Med. Chem.* 2009, 44, 2606. [CrossRef]
- [4]. Wanare, G.; Aher, R.; Kawathekar, N.; Ranjan, R.; Kaushik, N. K.; Sahal, D. *Bioorg. Med. Chem. Lett.* 2010, 20, 4675. [CrossRef]
- [5]. Shivakumar, P. M.; Seenivasan, S. P.; Kumar, V.; Doble, M. *Bioorg. Med. Chem. Lett.* 2010, 20, 3169. [CrossRef]
- [6]. Zhang, X. H.; Wu, S. K.; Gao, Z. Q.; Lee, S. T.; Kwong, H. L. *Thin Solid Film* 2000, 371, 40. [CrossRef]
- [7]. Ahn, J. H.; Kim, H. M.; Jung, S. H.; Kang, S. K.; Kim, K. R.; Rhee, S. D.; Yang, S. D.; Cheon, H. G.; Kim, S. S. *Bioorg. Med. Chem. Lett.* 2004, 14, 4461. [CrossRef]
- [8]. Archana Srivastava, V. K.; Chandra, R.; Kumar, A. *Ind. J. Chem. Sec. B.* 2002, 41, 2371.
- [9]. Elguero, J. In *Comprehensive Heterocyclic Chemistry*. Karitzky, A. R.; Ress, C. W. (Eds.) Pergamon: Oxford, 1984, 5, 167-303.
- [10]. Elguero, J. In *Comprehensive Heterocyclic Chemistry II*. Karitzky, A. R.; Ress, C. W.; Scriven, E. F. (Eds.) Pergamon: Oxford, 1996, 3, 1-76.
- [11]. Seebacher, W.; Michi, G.; Belaj, F.; Brun, R.; Saf, R.; Weis, R. *Tetrahedron* 2003, 59, 2811. [CrossRef]

Synthesis and Antimicrobial Evaluation of Some Novel 2, 4-(Substituted-Phenyl)-2, 3-Dihydro-1H-1, 5-Benzodiazepine Derivatives

Kendre M. M.*, Vidule R. R.

Department of Chemistry, Shri Sant Gadge Maharaj Mahavidyalaya Loha, Dist. Nanded -431708,
Maharashtra, India

ABSTRACT

In the present investigation, a series of some novel 2, 4-[substituted-phenyl]-2, 3-dihydro-1H-1, 5-benzodiazepines (**3a-1**) have been synthesized by the treatment of 1-(substituted-2-hydroxy-phenyl)-3-(4'-dimethylamino-phenyl)-prop-2-en-1-ones (chalcones) (**1a-1**) with orthophenylene diamine (**2**) using absolute ethanol as solvent in the presence of catalytic amount of Lanthanum Nitrate in short reaction time with excellent yield (60-70%) by conventional method. The products were tested for purity by TLC and structures of newly synthesized compounds were confirmed by IR, ¹H NMR and Mass spectral analysis. All these newly synthesized compounds were evaluated for their antimicrobial activity. Most of the compounds showed potent activity against the pathogens used.

Key words: O-Hydroxychalcones, orthophenylene diamine, Lanthanum Nitrate, 1, 5-Benzodiazepines, Antimicrobial activity.

I. INTRODUCTION

1, 5- Benzodiazepines retained the interest of researchers due to the unique structural properties and broad spectrum of biological activities¹. 1, 5 benzodiazepine derivatives showed a larg number of pharmacological properties such as antibacterial²⁻³, antifungal⁴, anticancer and antioxidant⁵⁻⁶, anti-Inflammatory and cytotoxic⁷⁻⁸, anticonvulsant⁹, CNS depressant¹⁰ etc. It is well known that halogen substituted 1, 5-Benzodiazepine compounds are also strongly biologically active¹¹. On the other hand, halogen and methyl groups substituted in benzene ring of 1, 5-benzodiazepine molecules also exhibit good biological activity¹²⁻¹³. Therefore there has been a particular interest in the synthesis of halogen; methyl and hydroxyl groups substituted benzodiazepines.

In view of these observations, in the present investigation we report here, the synthesis of a number of novel 1, 5-Benzodiazepines(**3a-1**), having halogen, hydroxy and methyl groups with an aim to find new most active antibacterial and antifungal agents. We have synthesized a novel series of 2-(4'-(Dimethylamino-phenyl)-4-(substituted-2-hydroxy-phenyl)-2, 3-dihydro- *1H*- 1, 5-Benzodiazepines as antimicrobial agents by refluxing the substituted 2'-hydroxychalcone with orthophenylene diamine in the presence of catalytic amount of Lanthanum Nitrate. The structures of the newly synthesized compounds (**3a-1**) were established on the basis

of IR, ^1H NMR, and Mass spectral data. All the newly synthesized compounds were tested for their antibacterial activity against *Escherichia coli*, *Salmonella typhi*, *Staphylococcus aureus* and *Bacillus subtilis* and antifungal activity against *Aspergillus niger*, *Penicillium chrysogenum*, *Fusarium moneliforme* and *Aspergillus flavus*, using Peniciline and Greseofulvin as standard drugs.

II. MATERIALS AND METHODS

All the solvents and reagents were obtained from commercial sources and were used without further purification. The melting points were determined by Open Capillary method and are uncorrected. The mass spectra were obtained with a Shimadzu GC-MS spectrophotometer.

The IR spectra in KBr were recorded on Shimadzu Spectrophotometer and ^1H NMR spectra were recorded in DMSO on Avance 300 MHz Spectrometer using TMS as internal standard. The chemical shift values are expressed in part per million (ppm) downfield from the internal standard and signals are quoted as s (singlet), d (doublet), t (triplet) and m (multiplet). TLC was used to monitor the progress of all reactions and to check the purity of compounds by using ethyl acetate and petroleum ether as an eluent in the ratio of (3:7 v/v) which were further purified by column chromatography [ethyl acetate: pet ether (7:3)]. All the compounds were tested for their antibacterial and antifungal activities by agar diffusion method.

General method for the Synthesis of 2, 4-(substituted-phenyl)-2, 3-dihydro-1H-1, 5-benzodiazepine:

An equimolar reaction mixture of orthophenylene diamine (0.001mol) and substituted 2'-hydroxy chalcone (0.001mol) in 10 ml absolute ethanol was mixed in round flask refluxed for 1 hours, in the presence of Lanthanum Nitrate (10 m mol %). The progress of the reaction was monitored by using TLC [eluent; ethyl acetate; pet ether (3:7)]. After completion of reaction, the reaction mixture was distilled to remove the excess of solvent and the reaction mixture was poured on crushed ice. The solid crude product obtained was filtered, washed with cold water, dried and recrystallized by using ethanol to get corresponding 2, 4-(substituted-aryl)-2, 3-dihydro-1H-1, 5-benzodiazepine in 60-70 % yield, which were further purified by column chromatography [ethyl acetate: pet ether (3:7)].

Scheme-1: Synthesis of 2, 4-(substituted-phenyl)-2, 3-dihydro-1H-1, 5-benzodiazepine

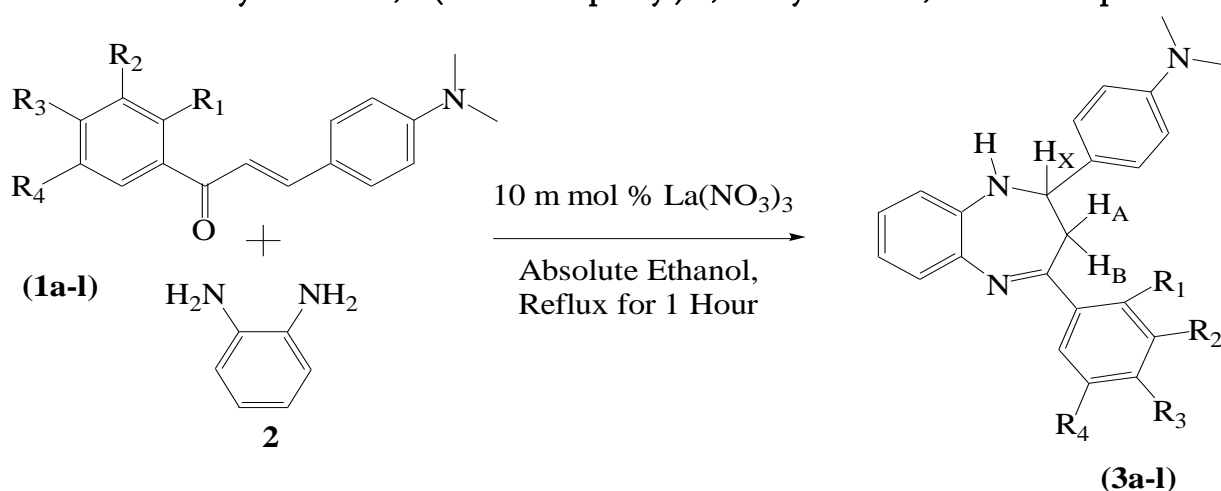


Table:- 1 Physical data of newly Synthesized 1, 5-Benzodiazepine derivatives (3a-l)

Sr. No	Entry	R ₁	R ₂	R ₃	R ₄	Molecular formula	Yield in %	M. P. in °C
1	3a	OH	I	H	I	C ₂₃ H ₂₁ N ₃ I ₂ O	62	152-153
2	3b	OH	I	H	CH ₃	C ₂₄ H ₂₄ N ₃ IO	67	102-103
3	3c	OH	Cl	H	Cl	C ₂₃ H ₂₁ N ₃ Cl ₂ O	70	145-146
4	3d	OH	I	H	Cl	C ₂₃ H ₂₁ N ₃ IClO	65	133-134
5	3e	OH	Br	H	CH ₃	C ₂₄ H ₂₄ N ₃ BrO	66	122-123
6	3f	OH	Br	H	Cl	C ₂₃ H ₂₁ N ₃ BrClO	67	105-106
7	3g	OH	Br	H	Br	C ₂₃ H ₂₁ N ₃ Br ₂ O	64	154-155
8	3h	OH	I	H	Br	C ₂₃ H ₂₁ N ₃ IBrO	66	142-143
9	3i	OH	H	CH ₃	Cl	C ₂₄ H ₂₄ N ₃ ClO	65	113-114
10	3j	OH	H	H	Br	C ₂₃ H ₂₁ N ₃ BrO	67	132-133
11	3k	H	Br	OH	Br	C ₂₃ H ₂₁ N ₃ Br ₂ O	70	115-116
12	3l	H	I	OH	I	C ₂₃ H ₂₁ N ₃ I ₂ O	68	158-159

III. RESULTS AND DISCUSSION

In recent years, one of the most important conventional methods used for the syntheses of 2,4-substituted-phenyl-2,3-dihydro-1*H*-1,5-benzodiazepines has been the reaction of α , β -unsaturated carbonyl compounds, such as substituted 2'-hydroxychalcone with 2-orthophenylene diamine¹⁴ (**2**) and α , β -unsaturated carbonyl compounds i.e. 2'-hydroxychalcone (**1a-l**) in absolute ethanol was refluxed for 1 hour, in the presence of Lanthanum Nitrate. The reaction mixture was distilled to remove the excess of solvent and the reaction mixture was poured on crushed ice and recrystallized by using ethanol to get 2,4-(substituted-phenyl)-2,3-dihydro-1*H*-1,5-benzodiazepine derivatives (**3a-l**) in 60-70 % yield. In the literature, orthophenylene diamine has been reported to react with α , β -unsaturated carbonyl compounds or 2'-hydroxychalcone to give a Michael addition type adduct formed by the nucleophilic attack of the electron rich Nitrogen atom of the β carbon atom of the chalcone, rendered electrophilic by a carbonyl group, when the reaction is carried out under milder conditions by using a basic medium¹⁵. It has also been reported that final products are obtained under basic reaction conditions. The Michael addition products, when isolated, were cyclized to obtain the final product thereby establishing the reaction product as formed in one steps to give the final product. We identified the synthesized product exclusively, based on spectral observations.

In the present work, a series of novel 1, 5-benzodiazepines (**3a-l**) were synthesized by cyclization of corresponding 2'-hydroxychalcones (**1a-l**). All the synthesized 1, 5-benzodiazepines didn't give positive Wilson test and red coloration with concentration H₂SO₄ which confirmed the formation of 1, 5-

benzodiazepine compounds. The newly synthesized compounds have been confirmed first by TLC and Melting Points of products were different from that of corresponding reactants. The structures of newly synthesized 2,4-substituted-phenyl-2,3-dihydro-1*H*-1,5-benzodiazepine derivatives were confirmed by IR, ¹H NMR and Mass spectral data. The IR spectrum of compound **3c** exhibited peaks due to group -C=N, at 1589 cm⁻¹. The ¹H NMR spectrum shows characteristic peaks dd at δ 3.0 of H_A and δ 3.40 of H_B respectively due to proton of methylene group of seven member diazepine ring, due to germinal and vicinal coupling of -CH₂ protons of the diazepine ring. Further, the -CH proton of the ring resonated as a triplet at δ 5.25 (t, 1H, H_X), due two vicinal coupling with the two non-equivalent protons of the methylene group at position three of the diazepine ring. The proton of >N-H singlet shows at pick δ 7.25 (s, 1H, >NH), and also sharp pick of -OH group at δ 11.1 (s, 1H, OH), these observations are in agreement with the spectral data reported by Anjali Saini.¹⁶⁻¹⁷

All the newly synthesized 1, 5-benzodiazepine compounds were evaluated for their antibacterial activity against the selected four different pathogens, such as *E. coli*, *S. typhi*, *S. aureus* and *B. subtilis*. The **3b**, **3c**, **3g** and **3i** of 1, 5-benzodiazepine compounds show maximum activity against *E. coli*. The compounds **3a**, **3e**, **3j**, and **3l** showed weak activity against *S. typhi*, while **3c**, **3d**, **3f**, **3i** and **3k** showed stronger activity in comparison with standard drugs (Penicilin). All the synthesized compounds of benzodiazepine except **3f**, **3g** showed moderate activity against *S. aureus*. The bromine substituted compounds **3b**, **3j** and **3k** showed significant activity against *B. subtilis* as compared with standard drugs. All the newly synthesized compounds were evaluated for their antifungal activity against the four different pathogens *Aspergillus niger*, *Penicillium chrysogenum*, *Fusarium moneliforme* and *Aspergillus flavus*. The antifungal activity of some 1, 5-benzodiazepine compounds showed good activity against four pathogens. The presence of more electronegative substituted halogen atoms were found responsible for increasing antimicrobial activity.

Spectral data of 1, 5-Benzodiazepine derivatives:-

Synthesis of 2-(4'-Dimethylamino-phenyl)-4-(3-bromo-5-methyl-2-hydroxy-phenyl)-2,3-dihydro-1*H*-1, 5-benzodiazepine (3e); IR (KBr) cm⁻¹: 3348 (>N-H str of benzodiazepine), 1519 (Ar >C=C< Str) 3027 (Ar C-H str), 817 (C-Br), 632 (C-N) cm⁻¹; **¹H NMR (DMSO):** δ 2.1 (s, 3H, CH₃), δ 2.85 (s, 6H, N-(CH₃)₂) δ 3.0 (dd, 1H, H_A), δ 3.40 (dd, 1H, H_B) δ 5.25 (t, 1H, H_X), δ 7.4 (s, 1H, >NH) δ 6.6-7.9 (m, 9H, Ar-H) δ 11.1 (s, 1H, OH, D₂O exchangeable); **MS (m/z):** 450 (M+1).

Synthesis of 2-(4'-Dimethylamino-phenyl)-4-(3-Bromo-5-Chloro-2-hydroxy-phenyl)-2, 3-dihydro-1*H*-1, 5-benzodiazepine (3f) ; IR (KBr) cm⁻¹: 3332 (>N-H str of benzodiazepine), 3194 (Ar-OH), 1610 (C=N), 1517 (>C=C<), 812 (C-Cl), cm⁻¹; **¹H NMR(DMSO) :** δ 2.82 (s, 6H, -N-(CH₃)₂), δ 3.0 (dd, 1H, H_A), δ 3.4 (dd, 1H, H_B), δ 5.30 (t, 1H, H_X), δ 7.35 (s, 1H, >NH), δ 6.7-8.5 (m, 10H, Ar-H), δ 11.50 (s, 1H, OH, D₂O exchangeable); **MS (m/z):**471 (M+1).

Synthesis of 2-(4'-Dimethylamino-phenyl)-4-(3, 5-dibromo-2-hydroxy-phenyl)-2, 3-dihydro-1*H*-1, 5-benzodiazepine (3g); IR (KBr) cm⁻¹:3344 (>N-H str. of benzodiazepine), 3178 (Ar-OH), 1612 (C=N), 1519 (>C=C<),817 (C-Br), cm⁻¹; **¹H NMR (DMSO) :** δ 2.80 (s, 6H, N(CH₃)₂), δ 3.0 (dd, 1H, H_A), δ 3.35 (dd, 1H, H_B), δ 5.35 (t, 1H, H_X), δ 7.38 (s, 1H, >NH), δ 6.8-8.8 (m, 10H, Ar-H), δ 11.55 (s, 1H, OH, D₂O exchangeable); **MS (m/z):** 515 (M+1).

Synthesis of 2-(4'-Dimethylimino-phenyl)-4-(4-methyl-5-Choro-2-hydroxy-phenyl)-2, 3-dihydro-1, 5-benzodiazepine (3i); IR (KBr) 3336 (>N-H str. benzodiazepine), 3172 (Ar-OH), 1588 (C=N), 1519 (>C=C<), 815 (C-Cl), cm^{-1} ; $^1\text{H NMR(DMSO)}$: δ 2.1 (s, 3H, CH_3), δ 2.85 (s, 6H, $-\text{N}-(\text{CH}_3)_2$), δ 3.05 (dd, 1H, H_A), δ 3.35 (dd, 1H, H_B), δ 5.4 (t, 1H, H_X), δ 7.35 (s, 1H, $>\text{NH}$), δ 6.7-7.7 (m, 10H, Ar-H), δ 11.55 (s, 1H, OH, D_2O exchangeable); **MS (m/z); 406 (M+1).**

Table 2: Antimicrobial activity of synthesized 1, 5-benzodiazepine derivatives (3a-l)

		Bacteria (Zone of Inhibition in mm)				Fungi (Zone of Inhibition in mm)			
Sr No.	Entry	A	B	C	D	E	F	G	H
1	3a	17	13	22	14	RG	-ve	-ve	-ve
2	3b	18	15	--	22	-ve	-ve	-ve	RG
3	3c	20	18	20	--	RG	RG	-ve	-ve
4	3d	--	16	22	18	-ve	-ve	-ve	-ve
5	3e	14	14	--	13	-ve	-ve	RG	-ve
6	3f	--	18	14	17	-ve	-ve	-ve	-ve
7	3g	18	--	16	--	-ve	RG	-ve	-ve
8	3h	16	16	19	22	RG	-ve	-ve	-ve
9	3i	18	17	22	15	-ve	-ve	-ve	-ve
10	3j	17	14	22	26	RG	-ve	-ve	-ve
11	3k	--	16	17	25	-ve	-ve	RG	-ve
12	3l	18	15	18	23	-ve	-ve	-ve	RG
+veControl DMSO		-ve	-ve	-ve	-ve	+ve	+ve	+ve	+ve
Penicilline		26	20	34	22	X	X	X	X
-ve Control (Griseofulvin)		X	X	X	X	-ve	-ve	-ve	-ve

(Zone of Inhibition in mm)

A= Escherichia coli, B=Salmonella typhi, C= Staphylococcus aureus,
D=Bacillus subtilis E= Aspergillusniger, F=penicilliumchrysogenum,
G=Fusariummoneliforme, H= Aspergillusflavus -- = No Antibacterial activity,
 RG= Reduced Growth (Moderate Activity), -ve = Growth (Antifungal Activity Observed),
 X= Not Applicable

IV. ANTIMICROBIAL ACTIVITIES

All the newly synthesized 1, 5-benzodiazepine compounds were evaluated for their antibacterial activity against the selected four different pathogens, such as *E. coli*, *S. typhi*, *S. aureus* and *B. subtilis*. The **3b**, **3c**, **3g** and **3i** of 1, 5-benzodiazepine compounds show maximum activity against *E. coli*. The compounds **3a**, **3e**, **3j**, and **3l** showed weak activity against *S. typhi*, while **3c**, **3d**, **3f**, **3i** and **3k** showed stronger activity in comparison with standard drugs (Penicilin). All the synthesized compounds of benzodiazepine except **3f**, **3g** showed moderate activity against *S. aureus*. The bromine substituted compounds **3b**, **3j** and **3k** showed significant activity against *B. subtilis* as compared with standard drugs. All the newly synthesized compounds were evaluated for their antifungal activity against the four different pathogens *Aspergillus niger*, *Penicillium chrysogenum*, *Fusarium moneliforme* and *Aspergillus flavus*. The antifungal activity of some 1, 5-benzodiazepine compounds showed good activity against four pathogens. The presence of more electronegative substituted halogen atoms were found responsible for increasing antimicrobial activity.

V. CONCLUSION

In conclusion it can be summarized that, we have successfully synthesized 2, 4-(substituted-hydroxyphenyl)-2, 3 dihydro-1H-1, 5-benzodiazepine derivatives. The reaction described is a simple and highly efficient condensation reaction between substituted 2'-hydroxychalcones with *orthophenylene diamine* using Lanthanum Nitrate in absolute ethanol as a solvent. The advantages of present protocol are simplicity of operation, time saving and high yield of products. The 1, 5-benzodiazepine compounds **3b**, **3c** show activity against *E. coli*. All the synthesized compounds of benzodiazepine except **3f**, **3g** showed moderate activity against *S. aureus*. The bromine substituted compounds **3b**, **3j** and **3k** showed significant activity against *B. subtilis* as compared with standard drugs. The antifungal activity of some benzodiazepine compounds showed good activity against four pathogens selected. The presences of more electronegative substituted halogen atoms were responsible for increasing antimicrobial activity.

VI. ACKNOWLEDGEMENT

The authors are thankful to the Principal, Yeshwant College, Nanded for providing necessary facilities for carrying out the research work. Authors are also thankful to Director IICT Hyderabad for providing necessary spectral analysis facilities for the research work and also thankful to Principal, N.S.B.College, Nanded for providing biological data

VII. REFERENCES

- [1]. Anjani Solankee and Riki Tailor. Synthesis, Characterisation, Antimicrobial Evaluation of Chalcones and its Cyclised Product: Phenyl Pyrazolines and Benzodiazepines, *Chemi. Sci. Trans.*, 4(4): 2015; 1057-

1065

- [2]. Shrikrishna D. Tupare and R. P. Pawar. Highly Efficient Synthesis and Antibacterial of 1, 5-Benzodiazepines under Microwave Irradiation, *Inter. J. Appli. Chem.*, 13(2): 2017; 369-376
- [3]. Shahid Shaikh and M. A. Baseer. Synthesis and Antimicrobial Activities of some new 2, 3-dihydro-1, 5-Benzodiazepine Derivatives, *Inter. J. Pharma. Scien.Res.*, 4(7): 2013; 2717-2720
- [4]. Pankaj Kumar, Abhishek Kumar, Jean Sandra Pinto, Sachin A. Kumbar, Nanditha Bhat, Prashant Nayak. Synthesis and antimicrobial evaluation of some novel 1, 5 benzodiazepine derivatives derived from pyrrolyl chalcones, *Res. J. Pharm. Techno.*, 15(4): 2022; 1811-1814
- [5]. Shahnavaaz V, Farahnaz KB. Iron (III) Phosphate as an Efficient and Reusable Catalyst for the Synthesis of 1, 5-Benzodiazepines. *Org. Chem. Ind. J.*, 12(4): 2016;103
- [6]. Bharatesh S. Kittur, Sadanand N. Masuti, Shreenivas R. Deshpande, Bhumika B. Kittur, Sharanbasav B. Biradar, Y. Srinivas, Guruprasad S. Chilakantmath, Synthesis, Investigation of Anticancer and Antioxidant Activity of Certain 2,4-Diaryl Substituted Benzodiazepine and Benzothiazepines Derived From Vanillin, *RGUHS J. Pharm. Sci.*,10(4): 2020; 13-22
- [7]. Ishwar Bhat K, Abhishek Kumar, Synthesis and Anti-inflammatory Activity of some novel 1,5 Benzodiazepine Derivatives, *Asian J. Pharm. Clin. Res.*, 9(4): 2016; 63-66
- [8]. Nalla Kapil Arya and Anshu Dandia. The expedient synthesis of 1, 5-benzothiazepines as a family of cytotoxic drugs., *Bioor. Medi. Chem. Lett.*, 18: 2008; 114-119
- [9]. Anna PN, Deepika V. Facile green synthesis of 2, 4-substituted -2, 3- dihydro-1,5-Benzothiazepine derivatives as novel anticonvulsant and central nervous system (CNS) depressant agents. *Afr. J. Pure Appl. Chem.*, 5(12): 2011; 422-428
- [10]. Barbui C, Cipriani A, Patel V, Ayuso-Mateos JL, van Ommeren M. Efficacy of antidepressants and benzodiazepines in minor depression: systematic review and meta-analysis. *The British J. Psychiatry.*, 198(1): 2011; 11-16
- [11]. Virupakshi Prabhakar, Kondra Sudhakar Babu , L.K. Ravindranath , M. Sahanoor Basha , J. Latha. Application of Chalcones in Synthesis of Novel 1, 5-Benzodiazepine Derivatives Containing Thieno [2, 3-d] Pyrimidine Core Unit and its Biological Activity Screening. *Asian J. Res. Chem.*, 10(2): 2017; 71-84
- [12]. Nachiket SD, Atul KW, Deepak SM. Solvent Free Synthesis and Biological Evaluation of 1, 5-Benzodiazepine. *Nano Sci Nano Technol.* 11(1): 2017; 1-6
- [13]. Ranjana Sharma , Amita Tilak, R. N. Thakur, Sudhir Singh Gangwar, and Ravindra C. Sutar. Synthesis and Pharmacological Evaluation of Substituted 1, 5-Benzodiazepine Derivatives for its Antidepressant Activity in Experimental Animals, *World J. Pharma. Res.*, 6(17): 2017; 925-931
- [14]. Gajanan Gopinath Mandawad , Baseer Mubeen Shaikh , Santosh Subhash Chobe and Shankaraiah Guruvaiah Konda . NaOH/PEG-400: An eloquent system for the synthesis of new thienyl benzo[b]1,4-diazepines, *Euro. J. Chemi.*, 11 (4): 2020; 276-279
- [15]. Kumaraswamy MN, Vaidya VP, Chandrashekhhar C., Synthesis of novel 2,5-dihydro-1H-1,5-benzodiazepines encompassing naphtha (2,1-B) furan and evaluation of their pharmacological activities. *Inter. J. Pharm. Chem. Bio Sci.*, 3(2): 2013; 281-287

- [16]. Anjali Saini, Vikramdeep Monga, Gurpreet Singh, Synthesis and antibacterial evaluation of naphthalene based 1,5-benzodiazepine derivatives. *Pharmaspire*, 13(4): 2021; 177-181
- [17]. K. Ishwar Bhat, Abhishek Kumar. Synthesis, Characterization, and Antioxidant Activity of Some New Benzodiazepine Derivatives, *Indi. J. Hetero. Chem.*, 28(03): 2018; 397-400

A Kinetic Study of Solvent Effect on Hydrolysis of Acetic Anhydride by Conductivity Method

Suresh D. Dhage¹, Mahesh B. Swami²

¹Department of Chemistry, SSJES, Arts, Commerce and Science College, Gangakhed, Dist. Parbhani, Maharashtra, India

²Department of Chemistry, Bahirji Smarak Mahavidyalaya, Basmat. Dist. Hingoli, Maharashtra, India

ABSTRACT

The rates of hydrolysis are greatly dependent on environmental factors such as solvent composition, temperature and ionic strengths of salts present. In this study, kinetic investigation on the hydrolysis of Acetic Anhydride has been undertaken conductometrically. To determine the effect of solvent ethanol on the hydrolysis of Acetic Anhydride, a series of reactions was conducted in different ethanol-water mixtures, keeping all other reaction conditions identical. The pseudo first order rate constants obtained in different ethanol-water mixtures increase with increasing percentage of water in the medium. In each solvent composition, the kinetics of hydrolysis of Acetic Anhydride was followed at varying substrate concentration, keeping all other experimental parameters identical. In all cases the reactions were followed under pseudo first order conditions. The constancy of the rate constant values indicate that the order of the reaction with respect to Acetic Anhydride in different ethanol-water mixtures is one. Solvation is an electrostatic phenomenon. Since increasing proportion of ethanol retards the rate of reaction, it is concluded that reaction proceeds faster in a more polar medium. Thus, we conclude that decrease in hydrolysis rate of acetic anhydride by addition of a less polar solvent ethanol is due to progressive increase in the solvation of the reactant compared to that of the transition state.

Keywords: Kinetics, Solvent Effect, Hydrolysis, Conductivity etc.

I. INTRODUCTION

Hydrolysis reactions have been extensively used in degradation of complex substances to produce harmless eco-friendly products. Solvent effect constitutes an interesting study in nucleophilic displacement reactions. So, in the present study, the kinetics of hydrolysis of Acetic Anhydride was investigated in ethanol-water system. A change of solvent may change the rate of a chemical reaction by many orders of magnitude¹. The relationship between the nature of the solvent and the reaction rate is very complex. Depending on the many possible interactions between the solvent and the reactants and solvent and the Transition State^{2,3}.

In the present study, effect of substrate concentration in various ethanol-water mixtures at 308 K was studied. To determine the effect of solvent on hydrolysis, a series of reactions was conducted in different ethanol-

water mixtures, keeping all other reaction conditions identical at 308 K. The pseudo first order rate constants increased with increasing percentage of water in the medium.

II. EXPERIMENTAL

Purified samples of Acetic Anhydride were used. Ethanol was shaken with quick lime and allowed to stand overnight. The supernatant liquid was decanted and fraction distilling at 350.9 K was collected. All solutions and reaction mixtures were prepared in conductivity water.

Kinetic Techniques

The kinetics of the hydrolysis was followed by continuous monitoring of the reaction mixture. The instrument used for this was a Systronics Digital Direct Reading Conductivity Meter which is designed for measuring the specific conductivity of a solution using a conductivity cell. The accuracy and reproducibility of the readings are $\pm 0.5\%$. The rate of hydrolysis was followed by noting the specific conductance of the solution at suitable intervals of time. As hydrolysis proceeded, weakly ionized acetic acid was produced which contributed to the increase in specific conductance of the solution. An electrically operated thermostat was used. Temperatures were recorded by means of an accurate, sensitive thermometer reading to tenths of a degree.

III. RESULTS AND DISCUSSION

The observed first order rate constants were obtained by plotting $\log(K_{\infty} - K_t)/v$ vs. time based on the expression

$$K = 2.303/t \log K_{\infty} / (K_{\infty} - K_t)$$

Log K values were also plotted against $\epsilon - 1 / (2\epsilon + 1)$ values. This plot is linear which indicates that the reaction is of dipole-dipole type.

Effect of Substrate on Reaction Rate in Ethanol – Water mixture

To find out the order of the reaction in Acetic Anhydride in Ethanol–water, experiments were conducted in 10% Ethanol at 305 K, by varying the initial Anhydride concentration, keeping all other experimental parameters identical. In all cases, reactions were followed under pseudo first order conditions, using large excess of solvent over substrate. For each reaction, satisfactory $\log(K_{\infty} - K_t)$ versus temperature plot was obtained, showing that reaction exhibits first order dependence with respect to Acetic Anhydride. The pseudo first order rate constant k_1 was obtained from the slope of this plot. The constancy of k_1 values indicates that order of reaction with respect to Acetic Anhydride is one.

Table 1

S.No.	$10^2[\text{substrate}]/\text{M}$	$10^3/K_1$
1.	0.95	1.90
2.	1.17	1.87

3.	1.85	2.15
4.	2.21	2.23
5.	4.30	2.34
6.	10.59	2.42

Effect of varying [Ethanol] on rate of hydrolysis of Acetic Anhydride at 308 K

To determine the effect of medium on hydrolysis, a series of reactions was conducted in different ethanol-water mixtures, viz., 10%, 25%, 50%, 75%, 90% and 100% Ethanol. The pseudo first order rate constants were obtained in different Ethanol-

Water mixtures. These k_1 values increased with increasing percentage of water in the medium. [Table 2].

Since solvation is an electrostatic phenomenon, an ion or polar molecule in a polar solvent, gets oriented and attracts the solvent molecules. Since the rate of hydrolysis is found to be highest in 100% water and increasing proportion of Ethanol retards the rate of the reaction, it is clear that reaction proceeds faster in a more polar medium. This leads to the conclusion that the Transition State is more polar than the reactants. If so, the rate of the reaction increases with increasing dielectric constant of the medium. The actual values of the dielectric constants for different percentages were collected. The plot of $\log k_1$ versus $\epsilon - 1/(2\epsilon + 1)$ is linear which indicates that the reaction is of dipole-dipole type. Dipolar Acetic Anhydride molecule and dipolar water are assumed as the reactants in the rate determining step.

Table 2: Effect of solvent Ethanol on the rate of hydrolysis of Acetic Anhydride at 308 K.

[Ac₂O] = 0.1059

S.No.	Percentage of Ethanol	10 ³ k ₁ /sec ⁻¹
1.	10	3.41
2.	25	3.32
3.	50	0.76
4.	75	0.54
5.	90	0.21
6.	100	0.05

The change in rate with the change in solvent composition can also be explained on the basis of solvent – reactant interaction and solvent – transition interaction according to Hughes and Ingold⁴,

- 1) Solvation will increase with the magnitude of the charge
- 2) Solvation will decrease with the increasing dispersal of a given charge.

This would mean that the transition state is more solvated than the reactants because of an increased magnitude of charge in the former. Therefore decrease in hydrolysis rate of Acetic Anhydride by the addition of a less polar solvent is due to the progressive increase in the solvation of the reactant compared to that of the transition state.

IV. CONCLUSION

The hydrolysis reaction of Acetic Anhydride exhibits first order dependence with respect to anhydride under pseudo first order conditions in 10% Ethanol- water mixture and 20% Ethanol- water mixture at 308K. The rate of hydrolysis increased with increasing polarity or increasing dielectric constant of the medium. A plot of $\log K_1$ versus $\epsilon^{-1}/(2\epsilon + 1)$ is linear indicating that reaction is of dipole-dipole type. The change in rate with change in solvent composition can be also explained on the basis of solvent-reactant interaction and solvent-transition state interaction. According to Hughes and Ingold⁴, solvation will increase with the magnitude of the charge and will decrease with increasing dispersal of a given charge. This would mean that the transition state is more solvated than the reactants because of an increased magnitude of charge in the former. Therefore, decrease in hydrolysis rate of Acetic Anhydride by the addition of a less polar solvent than alcohol is due to the progressive increase in the solvation of the reactant compared to that of the transition state.

V. REFERENCES

- [1]. Ingold, C.K., 'Structure and Mechanism in Organic Chemistry', 2nd Edn, p.457 (Bell.: London 1969).
- [2]. Hammett, L.P., 'Physical Organic Chemistry', 2nd Edn, p.221, (McGraw-Hill: New York 1970).
- [3]. Parkar, A.J., Chem Rev., 69, 1 (1969).
- [4]. Ingold, C.K., Hughes, E.D., J. Chem. Soc., 252 (1935).

Oxidation of Methanol by Benzimidazolium Fluorochromate in Aqueous Acetic Acid Medium : A Kinetic Study

M. H. Gagare¹, Mahesh B. Swami², Suresh D. Dhage³

¹Research Scholar, Dept. of Chemistry, Maharashtra Udayagiri Mahavidyala, Udgir. Dist. Latur, Maharashtra, India

²Department of Chemistry, Bahirji Smarak Mahavidyalaya, Basmat. Dist. Hingoli, Maharashtra, India

³Department of Chemistry, SSJES's Arts, Commerce and Science College, Gangakhed-431514. Dist. Parbhani, Maharashtra, India

ABSTRACT

The kinetics study of oxidation of Primary Aliphatic alcohols by Benzimidazolium Fluorochromate (BIFC) in composition of Acetic Acid in water varying proportion at 303K. The oxidation of Aliphatic Alcohol with BIFC leads to the formation of the corresponding Aldehyde was followed by spectrophotometrically. The reaction is first order towards the reagent (BIFC), Oxidant (CH₃-OH) under pseudo first order reaction has been catalyzed by hydrogen ions(H⁺). Several kinetics parameters were determined at different Acetic acid-water mixture.

Keywords: Benzimidazolium Fluorochromate, Methanol, Kinetics and Mechanism, Acetic Acid, HClO₄, Spectrophotometer.

I. INTRODUCTION

A survey of literature gives the kinetics of oxidation of alcohols by various oxidizing reagent have been studied¹. Large number of alcohols is commercially available as well as can be early prepared. The rate of change of concentration of any one of the reactants or products per unit time known as rate of reaction. Many Kinetic parameters such as concentration, catalyst, dielectric constant⁶⁻¹¹, salt¹⁴⁻¹⁸, ionic strength, and temperature²³ were accounted by various Researchers. The study of organic compounds is of immense importance both from mechanistic and synthetic point of view. Halochromates²⁻⁵ have been used as mild and selective oxidizing reagent in synthetic organic chemistry. A number of new Halochromates like Pyridinium Halochromate⁶, Quinolinium Chlorochromate⁷, 2-Bipyridinium Chlorochromates⁸, Pyridinium Fluorochromates⁹, Quinolinium Fluorochromates¹⁰, Quinolinium bromochromate¹¹, pyridinium Chlorochromate¹², Imadazolium Fluorochromates^{13,21} have been used to study the kinetics and mechanism of oxidation of various organic compounds. But a newly synthesized and developed oxidizing agent is Benzimidazolium Fluorochromates². This reagent is more efficient and mild oxidizing agent. BIFC is less hygroscopic mild and quite stable oxidizing reagent for proposed kinetic study. In the present paper we report the kinetics of oxidation of Methanol by BIFC in aqueous acetic acid 50% and water 50% medium.

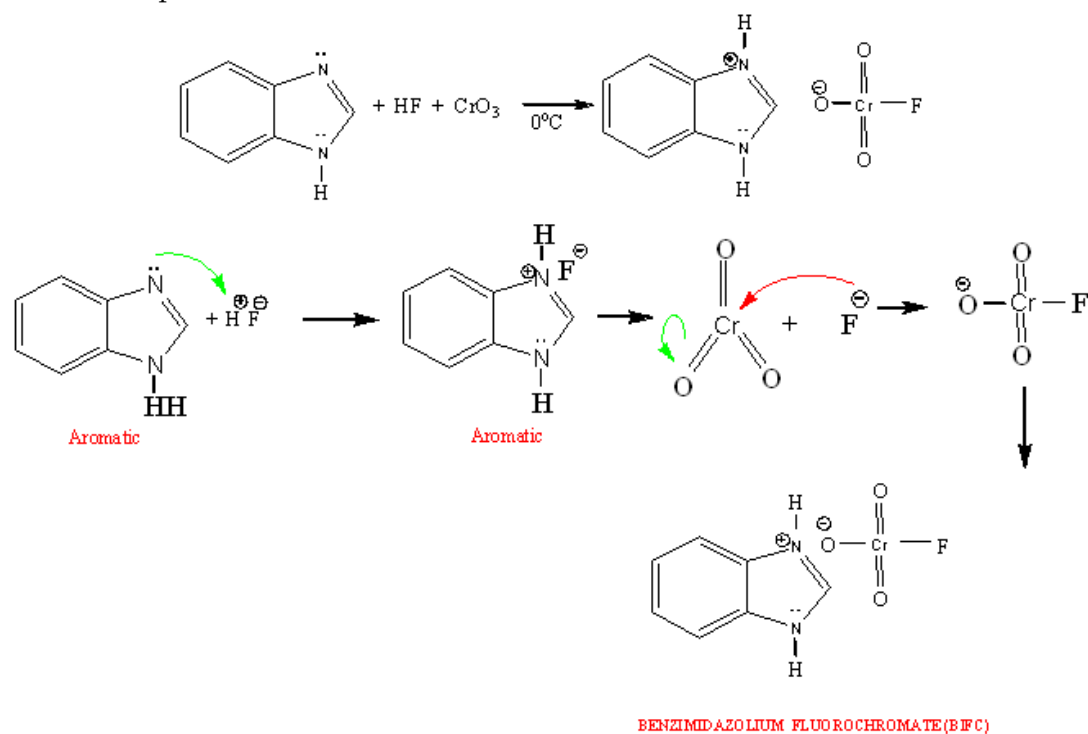
II. METHODS AND MATERIALS

Stoichiometry and Product Analysis

Stoichiometric studies for the product analysis of oxidation of Methanol over BIFC are made. Alcohols are used in this oxidation, are of extrapure quality received from Merck, Qualigens and Sigma Aldrich analyser was carried out its elemental analysis. Methanol [0.01M] was dissolved in acetic acid [10M], BIFC in acetic acid [0.01M] was added to the reaction mixture and refluxed for time ranging from around 1.5 to 2 hrs. After evaporation of the solvent, mixture was extracted by using ether. The resulted product was confirmed by TLC and Melting point. The structure of the compound also confirmed by taken through digital apparatus. In a typical experiment, Methanol [0.05M] and BIFC [0.01M] were produced upto 50 ml Acetic acid and keeping in dark for 10 hrs. to ensure completion of the reaction. The solution was treated by an excess of [150ml] solution of DNP in 1 M HCl kept in whole night at 0°C. The precipitated of DNP was filtered, dried, weighed and recrystallized from ethanol and taking weighed again. The corresponding yields of the DNP initial and final after recrystallizations were 85% and 72% sequentially. DNP has been found to be identical with DNP with formaldehyde.

Synthesis of Benzimidazolium Fluorochromate

BIFC has been prepared by the method described in the literature¹, from benzimidazole (Sigma Aldrich) 40% (23.6 gm; 0.2 mole), hydrofluoric acid (Qualigens) (4mL; 0.23mole) and chromium trioxide (Qualigens) (20gm; 0.2 mole) in the molar ratio 1:1.3:1 at 0°C. BIFC is obtained as yellow orange crystals. It is non hygroscopic, light insensitive and stable on storage. The structure was confirmed by TLC, XRD, digital M.P., IR spectra..

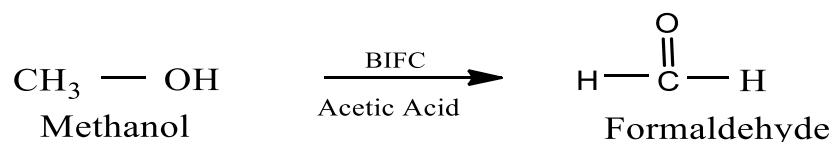


Characteristics of Benzimidazolium Fluorochromate (BIFC)

Molecular formula of BIFC¹ is $C_7H_7N_2CrFO_3$, Its Molar mass is 238 g/mol, BIFC is appeared in Yellow-orange crystals, Melting point -195°C , Solubility-slightly soluble in alcohol, acid and water, Its crystal structure-Heterocyclic, Flash point-Non-flammable. It is non-hygroscopic, light insensitive and stable on storage. BIFC is an effective and clean oxidant for alcohols.

Oxidation of Methanol by BIFC

Oxidation of alcohol $\text{CH}_3\text{-OH}$ by BIFC is an acid catalysed reaction. The oxidation of alcohols yields the corresponding Formaldehyde as the product.



III. RESULT AND DISCUSSION

Effect of varying Methanol Concentration

The effect of concentration of the substrate ($\text{CH}_3\text{-OH}$) was varied in the range 2×10^{-2} to 8×10^{-2} mol dm^{-3} and keeping $[\text{BIFC}]$, $[\text{H}^+]$ concentration as constant and constant temperature 303K (Table-1). The graph of $\log K_{\text{obs}}$ versus $\log[\text{Methanol}]$ with slope ($r=0.9837$) (Fig-1). The slope of graph indicates that the oxidation reaction was first order.

Effect of varying BIFC Concentration

The effect of BIFC concentration on rate of reaction were studied by changing the concentration of BIFC between the range 0.75×10^{-3} to 2×10^{-3} mol dm^{-3} and fixed $[\text{H}^+]$ and keeping substrate in excess (Table-1). The Positive slope of the graph $\log[\text{titre}]$ versus time confirmed that the reaction should be first order with respect to BIFC.

Effect of varying Perchloric Acid Concentration

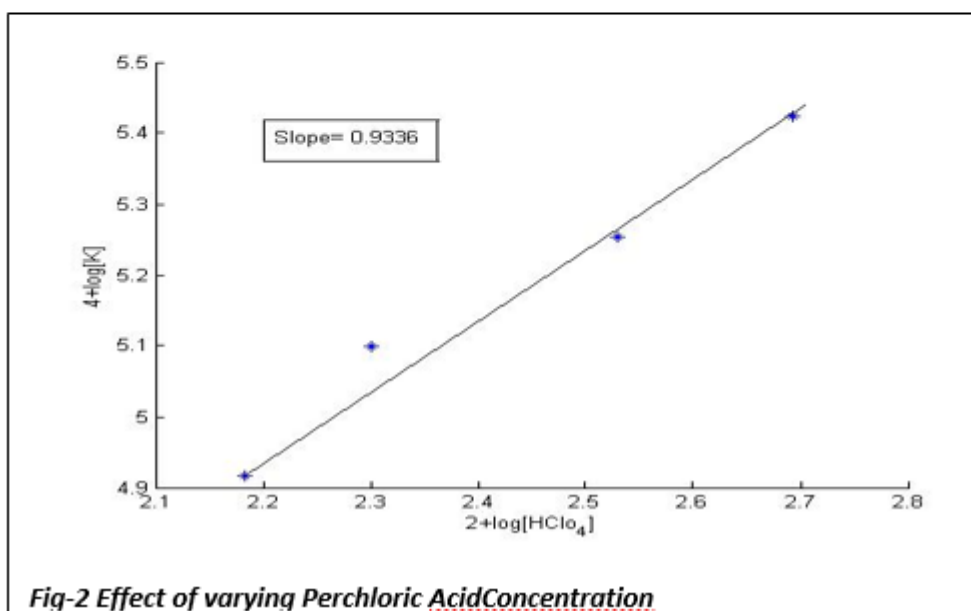
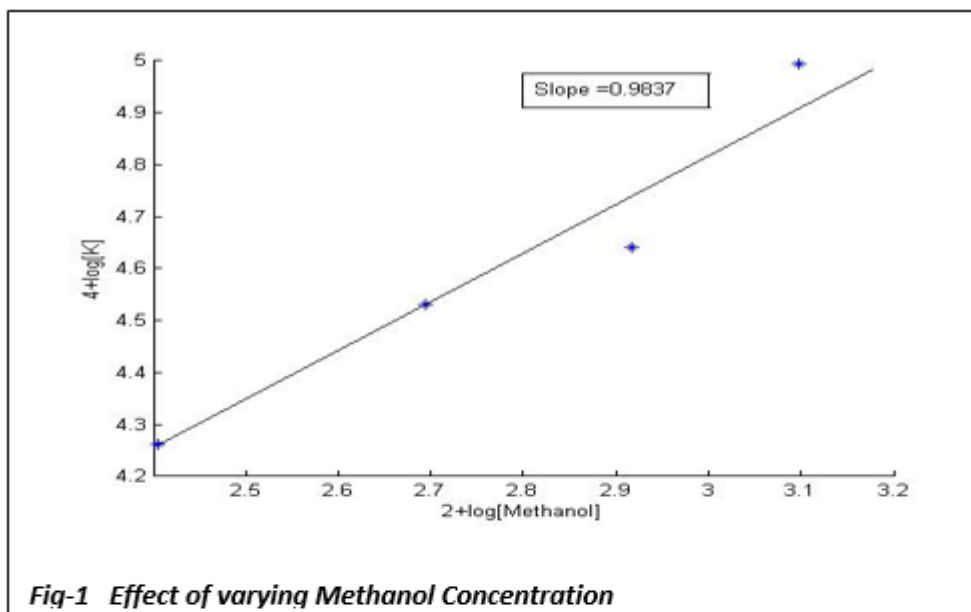
The range of concentration of Perchloric acid were varied between range 2×10^{-2} to 8×10^{-2} mol dm^{-3} and keeping all other concentrations as constant, the rate was studied (Table-1). The slope of graph $\log K_{\text{obs}}$ versus $\log[\text{H}^+]$ was around ($r=0.9336$) which indicates the reaction is pseudo first order with $[\text{H}^+]$ (Fig-2).

Table-1: Effect of Variation of Concentration of [Methanol], [BIFC] and $[\text{HClO}_4]$

$10^2[\text{Substrate}] \text{mol dm}^{-3}$	$10^3[\text{BIFC}] \text{mol dm}^{-3}$	$10^2[\text{HClO}_4] \text{mol dm}^{-3}$	$10^4 K_{\text{obs}} \text{S}^{-3}$
1.5	2	2	1.34
2	2	2	1.73
2.5	2	2	1.98
3	2	2	2.79
2	1.20	2	2.50

2	1.35	2	3.15
2	1.70	2	3.50
2	2	2	3.78
2	2.25	2	3.97
2	2	4	2.97
2	2	6	3.35
2	2	8	3.67

Acetic acid:H₂O [50:50], T=303 K



Effect of varying Ionic Strength

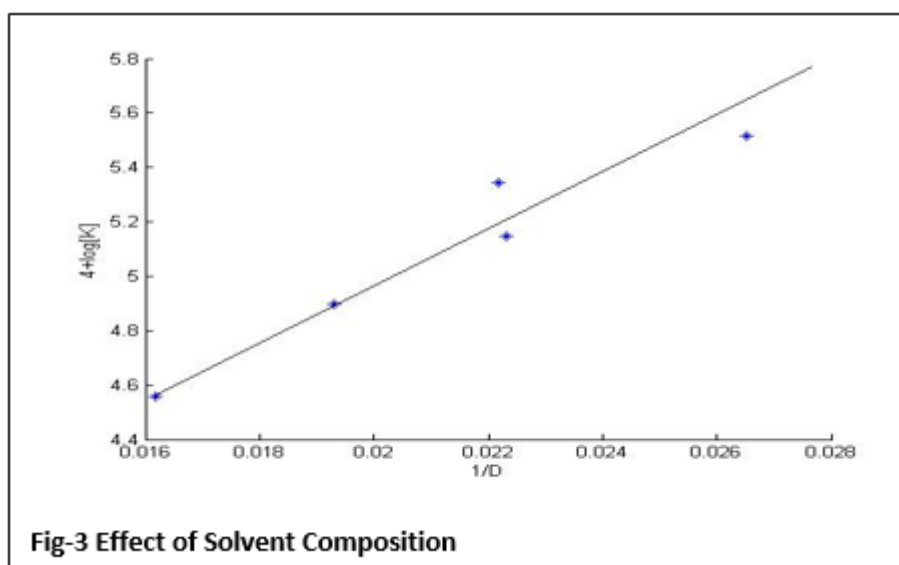
The effects of ionic strength were studied by varying the concentration of HClO_4 and keeping other concentration as constant. By observation we concluded the rate constant increase by increasing HClO_4 concentration. This effect suggests that the involvement of an ion and a neutral molecule in the rate determination step.

Effect of Solvent Composition

In the study of effect solvent composition dielectric constant are calculated approximately from the pure solvent. The less value of dielectric constant of solvent composition favours the oxidation of reaction process (Table-2). It was found that the reaction rate increases with increase in the percentage of Acetic acid.

Table-2: Dependence of Rate on Solvent Composition

% Acetic Acid: Water	Dielectric constant	$K_{\text{obs}} \times 10^4 (\text{S}^{-1})$
40-60	61.8	6.35
45-55	55.8	4.95
55-45	49.8	4.15
60-40	43.7	3.56
50-50	50.1	2.34



Effect of Temperature

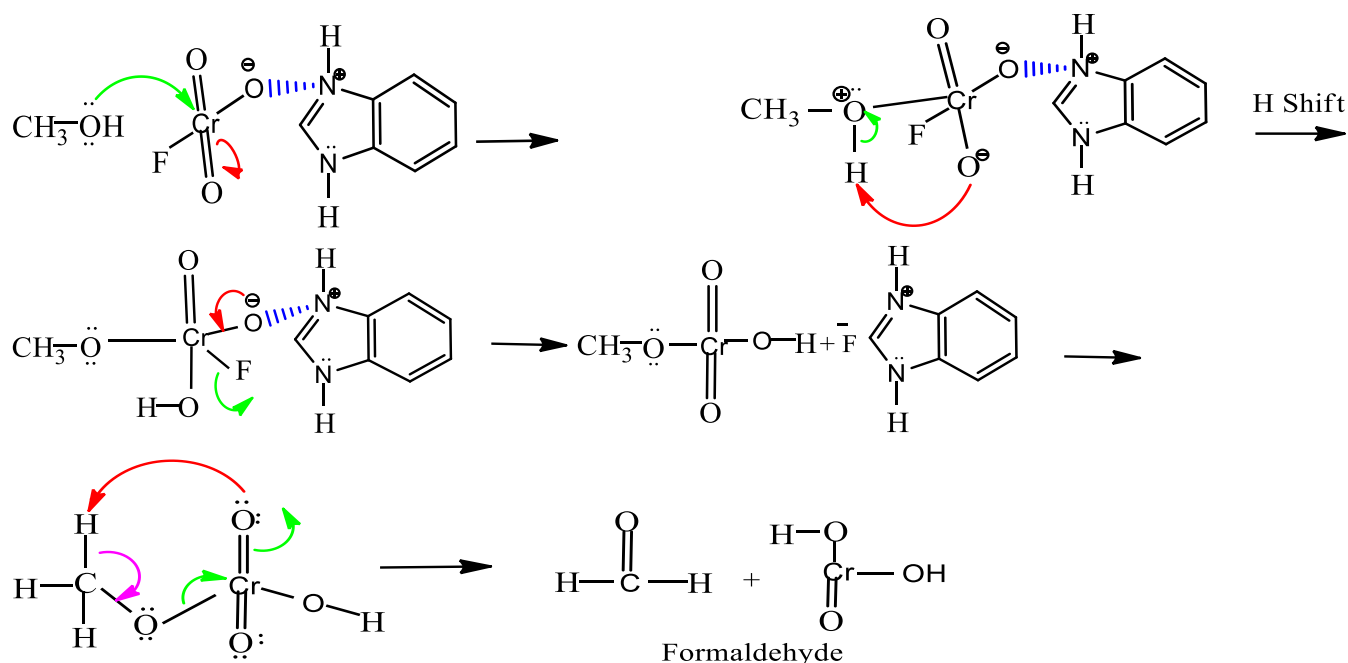
The oxidation reaction was conducted on different temperatures like 298, 303, 308 and 318K and rate of reaction values are given in Table-3. Eyring's²⁴⁻²⁵ graph of $\log K_{\text{obs}}/T$ versus $1/T$ getting linear with slope ($r=0.988$) and $\Delta H^\ddagger = 54.36 \text{ KJ mol}^{-1}$ and $\Delta S^\ddagger = -143.23 \text{ JK}^{-1} \text{ mol}^{-1}$ are obtained from intercept and slope of the graph.

Table-3 Effect of Temperature

Temperature K	$K_{obs} \times 10^4 (S^{-1})$
298	1.47
303	1.85
308	2.89
318	3.94

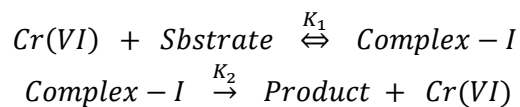
IV. MECHANISM

On the basis of the results, the following reaction mechanism is proposed. The oxidation of methanol gives formaldehyde as a product.



V. RATE LAW

The rate law derived on the basis of above mechanism as follows



The proposed mechanism was followed by the rate law as

$$\text{Rate} = K_1 K_2 [Cr(VI)][\text{Substrate}]$$

$$K_{obs} = K_1 K_2 [\text{Substrate}]$$

VI. CONCLUSION

In this oxidation kinetic parameters the effect of ionic strength and solvent polarity suggest the participation of an ion and a neutral molecule in the mechanistic step. The present method of estimation of alcohol is expected to be based on the oxidation of primary alcohol to aldehyde and associated reduction of oxidation state Cr(VI) to Cr(III). The reaction were performed by monitoring the increasing the concentration of Benzimidazolium fluorochromate spectrophotometrically using UV spectrophotometer. The reaction was studied under Pseudo- First order condition by using an excess of substrate over Benzimidazolium Fluorochromate. k_{obs} are independent of initial concentration of Benzimidazolium Fluorochromate, the rate of reaction increases with increase in the concentration of Methanol linearly. Reaction rate depend on reductant concentration at different temperature and it calculated from double reciprocal plots. The rate of reaction constants, k_{obs} , are evaluated from the linear plots of $\log [BIFC]$ vs time. The observed multivariate and simple linear regression analysis data was carried out by using the least-squares method.

Acknowledgement: The authors are thankful to Department of Chemistry, Maharashtra Udyagiri Mahavidyalaya Udgir and Dayanand Science College Latur for providing the laboratory facilities.

VII. REFERENCES

- [1]. Laidler Keith J -Chemical kinetics, third edition, Pearson Education Ltd (Indian reprint) Delhi. 2004, 1-2.
- [2]. Sivamurugan V., Abraham Rajkumar G., Arabindo B., Murugesan V., Indian J. Chem., 2005,44,144.
- [3]. Wiberg K. B., Physical Organic Chemistry, Wiley New York, 1964.
- [4]. Connors K.A. The study of reaction rates in solution. Chemical Kinetics. VCH, Weinheim. 1990.
- [5]. Wilkinson F., Chemical Kinetics and Reaction Mechanism, VNR Company, New York 1980.
- [6]. Dhariwal V., Yuvajurvedi D., Sharma P.K.; J. Chem. Res., 194(1997).
- [7]. Gurumurthy R., Gopalkrishnan M., Karthikeyan B., Asian J. Chem., 10, 476(1998).
- [8]. Kubhat V., Sharma P.K., Banerji K.K., Ind. J. chem., 39A, 1169(2000).
- [9]. Patil S.G., Joshi S.B., Asian J. chem., 14, 130(2002).
- [10]. Dave I., Sharma V., Banerji K.K., Indian J.Chem. Soc., 79, 347(2002).
- [11]. Nalawaya N., Jain A., J. Indian Chem. Soc., 79,587(2002).
- [12]. Kavita S., Pandurangan A., Indian J. chem., 44A, 715(2005).
- [13]. Bhuvaneshwari D.S., Elengo K.P., Int. Chem. Kintetics, 37,160(2005).
- [14]. Amis E. S., Solvent Effect on Reaction Rates and Mechanism, Academic Press: New York, 1967: 42.
- [15]. Scatchard G. Statistical Mechanics and Reaction Rates in Liquid Solutions. Chemical Reviews. , 1932, 10(1), 229-40.
- [16]. Amis E.S., Lamer V.K. The Gelatin of Brom Phenol Blue, Science. 1939 , 90(2326), 90-1.
- [17]. LaMer V.K., Frank J. Inst. 225, 709 (1938). Google Scholar Crossref., CAS. 1939.
- [18]. Laidler K.J., Eyring H. The effect of solvents on reaction rates. Annals of the New York Academy of

- Sciences. 1939 , 39(1), 303-40.
- [19]. Amis E.S. Selective Solvation and Dielectric Saturation as Related to Electron Exchange Reactions. *The Journal of Chemical Physics*. 1957, 26(4), 880-1.
- [20]. Basim H. Asghar, S. Sheik Mansoor, A. Mohamad Hussain, V. Saleem Malik, K. Aswin, S.P.N. Sudhan. *Arabian Journal of Chemistry*., 2013, 1878-5352
- [21]. Hallale S.N., Patwari S.B., Mandawad G.G., *International Journal of Science and Research*, 2015, Vol-4, Issue-12, pp-1062-1066.
- [22]. Olson A.R., Simonson T.R. Rates of ionic reactions in aqueous solutions. *The Journal of Chemical Physics*. 1949, 17(12), 1167-73.
- [23]. Arrhenius S. Über die, Reaktionsgeschwindigkeit bei der Inversion von Rohrzucker durch Säuren. *Zeitschrift für physikalische Chemie*. 1889, 4(1), 226-48.
- [24]. J. Dharmaraja, K. Krishnasamy and M. Shanmugam. *E-Journal of Chemistry*, Vol.5, No.4, pp.754-760, Oct-2008.
- [25]. I. Vannamuthu, V. Saleem Malik, S. Syed Shafi and S. Sheik Mansoor, *Chemical Science Transactions E-Journal*, 2015, 4(3), 694-703.
- [26]. Dogra S K and Dogra S. *Physical Chemistry through problems*-New Age International Publisher-2001, 587.
- [27]. Boekel M.A., T.S. Van, Tijssken L.M. *Kinetic modeling in Food process*, Woodhead publishing Ltd., 2001, 35-59.
- [28]. Donala A., M.C. Quarrie & Simon John D -*physical chemistry-A molecular approach*-viva Low priced Student edition, New Delhi., 2003, 1047.

A Brief Review on Synthesis of Meldrum Acid Chalcone Derivatives and It's Pharmacological Studies

Kuldeep T. Padhyar, Nandkishor Shirsath, Navanand B. Wadwale, Milind C. Nagare, Avinash U. Nerkar,
R.S. Nirwan*

Department of Chemistry, MGVs M.S.G. College Malegaon Camp Malegaon, Maharashtra, India

ABSTRACT

This review presents a arranged and complete investigation of the method of preparation, the chemical reactivity, and the anti-microbial properties linked with this system Meldrum acid and its chalcones are possible pharmacological and biologically active molecules got from the ordinary source. Meldrum's acid has been used in the plan and synthesis of various types of heterocyclic compounds and considered as a activehouseslab in organic synthesis activity. Meldrum acid is a useful stage in irregular organocatalysis. This work clarifies the current information about synthesis applies, pharmacologic importance, and scientific applications of Meldrum acid chalcone derivatives. Meldrum's acid and its derivatives have established their effectiveness and flexibility in organic synthesis. Showing very unusual properties and multiple sides of reactivity, this small construction has become the grounding of many synthetic methodologies. The DFT worldwide chemical awareness signifiers were calculated for the created compounds and used to predict their relative stability and reactivity.

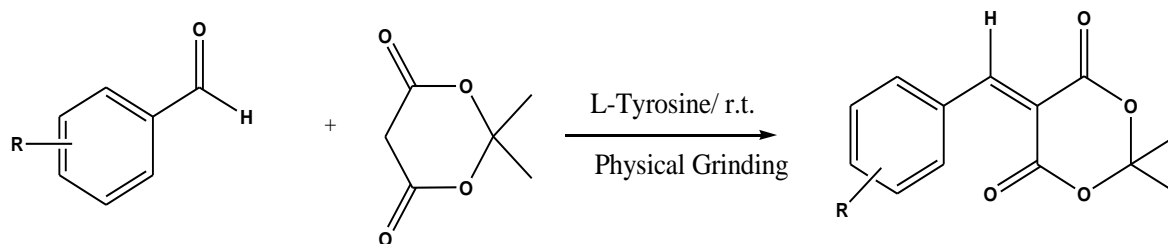
Keywords: Meldrum acid, Chalcone, Aldehyde, Knoevenagel Condensation, Biological Application.

I. INTRODUCTION

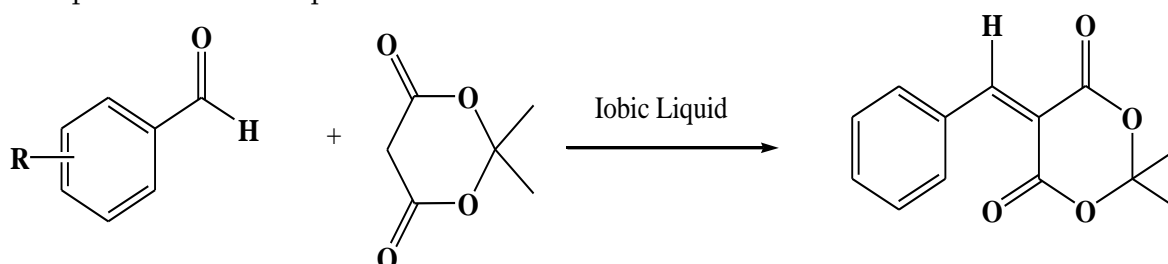
The Structural easiness of Meldrum's combined with is single properties has made this a adaptable reagent inorganic synthesis. The CH_2 group of Meldrum acid is place in between two carbonyl group shows more acidic properties and configuration to approach to hypothesis c-c linkage in organic compounds(1) The condensation of various derivative of aldehyde compounds and Meldrum acid is catalyzed by different bases such as piperidine ,pyridine(2) Knoevenagel condensation of Meldrum's acid and aldehydes gives rise to corresponding alkylidene derivatives. The alkylidene derivatives obtained are versatile substrates for variability of reactions. (3)

Synthesis:

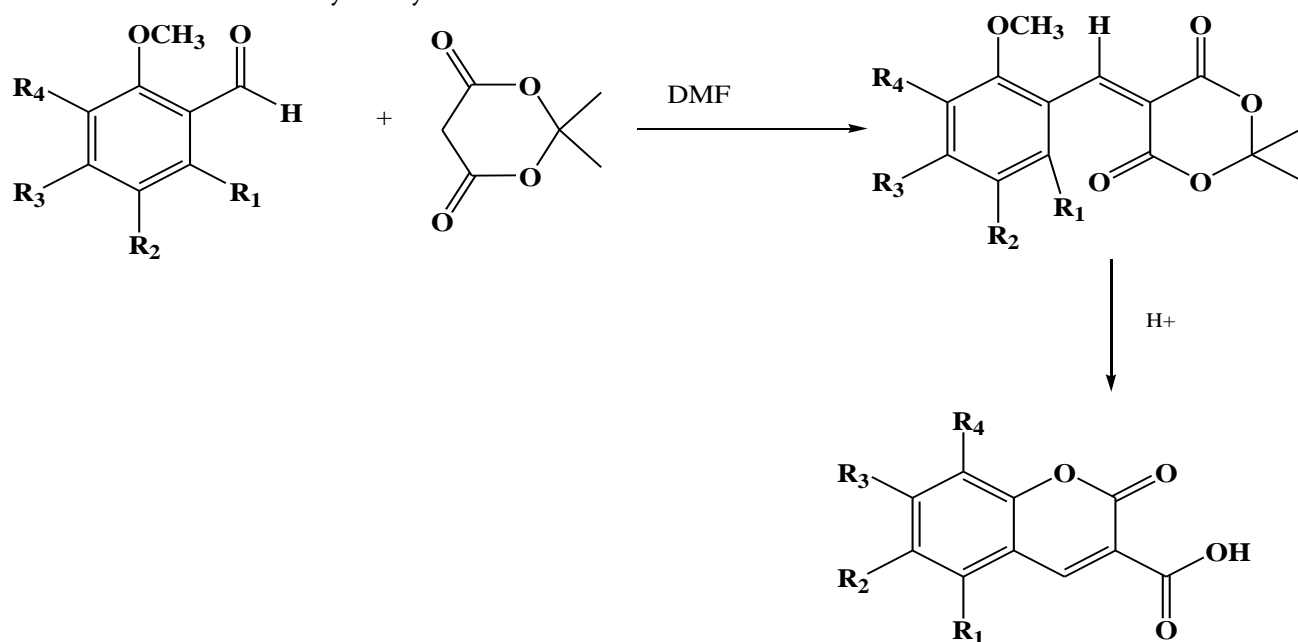
G.Tirupati et al. (4) have synthesized Meldrum acid chalcone derivatives by using L-Tyrosine as an Recyclable and Effectual Catalyst for Knoevenagel Condensation of Arylaldehydes with Meldrum's Acid in Solvent-Free Condition under Grinder Method.



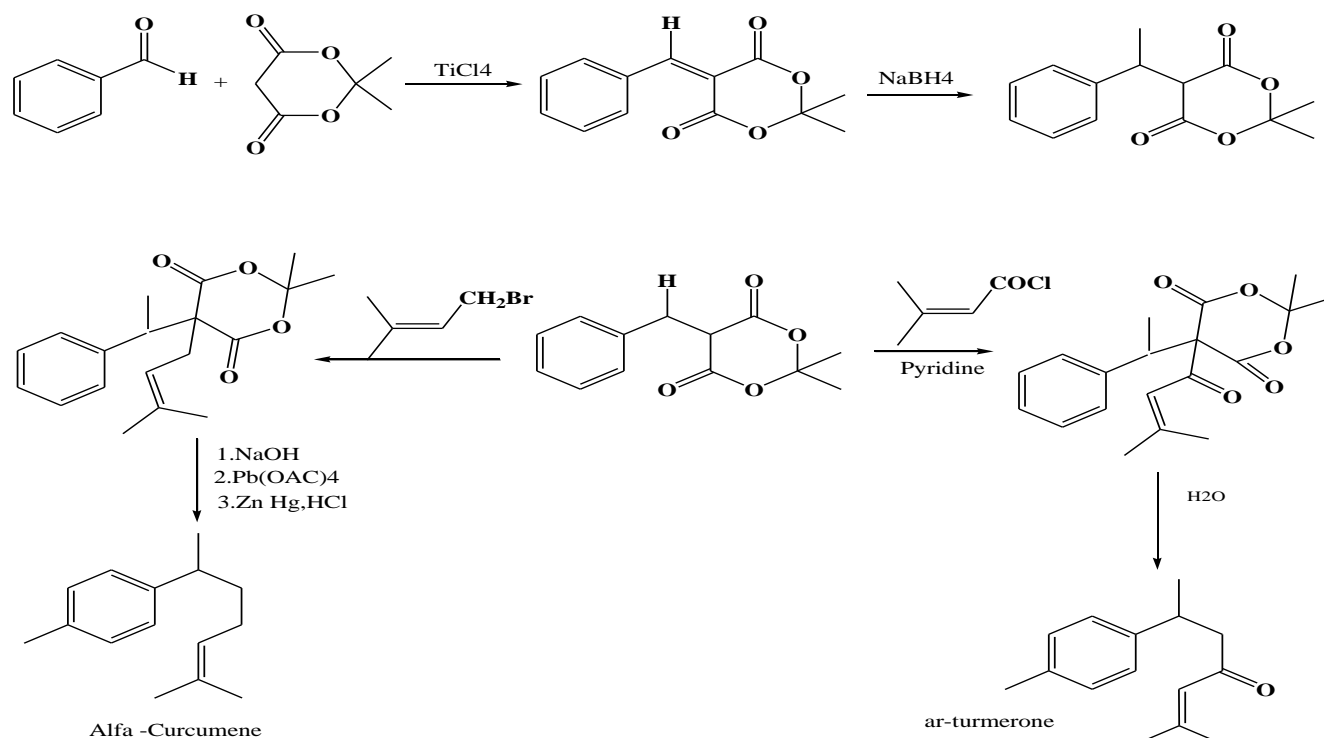
Nitin Darvatkar et al.(5) reported the Knoevenagel condensation of Meldrum acid and different derivatives of aldehyde in presence of ionic liquid at R.T.



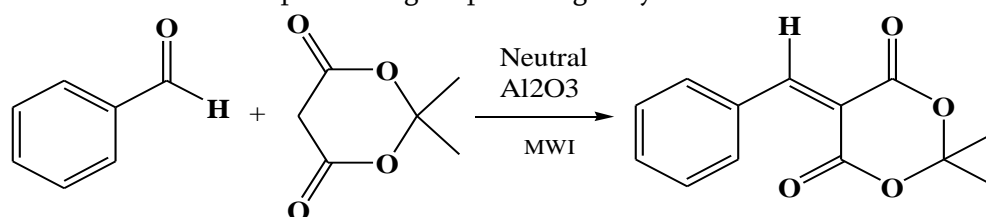
Veronica Armstrong et al (6) synthesized the 3-Carboxycoumarins from O-methoxy benzaldehyde and Meldrum acid via o-Methoxy benzylideneMeldrum acid derivatives



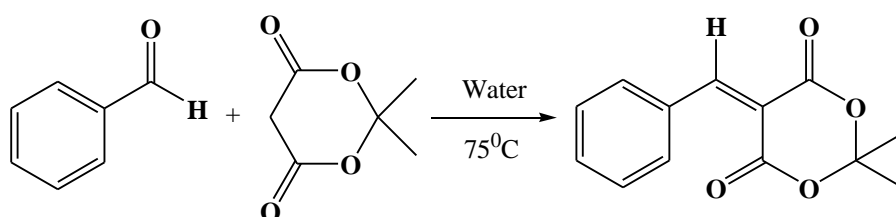
Mahulikar et al. (7) explains the application of Meldrum acid in synthesis of natural product i.e., alfa curcumin and ar-turmerone



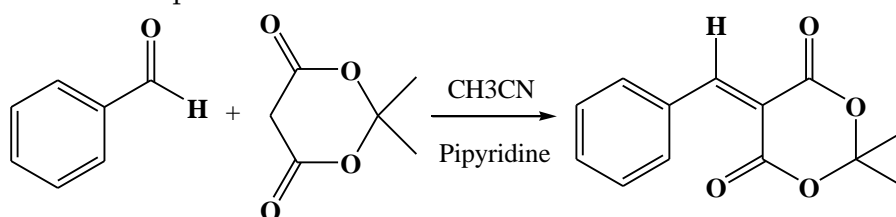
Manas Chakrabarty et al (8) reported Knoevenagel condensation of Meldrum acid by using Neutral Alumina in Microwave Irradiation and developed the higher percentage of yield and short reaction time.



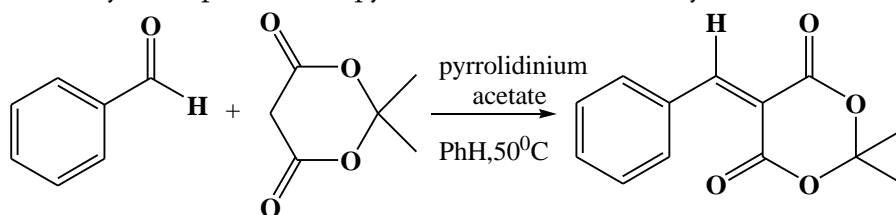
Till Drennhaus et al. (9) synthesized the Meldrum acid chalcone derivative by using aldehyde and Meldrum's acid were suspended in water and heated up to 75°C . The reaction mixture was stirred until the condensation was completed.



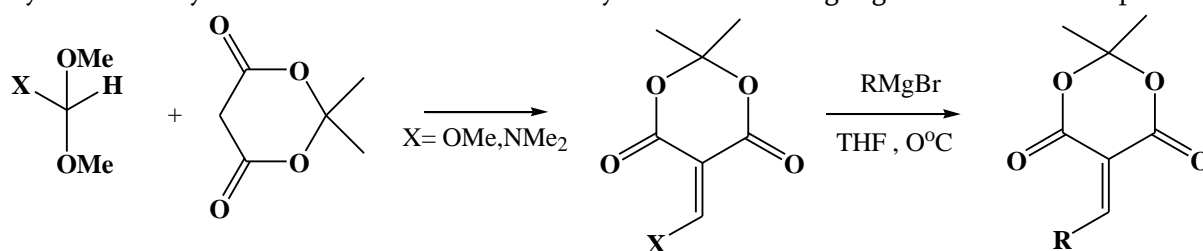
Till Drennhaus et al. (9) also developed the synthesized Meldrum acid chalcone derivatives by Meldrum's acid was dissolved in CH_3CN (10 mL), then aldehyde and piperidine were added. The reaction was stirred until the condensation was completed.



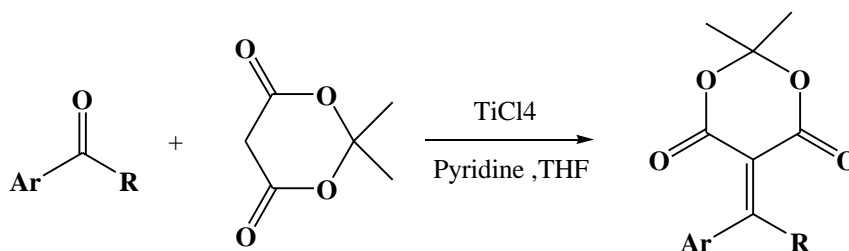
Aaron M.Dumas et al. (10) Synthesis of alkylidenes derived from aldehydes can be achieved under a large variety of conditions Alkylidene Meldrum's acids are prepared by the Knoevenagel condensation of Meldrum's acid and aldehydes in presence of pyrrolidinium acetate-catalysed condensation in benzene .



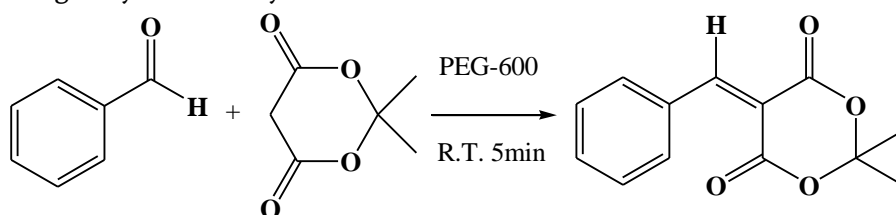
Aaron M.Dumas et al. (10) discovered the alternative route is the preparation of methoxy- or dimethylaminomethylene Meldrum's acids followed by elimination using organometallic nucleophiles .



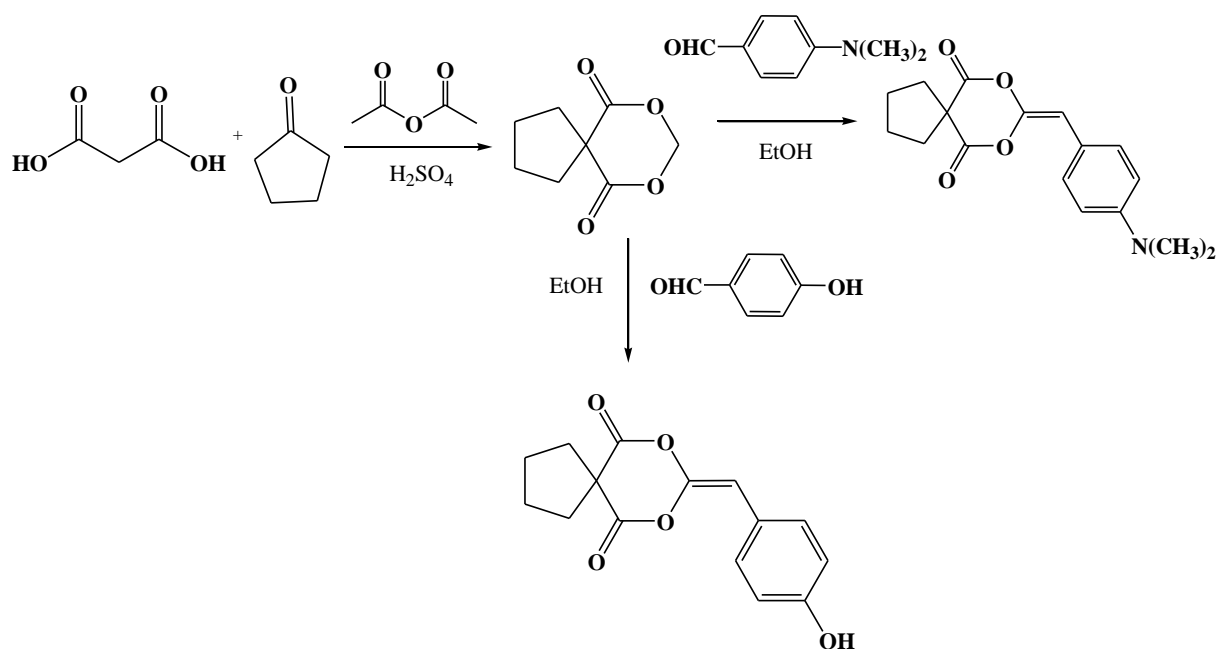
Alkylidenes derived from ketones are nearly always prepared by using the TiCl_4 -mediated condensation in presence of pyridine of ketones with Meldrum's acid.



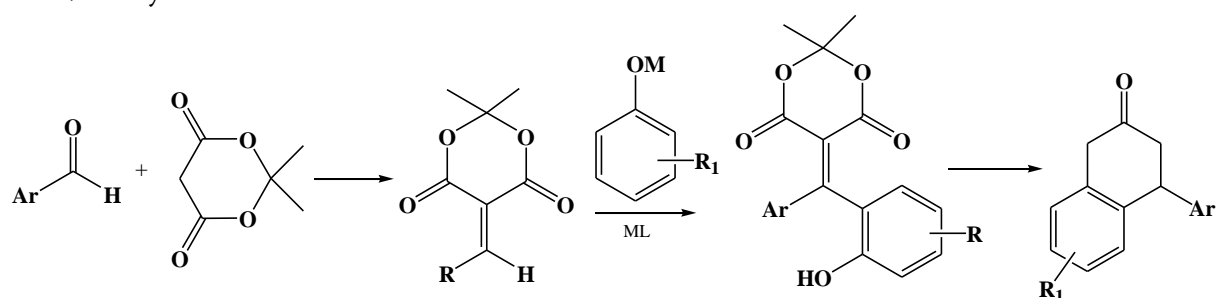
Babasaheb Bandgar et al (11) developed eco-friendly protocol for the uncatalyzed Knoevenagel condensation in PEG-600 at R.T. with good yields of alkylidenes derivatives of Meldrum acid



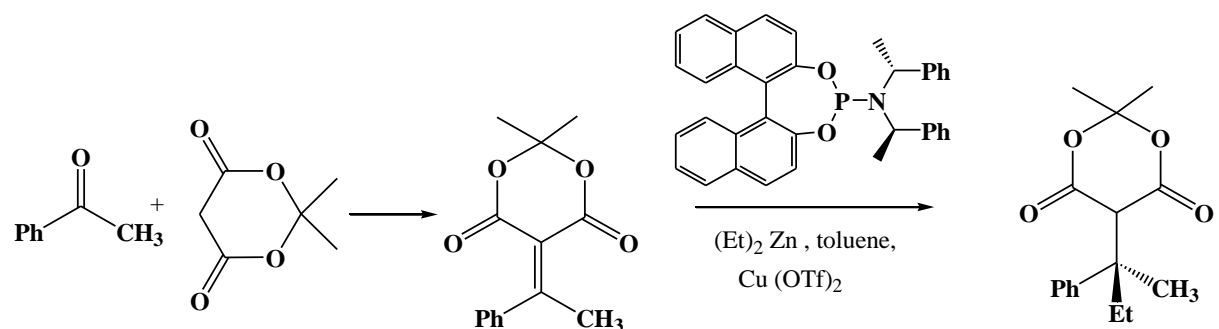
Jinhe Jiang (12) synthesized the Ox spirocyclic compound by using a mixture of malonic acid and acetic anhydride in strong sulfuric acid was stirred at 303K then added cyclopentanone dropwise and allowed to proceed for 3 h. after completion of reaction cool and filtered then above compound was react with benzaldehyde in ethanol to formed oxacyclic compounds.



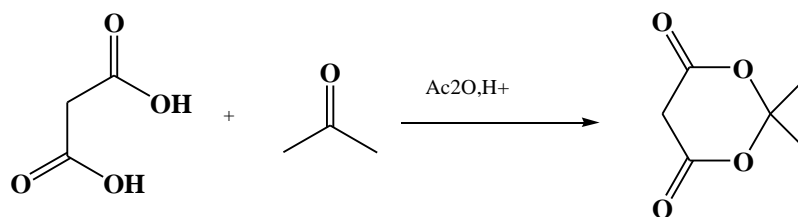
The David Thmpson (13) Moon was worked in his Master of Science degree thesis on the conjugate addition of Novel Nucleophiles and catalytic Intramolecular Tandem cyclization and Friedel-Crafts acylation with alkylidene Meldrum acid Derivatives. Addition of Metal Phenolates on to Alkylidene Meldrum's Acids by C-Alkylation/O-Acylation as shown in below



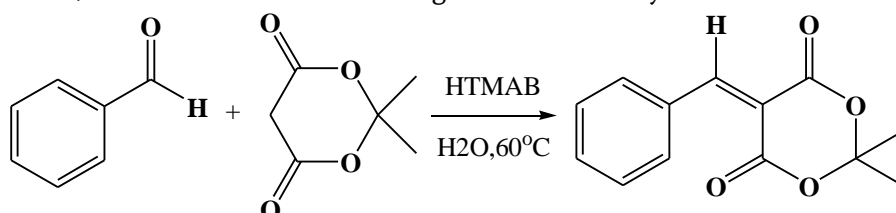
The David Thmpson Moon (13) was also work on Conjugate Addition of Dialkylzinc Reagents onto Alkylidene Meldrum's Acids via a Chiral Copper catalyst



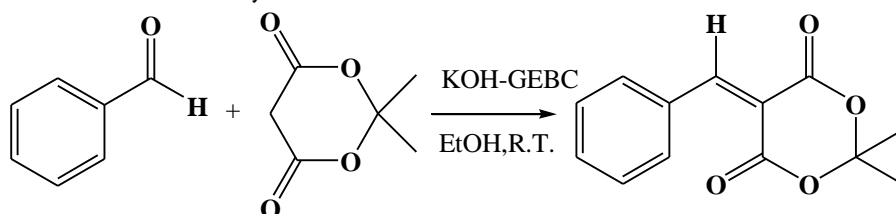
Tong-Shou Jin(14) to a solution of malonic acid in 4.8 mL of acetic anhydride, sulfuric acid was added while stirring and cooling in ice water. Acetone (4.0 mL) was added after 20 minutes, the mixture was stirred for 6 hours, and was then allowed to stand overnight in the refrigerator, and the resulting crystals filtered off.



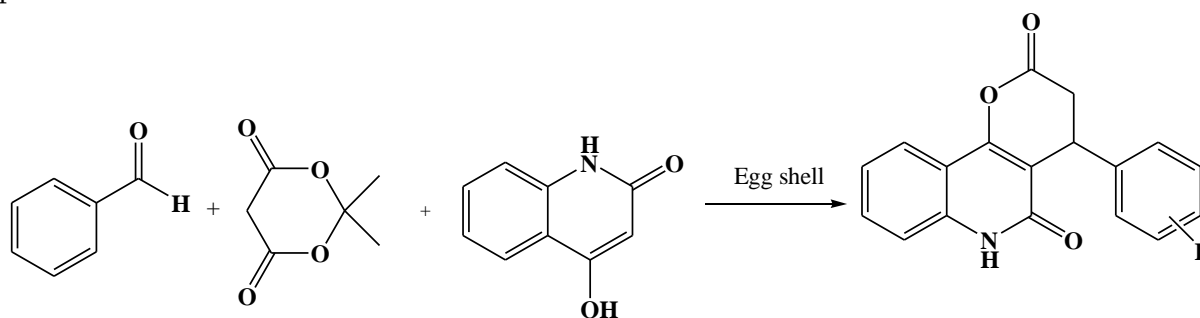
Tong-Shou Jin(14) was worked on a solution of an aromatic aldehyde and isopropylidene malonate in water was heated in the presence of a catalytic amount of HTMAB, and the corresponding 5-arylmethylene-2,2-dimethyl-1,3-dioxane-4,6-diones 3 were obtained in good to excellent yields



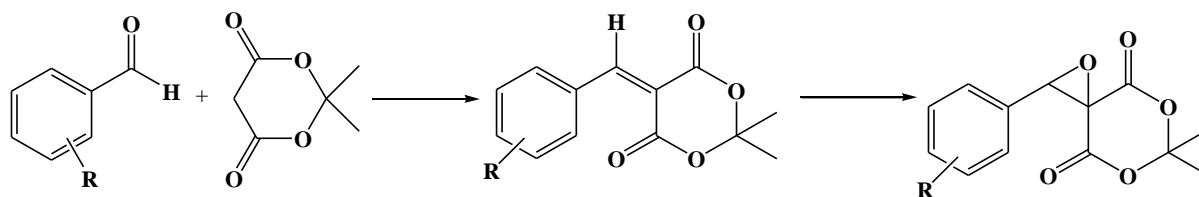
Shital Shinde et al (15), was take equimolar mixture of Meldrum acid and benzaldehyde was stirred in the presence of 1 g of various GEBCs (Gel Entrapped Base Catalysis) in EtOH at Room temperature until the completion of reaction as monitored by TLC.



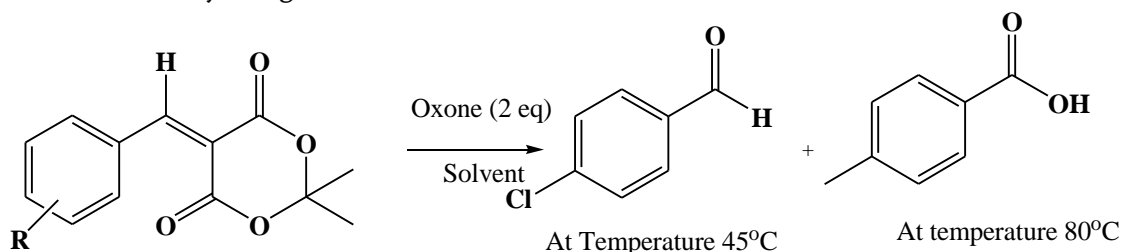
Leila Youseftabar Miri et al (16) reported a green and efficient heterogeneous catalyst for the synthesis of pyrano [3,2-c] quinoline derivatives by using a mixture of aromatic aldehyde and Meldrum's acid with eggshell in 3 ml EtOH stirred at 60 ° C (oil bath) and then added of 4-hydroxyquinolin-2(1H)-one 3 (1 mmol) to mixture of the starting materials. After completion, the reaction mixture was filtered and the obtained precipitate washed with hot ethanol.



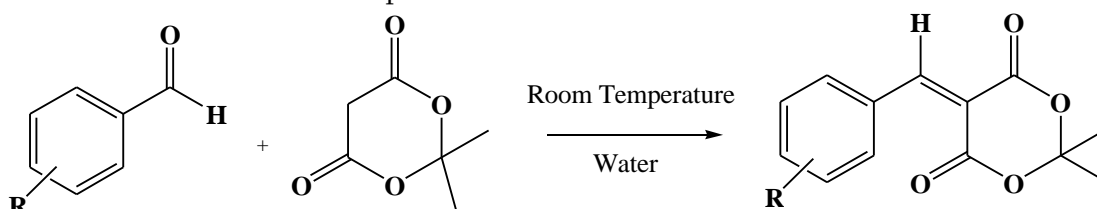
Harmeet Sandhu et al (17) reported the synthesis of arylidene derivatives of meldrum acid and its biological evaluation of meldrum acid as a antimalarial and antioxidant agent. Harmeet Sandhu et al proposed the synthetic route of arylidene and epoxide derivatives of meldrum acid.



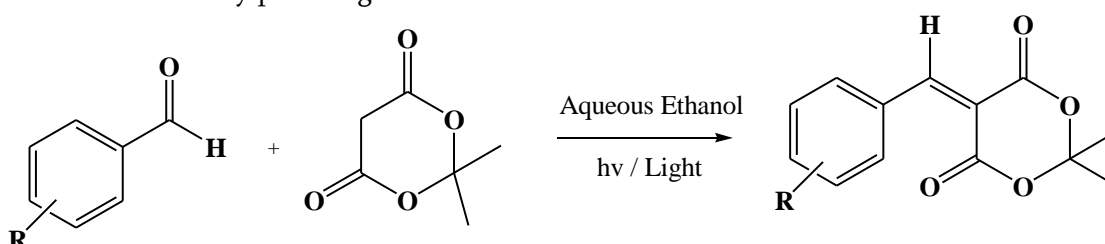
Muthish Suresh et al (18) reported the transition metal free expedient approach for the c=c bond cleavage of arylidene meldrum acid by using various oxidant.



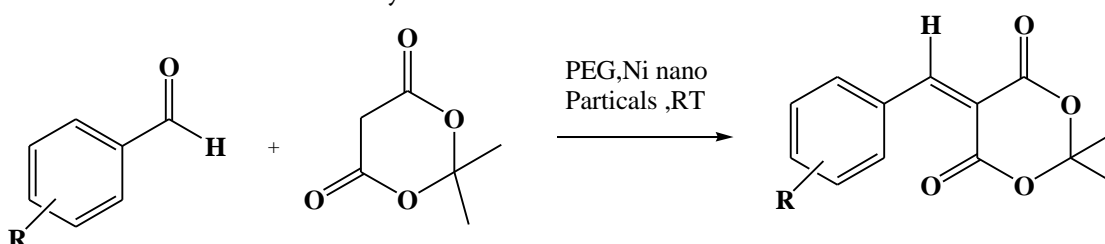
Mohit Deb et al (19) synthesized the arylidene Meldrum acid derivatives from aldehydes and meldrum acid by using water as a solvent at Room Temperature.



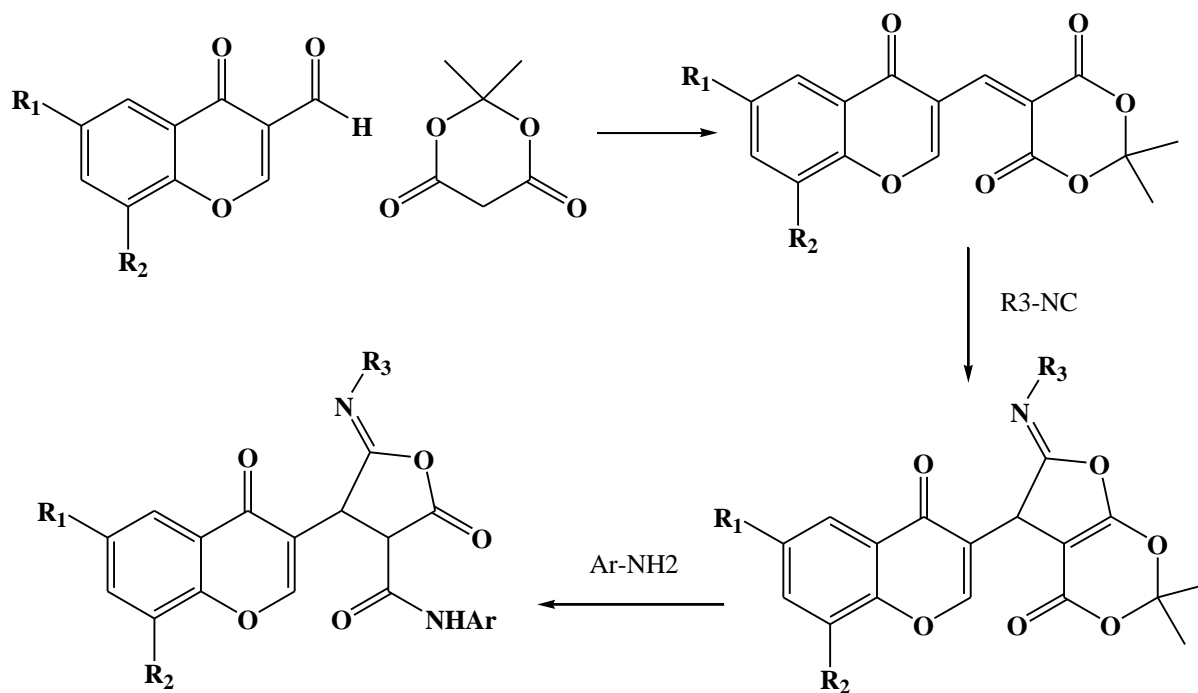
Somnath Ghosh et al (20) reported Knoevenagel condensation of meldrum acid with aromatic aldehydes in aqueous ethanol initiated by photo-light.



Jitender Khurana et al (21) reported Nickel nanoparticles catalyzed chemoselective Knoevenagel condensation of Meldrum's acid and substituted aldehyde.



Mohammad Bagher et al. (22) we have developed a pseudo-five-component condensation reaction for the formation of biologically interesting tripeptide-bound chromones, which is one-pot and atom and step economic.



II. CONCLUSION

The purpose of this review is to cover systematically work on the Meldrum acid chalcone derivatives of the Meldrum's acid and the application of these processes in synthetic organic chemistry. The present study was initiated with the aim of providing an efficient and convenient method for the synthesis of arylidene analogues of Meldrum's acid. The optimization of the synthetic procedure was carried out.

III. REFERENCES

- [1]. Uday V. Desai, D. M. Pore, R. B. Mane, S. B. Solabannavar, and P. P. Wadgaonkar synthetic communications Vol. 34, No. 1, pp. 25–32, 2004
- [2]. M.A.P. Martins, C.P. Frizzo, D.N. Moreira, L. Buriol, P. Machado, Chem. Rev. 109, 4140 (2009)
- [3]. L.R. Madivada, R.R. Anumala, G. Gilla, S. Alla, K. Charagondla, M. Kagga, A. Bhattacharya, R. Bandichhor, Org. Process Res. Dev. 13, 1190 (2009)
- [4]. G. Thirupathi, M. Venkatanarayana, P. K. Dubey, and Y. Bharathi Kumari, Hindawi Publishing Corporation Organic Chemistry International Volume 2012, Article ID 191584.
- [5]. Nitin B. Darvatkar, Amol R. Deorukhkar, Sachin V. Bhilare, and Manikrao M. Salunkhe Synthetic Communications, 36: 3043–3051, 2006, Taylor & Francis Group, LLC
- [6]. Veronica Armstrong, Oriana Soto, Jaime A. Valderrama and Ricardo Tapia synthetic communications, 18(7), 717-725 (1988)
- [7]. P.P. Mahulikara and R.B. Maneb, Journal Of Chemical Research 2006
- [8]. Manas Chakrabarty, Ratna Mukherjee, Manju Chakrabarty, Shiho Arimac and Yoshihiro Harigayac

Letters in Organic Chemistry, 2006, 3, 868-871

- [9]. Till Drennhaus, Laura ohler, SavehDjalali, Svenja Hofmann,a Clemens Mjuller,aJorgPietruszka, and Dennis Worgull *Advanced Synthesis & Catalysis* 10.1002/adsc.202000039
- [10]. Aaron M. Dumas And Eric Fillion *Accounts Of Chemical Research* Vol. 43, No. 3 March 2010 440-454
- [11]. Babasaheb P. Bandgar, A,B Balaji L. Korbadi, A Sachin A. Patil, A Sunita B. Bandgar, A Hemant V. Chavan, A and Baliram S. Hote , *Aust. J. Chem.* 2008, 61, 700–703
- [12]. Jinhe Jiang and Wulan Zeng , *Crystals* 2016, 6, 134
- [13]. David Thompson Moon A thesis presented to the University of Waterloo in fulfilment of the thesis requirements for the degree of Master of Science in Chemistry , 2008
- [14]. Tong-Shou Jin, Rui-Qiao Zhao, Meng Li, Ying Zhao, and Tong-Shuang Li , *ARKIVOC* 2006 (xiv) 53-58
- [15]. Shital Shinde, Gajanan Rashinkar, Arjun Kumbhar, Santosh Kamble, and RajashriSalunkhe , *Helvetica Chimica Acta – Vol. 94* (2011)
- [16]. Leila Youseftabar-Miri, Fatemeh Akbarib , FarshidGhraghsahar *Iranian Journal of Catalysis* 4(2), 2014, 85-89
- [17]. Harmeet S. Sandhu , Sameer Sapra , Mukesh Gupta , Kunal Nepali , Raju Gautam , Sunil Yadav , Raj Kumar , Sanjay M. Jachak , Manoj Chugh , Manish K. Gupta, Om P. Suri , K. L. Dhar *Bioorganic & Medicinal Chemistry* 18 (2010) 5626–5633.
- [18]. Muthiah Suresh, Anusueya Kumari, Raj Bahadur Singh , *Tetrahedron* 75 (2019) 130573
- [19]. Mohit L. Deb and Pulak J. Bhuyan , *Tetrahedron Letters* 46 (2005) 6453–6456
- [20]. Somnath Ghosh , Jhantu Das, Subhagata Chattopadhyay, *Tetrahedron Letters* 52 (2011) 2869–2872.
- [21]. Jitender M. Khurana , Kanika Vij *Tetrahedron Letters* 52 (2011) 3666–3669
- [22]. Mohammad Bagher Teimouri, Peyman Akbari-Moghaddam, and GolaraGolbaghi , *ACS Comb. Sci.* 2011, 13, 659–66

A Short Review on The Application of Phase Transfer Catalyst (PTC) Towards the Synthesis of Heterocyclic Compounds

Sindhu A. Bhosale¹, Akshaykumar B. Harepatil¹, Rajendra P. Pawar^{3*}, Vidya S. Dofe¹, Vivekanand B. Jadhav^{2*}

¹Department of Chemistry, Deogiri College, Aurangabad, Pin-431003, Maharashtra, India

²Department of Chemistry, Shri Muktanand College Gangapur, Dist.-Aurangabad, Pin-431109, Maharashtra, India

³Department of Chemistry, Shivchhatrapati College, Aurangabad, Pin-431003, Maharashtra, India

ABSTRACT

Phase Transfer Catalyst is a capable and one of the exceptional methods for the synthesis of organic compounds. It enables the migration of reactants from one phase to another phase. PTC is used to relocate the required active form of an anion from the aqueous phase to the organic phase, where the reaction occurs. One of the foremost tasks for the process design of the PTC system is to launch a dependable thermodynamic model capable of describing the phase behavior of all components i.e. organic solvents, inorganic salt, water, and the PTC. Many reactions and experiments are evidence of the applications of Phase Transfer Catalysis. It can reduce number of cycle times and also increases the yield. Some experiments also proved that PTC also eliminates harmful or expensive reagents and solvents, and provide many other benefits to organic chemical manufacturers, so much effort has been directed towards the utilization of PTC in varioussyntheses. There are major advantages of PTC in industrial applications, which can be easily recognized in the mentioned examples. To identify the structures of products, physical and spectroscopic methods were used. Many approaches to Phase Transfer Catalysis are discussed here in this Chemical Literature review.

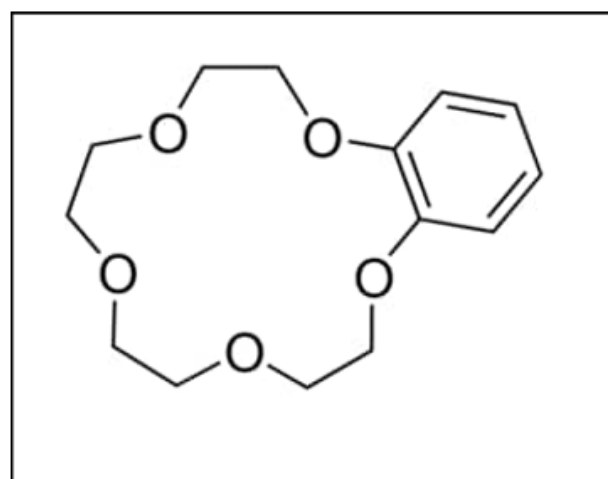
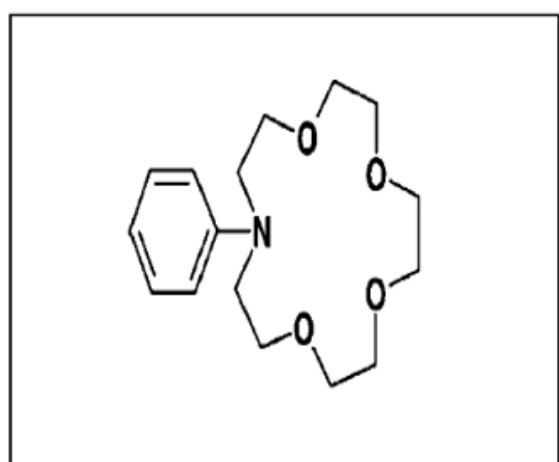
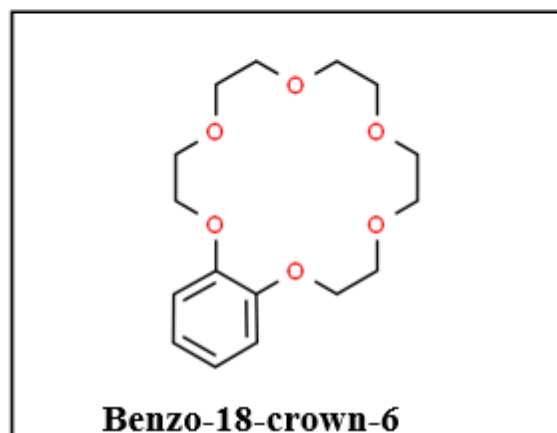
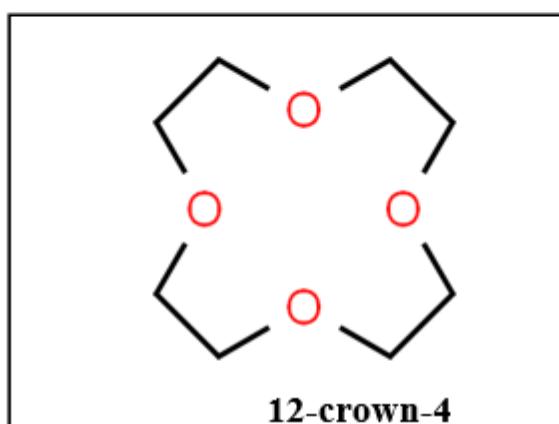
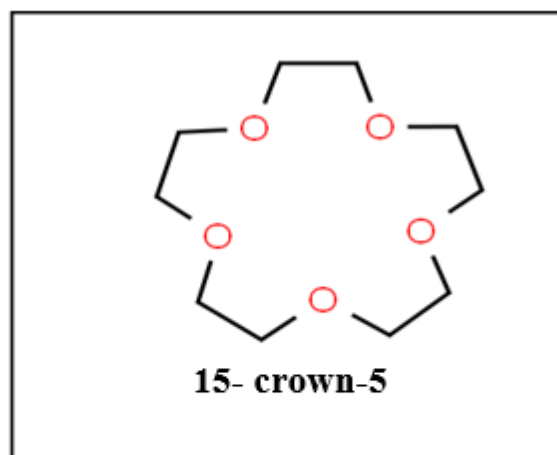
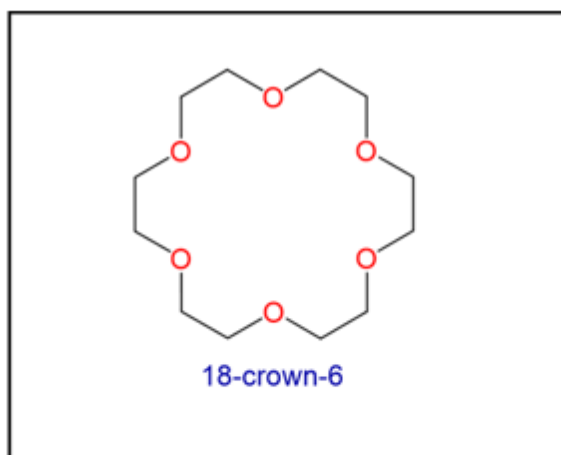
I. INTRODUCTION

We can see lots of industrial applications of PTC. Various processes of organic synthesis. Chemical products of practical applications can be yield by using organic synthesis such as Polymers, dyes, pharmaceuticals, photographic chemicals. Because of the Biological activity of the heterocyclic compounds achieved from some reactions, the compounds have important values in industry.

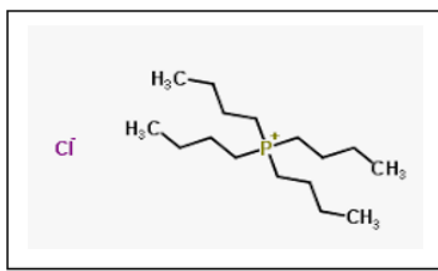
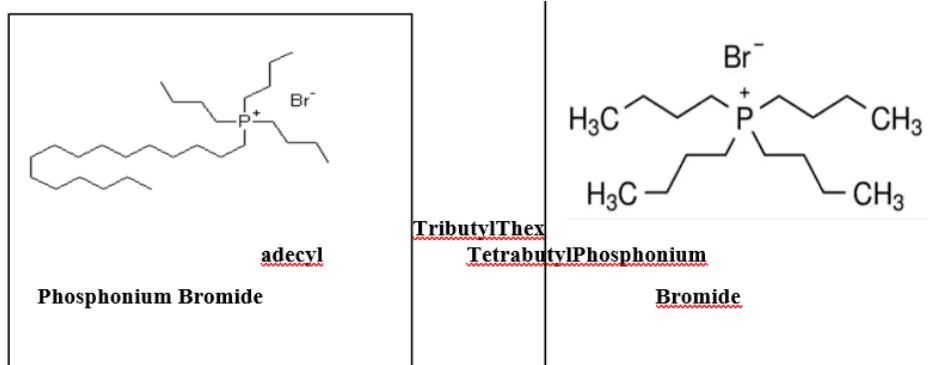
The wastes formed during various chemical reactions can be regenerated, destroyed and disposed, consuming much energy and creating major problem to the environment. It is Essential to use and develop synthetic methodologies that decrease these problems. PTC (Phase Transfer Catalyst) is the most common and effective methodologies that fulfil this requirement.it is identified that number of reactions progressed *via* carbanions, can be Performed competently by using phase transfer catalysts technique. Phase transfer catalysis is beneficial in many industrial approaches. A large number of PTC measures use the liquid-liquid phase transfer catalysis (L-L PTC) mode of procedure.

Types of Phase Transfer Catalysts:-

- 1) Crown Ethers:- (Pugia 1986, Mathias and Carraher 1984, Ganboa 1986, Valentine 1975, Artamkina et al 1984, Salisova 1979, Vogtle 1803, Gockel 1976, Izatt et al 1971, Baker 1981, Wingfield 1980)

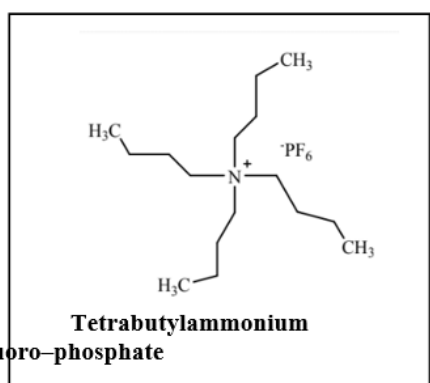
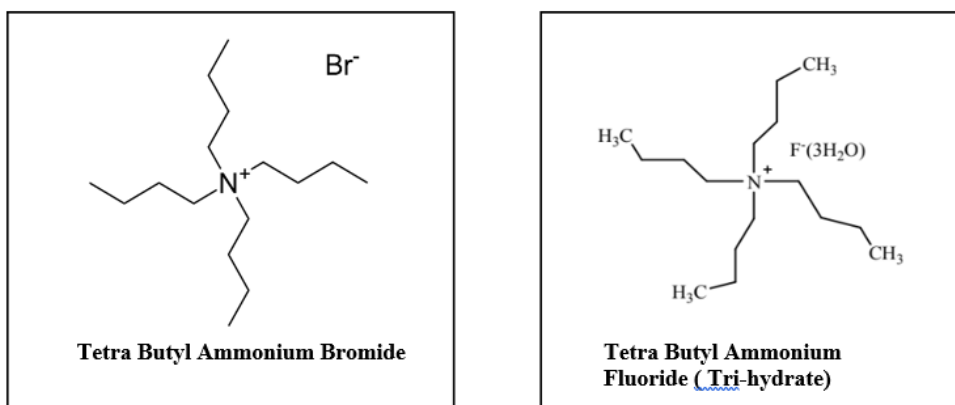


2) **Quaternary Phosphonium salts**(Kisch et al 1986, Alper 1981, McNulty et al 2004, Dehmlov 1977)



Tetra Butyl Phosphonium-Chloride

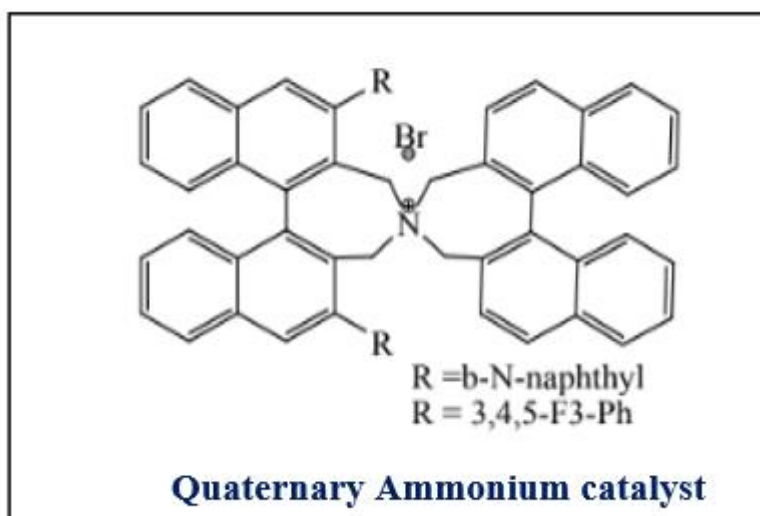
3) **Quaternary Ammonium Salts :-**



Tetra Butyl Ammonium Hexafluoro-phosphate

4) Maruoka Catalyst (Quaternary Ammonium catalysts)

Maruoka (Ooi et al 1999) designed an array of C₂-symmetric, biarylspiro ammonium catalysts.



II. MODES OF OPERATIONS OF PHASE TRANSFER CATALYSIS

There are two modes of operations in PTC

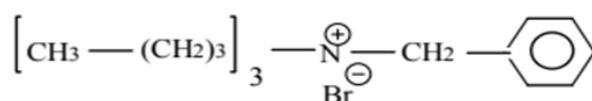
1- Liquid-liquid phase transfer catalysis (L-L)PTC(Lygo et al 1999)

2- Solid-liquid phase transfer catalysis (S-L)PTC (Yadav 2004)

Phase transfer catalysis has been applied in many industrial processes. A large number of PTC processes use the liquid-liquid phasetransfer catalysis (L-L PTC) mode of operation. PTC has been quite successful for C,N,O and S-alkylations involving S_N2 typeractions in fine chemical industries, apart from dehydrohalogenations. The benefits of solid-liquid phase transfer catalysis (S-L PTC) are,the reaction is directed at manageabletemperature, the reaction rate are improved by orders of magnitude and the reaction is 100% selective, in comparison with liquid-liquid phase transfer catalysis (L-L PTC) which is very slow and yields by-products. The mechanism based on homogenous solubilisation of solid resulting in the development of an active ion-pair with nucleophile, was found to prevail in the system.

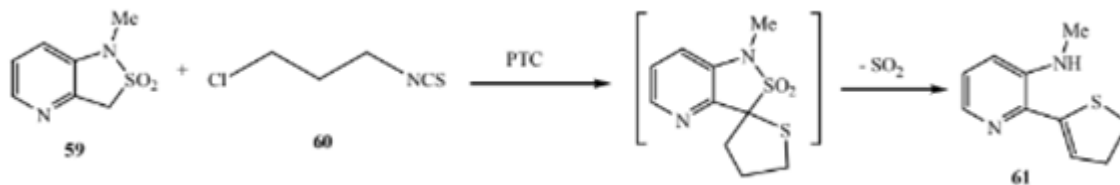
Preparation of the phase transfer catalyst(tributylbenzylammonium bromide) (Amera M. AL-Rubay)

(TBBAB) General Procedure: (AL-Nakshabandy,2005) 10 gm of (0.053 mole) A mixture of tri-butylamine, 9.22 gm (0.053 mole) benzyl-bromide and (50 ml) of dry benzene was positioned in a (250 ml) dry round-bottomed flask which is fitted with a condenser. After refluxing the mixture for (30) minutes, it resulted in a thick solution. Afterwards the precipitate was cooled, filtered and the subsequent white powderwas washed with benzene and recrystallized from a mixture of ethyl acetate and ethanol,giving white crystals of tributylbenzylammonium bromide, m.p(174-175 oC) agrees withthe reported m.p (176 oC) (Aldrich,1989).



III. APPLICATIONS OF PTC

1. Uses of PTC in syntheses of five-membered heterocyclic compounds The reaction of pyridosultam 59 with 3-chloropropylthiocyanate 60 under the condition (toluene/aq. NaOH / TBAB) yielded the corresponding dihydrothiophene derivative 61 (Modrzejewska 2005)



2. Homogenous PTC applications:-

Quaternary ammonium, phosphonium & arsonium salts (generally termed “onium” salts) deliver a source of singly charged lipophilic cations. Overall, catalyst productivity is subjective by the large number of carbon atoms (high lipophilicity) and the symmetry of the carbon atom chains about the heteroatom.

3. PTC for the analysis of carboxylic acids:-

Acidic herbicides, diuretics, urinary acidic moieties and buprenorphine, ethylene thiourea, sulphide, polysulphides, cyanide, and thiocyanate, nitrate, nitrite, methanol, iodide, cyanide, nitrite and thiocyanate, levorphanol, phenols, phenoxyacetic acids and perfluoro-octanoic acid.

4. Heterogenous PTC applications:-

PTC linked to a polymer matrix are described as heterogenous catalysts [59]. Many materials have been developed in this context, some of them specialized to catalyze specific reactions. In this case, the catalyst is bonded to a matrix forming a third immiscible solid phase between the organic and aqueous ones involving a swelling, mixing and diffusion during the reaction. Due to diffusion retardation, reactions with slow intrinsic reaction rates are much slower with a tri-phase catalyst than with its homogeneous counterpart [11,32]. On the other hand, the use of tri-phase PTC simplifies the removal of the catalyst after the reaction which can be re-used until they lose their mechanical stability [9,63,64]. In general, a polymer-supported catalyst consists of a hydrophobic polymer backbone solvated in the organic solvent and a hydrophilic part containing water and the nucleophile. In agreement to the extraction mechanism for homogenous PTC reactions, phase-transfer cycle in a tri-phase PTC consists of an ion-exchange step in the aqueous phase followed by the reaction in the organic-phase. A major difference between the two mechanisms is that in a tri-phase PTC system the catalyst movement is restricted and the organic and aqueous reagents must be brought to the catalyst cation. The catalyst structure and loading, the spacer chain, the polymer structure, the agitation and the swelling power of the solvent, the concentration of reactant, the type of the anion, the organic leaving group and the catalyst cation are some of the criteria that should be considered in tri-phase PTC.

5. PTC has been quite successful for C,N,O and S-alkylations involving S_N² type reactions in fine chemical industries, apart from dehydrohalogenations. *o*-Nitrodiphenyl ether (Yadav 2004) is an important intermediate in the fine chemical industry and used in a number of drugs.

IV. CONCLUSION

As per the literature survey, some reactions were observed. A reaction was accomplished in phase transfer catalysis conditions using solid-liquid phase system [dioxin/ K_2CO_3 /tetrabutyl ammonium bromide (TBAB)], where the reactants in dioxane made the organic phase in which potassium carbonate was suspended. The reaction was synthesized with Tetra butyl ammonium bromide (TBAB). The reaction mechanism contains two consecutive catalytic cycles, the first one specifically proton abstraction of the nucleophile, takes place on the surface of solid carbonate. The anion is formed and it migrates as an ion pair with the catalytic cation into the organic phase, where the second step concerned with the substitution reaction was occurred. The two cycles occur again to give the final cyclized product.

V. REFERENCES

- [1]. Tremillon, In: Reactions in solutions. An applied analytical approach. J. Wiley (Eds.), Chichester, (1997).
- [2]. A. Bunton, In: Surfactant Science Series; M. Gratzel, K. Kalyanasundaram, Eds.; Marcel Dekker, Inc.: New York, Vol. 38 (1991).
- [3]. V. Dehmlow, *Angew. Chem.Int. Ed. Eng.*, 16 (1977) 493.
- [4]. R. Knapp, In: Analytical Derivatization Reactions. J. Wiley (Eds.), New York, 1979.
- [5]. S. Kuo, J. -J. Jwo, *J. Org. Chem.*, 57 (1992) 1991.
- [6]. Boyer, A. Hambardzoumian, G. Lamaty, A. Leydet, J. -P. Roque, P. Bouchet, *New J. Chem.*, 20 (1996) 985.
- [7]. Guazzelli, G. and Settambolo, R. (2007) 4-Indolylbutanals from Rhodium-catalyzed hydroformylation of allylindoles as precursors of benzofused indolizines. *Tetrahedron Lett.*, 48, 34, 6034–6038.
- [8]. Coupling using a chiral quaternary ammonium salt as catalyst. *Tetrahedron Lett.*, 40, 3843-3846. Izatt, R.M. Nelson, D.P. Rytting, J.H. Haymore, B.L. and Christensen, J.J. (1971).
- [9]. Calorimetric study of the interaction in aqueous solution of several uni- and bivalent metal ions with the cyclic polyether dicyclohexyl 18-crown-6 at 10, 25, and 40 deg. *J. Am. Chem. Soc.*, 93, 1619-1623.
- [10]. Jonczyk A. and Gierczak, A. H. (2000) Direct Dichlorovinylolation of Some Carbonyl Compounds by Trichloroethylene Under Conditions of Phase-Transfer Catalysis. *Tetrahedron*, 56, 6083-6087.
- [11]. Whitehouse, M.W. and Leader, J. E., Biochemical properties of anti-inflammatory Drugs-IX. *Biochemical Pharmacology*, 16, 537 (1967).
- [12]. Lombardino, J.G. and Wiseman, E. H., Antinflammatory 2-aryl-1,3-indandiones. *J. Med. Chem.* 11 (2), 342 (1968).
- [13]. Courant, J., Leblois, D., Tandon, M., Robert-Piessard, S., Le Baut, G. Juge, M., Petit, J.Y. and Welin, L. 1,3-Indandion VIII. 2-Hydroxy-2-indolyl-1,3-indandions, 2-(indol-3-yl methylene indandion and derivatives: Search for anti-inflammatory activity. *European Journal of Medicinal Chemistry*, 24, 145, (1989).
- [14]. Caruso, A., Garofalo, A., Grande, F., Aiello, F., Anzini, M. Ortuso, F., Alcaro, A., Panno, A., Saturnino, C.

- and Sinicropi, M. S. A. L.4) Synthesis And biological evaluation of 1,3-Indandione derivatives as acetylcholinesteraseinhibitors. *Pharmacology Online*, 264 (2009).
- [15]. Jeyachandran, M. and Ramesh, P., Synthesis, antimicrobial, and anticoagulant activities of 2-(arylsulfonyl) indane-1,3-diones. *Organic Chemistry International* (2011).
- [16]. Köhler, F., Fickentscher, K., Halfmann, U. and Koch, H., Embryotoxicität und teratogenität von derivaten des 1, 3- indandion. *Archiv für Toxikologie*, 33, 191 (1975).

A Review on Schiff Base Ligands and Their Biologically Important Metal Complexes

Nirmal R. Joshi¹, Saroj R. Bembalkar^{1*}, Rajendra P. Pawar^{2*}

¹Department of Chemistry, Deogiri College, Aurangabad, Maharashtra, India

²Department of Chemistry, Shiv Chhatrapati College, Aurangabad, Maharashtra, India

ABSTRACT

Herein, this review paper includes introduction to Schiff base ligands, history of Schiff base Preparation of Schiff base ligand, Metal complexes of Schiff base and biological importance of Schiff Base Metal Complexes.

Keywords: Schiff Base, Metal Complexes, Anti-Bacterial, Anti-Fungal, Anti-Cancer Activity

I. INTRODUCTION

Schiff bases

Co-ordination chemistry is the study of coordinate covalent bond formation between the ligand and metal ion. Schiff bases are aldehyde or ketone like compounds in which the carbonyl group is replaced by an imine or azomethine (C=N) group. Schiff-base ligands and their metal complexes have received much attention in recent years due to their wide use as catalysts, dyes and pigments, polymer stabilizers and they possess broad range of biological activities, such as anti-malarial, anti-fungal, anti-bacterial, anti-tubercular anti-inflammatory, anti-viral, and anti-pyretic activities [1-2]. It contains a carbon-nitrogen double bond with the nitrogen atom connected to an aryl or alkyl group but not hydrogen (**Figure 1**).

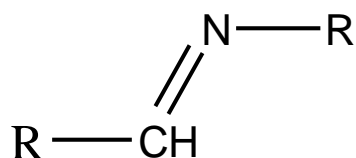


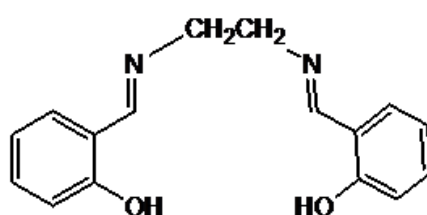
Figure 1: Structure of a Schiff base.

Schiff bases have general formula $\text{R}_1\text{N}=\text{CR}_2\text{R}_3$, where R is a phenyl or alkyl group which gives the Schiff base its stability [3]. Since formation of Schiff bases is reversible, due to the hydrolysis of the imine under certain conditions, it is still straight forward for the reaction to complete while others are very sensitive to water and easily hydrolyse back to aldehyde. To overcome this hydrolysis, the reaction of Schiff bases should be undertaken under dry solvent conditions or using some additional procedure to remove the side product water, in the imine formation. The lone pair of electron on the nitrogen atom of the imine group can enable the formation of a proper donor bond to a metal ion for metal-ligand complex formation. Many Schiff bases have a second functional group like OH, SH groups or another N atom, which are near to imine group. These

functional groups can allow the formation of five or six member chelate rings when coordinated with different metal ions.

II. HISTORY OF SCHIFF BASES

Schiff bases are named after Hugo (Ugo) Schiff (1834-1915), a German chemist. He discovered Schiff bases in 1864 [4] and other imines, and was also responsible for research in aldehydes and had the Schiff test named after him. A well-known Schiff base ligand is a salen (Figure- 2) with a bi-functional and tetradentate(ONNO) ligand.



Salen

Figure 2 Schiff base ligand

III. PREPARATION OF SCHIFF BASE LIGAND

Schiff base (HC=N-R) is the nitrogen analogue of an aldehyde or ketone, where the carbonyl group is replaced by an imine group (Figure 3).

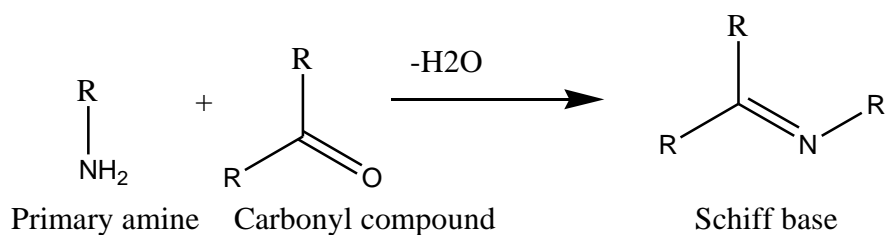


Figure 3 Synthesis of Schiff base ligand.

Schiff bases which contain aryl substituents are more stable and more easily synthesized than those that contain alkyl substituents. It means that Schiff bases of aliphatic aldehydes are relatively unstable and they readily undergo polymerisation in comparison to products from conjugation of aromatic aldehydes [5-8].

A Schiff base reaction is a reversible, acid-catalysed condensation between a primary amine (not ammonia) and either an aldehyde or ketone.

The formation of Schiff bases from aldehydes or ketones requires a protic solvent which is sufficiently dry in order to prevent potential hydrolysis of the newly formed imine bond. The formation is generally undertaken

under acid or base catalysis, or upon heating. The completion of imine formation is controlled by the separation of the product or removal of water, or both.

IV. METAL COMPLEXES OF SCHIFF BASE

As ligands, Schiff bases are very efficient. The presence of the lone pair of electrons on the nitrogen atom of the imine bond can be donated to the appropriated metal ion. Many Schiff base ligands have a second or even third functional group, such as OH of salicylaldehyde or its derivatives and the nitrogen atoms from heterocyclic rings, e.g. pyridine. This electron donation, in conjunction with a functional group, means that a vast number of transition metal complexes could be prepared. A large number of Schiff base complexes have been used in catalytic activities, polymer [9]-17]

V. BIOLOGICAL IMPORTANCE OF SCHIFF BASE METAL COMPLEXES

Due to the improvement in the area of bio-inorganic chemistry, there is an increase in the interest in Schiff base complexes, since it has been recognized that many of these complexes may serve as models for biologically important species. They act as anti bacterial, anti fungal, anti malarial etc agents [18-19]. Thus, they are, reported as follows.

A. Anti-bacterial activity of Schiff base complexes

Metal complexes of Schiff base derived from 2-thiophene carboxaldehyde, 2-amino benzoic acid (HL) and Fe(III) or Co(II) or Ni(II) or UO₂(II) showed a good anti-bacterial activity against, Escherichia Coli, Pseudomonas Aerogimus and Staphylococcus Pyogenes. Fe(III), Cu(II), Zn(II) and UO₂(II) complexes caused inhibition for E. Coli The importance of this lies in the fact that these complexes could be applied fairly in the treatment of some common diseases caused by E. coli. However, Fe(III), Co(II), Cu(II), Zn(II) and UO₂(II) complexes were specialized in inhibiting Gram-positive bacterial strains (Staphylococcus pyogenes and P. Aeroginosa). The importance of this unique property of the investigated Schiff base complexes lies in the fact that, it could be applied safely in the treatment of infections caused by any of these particular strains.

B. Anti-fungal activity of Schiff base complexes

A Schiff base ligand derived from 1,4-dicarbonyl-phenyl-dihydrazide and chromene-2,3-dione formed complexes with Cr(III), Mn(III), and Fe(III) metal salt in methanolic medium, then tested for their antimicrobial activities to assess their inhibiting potential. The antifungal experimental results of the compounds were compared with the standard antifungal drug (Miconazole) at the same concentration. All the metal complexes exhibited greater anti-fungal activity against Aspergillus sp. However, they show slightly lesser activity against Rhizoctonia sp. than standard drug micorazole. The Cr(III) and Fe(III) complexes are more effective against penicilium sp. than the standard drug. From the data it has been also

observed that the activity depends upon the type of metal ion and varies in the following order of the metal ion: Cr > Fe > Mn

C. Anti-cancer activity of Schiff base complexes

Cancer or malignant neoplasm is a class of diseases in which a group of cells display uncontrolled growth, invasion and even sometimes Metastasis, It continues as a serious public health problem throughout the world as the most feared diagnosis. It is the second leading cause of human death after cardiovascular diseases in developing as well as in developed countries. Currently, the treatment for cancer primarily includes surgery and chemotherapy, but the curative effects of the existing chemotherapeutic drugs are not good enough and they have plentiful side effects. The development of more effective drugs for treating patients with cancer has been a main attempt over the past 50 years. In recent years, various Schiff bases derivatives have been found to be associated with anticancer properties [20].

VI. CONCLUSION

- 1) Schiff bases act as ligand for complexation with metal ions.
- 2) Schiff base metal complexes can be used as catalysts.
- 3) Schiff base metal complexes exhibit biological activities like anti bacterial, anti fungal etc. activities.

VII. REFERENCES

- [1]. K.C. Gupta and A.K. Sutar, *Coord. Chem. Rev.* 2008, 252, 1420.
- [2]. K.C. Gupta, A. Kumar Sutar and C.-C. Lin, *Coord. Chem. Rev.* 2009, 253, 1926.
- [3]. A. Zoubi and Wail, *J. Coord. Chem.*, 2013, 66, 2264.
- [4]. H. Schiff, *Justus Liebig's Annalen der Chemie*, 1864, 131.
- [5]. R. Atkins, G. Brewer, E. Kokot, G.M. Mockler and E. Sinn, *Inorg. Chem.*, 1985, 24, 127.
- [6]. C.M. Brewster, *J. Am. Chem. Soc.*, 1924, 46, 2463.
- [7]. I.A. Savich, A.K. Pikaev, I.A. Lebedav and V.I. Spitsyn., *Vestnik. Moskov. Univ*, 1956, 11, 225.
- [8]. K.N. Campbell, A.H. Sommers and B.K. Campbell, *J. Am. Chem. Soc.*, 1944, 66, 82 .
- [9]. A. Earnshaw and N. Greenwood, *Chemistry of the Elements* (2nd ed.) Butterworth–Heinemann., 1997 .
- [10]. C.E. Housecroft and A.G. Sharpe, *Inorganic Chemistry* (2nd Ed), 2005, 694.
- [11]. G.C. Congress, *Green Car Congress*, 2008.
- [12]. P.J. McCarthy, R.J. Hovey, K. Ueno and A.E. Martell, *J. Am. Chem. Soc*, 1955, 77, 5820
- [13]. M. Franks, A. Gadzhieva, L. Ghandhi, D. Murrell, A.J. Blake, E.S. Davies, W. Lewis, F. Moro, J. McMaster and M. Schroder, *Inorg. Chem.*, 2013, 52, 660.
- [14]. M. Jian-Ying, *Synthesis and Reactivity in Inorganic, Metal-Organic, and Nano-Metal Chemistry*, 2013, 43, 1361
- [15]. P. Mukherjee, M.G.B. Drew and A. Ghosh, *Eur. J. Inorg. Chem.*, 2008, 2008, 3372.

- [16]. V.C. Gibson and E.L. Marshall, *Comprehensive Coordination Chemistry II*, 2003, 9, 1.
- [17]. E.N. Jacobsen, W. Zhang, A.R. Muci and L.D. James R. Ecker *J. Am. Chem. Soc.*, 1991,
- [18]. G.J.P. Britovsek, V.C. Gibson, B.S. Kimberley, P.J. Maddox, S.J. Mctavish, G.A. Solan, A.J.P. White and D.J. Williamsa, *Chem. Commun.*, 1998, 849.
- [19]. S Arulmurugan, H.Kavitha and B.R Venkatraman: *Rasayan J.Chemistry* , 2010, 3, 385-410.
- [20]. Ahmed M. Abu –Dief and Ibrahim M.A Mohamed. *Beni-Suef University J.Basic and Applied Sci*, 2015, 4, 119-113.

The Numerous Pharmacological Activity of *Curcuma longa* : A Review

Mahesh Walle^{*1}, S.P. Gawali¹, S.S. Kamble¹, R.P. Pawar², R.D. Ingle³

^{*1}Department of Chemistry Sundarrao More College Poladpur-Raigad, Maharashtra, India

²Department of Chemistry, Shiv Chatrapati College Aurangabad, Maharashtra, India

³Department of Chemistry, Deogiri College Aurangabad, Maharashtra, India

ABSTRACT

Curcuma longa (Turmeric) is widely used popular Indian medicinal plant from ancient era which belongs to the Zingiberaceae family. *Curcuma longa*, an important constituent of turmeric, is known for various pharmacological activities. Some of the Chemical in turmeric that has been studied are curcuminoids, turmerone, cineole etc. turmerone stimulate stem cells to make new brain cells and helps in neurodegenerative conditions like Alzheimer's disease. Turmeric also renders other protective biological effects in humans like antidiabetic, anti-inflammatory, anti-carcinogenic, anti-oxidant, wound healing and anti-cancer effects. This review summarizes the important pharmacological effects of curcumin.

Keywords: *Curcuma Longa*, Turmeric, Pharmacological activity.

I. INTRODUCTION

Curcuma longa is an Indian rhizomatous herbal plant (turmeric) of the ginger family (Zingiberaceae) of various pharmacological effects¹⁻². The medicinal benefits of turmeric could be attributed to the presence of active principles called curcumin-oids. One of the most interesting components of curcumin-oid is curcumin, which is a small molecular weight polyphenol compound and lyophilic in nature, hence insoluble in water and also in ether but soluble in ethanol, dimethylsulfoxide, and other organic solvents³.

Turmeric is an herbaceous perennial plant that grows up to 1 meter tall with many branches with yellow to orange, cylindrical, aromatic rhizomes. The leaves are alternate and arranged in two rows. They are divided into leaf sheath, petiole, and leaf blade. From the leaf sheaths, a false stem is formed. The rhizomes are the most widely used part of the plant as cooking ingredient, medicine and color dye though the leaves and the stems are used for many purposes mainly cooking.⁴

Turmeric as an aromatic medicinal plant was known to Indians since ancient times. Many scientists and historians argue that the South Asia is the original home of turmeric; from there it might have spread to countries in the South East Asia and Pacific islands where Turmeric is cultivated. It was recorded that turmeric was grown wild in the forest regions of Java, Indonesia as early as 5th century AD. There are Sanskrit texts belong to 5th and 6th centuries AD describe the usages of turmeric. Marco Polo mentions the

usages of turmeric in China. Turmeric is widely cultivated mainly in India, China, Taiwan, Indonesia, Sri Lanka, Java, Brazil, Peru, many parts of Africa and Australia.⁵

Relatively low dose of the complex can provide health benefits for people that do not have diagnosed health conditions. Most of these benefits can be attributed to its antioxidant and anti-inflammatory effects. Ingesting curcumin by itself does not lead to the associated health benefits due to its poor bioavailability, which appears to be primarily due to poor absorption, rapid metabolism, and rapid elimination. There are several components that can increase bioavailability. For example, piperine is the major active component of black pepper and, when combined in a complex with curcumin, has been shown to increase bioavailability by 2000%.⁶

II. DISCOVERY OF STRUCTURE OF CURCUMIN

Curcumin (1, 7-bis (4-hydroxy-3-methoxyphenyl)-1, 6-heptadiene-3,5-dione) is also called diferuloylmethane. Turmeric production in India of in the world is 78%. Turmeric known as *Haldīn* Hindi is a popular and sacred spice from India is nickname as 'Indian saffron' due to its golden yellow colour. It has profound significance as a condiment, dyeing agent, flavoring agent and even as a medicine, it is a very important ingredient in Asian cuisine is especially in Indian curry preparation. A byproduct of turmeric is 'kumkum' or the sacred vermilion, it has a place of importance in many Hindu religious ceremonies, offering and festivals, the increasing demand of pure, organic food product, and turmeric is an important food coloring agent⁷.

Vogel and Pelletier reported the isolation of "Yellow colouring matter", from the rhizomes of *curcuma longa* and named it Curcumin. The curcumin is found mixture of resin and turmeric oil. The pure preparation of curcumin are obtained Vogel Jr. in 1842 but formulae were not report in the decades that followed, several chemists reported possible structures of curcumin The chemical structure of curcumin are identified. In 1910 Milobedzka and Lampe as 1,6-heptadiene-3,5-dione-1,7 bis-(4-hydroxy-3-methoxyphenyl) by the same group in 1913 resulted in the synthesis of the compound. Subsequently, Srinivasan separated and quantified the components of curcumin by chromatography. Although turmeric, the major source of curcumin has been consumed as a dietary spice and a cure for human ailments for thousands of years in Asian countries, the biological characteristics of curcumin were not scientifically identified, until the mid-twentieth century. In a paper published in Nature in 1949, schraufstatter and colleagues reported that curcumin is a biologically active compound that has antibacterial properties. After that many scientist worked on turmeric and it showed many useful properties as like cholesterol lowering, anti-diabetic, anti-inflammatory, antioxidant and later anticancer activity, anti-inflammatory and thus the interest in curcumin research has increased dramatically over the years in human clinical trials curcumin has been found to be safe and efficacious and the U.S food and drug administration has approved curcumin as a "generally regarded as a safe" compound⁸.

III. MECHANISM OF ACTION

As curcumin is lead natural compound in drug discovery it already bears tremendous bioactivity and its functional modification synthesized many new derivatives which increases the potency of curcumin towards the different physiological functions and pathological state of human being. The Functionalities in the curcumin structure has great activity as shown in Figure 1.

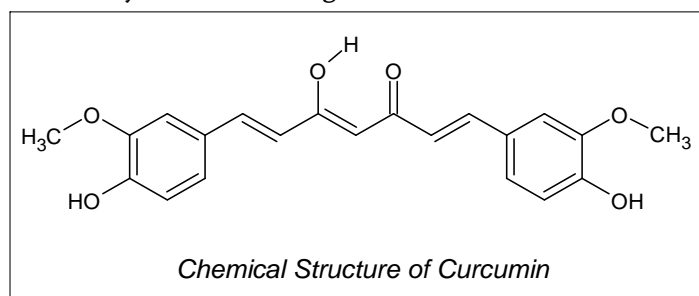


Figure 1

Anti-Alzheimer activity: Alzheimer disease is the most common cause of dementia globally. This neurodegenerative disorder of the brain is chronic and progressive, characterized clinically by the deterioration in the key symptoms of behavioral and cognitive abilities. Researchers reported the advantages of curcuminoids as anti-alzheimer agents⁹.

Anti-Diabetic activity: Curcumin was reported to possess anti-diabetic activity. The effect of anti-diabetic activity could be attributed to the antioxidant property of curcumin¹⁰. In their study, researchers demonstrated curcumin positive effect through the improvement of diabetes-induced endothelial dysfunction by decreasing superoxide production and vascular protein kinase C inhibition. Interestingly, recent studies demonstrated the ability of curcumin to have the capacity to directly quench reactive oxygen species (ROS) that can contribute to oxidative damage¹¹.

Anti-Oxidant activity: Curcumin demonstrated the antioxidant activity by evaluation curcumin using various in-vitro antioxidant assays such as 1,1-diphenyl-2-picryl-hydrazyl free radical (DPPH) scavenging, 2,2'-azino-bis(3-ethylbenzthiazoline-6-sulfonic acid) (ABTS) radical scavenging activity, N,N-dimethyl-p-phenylenediaminedihydrochloride (DMPD) radical scavenging activity, total antioxidant activity determination by ferric thiocyanate, total reducing ability determination by the Fe³⁺ – Fe²⁺ transformation method, superoxide anion radical scavenging by the riboflavin/ methionine/illuminate system, hydrogen peroxide scavenging and ferrous ions (Fe²⁺) chelating activities¹².

Anti-inflammatory activity: Curcumin possesses significant anti-inflammatory activity in acute as well as in chronic models of inflammation. It is as potent as phenylbutazone in the carrageenan edema test but only half as potent in chronic tests¹³. Curcumin has been demonstrated to be safe in six human trials and has demonstrated anti-inflammatory activity. It may exert its anti-inflammatory activity by inhibition of a number of different molecules that play a role in inflammation. Curcumin has been shown to regulate numerous transcription factors, cytokines, protein kinases, adhesion molecules, redox status and enzymes that have been linked to inflammation¹⁴.

Anticarcinogenic activity: Animal studies involving rats and mice, as well as *in vitro* studies utilizing human cell lines, have demonstrated curcumin's ability to inhibit carcinogenesis at three stages: tumor promotion, angiogenesis, and tumor growth. In two studies of colon and prostate cancer, curcumin inhibited cell proliferation and tumor growth. Turmeric and curcumin are also capable of suppressing the activity of several common mutagens and carcinogens in a variety of cell types in both *in vitro* and *in vivo* studies. The anticarcinogenic effects of turmeric and curcumin are due to direct antioxidant and free-radical scavenging effects, as well as their ability to indirectly increase glutathione levels, thereby aiding in hepatic detoxification of mutagens and carcinogens, and inhibiting nitrosamine formation¹⁵.

Antimicrobial activity: Turmeric extract and the essential oil of *Curcuma longa* inhibit the growth of a variety of bacteria, parasites, and pathogenic fungi. In a study guinea pig were infected with either dermatophytes, pathogenic molds or yeast, found that topically applied turmeric oil inhibited dermatophytes and pathogenic fungi. Curcumin has also been found to have moderate activity against plasmodium, falciparum and leishmania major organisms. The antifungal, antibacterial, phytotoxic, cytotoxic and insecticidal activity of ethanolic extract of turmeric shows antifungal activity toward *Trichophyton longifusus* and *Microsporum aureus*¹⁶.

Wound Healing activity: Wound healing includes the repair of tissues in a complex process that involves inflammation, granulation, and remodeling of the tissue¹⁷. Enhancement of wound healing was reported by curcumin in animals. The mechanisms of action of wound healing effect of curcumin include: immune histochemical localization of transforming growth factor- β 1 showed an increase in curcumin-treated wounds as compared with untreated wounds¹⁸ and modulating collagen and decreasing reactive oxygen species¹⁹. In addition, curcumin showed earlier re-epithelialization, improved neovascularization, increased migration of various cells including dermal myofibroblasts, fibroblasts, and macrophages into the wound bed, and higher collagen content²⁰.

IV. CHEMICAL CONSTITUTION OF CURCUMIN

Major constituents: 1) Curcuminoids (5%) the chief one is curcumin which has antioxidant property. Other curcuminoids are dicaffeoyl methane, caffeoylferuloyl methane and dihydrocurcumin. 2) Volatile oil (5%), containing chiefly of sesquiterpenezingiberone (25%), turmerone and arturmerone, alcohol-poly methylcarbinol, d-phelandrene, sabinene, cineole, borneol, etc.

Minor constituents: Sugars- arabinose, fructose, glucose and starch grains The active constituents of turmeric are the flavonoid curcuminoids which is a mixture of curcumin (diferuloylmethane), monodesmethoxycurcumin and bisdesmethoxycurcumin curcumin makes up approximately 90% of the curcuminoids content in turmeric. Active constituent is curcumin, which comprises 0.3-5.4 % of raw material
Compound/extract biological activity 1) Turmeric powder - Antitumor, Antiprotozoan, Anti-inflammatory and wound-healing 2) Methylcurcumin - Antiprotozoan 3) Demethoxycurcumin and Bisdemethoxycurcumin- Antioxidant 4) Volatile oil- Anti-inflammatory, Antibacterial, Antifungal e) Curcumin-Antibacterial and Antiprotozoan.

V. CONCLUSION

Curcumin can be considered a great potential therapeutic agent for a variety of inflammatory conditions and cancer types. Consequently, there is extensive interest in its therapeutic potential as evidenced by the number of ongoing phase II and III clinical trials. The primary obstacle to utilizing curcumin therapeutically has been its limited systemic bioavailability, but researchers are actively involved in trying to find the most efficient method of application.

VI. REFERENCES

- [1]. Panpatil, Virendra V., et al. "In vitro evaluation on antioxidant and antimicrobial activity of spice extracts of ginger, turmeric and garlic." *Journal of Pharmacognosy and phytochemistry* 2.3 (2013): 143-148.
- [2]. Pawar, Harshal, et al. "Phytochemical evaluation and curcumin content determination of turmeric rhizomes collected from Bhandara District of Maharashtra (India)." *Med. Chem* 4.8 (2014): 588-591.<http://dx.doi.org/10.4172/2161-0444.1000198>
- [3]. Aggarwal, Bharat B., Anushree Kumar, and Alok C. Bharti. "Anticancer potential of curcumin: preclinical and clinical studies." *Anticancer research* 23.1/A (2003): 363-398.
- [4]. Alsamydai, Ali, and NisreinJaber. "Pharmacological aspects of curcumin." *Int J Pharm* 5.6 (2018): 313-26.[http://dx.doi.org/10.13040/IJPSR.0975-8232.IJP.5\(6\).313-26](http://dx.doi.org/10.13040/IJPSR.0975-8232.IJP.5(6).313-26)
- [5]. DebjitBhowmik, Chiranjib, et al. "Turmeric: a herbal and traditional medicine." *Archives of applied science research* 1.2 (2009): 86-108.
- [6]. Hewlings, Susan J., and Douglas S. Kalman. "Curcumin: A review of its effects on human health." *Foods* 6.10 (2017): 92.<https://doi.org/10.3390/foods6100092>
- [7]. Krup, Vasavda, L. Hedge Prakash, and A. Harini. "Pharmacological activities of turmeric (*Curcuma longa* Linn): a review." *J HomeopAyurv Med* 2.133 (2013): 2167-1206.<http://dx.doi.org/10.4172/2167-1206.1000133>
- [8]. http://www.indianetzone.com/41/history_turmeric.htm
- [9]. Ghosh, S. "Gomes A." Russell's viper (*DaboiaRusselliRusselli*) venom toxicity neutralizing efficacy of Curcumin-Gold Nanoparticle (C-GNP) in experimental animal model. *J Toxins* 3.2 (2016): 6.
- [10]. Panchatcharam, Manikandan, et al. "Curcumin improves wound healing by modulating collagen and decreasing reactive oxygen species." *Molecular and cellular biochemistry* 290.1 (2006): 87-96.<https://doi.org/10.1007/s11010-006-9170-2>
- [11]. Chereddy, Kiran Kumar, et al. "Combined effect of PLGA and curcumin on wound healing activity." *Journal of controlled release* 171.2 (2013): 208-215.
- [12]. David, Bruno, Jean-Luc Wolfender, and Daniel A. Dias. "The pharmaceutical industry and natural products: historical status and new trends." *Phytochemistry Reviews* 14.2 (2015): 299-315.<https://doi.org/10.1007/s11101-014-9367-z>

- [13]. Naik, Suresh R., Vishnu N. Thakare, and Snehal R. Patil. "Protective effect of curcumin on experimentally induced inflammation, hepatotoxicity and cardiotoxicity in rats: evidence of its antioxidant property." *Experimental and Toxicologic Pathology* 63.5 (2011): 419-431. <https://doi.org/10.1016/j.etp.2010.03.001>
- [14]. Kim, Jiyoung, HyongJoo Lee, and Ki Won Lee. "Naturally occurring phytochemicals for the prevention of Alzheimer's disease." *Journal of neurochemistry* 112.6 (2010): 1415-1430. <https://doi.org/10.1111/j.1471-4159.2009.06562.x>
- [15]. Somasundaram, Sivagurunathan, et al. "Dietary curcumin inhibits chemotherapy-induced apoptosis in models of human breast cancer." *Cancer research* 62.13 (2002): 3868-3875.
- [16]. Adamczak, Artur, Marcin Ożarowski, and Tomasz M. Karpiński. "Curcumin, a natural antimicrobial agent with strain-specific activity." *Pharmaceuticals* 13.7 (2020): 153.
- [17]. Chandran, Binu, and Ajay Goel. "A randomized, pilot study to assess the efficacy and safety of curcumin in patients with active rheumatoid arthritis." *Phytotherapy research* 26.11 (2012): 1719-1725. <https://doi.org/10.1002/ptr.4639>
- [18]. Jackson, J. K., et al. "The antioxidants curcumin and quercetin inhibit inflammatory processes associated with arthritis." *Inflammation Research* 55.4 (2006): 168-175. <https://doi.org/10.1007/s00011-006-0067-z>
- [19]. Kloesch, Burkhard, et al. "Anti-inflammatory and apoptotic effects of the polyphenol curcumin on human fibroblast-like synoviocytes." *International immunopharmacology* 15.2 (2013): 400-405. <https://doi.org/10.1016/j.intimp.2013.01.003>
- [20]. Villaflores, Oliver B., et al. "Curcuminoids and resveratrol as anti-Alzheimer agents." *Taiwanese Journal of Obstetrics and Gynecology* 51.4 (2012): 515-525. <https://doi.org/10.1016/j.tjog.2012.09.005>

An Efficient and Reusable ZnS NPs Catalyst for Synthesis of α -Hydroxyphosphonates

Tidke Vishwamber Angadrao

Department of Chemistry, Vai. Dhunda Maharaj Degloorkar Mahavidhyalay, Degloor Nanded-431717,
Maharashtra, India

ABSTRACT

Synthesis of series of bioactive α -hydroxy phosphonates (2a-i) stirred with the benevolent heterogeneous ZnS nano catalyst was employed as an efficient catalyst for at room temperature. The current approach to generate sustainable catalyst in place of volatile organic compounds to 2-chloroquinoline-3-carbaldehyde (1a-j) with triethylphosphite. The reaction is furnished in short time and products were obtained in good yield.

Keyword- α -hydroxy phosphonates, nano particles, volatile organic compounds.

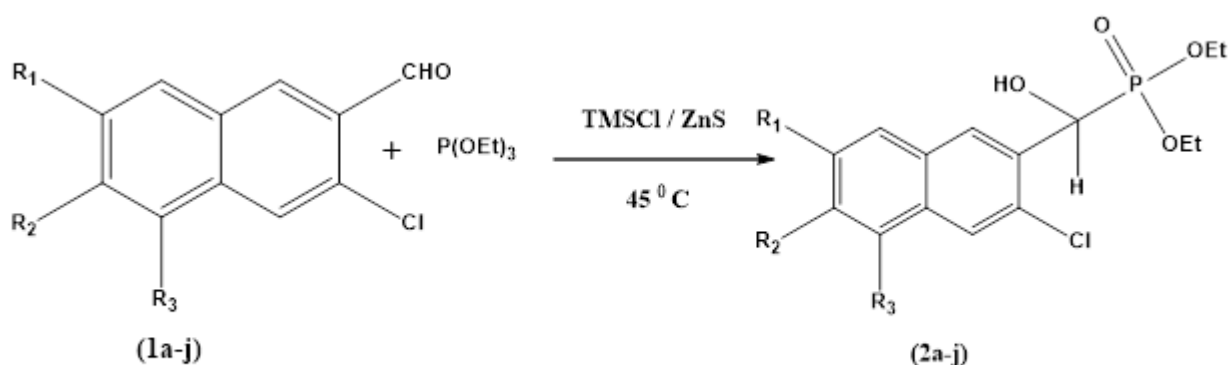
I. INTRODUCTION

The α -hydroxyphosphonates have received much attention due to their wide range of applications and their importance as synthetic transition products of other biologically important α -substituted phosphoryl compounds¹. Surprisingly, attempts have been made to formulate hydroxyphosphonates, and the Abramov reaction represents one of the most useful methods for synthesizing α -hydroxyphosphonates². This process involves aldehydes condensation with triethyl phosphite³, I_2 catalysts functioned as acid catalysts⁴, $ZnBr_2$ ⁵, β -cyclodextrin, ammonium metavanadate and bismuth (III) nitrate pentahydrate⁶, and $TMSCl$ was an efficient catalytic system has been shown⁷. Therefore, some drawbacks such as extended reaction times, use of volatile hazardous organic compounds and expensive catalysts, and low product yields after harsh reaction conditions are not recognized in chemistry. Therefore, many synthetic methods have been developed to build α -hydroxyphosphonates in the presence of catalysts or activators.

To overcome these shortcomings, a new method based on the use of ultrasonic microwaves and nano catalysts has recently been employed. Advances towards the ecologically benign synthesis of α -hydroxyphosphonates are desirable because of their important role in the synthesis of biologically active components. New developments in chemical synthesis, a broad focus on reaction efficiency, waste reduction, abandonment of hazardous reagents, and precise use of resources are the main goals. The ZnS nano particles⁸ have been performed as a powerful alternate for the usually active risky ionic liquid to carbonyl oxygen, crafting the $C=O$ bond extra electrophilic. We report here our results of ZnS Nano catalyzed modified Abramov reaction. Mesoporous ZnS nanospheres were previously used as heterogeneous catalysts for synthesis of 5-substituted 1H-tetrazoles from various nitriles such as Substrates and sodium azide (Lang et al. 2010, 2013)⁹. However, these steps performed in N, N-dimethylformamide (DMF) solvent and acidic conditions are

essential to obtain the desired product¹⁰. In this research, we developed a more efficient and convenient method toward synthesis of α -hydroxy phosphonates through aldehyde, triethyl phosphite, and TMSCl in the presence of ZnS nanoparticles as a new heterogeneous catalyst under solvent-free conditions.

Quinolines are an important class of heterocyclic compounds¹¹ have been screened for numerous biological activities such as bactericidal¹², antitumor¹³, anti-inflammatory¹⁴, and antimalarial¹⁵. Quinolines such as 2-chloroquinoline-3-carbaldehyde capture a noticeable position as they are key intermediates for extend annellation and for several functional group interconversions. It is furthermore reported that organophosphates are effective pesticides which have wide variety of application¹⁶. Recently, some new vinyl phosphates have been reported as convincing inhibitors of phosphatase and phosphodiesterase¹⁷.



Scheme: Synthesis of [2a-j] from [1a-j] by using ZnS NPs catalyst

II. RESULTS AND DISCUSSION

The original work of Abramov reaction involved the heating under microwave of an aldehyde or a ketone with trialkylphosphite at 70-100°C for several hours in sealed tube¹⁸. Under these stringent conditions dialkyl- α -alkoxyalkylphosphonates could be isolated in various yields. To overcome these difficulties in attempting Abramov reaction silyl halide can be used along with the carbonyl compounds and the phosphorous reagent¹⁹. Removal of the residual silyl-ester linkages at the phosphonate Centre is accomplished with water or alcohol under mild conditions. Hence the Abramov reaction with such modification is referred as “Modified Abramov Reaction”. α -hydroxyphosphonates may serve as precursors for the synthesis of alpha aminophosphonates which are analogs of alpha amino acid²⁰. Hence a search for new biological active compound has stimulated recent studies on the synthesis of α -substituted phosphonates. In continuation of our work on phosphorus chemistry,²¹ herein several examples of modified Abramov reaction on 2-chloroquinoline-3-carbaldehydes (1a-j) are presented to afford α -hydroxyphosphonates (2a-j) compounds.

The one pot two-component reaction between triethyl phosphite (2 mmol), and quinoline 3-carbaldehyde (2 mmol), was chosen as a model reaction. All the reaction conditions were optimized using ZnS nano particles as a catalyst²². The reaction mixture was stirred at room temperature under solvent-free condition. It was observed that initially the reaction mixture was clear and after 10 min the solid product formation started. It

is noteworthy that, no significant product formation was observed under similar reaction conditions in the absence of catalyst even after 5 h (Table 1).

Table 1. ZnS NPs facilitated synthesis of α -hydroxyphosphonates.

<i>Entry</i>	<i>R₁</i>	<i>R₂</i>	<i>R₃</i>	<i>Time (min)</i>	<i>Yield (%)</i>	<i>MP ($^{\circ}$C)</i>
2a	H	H	H	10	95	128-130 $^{\circ}$ C
2b	CH ₃	H	H	15	98.8	145-147 $^{\circ}$ C
2c	H	CH ₃	H	20	92.6	141-143 $^{\circ}$ C
2d	H	H	CH ₃	12	89.6	172-174 $^{\circ}$ C
2e	OCH ₃	H	H	17	94.15	156-160 $^{\circ}$ C
2f	H	OCH ₃	H	18	91.2	166-170 $^{\circ}$ C
2g	H	H	OCH ₃	16	95.2	149-151 $^{\circ}$ C
2h	OCH ₂ CH ₃	H	H	18	92.9	168-170 $^{\circ}$ C
2i	H	H	CH ₂ CH ₃	18	83.2	149-151 $^{\circ}$ C
2j	Cl	H	H	18	88.9	115-119 $^{\circ}$ C

III. EXPERIMENTAL SECTION

General Procedures.

2-Chloroquinoline-3-carbaldehydes were prepared in the laboratory by the reported method.⁽²³⁾ triethylphosphite were procured from Sigma Andrich. methanol and hexane, ZnS, were procured from Merk D. Fine-chem. All melting points were determined in open capillaries on Kumar's melting point apparatus. The products were characterized by their spectral data. ¹H NMR spectra were recorded on a Varian INOVA-500 (500 MHz) spectrometer. Chemical shifts are reported in ppm from the solvent resonance as the internal standard (DMF-d₇; 8.03 ppm) or tetramethylsilane (0.0 ppm) resonance as the internal standard (CDCl₃). Data are reported as follows: chemical shift, integration, multiplicity (s = singlet, d = doublet, t = triplet, br = broad) and coupling constants (Hz). Infrared spectra were recorded on a FT/IR-300E spectrometer. Mass spectra were recorded Micromass Quattro-II using electrospray Ionization technique, showing (m+1) peak as a base peak. Analytical thin layer chromatography (TLC) was performed on Merck precoated TLC plates (silica gel 60 GF254, 0.25 mm). Other simple chemicals were purchased and used as such.

General procedure. Diethyl (2 -chloro-quinolin-3-yl) (hydroxy) methylphosphonate. (2a)

A mixture of 2-chloroquinoline-3-carbaldehyde (0.96 gm, 3 mmol) and triethylphosphite (1.68 gm, 6 mmol) and TMSCl all the reaction conditions are optimized ZnS as catalyst. The reaction was added with constant stirring. Progress of reaction was monitored on TLC. After completion of reaction (15 min.), the mixture was concentrated on rotary-evaporator under reduced pressure, to obtain an oily residue. The oily residue was dissolved in methanol. This methanolic solution was concentrated, dissolved in dichloromethane and

reprecipitated with hexane. Thus, obtained solid was filtered, washed with hexane and dried in oven at 40°C. All of the α -hydroxyphosphonates is known compounds to which the spectroscopic data were compared.

(2a). diethyl ((2-chloroquinolin-3-yl) (hydroxy)methyl) phosphonate-

.IR (KBr), cm^{-1} : 3245 (-OH); 1218 (-P=O); 104(-P-O-C). ^1H NMR (CDCl_3), δ ppm: 1.2 (t, 3H, O-CH₂-CH₃); 1.4 (t, 3H, O-CH₂-CH₃); 2.1 (s, 1H, -CH-OH); 4.1 (m, 4H, O-CH₂-CH₃ and OCH₂-CH₃); 5.5 (d, 1H, -CH-P=O); 7.4 (t, 1H, Ar-H, C₆); 7.9 (t, 1H, Ar-H, C₇); 7.7 (d, 1H, Ar-H, C₅); 8.1 (d, 1H, Ar-H, C₈); 8.5 (s, 1H, Ar-H, C₄). ES-MS: m/z 330 (m+1) base peak and 332(m+3). Elemental analysis: C₁₄H₁₇ClNO₄P Calculated: C: 51.01 %, H: 5.19%, N: 4.25 %; Found: C: 51.03%, H: 5.389 %, N: 4.355%.

(2b). diethyl ((2-chloro-6-methylquinolin-3-yl)(hydroxy)methyl) phosphonate-

IR (KBr), cm^{-1} : 3278 (-OH); 1218 (-P=O); 1037 (-P-O-C). ^1H NMR (CDCl_3), δ ppm: 1.2 (t, 3H, O-CH₂-CH₃); 1.3 (t, 3H, O-CH₂-CH₃); 2.4 (s, 1H, -CH-OH); 2.5 (s, 3H, ArCH₃); 4.1 (q, 2H, O-CH₂-CH₃); 4.2 (q, 2H, O-CH₂-CH₃); 5.6 (d, 1H, CH-P=O); 7.5 (s, 1H, Ar-H, C₅); 7.6 (d, 1H, Ar-H, C₇); 7.9 (d, 1H, Ar-H, C₈); 8.5 (s, 1H, Ar-H, C₄). ES-MS: m/z 344 (m+1) base peak and 345.9 (m+3). Elemental analysis: C₁₅H₁₉ClNO₄P Calca.: C: 52.41 %, H: 5.57 %, N: 4.07 %; Found: C: 52.50 %, H: 5.67 %, N: 4.17 %.

(2c). diethyl ((2-chloro-7-methylquinolin-3-yl) (hydroxy)methyl) phosphonate -

IR (KBr), cm^{-1} : 3278 (-OH); 1218 (-P=O); 1037 (-P-O-C). ^1H NMR (CDCl_3), δ ppm: 1.2 (t, 3H, O-CH₂-CH₃); 1.3 (t, 3H, O-CH₂-CH₃); 2.4 (s, 1H, -CH-OH); 2.5 (s, 3H, ArCH₃); 4.1 (q, 2H, O-CH₂-CH₃); 4.2 (q, 2H, O-CH₂-CH₃); 5.6 (d, 1H, CH-P=O); 7.5 (s, 1H, Ar-H, C₅); 7.6 (d, 1H, Ar-H, C₇); 7.9 (d, 1H, Ar-H, C₈); 8.5 (s, 1H, Ar-H, C₄). ES-MS: m/z 344 (m+1) base peak and 345.9 (m+3). Elemental analysis: C₁₅H₁₉ClNO₄P Calca.: C: 52.41 %, H: 5.57 %, N: 4.07 %; Found: C: 52.50 %, H: 5.67 %, N: 4.17 %.

(2d). diethyl ((2-chloro-8-methylquinolin-3-yl)(hydroxy)methyl)phosphonate-

IR (KBr) cm^{-1} : 3277 (-OH); 1222 (-P=O); 1037(-P-O-C)., δ ppm ^1H NMR(CDCl_3): 1.1 (t, 3H, O-CH₂-CH₃); 1.3 (t, 3H, O-CH₂-CH₃); 2.7 (s, 1H, -CH-OH); 3.9 (s, 3H, Ar-O-CH₃); 4.2 (q, 2H, O-CH₂-CH₃); 4.3 (q, 2H, O-CH₂-CH₃); 5.8 (d, 1H, CH-P=O); 7.0 (s, 1H, Ar-H, C₅); 7.5 (d, 1H, Ar-H, C₇); 8.1 (d, 1H, Ar-H, C₈); 8.8 (s, 1H, Ar-H, C₄). ES-MS: m/z 360(m+1) base peak and 362 (m+3). Elemental analysis: C₁₅H₁₉ClNO₅P Calculated: C: 50.08 %, H: 5.32 %, N: 3.89 %; Found: C: 50.10%, H: 5.42 %, N: 3.99 %.

(2e). diethyl ((2-chloro-6-methoxyquinolin-3-yl) (hydroxy)methyl) phosphonate-

IR (KBr) cm^{-1} : 3265 (-OH); 1219 (-P=O); 1034 (-P-O-C). ^1H NMR (CDCl_3), δ ppm: 1.1(t, 3H, O-CH₂-CH₃); 1.3 (t, 3H, O-CH₂-CH₃); 2.7 (s, 1H, -CH-OH); 4.0 (s, 3H, Ar-OCH₃); 4.3 (q, 2H, O-CH₂-CH₃); 4.4 (q, 2H, O-CH₂-CH₃); 5.7 (d, 1H, CH-P=O); 7.2 (d, 1H, Ar-H, C₆); 7.4 (s, 1H, Ar-H, C₈), 7.8 (d, 1H, Ar-H, C₅); 8.7 (s, 1H, Ar-H, C₄). ES-MS: m/z 343.9 (m+1) base peak and 346 (m+3). Elemental analysis: C₁₅H₁₉ClNO₅P Calculated.: C: 50.08 %, H: 5.32 %, N: 3.89 %; Found: C: 50.27%, H: 5.52 %, N: 4.21 %.

(2f). diethyl ((2-chloro-7-methoxyquinolin-3-yl) (hydroxy)methyl) phosphonate-

IR (KBr) cm^{-1} : 3258 (-OH); 1235 (-P=O); 1049 (-P-O-C). ^1H NMR (CDCl_3), δ ppm: 1.2 (t, 3H, O-CH₂-CH₃); 1.4 (t, 3H, O-CH₂-CH₃); 1.3(t, 3H, Ar-O-CH₂-CH₃); 3.3 (bs, 1H, -CH-OH); 4.2 (q, 2H, O-CH₂-CH₃); 4.3 (q, 2H, O-CH₂-CH₃); 4.3 (q, 2H, O-CH₂-CH₃); 5.5 (d, 1H, CH-P=O); 7.2 (s, 1H, Ar-H, C₅); 7.4 (d, 1H, Ar-H, C₇); 7.7 (d, 1H, Ar-H, C₈); 8.5 (s, 1H, Ar-H, C₄). ES-MS: m/z 374 (m+1) base peak and 376 (m+3). Elemental

analysis: C₁₆H₂₁ClNO₅P Calculated.: C: 51.41 %, H: 5.66 %, N: 3.75 %; Found: C: 51.581 %, H: 5.772 %, N: 3.91 %.

(2g). diethyl ((2-chloro-8-methoxyquinolin-3-yl) (hydroxy)methyl) phosphonate-

IR (KBr) cm⁻¹: 3252 (-OH); 1223 (-P=O); 1041 (-P-O-C). ¹H NMR (CDCl₃), δ ppm: 1.2 (t, 3H, O-CH₂-CH₃); 1.35 (m, 6H, O-CH₂-CH₃ and Ar-CH₂-CH₃); 2.3 (s, 1H, -CHOH); 3.25 (q, 2H, Ar-CH₂-CH₃); 4.2 (m, 4H, O-CH₂-CH₃ and O-CH₂-CH₃); 5.6 (d, 1H, CH-P=O); 7.5 (t, 1H, Ar-H, C₆); 7.6 (d, 1H, Ar-H, C₇); 7.7 (d, 1H, Ar-H, C₅); 8.5 (s, 1H, Ar-H, C₄). ES-MS: m/z 359 (m+1) base peak and 361 (m+3). Elemental analysis: C₁₅H₁₉ClNO₅P Calculated.: C: 53.71 %, H: 5.92 %, N: 3.92 %; Found: C: 53.82 %, H: 5.99 %, N: 4.05 %.

(2h). diethyl ((2-chloro-5-ethoxyquinolin-3-yl) (hydroxy)methyl) phosphonate.

IR (KBr) cm⁻¹: 3255 (-OH); 1234 (-P=O); 1049 (-P-O-C). ¹H NMR (CDCl₃), δ ppm: 1.2 (t, 3H, O-CH₂-CH₃); 1.3 (t, 3H, O-CH₂-CH₃); 1.4 (t, 3H, Ar-O-CH₂-CH₃); 3.4 (bs, 1H, -CH-OH); 4.1 (q, 2H, O-CH₂-CH₃); 4.2 (q, 2H, O-CH₂-CH₃); 4.3 (q, 2H, O-CH₂-CH₃); 5.6 (d, 1H, CH-P=O); 7.0 (s, 1H, Ar-H, C₅); 7.4 (d, 1H, Ar-H, C₇); 7.9 (d, 1H, Ar-H, C₈); 8.4 (s, 1H, ArH, C₄). ES-MS: m/z 374 (m+1) base peak and 376 (m+3). Elemental analysis: C₁₆H₂₁ClNO₅P Calcd.: C: 51.41 %, H: 5.66 %, N: 3.75 %; Found: C: 51.527 %, H: 5.793 %, N: 3.85 %.

IV. CONCLUSION

We have demonstrated a simple and efficient method for the one-pot synthesis of α-hydroxyphosphonates using nanoparticles as catalysts. This method does not require the use of acidic, highly toxic reagents as catalysts. Furthermore, the simplicity of operation, mild reaction conditions, fairly short reaction times, high yields, catalyst reusability and cost efficiency make this protocol an important complement to existing methods for α-hydroxyphosphonate synthesis. Further work is underway to extend the scope of nanoparticles to other organic transformations. In addition to short reaction times, a wide range of substrates, and the use of biodegradable solvents and catalysts, this process is characterized.

V. REFERENCES

- [1]. Faille, S.; Finocchiaro, P.; Consiglio, G.A. Syntheses, characterization, stereochemistry and complexing properties of acyclic and macrocyclic compounds possessing α-amino- or α-hydroxyphosphonate units: A review article. *Heteroatom. Chem.* 2000, 11, 493–504.
- [2]. Olszewski, T.K. Environmentally benign syntheses of α-substituted phosphonates: Preparation of α-amino and α hydroxyphosphonates in water, in ionic liquids, and under solvent-free conditions. *Synthesis* 2014, 46, 403–429. [CrossRef] b) Lipshutz, B. H.; Buzard, D. J.; Yun, C. S. *Tetrahedron Lett.* 1999, 40, 201–204.
- [3]. Heydari, A.; Arefi, A.; Khaksar, S.; Tajbakhsh, M. Hydrophosphonylation of aldehydes catalyzed by guanidine hydrochloride in water. *Catal. Commun.* 2006, 7, 982–984.
- [4]. Vangala, V.B.; Pati, H.N. Efficient synthesis of β-lactam containing α-hydroxy phosphonates using tartaric acid and fumaric acid as mild catalysts. *Synth. Commun.* 2016, 46, 374–378.

- [5]. Wang, H.S.; Zeng, J.E. Iodine-catalyzed, efficient synthesis of α -hydroxy phosphonates in water. *Phosphorus Sulfur Silicon Relat. Elem.* 2010, 185, 1425–1428. [CrossRef] (b) Wang, T.; Lei, D. Y.; Huang, Y.; Ao, L. H. *Phosphorus Sulfur Silicon Relat. Elem.* 2009, 184, 2777. (c) Jin, C.; He, H. *Phosphorus Sulfur Silicon Relat. Elem.* 2011, 186, 1397.
- [6]. Raju, P.; Rajeshwaran, G.G.; Nandakumar, M.; Mohanakrishnan, A.K. Unusual reactivity of aryl aldehydes with triethyl phosphite and zinc bromide: A facile preparation of epoxides, benzisoxazoles, and α -hydroxy phosphonate esters. *Eur. J. Org. Chem.* 2015, 2015, 3513–3523.
- [7]. Ramesh, K.; Madhav, B.; Murthy, S.N.; Nageswara, Y.V.D. Aqueous-phase synthesis of α -hydroxyphosphonates catalyzed by β -cyclodextrin. *Synth. Commun.* 2012, 42, 258–265.
- [8]. Morales, R. C.; Tambyrajah, V.; Jenkins, P. R.; Davies, D. L.; Abbott, A. P. *Chem. Commun.* 2004, 158.
- [9]. Lang L, Li B, Liu W, Jiang L, Xu Z, Yin G (2010) Mesoporous ZnS nanospheres: a high activity heterogeneous catalyst for synthesis of 5-substituted 1H-tetrazoles from nitriles and sodium azide. *Chem Commun* 46(3):448–450.
- [10]. Lang L, Zhou H, Xue M, Wang X, Xu Z (2013) Mesoporous ZnS hollow spheres-catalyzed synthesis of 5-substituted 1H-tetrazoles. *Mater Lett* 106:443–446.
- [11]. F.H. Westheimer, *Science* 235 (1987) 1173–1178.
- [12]. O.J. Kolodiazny, *Tetrahedron Asymmetry* 16 (2005) 3295–3340.
- [13]. M.J. Brenne, J. Jacques, M.C. Briano, E. Surcouf, *Nouv. J. Chim.* 2 (1978) 19–20.
- [14]. D.Y. Kim, D.F. Wiemer, *Tetrahedron Lett.* 44 (2003) 2803–2805.
- [15]. J. Neyts, E. De Clercq, *Antimicrob. Agents Chemother.* 41 (1997) 2754–2756.
- [16]. P. Kafarski, B. Lejczak, *J. Mol. Catal. B Enzym.* 29 (2004) 99–104.
- [17]. M.V. Lee, E.M. Fong, F.R. Singere, R.S. Guenette, *Cancer Res.* 61 (2001) 2602–2608.
- [18]. Abramov, V. S.; *Dokl. Akad. Nauk S. S. S. R.* 1954, 95, 991. b] William, A. D.; Tokoro, Y. *J. Org. Chem.* 2001, 66, 7903.
- [19]. Evans, D. A.; Hurst, K. M.; Truesdale, L. K.; Takacs, J. M. *Tetrahedron Lett.*, 1977, 2495. R.U. Pokalwar, R.V. Hangarge, B.R. Madje, M.N. Ware, M.S. Shingare, *Phosphorus Sulfur Silicon Relat. Elem.* 183 (2008) 1461–1470
- [20]. Dhawan, B.; Redmore, D. *Phosphorus and Sulfur* 1987, 32, 119 [13] J.M. Hwang, S.H. Yeom, K.Y. Jung, *Bull. Korean Chem. Soc.* 28 (2007) 821–826.
- [21]. Mane, A. S.; Chavan, V. P.; Karale, B. K.; Hangarge, R. V.; Gaikwad, M. S.; Shingare, M. S. *Synthetic Commun.* 2002, 32 (17), 2633.
- [22]. Dighe SN, Jain KS, Srinivasan KV (2009) A novel synthesis of 1-aryl tetrazoles promoted by employing the synergy of the combined use of DMSO and an ionic liquid as the solvent system at ambient temperature. *Tetrahedron Lett* 50(45):6139–6142.

PEG-400 Mediated Synthesis of Pyranopyrazole Derivatives Via a Three-Component One Pot Reaction

Yogesh Nalwar¹, Trambak Kendre¹, Arvind Patil², Charushila Nerkar³, Santosh Chobe^{4*}

¹Department of Chemistry, Toshniwal A.C.S. College, Sengaon-431542, Maharashtra, India

²SNJB's KKHA Arts, SMGL Commerce and SPHJ Science College Chandwad Dist Nashik, Maharashtra, India

³Department of Chemistry, Arts, Science and Commerce College, Manmad, Dist. Nashik, Maharashtra, India

⁴Research Centre in chemistry, MGV's Loknete Vyankatrao Hiray Arts, Science and Commerce College, Panchavati, Nashik-03, Maharashtra, India

ABSTRACT

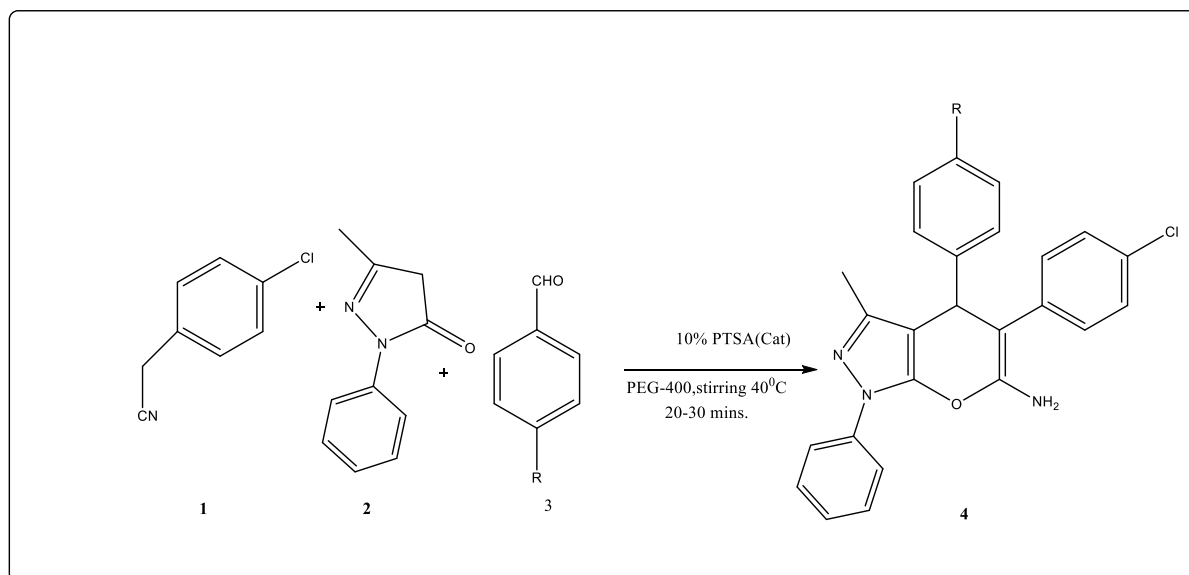
Three-component efficient synthesis of pyranopyrazoles derivatives by reacting substituted aromatic aldehydes [1], (4-chlorophenyl) acetonitrile [2] and 3-methyl-1-phenyl-pyrazol-5(4H)-one [3] using catalytic amount of PTSA, PEG-400 as a green solvent. The use of PEG as a reaction medium in organic reactions is one of the fantastic methods of green chemistry, as reactions can be performed under conditions that minimize environmental risk and chemical waste. PEG-400 is widely recognized as a low-cost, nonflammable, eco-friendly, recyclable, and abundantly accessible green solvent. Using the environmentally friendly properties of PEG-400 solvent. It is easy to get the catalyst and solvent back and use them again. It is easy, green, and quick to make pyranopyrazoles derivatives with this method.

Keywords: PEG-400; Pyrano[2,3-c]pyrazole; PTSA(cat); multi-component reaction.

I. INTRODUCTION

The class of pyranopyrazole derivatives is fascinating heterocyclic compounds with nitrogen and oxygen¹. It is known that multicomponent reactions are selective, Effective, atomically-efficient, time-saving, and simple to use perform reaction². The synthesis of heterocyclic compounds from relatively simple starting material in a convergent way is to use tandem C–C bond formations^{3,4}. In the era of the development of multi-component reaction (MCR) protocols for the synthesis of heterocyclic compounds, this attracted considerable interest. In addition, MCRs adhere to the principles of green chemistry in terms of atom economy of steps as well as numerous stringent criteria for an ideal organic synthesis. The reactions are efficient at constructing highly functionalized small organic molecules from readily available starting materials in a single step, with inherent flexibility for creating molecular complexity and diversity, while minimizing time, labour, cost, and waste generation^{5,6}. Compounds with a pyrazole scaffold have been shown to inhibit HIV-1 reverse transcriptase and IL-1 synthesis⁷, as well as possess antihyperglycemic, antibacterial, sedative-hypnotic, anti-inflammatory, antipyretic, and analgesic properties⁸. These results prompted the synthesis of a new series of bioactive, functionalized pyrazoles. Compared to conventional homogeneous catalysts, heterogeneous catalysts' simple

filtration-based recovery from the reaction mixture is advantageous. In addition, it is reusable after activation, making the process economically viable. The physical and chemical properties of naturally occurring clay include shape selectivity, an acidic, basic nature, and thermal stability. Several base-catalyzed organic transformations⁹. In present work, in order to establish a quick and efficient approach to this class of compounds we have investigated the catalytic amount of PTSA of is used in synthesis of pyranopyrazoles and its derivative via tandem three component one-pot reactions in PEG-400 as a green reaction solvent.



Scheme: One pot synthesis of pyranopyrazoles derivatives

Table I: Comparison of various solvents for synthesis of pyrano[2,3-c]pyrazoles.

Sr. No.	Solvent	Time (min)	Yield in %
1	Methanol	120	30
2	Ethanol	100	35
3	Acetonitrile	100	40
4	PEG-200	70	55
5	PEG-300	50	70
6	PEG-400	30	>85

Table II: Catalytic activity of PTSA

Sr.No	Wt % of catalyst PTSA	Condition	Time	Yield in %
1	0	Reflux	1 hrs	No reaction
2	5	Stirring	2 hrs	30-40
3	5	Reflux	2 hrs	60
4	10	Stirring	20-30 min	85-90

Table III: Physical data of synthesized compounds.

Entry	R	Time in Min.	Yield in (%)	MP(°C)
1	4-OH	28	78	210
2	4-Cl	30	88	190
3	4-F	35	86	222
4	3-Br	25	81	218
5	4-NO ₂	32	82	232
6	3-OH	35	73	212
7	4-OMe	35	80	208
8	2-Cl	28	77	198

II. EXPERIMENTAL

The melting points were determined in an uncorrected open capillary tube. All chemical solvents were purified. The gift of bleaching earth clay came from Supreme Silicones Pune. Using a pre-coated sheet of silica gel-G and iodine vapors as a detector, the completion of the reaction was monitored by thin layer chromatography. On a Shimadzu spectrometer, KBr was used to record IR spectra. ¹H-NMR was recorded in DMSO-d₆ using a 300-MHz Avance spectrometer and TMS as the internal standard. On an EI-Shimadzu QP2010PLUS GC-MS, mass spectra were collected.

Spectra of selected compounds:

Entry 1.4-(6-amino-5-(4-chlorophenyl)-3-methyl-1-phenyl-1,4-dihydropyrano[2,3-c]pyrazol-4-yl)phenol
white powder, IR (KBr in cm⁻¹): 3420, 3336, 3150, 1630, 1538; ¹H NMR (DMSO-d₆): δ 1.9 (s, 3H, CH₃), δ 4.30 (s of -C-H proton of pyrano) δ 5.18 (brs, 2H -NH₂), δ 6.9-7.89 (m, 13H, Ar-H), MS, m/z: 429.12 (100.0%)

Entry 2. 4,5-bis(4-chlorophenyl)-3-methyl-1-phenyl-1,4-dihydropyrano[2,3-c]pyrazol-6-amine:
C₂₅H₁₉Cl₂N₃O: Yellow powder, IR (KBr) in cm⁻¹: 3358, 3156, 3010, 1640, 1535; ¹H NMR (DMSO-d₆): δ 2.16 (s, 3H, CH₃), δ 4.22 (s of -C-H proton of pyrano) δ 5.41 (brs, 2H -NH₂), δ 6.9-7.89 (m, 13H, Ar-H), MS, m/z: 447.09 (100.0%).

Entry 4.4-(3-Bromo-phenyl)-5-(4-chloro-phenyl)-3-methyl-1-phenyl,4-dihydro-pyrano[2,3-c]pyrazol-6-ylamine
C₂₅H₁₉BrClN₃O: Light brown powder, IR (KBr) in cm⁻¹: 3336, 3176, 3150, 1650, 1535; ¹H NMR (DMSO-d₆): δ 2.18 (s, 3H, CH₃), δ 4.18 (s of -C-H proton of pyrano) δ 5.40 (brs, 2H -NH₂), δ 6.9-7.80 (m, 13H, Ar-H), MS, m/z: m/z: 491.04 (100.0%)

Entry 7.5-(4-chlorophenyl)-4-(4-methoxyphenyl)-3-methyl-1-phenyl-1,4-dihydropyrano[2,3-c]pyrazol-6-amine
Pale yellow powder, IR (KBr) in cm⁻¹: 3358, 3150, 3176, 1650, 1520; ¹H NMR (DMSO-d₆): δ 2.19 (s, 3H, CH₃), δ 4.20 (s of -C-H proton of pyrano) δ 5.42 (brs, 2H -NH₂), δ 6.9-7.80 (m, 13H, Ar-H), MS, m/z: 443.14 (100.0%)

III. RESULT AND DISCUSSION

The development of multi-component reaction (MCR) protocols for heterocyclic Conclusions. Considering the importance of green chemistry, the reaction was performed solvent- and catalyst-free at room temperature and 80°C for 60 min. No desired product formed. Organic chemists' increasing interest in PEG-400 as a solvent of choice^{10,11} use it as a green solvent in the present study. In subsequent optimization experiments, PEG-400 was used as a reaction solvent. The reaction went smoothly, and the solvent can be recycled. We studied the one-pot, three-component reaction protocol with PTSA(cat). PEG-400 was the most effective, green, and environmentally friendly solvent we observed.

To synthesize the desired product in quantitative yield, we added 5% of PTSA(cat). even after two hrs of reflux, the reaction wasn't complete. Adding 5% more catalyst to the same reaction mixture completed it in 10 minutes. With 10% catalyst, the same reaction takes 20-30 minutes. 10 weight % of catalyst is needed to convert all three reactants into a product smoothly and quickly.

IV. CONCLUSION

At last, 10% PTSA and PEG-400 as a green solvent, we have developed a general and simple method for the synthesis of pyrano-pyrazoles derivatives. PEG-400 is a biodegradable and reusable solvent that helps protect the environment. Up to three cycles, the catalyst has been seen to perform well in throughout the reaction.

V. ACKNOWLEDGEMENTS

Authors are thankful to principal M.G.Vs. L.V. H College for providing laboratory facilities. One of the authors SSC thankful to SPPU, BOD, Research Cell for Financial support for project under Aspire Mentorship scheme.

VI. REFERENCES

- [1]. Ghodke, Swati S., et al. "One-pot synthesis of pyrano [2, 3-c] pyrazoles using lemon peel powder as a green and natural catalyst." *European Chemical Bulletin* 9.2 (2020): 38-42.
- [2]. Patil, Ravindra M., and A. P. Rajput. "Synthesis of 6-Amino-2, 4-Dihydropyrano-[2, 3-c] Pyrazol-5-Carbonitriles Catalyzed by Cerium (IV) carboxymethylcellulose under Solvent-Free Conditions." *Applicable Chem* 7.3 (2018): 553-558.
- [3]. Ji, Ke-Gong, et al. "PtCl₂-catalyzed tandem triple migration reaction toward (Z)-1, 5-dien-2-yl esters." *Organic Letters* 10.17 (2008): 3919-3922.
- [4]. Miura, Tomoya, and Masahiro Murakami. "Formation of carbocycles through sequential carboration triggered by addition of organoborons." *Chemical communications* 3 (2007): 217-224.
- [5]. Vasuki, Gnanasambandam, and KandhasamyKumaravel. "Rapid four-component reactions in water:

- synthesis of pyranopyrazoles." *Tetrahedron Letters* 49.39 (2008): 5636-5638.
- [6]. Ugi, Ivar. "Recent progress in the chemistry of multicomponent reactions." *Pure and Applied Chemistry* 73.1 (2001): 187-191.
- [7]. Kees, Kenneth L., et al. "New potent antihyperglycemic agents in db/db mice: Synthesis and structure-activity relationship studies of (4-substituted benzyl) (trifluoromethyl) pyrazoles and-pyrazolones." *Journal of medicinal chemistry* 39.20 (1996): 3920-3928.
- [8]. Genin, Michael J., et al. "Novel 1, 5-diphenylpyrazole nonnucleoside HIV-1 reverse transcriptase inhibitors with enhanced activity versus the delavirdine-resistant P236L mutant: lead identification and SAR of 3-and 4-substituted derivatives." *Journal of medicinal chemistry* 43.5 (2000): 1034-1040.
- [9]. Dawane, B. S., et al. "One-pot multicomponent synthesis and antimicrobial evaluation of some novel pyrano-[2, 3-c]-pyrazoles derivatives." *Der Pharma Chemica* 3.3 (2011): 300-305.
- [10]. Wang, Liang, et al. "PEG-supported imidazolium chloride: a highly efficient and reusable reaction medium for the Heck reaction." *Synlett* 2005.12 (2005): 1861-1864.
- [11]. Chobe, Santosh S., et al. "Poly (ethylene glycol) (PEG-400): A green approach towards synthesis of novel pyrazolo [3, 4-d] pyrimidin-6-amines derivatives and their antimicrobial screening." *Archives of Applied Science Research* 6.2 (2014): 61-66.

Thienodiazepine - A Comprehensive Review of Their Synthesis and Diverse Biological Importance

Vidya S. Dofe¹, Anant B. Kanagare¹, Dattatraya N. Pansare¹, Ravindra D. Suryawanshi², Rajendra P. Pawar^{2*}

¹Department of Chemistry, Deogiri College, Aurangabad-431 005, Maharashtra, India

²Department of Chemistry, Shivchhatrapati College, Aurangabad-431 003, Maharashtra, India

ABSTRACT

The concept of privileged structure, which is defined as “a single molecular framework able to provide ligands for diverse receptors”, has emerged as a powerful approach to increase the chances of discovering lead compounds. The thienodiazepine scaffold is one of the classical examples of privileged structures, which has proved its effectiveness in a number of pharmaceutical drugs and still continues to attract much interest today in medicinal chemistry. The discovery of thienodiazepine as central nervous system depressants, many synthetic derivatives that display a wide range of therapeutic applications. This review outlines the biological importance and synthesis of various types of thienodiazepine derivatives from various heterocyclic moiety.

I. INTRODUCTION

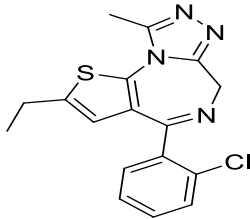
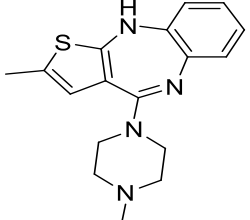
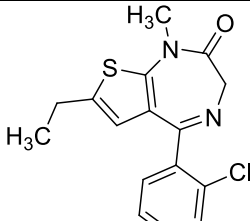
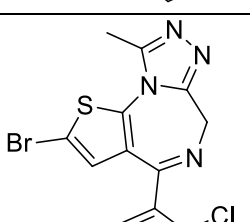
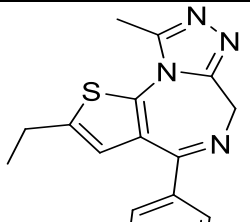
Benzodiazepines play an important role in pharmacotherapy for anxiety and depressive psychosis. Most of them have a bicyclic core consisting of benzene and 1,4-diazepine (i.e., 1,4-benzodiazepine), but 2,3-benzodiazepines including tofisopam are also used as anti-anxiety drugs. Furthermore, a bioisosteric replacement of benzene by thiophene created several anxiolytic thienodiazepines represented by etizolam (Garg, B et al. 2014).

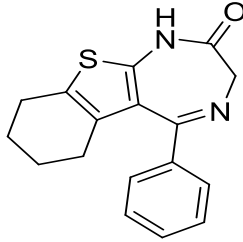
1,4-Thienodiazepine-2,5-diones have been synthesized via the Ugi-Deprotection-Cyclization (UDC) approach starting from 2-aminothiophenes in a convergent and versatile manner. 1,4-thienodiazepine-2,5-diones have been screened for the activity against p53-Mdm2 interaction. Biological evaluations demonstrated that some compounds exhibited promising antagonistic activity (Huang, Y. et al. 2010). Acid-promoted condensation of a hydrazonoester derived from phenylalanine afforded an azine which was converted to a pyrrole through 3 steps: isomerization to dienamine, [3,3]-sigmatropic rearrangement, and cyclization. In this study, reaction behavior of the intermediate proved to be switched depending on the type of the aromatic ring. Hydrazonoesters derived from thienylalanines afforded various thienodiazepine derivatives under thermal acidic conditions. A more reactive thiophene ring is likely to undergo Friedel-Crafts reaction prior to isomerization to dienamine (Ohtake, K. et al. 2021). 4-aryl-thieno[1,4]diazepin-2-ones were synthesized and evaluated for their antiproliferative activities against the A375P melanoma and U937 hematopoietic cell lines (Lee, J. et al. 2018). A series of 5-substituted thieno[3,2-e][1,4]diazepin-2-ones was synthesized in four steps from methyl 3-aminothiophene-2-carboxylate. After the coupling of 3-aminothiophene with α -amino acids,

the key final step that involves an uncatalysed Pictet–Spengler reaction allowed the cyclization of the seven-membered diazepinone ring (Denoyelle, S. et al. 2015).

Thiophene isoster (namely thieno- [1,4]diazepine) scaffold has shown interesting properties over the past years. The drugs containing thienodiazepinemoiety and their biological activities are shown in **Table 1**.

Table 1. Drugs containing thienodiazepine moiety

Sr. No.	Name of Compound	Structure	Uses	Reference
1	Etizolam		Anxiolytic	Garg, B et al. (2014)
2	Olanzapine		Bipolar disorder and antipsychotic agent	Pryor, K. et al. (2019), Clarke, Z. et al. (2007)
3	clotiazepam		Insomnia, anxiety and anesthesia before	Kawakami Y, et al (2015)
4	brotizolam		hypnotic in the management of insomnia, anticonvulsant, antianxiety and muscle relaxant properties	Langley, M. S. et al. (1988)
5	Deschloroetizolam		stimulates GABA-A receptors	Sommerfeld-Klatta, K. et al. (2020)

6	Bentazepam		CNS depressant	Otero, F. J. et al. (1994)
---	------------	---	----------------	----------------------------

II. CONCLUSION

Thienodiazepine have a high significance in the field of medicinal chemistry with broad-spectrum of pharmacological activities. Thus, thienodiazepine can be useful for design and formation of novel drugs. Thienodiazepine may lead to potent type drugs with range of therapeutic applications as compared to presently available pharmacological agents.

III. ACKNOWLEDGMENT

The authors are thankful to Dr. Rajendra Pawar, Principal, Shivchhatrapati College, Aurangabad, Maharashtra, India for providing a platform to work on Heterocyclic moieties.

IV. REFERENCES

- [1]. Denoyelle, S., Tambutet, G., Masurier, N., Maillard, L. T., Martinez, J., & Lisowski, V. (2015). Synthesis of Thieno[3,2-e][1,4]diazepin-2-ones: Application of an Uncatalysed Pictet-Spengler Reaction. *European Journal of Organic Chemistry*, 2015(32), 7146–7153. doi:10.1002/ejoc.201500943
- [2]. Garg, B., & Gupta, S. (2014). A case of etizolam dependence. *Indian Journal of Pharmacology*, 46(6), 655. doi:10.4103/0253-7613.144943
- [3]. Huang, Y., Wolf, S., Bista, M., Meireles, L., Camacho, C., Holak, T. A., & Dömling, A. (2010). 1,4-Thienodiazepine-2,5-diones via MCR (I): Synthesis, Virtual Space and p53-Mdm2 Activity. *Chemical Biology & Drug Design*, 76(2), 116–129. doi:10.1111/j.1747-0285.2010.00989.x
- [4]. Kane O. Pryor, Kingsley P. Storer, in *Pharmacology and Physiology for Anesthesia* (Second Edition), 2019
- [5]. Kawakami Y, et al: Refractory case of adrenergic urticaria successfully treated with clonazepam. *J Dermatol* 2015; 42: 635.
- [6]. Langley, M. S., & Clissold, S. P. (1988). Brotizolam. *Drugs*, 35(2), 104–122. doi:10.2165/00003495-198835020-00002
- [7]. Lee, J., Jung, H., Kim, M., Lee, E., Im, D., Aman, W., & Hah, J.-M. (2018). Discovery of novel 4-aryl-thieno[1,4]diazepin-2-one derivatives targeting multiple protein kinases as anticancer agents. *Bioorganic & Medicinal Chemistry*, 26(8), 1628–1637. doi:10.1016/j.bmc.2018.02.009
- [8]. Ohtake, K., Tsuda, J., Takatori, K., Nagumo, S., & Yasui, E. (2021). Chemical switching in reaction

- behavior of azine: Synthesis of a novel thienodiazepine derivative. *Tetrahedron Letters*, 71, 153043. doi:10.1016/j.tetlet.2021.153043
- [9]. Otero, F. J., Hernandez-Herrero, C., Martinez-Arevalo, M.-J., Garrido, J., Armenteros, S., & Velasco, J. (1994). Fluoxetine/benzazepam combination in the treatment of dysthymic disorders. *Current Therapeutic Research*, 55(5), 519–531. doi:10.1016/s0011-393x(05)80182-1
- [10]. Sommerfeld-Klatta, K., Łukasik-Gł ębicka, M., Tezyk, A.; Panie ński, P., Zaba, C., Zieli ńska-Psuja, B. (2020) Clonazolam a new designer benzodiazepine intoxication confirmed by blood concentration. *Forensic Sci. Int.*, 310, 110237
- [11]. Thomas Kraemer, Hans H. Maurer, in *Handbook of Analytical Separations*, 2008
- [12]. Zoe Clarke, in *xPharm: The Comprehensive Pharmacology Reference*, 2007

Green And Efficient Synthesis of Bis (Indolyl) Methanes Using Zinc Triflate

Nakkalwar S. L., Kasralikar H. M., Kaminwar N. S.*

Department of Chemistry, Lal Bahadur Shastri Mahavidyalaya, Dharmabad-431809, Maharashtra, India

ABSTRACT

Zinc triflate has been successfully used as catalyst for efficient and green synthesis of pharmaceutically valued bis (indolyl) methanes by the reaction of aromatic aldehydes with indole in aqueous ethanol as a green solvent. Excellent yield of products within a short period of time at reflux temperature were obtained.

Keywords: Aldehydes, Indole, Bis (indolyl) methane, Zinc triflate

I. INTRODUCTION

The heterocycles containing indole motif owe their existence in various natural commodities like agrochemicals and pharmaceuticals [1-3]. Especially, the nitrogen containing 3,3'-bis(indolyl)methanes (BIMs) with two indole motifs united by a single carbon at 3-position are the well-known class of alkaloids [4] and isolated from plant and marine sources [5]. The various activities that they exhibit, includes cytotoxic, insecticidal, antibacterial, antioxidative and activities. Because of their vast biological activity various methods of their synthesis have been reported in the literature. Most of the methods involve the use of conventional Lewis acids as well as protic acids as catalysts to promote electrophilic substitution reaction of indoles with various aldehydes or carbonyl compounds [6]. A variety of other catalysts such as sulphamic acid [7], $\text{In}(\text{OTf})_3$ [8], LiClO_4 [9], bis(cyclopentadienyl) ZrCl_2 [10], CuBr_2 [11], ZrCl_4 [12], $\text{Zn}(\text{HSO}_4)_2$ [13], polyindole salt [14], CAN [15], N-tert-butanefulfinyl aldimines [16], ion exchange resin [17], acetic acid [18], InCl_3 [19], InF_3 [20], $\text{Dy}(\text{OTf})_3$ [21], $\text{Ln}(\text{OTf})_3$ [22], $\text{FeCl}_3 \cdot 6\text{H}_2\text{O}$ [23], $\text{V}(\text{HSO}_4)_3$ [24], SBA-15/ SO_3H [25], oxalic acid [26], $\text{CF}_3\text{COONH}_4$ [27] vanadomolybdo phosphoric acid [28] have been reported for the synthesis of bis(indolyl) methanes. These reported synthetic methods are considered to be highly atom-efficient, but it has some major demerits like the use of toxic reagents and solvents, longer reaction time, tedious workup procedure, elevated reaction temperature, poor yield of products etc., are drawbacks that limit the scale-up of most of these procedures.

Considering these various points, herein we put forward a simple synthetic protocol, for the synthesis of the bis (indolyl) methanes in excellent yield, utilizing zinc triflate as an efficient catalyst. Zinc trifluoromethane sulfonate (zinc triflate) is commercially available as zinc salt of trifluoromethane sulfonic acid, which is commonly used as a Lewis acid catalyst. It is better catalyst amongst most of the Lewis acid catalysts. For different chemical transformations zinc triflate is successfully applied^{39,40, 41}.

So in this present report, we have developed a new synthetic protocol for the facile synthesis of bis (indolyl) methanes from the corresponding aromatic aldehydes and indoles *via* the electrophilic substitution of indoles with different aromatic aldehydes using zinc triflate, an eco-friendly catalyst at reflux temperature in (1:1) water: ethanol. The method includes comfortable handling, easy separation of the products.

II. RESULTS AND DISCUSSION

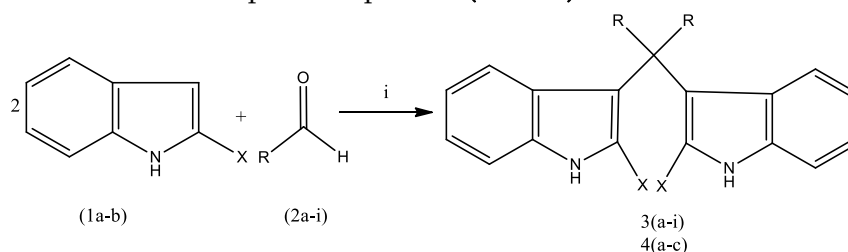
The synthesis of bis (indolyl) methane derivatives in 1:1 aqueous ethanol by one pot reaction of indole with aromatic aldehyde catalyzed by zinc triflate is presented in this paper (**Scheme 1**). The reaction of indole (2 mmol) and benzaldehyde (1 mmol) was selected as a model reaction in 1:1 aqueous ethanol in order to optimize the reaction conditions. The model reaction was converted to 3a in higher yield using Zn(OTf)₂ catalyst (**Table 1**).

Table 1: Optimization of reaction between indole and aromatic aldehyde under reflux.

Entry	Solvent	Time (min)	Catalyst (mol%)	Isolated yield (%)
1	DMF	38	10	48
2	THF	30	10	52
3	MeOH	24	10	82
4	EtOH	22	10	84
5	EtOH:H ₂ O (1:1)	10	10	90

A set of reaction was examined in various solvents under reflux (**Table 1**). Firstly, the reactions were conducted in five different solvents (entries 1-5, **Table 1**). The best deal was obtained in EtOH:H₂O (1:1) (entry 5, **Table 1**) using 10 mol% of the catalyst. The reactions using other solvents gave moderate to low yield of product (entries 1-4, **Table 1**). Different catalytic conditions were also applied in EtOH:H₂O (1:1); high yield was found when 10 mol% of the catalyst is used (entry 5, **Table 1**). Therefore, we confirmed the same reaction conditions for the synthesis of different bis (indolyl) methane derivatives. The workup of reaction involves only filtration and washing with hot ethanol. The catalyst was separated from the product by filtering it with hot ethanol.

All reactions were conducted under reflux for 10-18 min in (1:1) aqueous ethanol in presence of 10 mol% of Zn(OTf)₂ catalyst. The products were obtained in good yields. Molecular structures of the products were characterized by ¹H NMR and ESI-MS spectroscopic data (**Table 2**).



Scheme 1: Reagent and conditions: (i) 10mol% Zn(OTf)₂, water:ethanol (1:1) 5 mL, reflux (0-80°C) for 08-18 min.

Table2: One pot synthesis of bis (indolyl) methane derivatives in 1:1 aqueous ethanol by Zn(OTf)₂^a.

Entry	Indole X= H, CH ₃	2 (a-i)	Product	Time (min.)	Yield ^b (%)	MP °C
1	H	Benzaldehyde	3a	10	92	98-99 ²⁷
2	H	4-Chloro Benzaldehyde	3b	13	88	78-79 ²⁷
3	H	4-Nitro Benzaldehyde	3c	16	87	224-225 ²⁷
4	H	4-Hydroxy Benzaldehyde	3d	10	91	123-125 ²⁷
5	H	4-Bromo Benzaldehyde	3e	12	86	110-112 ²⁷
6	H	4-Dimethyl amino Benzaldehyde	3f	10	90	180-181 ²⁷
7	H	Vaniline	3g	09	86	110-112 ²⁷
8	H	4-Anisaldehyde	3h	08	90	190-191 ²⁷
9	H	Furfuraldehyde	3i	11	88	>300 ²⁷
10	CH ₃	Benzaldehyde	4a	11	87	246-248 ²⁷
11	CH ₃	4-Anisaldehyde	4b	10	90	210-211 ²⁷
12	CH ₃	4-Nitro Benzaldehyde	4c	18	91	240-242 ²⁷

^aSubstituted Indol (2 mmol), aromatic aldehyde (1 mmol), H₂O:EtOH (1:1) (5 mL), reflux.

^bisolated yield

III. EXPERIMENTAL

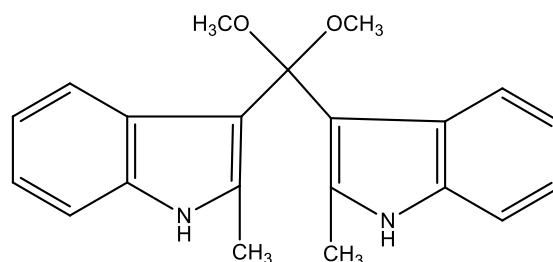
General details

Chemicals were Sigma Aldrich, Alpha Aiser and Spectochem made and used as such without further purification. ¹H NMR spectra was recorded on a Bruker (400 MHz) spectrophotometer using DMSO-d₆ as deuterated solvent with tetramethylsilane (TMS) as the internal standard. Reactions were monitored by TLC using Merk silica gel plates. Products were characterized by ¹H NMR and Mass spectra.

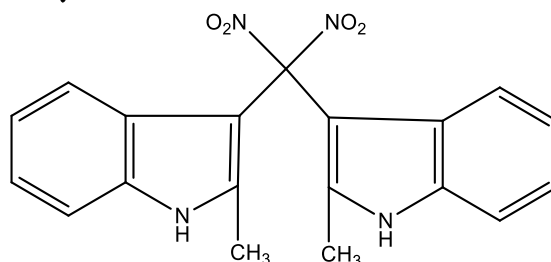
General procedure for the synthesis of bis (indolyl) methane derivatives:

A mixture of indole (2 mmol), aromatic aldehyde (1 mmol) were refluxed (70-80°C) with stirring in the presence of Zn(OTf)₂ (10 mol%) in solvent system in (1:1) aqueous ethanol on oil bath. The progress of reaction was monitored by TLC. After completion of reaction, the mixture was filtered. The residue was washed with warm ethanol to separate the Zn(OTf)₂ catalyst. After cooling the ethanolic reaction phase, the precipitate was filtered. The crude products were purified by recrystallization from 95% ethanol.

Characterization Data:



3,3'-((4-Methoxy phenyl) methylene) bis(2-methyl-1H-indole) (Table 2, entry 4b) Brown solid, **m.p.** 210-211°C, IR (KBr) cm^{-1} 3392, 3043, 2960, 2998, 1610, 1514, 1460, 1342, 1216, 1035; **$^1\text{H NMR}$ (400 MHz CDCl_3) δ ppm** 2.1(s, 6H), 3.75 (s, 3H), 5.90 (s, 1H), 6.85 (dd, 2H), 6.9 (dd, 2H), 7.05 (m, 6H), 7.2(d, 2H), 7.75 (2H, br's, NH); **ESMS** 409(M⁺); **Elemental analysis Cal.** C=82.07, H=6.36, N=7.36, found C= 81.9, H= 6.089, N=7.02.



3,3'-((4-Nitro phenyl) methylene) bis(2-methyl-1H-indole) (Table 2, entry 4c) Yellow solid, **m.p.** 240-242°C, IR (KBr) cm^{-1} 3388, 3058, 2911, 2848, 1620, 1596, 1518, 1460, 1426, 1388, 1340, 1221, 850; **$^1\text{H NMR}$ (400 MHz CDCl_3) δ ppm** 2.11(s, 6H), 6.6 (s, 1H), 6.85-6.95 (m, 4H), 7.1 (d, 2H), 7.25 (d, 2H), 7.5(d, 2H), 7.8 (s, 2H), 8.1 (s, 2H) **ESMS** 395 (M⁺); **Elemental analysis Cal.** C=75.93, H= 5.35, N= 10.63; found C=73.77, H=5.31, N=10.64.

IV. CONCLUSION

An efficient and simple method for the synthesis of spiro [indoline3,4' pyrano [2,3-c] pyrazole] derivatives was developed via one pot three component reaction of isatins, malononitrile and enolisable 1,3 dicarbonyl compounds under reflux in 1:1 aqueous ethanol using $\text{Zn}(\text{OTf})_2$ as a heterogeneous catalyst. This procedure offers several advantages like higher yields, quick reactions, convenient and simple procedure and ecofriendly reaction conditions.

V. ACKNOWLEDGEMENTS

We are thankful to the Principal, L.B.S. College, Dharmabad and Dharmabad Shikshan Sanstha for providing us the research facilities.

VI. REFERENCES

- [1]. Singh, T.P.; Singh, O.M. Mini-Reviews. Med. Chem., 2017, 18(1), 9-25.
- [2]. Sharma, V.; Kumar, P.; Pathaka, D. J. Heterocycl. Chem., 2010, 47(3), 491-502.
- [3]. Segraves, N.L.; Crews, P. J. Nat. Prod., 2005, 68(10), 1484-1488.
- [4]. Praveen, P.J.; Parameswaran, P.S.; Majik, M.S. Synthesis, 2015, 47(13), 1827-1837.
- [5]. (a) R. J. Sundberg, The Chemistry of Indoles, Academic Press, New York, 1996; (b) A. Casapullo, G. Bifulco, I. Bruno and R. Riccio, J. Nat. Prod., 2000, 63, 447; (c) T. R. Garbe, M. Kobayashi, N. Shimizu, N. Takesue, M. Ozawa and H. Yukawa, J. Nat. Prod., 2000, 63, 596.
- [6]. (a) P. T. Perumal and R. Nagarajan, Tetrahedron, 2002, 58, 1229; (b) M. Chakrabarty, N. Ghosh, R. Basak

- and Y. Harigaya, *Tetrahedron Lett.*, 2002, 43, 4075; (c) D. Chen, L. Yu and P. G. Wang, *Tetrahedron Lett.*, 1996, 37, 4467; (d) J. S. Yadav, B. V. Reddy, C. V. Murthy, G. M. Kumar and C. Madan, *Synthesis*, 2001, 783.
- [7]. P. R. Singh, D. U. Singh and S. D. Samant, *Synth. Commun.*, 2005, 35, 2133.
- [8]. Shun-Jun Ji, Min-Feng Zhou, Da-Gong Gu, Shun-Yi Wang and Teck-Peng Loh, *Synlett*, 2003, 13, 2077.
- [9]. J. S. Yadav, B. V. S. Reddy, V. S. R. Murthy and G. M. Kumar, *Synthesis*, 2001, 783.
- [10]. M. Lakshmi Kantam, K. Aziz and P. R. Likhari, *Catal. Lett.*, 2004, 98, 117.
- [11]. L. Mo, Z. Ma and Z. Zhang, *Synth. Commun.*, 2005, 35, 1997.
- [12]. R. R. Nagawade and D. B. Shinde, *Bull. Korean Chem. Soc.*, 2005, 26(12), 1962.
- [13]. K. Niknama, M. A. Zolfigolb, T. Sadabadi and A. Nejati, *Journal of the Iranian Chemical Society*, 2006, 3, 318.
- [14]. S. Palaniappan and A. John, *J. Mol. Catal. A: Chem.*, 2005, 42, 168.
- [15]. X. Zeng, S. Ji and S. Wang, *Tetrahedron*, 2005, 61, 10235.
- [16]. B. Ke, Y. Qin, Q. He, Z. Huang and P. Wang, *Tetrahedron Lett.*, 2005, 46, 1751.
- [17]. F. Xin-Liang, G. Chuan-Jin and Z. Cheng-Xue, *Synth. Commun.*, 2004, 34, 487.
- [18]. A. Kamal and A. A. Qureshi, *Tetrahedron*, 1963, 19, 513.
- [19]. G. Babu, N. Sridhar and P. T. Perumal, *Synth. Commun.*, 2000, 30, 1609.
- [20]. B. P. Bandgar and K. A. Shaikh, *J. Chem. Res. Synop.*, 2004, 34.
- [21]. X.-L. Mi, S.-Z. Luo, J.-Q. He and J.-P. Cheng, *Tetrahedron Lett.*, 2004, 45, 4567.
- [22]. D. Chen, L. Yu and P. G. Wang, *Tetrahedron Lett.*, 1996, 37, 4467.
- [23]. Shun-Jun Ji, Min-Feng Zhou, Da-Gong Gu, Zhao-Qin Jiang and Teck-Peng Loh, *Eur. J. Org. Chem.*, 2004, 1584.
- [24]. F. Shirin, A. Yahyazabeh, M. Abedini and D. Imami, *Bull. Korean Chem. Soc.*, 2010, 31, 1715.
- [25]. M. A. Naik, D. Sachdev and A. Dubey, *Catal. Commun.*, 2010, 11, 1148.
- [26]. R. G. Vaghei, H. Veisi, H. Keypour and A. A. Firouzabadi, *Mol. Diversity*, 2010, 14, 87.
- [27]. Vivekanand B. Jadhav¹, Srinivas L. Nakkalwar, Sunil U. Tekale, Shivaji B. Munde and S. B. Patwari, *Der Chemica Sinica*, 2015, 6(2):20-24
- [28]. E. Rafiee, Z. Zolfagharifar, M. Joshaghani and S. Eavani, *Appl. Catal., A*, 2009, 365, 287
- [29]. Yamazaki, S.; Takebayashi, M.; Miyazaki, K. *J. Org. Chem.* 2010, 75(4), 1188-1196.
- [30]. Nisa, R. U.; Ayub, K. *New J. Chem.* 2017, 41(12), 5082-5090. Doi10.1039/c7nj00312a
- [31]. Uday Kumar, N.; Sudhakar Reddy, B.; Prabhakar Reddy, V.; Bandichhor, R. *Tetrahedron Letters*, 2014, 55, 910-912.

Synthesis, Characterization and Biological Activity of New Schiff Bases Derived from Aminopyrimidine and Their Metal Complexes

D. T. Sakhare

U.G, P.G. & Research Centre, Department of Chemistry, Shivaji, Art's, Commerce & Science College Kannad,
Dist. Aurangabad-431103, Maharashtra, India

ABSTRACT

The new Schiff bases derived from 2-amino-4,6-dimethylpyrimidine with 2,4-dihydroxybenzaldehyde (L_1) and their complexes with Cu (II) has been prepared. These complexes were characterized by elemental analysis, 1H NMR, IR and electronic spectra, and with the aid of magnetic moment, molar conductivity and mass spectrometry. We further determined some of their size on the nanoscale. The results indicated that Schiff bases behaved as a bidentate NO chelator that coordinates to the metal ions by azomethine nitrogen, pyrimidine nitrogen and phenolic oxygen, demonstrating 1: 2 (metal to ligand) ratios. The measurements of conductivity revealed a nonelectrolytic nature of the complexes. The ligand and its complexes were screened for their antifungal and antibacterial activity against *Aspergillus niger*, *Penicillium chrysogenum*, *Fusarium moneliforme* and *Aspergillus flavus* and *Escherichia coli*, *Salmonella typhi*, *Staphylococcus aureus*, *B. subtilis*. The result indicated that the complexes exhibited good antifungal and antibacterial activities.

Keywords: Heterocyclic Schiff bases, 2-amino-4,6-dimethylpyrimidine, 2,4-dihydroxybenzaldehyde, Biological Activity.

I. INTRODUCTION

Pyrimidine constitutes major nucleotides of deoxyribonucleic acid (DNA) and ribonucleic acid (RNA). However, derivatives of pyrimidine are widely distributed in nature. e.g. thiamine (vitamin B_2) and olloxan. Pyrimidine compounds are known to play vital roles in coordination chemistry as they easily form Schiff bases with carbonyl (aromatic and non-aromatic) compounds. Coordination chemistry is undoubtedly the most active research area in inorganic chemistry. Several thousands of coordination complexes have been synthesized and investigated during the past few decades. Ever since the importance of coordination phenomenon in biological processes was realized, lot of metal containing macromolecules have been synthesized and studied to understand the role of these ligands in biological systems, and they also contribute to the development of new metal-based chemotherapeutic agents. These have resulted in the emergence of an important branch of inorganic chemistry viz. bioinorganic chemistry because in several cases, the metal chelates have been found to be more antimicrobial than the chelating agents themselves.

phosphorylation of tyrosine residues in proteins. There are usually functional modifications of the proteins and mutations of this kinase can cause cancer [15]. Cryptogein (1LRI) is a small protein that has a sterol carrier activity as it acts as a sterol shuttle that helps the pathogen grow and complete its life cycle [16]. ATPase (2OBM) is a type III secretion system (T3SS) that is involved in the initial stages of selective secretion of specialized T3SS virulence effector proteins from the bacterial cytoplasm to the infected host cell, a process crucial to subsequent pathogenicity. In addition, zidovudine and pyrrolo-pyrimidine nucleoside derivatives are in use as anti-HIV and anti-hepatitis-c drugs [17]. The many therapeutic activities exhibited by pyrimidinyl containing drug/compounds could be attributed to their low toxicity and structural diversity [18]. Pyrimidine bioactive derivatives reportedly form stable Schiff bases which can be used as molecular metal ion chelators [19]. It has also been shown that the efficacy of pyrimidine bioactive molecules is enhanced in its coordination to metal ions [20-22]. Heteroleptic metal complexes of pyrimidinyl Schiff bases bearing hetero (N and O) atoms show high kinetic and thermodynamic stabilities, mixed chelation abilities in biological fluid systems and have the ability to prevent induced cellular oxidative stress damages [23].

Heterocyclic Schiff base ligands containing O- or N-donors and their metal complexes have been shown to exhibit interesting properties [24] and those containing pyrimidine rings represent a promising class of compounds due to their inherent biological and pharmaceutical properties [25]. Pyrimidine based compounds exhibit a broad spectrum of biological activities [26]. Pyrimidine with its interesting heterocyclic structure has extensively been used in drug design due to its potential antimicrobial, antifungal, antiviral and antitumor properties. Many ligands containing the pyrimidine ring and their transition metal complexes have been synthesized and tested for biological and therapeutic properties where they sometimes act as models for the active sites of biomolecules [27]. The importance of 2-benzoylpyridine metal complexes, for example, is due to their ability to facilitate substrate binding thus stabilizing the reactive intermediates of transition metals [28]. Copper complexes have recently been the subject of intense research because of their potentials as radiopharmaceuticals for targeting hypoxic tissues and as effective drugs for the treatment of refractory neuroblastoma in children. Copper is an important trace element for plants and animals and is involved in mixed ligand complex formation in a number of biological processes [29]. Many cobalt(II) complexes of Schiff base ligands containing 2-benzoylpyridine behaved as a growth inhibitor for microorganisms. Binuclear copper(II) complexes with monoatomic bridges, such as halides, have attracted recent attention due to their structural diversity and interesting catalytic, magnetic and biological properties [30]. The crystalline architectures of these compounds are found to be interesting due to variations in the nature of intervening intermolecular forces.

In the present work, we report a synthesis, characterization, antibacterial and antifungal studies of a Schiff base derived from 2-amino-4,6-dimethylpyrimidine and 2,4-dihydroxybenzaldehyde and its iron (III) complexes. Also, the structure of prepared ligands were checked by FT-IR, ¹H- NMR, UV-Vis techniques and prepared complexes were characterized by FT-IR, UV-Vis, molar conductivity and magnetic susceptibility measurements.

II. EXPERIMENTAL SECTION

2.1. Materials:

Chemicals and reagents used in this work: 2-amino-4,6-dimethylpyrimidine, 2,4-dihydroxybenzaldehyde, $\text{Cu}(\text{NO}_3)_2 \cdot 2\text{H}_2\text{O}$, were obtained from Sigma-Aldrich Chemical Company.

2.2. Instrumentation:

IR spectra were recorded on FTIR (ATR)-BRUKER-TENSOR37 spectrometer using KBr pellets in the range of 4000-400 cm^{-1} . ^1H -NMR (Varian mercury 300MHZ) spectra of ligand were measured in DMSO using TMS as internal standard. X-RD was recorded on BRUKER D8 Advance. TGA- DTA was recorded on Shimadzu. The carbon, hydrogen and nitrogen contents were determined on Elemental model vario SHIMADZU spectrometer. Molar conductance of complexes was measured on Elico CM 180 conductivity meter using 10⁻⁴ M solution in DMSO. Magnetic susceptibility measurements of the metal chelates were done on a Guoy balance at room temperature using $\text{Hg}[\text{Co}(\text{SCN})_4]$ as a calibrant.

2.3. Procedures:

2.3.1. Synthesis of schiff base ligand (L_1):

The ligand was prepared by a modification of the reported methods [31]. The Schiff base ligand has been synthesized by refluxing a mixture of 0.01 mol (1.2015g) of 2,4-dihydroxybenzaldehyde, and 0.01 mol (1.2710 g) of 2-amino-4,6-dimethylpyrimidine, in 50 ml super dry ethanol refluxed for about 4h. Schiff base thus formed was cooled to room temperature and collected by filtration, followed by recrystallization in ethanol and dried in vacuo over anhydrous calcium chloride (Yield:76%).

2.3.2. Synthesis of metal complexes $[\text{M}(\text{L}_1)_2]$:

To a hot ethanol solution (25ml) of the ligand (2 mol) and (25ml) of metal Nitrate (1mol) was added with constant stirring. The pH of reaction mixture was adjusted to 7-8 by adding 10% alcoholic ammonia solution and refluxed for about 3 h. The precipitated solid metal complex was filtered off in hot condition and washed with hot ethanol and dried over calcium chloride in vacuum desiccators. (Yield: 75%) [32].

III. RESULTS AND DISCUSSION

Some of physical properties of Schiff bases ligands and their metal complexes are given in (Table 1).

Table 1: Physical properties of Schiff base ligands (L_1) and their metal complexes.

Compound Molecular formula	Mol. Wt.	M.P. Decomp temp. $^{\circ}\text{C}$	Colour	Molar Conduc. Mho. $\text{Cm}^2\text{mol}^{-1}$
L_1	244	98	Yellow	---
Cu-L_1	587	>300	Dark Yellow	19.27

Table: 2. Elemental Analysis of Fe(III) Complex

Compound	% Found (Calculated)			
	C	H	N	M
L ₁	52.54 (53.23)	3.53 (3.82)	16.60 (16.85)	----
Cu-L ₁	44.45 (44.32)	3.38 (3.30)	14.17 (14.16)	9.91 (9.87)

3.1. ¹H-NMR spectra of ligand:

The ¹H-NMR. Spectra of free ligand at room temperature show the following signals. 5.9 δ (s, 2H, Phenolic (OH) hydrogen of pyrimidine ring), 6.66 δ(s, 1H, Hydrogen bonded to pyrimidine ring), 7.94 δ (s, 1H, hydrogen bonded to azomethine carbon), 7.69-7.28 δ (D,4H, Aromatic Ha, Hb, protons of phenyl ring).

3.2. IR Spectra:

The IR spectrum in Fig.2 & 3 of free ligands shows characteristic bands at 3325, 1638, 1487,1207 and 1089 cm⁻¹ assignable to νOH (intramolecular hydrogen bonded), ν C=N (azomethine), ν C=C(aromatic), ν C-N (aryl azomethine) and ν C-O (Enolic) stretching modes respectively [3324] The absence of a weak broad band in the 3200-3400 cm⁻¹ region, in the spectra of the metal complexes suggests deprotonation of the intermolecular hydrogen bonded OH group on complexation and subsequent coordination of phenolic oxygen to the metal ion. This is further supported by downward shift in ν C-O (phenolic) [34] with respect to free ligand. On complexation, the ν (C=N) [35] band is shifted to lower wave number with respect to free ligand, denoting that the nitrogen of azomethine group is coordinated to the metal ion. The ν C-N band is shifted to lower wave number with respect to free ligand, The IR spectra of metal chelates showed new bands in between the 500-600 and 400-500 cm⁻¹ regions which can be assigned to ν M-O and M-N [36] vibrations respectively The IR spectra of Fe(III) show a strong band in the 3050-3600 cm⁻¹ region, suggesting the presence of coordinated water in these metal complexes. The presence of coordinated water is further confirmed by the appearance of non-ligand band in 830-840 cm⁻¹ region, assignable to the rocking mode of water. The presence of coordinated water is also established and supported by TG/DTA analysis of these complexes. Hence it is concluded that the coordination takes place via phenolic oxygen and azomethine nitrogen of ligand molecule in below Table 3.

Table: 3 Salient features of IR spectral data of ligands & Metal complex

Bond vibrational modes	O-H Free Stretching (cm ⁻¹)	C = N Azomethine Stretching (cm ⁻¹)	C = C Aromatic ring stretching (cm ⁻¹)	C -- N Aryl azomethine stretch (cm ⁻¹)	C -- O Enolic stretching (cm ⁻¹)	M--O	M--N
L ₁	3335	1648	1483	1205	1087	--	--
Cu-L ₁	1625.51	1433.20	1351.24	1190.22	1210.32	501.31	451.25

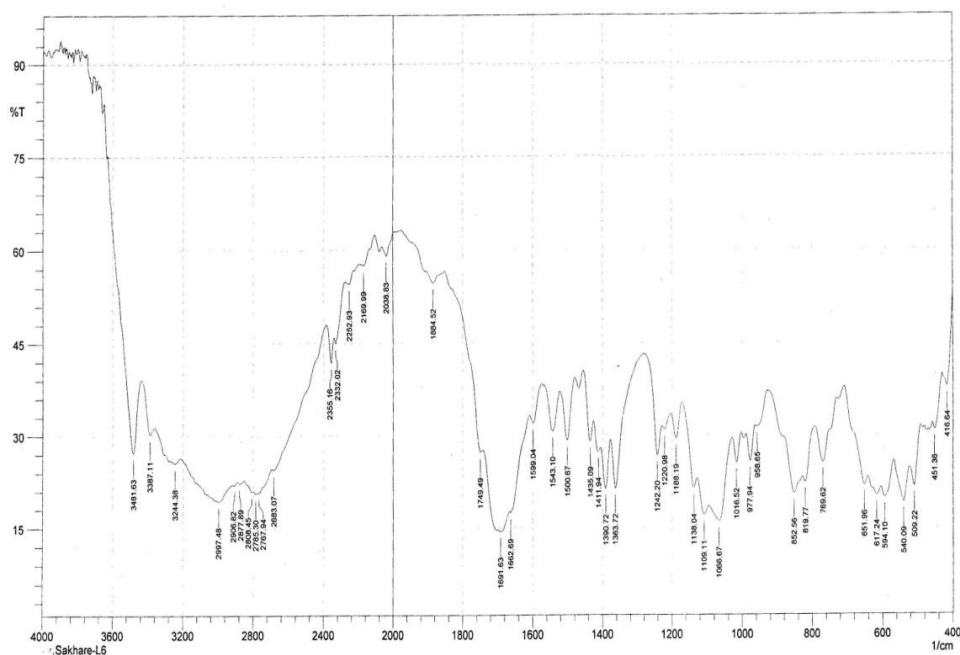


Fig. 2 Infrared Spectra of Ligand L

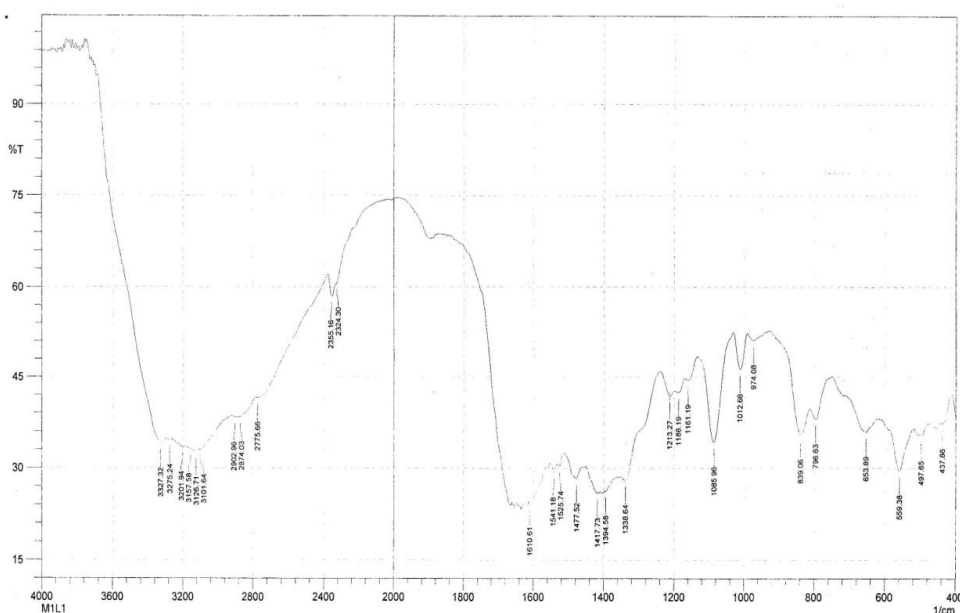


Fig. 3 Infrared Spectra of Cu(II) Complex of Ligand L

3.3. Molar conductance measurements:

The conductivity measurements of the complexes were recorded for (10^{-3} M), the solution of the samples was in (DMSo) at room temperature. The molar conductance values of the complexes showed in (Table 4). We concluded from the results that the Ni(II) complexes of the ligand (L₁) have a molar conductivity values in the range ($10.5 - 72.4 \Omega^{-1} \text{ mol}^{-1} \text{ cm}^2$). Which indicates that complexes are non-ionic therefore, they are considered as non-electrolytes[37].

3.4. Magnetic susceptibility:

The values of effective magnetic moment of metal complexes were summarized in (Table 1), which were measured at room temperature. The complexes [Fe(L₁)] have (μ_{eff}) in the range (2.81-2.97 B.M) this value is within the range of octahedral geometry[38].

3.5. Thermogravimetric analysis:

Thermal decomposition studies of complex have been carried out as to corroborate the information obtained from the IR spectral studies to know the presence of water molecule in these complexes as well as to know their decomposition pattern. The simultaneous TGA/DTA analysis of Fe(III) was studied from ambient temperature to 1000°C in nitrogen atmosphere using α -Al₂O₃ as reference. An analysis of the thermogram of the complexes indicated that Fe(III) complexes Fig. 4 shows two step decomposition. The first weight loss 6.66 0%, in between temp. 55-230°C could be correlated with the loss of two coordinated water (calculated 6.01 %). The anhydrous compound does not remain stable at higher temperature; it undergoes rapid decomposition in the range 230-650°C with 79.72 % mass loss corresponds to decomposition of the complex (calcd. 80.70%) in second step.

The decomposition is completed leading to the formation of stable residue of metal oxide Fe₂O₃ obs. 13.12 % (calcd. 13.28 %). The kinetic and thermodynamic viz the energy of activation (E_a), frequency factor (Z), entropy change (- ΔS) and free energy change (ΔG) for the non-isothermal decomposition of complexes have been determined by employing Horowitz-Metzger method [39] values are given in Table 3. The Calculated values of the given activation energy of the complexes are relatively low, indicating the autocatalysis effect of metal ion on the thermal decomposition of the complex. The negative value of activation entropy indicates that the activated complexes were more ordered than the reaction was slow. The more ordered nature may be due to the polarization of bonds in the activated state, which might occur through charge transfer transitions [40].

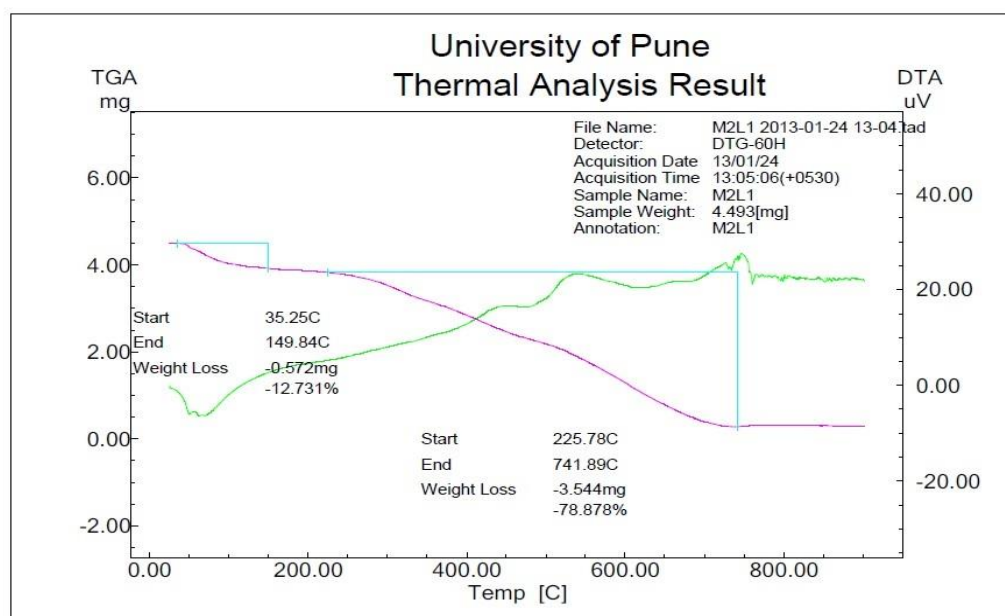


Fig. 4 TGA-DTA Curve of Cu (II) Complex of Ligand L₁

3.6. Electronic Spectra:

The electronic spectra of Schiff base ligand (L_1) show absorption bands at (42553cm^{-1} and 27027cm^{-1}) which are attributed to ($\pi \rightarrow \pi^*$) and ($n \rightarrow \pi^*$) transitions respectively, the complex of Ni(II) shows band at (42553cm^{-1}) which due to ($\pi \rightarrow \pi^*$) transition, the band at (23255cm^{-1}) is due to charge transfer (C.T), the band at (14814cm^{-1}) is due to the transition ${}^3A_{2g} \rightarrow {}^3T_{2g}$ the complexes are octahedral geometry[41].

3.7. X – Ray Diffraction Studies of Metal Complexes:

The Fe(III) complexes of ligand L_1 was selected for X-ray powder diffraction studies (Fig.5). X-ray powder data of all the main peaks have been indexed independently by trial and error method. The unit cell data crystal lattice parameters and the data obtained after indexing the powder data is presented in Table 4

The Fe(III) complex of ligand L_1 showed fourteen reflections with maxima at $2\theta = 9.77^\circ$ corresponding to d value 4.54\AA . The unit cell values of lattice constants are $a = 6.8760\text{\AA}$, $b = 9.2456\text{\AA}$, $c = 24.234\text{\AA}$, $\alpha = \beta = 90^\circ$ $\gamma = 120^\circ$ and unit cell volume $V = 1334.21763 (\text{\AA})^3$. The Ni(II) complex of ligand L_5 showed nine reflections with maxima at $2\theta = 6.49^\circ$ corresponding to d value 6.80\AA . The unit cell values of lattice constants are $a = 8.765\text{\AA}$, $b = 11.234\text{\AA}$, $c = 15.345\text{\AA}$, $\alpha = \beta = 90^\circ$ $\gamma = 120^\circ$ and unit cell volume $V = 1308.53064 (\text{\AA})^3$

Table: 4 Indexed X-ray Diffraction Data of Cu(II) Complex of Ligand L_1

Peak No.	2θ (observed)	2θ (calculated)	d (observed)	d (calculated)	Miller indices of Planes			Relative intensities (%)
					h	k	l	
1	6.63185	6.6037	6.68052	6.69818	1	1	0	100
2	8.05543	8.0484	5.5042	5.50176	0	1	2	2.75
3	9.29527	9.28274	4.7744	4.77537	1	1	2	29.15
4	10.38016	10.38215	4.27953	4.27439	2	1	0	38.77
5	13.88418	13.88596	3.21252	3.20971	1	0	4	50.77
6	16.09511	16.09389	2.78032	2.77873	2	0	4	3.59
7	17.46374	17.46372	2.5683	2.56679	0	3	3	11.51
8	18.85989	18.82103	2.38424	2.38769	2	2	4	5.55
9	21.01088	20.99559	2.14944	2.14989	1	1	6	5.43
10	25.76993	25.76125	1.77247	1.77234	0	4	5	1.58
11	28.94887	28.94172	1.59197	1.59179	3	3	6	1.78
12	31.47362	31.4613	1.47582	1.47589	1	3	8	2.15

Unit cell data and crystal lattice parameter

$a (\text{\AA}) = 9.59$	Volume(V) = $1219.0558 (\text{\AA})^3$
$b (\text{\AA}) = 9.34$	Density(obs.) = 1.0884gcm^{-3}
$c (\text{\AA}) = 13.61$	Density(cal.) = 1.0774gcm^{-3}
$\alpha = 90.00$	Z = 1
$\beta = 90.00$	Crystal system = Orthorhombic
$\gamma = 90.00$	Standard deviation (%) = 0.062 Porosity = 1.02%

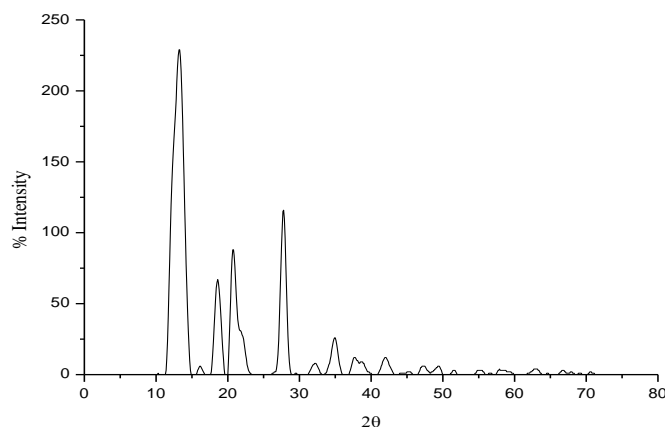


Fig. 5 X-ray Diffractogram of Cu(II) complex of L₁

IV. BIOLOGICAL ACTIVITY

4.1. Antibacterial activity & Antifungal Activity:

Antifungal activity and Antibacterial activity of ligand and metal complexes were tested in vitro against fungal such as *Aspergillus niger*, *Penicillium chrysogenum*, *Fusarium moneliforme*, *Aspergillus flavus* and bacteria such as *E. Coli*, *B.Subtilis*, *Staphylococcus aureus* and *Bacillus subtilis* by paper disc plate method [42]. The compounds were tested at the concentrations 1% and 2% in DMSO and compared with known antibiotics viz *Griseofulvin* and *Penicillin*. (Table 5 and 6). From Table 5 and 6, it is clear that the inhibition by metal chelates is higher than that of a ligand and results are in good agreement with previous findings with respect to comparative activity of free ligand and its complexes [42]. Such enhanced activity of metal chelates is due to the increased lipophilic nature of the metal ions in complexes. The increase in activity with concentration is due to the effect of metal ions on the normal cell process. The action of compounds may involve the formation of hydrogen bond with the active centre of cell constituents, resulting in interference with the normal cell process [43].

Table 5. Antifungal activity of ligands

Test Compound	Antifungal Growth								
	<i>Aspergillus niger</i>		<i>Penicilliumchrysogenum</i>		<i>Fusarium moneliforme</i>		<i>Aspergillus flavus</i>		
	1%	2%	1%	2%	1%	2%	1%	2%	
L ₁	-ve	-ve	-ve	-ve	-ve	-ve	-ve	-ve	-ve
Cu-L ₁	-ve	-ve	-ve	-ve	-ve	-ve	RG	+ve	+ve
+ve control	+ve	+ve	+ve	+ve	+ve	+ve	+ve	+ve	+ve
-ve control (Griseofulvin)	-ve	-ve	-ve	-ve	-ve	-ve	-ve	-ve	-ve

Ligand & Metal : +ve – Growth (Antifungal Activity absent)

-ve - Growth (Antifungal Activity present)

RG - Reduced Growth (More than 50% reduction in growth observed)

Table 6. Antibacterial activity of ligands and their metal complexes

Test Compound	Diameter of inhibition zone (mm)							
	<i>E. coli</i>		<i>Salmonella typhi</i>		<i>Staphylococcus aureus</i>		<i>Bacillus subtilis</i>	
	1%	2%	1%	2%	1%	2%	1%	2%
L	13mm	17mm	-ve	14mm	-ve	18mm	16mm	19mm
Cu-L	12mm	14mm	13mm	15mm	18mm	21mm	11mm	14mm
DMSO	-ve	-ve	-ve	-ve	-ve	-ve	-ve	-ve
Penicillin	14mm	14mm	18mm	18mm	31mm	31mm	19mm	19mm

Ligand & Metal: -ve - No Antibacterial Activity

Zone of inhibition - --mm

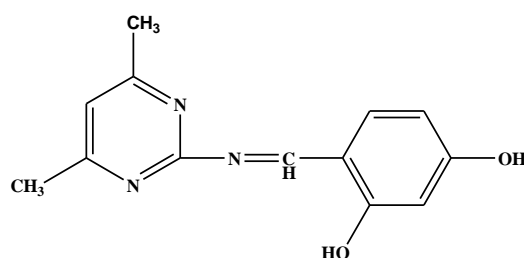


Fig. 6 Structure of Schiff Base Ligand L₁

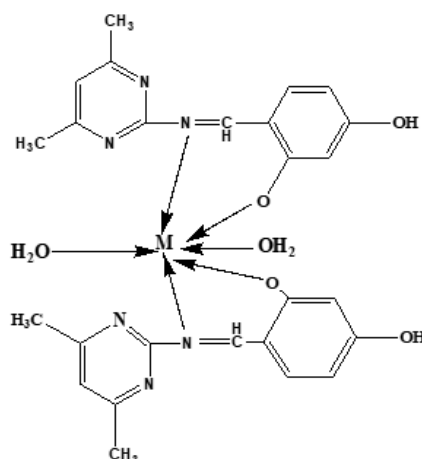


Fig. 7. The proposed Structure of the Metal complexes. [When M= Cu(II)]

V. CONCLUSION

In the light of above discussion we have proposed octahedral geometry for Cu(II) complexes. On the basis of the physico-chemical and spectral data discussed above, one can assume that the ligand behave as dibasic, NO bidentate, coordinating via phenolic oxygen and imino nitrogen as illustrated in Fig.7. The complexes are biologically active and show enhanced antimicrobial activities compared to free ligand. Thermal study reveals thermal stability of complexes. The X-ray study suggests monoclinic crystal system for Cu(II) complexes.

VI. ACKNOWLEDGEMENTS

The authors are grateful thank to sophisticated analytical instrument facility (SAIF), sophisticated test and instrument center (STIC), Kochi for providing elemental analysis (CHN). We are also grateful thank to Department of Chemistry, Pune University Pune for providing IR, NMR spectroscopy and TGA-DTA facilities, Department of Physics, Pune University Pune for providing X-RD facilities and we are also grateful thank to Department of Microbiology N. S. B. College, Nanded for providing Antibacterial and Antifungal activities.

VII. REFERENCES

- [1]. D.T.Sakhare, Copper Metal Complexes of a Pyrimidine Based Schiff Base Ligand Synthesis, Characterization and Biological Activity, Journal of Xidian University, 16(3), 191-201,2022,
- [2]. D.T.Sakhare, Synthesis, characterization of some transition metal complexes of bidentate Schiff base and their antifungal and antimicrobial studies,Advances in Applied Science Research, 6(6):10-16,2015.
- [3]. Ibrahim F. M.; Jassim A. H. and Muhyedeen B. R. J., "Synthesis and AB initio study of biologically important thioamide". LAP LAMBERT Academic Publishing, 2018.
- [4]. Gavalyan V. B., "Synthesis and characterization of new chitosan-based Schiff base compounds",Carbohydr. Polym., 145, 37-47, 2016.
- [5]. Theivendren P.S. James C.R., Dniandev P.V., Valzita S.K., A mini review of pyrimidine and fused pyrimidine marketed drugs, Research in Pharmacy, 2012, 2, 1-09.
- [6]. Sharma V., Chitranshi N., Agarwa A.K., Significance and biological importance of pyrimidine in the microbial world, Inter. J. Med. Chem., 2014, 1-31.
- [7]. Vega S., Alonso J., Diaz J. A., Junquera F., Synthesis of 3-substituted-4-phenyl-2-thioxo-1,2,3,4,5,6,7,8-octahydrobenzo[4,5]thieno[2,3-á]pyrimidines. J. Hetero. Chem., 1990, 27, 269-273.
- [8]. Harshalata D., Dhongade H.J., Kavita C., Pharmacological potentials of pyrimidine derivatives: A review, Asian J. Pharm. Clin. Res., 2015, 8, 171-177.
- [9]. Balzarini J., McGuigan C., Bicyclic pyrimidine nucleoside analogues (BCNAs) as highly selective and potent inhibitors of varicella-zoster virus replication, J. Antimicrob. Chemother., 2002, 50, 5-9.
- [10]. Rana K., Kaur B., Kumar B., Synthesis and antihypertensive activity of some dihydropyrimidines, Indian

- J. Chem. B, 2004, 43, 1553–1557.
- [11]. Atkins M., Jones C.A., Kirkpatrick P. Sunitinib maleate. *Nat. Rev. Drug Discov.*, 2006, 5, 279-280.
- [12]. Wilhelm S., Carter C., Lynch M., Lowinger T., Dumas J., Smith R.A., et al., Discovery and development of sorafenib: a multikinase inhibitor for treating cancer, *Nat. Rev. Drug. Discov.*, 2006, 5, 835-844.
- [13]. Ramaling S., Belani C.P., Role of bevacizumab for the treatment of non-small-cell lung cancer. *Future oncology*, 2007, 3, 131-139.
- [14]. Harris P.A., Bolor A., Cheung M., Kumar R., Crosby R.M., Davis-Ward R.G., et al., Discovery of 5-[[4-[(2,3-dimethyl-2Hindazol-6-yl)methylamino]-2-pyrimidinyl] amino]-2-methylbenzenesulfonamide (Pazopanib), a Novel and potent vascular endothelial growth factor receptor inhibitor, *J. Med. Chem.*, 2008, 51, 4632-4640.
- [15]. Smietana M., Clayette P., Mialocq P., Vasseur J.-J., Joe O., A Synthesis of new N-isobutyryl-L-cysteine/MEA conjugates: Evaluation of their free radical-scavenging activities and antiHIV properties in human macrophages, *Bioorganic Chem.*, 2008, 36, 133–140.
- [16]. Lascombe M.B., Ponchet M., Venard P., Milat M.L., Blein J.P., Prange T., The 1.45 Å resolution structure of the cryptogeincholesterol complex: a close-up view of a sterol carrier protein (SCP) active site, *Acta Crystallogr. Sect. D*, 2002, 58, 1442-1447.
- [17]. Kappe C.O., 100 years of the biginelli dihydropyrimidine synthesis, *Tetrahedron*, 1993, 49, 6937-6963.
- [18]. Espinet P., Esteruelas M.A., Oro L.A., Serrano J.L., Sola E., Transition metal liquid crystals: advanced materials within the reach of the coordination chemist, *Coord. Chem. Reviews*, 1992, 117, 215-274.
- [19]. antibacterial activities of some metal(II) complexes of 3-(1-(2-pyrimidinylimino)methyl-2-naphthol, *Elixir Appl. Chem.*, 2013, 59, 15843-15847.
- [20]. D.T.Sakhare, Synthesis, characterization of some transition metal complexes of bidentate Schiff base and their antifungal and antimicrobial studies, *Advances in Applied Science Research*, 2015, 6(6):10-16.
- [21]. Sönmez M., Sogukomerogullari H. G., Öztemel F., Berber İ., Synthesis and biological evaluation of a novel ONS tridentate Schiff base bearing pyrimidine ring and some metal complexes, *Med. Chem. Res.*, 2014, 23, 3451–3457.
- [22]. Gulcan M., Özdemir S., Dündar A., Ispir E., Kurtoglu M., Mononuclear complexes based on pyrimidine ring azo Schiff-Base ligand: synthesis, characterization, antioxidant, antibacterial, and thermal investigations, *Z. Anorg. Allg. Chem*, 2014, 640, 1754-1762.
- [23]. Mildvan A.S., Cohn M., Kinetic and magnetic resonance studies of the pyruvate kinase reaction II complexes of enzyme, metal and substrates, *J. Bio. Chem.*, 1966, 241, 1178-1193.
- [24]. Fromm, K.M. (2013) Silver Coordination Compounds with Antimicrobial Properties. *Applied Organometallic Chemistry*, 27, 683-687. <https://doi.org/10.1002/aoc.3047>
- [25]. Alwan, S.M. and Al-Kaabi, J.A-S. (2014) Synthesis and Preliminary Antimicrobial Activity of New Schiff Bases of Pyrido[1,2-a] Pyrimidine Derivatives with Certain Amino Acid. *Medicinal Chemistry*, 4, 635-639. <https://doi.org/10.4172/2161-0444.1000206>
- [26]. Amr, E.A., Ashraf, M.M., Salwa, F.M., Nagla, A.A. and Hammam, A.G. (2006) Anticancer Activities of Some Newly Synthesized Pyridine, Pyrane, and Pyrimidine Derivatives. *Bioorganic and Medicinal*

- Chemistry, 14, 5481-5488. <https://doi.org/10.1016/j.bmc.2006.04.045>
- [27]. Srivastva, A.N., Singh, N.P. and Shriwastaw, C.K. (2016) In Vitro Antibacterial and Antifungal Activities of Binuclear Transition Metal Complexes of ONNO Schiff Base and 5-Methyl-2,6-pyrimidine-dione and Their Spectroscopic Validation. *Arabian Journal of Chemistry*, 9, 48-61. <https://doi.org/10.1016/j.arabjc.2014.10.004>
- [28]. Arun, T., Subramanian, R. and Raman, N. (2016) Novel Bio-Essential Metal Based Complexes Linked by Heterocyclic Ligand: Synthesis, Structural Elucidation, Biological Investigation and Docking Analysis. *Journal of Photochemistry and Photobiology B*, 154, 67-76. <https://doi.org/10.1016/j.jphotobiol.2015.11.011>
- [29]. Garagorri, D.B. and Kirchner, K. (2008) Modularly Designed Transition Metal PNP and PCP Pincer Complexes Based on Aminophosphines: Synthesis and Catalytic. *Accounts of Chemical Research*, 41, 201. <https://doi.org/10.1021/ar700129q>
- [30]. Gruenwald, K.R., Kirillov, A.M., Haukka, M., Sanchiz, J. and Pombeiro, A.J.L. (2009) Mono-, Di- and Polynuclear Copper(II) Compounds Derived from N-butyldiethanolamine: Structural Features, Magnetism and Catalytic Activity for the Mild Peroxidative Oxidation of Cyclohexane. *Dalton Transactions*, 12, 2109-2120. <https://doi.org/10.1039/b813160k>
- [31]. D.T. Sakhare, Synthesis, characterization and in-vitro biological activities of Co (II) complexes of 2-(4-Methylbenzylideneamino) Pyrimidine-4, 6-Diol. *Current Pharma Research.*, 9(4), 3335-3344, 2019.
- [32]. D.T. Sakhare, Synthesis, Spectral, Thermal And Antimicrobial Activities of Mn (II) And Fe (III) Schiff Base Metal Complexes. *International Journal of Current Research In Chemistry And Pharmaceutical Sciences*, 2(7), 1-8, 2015.
- [33]. A A Osowole¹, R Kempe , R Schobert and S A Balogun , *Candian journal of pure and applied sciences* ,2010; 4(2) 1169-1178.
- [34]. A A Osowole . and R O Yoade , *Scientific Journal Of Applied Research* . 2013; 4: 101-106
- [35]. D. T. Sakhare , Synthesis, characterization and antimicrobial activities of some Mn(II) and Fe(III) complexes of biologically active bidentate ligands, *Journal of Chemical and Pharmaceutical Research*, 7(6), 198-204, 2015.
- [36]. M Usharani. E Akila, And R Rajavel. *International Journal of Recent Scientific Research* ,2013; 4(9): 1385- 1390.
- [37]. J.A. Dean, *Lange's Hand Book of Chemistry*, 14th ed., Megraw-Hill, New York,1992, p. 35.
- [38]. Housecroft, C.E., Sharpe, A.G.: *Inorganic Chemistry*, 2nd edn. Pearson, England (2005).
- [39]. D.T. Sakhare, Synthesis, Characterization And Antimicrobial Studies of Some Transition Metal Complexes of Schiff Bases, *International Journal of Current Research In Chemistry And Pharmaceutical Sciences*, 2(6), 28-34, 2015.
- [40]. Avaji P G, Reddy B N and Patil S A, *Trans. Met. Chem.*, 2006, 31, 842.
- [41]. Omar, M. M., Mohamed, G. G., & Ibrahim, A. A., Spectroscopic characterization of metal complexes of novel Schiff base. Synthesis, thermal and biological activity studies. *Spectrochimica Acta Part A: Molecular and Biomolecular Spectroscopy*, 73(2), 358-369,2009.

- [42]. D. T. Sakhare, Syntheses, characterization of some transition metal complexes of bidentate schiff base and their antimicrobial activities, *Der Chemica Sinica*, 6(6):1-6, 2015.
- [43]. D.T. Sakhare, Synthesis, Characterization And Antimicrobial Studies On Schiff Base Derived From 2-Amino 4,6- Dihydroxypyrimidine And Benzaldehyde And Its Cobalt Complexes , *International Journal of Food and Nutritional Sciences*, 11(1), 170-182, 2022.

Synthesis of β -amino Carbonyl Compounds by Michael Reaction

Dr. Jaishri Somwanshi¹, Dr. M.B Swami²

¹Department of Chemistry, Shri Madhavrao Patil Mahavidyalaya, Murum, dist. Osmanabad, Maharashtra, India

²Department of Chemistry, B. S College, Basmath. Dist. Hingoli-431512, Maharashtra, India

ABSTRACT

Over the past several years tremendous progress has been achieved by employing new nitrogen nucleophiles and suitable acceptors as well as more efficient catalytic systems for this important transformation. In the following, we have taken a brief account of aza-Michael addition reaction¹ with special emphasis on the development of the new catalysts. Catalysts for aza-Michael addition reaction

The role of aza Michael reaction in the synthesis of pharmacologically important family of β - amino carbonyl compounds and its derivatives is well documented in the literature.⁴

The Aza Michael reaction is widely recognized as one of the most important carbon- nitrogen bond forming reactions in organic synthesis ⁶. In general, this transformation is a heteroatom (Nitrogen) nucleophilic (donor addition to a β -carbon of electro poor alkenes acceptor) giving a stabilized carbanion intermediate, which after protonation with another electrophile furnishes the final addition product. The obtained β -amino ketones owing to their wide range of biological activities⁶ and pharmacological properties⁷. Carbonyl compounds (aza- Michael addition) is one of the simplest and most effective methods for preparing β - amino carbonyl compound. In recent years a number of catalysts such as SmI_2 $\text{CuO} \cdot 7\text{f}_2$, $\text{Bi}(\text{NO}_3)_3$, $\text{Bi}(\text{OTf})_2$, LiClO_4 , $\text{FeCl}_3 \cdot 6\text{H}_2\text{O}$. TMSCl , boric acid and clay have been developed for this reaction.

Material and Methods: To a mixture of α, β -unsaturated compound (2 mmol) and amine (2 mmol) in CH_2Cl_2 (10 mL) was added AgOTf (0.2 mol%) at room temprature. The resulting mixture was stirred at the same temperature for a specified period. The progress of the reaction was monitored by TLC. After completion of the reaction as indicated by TLC, the mixture was diluted with CH_2Cl_2 (20 mL) and washed with H_2O and brine, and the organic layer was dried (anhyd Na_2SO_4) and concentrated under reduced pressure. Thus obtained crude products were purified by column chromatography (silica gel, 60–120 mesh, EtOAc –hexane, 2:8).

Result:

Most effective methods for preparing β - amino carbonyl compound. In recent years a number of catalysts such as SmI_2 $\text{CuO} \cdot 7\text{f}_2$, $\text{Bi}(\text{NO}_3)_3$, $\text{Bi}(\text{OTf})_2$, LiClO_4 , $\text{FeCl}_3 \cdot 6\text{H}_2\text{O}$. TMSCl , boric acid and clay have been developed for this reaction. β -amino carbonyl compounds are useful building blocks for the molecules with applications in pharmaceuticals and fine chemicals⁹⁻¹⁴. They are versatile intermediates for the synthesis of biologically important natural products and antibiotics

β - amino carbonyl ingredients, which have attracted great attention for their use as key intermediates of anticancer agents, antibiotics and other drugs¹⁵ β -amino carbonyl compounds used as essential intermediates in the synthesis of β - amino acid and β - lactam antibiotic¹⁷.

Conclusion

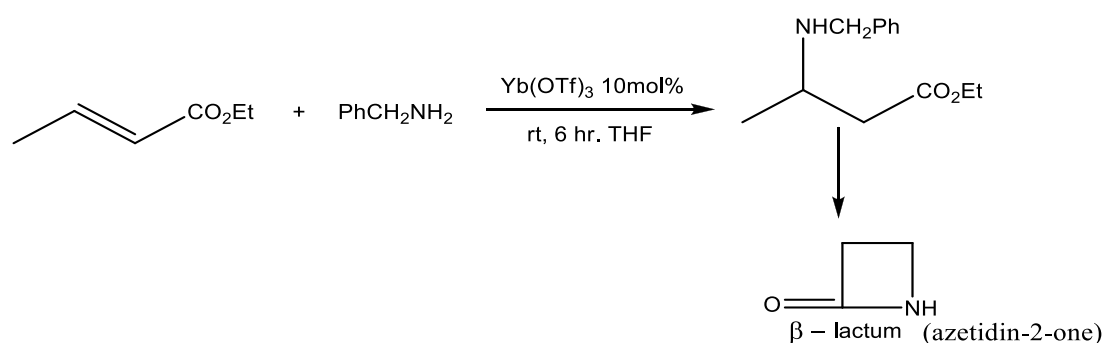
In conclusion, the present procedure provides an efficient methodology for the synthesis of β -amino carbonyl compounds via aza- Michael reaction. The notable advantages offered by this method are simple operation, mild (room temperature) and environment friendly reaction conditions, much faster (20-50min) reaction, high yields of products and cost effectiveness.

Most significantly, this demonstrates the potential of water as an efficient promoter and provides much promise for the use of water in other chemical transformations.

Key words: Synthesis of β - amino carbonyl compound, catalysts such as SmI₂ CuO₇f₂, Bi (NO₃), Bi (OTf)₂, LiClO₄, FeCl₃-6H₂O. TMSCl, boric acid and clay. The obtained β -amino ketones owing to their wide range of biological activities⁷ and pharmacological properties⁷.

I. INTRODUCTION

Precision Organic chemistry is an innovative science and the glory organic chemistry continues to improve after each discovery. One of such path breaking discovery was Michael reaction¹. Which involved a base promoted addition of various active methylene compounds to electron deficient alkenes. The Aza Michael reaction is widely recognized as one of the most important carbon- nitrogen bond forming reactions in organic synthesis ⁵ . The synthesis of β -amino carbonyl compounds has become a field of increasing interest in organic synthesis during the past few decades.⁹ Carbonyl compounds (aza- Michael addition) is one of the simplest and most effective methods for preparing β - amino carbonyl compound. In recent years a number of catalysts such as SmI₂ CuO₇f₂, Bi (NO₃), Bi (OTf)₂, LiClO₄, FeCl₃-6H₂O. TMSCl, boric acid and clay have been developed for this reaction. However, most of these catalytic systems are restricted to only aliphatic amines since aromatic amines are poor nucleophiles. Authors have established general protocol using Ytterbium triflate as a catalyst which is relatively expensive compared to other lanthanide triplets. The method was further extended to yield optically active B-lactum.



Synthesis of β -amino carbonyl compounds via aza-Michael reaction

A) Procedure

To a mixture of α - β -unsaturated compound (2 mmol) and amine (2 mmol) in CH_2Cl_2 (10 ml) was added AgOTf (0.2 mol %) at room temperature. The resulting mixture was stirred at the same temperature for a specified period. The progress of the reaction was monitored by TLC. After completion of the reaction as indicated by TLC, the mixture was diluted with CH_2Cl_2 (20 mL) and washed with H_2O and brine, and the organic layer was dried (anhyd Na_2SO_4) and concentrated under reduced pressure. Thus obtained crude products were purified by column chromatography (silica gel, 60–120 mesh, EtOAc –hexane, 2:8).

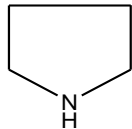
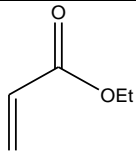
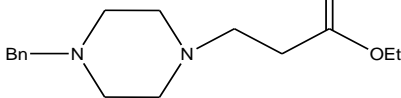
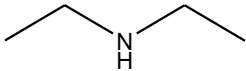
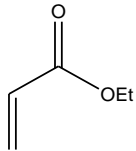
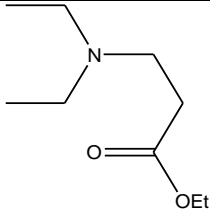
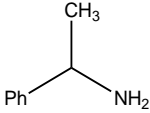
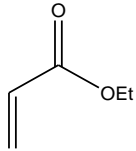
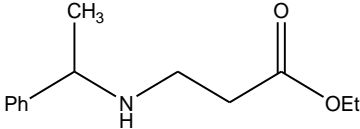
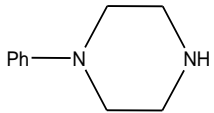
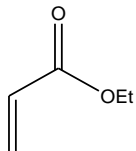
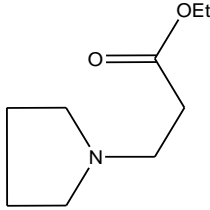
B) Reaction

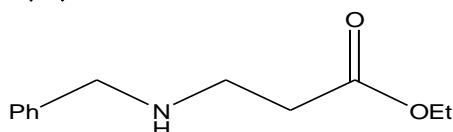


II. RESULT AND DISCUSSION

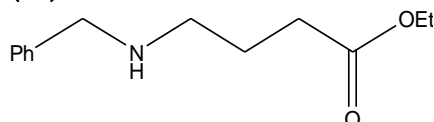
Melting points were recorded on Buch R-533 apparatus and uncorrected. IR spectra were recorded on a Perkin-Elmer FT-IR 240-c spectrophotometer using KBr optics. ^1H NMR and ^{13}C spectra were recorded on Gemini-200 MHz, Bruker Avance 300M Hz and Unity-400M Hz spectrometer in CDCl_3 using TMS as internal standard. Mass spectra were recorded on a Finnigan MAT 1020 mass spectrometer operating at 70eV. Column chromatography was performed using E. Merck 60-120, mesh silica gel. All the solvent were distilled, dried and stored under nitrogen prior to use.

Entry	Nucleophile	Olefin	Product	Reaction Time (h)	Yield (%)
3a				2.2	95
3b				2.8	93
3c				3.0	90

3d				3.2	92
3e				1.8	95
3f				2.5	88
3g				1.8	90

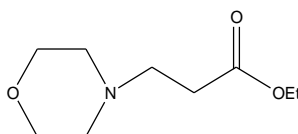
Spectral Data:**Ethyl-3-(N-benzylamino)-propionate (3a):**

Sr. No.		
1	State	
2	M.P.	
3	IR	V 3253, 3042, 2967, 2834, 1728, 1614, 1590, 1505, 1473, 1356, 1285, 1130, 1057, 1017, 983, 869, 820, 793, 738 Cm^{-1}
4	^1H NMR (CDCl_3)	\square 1.23 (t, 3H, J = 7.0 Hz), 2.15 (brs, 1H), 2.50 (t, 2H, J = 6.2 Hz), 2.85 (t, 2H, J = 6.2 Hz), 3.70 (s, 2H), 4.15 (q, 2H, J = 7.0 Hz), 7.22 – 7.40 (m, 5H)
5	EIMS (m / z) %	2.7 (m + 25), 178, (18), 134 (100), 106 (31), 77 (56), 52 (15)

Ethyl-3-(phenethylamino) butanoate (3b):

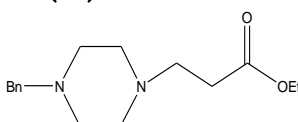
Sr. No.		
1	State	Colorless liquid
2	M.P.	
3	IR	V 3430, 3027, 2930, 2852, 1730, 1601, 1457, 1375, 1253, 1171, 1121, 1030, 748, 699, 638, 580 Cm^{-1}
4	^1H NMR (200 MHz, CDCl_3)	δ 1.23 (t, 3H, J = 6.5 Hz), 2.15 (s, 1H), 2.47 (t, 2H, J = 0 Hz), 2.75 – 2.95 (m, 6H), 4.10 (q, 4H, J = 0 Hz), 7.12 – 7.30 (m, 5H)
5	EIMS (m / z) %	221 (95), 220 (10), 209 (20), 208 (100), 205 (10), 160 (12), 140 (10), 102 (10), 88 (10), 73 (13)

Ethyl-3-(Morpholin-4-yl) propanoate (3c):

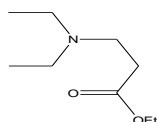


Sr. No.		
1	State	Colourless liquid
2	M.P.	
3	IR	V 2841, 1722, 1615, 1592, 1506, 1463, 1410, 1376, 1230, 1108, 1036, 1005, 981, 912, 871, 824, 766, 742, 691 Cm^{-1}
4	^1H NMR (200 MHz, CDCl_3)	δ 1.30 (t, J = 7.0 Hz, 3H), 2.45 – 2.52 (m, 6H), 2.68 (t, J = 6.8 Hz, 2H), 3.70 (t, J = 4.5 Hz, 4H), 4.20 (q, J = 7.0 Hz, 2H)
5	EIMS (m / z) %	187 (18), 158 (22), 114 (100), 86 (15), 58 (30)

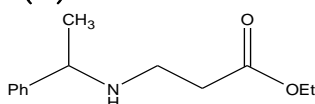
Ethyl- 3-(4-benzylpiperazin-1-yl) propanoate (3d)



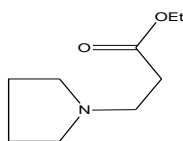
Sr. No.		
1	State	Light red colored liquid
2	M.P.	
3	IR	V 3432, 2928, 1727, 1630, 1518, 1458, 1343, 1216, 1163, 1108, 1024, 961, 845, 761, 732 Cm^{-1}
4	^1H NMR (200 MHz, CDCl_3)	δ 1.30 (t, 3H, J = 7.5 Hz), 1.78 – 1.88 (m, 4H), 2.48 – 2.60 (m, 6H), 2.82 (t, 2H, J = 7.5 Hz), 4.15 (q, 2H, J = 7.5 Hz)
5	EIMS (m / z) %	171 (M^+ 20), 142 (25), 98 (100), 70 (15), 46 (10)

Ethyl 3-(diethyl-amino) propanoate (3e):

Sr. No.		
1	State	
2	M.P.	
3	IR	V 2843, 1722, 1612, 1588, 1506, 1456, 1410, 1366, 1222, 1108, 1036, 1005, 978, 912, 860, 824, 766, 742, 691 Cm^{-1}
4	^1H NMR (CDCl_3)	\square 1.02 (t, 6H, J = 7.0 Hz), 1.26 (t, 3H, J = 7.0 Hz), 2.38 (t, 2H, J = 7.0 Hz), 2.50 (q, 4H, J = 7.0 Hz), 2.75 (t, 2H, J = 7.0 Hz), 4.12 (q, 2H, J = 7.0 Hz)
5	EIMS (m / z) %	

Ethyl- 3-(1-phenylethylamino) propanoate (3f):

Sr. No.		
1	State	Liquid
2	M.P.	
3	IR	V 3446, 3062, 3027, 2973, 2929, 2863, 1731, 1451, 1373, 1256, 1182, 1121, 1029, 953, 861, 760 cm^{-1}
4	^1H NMR (200 MHz, CDCl_3)	\square 1.25 (t, 3H, J = 6.5 Hz), 1.32 (d, 3H, J = 6.0 Hz), 1.85 (brs, 1H), 2.42 (t, 2H, J = 6.0 Hz), 2.60 – 2.80 (m, 2H), 3.75 (q, 1H, J = 6.5 Hz), 4.12 (q, 2H, J = 6.5 Hz), 7.15 – 7.30 (m, 5H)
5	EIMS (m / z) %	221 (M^+ 10), 207 (80), 179 (10), 161 (12), 135 (20), 119 (55), 106 (100), 92 (25), 78 (32), 51 (40), 43 (35)

Ethyl- 3-(pyrrolidin-1-yl) propanoate: (3g):

Sr. No.		
1	State	
2	M.P.	
3	IR	V 3444, 2975, 2821, 1930, 1732, 1618, 1599, 1500, 1455, 1380, 1231, 1056, 1015, 927, 864, 760, 694 cm^{-1}

4	¹ H NMR (200 MHz, CDCl ₃)	δ 1.26 (t, 3H, J = 7.0 Hz), 2.45 – 2.55 (m, 8H), 2.68 (t, 2H, J = 7.5 Hz), 3.48 (s, 2H), 4.12 (q, 2H, J = 7.0 Hz), 7.18 – 7.30 (m, 5H)
5	EIMS (m / z) %	262 (M ⁺ 40), 233 (21), 189 (100), 161 (15), 119 (26), 91 (10), 84 (36), 77 (85), 65 (14), 52 (12), 42 (20)

All the above synthesized β -amino carbonyl compounds are useful building blocks for the molecules with applications in pharmaceuticals and fine chemicals⁹⁻¹⁴. They are versatile intermediates for the synthesis of biologically important natural products and antibiotics and chiral auxiliaries and other nitrogen containing molecules.

They are also useful precursors for the generation of β - amino alcohols, which are common reagents in the preparation of fine chemicals⁷ pharmaceuticals¹⁶.

III. CONCLUSION

In conclusion, the present procedure provides an efficient methodology for the synthesis of β -amino carbonyl compounds via aza- Michael reaction. The notable advantages offered by this method are simple operation, mild (room temperature) and environment friendly reaction conditions, much faster (20-50min) reaction, high yields of products and cost effectiveness

IV. REFERENCES

- [1]. (a) Michael, A. J. Prakt. Chem. 1887, 3, 349. (b) Michael, A. Am. Chem. J. 1887, 9, 112.
- [2]. For review: Bergmann, E. D.; Ginsburg, D.; Pappo, R. Org. React. 1959, 10, 179.
- [3]. Perlmutter, P. Conjugate Addition Reaction in Organic Synthesis Pergamon Press. Oxford. 1992.
- [4]. (a) Reviews: Liu, M.; Sibi, M. P. Tetrahedron. 2002, 58, 7991. (b) Vicario, J. L.; Badia, D.; Carrillo, L. Org. Prep. Proc. Int. 2005, 37, 513. (c) Xu, L.-W.; Xia, C.-G. Eur. J. Org. Chem. 2005, 633.
- [5]. a] perimutter, p.conjugated Addition Reactions in organic synthesis; Pergamum press; oxford,1992, p.114
b] Yadav, J.S. Reddy, B.V.S. Basak, A.K. Narsaiah, A.V. chemistry Lett.2003, 988, c] xu,L, W; XIA, C. G. Eur.J. org.chem. 2005,633.
- [6]. a] Frackenponi J; Arvidsson, J.V. seevach. K.chem.soc. Rev. 1996,25,117-128
- [7]. Hayashi,Y;Karada, J; Harada. R; Rachiki. A;lijima, K ; Takiguch, Harada. R;Rachiki. A; Lijima, K; Takiguch, Y; Muramtsu. M. Miyazaki, H ; Asari, T; OKAZAKI t, sato y; yasuda, E. Yano, M. Uno; ojima I , J. Med. Chem. 1998,41,2345-2360
- [8]. For review; Juaristi, E,soloshon, V.A. Enantioselective synthsis of B- Amino acid 2nd ed. John wiley and sons, New York Ny,2005. J.Tetrahedron Lett. 2005 46-7761
- [9]. Saidi, M. R.; Pourshojaei, Y.; Aryansab, F. Synth. commun. 2009, 39, 1109.
- [10]. Bartoli, G.; Bosco, M.; Marcantoni, E.; Sambri, L.; Torregiani, E. J. Org. Chem. 2001, 66, 9052.

- [11]. (a) Mukherjee, C.; Misra, A. K. *Lett. In Org. Chem.* 2007, 4, 54. (b) Singh, S. P.; Vijaya Kumar, T.; Chandrashekaram, M.; Giribabu, L.; Yella Reddy, P. *Synth. commun.* 2009, 39, 3982.
- [12]. Nath, J.; Chaudhuri, M K. *Catalysis Letters.* 2009.
- [13]. Wang, Y.; Yuan, Y.-Q.; Guo, S.-R. *Molecules*, 2009, 14, 4779.
- [14]. Amore, K. M.; Leadbeater, N. E.; Miller, T. A.; Schmink, J. R. *Tetrahedron Lett.* 2006, 47, 8583.
- [15]. Raje, V. P.; Bhat, R. P.; Samant, S. D. *Synlett.* 2006, 16, 2676.
- [16]. Hussain, S.; Bhardwaj, S. K.; Chaudhuri, M. K.; Kalita, H. *Eur. J. Org. Chem.* 2007, 374.
- [17]. Surendra, K.; Shrilakshmi krishnaveni, N.; Sridhar, R.; Ramarao, K. *Tetrahedron Lett.* 2006, 47, 2125.

Silica Supported PPA : An Efficient and Recyclable Catalyst for Benzimidazoles Synthesis at Room Temperature

Sushil R Mathapati¹, Sujit S Mathakari¹, Mahesh B Swami², Mantosh B Swami^{3*}

¹Department of Chemistry, Shri Madhavrao Patil Mahavidyalaya, Murum-413605, Dist: Osmanabad, Maharashtra, India

²Department of Chemistry, Bahirji Smarak Mahavidyalaya, Basmat-431512, Dist: Hingoli, Maharashtra, India

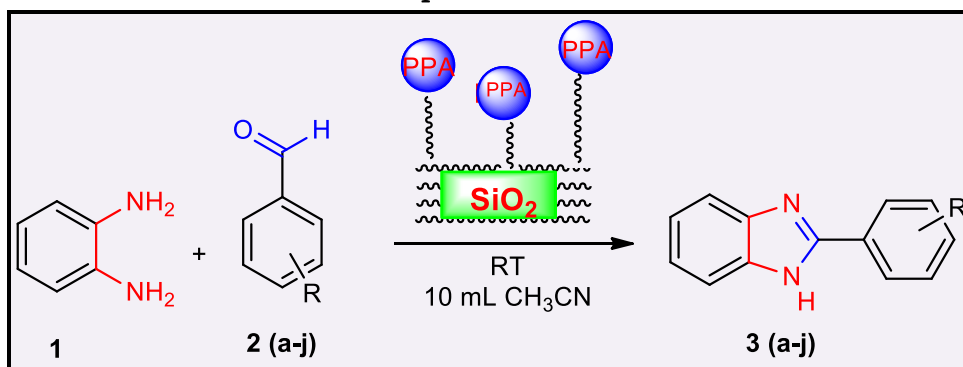
³Department of Chemistry, Mahatma Basweshwar Mahavidyalaya, Latur-413512, Maharashtra, India

ABSTRACT

Benzimidazoles are well known heterocyclic moiety in the field of pharmacological and organic synthesis. We have designed the efficient protocol for 2-phenyl benzimidazoles synthesis. A simple, highly efficient and environmental being procedure for the condensation of *o*-phenylenediamine with aromatic aldehydes in the existence of catalytic amount of SiO₂-PPA have been designed. Prepared SiO₂-PPA catalyst has remarkably efficient up to fifth cycles, reported excellent to good yield of target molecule. The mild reaction conditions, the high yield of the products and recyclability of catalyst are the attractions of reported methodology. Such advantages make it ecofriendly and proficient route for synthesis of benzimidazoles under prescribed reaction conditions.

Keywords: Diamine, Benzimidazoles, SiO₂-PPA catalyst, Room Temperature, Recyclability etc.

Graphical Abstract



I. INTRODUCTION

Recently, (SiO₂- PPA) has been used as an efficient heterogeneous catalyst for many organic transformations. PPA/SiO₂ has some advantages including its low cost, ease of preparation, and ease of handling [1]. In addition, the catalyst can be easily separated from the reaction mixtures by simple filtration and is reusable.

Previously [2], the conversion of carbonyl compounds into oxathioacetals or dithioacetals using PPA/SiO₂ and a convenient method for the synthesis of isoxazole derivatives using PPA/SiO₂ as a reusable catalyst have been reported [3]. In the last several years the development of non-toxic, low cost, eco-friendly, recyclable catalyst systems which give high productivity under mild reaction conditions has received much attention in organic synthesis [4]. Solid supported catalysts [5,6] have gained much prominence due to their inherent economic and environmental benefits, ease of handling, easy catalyst separation and regeneration, thermal stability and long catalytic life [7]. Since the activity and selectivity of a reagent dispersed on the surface of the support is improved, as the effective surface area of reagent can be increased manifold, they are expected to perform better than the individual reagents [8]. Low toxicity, moisture, air tolerance and low price are other common features that make the use of solid supported reagents attractive alternative to the conventional catalysts.

As we know, N-heterocyclic compounds are the most abundant and integral scaffolds that occur ubiquitously in a large number of bioactive natural products, drug intermediates, pharmaceuticals, and agrochemicals. Benzimidazoles are a privileged class of compounds among the N-heterocycles with a diverse spectrum of biological activities and therapeutic potentialities including anti-ulcers, anti-hypertensives, anti-virals, anti-fungals, anti-cancers, anti-histaminics also it exhibits medicinal properties such as serotonergic 5-HT₃ and 5-HT₄ receptors in the CNS [9, 10]. In addition, the unique benzimidazole moiety is “Master key” in anti-inflammatory, anti-analgesic, antioxidant, anti-diabetic, selective neuro peptide YY1 receptor antagonists, anti-malarial, anti-tubercular, etc., drugs [11-15]. Moreover, benzimidazoles are very important intermediates in dyes and polymer synthesis and widespread applications in fluorescence, chemo sensing, crystal engineering, and corrosion science [16]. Furthermore, with their biological consequence, benzimidazoles form unvarying complexes with diverse metals in transition group [17]. Metal chelations of 2-substituted imidazole and benzimidazole based structures with various ligands have been published with mono, bi and tri dentate co-ordination structures [18]. Some of the commercially important benzimidazole product structures, which are industrially very important, are illustrated in **Fig.1**.

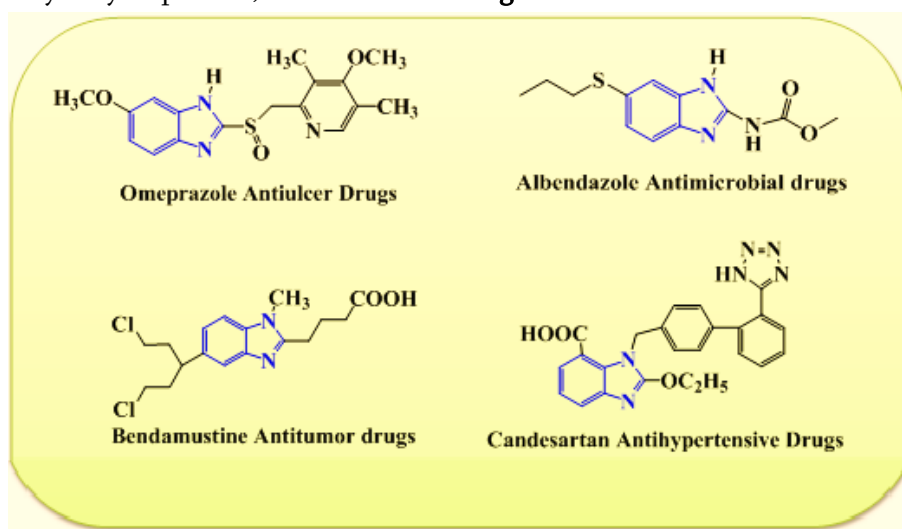


Fig. 1. Examples of important commercial drugs containing benzimidazole structural moiety.

Recently, benzimidazole derivatives have also been prepared from the oxidative condensation of 1,2-arylenediamines with aldehydes using different oxidative and catalytic reagents such as sulphur, Sc(OTf)₃ or Yb(OTf)₃[19], Silica-Sulphuric acid [20-21], NH₄Br [22], Lewis acids like pyridinium-p-toluene sulfonate, ionic liquids [23] like polyaniline-sulfate and zeolite. SiO₂/ZnCl₂ [24], nitrobenzene (high boiling oxidant/solvent) [25], silphox [POCl₃-n(SiO₂)_n] [26], Fe₃O₄@SiO₂/(NH₄)₆-Mo₇O₂₄ magnetic core-shell nano composite, boron tri-fluoride etherate (BF₃.OEt₂), Cu-nano particles/SiO₂, LiBr, GO-HSO₄ [27-30], PPA [31], fluorinated phosphoric Acid [32], methane sulfonic acid [33] these catalysts were utilized in the same procedure.

However, many of these protocols have not been entirely satisfactory because of some drawbacks such as low yields, long reaction time, strong acidic conditions, tedious workup procedures, requirement of excess amounts of catalyst and use of toxic reagents, catalysts or solvent, cumbersome experimental processes, and use of moisture-sensitive and costly catalysts. The development of simple, efficient, high yield green synthetic approach for the synthesis of biological active compounds is one of the major challenges in organic synthesis. Therefore, it is necessary to find a new catalyst or path for this important synthesis reaction. In addition, to overcome from all these disadvantages here we report a practical, inexpensive and green method for the synthesis of benzimidazole derivatives with reusable catalyst.

Herein, we present an efficient, simple, and economical cheap method for the preparation of benzimidazole derivatives catalyzed by Heterogeneous SiO₂@PPA catalyst. Present method obtained selective, efficient, and high yield of respective product in short reaction period. Furthermore, we have also studied the influence of concentration of catalyst, effect of solvent as well as temperature on benzimidazole yield. Various substituted benzimidazole derivatives were prepared by using o-phenylenediamine and various substituted aldehydes in the presence of SiO₂@PPA in ethanol at room temperature. We found that, the present protocol has easy and simple workup procedure with the separation of products and catalyst from reaction mixture, which shows one of the efficient alternative protocol for the benzimidazole derivative preparation.

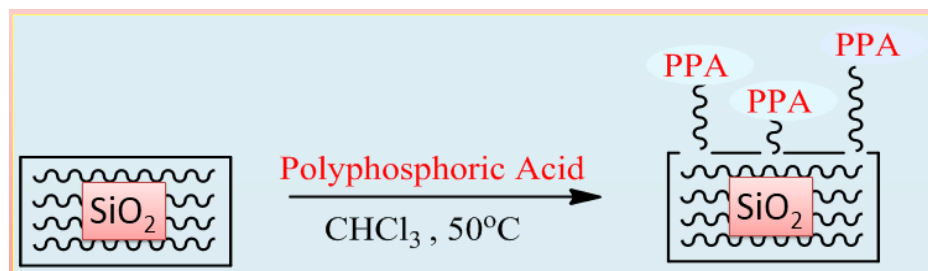
II. EXPERIMENTAL

2.1 General

All the chemicals used for synthesis were of LR (laboratory reagent) grade. Silica used for catalyst synthesis is of 70– 230 mesh size. TLC (thin layer chromatography) was performed on microscopic glass slides coated with silica gel-G using, petroleum ether:ethyl acetate (8:2) as a solvent system and the spot were visualized by exposure to iodine vapours. The XRD pattern acquired on a multi -purpose x-ray diffractometer at a scan rate of 0.17-2qs⁻¹. All the melting points of prepared compounds were determined in open capillary tubes and are uncorrected. The FT-IR spectra were recorded on a Perkin-Elmer spectrophotometer using KBr pellets. ¹HMR spectra were recorded on Varian Gemini (200 MHz) spectrometer using DMSO-d₆ as solvent and TMS as internal standard. ¹³C-NMR spectra were recorded on 50 MHz in DMSO-d₆ solvent, in δ ppm. All chemical shifts values are reported in δ scale downfield from TMS. Homogeneity of the compound was checked by TLC on silica gel plates.

2.2 General procedure for the synthesis of PPA/SiO₂ catalyst

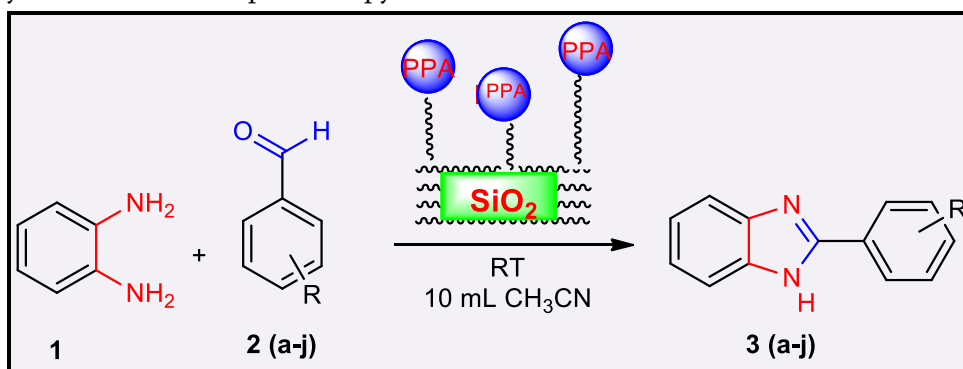
PPA (4.0 gm) was charged in the round-bottom flask, and CHCl₃ (100 mL) was added. After the mixture was stirred at 50 °C for 1 h, followed by SiO₂ (16.0 gm, 70– 230 mesh) was added to the solution, and the mixture was stirred for another 1 h. CHCl₃ was removed by evaporation, and the resulting solid was dried in vacuum at room temperature for 3 h. Used PPA/SiO₂ was regenerated as follows: PPA/SiO₂ was recovered by filtration from the reaction mixture, and then it was put in the 50 mL round-bottom flask and dried in vacuum at 100 °C for 2 hr.



Scheme 1: Preparation of SiO₂ supported PPA catalyst.

2.3 General procedure for the synthesis of benzimidazole derivatives

To a mixture of o-phenylenediamine (0.01 mol.) and aromatic aldehydes (0.01 mol.), ethanol (10 mL) were added in 50 mL round bottom flask. To this solution, added a known amount of catalyst SiO₂@PPA(0.5 gm). Resulting reaction mixture was stirred at room temperature. The progress of reaction was traced by TLC. After completion of the reaction vessels pour in 50 mL H₂O and extracted with ethyl acetate (10 mL X 3), catalyst was filter out and separated from the above solution. The collected organic layer was concentrated and the crude product was obtained and it was purified by recrystallization. pure benzimidazole products and further characterized by ¹H and ¹³C NMR spectroscopy.



Scheme 2: Synthesis of benzimidazole derivatives using SiO₂@PPA catalyst.

2.4 Spectral study of specified synthesized products 3 (a-j)

2.4.1 2-Phenyl- 1H-benzimidazole (3a): ¹H-NMR spectrum (200MHz, DMSO-d₆, in δ ppm): 12.86 (s, 1H, NH), 8.12 (m, 2H), 7.50-7.62 (m, 5H), 7.18 (m, 2H); ¹³C-NMR (50 MHz, DMSO-d₆, in δ ppm): 114.7, 118.9, 121.4, 123.4, 126.4, 129.0, 129.8, 130.1, 136.4, 145.5, 153.0. FT-IR (KBr) in cm⁻¹: 3048, 1460, 1418, 1280, 972, 745; Analy. Calcd. for C₁₃H₁₀N₂: C 80.39, H 5.19, N 14.42; Observed: C 80.42 H 5.18 N 14.40.

- 2.4.2 2-(4- Methoxyphenyl)-1H- benzimidazole (3b):** ¹H NMR (in δ ppm): 12.52 (s, 1 H, NH), 8.19 (dd, 2 H, J = 8.0 Hz), 7.66 (d, 1 H), 7.45 (d, 1 H), 7.24–7.10 (m, 2 H), 7.13 (d, 2 H, J = 8.0 Hz), 3.86 (s, 3 H). ¹³C NMR (in δ ppm): 158.38, 152.86, 139.88, 129.22, 124.67, 124.19, 122.20, 120.46, 114.30, 113.16, 58.31; IR (in cm^{-1}): 3450, 2242, 2120, 1655, 1045; Analy. Calcd. for $\text{C}_{14}\text{H}_{12}\text{N}_2\text{O}$: C 74.98, H 5.39, N 12.49, O 7.13; Observed: C 75.02, H 5.37, N 12.50, O 7.11.
- 2.4.3 2- [4- (2-propyl) phenyl]- 1H-benzimidazole (3d):** ¹H NMR (in δ ppm): = 12.86 (br. s, 1 H, NH), 8.15 (d, 2 H, J = 8 Hz), 7.72 (d, 1 H), 7.58 (d, 1H) 7.36 (d, 2 H, J = 8 Hz), 7.22–7.15 (m, 2H), 2.95 (m, 1 H), 1.26 (d, 6H). ¹³C NMR (in δ ppm): 151.33, 149.40, 143.85, 136.16, 128.77, 126.94, 126.43, 122.23, 120.65, 116.56, 112.20, 40.20, 24.00; IR (in cm^{-1}): 3456, 2350, 2127, 1665, 1073; Analy. Calcd. for $\text{C}_{16}\text{H}_{16}\text{N}_2$: C 81.32, H 6.82, N 11.85; Observed: C 81.32, H 6.80, N 11.87.
- 2.4.4 2-(3- Nitrophenyl)-1H- benzimidazole (3g):** ¹H-NMR (in δ ppm): 13.2 (s, 1H, NH), 8.86(s, 1H), 8.46 (d, 1H, J=6 Hz), 8.24 (d, 1H, J=7 Hz), 7.89 (m, 1H, J=7 & 6 Hz), 7.53 (m, 2H), 7.24(m, 2H); ¹³C-NMR (in δ ppm): 115.3, 123.1, 123.6, 124.4, 126.2, 127.4, 128.1, 133.4, 134.6, 135.2, 143.8, 149.7, 150.2; IR (KBr in cm^{-1}): 3060, 1524, 1450, 1357, 973, 746; Analy. Calcd. for $\text{C}_{13}\text{H}_9\text{N}_3\text{O}_2$: C 65.27, H 3.79, N 17.56, O 13.38; Observed: C 65.32, H 3.77, N 17.55, O 13.36.
- 2.4.5 2-(4- Chlorophenyl)-1H- benzimidazole (3i):** ¹H-NMR (in δ ppm): 12.9 (s, 1H, NH), 8.25(d, 2H, J=8.5 Hz), 7.6 (d, 2H, J=8.5 Hz), 7.45 (m, 2H), 7.20 (m, 2H). ¹³C-NMR (in δ ppm): 116.4, 124.1, 126.3, 128.9, 128.2, 129.7, 130.4, 134.3, 145.9, 152.6; IR (KBr in cm^{-1}): 3041, 1450, 1402, 1280, 965, 750; Analy. Calcd. for $\text{C}_{13}\text{H}_9\text{ClN}_2$: C 68.28, H 3.97, Cl 15.50, N 12.25; Observed: C 68.25, H 3.96, Cl 15.55, N 12.24.
- 2.4.6 2-(4- Bromophenyl)-1H- benzimidazole (3k):** ¹H NMR (in δ ppm): 12.65 (s, 1H, NH), 8.20(d, 2H J = 8.5 Hz), 7.66 (d, 2 H J = 8.5 Hz), 7.66–7.48 (m, 2 H), 7.23–7.12 (m, 2H). ¹³C NMR (in δ ppm): 155.14, 142.06, 133.85, 131.74, 130.47, 124.56, 123.37, 115.22; IR (in cm^{-1}): 3325, 2167, 2119, 1650, 1035, 827; Analy. Calcd. for $\text{C}_{13}\text{H}_9\text{BrN}_2$: C 57.17, H 3.32, Br 29.26, N 10.26; Observed: C 57.20, H 3.32, Br 29.24, N 10.25.

III. RESULTS AND DISCUSSION

We have worked on design an efficient protocol for the synthesis of benzimidazoles, various Lewis acid, heterogeneous, recyclable catalysts have been utilized for synthesis of benzimidazole preparation by the cyclization reaction of diamine and aldehydes. In the present work, we explored the potential of silica supported PPA as a catalyst for the synthesis of benzimidazoles. $\text{SiO}_2@\text{PPA}$ showed remarkable efficiency at room temperature under optimized conditions. We have prepared ten derivatives of benzimidazoles from various substituted aldehydes and diamine in the presence of catalytic amount of $\text{SiO}_2@\text{PPA}$ in 10 mL ethanol at room temperature.

Reaction parameters were finalized after optimization of amount of catalyst, effect of solvent and temperature, for this we flameout the model reaction as diamine (0.01 mol) and benzaldehyde (0.01 mol) were stirred in 10 mL solvent. The effect of different solvents have been studied under the same reaction conditions, as shown in table. The yield of the product varied with the nature of the solvents, better conversion and easy isolation

of product was found with acetonitrile. Acetonitrile dissolves a wide range of ionic and non-polar compounds. In a similar manner, the reaction with *O*-phenylenediamine and aldehydes was carried out without any solvents. The observation shows that the reaction was not brought into completion, even after starting for a period 12 hrs at room temperature, and the reaction mixture showed a number of spots in thin layer chromatography (TLC).

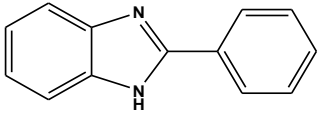
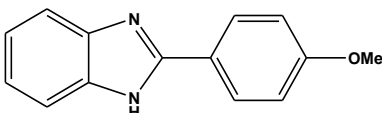
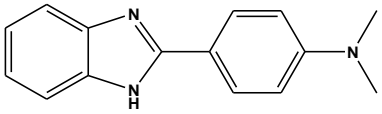
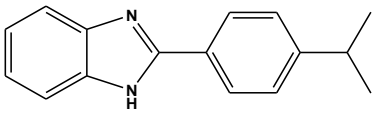
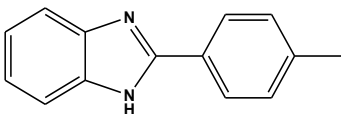
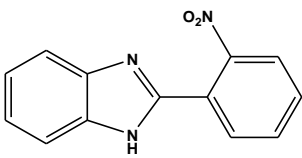
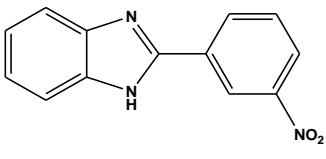
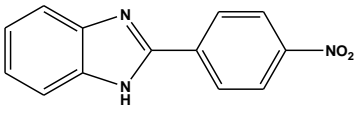
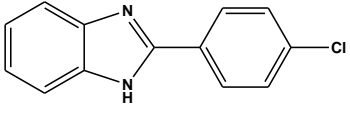
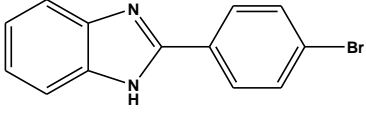
After the screening of solvents, we have finalized acetonitrile as solvent; we have screened same reaction under varying temperature. After the study, we have concluded as the studied reaction gave excellent output at room temperature for given transformation in presence of SiO₂-PPA, stirred in 10 mL acetonitrile. Additionally, the effect of amount of catalyst on present reaction also studied and we have found (0.5 gm) of SiO₂-PPA catalyst showed remarkable efficiency for the studied transformation. After the screening of all parameters, we have outlined optimized conditions as *o*-phenylenediamine (0.01 mol.) and aromatic aldehydes (0.01 mol.), ethanol (10 mL) stirred at room temperature in presence of 0.5 gm of SiO₂-PPA catalyst.

Table 1: Influence of various reaction parameters on reaction outcomes.

Sr. No.	Catalyst SiO ₂ PPA (in gm)	Solvent	Temp. (in C°)	Reaction Time (in hr)	Yield (In %)
1	0.5	Solvent free	R.T	12	30
2	0.5	ETOH	R.T	12	56
3	0.5	DMF	RT	14	62
4	0.5	CH ₃ -CN	RT	6	92
5	0.5	Toluene	RT	16	50
6	0.5	CH ₃ -CN	40	6	80
7	0.5	CH ₃ -CN	60	6	72
8	0.5	CH ₃ -CN	Reflux	6	45
9	0.7	CH ₃ -CN	RT	6	92
10	0.4	CH ₃ -CN	RT	6	85

With this optimized reaction condition, we have proceeded to investigate the scope and generality of this protocol using collection of various substituted aromatic aldehydes and diamine in ethanol as solvent. Consequently, a diversity of commercially accessible different structurally substituted aldehydes were treated in the optimized reaction conditions to obtain benzimidazole derivatives and obtained results are summarized in Table 2. As shown in Table 2, all substituted aldehydes participated well in this cyclization reaction and afforded the desired products of benzimidazole in good to efficient yields using catalytic amount of SiO₂-PPA and all the functionality of reactants were preserved throughout the transformation.

Table 2: Synthesis of benzimidazole compounds 3(a-j) from diamine and aldehydes under optimized conditions^(a)

Entry	Product	Time (h)	M.P.(°C)	Yield (%) ^(b)
1		6.00	291	92
2		4.10	232	94
3		3.40	238	90
4		3.50	243	93
5		2.50	224	92
6		4.40	255	82
7		5.30	145	85
8		4.10	316	92
9		3.40	293	90
10		4.10	258	88

Reaction conditions: diamine (0.01 mol), aldehyde (0.01mol), 10 mL CH₃CN, 0.5 gm SiO₂@PPA, stirred at room temperature. Reaction time is monitored by TLC. **(b) Isolated yield.**

IV. RECYCLABILITY OF SiO₂-PPA

We have also studied the reusability of reported catalyst to the course of benzimidazole from substituted aldehyde and O-phenylenediamine in 10 mL acetonitrile solvent. Result showed that prepared catalyst were give remarkable yield of target molecule up to 5th cycle (shown in figure 2). It was easily separated from reaction vessels and reuse after just washing with water, heated at 100 °C for 2 hr.

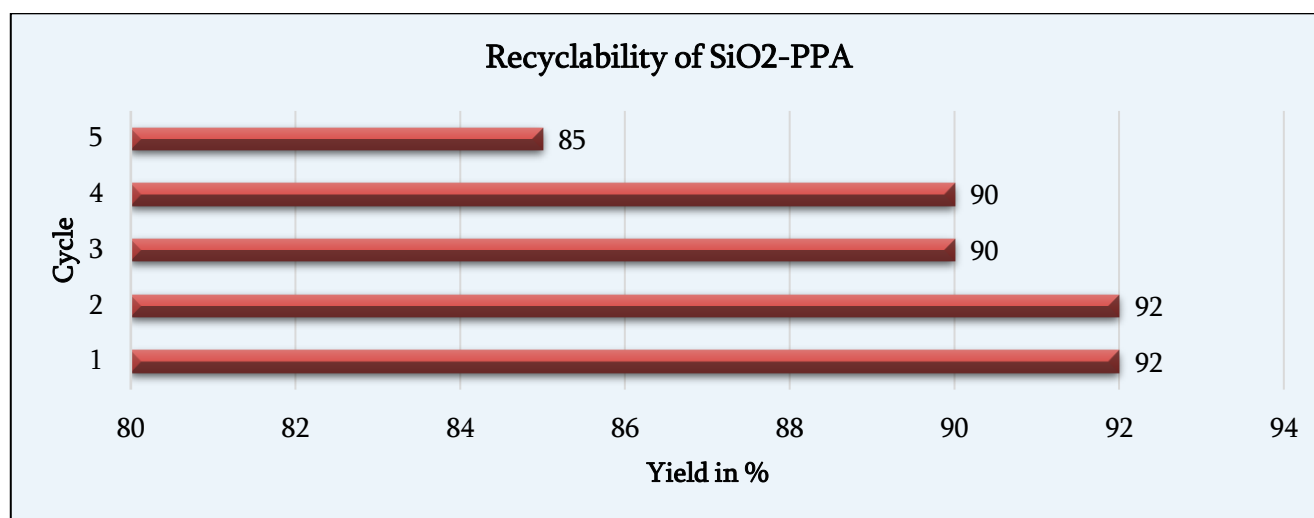


Fig. 2: Study of recyclability of SiO₂-PPA catalyst for synthesis of benzimidazoles.

V. CONCLUSIONS

In conclusion, we have developed a simple and efficient method for the synthesis of benzimidazole derivatives using silica supported poly phosphoric acid catalyst under mild reaction conditions with competitive and high yield. The advantages of the present technique are the operational simplicity, high efficiency, no side products formation, easy of workup procedure, less reaction time, thus suitable for large-scale production of benzimidazole derivatives. Reported catalyst was easily synthesised from available starting material and has stress-free workup process with outstanding productivity up to five cycles.

Acknowledgment:

Authors are thankful to the management and Principals of their respective colleges for encouragement & assistance. They are also thankful to IICT Hyderabad and Solapur University for proving spectral data.

VI. REFERENCES

[1]. R.H. Vekariya, N.P. Prajapati, H.D. Patel, Syn. Comm., 46 (2015) 197-219.

- [2]. T. Aoyama, T. Takido, M. Kodomari, *Synlett.*, 13 (2004) 2307–2310.
- [3]. K.I. Itoh, T. Aoyama, H. Satoh, Y. Fujii, H. Sakamaki, T. Takido, M. Kodomari, *Tetrahedron Lett.*, 52 (2011) 6892–6895.
- [4]. Q. Zhang, S. Zhang, Y. Deng, *Green. Chem.*, 13 (2011) 2619–2637.
- [5]. M.I. Ansari, M.K. Hussain, N. Yadav, P.K. Gupta, K. Hajela, *Tetrahedron Lett.*, 53 (2012) 2063–2065.
- [6]. R.S. Verma, *Green. Chem.* 1 (1999) 43–55.
- [7]. A. Corma, H. Garcia, *Adv. Synth. Catal.*, 348 (2006) 1391–1412.
- [8]. S. Kantevari, R. Bantu, L. Nagarapu, *J. Mol. Catal. A-Chem.*, 269 (2007) 53–57.
- [9]. M. Wang, X. Han, Z. Zhou, *Expert Opin. Ther. Pat.*, 25 (2015) 595–612.
- [10]. L. María, R. López, B. Bellinda, M.J. Morcillo, I.D. Tejada, L. Orensanz, M.J. Alfaro, M.I. Martín, *J. Med. Chem.*, 42 (1999) 5020–5028.
- [11]. S.M. Sondhi, N. Singh, A. Kumar, O. Lozachc, L. Meijer, *Bioorganic & medicinal chemistry*, 14 (2006) 3758–3765.
- [12]. C. Kus, G.A. Kilcigil, S. Ozbey, F.B. Kaynak, M. Kaya, T. Coban, B. Can-Eke, *Bioorg. Med. Chem.*, 16 (2008) 4294–4303.
- [13]. R. Vinodkumar, S.D. Vaidya, B.V. Kumar, U. N. Bhise, S. B. Bhirud, U. C. Mashelkar, *Eur. J. Med. Chem.*, 43 (2008) 986–995.
- [14]. H. Zarrinmayeh, D.M. Zimmerman, B.E. Cantrell, E.C.R. Smith, J.A. Nixon, R.F. Bruns, B. Gitter, P.A. Hipskind, P.L. Ornestein, H. Zarrinmayeh, T.C. Britton, D.A. Schober, D.R. Gehlert, *Bioorg. Med. Chem. Lett.*, 9 (1999) 647–652.
- [15]. J. Camacho, A. Barazarte, N. Gamboa, J. Rodrigues, R. Rojas, A. Vaisberg, R. Gilman, *Bioorg. Med. Chem.*, 19 (2011) 2023–2029.
- [16]. M. Berrada, F. Carriere, Y. Abboud, A. Abourriche, A. Benamara, N. Lajrhed, M. Kabbaj and M. Berrada, *J. Mater. Chem.*, 12 (2002) 3551–3559.
- [17]. H. A. Barker, R.D. Smyth, H. Weissbach, J.I. Toohey, J.N. Ladd, B.E. Volcani, *J. Biol. Chem.*, 235 (1960) 480–488.
- [18]. M. Kidwai, A. Jahan, D. Bhatnagar, *Journal of Chem. Scie.*, 122 (2012) 607–612.
- [19]. K. Nagata, T. Itoh, H. Ishikawa, A. Ohsawa, *Heterocycles*, 61 (2003) 93–96.
- [20]. Z.H. Zhang, T.S. Li, J.J. Li, *Monatsh. Chem.*, 138 (2007) 89–94.
- [21]. M. Chakrabarty, S. Karmakar, M. Ajanta, S. Arima, Y. Harigaya, *Heterocycles*, 68 (2006) 967–974.
- [22]. M.B Swami, S.G Patil, S.R Mathapati, H.G.Ghuge, A.H. Jadhav, *Der PharmaChemica*, 7 (2015) 533–535.
- [23]. A.H. Jadhav, H. Kim, *RSC Adv.*, 15 (2013) 5131–5140.
- [24]. R.G. Jacob, L.G. Dutra, C.S. Radatz, S.R. Mendes, G. Perin, E.J. Lenardão, *Tetrahedron Lett.*, 50 (2009) 1495–1497.
- [25]. V. Narsaiah, A.R. Reddy, J.S. Yadav, *Synth. Commun.*, 41 (2011) 262–267.
- [26]. A. Hasaninejad, K. Niknam, A. Zare, E. Farsimadan, M. Shekouhy, *Phosphorus Sulfur Silicon Relat. Elem.*, 184(2009) 147–155.
- [27]. K. Bahrami, M.M. Khodaei, A. Nejati, *Green Chem.* 12, (2010) 1237–1241.

- [28].A.H. Jadhav, G.M. Thorat, K. Lee, A.C. Lim, H. Kang, J.G. Seo, *Catalysis Today*, 265(2016) 56-57.
- [29].M.B. Swami, A.H. Jadhav, S.R. Mathpati, H.G. Ghuge, S.G. Patil, *Res Chem. Intermed*, 1164 (2016)2745-2053.
- [30].M.R. Mohammadizadeh, S. ZeinakhatounTaghavi, *E-Journal of Chemistry*, 8 (2011), 101-106.
- [31].J. Lu, B. Yang, Y. Bai, *Syn. Comm.*, 32 (2002) 3703–3709.
- [32].S.R. Mathapati , K.N. Patil , S.S. Mathakari , A.W. Suryawanshi, A.H. Jadhav, *Phosphorus Sulfur Silicon Relat. Elem.*, 169 (2021) 538-547.
- [33].S.R. Mathapati, *WJPR*, 11 (2022) 942-950.

Study of Nickel (II) and Mercury (II) Schiff Bases Metal Complexes

S. Anjanikar¹, S. Chandole^{*2}

¹Department of Chemistry, Sharadchandra College, Naigaon, District- Nanded- 431709, Maharashtra, India

^{*2}Department of Chemistry, S.G.B. College, Purna Jn- 431511, Maharashtra, India

ABSTRACT

Novel heterocyclic based metal complexes of Ni (II) and Hg (II) were synthesized from Schiff bases of 3-Actyl 4-Hydroxy Quinolin-2(1H)-one (AHQ). The Schiff bases 4-hydroxy-3-(1-((4-methylpyridin-2-yl)imino)ethyl)quinolin-2(1H)-one(L₁), 4-hydroxy-3-(1-((5-methylpyridin-2-yl)imino)ethyl)quinolin-2(1H)-one(L₂) were prepared by condensation of AHQ with substituted pyridine moiety. These complexes were characterized by elemental analysis, magnetic moment, electronic and IR spectral analysis. In vitro biological screening effects of the synthesized Complexes were tested for their antibacterial and antifungal activity. For antibacterial activity the bacterial species used were *Bacillus subtilis*, *Escherichia coli*, *Salmonella typhi*, and *Staphylococcus aureus* while fungal species used were, *Aspergillus flavus*, *Penicillium chrysogenum*, *Aspergillus niger* and *Fusarium moniliforme*. The antibacterial activity was screened using agar well diffusion method and antifungal activity with poison plate method.

Keywords: AHQ, substituted pyridine, Metal Complexes, Spectral Analysis, Biological Activity.

I. INTRODUCTION

Many Schiff base have drawn wide attention because of their diverse biological and pharmaceutical activities.¹ Azomethine nitrogen in the Schiff base has significant chemical and biological relevance since it not only facilitates binding sites for metal ions but also associate with different substrates of biomolecules, such as proteins and amino acids which are essential components of biological systems.^{2,3} Many Schiff bases derived from heterocyclic moiety possess a wide spectrum of medicinal properties and thus, have been studied for activity against antituberculosis,⁴ anti-inflammatory,⁵ antibacterial,⁶ antifungal,⁷ anticancer,⁸ antioxidant,⁹ and many more. Transition metals like nickel, iron, cobalt and copper among others, can form extremely stable complexes with the dynamic schiff base molecule, which can also be a chelating ligand.¹⁰ Usually metal chelates are more effective against bacteria and fungi than the isolated ligands.¹¹ Metal complexes biological potential and chelating power have attracted a lot of attention. The pharmacological activity of metal complexes is highly dependent on the nature of the metal ions and the donor sequence of the ligands because different ligands exhibit different biological properties.¹² The catalytic function of Schiff base metal complexes are observed in various reactions such as oxidation,¹³ epoxidation,¹⁴ polymerisation,¹⁵ condensation,¹⁶ reduction,¹⁷ and other reactions.

The present investigation deals with the synthesis, spectral characterization (IR, electronic) and antimicrobial activities (antibacterial and antifungal) of Schiff base ligand metal complexes of Ni (II) and Hg(II) derived from AHQ and substituted amino pyridine.

II. EXPERIMENTAL

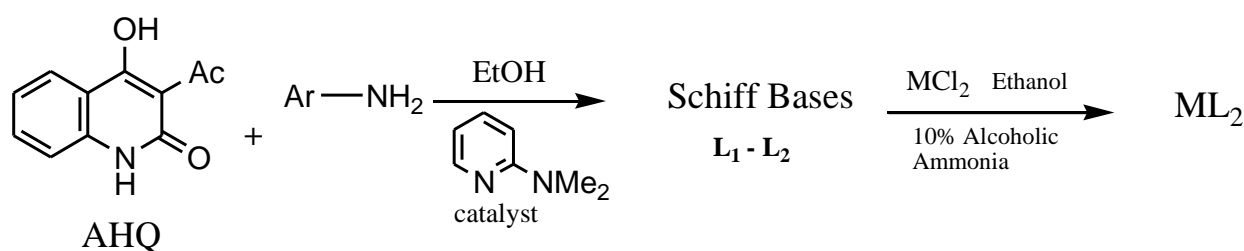
Melting points were determined by open capillary method and were uncorrected. IR spectra were carried out as KBr discs on a Shimadzu, IR-470 Spectrometer. The elemental analysis was determined using the Thermo Fisher Scientific CHN/S/O analyzer instrument. The magnetic susceptibilities of complexes were measured by the Gouy's method at room temperature using the Sherwood scientific magnetic susceptibility balance and using distilled water as the calibrant. Molar conductance of the metal complexes was measured using the Fisher Scientific PH/conductivity meter. The molar conductance measurements were performed using 0.001 M solutions of the complexes in DMSO at room temperature.

GENERAL PROCEDURE FOR SYNTHESIS OF COMPLEXES:

Each complex is synthesized by placing 0.02 moles of ligand (L_1 - L_2) in a flask with a flat bottom and 50 milliliters of ethanol. After a brief period of heating, 0.01 moles of a metal salt solution that has been dissolved in 20 milliliters of ethanol is added gradually to the hot ligand solution. After two hours of refluxing, the mixture is chilled. In a cold container with refluxed contents, a freshly made 10% alcoholic ammonia solution is gradually added while being constantly stirred. Precipitation starts to form at pH eight.

For an hour, the precipitated complex is digested. If a pH shift is seen, it is corrected and digested for a further hour. The digested precipitate of complex is filtered in hot water, washed with hot ethanol, followed by hot petroleum ether, and dried in vacuum desiccators over calcium chloride.

REACTION SCHEME:



Where Ar_{i-ii} is $Ar_i = 2\text{-amino } 4\text{-methyl Pyridine}$
 $Ar_{ii} = 2\text{-amino } 5\text{-methyl Pyridine}$

$M = Ni(II) \text{ \& } Hg(II)$

Fig. 1 Synthesis of Metal Complexes of Ni(II) and Hg (II)

III. ANTIMICROBIAL STUDY

ANTI BACTERIAL ACTIVITY:

The agar well diffusion method was used to test the antibacterial activity.¹⁸Mueller Hinton Agar for bacteria was used for all tests for antibacterial activity. For positive control of bacteria Ampicillin was used. The solvent and positive control used was DMSO. Antibiotics and dehydrated media powder were brought from Hi-Media, India. Using sterile wire-loop, test organisms were aseptically added to sterile MH broth before being incubated at 37°C for 18 hours. This suspension was utilized as an inoculant. Wells in the media plates with a 10mm diameter were made using a sterile cork borer for the addition of compound solutions and controls. With the aid of a micropipette, 100 µl of the compound solution was aseptically added to the wells to reach a final concentration of 10 g of compound in each well. As controls, the same quantity of DMSO and ampicillin solution were introduced. The plates were cooled for 30 minutes to allow solutions to diffuse through the agar substrate. Plates were then incubated for 24 hours at 37°C. *Bacillus subtilis* and *Salmonella typhi* were gram positive bacteria that were utilized as test organisms, whereas *Staphylococcus aureus* and *Escherichia coli* were gram negative microorganisms. The zone margin should be regarded as the region that does not clearly display any expansion that the unaided eye can see. With a measuring scale in millimetres, the clean zone was measured.

ANTIFUNGAL ACTIVITY

The poison plate approach was used to provide antifungal activity.¹⁹For the evaluation of antifungal activities, *Aspergillus niger*, *Aspergillus flavus*, *Fusarium moniliforme*, and *Penicillium chrysogenum* species were selected. Potato Dextrose Agar (PDA) media was utilized as a culture. To sterilize the medium, it was autoclaved at 121°C for 25 minutes under 15 psi of pressure. 20 ml of sterilized, melted PDA was added to sterilized petri plates with 2 ml of each component, and the mixture was then gently stirred in a circular motion to get homogenized. With positive Neomycin and negative DMSO controls, the identical process was followed. The fungal spores from the slant culture were transferred to a test tube containing sterile saline and thoroughly mixed with a sterile wire loop. As an inoculant, this spore solution was employed. The plates were incubated for four days at room temperature. After incubation, the growth of the infected fungi was monitored on the plates. The outcomes were noted.

IV. RESULT AND DISCUSSION

The Ni (II) complexes prepared in the present work are greenish-yellow. These are stable to air and moisture. All Ni(II) complexes are not soluble in water, common polar and non-polar solvents but are sparingly soluble in methanol, ethanol and chloroform. They are appreciably soluble in dimethyl sulphoxide (DMSO). The observed solution conductivities of Ni (II) complexes are given in Table 1. The low solution conductivity values of the complexes in DMSO indicate their non-electrolytic nature.²⁰The elemental analysis data (Table 1) of metal complexes confirm the ligand to the metal ratio for Nickel complexes as 2:1, proposing a monomeric

complex. The electronic spectra of Ni(II) complexes observed in the present work show absorption bands in three regions. $V_1 = 11495 - 11360 \text{ cm}^{-1}$, $V_2 = 16530 - 16390 \text{ cm}^{-1}$ and $V_3 = 26315 \text{ cm}^{-1}$. These observed bands may be assigned to three spin allowed transition ${}^3A_{2g} \rightarrow {}^3T_{2g}$, ${}^3A_{2g} \rightarrow {}^3T_{1g} (F)$ and ${}^3A_{2g} \rightarrow {}^3T_{1g}(F)$ charge transfer band respectively, which are characteristic of the distorted octahedral field.^{21,22}The electronic spectral data are presented in Table 2.

Mercury complexes Prepared in the present research work are white. They are stable in air and moisture. The Hg(II) complexes decompose at high temperature (above 300°C).²³They are insoluble in non-polar and common polar solvents. At a very low concentration, solutions can be prepared in CH_3OH and DMSO. The molar conductance value of the complexes in DMSO (10^{-3}M) is very low ($16.02 - 16.61 \text{ mhos}^{-1} \text{ cm}^2\text{mol}^{-1}$), indicating the non-electrolytic nature of complexes.²⁴The metal to ligand ratio was shown as 1:2, predicting a monomeric structure. All Hg (II) complexes are diamagnetic. These findings agree with the previously reported experimental work.²⁶

In the present investigation IR spectrum data of Ni (II) and Hg (II) was given in table-4. The stretching vibration for lactum $\text{C}=\text{O}$ observed in range of $1664 - 1660 \text{ cm}^{-1}$ for Ni (II) while in Hg (II) complexes found within the range $1665 - 1663 \text{ cm}^{-1}$.

The band assigned to the azo-methine $\text{C}=\text{N}$ stretching frequencies in the free ligand were observed around $1617 - 1600 \text{ cm}^{-1}$. In the IR spectra of the Ni (II) and Hg (II) complexes, medium to weak bands appeared in the region $1599 - 1590 \text{ cm}^{-1}$ were assigned to azo-methine $\text{C}=\text{N}$ stretching vibration mode. A decrease in a shift of this band observed on complexation indicates that the imine group of each ligand is coordinated to metal ion via its nitrogen.²⁷

The medium intensity absorption bands in the region $1276 - 1270 \text{ cm}^{-1}$ in the spectra of metal complexes were predictable to enolic $\text{C}-\text{O}$ stretching frequency. These bands in the corresponding free ligands spectra were observed in the range $1269 - 1224 \text{ cm}^{-1}$. Thus the observed upward shift of this band by $18 - 22 \text{ cm}^{-1}$ and the disappearance of broad absorption due to phenolic $-\text{OH}$ in metal complexes confirms the participation of enolic oxygen bonded to 4C of 4-hydroxyquinolin-2(1H)-one part in the formation of the complex.

The band in the range $498 - 472 \text{ cm}^{-1}$ were assigned for Metal Oxygen bond while band in the range $448 - 428 \text{ cm}^{-1}$ were assigned to Metal Nitrogen bond.²⁸

The antibacterial activity was tested for the synthesized Ni (II) and Hg (II) complexes. The outcomes are summarized in Table 5. Across all bacterial species under study, metal complexes of Ni (II) and Hg (II) have shown good antibacterial activity in zones of inhibition ranging from 14 to 19 mm in diameter. Metal complexes with all ligands showed substantial activity in the antifungal test. It has been found that complexes of Ni (II) complexes have shown higher antibacterial and antifungal activity as compare to Hg (II) complexes.²⁹

V. CONCLUSION

In conclusion, we reported the synthesis, characterization, and antimicrobial properties of metal complexes of Ni (II) and Hg (II) with Schiff bases obtained from heterocyclic moieties such as pyridine and AHQ with the

goal of developing a contribution to coordination chemistry. Ni (II) metal complexes that have been prepared are monomeric and have an octahedral orientation, whereas Hg (II) metal complexes are monomeric and have a tetrahedral geometry. Thus according antimicrobial studies all complexes have significant antibacterial and antifungal action.

Table No. 1 Elemental Analysis of Ni (II) and Hg(II)Complexes

S. No.	Complexes	Molecular formula	Colour	M.P.°C	Mol. Wt.	Soln cond. μ v	Elemental analysis Found(Calculated)			
							%C	%H	%N	%M
1	[Ni (L ₁) ₂]	[Ni(C ₁₇ H ₁₄ N ₃ O ₂) ₂ (H ₂ O) ₂]	Greenish Yellow	265	679.36	16.21	60.06 (60.11)	4.66 (4.75)	12.38 (12.37)	8.50 (8.64)
2	[Ni (L ₂) ₂]	[Ni(C ₁₇ H ₁₄ N ₃ O ₂) ₂ (H ₂ O) ₂]	Greenish Yellow	248	679.36	16.26	60.02 (60.11)	4.54 (4.75)	12.30 (12.37)	8.58 (8.64)
3	[Hg (L ₁) ₂]	[Hg(C ₁₇ H ₁₄ N ₃ O ₂) ₂]	White	>300	785.23	16.61	51.90 (52.01)	3.65 (3.59)	10.74 (10.70)	25.51 (25.55)
4	[Hg (L ₂) ₂]	[Hg(C ₁₇ H ₁₄ N ₃ O ₂) ₂]	White	>300	785.23	16.02	51.88 (52.01)	3.63 (3.59)	10.60 (10.70)	25.61 (25.55)

Table No. 2 Electronic Spectral Data of Ni (II) Complexes

Sr. No.	Complexes of Ligand (L ₁ -L ₂)	Absorption Maxima cm ⁻¹ (nm)		
		V ₁	V ₂	V ₃
1	Ni [(L ₁) ₂ (H ₂ O) ₂]	11495 (870)	16530 (605)	26315 (380)
2	Ni[(L ₂) ₂ (H ₂ O) ₂]	11360 (880)	16390 (610)	26315 (380)

Table No. 3Magnetic Susceptibility Data of Ni (II) Complexes

Sr. No.	Ni (II) Complexes of ligand	$\chi_M \times 10^6$ (CGS)	$\chi_A \times 10^6$ (CGS)	μ_{eff} (B.M.)
1	Ni [(L ₁) ₂ (H ₂ O) ₂]	3964.55	4263.75	3.19
2	Ni[(L ₂) ₂ (H ₂ O) ₂]	3675.57	3974.77	3.08

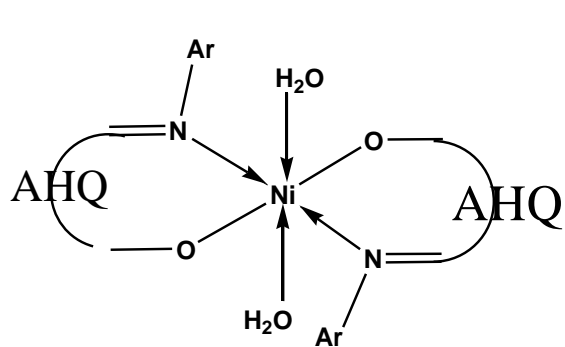
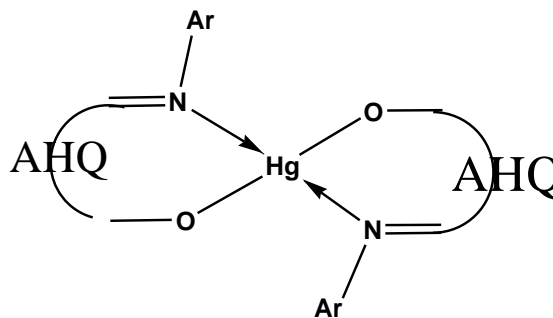
Table No. 4 Infrared Absorption Frequencies (cm⁻¹) of

Sr. No.	Ligand / Complex	Bond vibrational modes (stretching – ν)						
		Lactam		Pyridine	Azo-methine	Enolic	New Peaks	
		(C=O)	(C=N)	(C=N)↓	(C-O)↑	M-O	M-N	
1	Ni [(L ₁) ₂ (H ₂ O) ₂]	1664	1605	1599	1270	498	448	
2	Ni[(L ₂) ₂ (H ₂ O) ₂]	1660	1600	1590	1272	492	440	
3	Hg(L ₅) ₂	1665	1603	1593	1276	472	430	
4	Hg(L ₅) ₂	1663	1600	1592	1270	475	422	

Table No.5 Anti- Bacterial and Anti-Fungal Activity

Synthesized Schiff base ligands	Antibacterial Study Zone of Inhibition(diameter in mm)				Antifungal Study Growth of Fungi			
	Gram Positive		Gram Negative		<i>A. niger</i>	<i>A. flavus</i>	<i>F. moniliforme</i>	<i>P. chrysogenum</i>
	<i>S. typhi</i>	<i>B. subtilis</i>	<i>E. coli</i>	<i>S. aureus</i>				
Ampicillin (Reference)	18	19	17	18	Neomycin (Reference)	-	-	-
Ni [(L ₁) ₂ (H ₂ O) ₂]	17	18	19	18	-	-	-	-
Ni[(L ₂) ₂ (H ₂ O) ₂]	18	18	18	19	-	-	-	-
Hg(L ₅) ₂	16	15	15	17	++	+	+	+
Hg(L ₅) ₂	16	17	14	14	+	+	-	-

Moderate growth (++) , Reduced growth (+) and No growth (-) of fungi

Structure I: Monomeric octahedral Structure of Ni(II) Complexes of Ligand L₁ & L₂

Structure II: Monomeric tetrahedral Structure of Hg(II) Complexes of Ligand L & L.

VI. REFERENCES

- [1]. Shekhawat A.S., Chauhan N. S., Singh G., Chundawat N. S., Int. J. Pharm. Sci. Res., 2022, 13(1), 192-196.
- [2]. Anush S. M., Vishalakshi B., Kalluraya B., Manju N., Int. J. Bio. Mac., 2018, 119, 446-452.

- [3]. Monier M., *Int. J. Bio. Mac.*, 2012, 50, 773–781.
- [4]. Murtaza S., Akhtar M.S., Kanwal F., Abbas A., Ashiq S., Shamim S., *J. Saudi Chem. Sco.*, 2017, 21, S359-S372.
- [5]. Meeran I. S., Tajudeen S.S., Azger V.N., Dusthakeer, Shabeer T. K., *J. Pharm. Chem. Bio. Sci.*, 2018, 6(3), 158-177.
- [6]. Da Silva C., Da Silva D.L., Modolo L.V., Alves R.B., Resende M.A., Martin C.V.B., Fatima A., *Journal of advanced Research*, 2011, 2, 1-8.
- [7]. Login C. C., Baldea J., Tiperciuc B., Benedec D., Vodnar D. C., Decea N., Suciuc S., *Oxidative Medicine and Cellular Longevity*, 2019, Article ID 1607903, 1-11.
- [8]. Saeed A. M., Neyadi S.S., Abdou I. M., *Heterocycl. Commun.*, 2020, 26, 192–205.
- [9]. Bakır T. K., Lawag J. B., *Research on Chemical Intermediates*, 2020, 46, 2542-2557.
- [10]. Singh J., Singh P., *ISRN Physical Chemistry*, 2012, Article ID 504038.
- [11]. Laiq E., Shahid N., *Biosci. Biotech. Res. Asia*, 2021, 18(3), p. 575-583.
- [12]. Soroceanu A., Bargan A., *Crystals*, 2022, 12, 1436.
- [13]. Gama A., Flores-Lopez L.Z., Aguirre G., Parra-Hake M., Somanathan R., Walsh P.J., *Tetrahedron Asymmetry*, 2002, 13, 149-154.
- [14]. Baojiao G., Jiying M., Yan Z., *Inorg. and nano metal chemistry*, 2015, (45) 6, 821-827.
- [15]. De Clercq B., Verpoort F., *Journal of Molecular Catalysis A: Chemical*, 2002, (180)1-2, 67-76.
- [16]. Walaa H. M., Gehad G. M., Hoda, A. E., Radwan M. A., *Applied Organometallic Chemistry*, 2018, 1-14.
- [17]. Liu S., Peng J., Yang H., Bai Y., Li J., Lai G., *Tetrahedron*, 2012, (68)5 1371-1375.
- [18]. Kenawy R., Azaam M. M., Khattab S. A., *Sci J B. A. S.*, 2019, 40, 69-77.
- [19]. Sonnekar V. S., Jadhav W. N., Dake S. A., Pawar R. P. *Res. J. Pharma. Bio. Chem. Sci.*, 2013, 4 (2), 1411-1418.
- [20]. Hasan M. R., Hossain M. A., Salam A. M., Uddin M., *Journal of Taibah University for Science*, 2016, 10, 766–773.
- [21]. Lever A. B. P., “*Inorganic Electronic spectroscopy*,” Elsevier, 1968, 356-359.
- [22]. Cotton, F.A., Wilkinson, G., *Advanced Inorganic Chemistry*,” Interscience, 1972, 3rd Edn. 896
- [23]. Halli B., Patil V. B., *Ind. J. of Chem.*, 2011, (50A)5, 664-669.
- [24]. Halli M.B., Reddy P.V., Sumathi R.B, K. Mallikarjun, *Indian j. of applied Res.* 2013 3(8), 82-84.
- [25]. Hernandez G., Bernes S., Portillo O., Ruíz A., Moreno G. E., Gutierrez R., *Acta Crystallogr E Crystallogr Commun.*, (E71), 2015, 1462–1466.
- [26]. Fernandez-g J.M., Arauz E.A., Rosado R.C., Toscano R.A., Maciasruvalcaba R.N., Martinez M, A., *Transition Metal Chem.*, 1999, 24(1), 18-24.
- [27]. Arumugam A.P., Guhanathan S., Elango G., *SOJ Materials Science & Engineering*, 2017, 5(2), 1-12.
- [28]. Geary W., *Coord. Chem. Rev.*, 1971, (7)1, 81-122.
- [29]. Reiss A., Caproiu T., Stanica N., *Bull. Chem. Soc. Ethiop.*, 2009, 23(1), 63-68.

Waste Plastic to Useful Fuel

B. P. Pingle¹, R. D. Suryawanshi², R. P. Pawar^{2*}

¹Hi Tech Institute of Technology, Aurangabad-431005, Maharashtra, India

²Department of Chemistry, Shivchhatrapati College, Aurangabad-431005, Maharashtra, India

ABSTRACT

Plastic become a universal material, used for everything from throw away bags to wings of aircraft. Worldwide, it is produced in massive scale due to its properties like light weight, high strength, inexpensive, etc.

Day by day, a huge amount of this non bio-degradable waste is increasing due to unlimited use of this plastic. Hence disposal of such material is essential from safety point of view. Simultaneously, with heavy consumption of fossil fuel, the world in future will face the energy shortage and environmental concern; if no other alternatives are found.

This paper reviews pyrolysis of waste plastic which is an economical method to solve waste plastic problem and to produce quality fuel which can have properties similar to commonly used fuels.

Keywords:-Waste plastic, disposal, pyrolysis, energy source, polymerization, degradation, Thermosets, thermoplastic, hydrocarbons etc.

I. INTRODUCTION

Plastic is a high molecular weight polymeric material. The term polymer means a molecule made up by repetition of simple unit.(1,2) It refers to their malleability or plasticity during manufacture, which allows them to be cast, pressed, or extruded into a variety of shapes such as films, fibers, plates, tubes, bottles, boxes, and much more.(3)

A. Most of the plastics mainly made up of.....

Petroleum: Non-Renewable Natural Resource

Coal: Non-Renewable Natural Resource

B. Types of plastic:

There are two main types of plastics: thermoplastics and thermosetting polymers. (4, 5)

Thermoplastics are softening if enough heat is applied and hardened on cooling. Thus they can be converted into new plastics products. Examples are polyethylene, polystyrene and polyvinyl chloride, etc.

Thermosets or thermosetting's plastics can melt and take shape only once. They are not suitable for repeated heat treatments; therefore after solidified, they remain as it is. Examples are phenol formaldehyde and urea formaldehyde.

II. WASTE PLASTIC POLLUTION

It is well known that most of the plastic materials are non-degradable polymers. These materials do not break without any chemical process; thus a huge amount of such waste material is increasing day by day on the earth. India generates 56 lakh tonnes of plastic waste annually, with Delhi accounting for a staggering 689.5 tonnes a day.

Total plastic waste which is collected and recycled in the country is estimated to be 9,205 tonnes per day (approximately 60% of total plastic waste) and 6,137 tonnes remain uncollected and littered. This waste is a source of continuing pollution as it is not bio-degradable and poisons for the environment. (7)

Major chemicals used in the manufacture of plastics are highly toxic. Plastic made from petroleum is a material that the earth cannot digest. These toxic chemicals (benzene, vinyl chloride, xylenes and biphenyls etc.) pose serious threat to living beings of all species on earth. (3, 6)

Environmental Issues Due to Disposal of Plastic Waste: (6-8)

- Plastic pollution on land is both physical and chemical. Plastic reduces soil fertility by forming the part of manure for years. Plastic spoil environmental aesthetics and hygiene. Plastics in landfills emit hazardous VOCs during incineration. Plastics in soil can lessen the growth of plants and trees by blocking the absorption of minerals, water and other nutrients.
- Choked drains cause flooding during monsoons. Plastic debris's clog the sewage drains and create stagnant water which will be an ideal habitat for mosquitoes and other parasites. Wastes dumped in water courses contaminate and poison freshwater life.
- Plastic is mistaken for food and can be eaten up by birds, turtles, seals, and whales. This may choke them, or impede digestion and causing starvation. Over a million sea birds and mammals die annually from ingestion of plastics.
- Toxic chemicals in plastics can cause neurological problems such as cancer, birth defects, hormonal changes gastric ulcer, thyroid problems and cardiovascular disease etc. The endocrine disrupting chemicals (EDCs) in plastics have been contributing to obesity and diabetes. The plastic bottles may leach cancer – causing chemicals such as phthalates (a component makes plastic pliable) and Bis – phenol A (a component harden plastic). Bis – phenol A (BPA) a synthetic estrogens can affect the hearts of the women and can permanently damage DNA of mice. (8,10)

An Overview of Plastic Waste Management:

Disposal of plastic waste is a serious concern in India. New technologies have been developed to minimize their adverse effect on the environment. Currently, worldwide accepted technology used for the plastic disposal is incineration. However, the incinerators were designed poorly, releases extremely toxic compounds (chlorinated dioxins and furans) and raising several environmental issues (2, 9). In India for safer disposal of plastic waste, various technologies have been experimented. Some of these are described as below;

Utilization of plastic waste in road construction:**Polymer Blended Bitumen Roads:**

The process of road lying using waste plastics is designed and the technique is implemented successfully for the construction of flexible roads at various places in India. (6)

Co-processing of Plastic waste in Cement Kiln (Link): (6)**Operating Manual for Co-processing of Plastic Waste in Cement Kilns:**

It is estimated approximately 15,342 tons/day (TPD) of plastic waste (on per capita basis) is generated in our country. To get rid of plastic waste disposal problems, Central Pollution Control board (CPCB) in association with MP Pollution Control Board has taken initiative to use the plastic waste in cement plant at ACC Kymore (Katni, MP). (1) The stack monitoring result revealed that emission values are found below the standard set for Common Hazardous Waste Incinerators. After getting encouraging results, CPCB has granted permission to many cement plants to co-process the hazardous and non-hazardous (including plastic) waste in their kilns after trial burns.

Processing of Plastic Waste as Alternative Fuel and Raw Material (AFR):

Co-processing refers to the use of waste materials in industry process such as cement, lime or steel production and power stations or any other large combustion plants. Co-processing indicates substitution of primary fuel and raw material by waste, recovering industry and material from waste. (1) Waste material such as plastic was used for co-processing are referred to an alternative fuels and raw material (AFR). In addition, one of the advantage recovery method used in existing facility, eliminating the need to invest on other plastic waste practices and to secure land filling.

Pre-processing of plastic waste:

The plastic waste should be received in segregated and bundled form in HDPE/Jute bags. Then the plastic waste will be sun dried and subjected to shredding before feeding into cement kilns. However, PVC containing plastic waste will not be accepted in cement kilns as it impairs the cement quality [6].

Plasma Pyrolysis Technology (PPT):

Plasma pyrolysis is a state of new technology, which integrates the thermo-chemical properties of plasma with the pyrolysis process. An intense and versatile heat generation capabilities of plasma pyrolysis technology enable it to dispose of all the types of plastic waste including polymeric, biomedical and hazardous waste in a safe and reliable manner. Pyrolysis is the thermal disintegration of carbonaceous material in oxygen-starved atmosphere. When optimized, the most likely compounds formed are methane, carbon monoxide, hydrogen, carbon dioxide and water molecule [1, 6].

Pyrolysis of Waste Plastics for Converting Waste Plastics into Diesel & Other Fuels:

Pyrolysis is a recycling technique converting plastic waste into fuels, monomers or other valuable materials by thermal & catalytic cracking processes. It allows the treatment of mixed, unwanted plastic waste. For many years research has been carried out on thermally converting waste plastics into useful hydrocarbons liquid such as crude oil & diesel fuel. Recently, the technology has matured to the point where commercial plants are now available. Pyrolysis recycling of mixed waste plastics into generator & transportation fuels is

seen as the answer for recovering value from unwashed, mixed plastics & achieving their desired diversion from landfill (1-5, 8, 10-14, 17-24).

Different methods are been used for pyrolysis of plastic. (5) Some of them are as follows

- 1) Thermal pyrolysis
- 2) Catalytic pyrolysis
- 3) Hydrous pyrolysis

Petroleum Products from the Crude Oil:-

Plastics are long chain of hydrocarbons. When they heated to melt down, their hydrocarbon bonds break down in to smaller number. Again, petroleum based compounds are depends on the number of hydrocarbons in the chain. Below there are some levels of hydrocarbons and there petroleum products:

Hydrocarbon Level	Product
C 1-4	Gas. Boiling Temperature below 0.
C 5-7	Very light so easily vaporized. These clear liquid is called naphtha, used as a solvent. Dry cleaning fluids, paint solvent, quick drying products are made from these liquids.
C 7-11	Gasoline. Vaporized below boiling point of water.
C 12-15	Kerosene.
C 16-18	Lubricating Oil. Does not vaporize at normal temperature level.
C 18>	Solid.

Source: http://science.howstuffworks.com/environmental/oil-refining_1.htm

III. CONCLUSION

Pyrolysis of waste plastic is a better solution over the problem of plastic pollution as well as shortage of fuel. The product from pyrolysis of mixed PE, PP and PS is very complex. Most of the major components are present in product of pyrolysis of individual plastics. The choice of catalyst, reaction temperature affects the oil quality and quantity. The implementation of this project can develop so many opportunities in the city. It can be a solution to control waste plastic, develop a new idea, and find out an alternative source of diesel for the country. This kind of project could be very promising and effective in the future.

IV. REFERENCES

- [1]. Anita Glazer, Sadun, Thomas F, Websler and Barry Commoner, Breaking down degradable plastics scam- A report prepared by Green peace.
- [2]. Feng Gao, "Pyrolysis of Waste Plastics into Fuels" –Ph.D. Thesis in Chemical & Process Engg; University of Canterbury, 2010.
- [3]. John Scheirs and Walter Kaminsky , "Feedstock Recycling & Pyrolysis of Waste Plastics".
- [4]. Osaka/Shiga, Converting Waste Plastics into a Resource ,Compendium of Technologies, United Nations

- Environmental Programme Division of Technology, Industry and Economics International Environmental Technology Centre , Japan.
- [5]. Cracking(Chemistry). Retrieved November 22, 2013, from Wikipedia.
- [6]. Central Pollution Control Board, An Overview of Plastic Waste Management, Delhi-110032: Central Pollution Control Board,Parivesh Bhawan, East Arjun Nagar, 2012.
- [7]. Central Pollution Control Board, An Overview of Plastic Waste Management. An Delhi-110032: Central Pollution Control Board,Parivesh Bhawan, East Arjun Nagar, 2013.
- [8]. Moinuddin Sarker, Mohammad Mamunor Rashid, Muhammad Sadikur Rahman, Mohammed Molla, "Alternative Diesel Grade Fuel Transformed from Polypropylene (PP) Municipal Waste Plastic Using Thermal Cracking with Fractional Column Distillation." Scientific Research-epe, 165-172, 2012.
- [9]. Burn dirty plastic safely! Its true, Robert G Tuss, file:///C:/ Document ~1/ Rock/ LOCALS~1/TEMP/Waste plastic technology, 2008.
- [10]. Pawar Harshal R & Lawanker shailendra M.,Waste plastic Pyrolysis oil Alternative fuel for CI Engine, A review paper, Research Journal of Engg. Sciences, 2 (2), 26-30, 2013.
- [11]. A. A. Garforth, Y. H. Lin, P. N. Sharratt, J. Dwyer, Production of hydrocarbons by catalytic degradation of high density polyethylene in a laboratory fluidised-bed reactor, Applied Catalysis A: General, 331-342, 11 May 1998.
- [12]. Lithner, Delilah, "Environmental and health hazards of chemicals in plastic polymers & products", Ph.D. Thesis, Sweden: Department of Plant and Environmental Sciences University of Gothenburg, Sweden, 2011.
- [13]. Sarthak Das S. P, "Pyrolysis & catalytic cracking of municipal waste for recovery of Gasoline range Hydrocarbons", B.Tech. Degree Thesis, Rurkela, 2007.
- [14]. Luis Noreña, Julia Aguilar, Violeta Mugica, Mirella Gutiérrez, Miguel Torres and Achilias Dr. Dimitris, Material Recycling-Trends and Perspectives, Europe: In Tech, 2012.
- [15]. P. V. Thorat, Miss. Sandhya Warulkar, Miss. Harshal Sathone, Thermofuel-Pyrolysis of waste plastic to produce Liquid Hydrocarbons: A review article, Advances in Polymer Science and Technology: An International Journal 3(1), 14-18, 2013.
- [16]. Pandian Sivakumar, Kamalakannan Anbarasu, Catalytic Pyrolysis of Dairy Industrial Waste LDPE Film Into Fuel, Academic Sciences-International Journal of Chemistry Research Vol 3(1), 1-4, 2012.
- [17]. Jenny Bo, Duke Ismael, R.T. Benbow, Dioxin Emission Reduction Program – Report, NSW, Australia, 2012.
- [18]. Dastanian, Seyed Mousa Fakhr Hoseini and Majid, Predicting Pyrolysis Products of PE, PP, and PET Using NRTL Activity Coefficient Model, Journal of Chemistry, 1-5, 2013.
- [19]. Neha Patni, Pallav Shah, Shruti Agarwal, and Piyush Singhal, Alternate Strategies for Conversion of Waste Plastic to Fuels, ISRN Renewable Energy, 1-7, 2013.
- [20]. Derrick, Matthew Johnson Sean, "Pyrolysis: A method for Mixed Polymer Recycling, Green Manufacturing Initiative, 21, 2010.
- [21]. Prof. Alka Zadgaonkar, Conversion of Waste Plastic in to Liquid Hydrocarbons/Energy, Project Report,

Nagpur, 2005.

- [22].M. Arandes, Iñaki Abajo, Danilo López-Valerio, Inmaculada Fernández, Miren J. Azkoiti, Martín Olazar and Javier Bilbao, Transformation of Several Plastic Wastes into Fuels by Catalytic Cracking,ACS, 4523-4529, 1997.
- [23].Jetjis,How to turn plastic waste into diesel fuel cheaply, Energetic forum, 85, 2007.
- [24].Achut kumar Panda, “Studies on process optimisation for production of liquid fuels from waste plastics”, Ph. D. Thesis, Rurkella, 2011.

Synthesis, Characterization and Microbial Activity of Aldimine Metal Complexes

Dinkar P. Kotwal

Department of Chemistry, Dnyanopasak Shikshan Mandal's Arts, Commerce and Science College, Jintur-431509, Maharashtra, India

ABSTRACT

Aldimine (E)-4-chloro-N-((thiophene-2-yl)methylene)benzenamine and its complexes with Cu (II), Ni (II), Co (II) and Zn (II) were prepared and characterized by analytical, spectroscopic techniques, magnetic measurements and electrical conductivity. The results indicate that the ligand coordinate through azomithine nitrogen and sulphur of thiophene moiety to the metal ions. The complexes were further screened for antimicrobial activity.

Keywords: Aldimine, metal complexes, Microbial activity.

I. INTRODUCTION

Aldimine are important class of ligand in coordination chemistry and their complex formation ability containing different donor atom is mostly reported. The chemistry of transition metal complexes containing heterocyclic donor atom are of interest on account of their biological importance¹. The aldimine metal complexes show fungicidal² antimicrobial³, anti-cancer⁴ and anti-inflammatory activity⁵. Thus the present study describe synthesis, characterization and microbial studies of some transition metal aldimine complexes.

II. EXPERIMENTAL

The ligand (E)-4-chloro-N-((thiophene-2-yl)methylene)benzenamine (L) has been characterized by IR studies. The complex characterized by infrared spectral studies, electronic spectral studies, magnetic moment, thermal analysis and conductivity measurement. The microbial activity of the investigated compound was tested by the paper diffusion method.

Synthesis of Aldimine:

The aldimine was synthesized by reported procedure⁶. To the solution of thiophene-2-carboxaldehyde 0.112 gm (0.001 mole) in 25 ml ethanol and 0.127 gm (0.001 mol) 4-chloroaniline in 25 ml ethanol was added. The solution was refluxed for 4.5 hrs. The solution was monitored on TLC, on completion of reaction the solution was concentrated, cooled and poured in water the separated solid was filtered, washed with water and recrystallized from ethyl alcohol and dried over calcium chloride in vacuum. The composition and yield of aldimine have shown in table no 1.

Synthesis of metal complexes:

The metal complexes of Cu (II), Ni (II), Co (II) and Zn (II) with ligand were prepared by refluxing the ethanolic solution of metal nitrate and ligand in 1:2 molar ratios. The pH of solution was adjusted by alcoholic ammonia.

Ligand (0.02 mole) in slight excess was taken in a round bottom flask containing 30 ml anhydrous ethanol and refluxed for few minutes with constant stirring to ensure complete dissolution, A solution of the appropriate metal nitrate (0.01 M) in 20 ml of anhydrous ethanol was then added drop by drop with constant-stirring in the hot solution of ligand. The content was refluxed five hours. After cooling, the pH of the mixture was maintained by the addition of alcoholic ammonia solution. The resultant precipitate was digested for one hour. The precipitate was filtered, washed with hot ethanol and dried in vacuum desiccators over anhydrous granular calcium chloride. The composition and yield of metal complexes have shown in table no 1.

III. RESULT AND DISCUSSION

The metal complexes are colored and stable to air and moisture. They are insoluble in water, sparingly soluble in benzene, chloroform, carbon tetrachloride etc. and completely soluble in dimethyl formamide and dimethyl sulfoxide. Elemental analysis suggests that the complex have 1:2(metal-ligand) stoichiometry. The conductivity value in dimethyl formamide ($1 \times 10^{-3}M$) reveals their electrolyte nature ^{7,8}. Based on elementary chemical analysis the formula, $ML_2(H_2O)_2(NO_3)_2$ were suggested for all compounds.

In infrared spectrum of ligand, a bond at 1654 cm^{-1} assigned to azomethine (C=N) stretching vibration ^{9,10}. A bond at 847.03 cm^{-1} L assigned to C-S-C stretching mode in thophin ring¹¹.

Table 1: Analytical data of ligand and metal complexes

Compound	Colour	Yield (%)	Formula	Mol Wt.	% Analysis Found(Calculated)			
					C	H	M	N
Ligand(L)	Pale yellow	63	$C_{11}H_8ClNS$	221.71	59.48 (59.59)	3.59 (3.64)	--	6.28 (6.28)
$(L)_2Cu(H_2O)_2(NO_3)_2$	Green	66	$C_{22}H_{20}Cl_2CuN_2O_2S_2$	542.99	48.58 (48.66)	3.65 (3.71)	11.43 (11.70)	5.09 (5.16)
$(L)_2Ni(H_2O)_2(NO_3)_2$	Pale Green	70	$C_{22}H_{20}Cl_2NiN_2O_2S_2$	538.14	49.02 (49.10)	3.64 (3.75)	10.65 (10.91)	5.19 (5.21)
$(L)_2Co(H_2O)_2(NO_3)_2$	Pink	53	$C_{22}H_{20}Cl_2CoN_2O_2S_2$	538.38	48.98 (49.08)	3.69 (3.74)	10.64 (10.95)	5.21 (5.20)
$(L)_2Zn(H_2O)_2(NO_3)_2$	Colour-less	52	$C_{22}H_{20}Cl_2ZnN_2O_2S_2$	544.83	48.42 (48.50)	3.62 (3.70)	11.79 (12.00)	5.08 (5.14)

In the spectra of Cu complexes the band at 1654 cm^{-1} is shifts to lower frequency (1628.53 cm^{-1}), indicating the co-ordination of azomethine nitrogen to metal atom. In spectra of complex the broad band at 3400 cm^{-1} , indicating the presence of coordinated water. The bands at 847.03 cm^{-1} shift to lower frequency and appear at

839.53 cm^{-1} , this shift refer the participation of sulphur of thiophen moiety in the complex formation^{7,11}, further confirmed by a new band. The new bands at 558.99 cm^{-1} and 526.82 cm^{-1} in the spectra of complex are assigned to stretching vibration of M-S and M-N bands respectively¹².

Table-2: IR frequency (cm^{-1}) of ligand and complexes

Ligand / Complex	ν (OH) Water	ν (C-S-C)	ν (C=N)	ν (M-N)	ν (M-S)
L	-	847.03	1654.00	-	-
L-Cu	3400.00	839.53	1628.53	526.82	558.99

The UV-Visible spectra of copper complexes of ligand exhibit bands at 15337 cm^{-1} , 26954 cm^{-1} attributed to ${}^3\text{E}_g \rightarrow {}^2\text{T}_{2g}$ and charge transfer transition which indicate distorted octahedral geometry of Cu (II) complexes, which further supported by μ_{eff} value 1.91 B.M.¹³.

The ligand field parameter values (Dq and LFSE) observed at 15337 cm^{-1} and 43.79 kcal mole^{-1} respectively and these are in good agreement with the distorted octahedral Cu (II) complexes

The electronic spectra of Ni (II) complex exhibit bands in the three regions as 9671 cm^{-1} 16000 cm^{-1} and 23752 cm^{-1} . This pattern of absorption may be assigned to transition ${}^3\text{A}_{2g} \rightarrow {}^3\text{T}_{2g}(\text{F})$, ${}^3\text{A}_{2g} \rightarrow {}^3\text{T}_{1g}(\text{F})$ and ${}^3\text{A}_{2g} \rightarrow \text{T}_{1g}(\text{P})$ respectively. This may be assigned to characteristic three spin allowed transition of octahedral complexes¹⁴, further supported by μ_{eff} value 2.98 B.M.

The reduction of B values for the Ni(II) complexes (715.93 cm^{-1}) as compared to the free ion value for Ni(II) ion (1030 cm^{-1}) reveals complex formation. The Nephelauxetic ratio (β) obtained are less than unity (0.695) in this case suggesting considerable amount of covalent character of the metal ligand bonds. The LFSE value (27.61 Kcal mole^{-1}) indicate considerable stability of Ni(II) complexes. The energy ratio ν_2/ν_1 (1.654) being close to reported values (1.6-1.82) as well as the 10Dq (9671 cm^{-1}) and percentage of β (43.88) found indicate that the Ni(II) complex is in octahedral geometry.

The electronic spectra of Co (II) complex exhibit bands at 9407 cm^{-1} , 18382 cm^{-1} and 21276 cm^{-1} . These bands may be assigned to ${}^4\text{T}_{1g}(\text{F}) \rightarrow {}^4\text{T}_{2g}$, ${}^4\text{T}_{1g}(\text{F}) \rightarrow {}^4\text{A}_{2g}(\text{F})$ and ${}^4\text{T}_{1g}(\text{F}) \rightarrow {}^4\text{T}_{1g}(\text{p})$ respectively, suggesting a high spin octahedral geometry around the cobalt ion. Octahedral geometry around cobalt ion¹⁵ further supported by μ_{eff} value 5.15B.M.

The reduction in B values for all the Co(II) complexes (762.46 cm^{-1}) as compared to the free ion value for Co(II) ion (971 cm^{-1}) reveals complexes formation thereby favoring the orbital overlap and delocalization of d orbitals. The Nephelauxetic ratio (β) in each case is less than unity (0.785) and their $\% \beta$ values (27.38 %) indicate partial covalent character in metal ligand bond. The LFSE value (25.62 Kcal mole^{-1}) indicates considerable stability of Co (II) complexes.

The electronic spectra of Zn (II) complex exhibits bands at 27932 cm^{-1} attributed to charge transfer transition suggesting a octahedral environment¹⁶. This complex is diamagnetic in nature.

The simultaneous use of TG and DTA show that the metal complexes are thermally quite stable. Thermograms of all the complexes indicate the presence of coordinated water molecules.

X-Ray powder pattern investigation suggests that all the complexes are crystalline in nature

IV. MICROBIAL ACTIVITY

The ligand and their metal complexes were tested for antibacterial activity Mueller Hinton agar was used for testing the susceptibility of microorganism by well diffusion method, using DMSO as solvent, at a concentration of 0.01 M against gram positive (*staphylococcus aureus*) and gram negative (*Escherichia coli*) bacteria. The zones inhibition against the growth of microorganisms was determined at the end of on incubation period 24 h at 37°C and the results are presented in table 3. It was found that the metal complexes are more active than the free ligand.

V. ACKNOWLEDGMENT

The author is thankful to Dr. W N. Jadhav, Ex principal, Sharda mahavidyalaya, Parbhani, , Dr. B. C. Khade Professor and Head, Dr. S.R. Bhusare DSM College, Parbhani, Dr. R. P. Pawar, C S Mahavidyalaya, Aurangabad, for their valuable guidance. Also thanks to Dr. S. G. Bhombe, Principal DSM College, Jintur, for providing the necessary facilities.

Table 3: Antimicrobial activities of Aldiminee and their complexes

compound	Zone of inhibition	
	Staphylococcus aureus	Escherichia coli
L	12	10
L-Cu	19	16
L-Ni	17	14
L-Co	16	15
L-Zn	14	12
Standard drug	26	30

VI. REFERENCES

- [1]. Antloin L., Febretel A C, Galtesti D, Giushi A and Sessoli R, Inorg.Chem,29, 143(1990) .
- [2]. Sudha Goyal and Keemati Lal. J. Indian Chem. Soc., 66-477 (1989).
- [3]. Jons,R.D.,Summerville, D.A.and Basolo,F.,Chem.Rev,79,130(1979).
- [4]. Wu. Zishen, Gui Ziqui and Yen Zhenhuan, Synth. React. Inorg. Met org. Che. 20.335 (1990)
- [5]. R.K. Parashar, R.C. Sharma, Anil Kumar and Govind Mohan, Inorg. Chim. Acta. 151, 201 (1988)
- [6]. Merchant, Jaysukhal R., Chothia D.S., J. Med. Chem., 13 (2), 335-36 (1970)
- [7]. M. Kumar, Orien. J. Chem.18(3) 559(2002).
- [8]. Geary, W.J., Coord. Chem, Rev, 7, 82(1971).
- [9]. Silverstein, M. R., Bassler, G. C. and Morrill, T. C., Spectrometric Identification Of Organic Compounds, John Wiley and Sons,4th ed., 1981,p- 111,130.
- [10]. Rao, N.R., Venkateshwar, P.R., Reddy. G.V. and Ganorkar, M.C., Indian J. Chem., 26A (10), 887 (1987).

- [11].Mohamad, G. G., Omar, M. M. and Hindy, A. M. Turk. J. Chem., 30,361,2006.
- [12].Nakamoto, K., "Infrared Spectra of Inorganic coordination compounds", John Wiley Publication, New York (1966; 1970).
- [13].Dash, D.C., Pansa, A.K., Jena, P., Potioshi, S.B. and Mahapatra A., J. Ind. Chem. Soc., 79, 48-50 (2002).
- [14].Sutton, D., "Electronic Spectra of transition metal complexes" McGraw Hill, 145-148 (1968)
- [15].Mahapatra, K., Rupini, B and Srihari, S., J. Ind. Chem. Soci, 81, (2004) 950-953.
- [16].Feggis, B.N. and J. Lewis, Prog. Inorg. Chem., 6, 87 (1964).

One-Pot Three Component Synthesis of Pyrimido Thiadiazolo Pyrimidine Dione Using 1-Butyl-3-Methyl Imidazolium Chloride with Their Antioxidant Activities

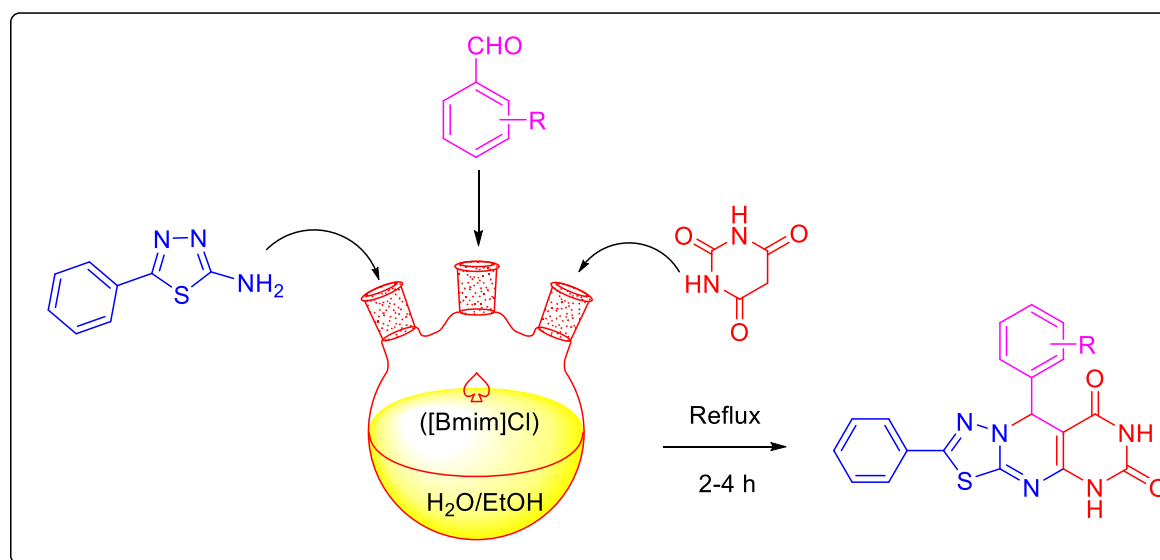
Gopinath S Khansole¹, Vijay N. Bhosale*²

¹D.A.B.N.A College, Chikhali, Sangali-415408, Maharashtra, India

²P. G., Department of Chemistry, Yeshwant Mahavidyalaya, Nanded, Maharashtra, India

ABSTRACT

A environment friendly, green, most efficient procedure has been developed for the synthesis of 9-substituted derivatives of 9-(4'-phenyl)-2-phenyl-5,9-dihydro-6 *H*-pyrimido[4,5-*d*][1,3,4] thiadiazolo [3,2-*a*] pyrimidine-6,8(7*H*)-dione from a multicomponent one pot three component condensation of 2-amino-5-phenyl 1,3,4-thiadiazole, A mixture of barbituric acid and different substituted aromatic aldehydes using 1-Butyl-3-methyl Imidazolium Chloride ([Bmim]Cl) in water-ethanol was refluxed for three to four hours. The formed compounds were screened potent Antioxidant activity.



Keywords: Green synthesis, Barbituric acid, Aromatic Aldehyde, MCR's.

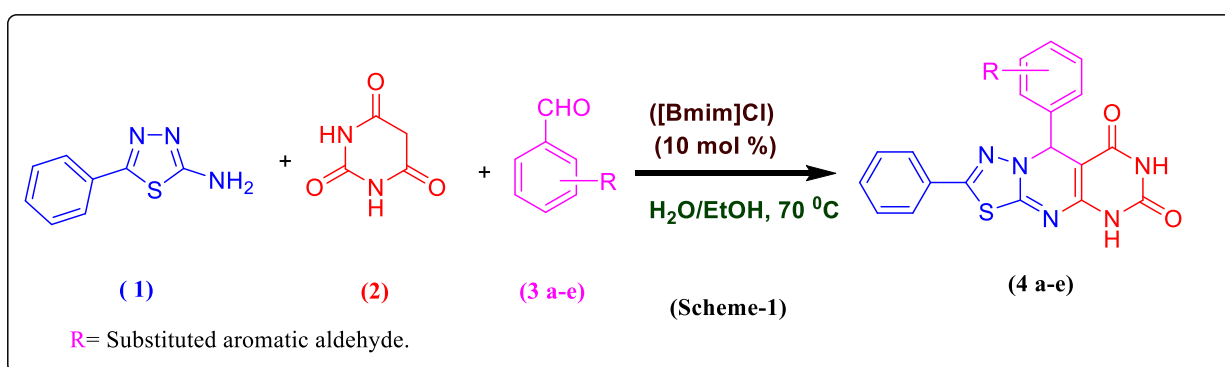
I. INTRODUCTION

Heterocyclic compounds have broad attention towards organic chemistry due to availability in natural products and medical field as well as biological properties[1]. The literature survey reveals that various thiadiazoles have resulted in many potential drugs and are known to exhibit a wide range of pharmacological and biological properties like antimicrobial [2], anti-inflammatory [3] and anticancer [4].

In a multicomponent reaction (MCRs) three or more reactant are converted into a higher molecular weight compound in a one pot method. The MCR has become very popular in the today's Chemistry. Thiadiazolo [3,2-*a*] pyrimidine dione derivatives occupies an important position in chemistry and biology. The most chemist widespread has growing interest to the development of Thiadiazolo [3,2-*a*] pyrimidine dione due to the diverse pharmacological as well as biological properties such as antifungal activity [5], antitumor [6], antioxidant [7], anticonvulsant[8], antihypertensive[9], analgesic[10], anti HIV activity[11], antibiotics[12]. In addition to these derivatives show diverse application in agrochemical industry and pharmaceutical industry Thiadiazolo [3,2-*a*] pyrimidine synthesis was reported using the various catalyst such as 2-[5-(4-methoxyphenyl) 4-*H*-1,2,4-triazole] acetic acid[13], NaOH in ethanol[14] , SBA-15 [15]. Some of the method reported above use expensive catalysts, strong acidic conditions, higher temperature, require long reaction time, resulting cumbersome product isolation procedure.

Recent days, 1-Butyl-3-methyl Imidazolium Chloride ([Bmim]Cl), act as a phase transfer catalyst (PTC) and it perform much organic transformation under mild condition. Thus new route utilizing a MCR protocol, for the synthesis of triazolo [1,5-*a*] pyrimidinedione can attacks considerable attention in the search of method for rapid entry of these heterocycles. Consequently, we thought that there is scope for further innovation towards milder reaction condition, short reaction time and better yield in choosing 1-Butyl-3-methyl Imidazolium Chloride ([Bmim]Cl) for this multicomponent reaction (MCRs). The mild Lewis acidity associated with 9-dihydro-6-*H*-pyrimido[4,5-*d*] [1,3,4] thiadiazolo [3,2-*a*] pyrimidine-6,8(7*H*)-dione having potent antioxidant activity.

II. RESULT AND DISCUSSION



Our efforts were focused on optimization reaction condition. The reaction mixture of 2-amino-5-phenyl 1,3,4-thiadiazole, barbituric acid was refluxed using 1-Butyl-3-methyl Imidazolium Chloride ([Bmim]Cl) in water-ethanol with different substituted aromatic aldehydes, was considered as a model reaction (**Scheme 1**) for investigating the effectiveness of different polar and non polar solvent using catalytic amount of molecular iodine (10 mol%). Solvent optimization clearly suggested that H₂O/EtOH is the best solvent for the desired transformation due to fast reaction rate and high yield (Table1, entry 6). The other polar protic solvents gives moderate yield (Table1, entry 5). While other aprotic solvent like THF, DMF, ethylene dichloride and 1,4-dioxane displayed slow reaction rates leading lower yield (Table1, entry 1-4).

We have carried out the model reaction using different stoichiometric amount of catalyst. The catalyst screening result are summarized in Table 2. It was observed that the excellent yield was achieved by using 10 mol% of 1-Butyl-3-methyl Imidazolium Chloride ([Bmim]Cl) (Table 2, entry 5).

After investigating the influence of different parameters on the model reaction, we turned our attention towards the 9-substituted derivatives of 9-(Substituted phenyl)-2-phenyl-5,9-dihydro-6*H*-pyrimido [4,5-*d*] [1,3,4] thiadiazolo [3,2-*a*] pyrimidine-6,8(7*H*) dione (**4a-e**) using one pot three component reaction of 2-amino-5-phenyl 1,3,4-thiadiazole (**1**) barbituric acid (**2**) was refluxed 1-Butyl-3-methyl Imidazolium Chloride ([Bmim]Cl) in water-ethanol with different substituted aldehydes (**3a-e**), and the result are summarized in Table 3. With the both electron-poor and electron-rich benzaldehydes (Table 3, entries 1-3 and 4-5), the corresponding 9-substituted of pyrimido [4,5-*d*] [1,3,4] thiadiazolo [3,2-*a*] pyrimidine-6,8(7*H*) dione derivatives (**4a-e**) were obtained to excellent yields. These synthesized products (**4a-e**) were completely characterized from IR, ¹H-NMR, Mass and ¹³C-NMR spectroscopic technique and also elemental analysis. The overall, mechanism takes place according to Knoevenagels-Micheal reaction (**Scheme-II**).

Table 1. Optimization of the reaction conditions using different solvents.^[a]

Entry	Solvent	Reaction Time (h)	Yield (%) ^[b]
1	1,4-dioxane	6.0	35
2	Ethylene dichloride	8.0	40
3	THF	9.0	45
4	DMF	6.0	50
5	EtOH	5.5	65
6	H2O/EtOH	4.0	80

^[a] **Reaction conditions:** 2-amino-5-phenyl 1,3,4-thiadiazole (1 mmol), barbituric acid (1 mmol) with substituted benzaldehydes (1 mmol) and 1-Butyl-3-methyl Imidazolium Chloride ([Bmim]Cl) in water-ethanol were refluxed at 70°C.

^[b] Isolated yields.

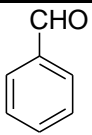
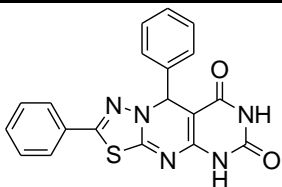
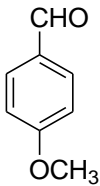
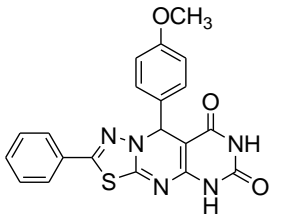
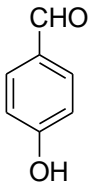
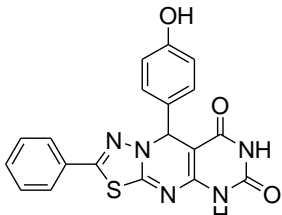
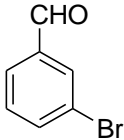
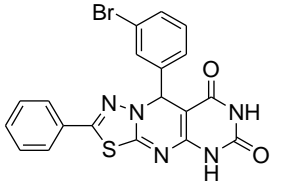
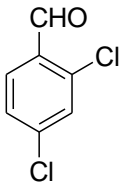
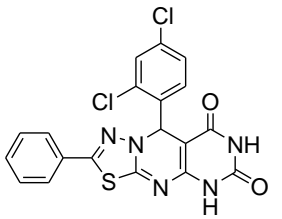
Table 2: Optimization Study for the amount of 1-Butyl-3-methyl Imidazolium Chloride ([Bmim]Cl) ^[a]

Entry	Catalyst (mole %)	Temperature (°C)	Reaction Time (h)	Yield % ^[b]
1	01	70	4.0	40
2	02	70	4.0	50
3	05	70	4.0	60
4	08	70	4.0	72
5	10	70	4.0	80
6	15	70	4.0	80
7	20	70	4.0	80

^[a] **Reaction conditions:** 2-amino-5-phenyl 1,3,4-thiadiazole (1 mmol), barbituric acid (1 mmol) with substituted benzaldehydes (1 mmol) and 1-Butyl-3-methyl Imidazolium Chloride ([Bmim]Cl) in water-ethanol were refluxed at 70°C.

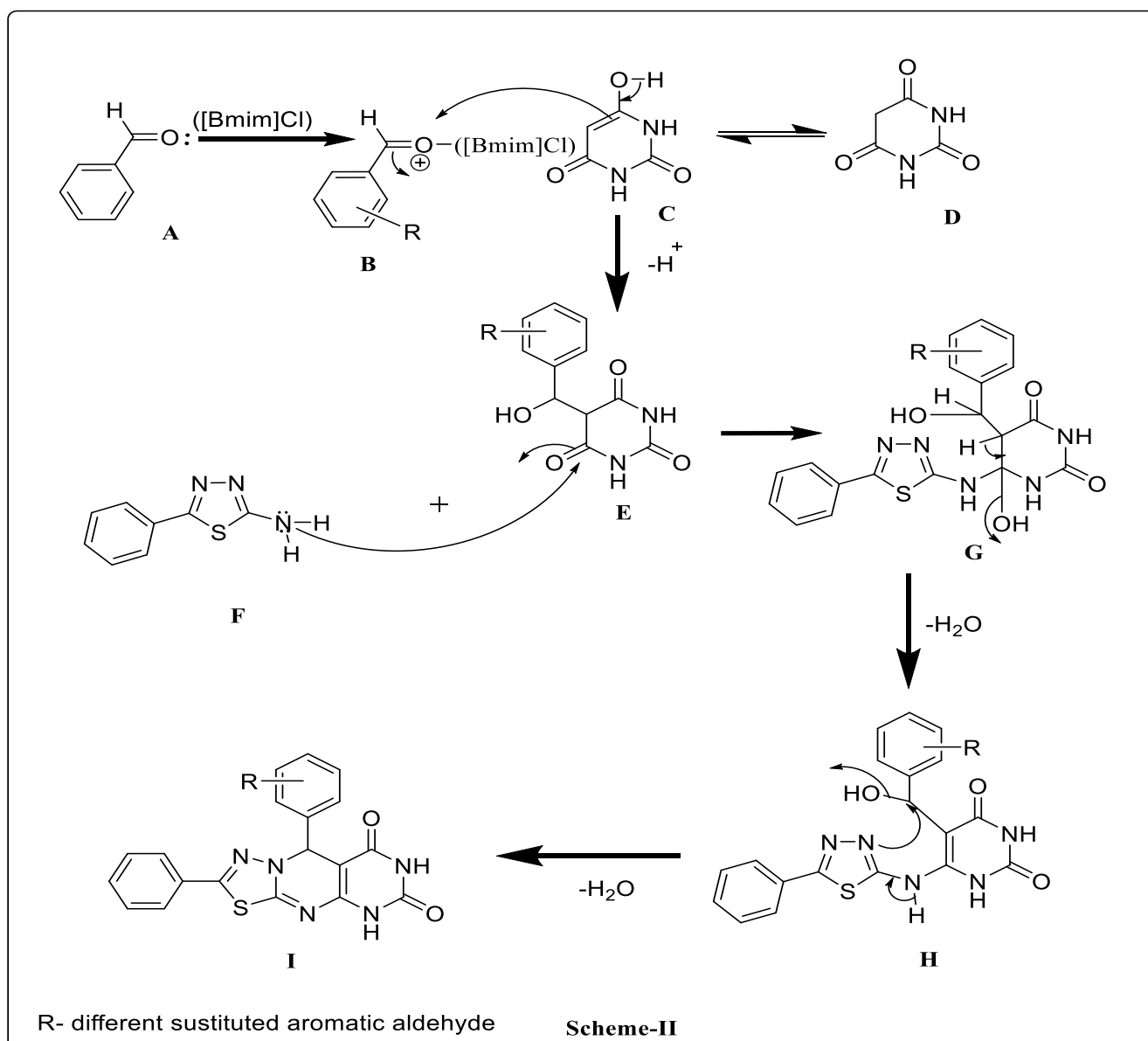
^[b] Isolated yields.

Table 3: Three component reaction of 2-amino-5-phenyl 1,3,4-thiadiazole (1), barbituric acid (2), and aromatic aldehydes (3a-e) for the synthesis of (4a-4e).^[a]

Entry	Aldehyde (3a-e)	Products (4a-4e)	Time (h)	Yield (%) ^[b]	M.P. (°C)
1			3.0	68	201-203
2			3.5	80	211-213
3			4.0	78	341-343
4			3.5	80	226-228
5			3.0	78	231-233

^[a] **Reaction conditions:** (1) (1 mmol), (2) (1 mmol), (3a-e) (1 mmol) and acetonitrile in Iodine were refluxed at 70°C.

^[b] Isolated yields.



III. EXPERIMENTAL

Open capillary tubes were used for melting points of isolated synthesized compounds and are uncorrected. Perkin-Elmer FTIR spectrophotometer was used for IR (KBr) spectra of compounds. Mass spectral data were recorded on liquid chromatography mass spectrometer (Shimadzu 2010Ev) using ESI probe. The ^1H and ^{13}C NMR spectra were recorded on various spectrometers at 300 & 400MHz using TMS as an internal standard.

General procedure for the synthesis of 9-substituted derivatives of 9-(4'-phenyl)-2-phenyl-5,9-dihydro-6H-pyrimido[4,5-d][1,3,4]thiadiazolo[3,2-a]pyrimidine-6,8(7H)-dione (4a-e) :

A mixture of 2-amino-5-phenyl 1,3,4-thiadiazole (1) barbituric acid (2) was refluxed using 1-Butyl-3-methyl Imidazolium Chloride ([Bmim]Cl) as an catalyst in water-ethanol with different substituted aldehydes (3a-e),

to isolate the respective products (**4a-e**). The reaction mixture was cooled to room temperature and poured into ice cold water. The solid obtained was filtered, washed with water and recrystallized by ethanol to give (**4a-e**). The reaction was monitored by TLC. These synthesized products (**4a-e**) were completely characterized from IR, ¹H-NMR, Mass and ¹³C-NMR spectroscopic technique and also elemental analysis.

Spectral Analysis:

2,9-diphenyl-5,9-dihydro-6H-pyrimido[4,5-d][1,3,4]thiadiazolo[3,2-a]pyrimidine-6,8(7H)-dione (4a) :

M.P. 201-203°C, Yield 68%. IR (KBr/ cm⁻¹) 3228 (-NH), 1701,1623 (2 C=O); ¹H NMR (400MHz, DMSO-d₆/ ppm) δ 6.8 (s, 1H, -CH), δ 6.7-7.9 (m, 10 H, Ar-H), δ 10.8 and δ 11.4 (2 bs, 2H, -NH); EI-MS (m/z: RA %): 375 (M⁺, 100%),. Elemental analysis calculated data for C₁₉H₁₃N₅O₂S ; C, 60.79; N, 18.86. Found: C, 60.81; N, 18.88.

9-(4'-methoxyphenyl)-2-phenyl-5,9-dihydro-6H-pyrimido[4,5-d][1,3,4]thiadiazolo[3,2-a] pyrimidine-6,8(7H)-dione (4b) :

M.P. 211-213 °C , Yield 80 %. IR (KBr/ cm⁻¹) 3209 (-NH), 1731,1674 (2 C=O),1269(-O-R); ¹H NMR (400MHz, DMSO-d₆/ ppm) δ 3.07 (s, 3H, -Ar-OCH₃), δ 6.40 (s, 1H, -CH), δ 7.0-8.5 (m, 9H, Ar-H), δ 11.1 and δ 11.3 (2 bs, 2H, -NH); EI-MS (m/z: RA %): 305 (M⁺, 100%). ¹³C NMR (400 MHz, DMSO-d₆/ ppm) δ: 163,160, 151, 150, 155, 143, 140, 128, 127,90 ,57, 51, 40, 39, 38. Elemental analysis calculated data for C₂₀H₁₅N₅O₃S ; C, 59.25; N, 3.73. Found: C, 59.26; N, 3.75.

9-(4'-hydroxyphenyl)-2-phenyl-5,9-dihydro-6H-pyrimido[4,5-d][1,3,4]thiadiazolo[3,2-a] pyrimidine-6,8(7H)-dione (4c) :

M.P. 341-343 °C, Yield 78% .IR (KBr/ cm⁻¹) 3450 (-OH), 3274(-NH) 1720, 1670 (2C=O); ¹H NMR (400MHz, DMSO-d₆/ ppm) δ 6.86 (s, 1H, -OH), δ 6.8 (s, 1H, -CH), δ 7.4-8.3 (m, 9H, Ar-H), δ 10.8 and δ 11.1 (2 bs, 2H, -NH); EI-MS (m/z: RA %): 391 (M⁺, 100%),. ¹³C NMR (400 MHz, DMSO-d₆/ ppm) δ: 168,164, 163,155, 150, 138, 132, 129, 123,115,114. Elemental analysis calculated data for C₁₉H₁₃N₅O₃S ; C, 58.30; N, 17.89. Found: C, 58.32; N, 17.92.

9-(3'-bromophenyl)-2-phenyl-5,9-dihydro-6H-pyrimido[4,5-d][1,3,4]thiadiazolo[3,2-a] pyrimidine-6,8(7H)-dione (4d) :

M.P. 226-228 °C, Yield 80%. IR (KBr/ cm⁻¹) 3136 (-NH), 1697,1604 (2C=O); ¹H NMR (400MHz, DMSO-d₆/ ppm) δ 5.7 (s, 1H, -CH), δ 7.0-8.2 (m, 9H, Ar-H), δ 10.4 and δ 11.1 (2 bs, 2H, -NH); EI-MS (m/z: RA %): 456 (M⁺+3, 100),. ¹³C NMR (400 MHz, DMSO-d₆/ppm) δ: 169, 168,167, 164, 161,156, 152, 150, 146, 135,134, 130, 129,126, 121, 120. Elemental analysis calculated data for C₁₉H₁₂N₅O₂BrS ; C, 50.23; N, 15.42. Found: C, 50.25; N, 15.44.

9-(2',4'-dichlorophenyl)-2-phenyl-5,9-dihydro-6H-pyrimido[4,5-d][1,3,4]thiadiazol[3,2-a] pyrimidine-6,8(7H)-dione (4e) :

M.P. 231-233 °C, Yield 75%.IR (KBr/cm⁻¹) 3132 (-NH), 1693,1600 (2C=O); ¹H NMR (400MHz, DMSO-d₆/ ppm) δ 5.7 (s, 1H, -CH), δ 7.11-8.39 (m, 8H, Ar-H), δ 10.47 and δ 11.29 (2 bs, 2H, -NH); EI-MS (m/z: RA %):

443 ($M^+ +1$, 100%), ^{13}C NMR (400 MHz, $\text{DMSO}-d_6/\text{ppm}$) δ : 168, 167 (C=O), 160,149 (C-4b), 135, 134,133,130,129 128, 126, 121, 78,40,39,38. Elemental analysis calculated data for $\text{C}_{19}\text{H}_{11}\text{Cl}_2\text{N}_5\text{O}_2\text{S}$; C, 51.36; N, 15.76. Found: C, 51.38; N, 15.78.

Antioxidant Activity:

A) DPPH (1, 1-diphenyl-2-picrylhydrazyl) radical scavenging assay:

DPPH (1,1-diphenyl-2-picrylhydrazyl) radical scavenging assay was performed as per earlier reported method^[16]. The reaction cocktail was prepared by mixing individual newly synthesized organic compounds is added to equal volume of 0.1 mM solution of DPPH radical in absolute ethanol. After 20 minutes of incubation at room temperature, the DPPH reduction was calculated by reading the absorbance at 517 nm using UV-Visible spectrophotometer. Ascorbic acid (1mM) was used as reference compound.

The compound (**4d and 4e**) shows remarkable antioxidant activity against DDPH radical scavenging activity with reference of ascorbic acid (91.4 ± 0.020).

B) OH radical scavenging assay:

Hydroxy radicals scavenging activity was measured with Fenton's reaction (Rollet –Labelle et al., 1998). The reaction mixture contained 60 μl of FeCl_2 (1mM), 90 μl of 1,10-phenanthroline(1mM), 2.4 ml of phosphate buffer (pH 7.8),150 μl of 0.17M H_2O_2 and 1.5 ml of individual newly synthesized organic compounds (1mM). The reaction mixture was kept at room temperature for 5 minutes incubation and the absorbance was recorded at 560 nm using UV-Visible spectrophotometer. Ascorbic acid (1mM) was used as the reference compound.

The compound (**4c, 4d and 4e**) shows good OH radical scavenging activity as compared with Ascorbic acid (89.5 ± 0.019).

Table 4: Antioxidant activity of tested compounds (4a-4e).

Entry	Compound Code	% Radical scavenging activity	
		DPPH radical scavenging	OH radical scavenging
1	4a	42.2 ± 0.80	56.1 ± 1.20
2	4b	68.6 ± 0.84	66.2 ± 1.65
3	4c	65.9 ± 1.79	75.2 ± 1.32
4	4d	88.4 ± 1.30	80.9 ± 0.22
5	4e	71.4 ± 0.71	79.2 ± 1.30
6	Ascorbic Acid (Standard)	91.3 ± 0.020	89.5 ± 0.019

IV. CONCLUSION

In conclusion, we have developed an efficient, green and easy protocol for synthesis of 9-substituted derivatives of 9-(Substituted phenyl)-2-phenyl-5,9-dihydro-6*H*-pyrimido[4,5-*d*] [1,3,4] thiadiazolo [3,2-*a*] pyrimidine-6,8(7*H*) dione by reaction of corresponding substituted aldehydes, 2-amino-5-phenyl 1,3,4-thiadiazole and barbituric acid in presence 1-Butyl-3-methyl Imidazolium Chloride ([Bmim]Cl) in water-ethanol. The product can be easily isolated by simple workup technique, short time, less expensive, requires ambient reaction condition, and give excellent yield. Among these synthesized compounds showed potent Antioxidant activity.

Acknowledgments

Authors are grateful to Principal, Yeshwant Mahavidyalaya, Nanded for providing laboratory facilities, UGC, New Delhi (File no.41-230/2012) (SR) for financial support and The Director, Panjab University, Chandigarh for providing spectra.

V. REFERENCES

- [1]. M. Jha, S. Guy, U.C. Ting, Tetrahedron Letters., 2011,52,4337-4371.
- [2]. K. Zamani, K. Faghli, M.S. Mehranjani, Polish J. Pharm. 2003, 55, 1111.
- [3]. A. Faroumadi, M. Mirzaei, A. Shafiee, Pharmazie. 2001, 56, 610.
- [4]. G. Sorba, A. Stilo, A.M. Gasco, M. Gill, Farmaco 1992, 47, 1992.
- [5]. Q. Chen, X.L. Zhu, Z.M. Liu, G.F. Yang, Eur. J. Med. Chem. 2008, 43(3): 595-603.
- [6]. X.L. Zhao, Y.F. Zhao, S.C. Guo, H.S. Song, D. Wang, P. Gong, Molecules, 2007,12, 1136-1146.
- [7]. V.N. Bhosale, G.S. Khansole, J.A. Angulwar, World J. Pharmacy and Pharmaceutical Sciences ., 2016,5(5),1434-1441.
- [8]. X.Yu. Dun, Xi-Wei Cheng, X.Q.Deng, Pharmacological reports, 2010, 62, 272-277.
- [9]. S. Sharma, M.C. Sharma, D.V. Kolhi, Journal of Optoelectronics and Biomedical Material, 2010; 1(3),151-160.
- [10].M.J. Hour, L.J. Huang, S.C. Kuo, Y. Xia, K. Bastow, Y. Nakanishi, E. Hamel, K.H.Lee, J. Med. Chem., 2000, 43 (23), 4479-4487.
- [11].V. Alagarsamy, R. Revathi, S. Meena, K.V. Ramashesu, S. Rajeshkarn, De E. Clercq, Indian Journal of Pharmaceutical Sciences, 2004, 459-462.
- [12].M. Cei , R. Pardelli , S. Sani , N. Mumoli , Clin.Exp.Med., 2014, 77-82.
- [13].S .Sahi, S. Paul, Medicinal Chemistry Research, 2016, 25 (5), 951-969.
- [14].S.V. Tiwari, J.A. Seijas, M.P. Vazquez, A.P. Sarkate, D.K. Lokwani, A.G. Nikalje, Molecules, 2016, 21,894.
- [15].G.M. Ziarani, P. Gholamzadeh, A. Badiel, S. Asadi, A.A. Soorki, J. Chile. Soc., 2015,60, 2975-2978.
- [16].R.G. Puligoundla, S. Karnakanti, R. Bantu, N. Kommu, S.B. Konda, L. Nagarapu, Tetrahedron, 2013,54,2480-2483.

An Overview of Green Synthesis & Biomedical Applications of Zinc Oxide (ZnO) Nanoparticles

Jagannath S. Godse¹, Santosh B. Gaikwad², Ravindra Suryawanshi³, Sanjay B. Ubale^{1*}, Rajendra P. Pawar^{3*}

¹Department of Chemistry, Deogiri College, Aurangabad - 431 005, Maharashtra, India

²Department of Chemistry, L P G Arts and Science College, Shirpur (Jain), Washim-444 504, Maharashtra, India

³Department of Chemistry, Shivchhatrapati College, Aurangabad – 431 005 (Maharashtra), India

ABSTRACT

Nanoparticles have been studied and used in a variety of modern industrial contexts over the last few decades. Zinc oxide nanoparticles have gotten a lot of attention because of their many properties, such as antifungal, photochemical, high catalytic, and antibacterial activities. This is even though the chemical and physical processes used to make nanoparticles involve harmful compounds and harsh environments. Methods for producing green nanoparticles from naturally occurring materials such as plants, fungi, bacteria, and algae have been developed. To demonstrate the utility, safety, and viability of zinc oxide nanoparticles in a variety of contexts, scientists have conducted extensive research into a variety of environmentally friendly production methods. As a result, we must rely on less reliable sources to compile useful reviews. Green synthesis appears to be safer and more environmentally friendly than chemical and physical preparation methods for nanoparticles. Nonetheless, it is frequently used in the medical field for things like bio-imaging, biosensors, drug administration, and gene delivery. Because of their low toxicity, zinc oxide nanoparticles can be used as smart weapons against drug-resistant microbes.

Keywords: zinc oxide nanoparticle, environmental benign, drug administration, biosensor.

I. INTRODUCTION

Nanotechnology is one of the fastest-growing fields in science and technology [1-2]. The unique physicochemical properties of nanomaterials enable cutting-edge systems, structures, nanoplatforms, and devices [3-4]. Nanomaterials have a high surface-to-volume ratio, are chemically stable, have good thermal conductivity, and have nonlinear optical properties [5]. This has led some scholars to seek alternative training. Conventional methods, which rely on physical and chemical processes, require the use of hazardous compounds as defensive agents, causing environmental toxicity [6]. Plant extract-mediated nanoparticle biogenesis is cheap and a rich source of protein caps. As a safe, non-toxic, and environmentally friendly alternative, plant-based green technology is gaining popularity. Plant extraction is a marginal technique for regulating chemical synthesis that, with careful synthesis, allows for a wide range of nanoparticle shapes and sizes and is used to normalise environmental chemical toxicity from side-by-side biological synthesis of

various metal oxides and metal nanoparticles [7]. Biocompatible, biodegradable, and functionalized nanomaterials are used in biomedical applications. For biological applications, magnetic nanoparticles, quantum dots, and carbon nanotubes, or nanoshells, have been studied [8-9]. Semiconductivity, piezoelectricity, and opticality are all properties of zinc oxide nanoparticles [10]. Zinc oxide nanoparticle-based nanomaterials are tested in nanosensors, energy storage, cosmetics, electronics, and optics [11]. Biodegradable and low-toxic zinc oxide nanoparticles are important. Zn^{2+} is involved in many processes in adults. Under basic and acidic conditions, zinc oxide nanoparticles dissolve slowly. Zn^{2+} ions emitted by soluble zinc oxide nanoparticles stress cells and harm a wide range of organisms [12]. Biological applications for zinc oxide nanoparticles [13]. Solubility is what harms zinc oxide nanoparticles. Dissolving extracellular zinc oxide nanoparticles increases intracellular Zn^{2+} . It is unknown what causes the increased dissolution of zinc oxide nanoparticles and intracellular Zn^{2+} [14]. This paper examines zinc oxide nanoparticles for biomedical applications, including their status, green manufacturing, and harmful effects. Based on their constituent elements, nanoparticles are classified as inorganic or organic [15]. Organic nanoparticles called fullerenes. Inorganic nanoparticles include gold, silver, semiconductors, magnetics, etc. Size, shape, and origin can classify nanoparticles. Nanomaterials can be synthetic or natural [16]. Zero-dimensional nanomaterials have no nanoscale dimensions outside the nanometer range; one-dimensional nanomaterials have one; and two-dimensional nanomaterials have two. Massive substances are divided into 1-100 nanometer units [6]. Nanodispersions are classified by molecular structure and particle size. Dendrimers are nanometer-scale branched macromolecules. These particles are mostly metal oxides (nanosilver and nanogold) and semiconductors (quantum dots). Carbon nanomaterials can be tubes, hollow spheres, or ellipsoids. Carbon nanomaterials are spherical or ellipsoidal, whereas nanotubes are cylindrical [17].

II. NANOPARTICLE SYNTHESIS METHODS

Bottom-up and top-down nanoparticle biogenesis [18]. Bottom-up approaches emphasise oxidation and reduction. Nanoparticle synthesis is a hot topic in science, with researchers seeking green processes and materials [19]. The synthesis solvent intermediate, the environmentally friendly reducing mediator, and the non-toxic material for nanoparticle stability should be evaluated for green chemistry. Most chemical and physical reactions use organic solvents. Water-repellent capping agents are to blame [20]. Green chemistry principles are compatible with bioorganism synthesis, including an eco-friendly method, agent reduction, and reaction rounding. Metal oxide inorganic nanoparticles synthesised using biological materials have unique optical, electrical, and chemical properties [21]. Metal oxides are used in piezoelectric devices, fuel cells, microelectronic circuits, sensors, and corrosion catalysts. Metal oxides are pollution absorbers. Zinc oxide nanoparticles are semiconducting metal oxides that can display unusual chemical features in nanotechnology due to their tiny mass and high limit density [22]. Zinc oxide nanoparticles stand out among metal oxides due to their refreshing properties [23], high catalytic activity, anti-inflammatory properties, wound healing, and UV filters [24]. Zinc oxide nanoparticles are biosensors for cholesterol, enzyme biochemistry, and other applications [25].

2.1. Green route for synthesis of ZnO Nanoparticles:

Chemical or physical synthesis is time-consuming and expensive. Chemical precipitation and reduction produce many byproducts. Chemical precipitation produces toxic chemical species that can adsorb on surfaces. Some reactions require heat, air mass, or poisonous substances like H_2S , poisonous models and stabilisers, and bimetallic precursors [26]. Nanoparticle synthesis and stabilisation involve toxic chemicals. Physical and chemical processes can quickly create nanoparticles. ZnO nanoparticle are made through chemical precipitation and sol-gel. Nanoparticle synthesis uses benign chemicals. Temperature also affected ZnO nanoparticle morphology. Green methods can synthesise nanoparticles using microorganisms, enzymes, plants, or plant extracts. Nanoparticle synthesis uses bacteria, fungi, and yeast. Using microorganisms to produce nanoparticles requires maintaining cell cultures, synthesising living things, and purifying [27-28]. Conventional chemical methods are expensive and often use chemical or organic solvents as reducing agents. ZnO nanoparticles powder treatments are available for mineral cream, anti-dandruff shampoo, antibiotic ointment, and bandages. ZnO nanoparticles are used in healthcare, beauty, antimicrobial, textile, and auto. ZnO nanoparticles are being studied as a micro- and nanoscale antibacterial agent. ZnO nanoparticles kill bacteria better than microparticles. Synthesis of ZnO nanoparticles uses natural materials and biopolymers, plant leaf extract, bacteria, fungi, and algae. Chemical and physical synthesis can be replaced with plant extracts. "Green" nanoparticle synthesis is appealing due to its eco-friendliness, economic potential, and applications in nanomedicine, chemically altered drugs, nano optoelectronics, etc. There is a lot of hope for this field because of how new it is and how quickly it is growing. There is a lot of hope for this field because of how new it is and how quickly it is growing. Flower-shaped ZnO nanoparticles are non-toxic, biosafe, and biocompatible due to biosynthetic and environmentally friendly technology. Most ZnO nanoparticle used in industry are synthetic and cheaper and whiter than silver nanoparticles [29-30]. various types of plant and bio media to use synthesis of ZnO nanoparticle to be maintaining green approach Fig 2.1.

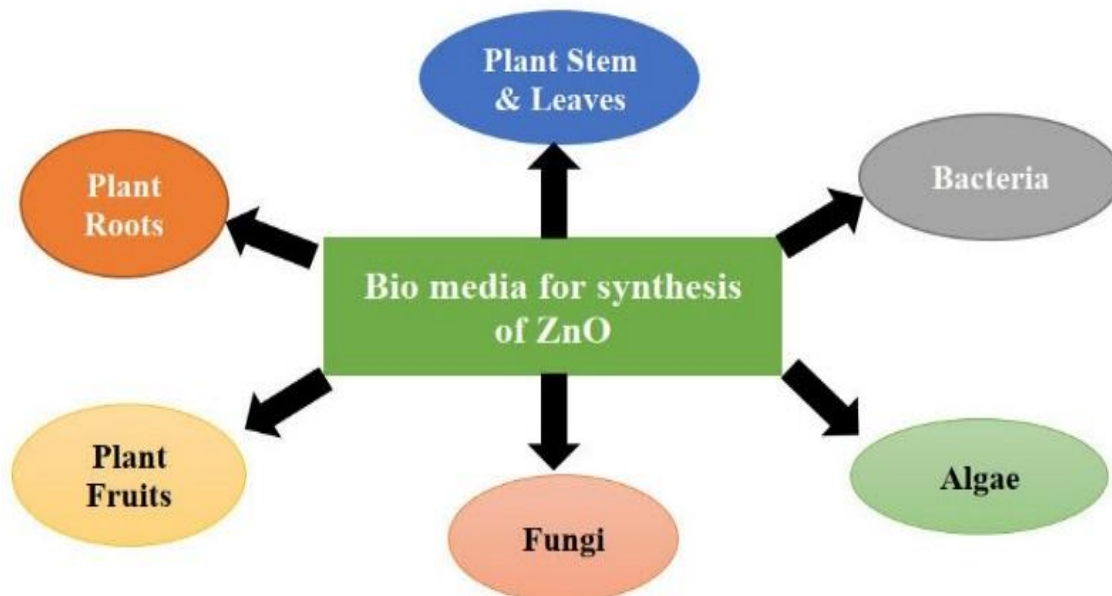


Fig.2.1 Different Bio media for synthesis of ZnO

Inexperienced ZnO nanoparticle synthesis uses plant extract. Barbadosis Sangeetha et al. synthesised ZnO nanoparticle using Miller leaf extract. Zinc nitrate and aloe vera extract form round ZnO nanoparticles. Above 25%, aloe vera leaf broth produces nanoparticles. SEM and TEM reveal that ZnO nanoparticles range in size from 25 to 40 nm. Spherical nanoparticles are obtained by adjusting leaf broth concentration [31] table 2.1.

Sr.No	Green Substrate	Name of Substrate	References
1	Plant	<i>Calotropis gigantea</i> , <i>Aloe barbadensis</i> , <i>Cassia auriculata</i> , <i>Acalypha indica</i> , <i>Parthenium hysterophorus</i> , <i>Camellia sinensis</i> , <i>Calotropis procera</i> , <i>Musa balbisiana</i> , <i>Citrus paradise</i> , <i>Medicago sativa</i>	[32-40]
2	Algae	<i>Marine macroalgae</i> , <i>Caulerpa peltate</i> , <i>Hypnea Valencia</i> , <i>Sargassum myriocystum</i> , <i>Sargassum muticum</i>	[41-44]
3	Bacteria	<i>Aeromonas hydrophila</i> , <i>Lactobacillus sporogen</i> , <i>Enterococcus faecalis</i> , <i>Bacillus cereus</i> ,	[45-48]
4	Fungi	<i>Aspergillus fumigates</i> , <i>Aspergillus aeneus</i> , <i>Fusarium spp.</i>	[49-51]

Table 2.1 Different Green substrate of ZnO Nanoparticles

III. CHARACTERIZATION OF ZINC OXIDE NANOPARTICLES

The FTIR, EDAX, AFM, XPS, ATR, UV-DRS, XRD, TEM, TG-DTA, and DLS are used to characterise the synthesised nanoparticles [52]. *Lamiaceae* plants, including *Vitex negundo* [44], *Plectranthus amboinicus* [53], and *Anisochilus carnosus* [54], produce NP in many different geometric forms, from hexagons and rods to agglomerates and spherical structures. Plant extract concentrations used in synthesis result in smaller NPs [55]. Different methods, such as transmission electron microscopy (TEM), X-ray powder diffraction (XRD), and field emission scanning electron microscopy (FE-SEM), were used to observe and compare the size range, and they all yielded similar results [56]. XRD analysis confirmed that the NPs synthesised from *Vitex negundo* flower and leaf were 100 nm using the Debye-Scherrer equation [44]. *Azadirachta indica* leaves are used to make ZnO NPs [57]. Nanobuds, hexagonal discs, and spherical NPs all showed the same size range in transmission electron microscopy and X-ray diffraction analysis. FTIR analysis established the presence of amine, carboxylic acid, carbonate moieties, alcohol, alkane, and amide during NP formation. The *Liliaceae* family includes the plants used to make *aloe vera* gel and juice [58]. NP agglomerates were formed from extracts of *Moringa oleifera*, *Calotropis gigantea*, *Plectranthus amboinicus*, *Agathosma betulina*, *Nephelium lappaceum*, and *Pongamia pinnata*. UV-visible spectrophotometry is used to validate the synthesis, and crystal NPs are obtained by centrifugation and drying in a hot air oven [44].

IV. APPLICATION OF ZINC OXIDE NANOPARTICLES

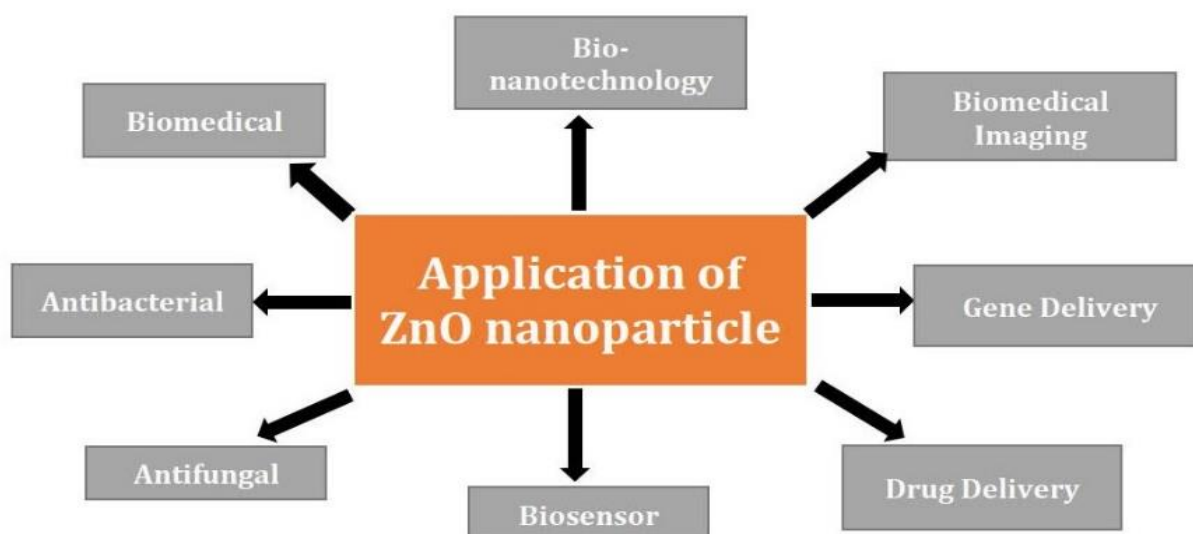


Fig.4.1 Application of Zinc Oxide Nanoparticles

Zinc oxide nanoparticles are drug carriers in biomedicine. Two factors drive their drug delivery application. Nanoparticles' small size allows them to pass through capillaries and enter cells, concentrating therapeutic substances where they're needed. Second, organic matter can be used to create nanoparticles that release drugs gradually. In studies on Zinc oxide nanoparticles and drug release, an antibiotic and its topical ointment were used. Zinc oxide nanoparticles in medicine harm the biological membrane. In biomedicine, zinc oxide nanoparticles transport drugs. Both are good for drug delivery[29, 59]. Nanoparticles enter capillaries and are absorbed by cells, directing therapeutic substances to injury sites. Organic nanoparticles are used to slow-release drugs. Zinc oxide nanoparticles affect biological membranes, study shows.

4.1. Drug Delivery:

The advantages of using ZnO nanoparticles for drug delivery stem from their two main basic properties. To begin with, because of their smaller size, nanoparticles can pass through smaller capillaries and be absorbed by cells, allowing for efficient drug accumulation at the target sites. Second, the use of biodegradable materials in the preparation of nanoparticles allows for the prolonged release of drugs within the targeted site over days or even weeks [60]. The role of synthesized ZnO nanoparticles in drug release was investigated [61] by observing its diffusion through egg membrane using the drug metronidazole benzoate. The presence of ZnO NPs with the drug has a significant effect on the biological membrane, according to the results.

4.2. Biosensors:

Biosensors have numerous applications in the fields of food science, ecology research, medicine, and analytical chemistry and biology. Some types of biosensors are electrochemical, photometric, piezoelectric,

and calorimetric [62]. These high-performance biosensors can be built on a platform of nanomaterials, either on their own or in combination with biologically active substances [63], which is why nanomaterials are becoming increasingly popular. Antibodies, enzymes, and other proteins, for instance, could be immobilized using the increased surface area of nanomaterials. In addition, they may be allowed to carry out direct electron transfers between the electrodes and the active sites of the biomolecules.

4.3. Antimicrobial Activity:

ZnO is being studied as a pharmaceutical agent in microscale and nanoscale forms[64]. Cell swelling may be caused by reactive oxygen species generated on particle surfaces, zinc ion release, membrane dysfunction, and nanoparticle acquisition. High temperatures affect ZnO nanoparticles' pharmaceutical activity, while intermediate temperatures reduce it. Evidence suggests that a mechanism study of ZnO nanoparticles' pharmacological behaviour may benefit from chemiluminescence and oxygen electrode analysis, suggesting that binding to the microorganism surface may be due to electrical forces. Metallic nanoparticles can be prepared with large surface areas, unusual crystalline and morphological forms, and edges, corners, and other reactive surface sites. ZnO nanoparticle ablation protocols are being studied. Nanoparticles will provide antineoplastic medicine with a synergistic antineoplastic impact in the presence of warmth and may be imaged to achieve medical precision and a greater thermal impact on neoplasm ablation. Several studies [65] suggested that a better understanding of the molecular mechanism involved in tumor-mediated nanoparticle ablation would aid in engineering nanoparticles of suitable composition and properties to synergize ablation.

4.4. Bioimaging:

ZnO is a notable semiconductor that is also used in electronics. It has the potential to replace Cd-related species in the biological and optical fields. ZnO nanostructures, such as nanoparticles, nanotubes, nanorods, and nanorings, are now widely understood to exist. Scientists are interested in ZnO nanoparticles as a potential bio-imaging tool [66]. There are potential biological and medical uses for this property at multiple levels. Consider the brightly glowing ZnO nanoparticles, also known as ZnO nanoparticles. Quantum yield (QY) may have favourable photophysical properties depending on its size and shape [67]. It was demonstrated that the surfaces of these nanoparticles could be easily altered. After careful modification, it has been found that ZnO nanoparticles can be very stable in aqueous solution, and their quantum yield (QY) can be increased to around 30% [68]. ZnO has a good reputation for being a secure material. Sunscreen products have incorporated ZnO, and it's also used as an additive in food packaging. As a result, the luminescent properties of ZnO nanoparticles could be used in a variety of medical and biological contexts [65]. Because of their small size, zinc oxide nanoparticles have unique properties that enable new advancements in biosensors, biomedicine, bioimaging, bio-nanotechnology, and many other fields.

V. CONCLUSION

Green ZnO nanoparticle synthesis is safer and more environmentally friendly than physical and chemical methods. ZnO nanoparticles are important and versatile due to their properties, benefits, and human applications. Green sources stabilise and reduce nanoparticle size and shape during synthesis. ZnO nanoparticles boost crop growth and yield. As food demand rises, staple crop yields fall. Sustainable agriculture requires commercialising metal oxide nanoparticles. Biomedical applications include bioimaging, drug delivery, biosensors, and gene delivery. ZnO nanoparticles can be used as smart weapons against drug-resistant microorganisms and as an antibiotic substitute. This review should help streamline methodological and clinical correlation research. In scientific and research reports, referencing this complex will suggest health solutions.

VI. REFERENCES

- [1]. Fakhari, S.; Jamzad, M.; Kabiri Fard, H., Green synthesis of zinc oxide nanoparticles: a comparison. *Green chemistry letters and reviews* 2019,12 (1), 19-24.
- [2]. Poole Jr, C. P.; Owens, F. J., *Introduction to nanotechnology*. John Wiley & Sons: 2003.
- [3]. Gattoo, M. A.; Naseem, S.; Arfat, M. Y.; Mahmood Dar, A.; Qasim, K.; Zubair, S., *Physicochemical properties of nanomaterials: implication in associated toxic manifestations*. BioMed research international 2014.
- [4]. Puzder, A.; Williamson, A.; Reboredo, F.; Galli, G., Structural stability and optical properties of nanomaterials with reconstructed surfaces. *Physical review letters* 2003,91 (15), 157405.
- [5]. Asha, A. B.; Narain, R., *Nanomaterials properties*. In *Polymer science and nanotechnology*, Elsevier: 2020; pp 343-359.
- [6]. Saleh, T. A., *Nanomaterials: Classification, properties, and environmental toxicities*. *Environmental Technology & Innovation* 2020,20, 101067.
- [7]. Jeevanandam, J.; Chan, Y. S.; Danquah, M. K., Biosynthesis of metal and metal oxide nanoparticles. *ChemBioEng Reviews* 2016,3 (2), 55-67.
- [8]. McNamara, K.; Tofail, S. A., *Nanoparticles in biomedical applications*. *Advances in Physics: X* 2017,2 (1), 54-88.
- [9]. Kannan, K.; Radhika, D.; Sadasivuni, K. K.; Reddy, K. R.; Raghu, A. V., Nanostructured metal oxides and its hybrids for photocatalytic and biomedical applications. *Advances in Colloid and Interface Science* 2020,281, 102178.
- [10]. Stan, M.; Popa, A.; Toloman, D.; Dehelean, A.; Lung, I.; Katona, G., Enhanced photocatalytic degradation properties of zinc oxide nanoparticles synthesized by using plant extracts. *Materials Science in Semiconductor Processing* 2015,39, 23-29.
- [11]. Chen, G.; Roy, I.; Yang, C.; Prasad, P. N., Nanochemistry and nanomedicine for nanoparticle-based diagnostics and therapy. *Chemical reviews* 2016,116 (5), 2826-2885.

- [12]. Raghupathi, K. R.; Koodali, R. T.; Manna, A. C., Size-dependent bacterial growth inhibition and mechanism of antibacterial activity of zinc oxide nanoparticles. *Langmuir* 2011,27 (7), 4020-4028.
- [13]. P Singh, R.; K Shukla, V.; S Yadav, R.; K Sharma, P.; K Singh, P.; C Pandey, A., Biological approach of zinc oxide nanoparticles formation and its characterization. *Advanced Materials Letters* 2011,2 (4), 313-317.
- [14]. Kao, Y.Y.; Chen, Y.C.; Cheng, T.J.; Chiung, Y.M.; Liu, P.S., Zinc oxide nanoparticles interfere with zinc ion homeostasis to cause cytotoxicity. *Toxicological Sciences* 2012,125 (2), 462-472.
- [15]. Ijaz, I.; Gilani, E.; Nazir, A.; Bukhari, A., Detail review on chemical, physical and green synthesis, classification, characterizations and applications of nanoparticles. *Green Chemistry Letters and Reviews* 2020,13 (3), 223-245.
- [16]. Li, Y.; Hu, J.; Yang, K.; Cao, B.; Li, Z.; Yang, L.; Pan, F., Synthetic control of Prussian blue derived nanomaterials for energy storage and conversion application. *Materials Today Energy* 2019,14, 100332.
- [17]. Venkataraman, A.; Amadi, E. V.; Chen, Y.; Papadopoulos, C., Carbon nanotube assembly and integration for applications. *Nanoscale research letters* 2019,14 (1), 1-47.
- [18]. Khandel, P.; Yadav, R. K.; Soni, D. K.; Kanwar, L.; Shahi, S. K., Biogenesis of metal nanoparticles and their pharmacological applications: present status and application prospects. *Journal of Nanostructure in Chemistry* 2018,8 (3), 217-254.
- [19]. Shah, M.; Fawcett, D.; Sharma, S.; Tripathy, S. K.; Poinern, G. E. J., Green synthesis of metallic nanoparticles via biological entities. *Materials* 2015,8 (11), 7278-7308.
- [20]. El-Seedi, H. R.; El-Shabasy, R. M.; Khalifa, S. A.; Saeed, A.; Shah, A.; Shah, R.; Iftikhar, F. J.; Abdel-Daim, M. M.; Omri, A.; Hajrahand, N. H., Metal nanoparticles fabricated by green chemistry using natural extracts: Biosynthesis, mechanisms, and applications. *RSC advances* 2019,9 (42), 24539-24559.
- [21]. Anselmo, A. C.; Mitragotri, S., A review of clinical translation of inorganic nanoparticles. *The AAPS journal* 2015,17 (5), 1041-1054.
- [22]. Osman, D. A. M.; Mustafa, M. A., Synthesis and characterization of zinc oxide nanoparticles using zinc acetate dihydrate and sodium hydroxide. *J. Nanosci. Nanoeng* 2015,1 (4), 248-251.
- [23]. Kalpana, V.; Devi Rajeswari, V., A review on green synthesis, biomedical applications, and toxicity studies of ZnO NPs. *Bioinorganic chemistry and applications* 2018.
- [24]. Fernández-García, M.; RODRIGUEZ, J. Metal oxide nanoparticles; Brookhaven National Lab.(BNL), Upton, NY (United States): 2007.
- [25]. Khan, R.; Kaushik, A.; Solanki, P. R.; Ansari, A. A.; Pandey, M. K.; Malhotra, B., Zinc oxide nanoparticles-chitosan composite film for cholesterol biosensor. *Analytica chimica acta* 2008,616 (2), 207-213.
- [26]. Sarkar, S.; Guibal, E.; Quignard, F.; SenGupta, A., Polymer-supported metals and metal oxide nanoparticles: synthesis, characterization, and applications. *Journal of Nanoparticle Research* 2012,14 (2), 1-24.
- [27]. Khan, M. F.; Ansari, A. H.; Hameedullah, M.; Ahmad, E.; Husain, F. M.; Zia, Q.; Baig, U.; Zaheer, M. R.; Alam, M. M.; Khan, A. M., Sol-gel synthesis of thorn-like ZnO nanoparticles endorsing mechanical

- stirring effect and their antimicrobial activities: Potential role as nano-antibiotics. *Scientific reports* 2016,6 (1), 1-12.
- [28]. Hosono, E.; Fujihara, S.; Kimura, T.; Imai, H., Non-basic solution routes to prepare ZnO nanoparticles. *Journal of Sol-Gel Science and Technology* 2004,29 (2), 71-79.
- [29]. Mirzaei, H.; Darroudi, M., Zinc oxide nanoparticles: Biological synthesis and biomedical applications. *Ceramics International* 2017,43 (1), 907-914.
- [30]. Prasad, A. R.; Williams, L.; Garvasis, J.; Shamsheera, K.; Basheer, S. M.; Kuruvilla, M.; Joseph, A., Applications of phytogenic ZnO nanoparticles: A review on recent advancements. *Journal of Molecular Liquids* 2021,331, 115805.
- [31]. Sangeetha, G.; Rajeshwari, S.; Venckatesh, R., Green synthesis of zinc oxide nanoparticles by aloe barbadensis miller leaf extract: Structure and optical properties. *Materials Research Bulletin* 2011,46 (12), 2560-2566.
- [32]. Chaudhuri, S. K.; Malodia, L., Biosynthesis of zinc oxide nanoparticles using leaf extract of *Calotropis gigantea*: characterization and its evaluation on tree seedling growth in nursery stage. *Applied Nanoscience* 2017,7 (8), 501-512.
- [33]. Naseer, M.; Aslam, U.; Khalid, B.; Chen, B., Green route to synthesize Zinc Oxide Nanoparticles using leaf extracts of *Cassia fistula* and *Melia azadarach* and their antibacterial potential. *Scientific Reports* 2020,10 (1), 1-10.
- [34]. Karthik, S.; Siva, P.; Balu, K. S.; Suriyaprabha, R.; Rajendran, V.; Maaza, M., *Acalypha indica*-mediated green synthesis of ZnO nanostructures under differential thermal treatment: Effect on textile coating, hydrophobicity, UV resistance, and antibacterial activity. *Advanced Powder Technology* 2017,28 (12), 3184-3194.
- [35]. Rajiv, P.; Rajeshwari, S.; Venckatesh, R., Bio-Fabrication of zinc oxide nanoparticles using leaf extract of *Parthenium hysterophorus* L. and its size-dependent antifungal activity against plant fungal pathogens. *Spectrochimica Acta Part A: Molecular and Biomolecular Spectroscopy* 2013,112, 384-387.
- [36]. Senthilkumar, S.; Sivakumar, T., Green tea (*Camellia sinensis*) mediated synthesis of zinc oxide (ZnO) nanoparticles and studies on their antimicrobial activities. *Int. J. Pharm. Pharm. Sci* 2014,6 (6), 461-465.
- [37]. Gawade, V.; Gavade, N.; Shinde, H.; Babar, S.; Kadam, A.; Garadkar, K., Green synthesis of ZnO nanoparticles by using *Calotropis procera* leaves for the photodegradation of methyl orange. *Journal of Materials Science: Materials in Electronics* 2017,28 (18), 14033-14039.
- [38]. Basumatari, M.; Devi, R. R.; Gupta, M. K.; Gupta, S. K.; Raul, P. K.; Chatterjee, S.; Dwivedi, S. K., *Musa balbisiana* Colla pseudostem biowaste mediated zinc oxide nanoparticles: Their antibiofilm and antibacterial potentiality. *Current Research in Green and Sustainable Chemistry* 2021,4, 100048.
- [39]. Nava, O.; Soto-Robles, C.; Gómez-Gutiérrez, C.; Vilchis-Nestor, A.; Castro-Beltrán, A.; Olivás, A.; Luque, P., Fruit peel extract mediated green synthesis of zinc oxide nanoparticles. *Journal of Molecular Structure* 2017,1147, 1-6.
- [40]. Król, A.; Railean-Plugaru, V.; Pomastowski, P.; Buszewski, B., Phytochemical investigation of *Medicago sativa* L. extract and its potential as a safe source for the synthesis of ZnO nanoparticles: The proposed

- mechanism of formation and antimicrobial activity. *Phytochemistry Letters* 2019,31, 170-180.
- [41]. Azizi, S.; Ahmad, M. B.; Namvar, F.; Mohamad, R., Green biosynthesis and characterization of zinc oxide nanoparticles using brown marine macroalga *Sargassum muticum* aqueous extract. *Materials Letters* 2014,116, 275-277.
- [42]. Anjali, K.; Sangeetha, B.; Raghunathan, R.; Devi, G.; Dutta, S., Seaweed Mediated Fabrication of Zinc Oxide Nanoparticles and their Antibacterial, Antifungal and Anticancer Applications. *ChemistrySelect* 2021,6 (4), 647-656.
- [43]. Nagarajan, S.; Arumugam Kuppasamy, K., Extracellular synthesis of zinc oxide nanoparticle using seaweeds of gulf of Mannar, India. *Journal of nanobiotechnology* 2013,11 (1), 1-11.
- [44]. Agarwal, H.; Kumar, S. V.; Rajeshkumar, S., A review on green synthesis of zinc oxide nanoparticles—An eco-friendly approach. *Resource-Efficient Technologies* 2017,3 (4), 406-413.
- [45]. Jayaseelan, C.; Rahuman, A. A.; Kirthi, A. V.; Marimuthu, S.; Santhoshkumar, T.; Bagavan, A.; Gaurav, K.; Karthik, L.; Rao, K. B., Novel microbial route to synthesize ZnO nanoparticles using *Aeromonas hydrophila* and their activity against pathogenic bacteria and fungi. *Spectrochimica Acta Part A: Molecular and Biomolecular Spectroscopy* 2012,90, 78-84.
- [46]. Mishra, M.; Paliwal, J. S.; Singh, S. K.; Selvarajan, E.; Subathradevi, C.; Mohanasrinivasan, V., Studies on the inhibitory activity of biologically synthesized and characterized zinc oxide nanoparticles using *Lactobacillus sporogens* against *Staphylococcus aureus*. *J Pure Appl Microbiol* 2013,7 (2), 1263-1268.
- [47]. Sukri, S. N. A. M.; Shameli, K.; Wong, M. M.T.; Teow, S.Y.; Chew, J.; Ismail, N. A., Cytotoxicity and antibacterial activities of plant-mediated synthesized zinc oxide (ZnO) nanoparticles using *Punica granatum* (pomegranate) fruit peels extract. *Journal of Molecular Structure* 2019,1189, 57-65.
- [48]. Hsueh, Y.H.; Ke, W.J.; Hsieh, C.T.; Lin, K.S.; Tzou, D.Y.; Chiang, C.L., ZnO nanoparticles affect *Bacillus subtilis* cell growth and biofilm formation. *PloS one* 2015,10 (6), e0128457.
- [49]. Rajan, A.; Cherian, E.; Baskar, G., Biosynthesis of zinc oxide nanoparticles using *Aspergillus fumigatus* JCF and its antibacterial activity. *Int J Mod Sci Technol* 2016,1, 52-7.
- [50]. Suba, S.; Vijayakumar, S.; Vidhya, E.; Punitha, V.; Nilavukkarasi, M., Microbial mediated synthesis of ZnO nanoparticles derived from *Lactobacillus* spp: Characterizations, antimicrobial and biocompatibility efficiencies. *Sensors International* 2021,2, 100104.
- [51]. Wani, A.; Shah, M., A unique and profound effect of MgO and ZnO nanoparticles on some plant pathogenic fungi. *Journal of Applied Pharmaceutical Science* 2012,(Issue), 40-44.
- [52]. Ealia, S. A. M.; Saravanakumar, M. In A review on the classification, characterisation, synthesis of nanoparticles and their application, IOP conference series: materials science and engineering, IOP Publishing: 2017; p 032019.
- [53]. Vijayakumar, S.; Vinoj, G.; Malaikozhundan, B.; Shanthi, S.; Vaseeharan, B., *Plectranthus amboinicus* leaf extract mediated synthesis of zinc oxide nanoparticles and its control of methicillin resistant *Staphylococcus aureus* biofilm and blood sucking mosquito larvae. *Spectrochimica Acta Part A: Molecular and Biomolecular Spectroscopy* 2015,137, 886-891.
- [54]. Anbuvaran, M.; Ramesh, M.; Viruthagiri, G.; Shanmugam, N.; Kannadasan, N., *Anisochilus carnosus*

- leaf extract mediated synthesis of zinc oxide nanoparticles for antibacterial and photocatalytic activities. *Materials Science in Semiconductor Processing* 2015,39, 621-628.
- [55]. Ali, M.; Kim, B.; Belfield, K. D.; Norman, D.; Brennan, M.; Ali, G. S., Green synthesis and characterization of silver nanoparticles using *Artemisia absinthium* aqueous extract—a comprehensive study. *Materials Science and Engineering: C* 2016,58, 359-365.
- [56]. Ghule, K.; Ghule, A. V.; Chen, B.J.; Ling, Y.C., Preparation and characterization of ZnO nanoparticles coated paper and its antibacterial activity study. *Green Chemistry* 2006,8 (12), 1034-1041.
- [57]. Bhuyan, T.; Mishra, K.; Khanuja, M.; Prasad, R.; Varma, A., Biosynthesis of zinc oxide nanoparticles from *Azadirachta indica* for antibacterial and photocatalytic applications. *Materials Science in Semiconductor Processing* 2015,32, 55-61.
- [58]. Basnet, P.; Chanu, T. I.; Samanta, D.; Chatterjee, S., A review on bio-synthesized zinc oxide nanoparticles using plant extracts as reductants and stabilizing agents. *Journal of Photochemistry and Photobiology B: Biology* 2018,183, 201-221.
- [59]. Vaseem, M.; Umar, A.; Hahn, Y.B., ZnO nanoparticles: growth, properties, and applications. *Metal oxide nanostructures and their applications* 2010,5 (1), 10-20.
- [60]. Rasmussen, J. W.; Martinez, E.; Louka, P.; Wingett, D. G., Zinc oxide nanoparticles for selective destruction of tumor cells and potential for drug delivery applications. *Expert opinion on drug delivery* 2010,7 (9), 1063-1077.
- [61]. Singh, T. A.; Das, J.; Sil, P. C., Zinc oxide nanoparticles: A comprehensive review on its synthesis, anticancer and drug delivery applications as well as health risks. *Advances in Colloid and Interface Science* 2020,286, 102317.
- [62]. Hwa, K.Y.; Subramani, B., Synthesis of zinc oxide nanoparticles on graphene–carbon nanotube hybrid for glucose biosensor applications. *Biosensors and Bioelectronics* 2014,62, 127-133.
- [63]. Wang, G.; Tan, X.; Zhou, Q.; Liu, Y.; Wang, M.; Yang, L., Synthesis of highly dispersed zinc oxide nanoparticles on carboxylic graphene for development a sensitive acetylcholinesterase biosensor. *Sensors and Actuators B: Chemical* 2014,190, 730-736.
- [64]. Sirelkhatim, A.; Mahmud, S.; Seeni, A.; Kaus, N. H. M.; Ann, L. C.; Bakhori, S. K. M.; Hasan, H.; Mohamad, D., Review on zinc oxide nanoparticles: antibacterial activity and toxicity mechanism. *Nano-micro letters* 2015,7 (3), 219-242.
- [65]. Wiesmann, N.; Tremel, W.; Brieger, J., Zinc oxide nanoparticles for therapeutic purposes in cancer medicine. *Journal of Materials Chemistry B* 2020,8 (23), 4973-4989.
- [66]. Carofiglio, M.; Barui, S.; Cauda, V.; Laurenti, M., Doped zinc oxide nanoparticles: synthesis, characterization and potential use in nanomedicine. *Applied Sciences* 2020,10 (15), 5194.
- [67]. Das, P. P.; Mukhopadhyay, S.; Agarkar, S. A.; Jana, A.; Devi, P. S., Photochemical performance of ZnO nanostructures in dye sensitized solar cells. *Solid State Sciences* 2015,48, 237-243.
- [68]. Sun, L.W.; Shi, H.Q.; Li, W.N.; Xiao, H.M.; Fu, S.Y.; Cao, X.Z.; Li, Z.X., Lanthanum-doped ZnO quantum dots with greatly enhanced fluorescent quantum yield. *Journal of Materials Chemistry* 2012,22 (17), 8221-8227.

Study of Polymer in the presence of Drug Using Dielectric Relaxation Spectroscopy

Ravikant Karale, Komal B. Kabara, Suad Alwaleedy, Saeed Mohemmed, Savita Kamble, Ashok C. Kumbharkhane, Arvind V. Sarode*

*School of Physical Sciences, Swami Ramanand Teerth Marathwada University, Nanded-431 606, Maharashtra, India

ABSTRACT

The present work reports structural and dynamical properties of aqueous Polyvinyl-pyrrolidone(PVP K-30) [C₆H₉NO]_n in the presence of Non steroidal anti-inflammatory drug (NSAID) Ibuprofen(IBP) [C₁₃H₁₈O₂] using time domain reflectometry (TDR) in the frequency region of 1 GHz to 30 GHz over the temperature range of 278.15 K-298.15 K. The frequency dependent complex dielectric permittivity has been analyzed by Havriliak-Negami equation. Cole-Davidson model is used for the description of the complex dielectric permittivity spectra $\epsilon^*(\nu)$. Dielectric parameters such as the static dielectric constant ϵ_0 , the high frequency limiting dielectric constant ϵ_∞ , relaxation time τ_0 and Kirkwood correlation factor were calculated.

Keywords: Polyvinyl-pyrrolidone, Ibuprofen, time domain reflectometry, dielectric relaxation.

I. INTRODUCTION

PVP an amorphous polymer may form complexes with a wide range of substances by forming hydrogen bonds between the hydroxyl groups of solvents and its carbonyl group[1].The water structure surrounding the coiled polymer was studied using PVP, a randomly coiled and flexible polymer that is easily soluble in water. For such a non-electrolytic solution, dielectric measurements are simple [2]. The dielectric relaxation amplitude ($\Delta\epsilon$),the dielectric relaxation time (τ_0) and the other thermodynamic parameters changes when the polymer is mixed with a polar solvent because these relaxation parameters are dependent on the structure of the solvent in the polymer-solvent mixture[3].As, PVP is non-harmful and biocompatible, it is used in drug delivery systems (DDSS), artificial organs, cosmetics, and other applications. It has excellent wetting properties in the solution state and easily produces films. As a result, it can be used as a coating or as a coating additive.PVP is also used as an adhesive in glue sticks and hot melts, as a special additive in batteries, ceramics, fiberglass, inks, inkjet paper and the chemical-mechanical planarization process, as emulsifiers and disintegrants in solution polymerization, photo-resists for cathode ray tubes, in aqueous metal quenching and in the production of membranes such as dialysis and water purification filters[4].

Ibuprofen (2-[4-(2-methylpropyl)phenyl]propanoic acid) is a non-steroidal anti-inflammatory drug(NSAID). It is used to treat pain and fever by millions of people worldwide. Ibuprofen's experimental solubility in

water (0.049 mg/ml) [5] makes this medicine as almost insoluble in water. The dissolution profile and bioavailability after oral administration of such a drug are relatively low. Preparing the poorly water soluble drugs in the amorphous form is one of the well established methods for increasing the solubility and bioavailability.

However, no research has been done on the dielectric and thermodynamic properties of aqueous PVP in presence of IBP solution. The solutions were prepared at room temperature for different molar concentrations of PVP viz. 0, 0.02, 0.04, 0.06, 0.08, 0.1 and ibuprofen viz. 0, 0.01, 0.02, 0.03, 0.04 and 0.05. We have measured the dielectric relaxation spectra for these solutions at 298.15 K, 288.15 K and 278.15 K using time domain reflectometry in the frequency range of 0.01 GHz-30 GHz. The purpose of the present research work is to carry out the microwave dielectric relaxation study of the poly(vinyl pyrrolidone)-Ibuprofen-Water mixtures of varying concentration and to investigate the impact of temperature and concentration on the structure and dynamics of water molecules in presence of PVP and IBP macromolecules as well as the intermolecular interactions between aqueous PVP and IBP molecules, in terms of various dielectric and thermodynamic parameters. We interpreted the obtained dielectric data by comparing with those of earlier dielectric studies.

II. EXPERIMENTAL

2.1. MATERIALS

Polyvinylpyrrolidone (PVP K-30) was purchased from sigma Aldrich and Ibuprofen was purchased from Hi Media Laboratories Pvt. Ltd. Mumbai, India and used without purification. Double distilled and deionized water was used for making the solution. The chemicals were weighed in an electronic digital balance (Mettler Toledo ME- 204) with a least count of 0.0001 gm. The solutions of 15 ml were prepared at room temperature for different concentrations of PVP and IBP and the dielectric measurement were carried out by using TDR.

III. RESULTS AND DISCUSSION

Dielectric dispersion and absorption curves obtained for the aqueous PVP at 0.02, 0.04, 0.06, 0.08 and 0.1 M concentration in presence of poor water soluble ibuprofen (IBP) with the concentrations 0.01, 0.02, 0.03, 0.04 and 0.05 M used at temperatures 278.15 K, 283.15 K, 288.15 K, 293.15 K and 298.15 K is shown in fig. 1 where only spectra at low and high concentrations and at all temperatures along with the spectra for water were depicted. The spectra show that there is a gradual decrease in dielectric permittivity for all the used concentrations and temperature and the loss peaks shift towards lower frequency side. This suggests molecular association between solute and solvent molecules.

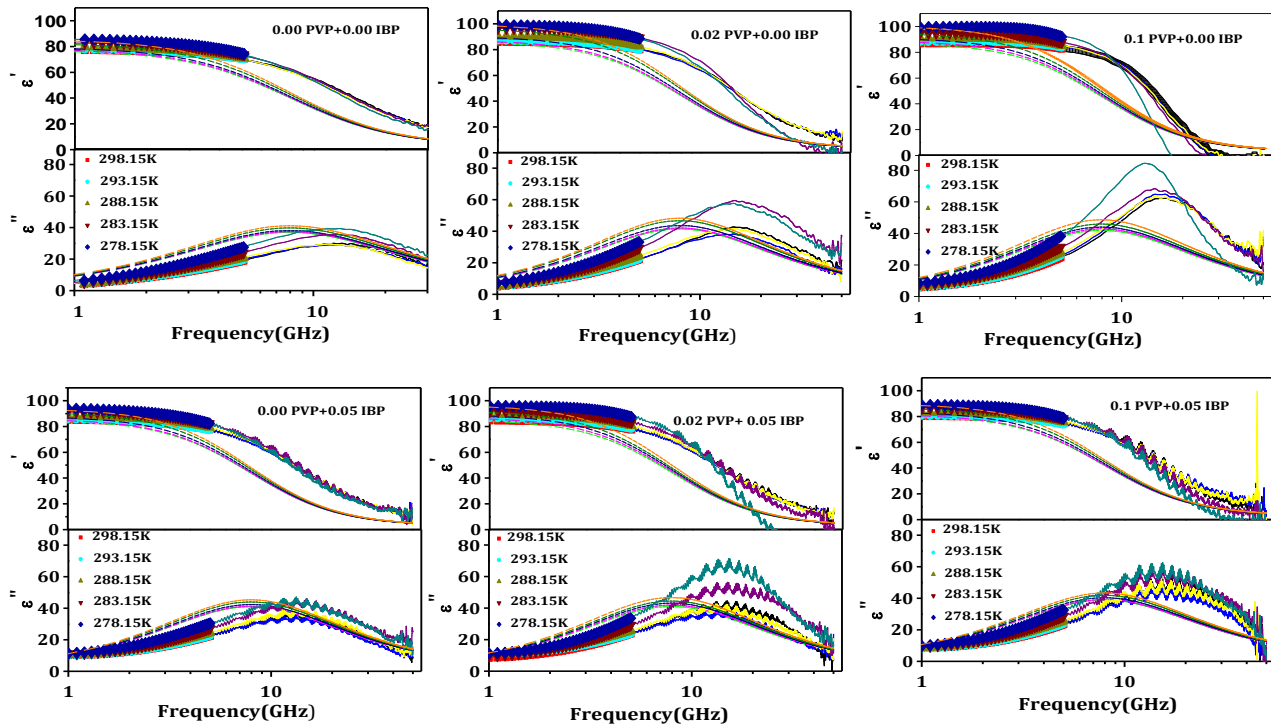


Figure 1: Permittivity spectra contains dielectric permittivity (ϵ') and loss (ϵ'') as a function of frequency for water and aqueous PVP in presence of IBP at different concentration and temperature. (Solid lines-observed data, Dotted lines-theoretical fitting and Symbols-fitted data).

Dielectric permittivity (ϵ') and loss (ϵ'') for PVP-IBP-Water system obtained for various concentrations in the temperature range of 278.15 K-298.15 K as a function of frequency is shown in fig. 1. The values of complex permittivity $\epsilon^* = \epsilon' - j\epsilon''$ as a function of frequency for the PVP-IBP-Water system have been analyzed and used for the evaluation of dielectric parameters at various temperatures and concentrations [6]. The process can be described by S. Havriliak -Negami [7] equation using least square fit method.

$$\epsilon^*(\omega) = \epsilon_\infty + \left[\frac{(\epsilon_0 - \epsilon_\infty)}{[1 + (j\omega\tau_0)^{1-\alpha}]^\beta} \right] \quad (1)$$

Where ϵ_0 is the static permittivity, ϵ_∞ the high frequency limiting static permittivity, τ_0 is the average relaxation time, ω is the angular frequency α and β are the distribution parameters. α ($0 < \alpha < 1$) indicates the broadness of the symmetric relaxation curve when the dielectric data are described by the Cole-Cole equation.

The data collected reveals that the static dielectric constant for aqueous PVP was found more than that of pure water and become almost constant for further increase in PVP concentration. This suggests that increasing PVP concentrations decreases the number of water molecules per PVP molecule that form hydrogen bonding at hydroxyl and methyl side group and thus form hydration layer around PVP molecule fig (a). This association between water and PVP increases the value of static dielectric constant only at lower PVP concentration but remain almost constant for further increases in concentration. As higher values of

dielectric constant has more significance for drugs stability in pharmacy which is directly related to solubility and stability of the products[8].

This suggests the complex or system is more stable towards lower temperature and lower PVP concentrations and will be more suitable for drug design and other pharmaceutical applications.

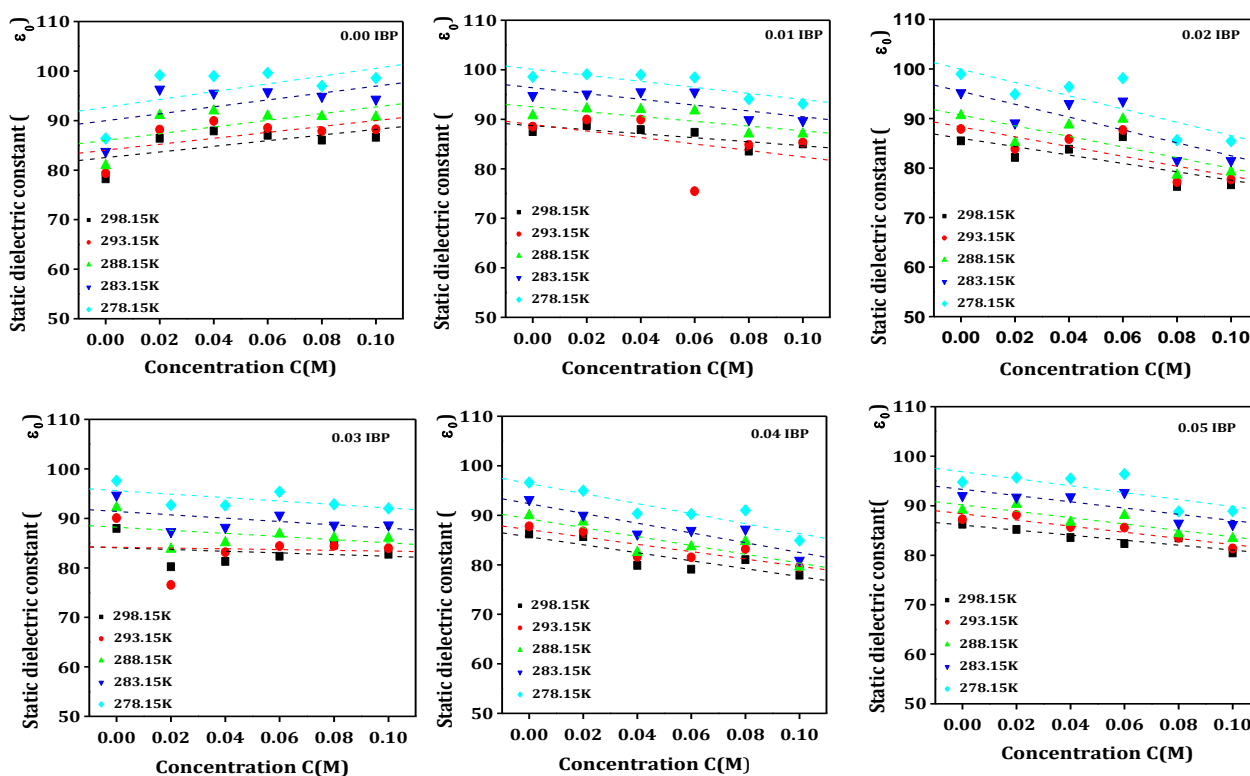


Figure3: Temperature and concentration dependent static dielectric constant of aqueous PVP in presence of different concentrations of ibuprofen.

The relaxation dynamics for the rotational motion of water molecules in the solute environment are given by dielectric relaxation time measured for aqueous PVP (fig. 4) and in the presence of ibuprofen. The relaxation time for aqueous PVP increased linearly with PVP concentration over all the measured temperatures, indicating a more heterogeneous / non-cooperative environment for water molecules that offers a large steric hindrance to the rotational motion of water molecules in the solvent rich (PVP) and in the low temperature region.

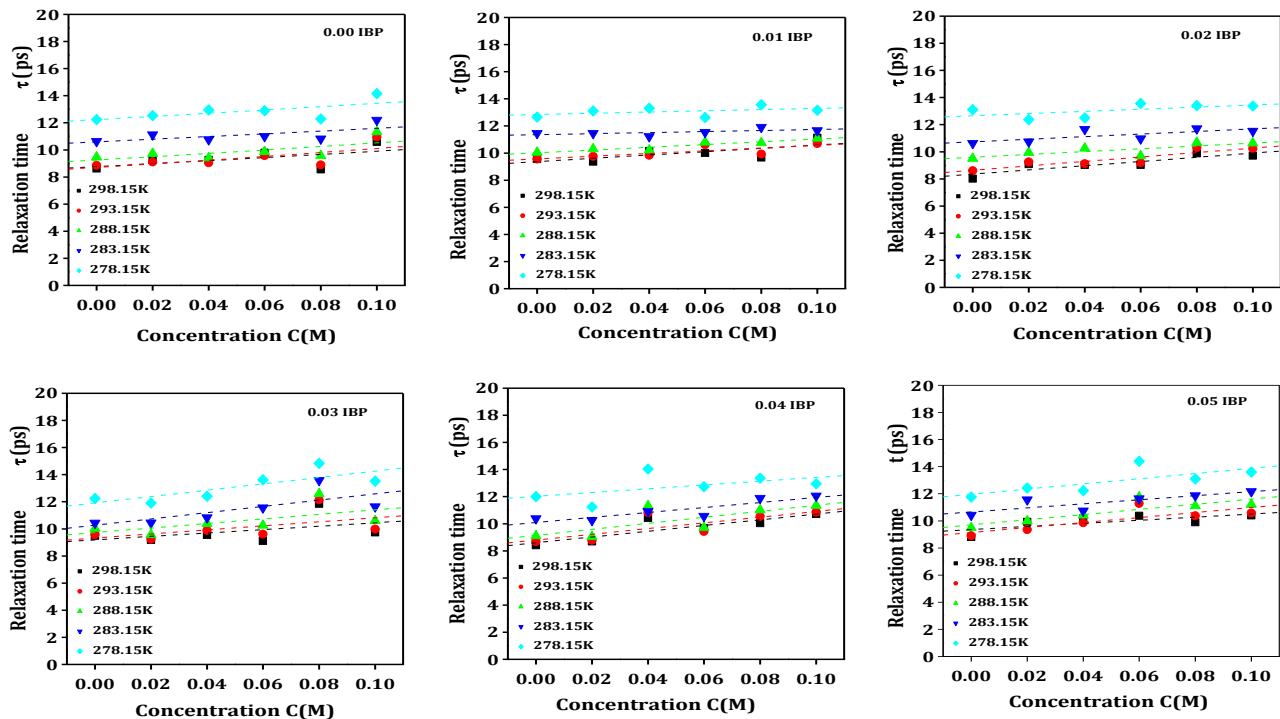


Figure 4: Dielectric relaxation time measured for aqueous PVP in the presence of Ibuprofen at different concentration and temperature.

Figure 4 depicts the relaxation time for aqueous PVP in the presence of ibuprofen at various PVP concentrations. For all the IBP concentrations it has been observed that relaxation time increases with PVP concentration and towards low temperature. This could be due to the formation of a hydration shell surrounding PVP, which interacts with IBP via the hydration shell, or to a dipole-dipole induced interaction between PVP and IBP via water molecules. As a result, rotational motion of water molecules gets restricted that results in increasing the values of relaxation time.

The information regarding orientation of electric dipoles in polar liquid is described by Kirkwood correlation factor ' g' '. The degree of intermolecular hydrogen bonding is measured by the deviation of the values of ' g' ' from unity. If ' g' ' is greater than 1 it means that molecules tend to direct themselves with parallel dipole moments; when g' is smaller than 1 then molecules prefer an ordering with antiparallel dipole moments. ' g' '=1 may be due to the cancellation of the effects of both kinds of parallel and anti-parallel multimers for associating molecules. Due to insufficient data available for the dipole moment at the measured temperature we used dipole moment for water $\mu=2.37$ D as calculated previously [9] to calculate the correlation factor ' g' ' from the measured $g\mu^2$ calculated using Kirkwood–Frohlich equation [10].

$$g\mu^2 = \frac{9K_B T M}{4\pi N \rho} \left[\frac{(\epsilon_s - \epsilon_\infty)(2\epsilon_s + \epsilon_\infty)}{\epsilon_s(\epsilon_\infty + 2)^2} \right] \quad (2)$$

The parameters used in eqn.(2) K_B is the Boltzmann constant, T is absolute temperature, M is the molecular weight, N is Avogadro's number and ρ is the density.

Since ' g ' is a measure of orientational correlation between a molecule and its nearest neighbors, the departure of ' g ' from unity could be an indication of molecular association due to short-range ordering interactions. In our case of aqueous PVP and IBP induced PVP, correlation factors are more than 1 (due to the parallel orientation of the dipoles) and decreases towards higher PVP concentrations suggesting increased correlation between solute dipole via hydration shell. The variation in the values of ' g ' with increasing IBP concentration in PVP at different temperatures is shown in fig 5. From the observed data, it has been concluded that the correlation (Parallel orientation) between water and the surrounding molecules decreases by the presence of ibuprofen for all the used PVP concentrations. This could be due to the reduced parallel correlation between solutes and solvent[11].

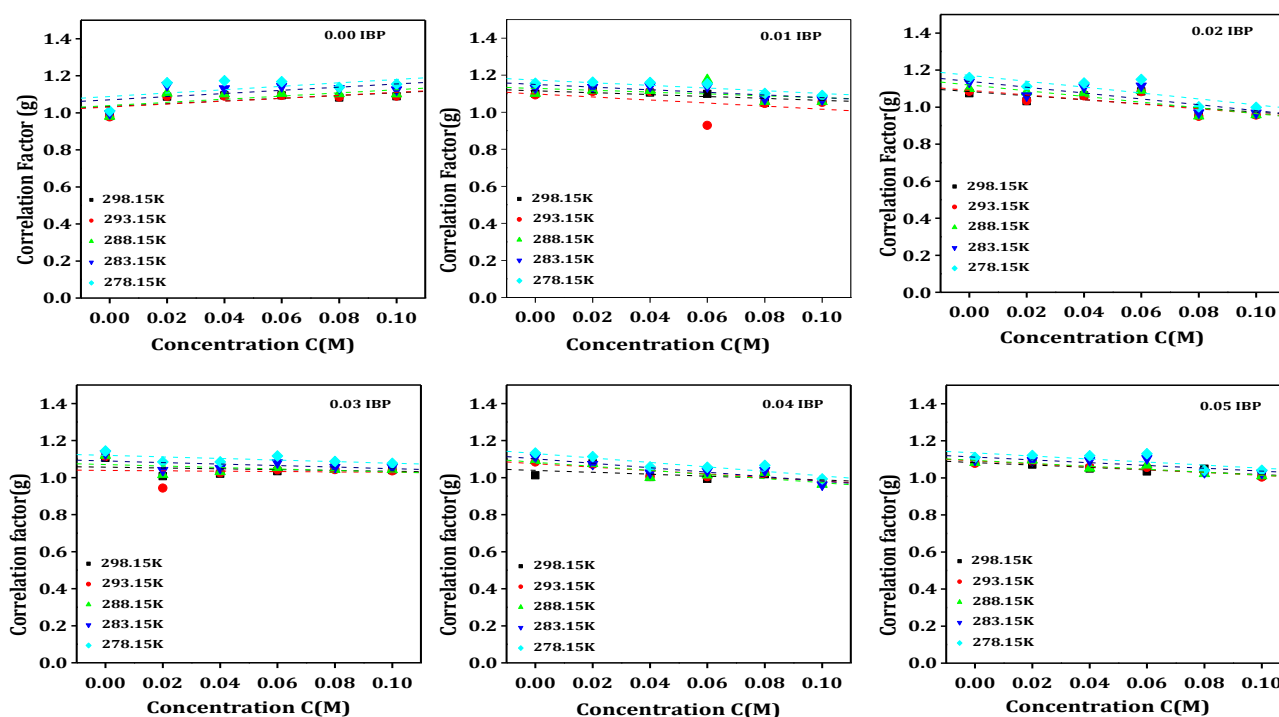


Figure 5: variation in correlation factor ' g ' for aqueous PVP and IBP induced PVP.

IV. CONCLUSIONS

From the overall study of dielectric and thermodynamical parameters we may conclude that

- Static dielectric constant for aqueous PVP was found more than that of pure water and become almost constant for further increase in PVP concentration.
- As higher values of dielectric constant has more significance for drugs stability in pharmacy which is directly related to solubility and stability of the products the addition of IBP to aqueous PVP gives surprising results that decreases the values of static dielectric constant towards higher PVP concentration.
- The presence of IBP with higher concentration in aqueous PVP makes the system less stable.

- The increase in the values of static dielectric constant for aqueous IBP in absence or at lowest PVP concentration clearly indicates that dipole-dipole parallel alignment must present between IBP and water molecules.
- Decreased values of correlation factor g and the factor $g\mu^2$ suggests reduced parallel correlation between the dipoles of aqueous PVP and IBP molecules to to formation of hydration layer or screening of PVP molecules by water molecules.
- This suggests the complex or system is more stable towards lower temperature and lower PVP concentrations and will be more suitable for drug design and other pharmaceutical applications.

V. ACKNOWLEDGEMENTS

Author Ravikant R. Karale is thankful to School of Physical Sciences, S.R.T.M.University Nanded for providing instrumentation facility, the TDR and other infrastructural facilities related to this work. The author is also gratefully acknowledged to Dept. of Science and Technology (DST), New Delhi for providing (TDR) facility through project sanctioned to Dr. A.V.Sarode (SERB/F/4632/2013-2015) and Dr.A.C.Kumbharkhane (SB/S2/LOP-032/2013). I am thankful to Dr.T.M.Kalyankar, School of pharmacy ,Swami Ramanand Teerth Marathwada University Nanded for their valuable support. I am also highly thankful to my research colleagues Mrs. Komal B. Kabara, Miss. Kamble Savita and Mrs.Suad Alwaleedy for timely support during my work.

VI. REFERENCES

- [1]. R.J.Sengwa and S. Sankhla. Dielectric dispersion study of poly (vinyl pyrrolidone)–polar solvent solutions in the frequency range 20 Hz–1 MHz. *Journal of Macromolecular Science, Part B: Physics*, 46(4) (2007) 717-747.
- [2]. N.Shinyashiki, Y. Matsumura, N. Miura, S. Yagihara, and S. Mashimo. Dielectric study of water structure in polymer solution. *The Journal of Physical Chemistry*, 98(51) (1994) 13612-13615.
- [3]. R.J.Sengwa, N.M. More, and S.C. Mehrotra. Dynamic structure of poly (vinyl pyrrolidone)/ethyl alcohol mixtures studied by time domain reflectometry. *Journal of Polymer Science Part B: Polymer Physics*, 43(9) (2005)1134-1143.
- [4]. A.V. Sarode, and A.C. Kumbharkhane. Dielectric relaxation and thermodynamic properties of polyvinylpyrrolidone using time domain reflectometry. *Polymer international*, 61(4) (2012)609-615.
- [5]. K.Adrjanowicz, K. Kaminski, Z. Wojnarowska,M. Dulski, L. Hawelek, S. Pawlus, M. Paluch, and W.Sawicki. Dielectric relaxation and crystallization kinetics of ibuprofen at ambient and elevated pressure. *The Journal of Physical Chemistry B*, 114(19) (2010) 6579-6593.
- [6]. A.V. Sarode, and A.C. Kumbharkhane. Dielectric relaxation and thermodynamic properties of polyvinylpyrrolidone using time domain reflectometry. *Polymer international*, 61(4)(2012) 609-615.
- [7]. K.B. Kabara, K.H. Wananje, A.C Kumbharkhane and A.V. Sarode. Dielectric behavior of indole in the

- GHz region using TDR. *Journal of Molecular Liquids*, 299 (2020) 112137.
- [8]. M.A.Abolghassemi Fakhree, D.R.Delgado, F. Martínez, and A. Jouyban. The importance of dielectric constant for drug solubility prediction in binary solvent mixtures: electrolytes and zwitterions in water+ ethanol. *Aaps Pharmscitech*, 11(4)(2010) 1726-1729.
- [9]. A. Luzar and J.Stefan.Dielectric behaviour of DMSO+water mixtures. A hydrogen-bonding model. *Journal of molecular liquids*, 46(1990) 221-238.
- [10]. V.V.Navarkhele. Static dielectric constant and excess properties of amino acids. *Journal of Chemical and Pharmaceutical Research*, 8(7)(2016) 930-935.
- [11]. R.J.Sengwa. Microwave dielectric relaxation and molecular dynamics in binary mixtures of poly (vinyl pyrrolidone)–poly (ethylene glycol) s in non-polar solvent. *Polymer international*, 52(9)(2003) 1462-1467.

Dielectric Relaxation Studies of Halo butanes in The Frequency Range 10 MHz to 30 GHz Using a Time Domain Reflectometry (TDR) Technique

Gubre Ashwini G.*, Kumbharkhane A.C

School of Physical Sciences, S. R. T. M. University, Nanded -431606, Maharashtra, India

ABSTRACT

The dielectric spectra for halobutanes (1-chlorobutane, 1-bromobutane, 1-iodobutane) in 1,4-dioxane (DX) in the frequency range 10 MHz to 30 GHz at 25°C with various concentrations have been determined using the time domain reflectometry (TDR) method. The dielectric spectrum of halobutanes have been fitted to the Debye model. The values of dielectric parameters such as static dielectric constant, Kirkwood correlation factor and Bruggeman factor signifies the molecular association and intermolecular hydrogen bonding in halobutanes.

Keywords: Halobutanes, Time Domain Reflectometry (TDR), complex permittivity spectra, static dielectric constant, Kirkwood correlation factor, Bruggeman factor.

I. INTRODUCTION

Time domain reflectometry technique covers an extensively wide frequency range which is mainly used for the determination of dielectric parameters with precisely accurate data in a single measurement. Dielectric study provides a way to understand the intermolecular interactions, especially in case of binary liquids. Also, the technique is a great platform for the understanding of the strength of relaxation processes in binary liquids.[1,2]Halobutanes plays an important role in many chemical reactions. They are a colourless, non-flammable liquid that has been shown to be effective in therapeutic settings. In particular, 1-Chlorobutane (CLB) is used as an intermediate for the production of other chemicals in the chemical industry. 1-Bromobutane (BMB) is commonly used as an alkylating agent, or in combination with magnesium metal in dry ether (Grignard reagent) to form carbon-carbon bonds. It can be used as a cleaning agent, an agent for chemical synthesis or as a solvent for extractions. 1-Iodobutane (IDB) is used as an alkylating agent in solvents and other intermediates. Used in the electronics industry as a subsurface preparation. 1-Iodobutane 98.0% minimum material available with or without copper stabilizer. Dielectric relaxation study of Dioxane with Haloalkanes provides important information regarding molecular interactions because of dipole-dipole interactions and bonding between the two different molecules. In a polar solvent like ethanol with various halogroups like Cl, Br, and I, R.V. Shinde et al. [3,4] have thoroughly investigated the dielectric studies of halopropanes within the frequency range of 10 MHz and 50GHz.

Understanding the structure of binary liquids in terms of hydrogen bonding is the main thrusts of the present study and also to reveal the effect of different halogroups in the molecular conformation of polar solute in the presence of non-polar solvent like dioxane.

II. EXPERIMENTAL DETAILS

2.1. Materials

The halobutanes were purchased commercially from LOBA CHEMIE PVT. LTD. with 99% purity. The 1, 4-dioxane was commercially obtained from SIGMA ALDRICH CHEMICALS PVT. LTD. with 99% purity and were used without additional purification.

2.2. Measurement

The experimental set up of TDR technique is as shown in Fig.1 The Tektronix Digital Serial Analyzer model DSA8300 with the sampling module 80E10B has been used. A sampling module 80E10B gives 12ps incident and 15ps reflected rise time pulse which was fed through a coaxial line system which is having 50 ohm impedance. Sampling oscilloscope records the change in step pulse after reflection from the end of line. The reflected pulse without sample $R_1(t)$ and with sample $R_x(t)$ were recorded in the time window of 5ns and are digitized in 2000 points. The Fourier transform of the pulse and data analysis was performed to determine complex permittivity spectra $\epsilon^*(\omega)$ using least square fit method.[5]

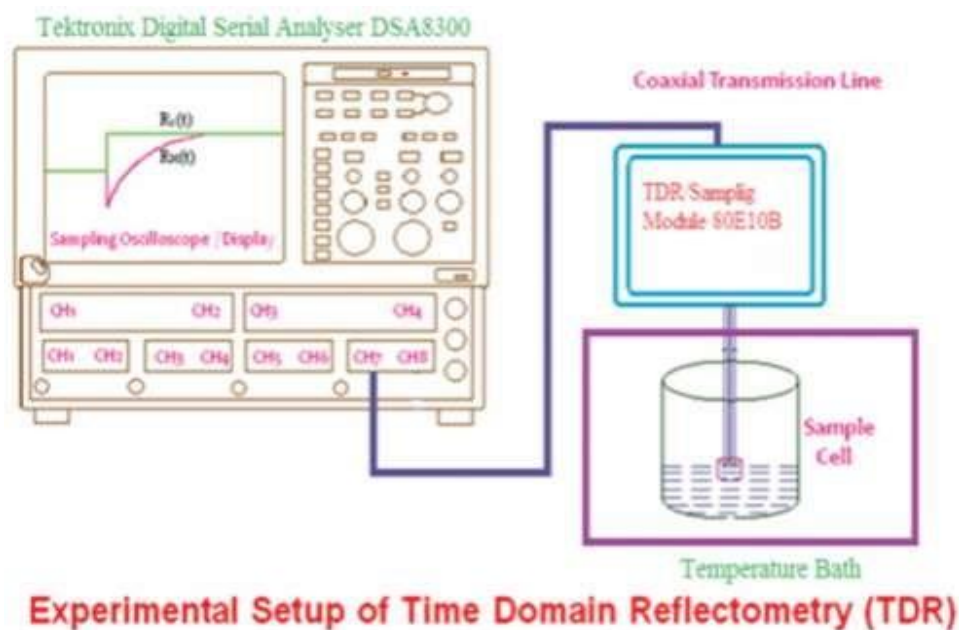


Fig.1 Experimental setup of Time Domain Reflectometry (TDR) technique

III. RESULTS AND DISCUSSION

3.1. Complex permittivity spectra

The frequency dependent dielectric behavior for CLB, BMB, IDB at 25 °C are shown in Fig.2 Complex permittivity $\epsilon^*(\omega)$ data were fitted to the Havriliak-Negami expression by using the non-linear least square fit method[6]:

$$\epsilon^*(\omega) = \epsilon_{\infty} + \frac{\epsilon_0 - \epsilon_{\infty}}{[1 + (j\omega\tau)^{1-\alpha}]^{\beta}} \quad (1)$$

where, ϵ_0 , τ , ϵ_{∞} respectively are the static dielectric permittivity, relaxation time, permittivity at high frequency and α and β are distribution parameters.

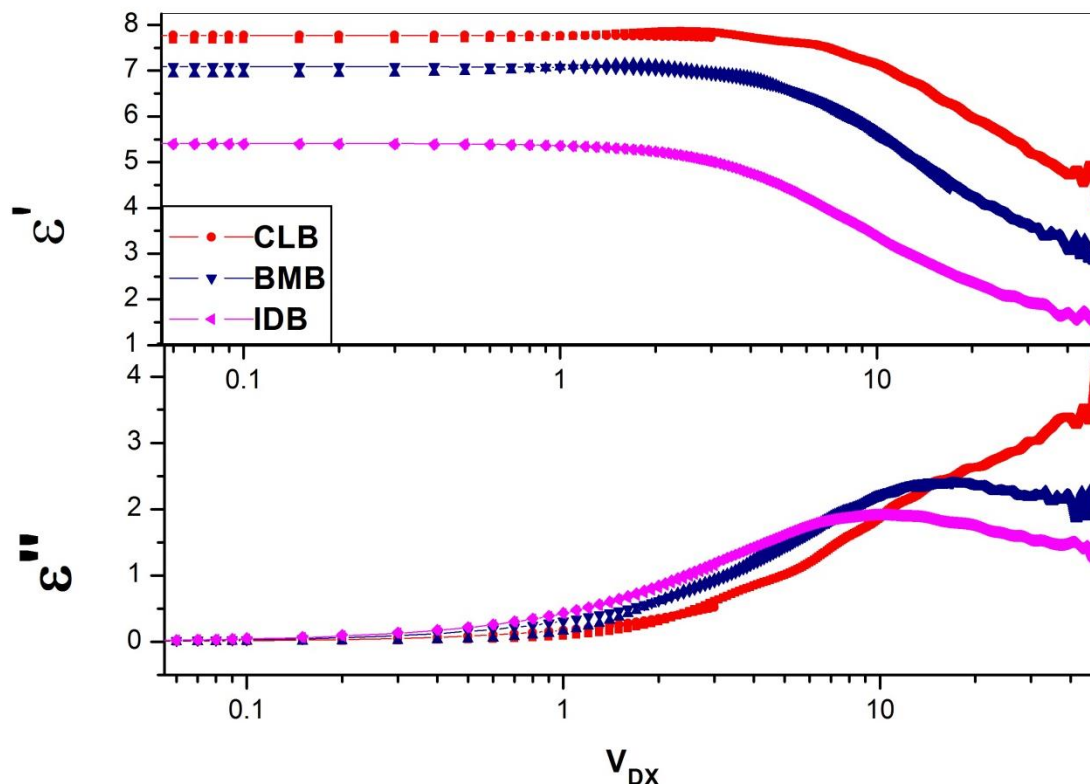


Fig.2 Complex permittivity spectra of halobutanes at 25°C

It is evident from fig.2 that when the frequency increases, the real part of the complex permittivity (ϵ') decreases. It is due to the fact that, the contribution of the charge carriers and the response of the permanent dipoles decreases at higher frequencies. It also can be seen that the response of permanent dipoles and the contribution of charge carriers in halobutanes is in the sequence of CLB > BMB > IDB. A peak in dielectric loss (ϵ'') shows the internal movements that include the reorientation of electric dipoles. The maximum value of dielectric loss is found in frequency range 20 GHz to 30 GHz for 1-chlorobutane, 10 GHz to 15 GHz for 1-bromobutane, 8 GHz to 10 GHz for 1-iodobutane.

For all halobutanes, the value of dielectric constant reduces with increase in concentration of dioxane in the mixture which is due to increase in the degree of disorder of the dipoles. [4]

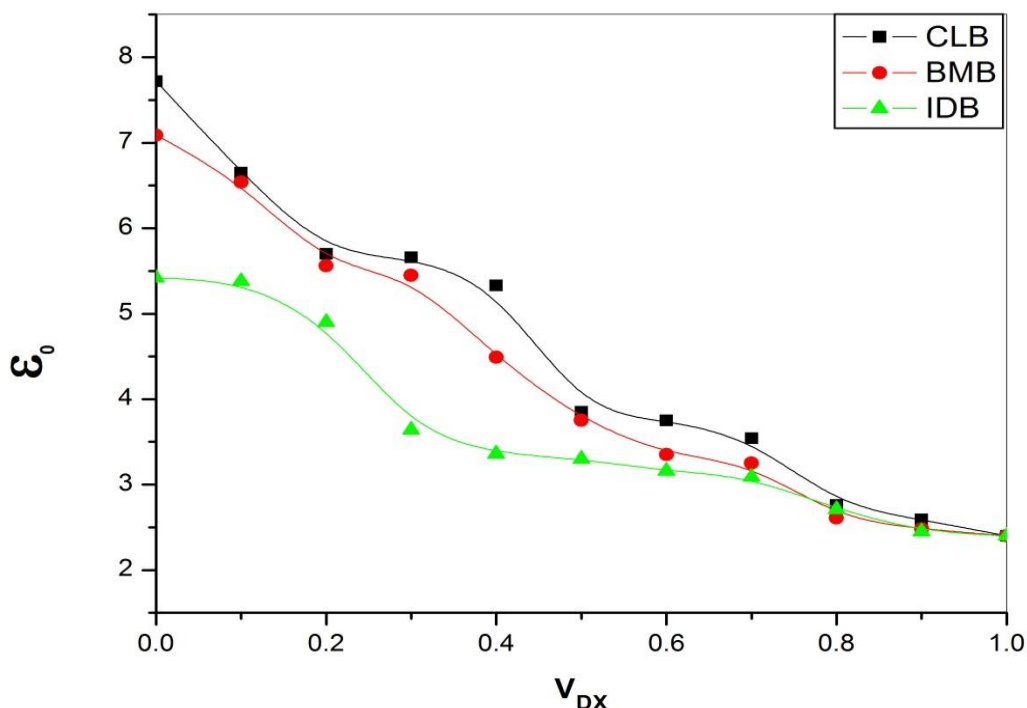


Fig.3 Static dielectric constant of Halobutanes at 25°C

3.2. Effective Kirkwood correlation factor:

The Kirkwood correlation factor gives information regarding the collective orientational correlation in the molecules. The deviation from unity of the Kirkwood correlation factor indicates the extent of intermolecular hydrogen bonding.[8]

The equation for pure liquid is given by the Kirkwood correlation factor 'g' as [8] -

$$g\mu^2 \frac{4\pi N\rho}{9kTM} = \frac{(\epsilon_0 - \epsilon_\infty)(2\epsilon_0 + \epsilon_\infty)}{\epsilon_0(\epsilon_\infty + 2)^2} \quad (2)$$

where, g is Kirkwood correlation factor, μ is dipole moment of the liquid, N is Avogadro’s number, M is molecular weight, ρ is density of the liquid, ε₀ is static dielectric constant, ε_∞ is dielectric constant at high frequency, k is Boltzmann constant and T is temperature.

The modified Kirkwood equation, which is based on the volume fraction mixture law, measures the effective angular Kirkwood correlation factor (g^{eff}) for various molecules in a binary mixture [9]:

$$\frac{4\pi N}{9kT} \left[\frac{\mu_D^2 \rho_D V_D}{M_D} + \frac{\mu_A^2 \rho_A (1-V_D)}{M_A} \right] \times g^{eff} = \frac{(\epsilon_{0m} - \epsilon_{\infty m})(2\epsilon_{0m} + \epsilon_{\infty m})}{\epsilon_{0m}(\epsilon_{\infty m} + 2)^2} \quad (3)$$

where, g^{eff} is the effective Kirkwood correlation factor, μ_D, μ_A, ρ_D and ρ_A are the dipole moments and densities of Dioxane and halobutanes respectively and V_D is the volume fraction of Dioxane.

Table.1 Kirkwood correlation factor for halobutane+ 1,4 dioxane mixture at 25°C

V_{DX}	CLB		BMB		IDB	
	g^{ff}	g^f	g^{ff}	g^f	g^{ff}	g^f
0	1.17	1	0.80	1	0.53	1
0.1	0.86	1.22	0.66	1.18	0.49	1.19
0.2	0.63	1.49	0.50	1.39	0.39	1.41
0.3	0.56	1.81	0.45	1.65	0.21	2.15
0.4	0.34	2.09	0.31	1.89	0.16	2.04
0.5	0.25	2.36	0.21	2.08	0.15	1.93
0.6	0.22	2.68	0.16	2.18	0.13	1.74
0.7	0.18	2.87	0.14	2.35	0.11	1.58
0.8	0.09	1.95	0.06	1.53	0.06	1.41
0.9	0.06	1.55	0.05	1.23	0.04	1.19
1	0.04	1	0.04	1	0.04	1

From Table.1 it can be seen that the g^{ff} value for pure CLB larger than unity, suggesting that the alignment of dipoles is parallel whereas for BMB, IDB as well as for mixture in dioxane are less than unity, confirming the dipoles with anti-parallel inclination. It also observed from Table.1 that the Kirkwood correlation factor of IDB is lower than the corresponding values of CLB and BMB, shows that the intermolecular hindrance in IDB molecules is much lower than that of CLB and BMB molecules.

3.3. Bruggeman factor:

The static permittivity of binary mixtures can be obtained by using the Bruggeman mixture formula[10]:

$$f_B = \left(\frac{\epsilon_{0m} - \epsilon_{0D}}{\epsilon_{0A} - \epsilon_{0m}} \right) \left(\frac{\epsilon_{0A}}{\epsilon_{0m}} \right)^{1/3} = (1 - V_D) \quad (4)$$

where, ϵ_{0m} , ϵ_{0D} , and ϵ_{0A} are the static dielectric constants of mixture, Dioxane and halobutane respectively. Bruggeman expression predicts a linear relationship between f_B and the volume fraction of water but the experimental values of f_B shows a non linear behavior i. e. experimental values have been deviated from unity (Table. 2).

To explain the non linear relationship the Eq(4) is modified as follows[11]:

$$f_B = \left(\frac{\epsilon_{0m} - \epsilon_{DX}}{\epsilon_{0A} - \epsilon_{DX}} \right) \left(\frac{\epsilon_{0A}}{\epsilon_{DX}} \right)^{1/3} = 1 - [a - (a - 1)V_{DX}]V_{DX} \quad (5)$$

where, a is an arbitrary parameter, the value of $a = 1$ means the ideal mixture with no interaction between solute and solvent. When we plot a graph between f_B and volume fraction of dioxane, the values of a are found

to be 1.44 for CLB, 1.40 for BMB and 1.53 for IDB which indicates that there is interaction between solute and solvent molecules.

Table. 2 : Bruggeman factor for halobutanes at 25°C

V_{DX}	f_B		
	CLB	BMB	IDB
0	1	1	1
0.1	0.85	0.86	0.85
0.2	0.72	0.73	0.71
0.3	0.60	0.61	0.58
0.4	0.49	0.50	0.47
0.5	0.38	0.39	0.36
0.6	0.29	0.30	0.27
0.7	0.20	0.21	0.18
0.8	0.12	0.13	0.11
0.9	0.05	0.06	0.05
1	0	0	0

IV. CONCLUSION

The study of the complex permittivity spectra of halobutanes on addition of nonpolar solvent (like dioxane) have been studied using TDR in the frequency range of 10 MHz to 50 GHz at 25°C and it is fitted to the Debye Model. The value of static dielectric constant decreases with increase in volume fraction of dioxane in the mixture. The Kirkwood correlation factors for halobutanes (BMB and IDB) are less than unity suggests antiparallel alignment of dipoles whereas for CLB it shows parallel alignments. Deviation of Bruggeman factor from unity indicates solute-solvent interaction.

V. ACKNOWLEDGEMENT

The financial support from Department of Science and Technology, New Delhi (Project number DST PROJECT SB/S2/LOP-032/2013) is gratefully acknowledged. Author AGG is thankful to Chhatrapati Shahu Maharaj Research Training and Human Development Institute (SARTHI), Pune, Maharashtra for financial assistance in the form of fellowship.

VI. REFERENCES

- [1]. Mehrotra, S.C., Kumbharkhane, A. and Chaudhari, A., 2017. Binary polar liquids: structural and dynamic characterization using spectroscopic methods. Elsevier.

- [2]. Hasted, J.B., 1973. Aqueous dielectrics (Vol. 122). London: Chapman and Hall.
- [3]. Shinde, R.V., Deshmukh, A.R., Ingole, S.A. and Kumbharkhane, A.C., 2019. Dielectric spectroscopy and hydrogen bonding studies of 1-chloropropane–ethanol mixture using TDR technique. *Journal of Advanced Dielectrics*, 9(02), p.1950018.
- [4]. Shinde, R.V. and Kumbharkhane, A.C., 2020. Temperature dependent dielectric relaxation studies of halopropane from 10 Mhz to 50 Ghz using a time domain reflectometry (TDR).
- [5]. Kumbharkhane, A.C., Puranik, S.M. and Mehrotra, S.C., 1991. Dielectric relaxation of tert-butyl alcohol–water mixtures using a time-domain technique. *Journal of the Chemical Society, Faraday Transactions*, 87(10), pp.1569-1573.
- [6]. Havriliak, S. and Negami, S., In *Journal of Polymer Science Part C: Polymer Symposia* 14(1) (1966) 99-117.
- [7]. Kirkwood, J.G., 1939. The dielectric polarization of polar liquids. *The Journal of Chemical Physics*, 7(10), pp.911-919.
- [8]. Kumbharkhane, A.C., Puranik, S.M. and Mehrotra, S.C., 1993. Dielectric relaxation studies of aqueous N, N-dimethylformamide using a picosecond time domain technique. *Journal of solution chemistry*, 22(3), pp.219-229.
- [9]. Bruggeman, V.D., 1935. Berechnung verschiedener physikalischer Konstanten von heterogenen Substanzen. I. Dielektrizitätskonstanten und Leitfähigkeiten der Mischkörper aus isotropen Substanzen. *Annalen der physik*, 416(7), pp.636-664.
- [10]. Puranik, S.M., Kumbharkhane, A.C. and Mehrotra, S.C., 1994. The static permittivity of binary mixtures using an improved Bruggeman model. *Journal of Molecular Liquids*, 59(2-3), pp.173-177.

Structural and Dielectric Relaxation Studies of Propionitrile-1,4 Dioxane Mixtures Using A TDR

D. G. Dongre, A. C. Kumbharkhane

School of Physical Sciences, S.R.T.M. University Nanded, 431606, Maharashtra, India

ABSTRACT

Dielectric relaxation properties of Propionitrile -1,4Dioxane binary mixtures have been measured over entire concentration at various temperatures using Time Domain Reflectometry (TDR) in the frequency range of 10 MHz to 30 GHz. The complex permittivity spectrum of Propionitrile-1,4Dioxane mixtures shows Debye type relaxation processes. The static dielectric constant (ϵ_s) and relaxation times (τ), in the mixture has been obtained using least square fit method. The molecular association is studied through the Kirkwood Correlation Factor.

Key Words: Complex Dielectric permittivity, Time Domain Reflectometry, Dielectric Relaxation Time, Kirkwood correlation factor, Excess Permittivity.

I. INTRODUCTION

There is great interest to study the dielectric relaxation behavior in liquids to understand the molecular structure and dynamics of molecules. The main interest of study to understand non hydrogen bonded aprotic solute in non-polar solvent which provides information about breaking of molecular multimer structures in the systems. The relaxation process is explained by microscopic heterogeneous structure based on three kind of intermolecular interactions. One is the interaction between solute molecules. The second is the interaction between solvent molecules. The last one is the interaction between the solute and solvent molecules. Nitriles are polar non-hydrogen bonded organic liquids with a large dipole moment and exist in the liquid state at room temperature. Due to large dipole moment the intermolecular interactions are strong and can cause association of the molecules. Propionitrile is one of the aliphatic nitriles whose behavior has been studied volumetrically in the presence of the non-polar toluene [1] as well as the polar highly associative 2-methyl-2-propanol[2]. 1,4dioxane(DX) is a non-hydrogen bonded liquid with very small electric dipole moment (0.45D) and the DX have been treated as a non-polar solvent.

Considerable experimental and theoretical dielectric relaxation studies have been done on binary mixtures of nitriles [3-7]. The dielectric permittivity varies as a function of frequency, temperature and concentration for the binary liquid mixtures [3-8]. Knowledge of frequency-dependent dielectric properties of binary liquid mixtures is important both in fundamental studies of liquid structure determination and its dynamics as well as in the practical applications. The frequency dependent dielectric behaviour of liquid mixtures also provides information on molecular interactions and mechanism of molecular process.

The present paper report the detailed study of dielectric behavior of Propionitrile (PPN) in 1, 4-dioxane (DX) over entire concentration range using time-domain reflectometry (TDR) at different temperatures in the frequency range 10 MHz to 30 GHz. From the measured dielectric spectra, the static dielectric constant and relaxation time were obtained by least squares fit method. Excess dielectric permittivity and Kirkwood correlation factor are also determined.

II. EXPERIMENTAL METHOD

a. Materials:

Propionitrile (PPN) and 1,4-dioxane (DX) obtained commercially (S. D. fine Chem. Ltd., Nanded, Maharashtra, India with purity 99%) and used without further purification. The solutions were prepared at different volume fraction of Propionitrile (PPN) in 1,4Dioxane.

b. Measurements:

The dielectric spectra were obtained by the TDR technique .The Tektronix Digital Serial Analyzer model no. DSA8300 sampling mainframe along with the sampling module 80E10B has been used for the time domain Reflectometry (TDR). A repetitive fast rising voltage pulse with 20ps incident rise time was fed through coaxial line system having 50 Ohm impedance. Sampling oscilloscope monitors change in step pulse after reflection from the end of line. The reflected pulse without sample $R_1(t)$ and with sample $R_x(t)$ were recorded in time window of 5 ns and digitized in 2000 points. The Fourier transformation of the pulse and data analysis were done earlier to determine complex permittivity spectra $\epsilon^*(\omega)$ using nonlinear least square fit method [9].

III. RESULTS AND DISCUSSIONS

3.1. Complex Permittivity Spectra:

The frequency dependent complex permittivity spectra of Propionitrile (PPN) in 1,4Dioxane (DX) at different temperatures are shown in Fig.1. It is observed that the real part of complex permittivity spectrum of Propionitrile in Dioxane mixtures is almost independent in high frequency region. As the frequency increases dielectric permittivity decreases for all concentration of Propionitrile in DX. These spectrums show the systematic variation of dielectric permittivity ϵ' and dielectric loss ϵ'' . In loss spectrum the loss peak shifted towards lower frequency .The complex permittivity spectra were fitted to Havriliak-Negami equation [10]

$$\epsilon^* = \epsilon_\infty + \frac{\epsilon_0 - \epsilon_\infty}{[1 + (j\omega\tau)^{1-\alpha}]^\beta} \quad (1)$$

where, ϵ_0 is the static dielectric constant, ϵ_∞ the permittivity at high frequency, α and β are the distribution parameters and τ is the relaxation time in picoseconds. The Havriliak-Negami function includes the Cole-Cole ($\beta = 1$)[11],Davidson-Cole($\alpha = 0$)[12] and Debye($\alpha = 0, \beta = 1$)[13] relaxation spectral function in limiting form. In this study Propionitrile with dioxane shows Debye type dispersion [13].

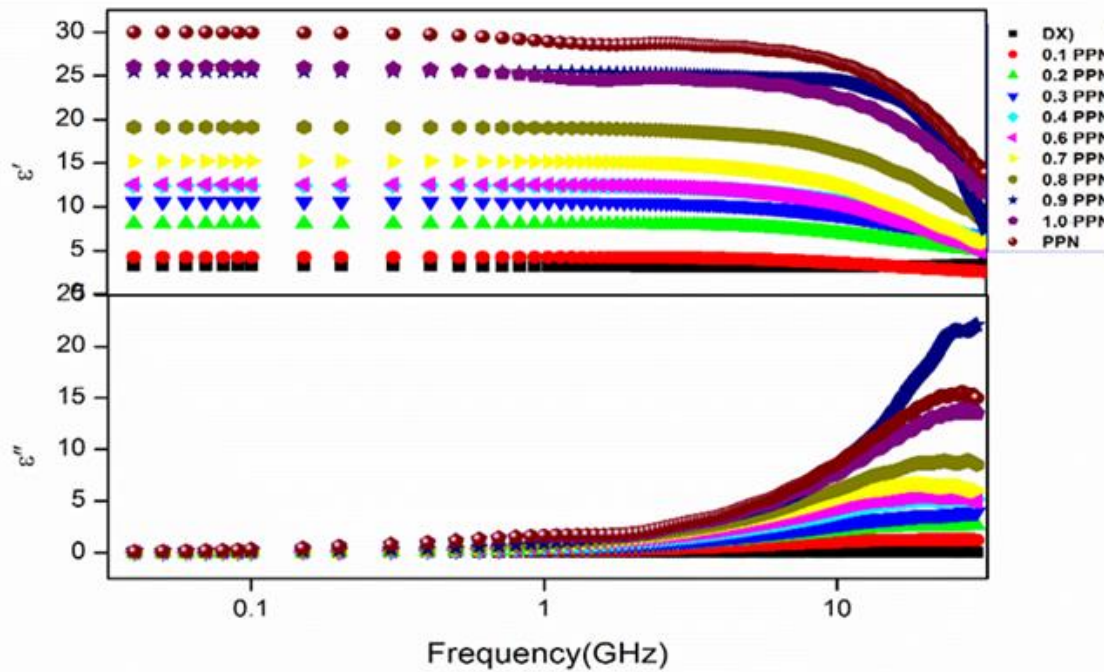


Figure 1: Complex Permittivity spectra for Propionitrile-1,4Dioxane mixtures at 25°C temperature.

3.2. Static Dielectric constant and Relaxation time

The values of dielectric parameters static dielectric constant (ϵ_0) and relaxation time (τ) in picoseconds are obtained from equation (1) and are reported in Table 1. The dielectric constant of liquids depends on many factors such as dipole moment, angular correlation of dipoles with neighboring dipole, nature of intermolecular forces, number of carbon atoms present in molecule, temperature [14]. The experimental values of dielectric parameters (ϵ_0 and τ) of the pure Propionitrile and 1,4Dioxane are in good agreement with the reported earlier [15,16]. It has been observed that static dielectric constant decreases with increase in the volume fraction of Dioxane in Propionitrile. In binary mixture of Propionitrile-1,4Dioxane it has been observed that the change in relaxation time is non-linear.

Table 1: Dielectric Parameters for PPN-1,4Dioxane Mixtures

V_{DX}	25°C		20°C		15°C		10°C		5°C	
	(ϵ_0)	(τ)	(ϵ_0)	(τ)	(ϵ_0)	(τ)	(ϵ_0)	(τ)	(ϵ_0)	(τ)
0.0	29.15(5)	5.77(1)	29.18(5)	5.91(1)	29.57(3)	6.13(8)	31.49(3)	6.17(6)	37.78(1)	6.22(1)
0.1	25.71(4)	6.28(3)	26.89(2)	6.31(3)	27.79(1)	6.34(1)	30.06(3)	6.46(1)	37.55(1)	6.64(1)
0.2	25.46(1)	6.29(3)	25.71(1)	6.52(3)	26.64(1)	6.58(2)	29.25(0)	6.59(3)	32.82(1)	6.75(8)

0.3	18.93(1)	6.87(1)	20.00(1)	6.89(1)	20.60(1)	7.02(1)	21.89(0)	7.24(0)	26.86(11)	7.35(8)
)									
0.4	15.07(1)	8.08(2)	15.79(1)	8.19(2)	16.39(1)	8.27(1)	16.84(0)	8.54(1)	19.80(1)	8.72(1)
)									
0.5	12.47(1)	8.76(1)	12.77(1)	8.79(2)	14.05(1)	8.91(9)	15.83(1)	9.04(2)	18.82(1)	9.26(15)
))
0.6	12.33(1)	7.58(2)	12.96(1)	7.61(1)	13.47(1)	7.64(2)	14.08(1)	7.71(2)	16.23(1)	7.72(2)
)									
0.7	10.39(1)	6.66(3)	10.62(1)	6.73(3)	11.38(1)	7.36(32)	12.14(2)	7.57(4)	12.37(3)	7.58(16)
)							4))
0.8	7.79(1)	6.38(4)	8.06(1)	6.51(1)	8.14(3)	6.55(86)	8.79(1)	7.49(3)	11.12(1)	7.50(5)
0.9	4.68(1)	5.16(1)	4.96(1)	6.29(1)	5.25(1)	7.14(3)	6.11(1)	7.16(6)	7.41(1)	7.22(6)
1.0	2.18(1)	-	3.19(1)	-	3.31(1)	-	4.38(1)	-	6.80(1)	-

3.3. Kirkwood Correlation Factor:

The Kirkwood-Frohlich equation provides useful information regarding the orientation correlation of dipole in the case of pure liquids [17]. The Kirkwood correlation factor determined from dielectric constant gives information on the collective orientation correlation between molecules. The deviation of the Kirkwood correlation factor “g” from unity is a measure of the extent of intermolecular bonding. The calculated theoretical dielectric constant using Kirkwood correlation factor provides a more detailed theoretical model for mixtures.

$$\frac{(\varepsilon_0 - \varepsilon_\infty)(2\varepsilon_0 + \varepsilon_\infty)}{\varepsilon_0(\varepsilon_\infty + 2)^2} = g\mu^2 \frac{4\pi N\rho}{9kTM} \quad (2)$$

Where, ε_0 is the static dielectric constant, ε_∞ is the dielectric constant at high frequency, g is the Kirkwood correlation factor, μ the dipole moment of liquid, N the Avogadro’s number, ρ the density of liquid and k, T has usual meanings.

The Kirkwood correlation factor determined from dielectric constant gives information on the collective orientational correlation between molecules. The deviation of the Kirkwood correlation factor “g” from unity is a measure of the extent of intermolecular bonding. The calculated theoretical dielectric constant using Kirkwood correlation factor provides a more detailed theoretical model for mixtures. The interpretation of the dielectric phenomena in the terms of the Kirkwood correlation factor is difficult for mixture of associating compound. It is impossible to determine average correlation factor g_1 and g_2 from a single value of the static dielectric constant without any assumption. Luzar suggested a theoretical model based on the mean field approximation for hydrogen bonded mixture [18]. The correlation factor g_1 and g_2 are calculated by the following equation [18]:

$$g_1 = 1 + Z_{11} \cos \varphi_{11} + Z_{12} \cos \varphi_{12} \left(\frac{\mu_2}{\mu_1} \right) \quad (3)$$

$$g_2 = 1 + Z_{21} \cos \varphi_{21} \left(\frac{\mu_1}{\mu_2} \right) \quad (4)$$

where $Z_{11} = 2\langle n_{HB}^{11} \rangle$, $Z_{12} = 2\langle n_{HB}^{12} \rangle$ and $Z_{21} = 2\langle n_{HB}^{21} \rangle V_{DX} / (1 - V_{DX})$ are the average number of particles forming the hydrogen bond with propionitrile-propionitrile, propionitrile - 1,4dioxane and 1,4dioxane-propionitrile pairs, respectively. X_{DX} is volume fraction of the 1,4dioxane. φ_{11} and φ_{21} are the angles between the neighboring dipoles of propionitrile and dioxane molecules. The Kirkwood-Frohlic theory must be applied to media containing two species of molecules, and the cross-correlation terms must be taken into account to separate g_1 and g_2 when considering only hydrogen bond contribution to the dipole-dipole correlation. The values of g_1 and g_2 are depends on volume fraction of 1,4DX in PPN-1,4DX mixtures as shown in **Figure 2**. The average number of hydrogen bonds $\langle n_{HB}^{11} \rangle$, $\langle n_{HB}^{12} \rangle$ and $\langle n_{HB}^{21} \rangle$ per propionitrile molecules for $1i$ pairs ($i = 1, 2$) have been determined according to the following relation [18]

$$\langle n_{HB}^{1i} \rangle = \frac{n_{1i}}{n_1} \omega_{1i} \quad (5)$$

where, $\omega_{1i} = \frac{1}{1 + \alpha^{1i} e^{-\beta E^{1i}}}$ is the probability of bond formation between propionitrile and 1,4dioxane. m number density of dioxane molecules. The value of $\beta = 1/kT$ and α^{1i} is the ratio of the two sub volume of the phase space, related to the non-hydrogen-bonded pairs have only two energy levels, E_{11} and E_{12} , for propionitrile -1,4-dioxane pair formed bonds, respectively. The values of $\langle n_{HB}^{11} \rangle$ and $\langle n_{HB}^{12} \rangle$ depending on the amount of hydrogen bonding pair densities between propionitrile-1,4-dioxane n_{12} and those between propionitrile - propionitrile molecule, i.e. $n_{11} = 2n_1 - n_{12}$. This can be calculated during which pair 11 and pair 12 is formed. The average number of hydrogen bonds between pairs 11 and 12 is plotted against V_{DX} as shown in **Figure 3**. The Luzar model [18] requires polarizability, the possible number of hydrogen bonds, dipole moments, and angles between dipoles $\cos\varphi_{11}$ and $\cos\varphi_{12}$ for the PPN and 1,4DX. **Table 2** contain the best possible molecular parameter values based on our analysis.

Table 2: Molecular parameters used in the computation of the static dielectric constant.

Molecular parameters	Propionitrile	1,4 Dioxane
Dipole moment (μ_1, μ_2)	4.02D	0.66D
Polarizability (α_1, α_2) (Å^3)	3.90	2.78
Bonding energy (E^{11}, E^{12}) (kJ/mol)	-13.3	-10.0
Molecular weight (gm/mol)	55.08	88.11
Density (gm/cm ³)	0.772	1.032

Note: 11- Propionitrile Pair 12- Propionitrile 1,4Dioxane pair

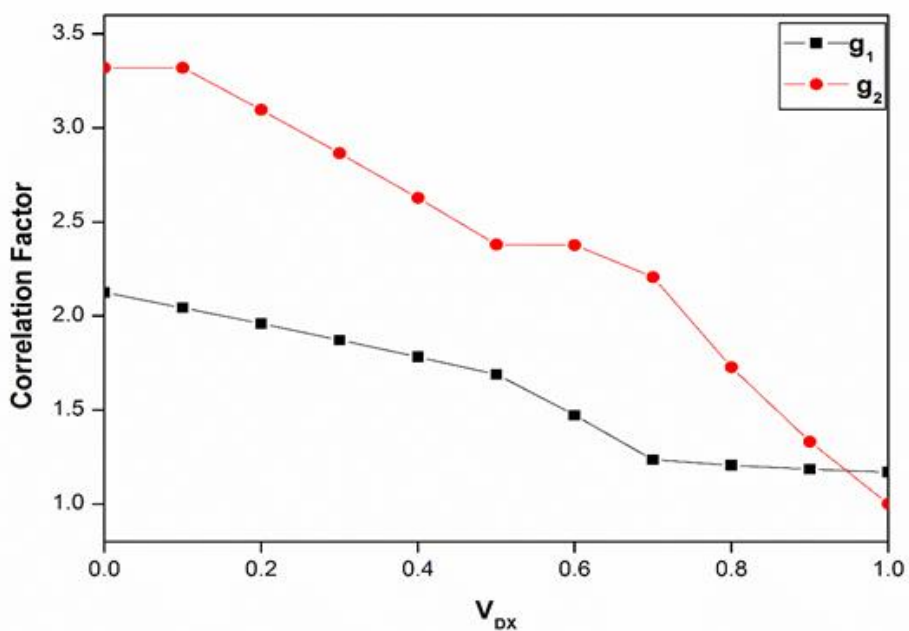


Figure 2: Correlation factor vs V_{DX}

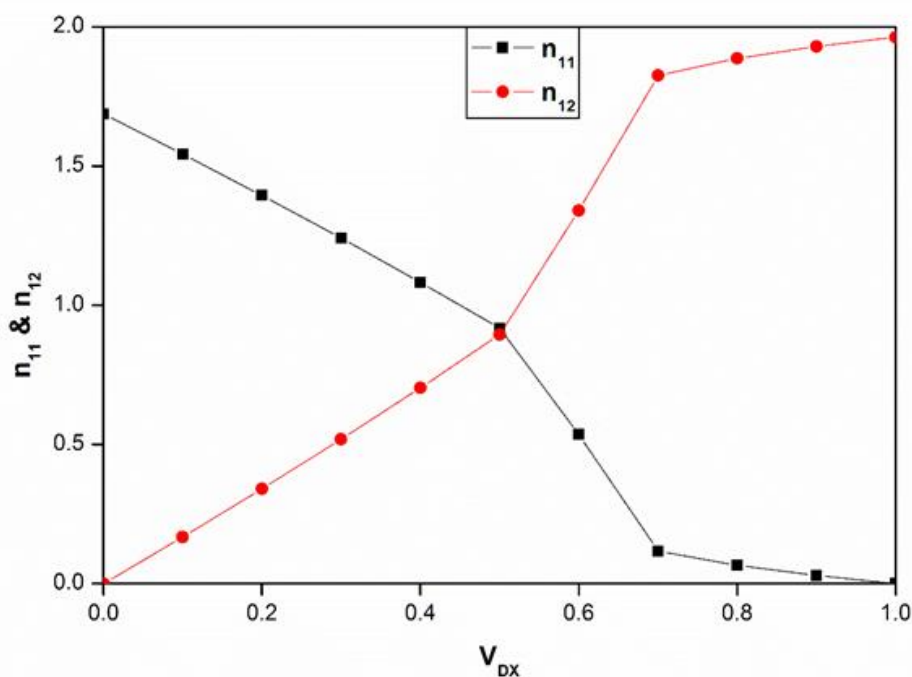


Figure 3: Plot of the average number of hydrogen bonds in PPN-PPN (pair 11) and PPN-1,4DX (pair 12) against V_{DX} .

IV. CONCLUSION

The complex dielectric spectra of Propionitrile- 1,4Dioxane mixture have been studied using time domain reflectometry technique in frequency range 10MHz to 30GHz at different temperatures. The values of static dielectric constant, relaxation time and Kirkwood correlation factor for Propionitrile-14Dioxane mixtures also calculated .As the concentration of DX in Propionitrile increases dielectric constant increases. The complex permittivity spectra for Propionitrile show systematic variation with frequency and concentration and shows Debye relaxation mechanism.

V. REFERENCES

- [1]. K.Rajagopal , S.Chenthilnath ,A.K. Nain J Mol Liq. 2010;151:23–29.
- [2]. K.Rajagopal K, S.Chenthilnath . J Mol Liq. 2011;160:72–80..
- [3]. S.N.Helambe,M.P.Lokhande,A.C.Kumbharkhane,S.C.Mehrotra,S.C. Doraiswamy,PRAMANA J. of Physics,44(1995)405-410.
- [4]. R. Jellema, J. Bulthuis, G. van der Zwan,Journal of Molecular Liquids, 73,74(1997)179-193.
- [5]. V.V.Ramana, A.B.V. Kiran Kumar, M. Ashok Kumar, M.K. Moodley,JournalofChemistry, Article ID 687106(2013)1-4.
- [6]. O. Mehmet, Bull. Korean Chem. Soc, 35(2014)1469.
- [7]. S.N. Helmbe, A.S. Chaudhari, S.C. Mehrotra, Journal of Molecular Liquids, 84(2000)235-244.
- [8]. S.N. Helmbe, M.P. Lokhande, A.C.Kumbharkhane,S.C.Mehrotra,PRAMANA J. of Physics,45(1995)19-24.
- [9]. R.H.Cole, J.G.Berberian, S.Mashimo,G.Chryssikos,A.Burns,E.Tombari,J ApplPhys,66(1989)793–802.
- [10]. S. Havriliak, S. Negami, J. Polym. Sci. C 14 (1966) 99–117
- [11]. K.S.Cole, R.H. Cole,J ChemPhys,9(1941)341
- [12]. D.W. Davidson, R.H. Cole RH,J ChemPhys,18(1950)1417-1490
- [13]. P.Debye, The Chemical Catalogue Company(1929).
- [14]. S.C.Mehrotra ,A.C. Kumbharkhane & A.S.Chaudhari AS: 'Binary Polar Liquids' Elsevier (2017) Netherlands.
- [15]. K.Rajagopal , S. Chenthilnath b, A.K. Nain Journal of Molecular Liquids 151 (2010) 23–29
- [16]. A. C. Kumbharkhane,M.N. Shinde,S.C. Mehrotra,N. Oshiki,N. Shinyashiki, S. Yagihara, and S. Sudo The Journal of Physical Chemistry A 2009, 113, 38, 10196-10201
- [17]. J.G.Kirkwood, J.Chem .Phys.7(1939) 911.
- [18]. A.Luzar,JMolLiq, 46(1990)221-238

Water Dynamics on The Structural Properties of Amino Acid in Presence of NSAID : An Approach Through Dielectric Spectroscopy

Suad Alwaleedy¹, Saeed Mohemmed¹, Ravikant Karale¹, Komal B. Kabara¹, Ashok C. Kumbharkhane¹, Bunty Rani Roy², Arvind V. Sarode^{1*}

¹School of Physical Sciences, Swami Ramanand Teerth Marathwada University, Nanded-431 606, Maharashtra, India

²Department of Physical Sciences, Kakatiya Institute of Technology and Science, Warangal, Telangana, India

ABSTRACT

Present work reports the dielectric response for non-steroidal anti-inflammatory drugs (NSAID) 2-[2-[2-[(2,6-dichlorophenyl)amino]phenyl]acetyl]oxyacetic acid (Aceclofenac) in the aqueous leucine solution at different concentrations and temperatures (298.15 K-283.15 K) using time domain reflectometry technique in the frequency region 1 GHz to 30 GHz. Dielectric parameters such as complex permittivity (ϵ^*), dielectric constant (ϵ), dielectric relaxation time (τ), dipole moment (μ) and Kirkwood correlation factor (g) have been calculated and the study is corroborated by the thermodynamic parameters such as molar enthalpy of activation (ΔH), entropy of activation (ΔS) and free energy of activation (ΔF) to give insight into the structural dynamics.

Keywords: Aceclofenac; leucine; Time Domain Reflectometry; Dielectric Relaxation; Thermodynamic Parameter.

I. INTRODUCTION

Aceclofenac, chemically known as 2-[2-[2-[(2,6-dichlorophenyl)amino]phenyl]acetyl]oxyacetic acid having molecular formula $C_{16}H_{13}Cl_2NO_4$ is a non-steroidal anti-inflammatory drug (NSAID) indicated for various painful indications and proved as effective as other NSAIDs [1]. Other applications includes treatment of rheumatoid arthritis, osteoarthritis, ankylosing spondylitis, tendinitis, and joint inflammation and reduces pain intensity and duration of morning stiffness and other inflammatory conditions [2, 3]

It possesses free carboxylic acid in the structure that can be found in a wide range of pharmaceutical compounds and plays an important role in drug design. Also, the carboxylic acids can act as both hydrogen bond acceptor and donor due to the simultaneous presence of carbonyl (C=O) and hydroxyl (O-H) groups. Hence carboxylic acids, which are quite polar in nature [4], can form dimers corresponding to homo-synthons well-known in supramolecular chemistry [5]. Aceclofenac is such a carboxylic acid derivative and one of the important non-steroidal anti-inflammatory drug (NSAID) molecules, which also possess analgesic

properties[6].It exhibits very slight solubility in water, and as a consequence, it exhibits low bioavailability after oral administration [7-9].

Due to wide range of applications continuous efforts have been taken by the scientific community to look into the structural conformation of aqueous leucine induced with aceclofenac (ACF) which directly relates to the applications of drug-amino acid and drug-proteins interaction as plasma protein binding is a very important factor in pharmacokinetics, pharmacodynamics, and drug interaction. Drug-protein interaction greatly influences the absorption, distribution, metabolism, and excretion properties of drugs [10]. A clear perception about the features of drug-protein interaction provides insights into drug therapy and drug design. As, amino acid is a basic building block of protein and amongst 20 different AA Leucine is a branched chain, nonpolar, aliphatic, hydrophobic amino acid having chemical formula $C_6H_{13}NO_2$ an essential amino acid required by our body as it is not synthesized in our body.

The amino acid leucine to be studied in the present work interacts with insulin signaling pathway to stimulate control of protein synthesis, maintenance of muscle protein during period of restricted energy intake, reduce postprandial glucose and insulin maintaining blood glucose level[11,12]. Due to such huge demand in the pharmaceutical and biological fields for numerous applications, it will be quite interesting to study molecular interaction between aqueous leucine and the drug aceclofenac as structural properties can be directly related to the applications.

After careful literature survey through various resources and to the best of my knowledge, no work on the interaction of concentration dependence of aceclofenac with aqueous leucine using time domain reflectometry in the GHz frequency, and in temperature region 298.15-283.15 K has been reported so far. But very little work has been carried out recently on the interaction of drug-amino acids[1]. Amino acids are important biomolecules through which the drugs interact inside the body. Solvent-mediated interactions in biological systems constitute the main determinants for regulating the structure, dynamics, and thermodynamics of bio-molecules, ultimately dictating their biological function and that of the cell. Because bio-molecules are embedded in a highly polar medium, electrostatics is a fundamental component of solvation effects at the molecular level. Though pure aceclofenac has poor solubility in water (0.015 mg/ml), but its solubility can be improved in nanoemulsion, solid lipid nanosuspension and polymeric nanosuspension (13). Therefore, in the present work priority is being given for the molecular interaction between the drug-aceclofenac with aqueous leucine.

The study not only finds applications in pharmaceutical and biological importance but also extends it to the interdisciplinary fields of molecular biology, physics and chemistry. Therefore, the present work aims at the investigation of molecular interaction in amino acid in presence of the water-insoluble drug, aceclofenac in aqueous leucine in terms of dielectric and thermodynamical parameters.

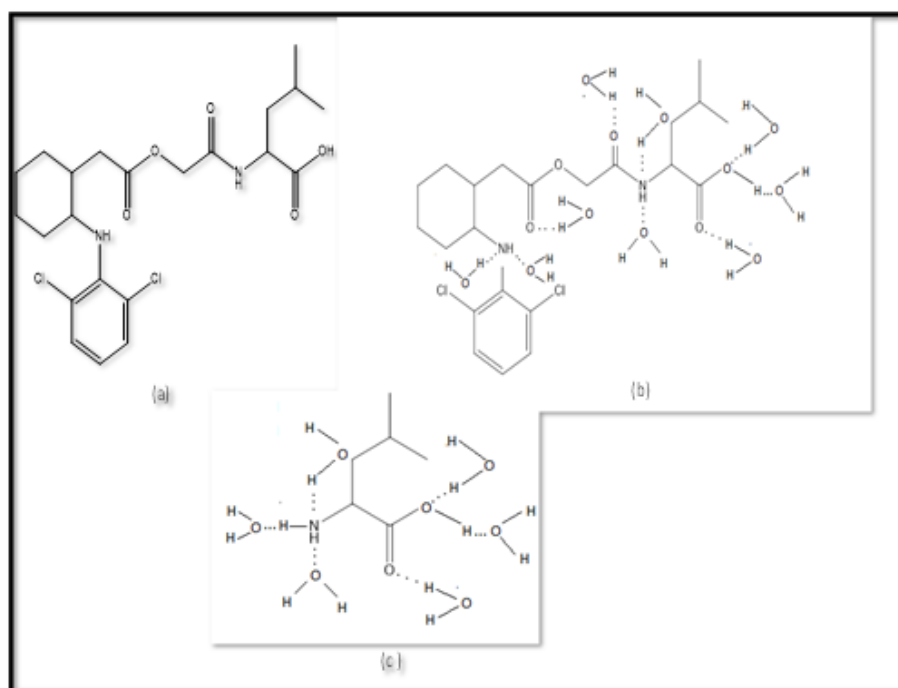


Fig.1 Different possible molecular conformations between a) Aceclofenac and leucine , b) aceclclofenc+leucine +water and (c) leucine+water.

II. EXPERIMENTAL DETAILS

2.1. Materials

Leucine was purchased from sigma Aldrich and Aceclofenac was purchased from Hi Media Laboratories Pvt. Ltd. Mumbai, India and used without purification. Doubly distilled and deionized water was used for making the solution. The chemicals were weighed in an electronic digital balance (METTLER TOLEDO ME- 204) with a minimum count of 0.0001 gm. The solutions of 15 ml were prepared at room temperature for different concentrations of leucine and ACF. The Aceclofenac and Leucine in different concentration in water was refluxed for 72 hour.

2.2. Measurements

The Tektronix Digital Serial Analyzer model no. DSA8300 sampling mainframe along with the sampling module 80E10B has been used for TDR. A sampling module provides 12 ps incident and 15 ps reflected rise time pulse was fed through a coaxial line system having 50 Ω impedance. Sampling oscilloscope monitors show change in step pulse after reflection from the end of line. The reflected pulse without sample $R_1(t)$ and with sample $R_x(t)$ were recorded in the time window of 5 ns and digitized in 2000 points. The Fourier transform of the pulse and data analysis was performed to determine complex permittivity spectra $\epsilon^*(\omega)$ using least square fit method [14-17]. Before measurements, the system was calibrated using different solvents with an accuracy ± 0.0026 as static dielectric constant for water at room temperature is 78.44 [18] and we observed the value 78.23 for water sample. To keep the temperature constant, a temperature controller system was

used. The sample cell is encased in a heat-insulating container, and the temperature inside the cell is measured with an electronic thermometer. The temperature of sample cell was maintained at desired value within the accuracy of ± 1 °C.

III. RESULT AND DISCUSSION

3.1. Dielectric Parameters

Dielectric dispersion and absorption curves obtained for aqueous leucinat 0.02, 0.04, 0.06, 0.08 and 0.1 M concentration in presence of poor water soluble aceclofenac(ACF) with concentrations 0.002, 0.004, 0.006, 0.008 and 0.01 M measured at temperatures 298.15 K, 293.15 K, 288.15 K and 283.15 K is shown in fig. 2 whereonly spectra at low and high temperatures and concentrations respectively were depicted to avoid rush of figures. The spectra show that there is a gradual decrease in dielectric permittivity for all the used concentrationstowards room temperature and the loss peaks shift towards lower frequency side when concentration is more. This suggests molecular association between solute and solvent molecules

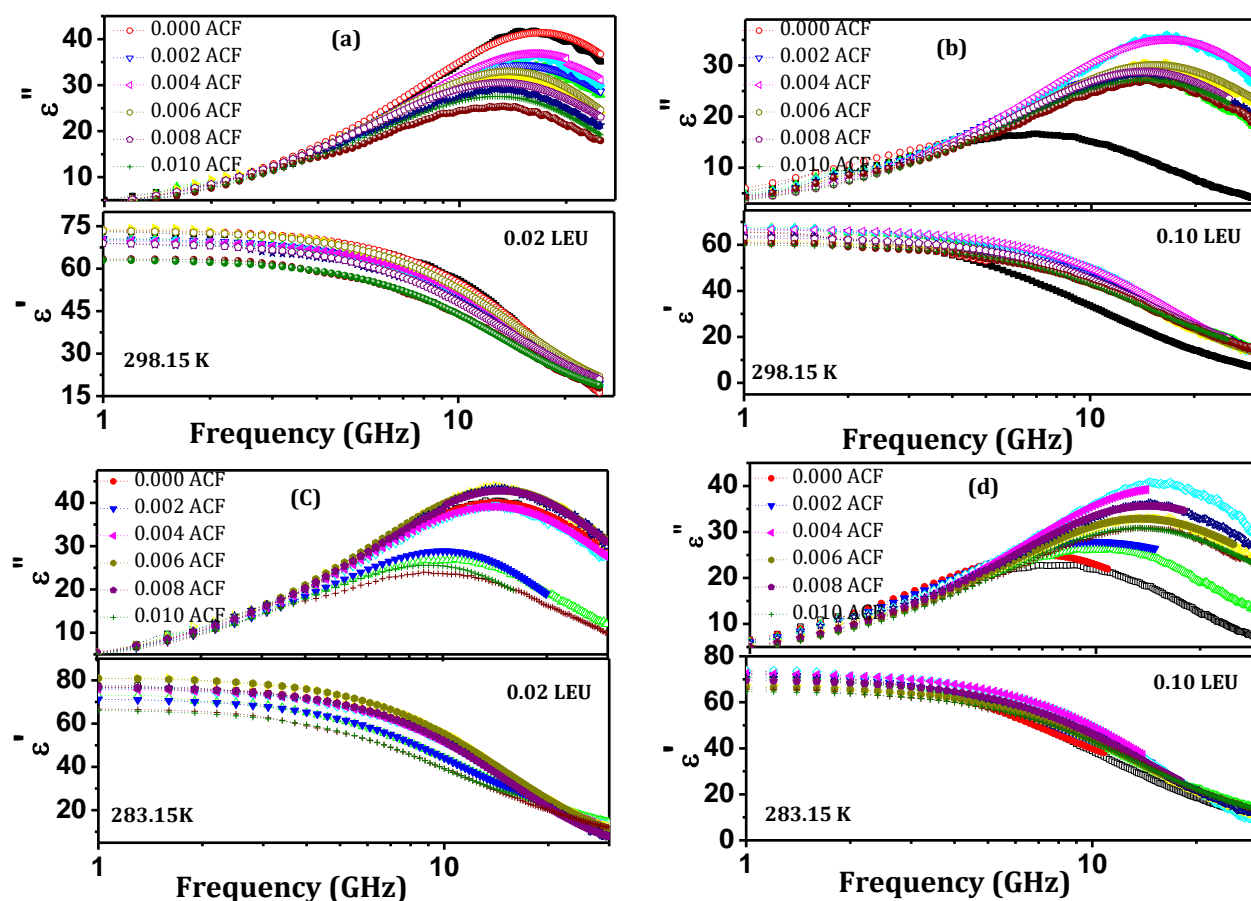


Fig.2. Permittivity spectra at temperature 298.15 K; for (a) 0.02 M and (b) 0.1 M leucine and at 283.15 K (c) and (d) at different aceclofenac concentration. solid symbols represents observed data while dotted lines indicates fitted data.

The process of complex permittivity spectra can be described by Havriliak-Negami equation [19] using least square fit method given below in equation 1.

$$\varepsilon_{(\omega)}^* = \varepsilon_{\infty} + \left[\frac{\Delta\varepsilon}{[1+(j\omega\tau)^{1-\alpha}]^{\beta}} \right] \quad (1)$$

For the relaxation process we use eq. (1), the parameters used are the relaxation strengths $\Delta\varepsilon = \varepsilon - \varepsilon_{\infty}$, ε_{∞} - the high-frequency limiting static dielectric constant, ω is the angular frequency and τ the relaxation time, α is the distribution parameter. α ($0 < \alpha < 1$) indicates the broadness of the symmetric relaxation curve when the dielectric data are described by the Cole-Cole equation. The relaxation curve with ($0 < \beta < 1$), $\alpha = 1$ corresponds to Debye-type of relaxation and a smaller value of α gives the broader symmetric relaxation curve, whereas the relaxation curve with $\beta = 1$ corresponds to a non-Debye type of relaxation in which the asymmetric relaxation ($0 < \beta < 1$), $\alpha = 0$ is associated with the cooperative mechanics of dielectric relaxation. It has been found that the dielectric data for the studied systems obey the Cole-Cole dispersion model [19]. As the frequency range of dielectric study in present work is from 1 GHz to 30 GHz, the value of ε_{∞} is just a fitting parameter. In the fitting procedure, ε_{∞} is not fitted and assumed to be 3.0. This is done because the data are not sensitive to ε_{∞} in the high frequency range.

Before we discuss more about the molecular interaction between amino acid leucine and the water insoluble drug aceclofenac, it will be more convenient to look into the water dynamics on the structural properties of amino acids. Observed data reveals that static dielectric constant for aqueous leucine decreases with increasing leucine concentration but increases towards lower temperature. The measured values of static dielectric constant with increasing concentrations of leucine were found to be less than that of pure water. Since at lower leucine concentration every leucine molecule is completely surrounded by water molecule and therefore interaction between leucine molecules is screened and thereby decreases the value of static dielectric constant. In other words we may say that this decrease may be due to the formation of hydration shell around leucine as mentioned in the previous study for aqueous amino acids studied [20]. With increasing leucine concentration more and more water molecules form hydration shell around leucine and loss of free water molecules that resulted in lowering the static dielectric constant. During this process hydrogen bonding network will be affected by the presence of leucine. As leucine has hydrophobic group present in it and therefore dynamics of surrounded water could be affected.

To see the effect of temperature on the structural behavior of aqueous leucine the study has been extended towards lower temperature. From the observed data, it has been noticed that by lowering the temperature from 298.15 K to 283.15 K static dielectric constant seems to be increasing for all the used concentrations. This rise in the values of static dielectric constant towards lower temperature over all the leucine concentrations may be due to the formation of induced dipoles via hydration layer with the neighboring or surrounding molecules as the molecules gained lower thermal energy and therefore amplitude of the random thermal motion is restricted. This gives perfect alignment (parallel or antiparallel) with the applied field so that dipoles are more closely aligned with each other; as a result the orientation polarization gets increased and so the static dielectric constant.

The alignment of dipoles can be well explained using dipole moment and correlation factor 'g' calculated and discussed in the next section.

The variation in static dielectric constant for aqueous leucine in presence of varying concentrations of aceclofenac (ACF) is shown in the fig 3. It has been observed that the overall trend for the static dielectric constant measured at 0.002, 0.004, 0.006, 0.008 and 0.01 M concentrations of aceclofenac at different temperatures was found to be decreasing with increasing aceclofenac concentrations. The presence of aceclofenac in aqueous leucine resulted in further decrease in the values of static dielectric constant and the variation was observed to be larger at 0.01 (M) concentration of aceclofenac. This variation in the values of static dielectric constant may be due to the molecular interaction between the amino group (NH_3) of the screened leucine by the water molecules and the H from the O-H group of ACF through weak induced dipole-dipole interaction and also due to intermolecular O-H...O H-bonds between aceclofenac and water. As, most drug modifications are based on the breakage of these H-bonds. As a result hydrogen bonding network affected which resulted in lowering the values of static dielectric constant with increasing ACF concentration. But for the highest used concentration of ACF there found very slight variation or almost constant values of static dielectric constant because at highest concentration all the possible hydrogen bonding sites are saturated and no site is available for bonding to be taking place; also intramolecular interactions in aceclofenac between N-H...O and N-H...Cl hydrogen bonds. It is seen that ACF is more stable, when both hydrogen bonds exist as a result there is no further change in the structural conformation which keeps the static dielectric constant almost constant over the used concentrations (0.01 M) and temperature.

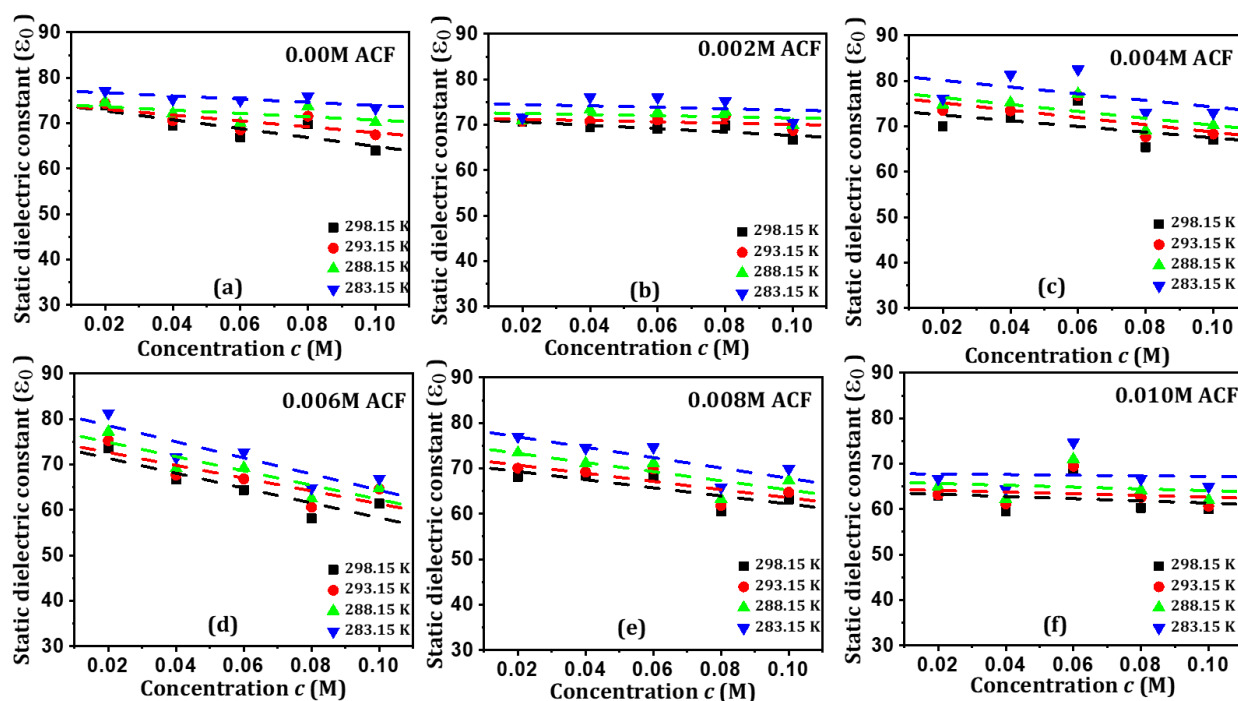


Fig. 3 Temperature and concentration dependent static dielectric constant of aqueous leucine for (a) 0.00 M, (b) 0.002 M, (c) 0.004 M, (d) 0.006 M, (e) 0.008 M and (f) 0.010 M aceclofenac at different temperature and concentration.

Increase in the values of static dielectric constant by lowering the temperature from 298.15 K to 283.15 K, may be due to increased dipole-dipole interaction (parallel or antiparallel) between leucine-aceclofenac molecules via hydration shell and is associated with the cooperative relaxation of bulk-like water.

Dielectric relaxation time measured for aqueous leucine (fig. 4) and in presence of aceclofenac gives relaxation dynamics for the rotational motion of water molecules in the solute environment. From the observed data relaxation time for aqueous leucine was found to be linearly increasing with leucine concentration over all the measured temperature indicating a more heterogeneous /non-cooperative environment for water molecules or we may say large steric hindrance to the rotational motion of water molecules in the solvent rich and low temperature region.

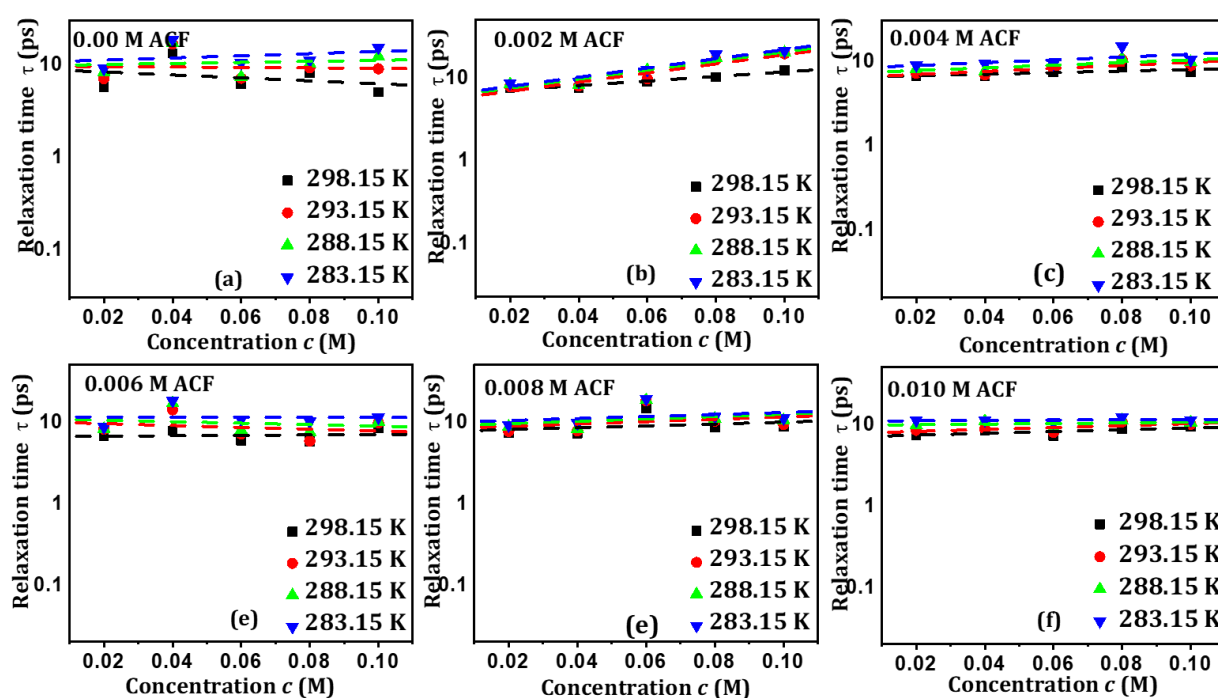


Fig. 4 Dielectric relaxation time measured of aqueous leucine for (a) 0.00 M ,(b) 0.002 M ,(c) 0.004 M ,(d) 0.006 M ,(e)0.008 M and (f) 0.010 M aceclofenac at different temperature and concentrations.

Increasing values of dielectric relaxation time reveals non cooperative environment for the molecular or rotational motion for water molecules. This may be due to association between water molecules that form hydration shell around leucine that interacts with ACF through hydration shell or dipole-dipole induced interaction between leucine and ACF through water. As a result rotational motion of water molecules gets restricted and observes only increased values of relaxation time.

In order to have deep insight into the structural conformation of water dynamics we may look into the orientational correlation between water–leucin–aceclofenac in terms of correlation factor ‘g’ or the factor ‘ $g\mu^2$ ’. Due to insufficient data available for the dipole moment at the measured temperature we used dipole moment for water $\mu=2.37$ D referenced previously [21, 22] to calculate the correlation factor ‘g’ from the measured ‘ $g\mu^2$ ’ using Kirkwood–Frohlich equation [23] given below.

$$g\mu^2 = \frac{9kTM}{4\pi N\rho} \left[\frac{(\epsilon_s - \epsilon_\infty)(2\epsilon_s + \epsilon_\infty)}{\epsilon_s(\epsilon_\infty + 2)^2} \right] \text{-----} \quad (2)$$

The variation of $g\mu^2$ and 'g' for the aqueous leucine and ACF induced leucine at different concentration and temperature is shown in fig. 5 and the values are reported in table 1. Since 'g' is a measure of orientational correlation between a molecule and its nearest neighbors, the departure of 'g' from unity could be an indication of molecular association due to short-range ordering interactions. In our case of aqueous leucine and ACF induced leucine, correlation factors are lower than 1 (due to the anti-parallel orientation of the dipoles) and decrease further towards higher leucine concentrations suggest increased correlation between solute dipole via hydration shell. The variation in the values of 'g' with increasing ACF concentration in leucine at different temperatures is shown in fig 5. From the closed observations, it has been concluded that the correlation between water and the surrounding molecules increases by the presence of aceclofenac for all the used leucine concentrations. This could be due to the alignment of antiparallel orientations of dipoles between solutes (ACF) and solvent (aqueous leucine). This may also be due to the fact that with increasing concentrations of both leucine and aceclofenac; number of water molecules attached to both the solutes under different conformations will be reduced. At higher ACF the g values are very much less than unity is the clear indication of highly aligned antiparallel conformation. The 'g' value was found to be increasing towards lower temperature which confirms the formation of weak interaction between ACF, leucine and water through hydration shell.

Table 1: correlation factor 'g' calculated from the factor $g\mu^2$ for the solution of leucine + water + aceclofenac at different temperature

leucine c(M)/T (K)	298.15	293.15	288.15	283.15	298.15	293.15	288.15	283.15
$g\mu^2$					g			
ACF 0 (M)								
0.02	5.12	5.04	4.99	5.06	0.91	0.90	0.89	0.90
0.04	4.81	4.80	4.82	4.94	0.86	0.85	0.86	0.88
0.06	4.63	4.66	4.67	4.93	0.82	0.83	0.83	0.88
0.08	4.83	4.86	4.93	4.98	0.86	0.87	0.88	0.89
0.10	4.42	4.58	4.67	4.80	0.79	0.82	0.83	0.85
ACF 0.002 (M)								
0.02	4.84	4.81	4.74	4.69	0.86	0.86	0.84	0.83
0.04	4.80	4.81	4.90	4.99	0.85	0.86	0.87	0.89
0.06	4.78	4.83	4.86	5.01	0.85	0.86	0.87	0.89
0.08	4.83	4.89	4.87	4.94	0.86	0.87	0.87	0.88

0.10	4.63	4.64	4.66	4.77	0.82	0.83	0.84	0.85
ACF 0.004 (M)								
0.02	4.84	4.97	4.94	4.99	0.86	0.88	0.88	0.89
0.04	4.98	5.00	5.02	5.35	0.89	0.89	0.89	0.95
0.06	5.24	5.20	5.17	5.43	0.93	0.93	0.92	0.97
0.08	4.52	4.60	4.61	4.79	0.80	0.82	0.82	0.85
0.10	4.62	4.67	4.71	4.77	0.82	0.83	0.83	0.85
ACF 0.006 (M)								
0.02	5.09	5.13	5.16	5.32	0.91	0.91	0.92	0.95
0.04	4.61	4.59	4.61	4.69	0.82	0.82	0.82	0.84
0.06	4.44	4.54	4.62	4.77	0.79	0.81	0.82	0.85
0.08	4.00	4.10	4.16	4.24	0.71	0.73	0.74	0.75
0.10	4.23	4.38	4.32	4.38	0.75	0.78	0.77	0.78
ACF 0.008 (M)								
0.02	4.71	4.76	4.90	5.05	0.84	0.85	0.87	0.90
0.04	4.74	4.70	4.75	4.89	0.84	0.84	0.85	0.87
0.06	4.72	4.75	4.75	4.90	0.84	0.85	0.85	0.87
0.08	4.17	4.19	4.21	4.31	0.74	0.75	0.75	0.77
0.10	4.36	4.39	4.46	4.57	0.78	0.78	0.79	0.81
ACF 0.01 (M)								
0.02	4.34	4.28	4.33	4.37	0.77	0.76	0.77	0.78
0.04	4.10	4.14	4.14	4.21	0.73	0.74	0.74	0.75
0.06	4.76	4.72	4.74	4.90	0.85	0.84	0.84	0.87
0.08	4.15	4.24	4.27	4.36	0.74	0.75	0.76	0.78
0.10	4.13	4.10	4.12	4.25	0.74	0.73	0.73	0.76

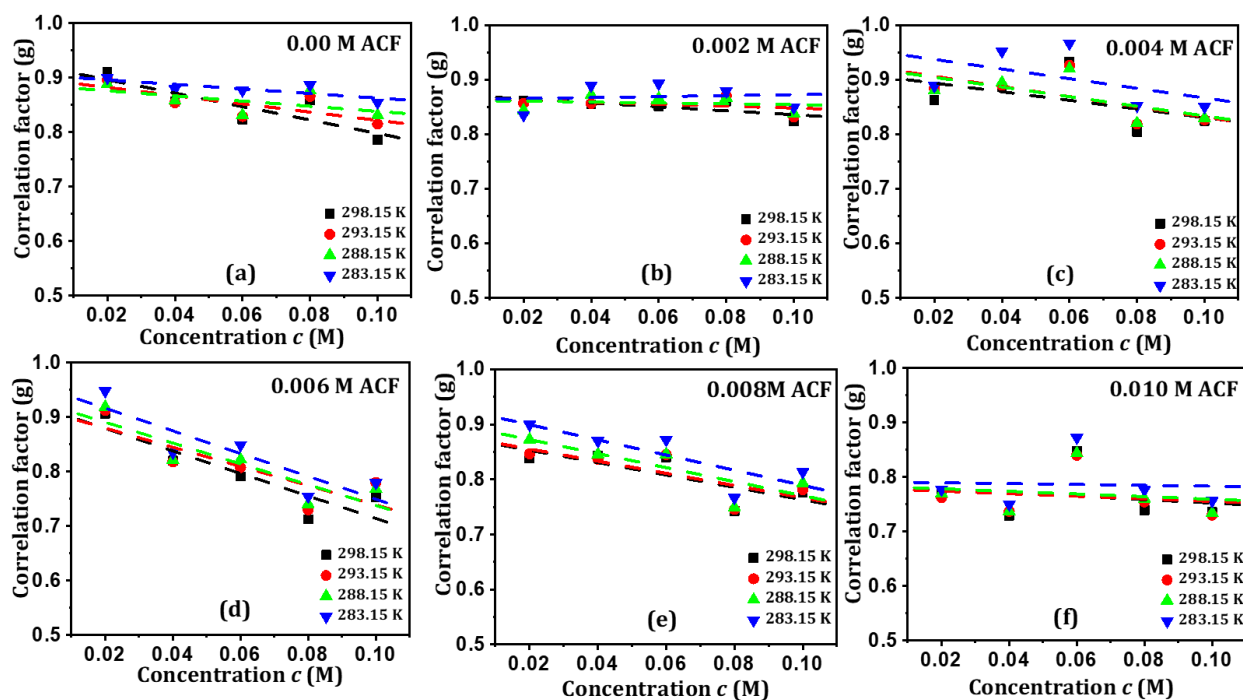


Fig. 5 variation in correlation factor 'g' of aqueous leucine for (a) 0.00 M ,(b) 0.002 M ,(c) 0.004 M,(d) 0.006 M ,(e)0.008 M and (f) 0.010 M aceclofenac at different temperature and concentration . .

3.2. Thermodynamical Parameters:

Thermodynamical parameters such as molar free energy of activation (ΔF), molar enthalpy (ΔH) and molar entropy of activations (ΔS) play a vital role in deciding water dynamics with amino acid and drug. Free energy of activation obtained for aqueous and ACF induced leucine is shown in fig.6. For aqueous leucine, the average molar free energy of activation was found in the range 2-3 kcalmol⁻¹. This energy is suggested for the weak hydrogen bonding. The free energy of activation was found almost independent upon temperature as it was found to be either slightly increased towards higher leucine concentrations or almost constant for all the ACF used .

The thermodynamic energy parameters ΔF and ΔS for dielectric relaxation as rate processes for the system under study were determined using Eyring's rate equations [24] as

$$\tau = \left[\frac{h}{kT} \right] \exp \left[\frac{\Delta F}{RT} \right] \quad (3)$$

and

$$\Delta F = \Delta H - T\Delta S \quad (4)$$

Where ΔF , ΔH , ΔS are the molar free energy, enthalpy and entropy of activation for the dipolar orientation.

For the aqueous leucine molar free energy of activation was observed to be in the range 2-3 kcal mol⁻¹ which was almost independent of concentration but was slightly increasing towards lower temperature for higher leucine concentration. This clearly suggests possibility of weak hydrogen bonding between water and leucine due to hydrophobic group present in leucine. This will form hydration layer around leucine molecule. For the ACF induced aqueous leucine, where NH₃ of leucine screened by the water molecules and hydrogen from the OH⁻ group of ACF interact weakly, the molecular interaction slightly increases with concentration and therefore dipoles require more energy in order to attain equilibrium with the applied field, and hence the ΔF increases with increasing leucine concentration for all the ACF concentrations. This indicates weak molecular association between leucine molecules screened by the water molecules and ACF molecules via hydration shell. As 4-5 kcal mol⁻¹ energy is suggested for breakage or formation of hydrogen bond the observed energy is lower than 4-5 kcal mol⁻¹ and can be attributed to the weak interaction.

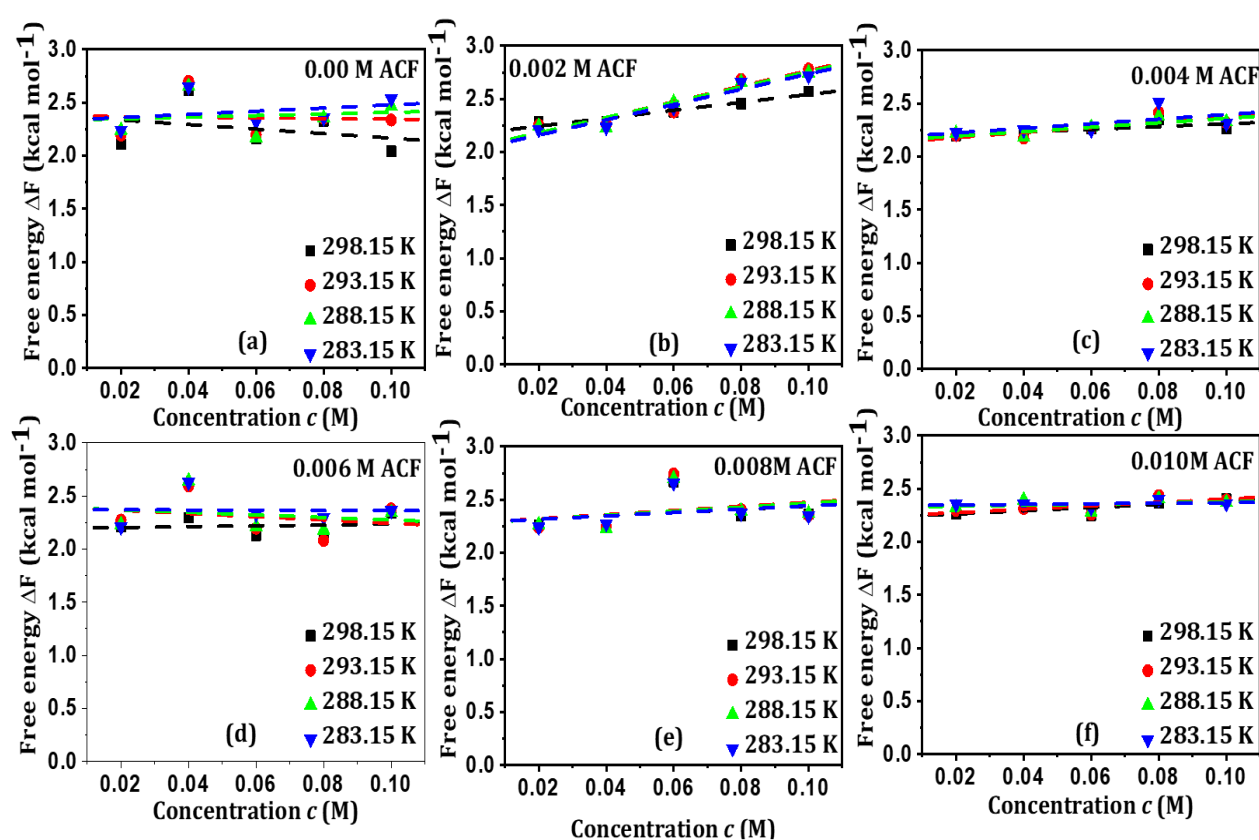


Fig.6 Molar free energy of of aqueous leucine for (a) 0.00 M ,(b) 0.002 M ,(c) 0.004 M,(d) 0.006 M ,(e)0.008 M and (f) 0.010 M aceclofenac at different temperature and concentration .

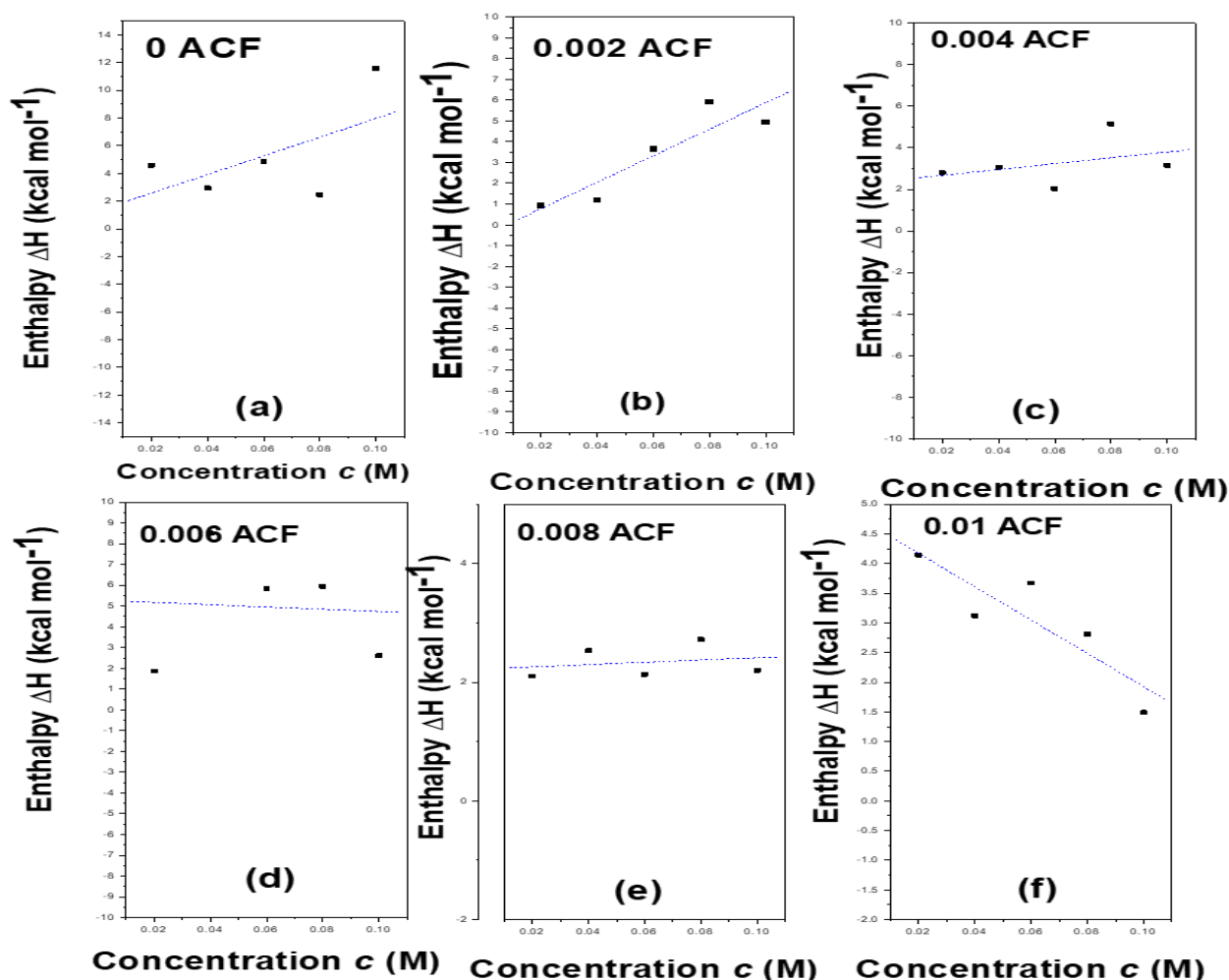


Fig. 7 Molar enthalpy of activation of aqueous leucine for (a) 0.00 M ,(b) 0.002 M ,(c) 0.004 M,(d) 0.006 M ,(e)0.008 M and (f) 0.010 M aceclofenac at different concentrations.

Enthalpy ΔH is a measure of the energy released when attractions are set up between positive or negative ions sites of solute and solvent molecules. With positive ions, there may only be loose attractions between the slightly negative oxygen atoms in the water molecules and the positive ions of leucine and ACF. With negative ions, hydrogen bonds are formed between lone pairs of electrons on the negative ions of leucine and ACF and the slightly positive hydrogen in water molecules.

Enthalpy for aqueous leucine was observed to be positive and increasing with leucine concentration (Fig. 7). This could be due to the formation of aggregations of liquids between solute and solvent molecules or due to the formation of hydration shell around leucine. This suggests that the process is slightly endothermic which

lowers the temperature of the solution than that of the original water. The rate of change of enthalpy for aqueous leucine was $67.5 \text{ kcal mol}^{-1}$ per molar concentration which was gradually decreases with the increase in ACF concentration and reaches to $-28.05 \text{ kcal mol}^{-1}$ per molar concentration for 0.01 M leaving the system exothermic. This suggests possibility of weak hydrogen bond formation between lone pairs of electrons on the negative ions of leucine and the slightly positive hydrogens in water molecules that forms hydration shell around leucine and the hydrogen from the $-\text{OH}$ group of ACF molecule through hydration shell. Thus, heat energy is released during the formation of new bonds between the ions of both solutes and water molecules leaving the process exothermic. The more the negative hydration enthalpy, the more favorable bonding at hydroxyl (OH) sites than the methyl (CH_3) or amino group (NH_3) group in the hydration process. In our case enthalpy measured at different leucine concentrations in presence of ACF was observed to be positive but relatively lower towards higher leucine concentration at higher ACF and suggests favorable bonding at $-\text{OH}$ site.

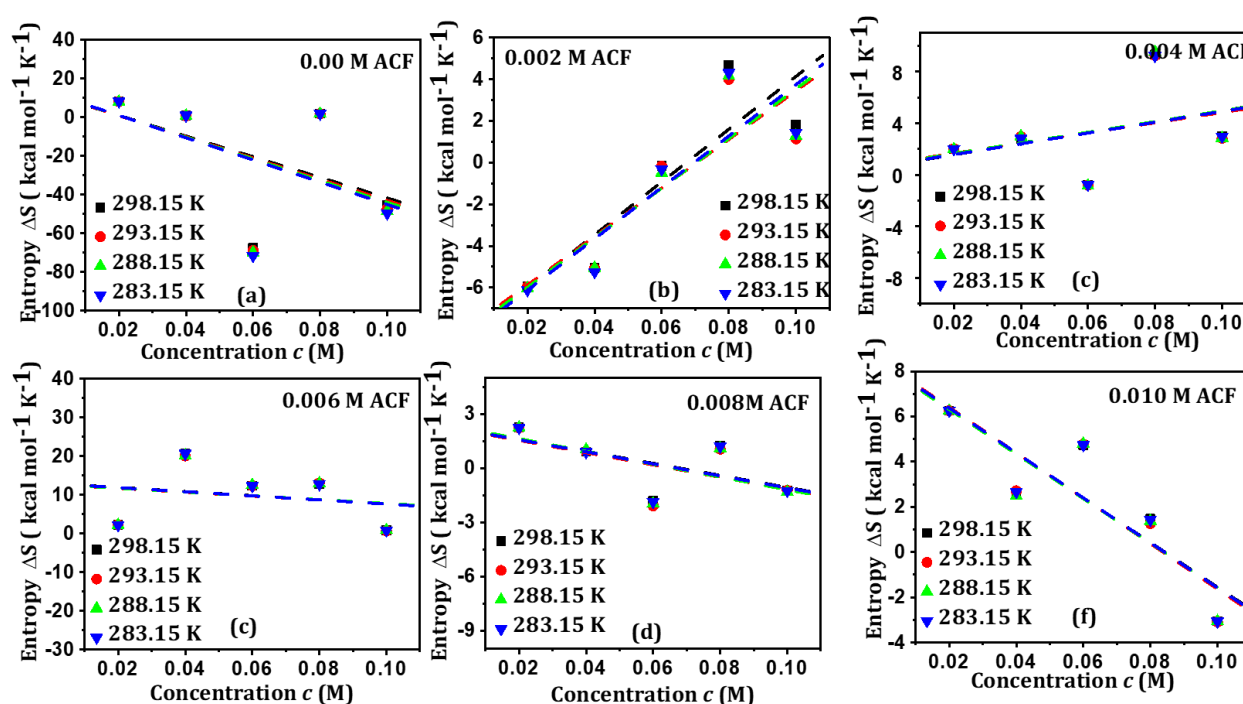


Fig. 8 Molar entropy of activation of aqueous leucine for (a) 0.00 M , (b) 0.002 M , (c) 0.004 M , (d) 0.006 M , (e) 0.008 M and (f) 0.010 M aceclofenac at different temperature and concentrations.

The molar entropy, ΔS of a system is a measure of its orderly nature. For favorable or cooperative environment, the activated system becomes more ordered than the normal one and the change in entropy is negative. For the aqueous leucine molar entropy of activation was observed to be decreasing over the used concentrations and temperature (Fig. 8). Negative entropy towards higher concentration suggests more ordered structure due to weak hydrogen bond formation between amino group of leucine and hydrogen from water molecules that form hydration shell around leucine. But the addition of small concentration of ACF to aqueous leucine make the system comparatively less order than that of aqueous leucine at lower leucine

concentration. The system looks disordered towards higher leucine concentrations due to unfavorable conformation. The magnitude of disorderness increases with the increasing ACF concentration but seems to be decreasing towards higher leucine concentrations. This suggests that ACF molecules make the system more disordered at lower leucine concentration but for higher leucine concentration the degree of disorderness becomes lower in presence of ACF. This may be due to the structural changes in leucine-water-aceclofenac in such a way that the overall entropy decreases and becomes negative.

IV. CONCLUSION

From the overall study we may conclude that static dielectric constant for aqueous leucine decreases with increasing leucine concentration may be due to the formation of hydration shell around leucine. Higher leucine concentration resulted in lowering the static dielectric constant. During this process hydrogen bonding network will be affected by the presence of leucine. Due to formation of hydration shell relaxation time for aqueous leucine was found to be linearly increasing with leucine concentration over all the measured temperature that indicates more heterogeneous /non-cooperative environment for water molecules or large steric hindrance to the rotational motion of water molecules in the solvent rich and low temperature region. From 298.15 K to 283.15 K static dielectric constant seems to be increasing for all the used concentrations may be due to the formation of induced dipoles via hydration layer with the neighboring or surrounding molecules as the molecules gained lower thermal energy and therefore amplitude of the random thermal motion is restricted. This gives perfect alignment (parallel or antiparallel) with the applied field so that dipoles are more closely aligned with each other; as a result the orientation polarization gets increased and so the static dielectric constant.

The presence of aceclofenac in aqueous leucine resulted in further decrease in the values of static dielectric constant and the variation was observed to be larger at higher ACF concentration. It is because of the molecular interaction between the amino group (NH_3) of the screened leucine by the water molecules and the H from the O-H group of ACF through weak dipole-dipole interaction as a result hydrogen bonding network affected due to the presence of aceclofenac which resulted in lowering the values of static dielectric constant. At highest concentration all the possible hydrogen bonding sites are saturated and no site is available for the bonding to be taking place; as a result there is no further change in the structural conformation which keeps the static dielectric constant almost constant over the used concentrations and temperature.

Increasing values of dielectric relaxation time with increasing ACF concentration reveals non cooperative environment for the molecular or rotational motion for water molecules. This may be due to association between water molecules that form hydration shell around leucine that interacts with ACF through hydration shell or dipole-dipole induced interaction between leucine and ACF through water. As a result rotational motion of water molecules gets restricted and observes only increased values of relaxation time. For aqueous leucine and ACF induced leucine, correlation factors are lower than 1 (due to the anti-parallel orientation of the dipoles) and decreases further towards higher leucine concentrations suggesting increased

correlation between solute dipoles via hydration shell. The correlation between water and the surrounding molecules increases by the presence of aceclofenac for all the used leucine concentrations could be due to the alignment of antiparallel orientations of dipoles between solutes and solvent. This may also be due to the fact that with increasing concentrations of both leucine and aceclofenac; number of water molecules attached to both the solutes under different conformations will be reduced. At higher ACF the g values are very much less than unity is the clear indication of highly aligned antiparallel conformation. The g value was found to be increasing towards lower temperature which confirms the formation of weak interaction between ACF, leucine and water through hydration shell.

For aqueous leucine, the average molar free energy of activation was found in the range 2-3 kcalmol⁻¹. This energy is suggested for the weak hydrogen bonding. The free energy of activation was found almost independent upon temperature as it was found to be either slightly increased towards higher leucine concentrations or almost constant for all the ACF used. This clearly suggests possibility of weak hydrogen bonding between water and leucine due to hydrophobic group present in leucine. This will form hydration layer around leucine molecule. For the ACF induced aqueous leucine, where NH₃ of leucine screened by the water molecules and hydrogen from the OH- group of ACF interact weakly, the molecular interaction slightly increases with concentration and therefore dipoles require more energy in order to attain equilibrium with the applied field, and hence the ΔF increases with increasing leucine concentration for all the ACF concentrations. This suggests possibility of weak hydrogen bond formation between lone pairs of electrons on the negative ions of leucine and the slightly positive hydrogens in water molecules that forms hydration shell around leucine and the hydrogen from the -OH group of ACF molecule through hydration shell.

Change in enthalpy (ΔH) measured at different leucine concentrations in presence of different ACF concentrations was observed to be positive but relatively lower towards higher leucine concentration at higher ACF and suggests favorable bonding at -OH site.

For the aqueous leucine molar entropy of activation was observed to be decreasing over the used concentrations and temperature. Negative entropy towards higher concentration suggests more ordered structure due to weak hydrogen bond formation between amino group of leucine and hydrogen from water molecules that form hydration shell around leucine. The system looks disordered towards higher leucine concentrations due to unfavorable conformation. This suggest that ACF molecules makes the system more disorder at lower leucine concentration but for higher leucine concentration the degree of disorderness becomes lower in presence of ACF. This may be due to the structural changes in leucine-water- aceclofenac in such a way that the overall entropy decreases and becomes negative.

V. ACKNOWLEDGEMENTS

Author SuadAlwaleedy is thankful to School of Physical Sciences, S.R.T.M.UniversityNanded for providing instrumentation facility, the TDR and other infrastructural facilities related to this work. The author is also gratefully acknowledged to Dept. of Science and Technology (DST), New Delhi for providing (TDR) facility through project sanctioned to Dr. A.V.Sarode (SERB/F/4632/2013-2015) and Dr. A.C. Kumbharkhane

(SB/S2/LOP-032/2013).I am also highly thankful to my research colleagues Mrs. Komal B. Kabara, Miss. KambleSaivta and Mr. PavanKachave for timely support during my work.

VI. REFERENCES

- [1]. S.P. Das, A. K.Sahoo, M. Das and A. K. Patnaik,S. K. Pradhan,Molecular interaction of non-steroid anti-inflammatory drug aceclofenac with leucine in dmsO medium: an ultrasonic study., *Int. J. Adv. Res.* 5(6), 1534-1545(2017)
- [2]. S.F. Koly, Kundu S.P., S.Kabir, M.S Amran, M.Z.Sultan, Analysis of aceclofenac and bovine serum albumin interaction using fluorescence quenching method for predictive,preventive, and personalized medicine,*PMA Journal*,6,24, (2015).
- [3]. R. Sathish, J.Ambu, A.Anjana, K.F.H.N.Ahamed, G. S. Rao, Pharmacokinetic And Pharmacodynamic Interaction Between Aceclofenac And Rosiglitazone In Rats,*International Journal of Pharma and Bioscience*,3(2),385-394, (2012)
- [4]. R.W. Gora, S.J. Grabowski & J. Leszczynski, Dimers of formic acid, acetic acid, Form amide and pyrrole-2-carboxylic acid: an ab initio study, *J.Phys.Chem.*109, 6397-6405, (2005) .
- [5]. Bhattacharya, Suman, Krishna S. Peraka, and Michael J. Zaworotko. "The role of hydrogen bonding in co-crystals." *Co-crystals: preparation, characterization and applications*: 33-79 (2018).
- [6]. C.Jelscha,R. N.Devib, C. Bruce, N. B.Guillota, I. Samuel,E.Auberta, Aceclofenac and interactions analysis in the crystal and COX protein active site, *Journalof Molecular Structure*, 1205, 127600, (2020).
- [7]. S. Suresh, S. Gunasekaran, S. Srinivasan,Studies of the molecular geometry, vibrational spectra, Frontier molecular orbital, nonlinear optical and thermodynamics properties of Aceclofenac by quantum chemical calculations, *SpectrochimicaActa Part A: Molecular and Biomolecular Spectroscopy*125 , 239–251,(2014).
- [8]. Makadia, Hiral A., et al. "Self-nano emulsifying drug delivery system (SNEDDS): future aspects." *Asian J. Pharm. Res* 3.1: 21-24 (2013).
- [9]. T. Kim, J Shin, B Lee Enhanced dissolution and bioavailability of poorly watersoluble aceclofenac using solid dispersion system. Denver, Colorado, USA: AAPS, Annual Meeting; October 21–25,(2001)
- [10]. S. F. Koly¹, S. P. Kundu, S. Kabir, M. S. Amran and Md. Z. Sultan, Analysis of aceclofenac and bovine serum albumin interaction using fluorescence quenching method for predictive, preventive, and personalized medicine *Article in EPMA Journal*, 6:24,(2015).
- [11]. Layman, Donald K., et al. "Defining meal requirements for protein to optimize metabolic roles of amino acids." *The American journal of clinical nutrition* 101.6 : 1330S-1338S(2015):
- [12]. Dillon, Edgar L., et al. "Amino acid supplementation increases lean body mass, basal muscle protein synthesis, and insulin-like growth factor-I expression in older women." *The Journal of Clinical Endocrinology & Metabolism* 94.5: 1630-1637. (2009).
- [13]. F.Shakeel, W. Ramadan and S.Shafiq, Solubility and Dissolution Improvement of Aceclofenac using Different Nanocarriers, *Journal of Bioequivalence & Bioavailability*, 1,(2009)

- [14]. T. Mohan, N. osamani, H. Ayachitand D. K. Deshpande *Physics and Chemistry of Liquids*, 46(3), 307–311, (2008).
- [15]. C. Kang, M. Timothy, Korter and David, W. Pratt, *The Journal Of Chemical Physics* 122, 174301-174308 (2005).
- [16]. K Kabara, K Wananje, R Sonsale, S Padghane, A Sarode *journal of pure and applied physics*, 56, 307-310 (2008)
- [17]. Deshmukh, S. D., et al. "Structural and dynamics study of polar liquid mixtures by dielectric and FTIR spectroscopic characterizations." *Journal of Molecular Liquids* 297: 111819(2020).
- [18]. T. Sato, R. Buchner, S. Fernandez, A. Chiba, W. Kunz, *J. Molecular Liquids* 117 93, (2005).
- [19]. Yurasov, Yu I., and A. V. Nazarenko. "Parameter of dielectric loss distribution in the new model for complex conductivity based on Havriliak–Negami formula." *Journal of Advanced Dielectrics* 10.01n02:2060006. (2020).
- [20]. I. Rodriguez-Arteche, S. Cervený, A. Alegria and J. Colmenero, *Dielectric spectroscopy in the GHz region on fully hydrated zwitterionic amino acids*, *Phys. Chem. Chem. Phys.*, 14, 11352–11362 (2012).
- [21]. Lyons, James R., Ehsan Gharib-Nezhad, and Thomas R. Ayres. "A light carbon isotope composition for the Sun." *Nature communications* 9.1: 1-10 (2018).
- [22]. D. Kang, J. Dai, and J. Yuan, *Changes of structure and dipole moment of water with temperature and pressure: A first principles study*, *The journal of chemical physics* 135, 024505 (2011)
- [23]. Gorji, Amin, and Nicola Bowler. "concentration and temperature dependent models of dielectric spectral parameters for low-concentration ionic aqueous solutions." *Precision radio-frequency and microwave dielectric spectroscopy and characterization of ionic aqueous solutions* 1001: 91 (2018).
- [24]. Vishwam, T., et al. "Microwave dielectric relaxation spectroscopy study of propylene glycol/ethanol binary mixtures: Temperature dependence." *Spectrochimica Acta Part A: Molecular and Biomolecular Spectroscopy* 179: 74-82(2017).

Study of the Characteristics of the Soil of Dindori at X-Band Frequency

Dr. Manisha Dhiware

Department of Physics, K. V. N. Naik Arts, Commerce and Science College, Canada Corner, Nasik, SPPU,
Pune, Maharashtra, India

ABSTRACT

Study of physical properties, chemical properties, dielectric properties of soils with varied organic and inorganic matter is utilizable in agriculture to prognosticate quality and fertility of soil. In the present study, the X-band microwave bench is setup in TE₁₀ mode with Reflex Klystron source operating at frequencies 9.56 GHz is used. The study of different physico-chemical characteristics of the soil samples from different location of nearby village of Dindori Tehsil is reported. The chemical, texture and physical properties of the samples under study are reported. The average pH of the soil from selected sites recorded in between 6.93 – 7.68. Organic carbon content ranges from 0.51% to 1.25%, the available nitrogen was recorded in the ranges from 79 to 169 kg/ha, available Potassium in the soil ranges from 205 to 342 kg/ha and available Phosphorus ranges from 43.8 to 138.05 kg/ha. The dielectric constant of soil of this region is 2.72.

Keywords: Dielectric constant, Microwave frequency, Emissivity

I. INTRODUCTION

Irrigation plays an important role in agricultural development. Crop production increases considerably if irrigation is provided to dry lands. Nashik district is well known for the grapes and onion production as well as export. Area under fruits and other cash crops show increase in recent time. One of the main reasons behind this cropping pattern change is the irrigation development in the district [1]. Soils are medium in which crops grow food and cloth. Soil is not only important for agriculture but also more useful for living organisms. Soil as a component of the terrestrial ecosystem fulfills many functions including those that are essential for sustaining plant growth [2].

Soil is the most vital and precious natural resource that sustains life on the earth. Soil is one of the most significant ecological factors, on which plants depend for their nutrients, water and mineral supply. Soil, as most people think, is not a dead inert matter of minerals. But a healthy soil is indeed alive and dynamic consisting of microorganisms. The top-most layer of soil is comparatively richer in nutrients and supports maximum bio-farms. The profile character varies distinctly from place to place, particularly with respect to their depth, colour and composition. The soil is a natural body of mineral and organic material differentiated into horizons [3]. Conventional agriculture has been largely dependent on intensive chemical inputs which

play an important role in improving food productivity to meet human demands. In recent years, most of the farmers are using the excess amount of fertilizers and pesticides. Due to excess use of chemicals soil quality decreases. Small crop also affected due to large use of fertilizers and pesticides. So it becomes essential to analysis of soil parameter [4].

Soil formation is a constructive as well as destructive process [5]. Soil is composed of particles of broken rock that have been altered by chemical and mechanical processes that weathering and erosion. Soil has a complex function which is beneficial to human and other living organism [3]. Soil is not merely a group of mineral particles. It has also a biological system of living organism as well as some other components. The climate and other factor largely affect the soil formation. The mineral composition of soil, the organic matter within it and the environment, all are determined by the chemical properties of soil [6]. It is also of variable depth, which differs from the parent material below in morphology, physical properties and constitution, chemical properties and composition and biological characteristics [7]. Chemistry of soil covers chemical reaction process in the soil pertaining to plant and animal growth and human development [8].

II. MATERIALS AND METHODS

Study Area

The soil quality is of lateritic type and has tiny gravel in it to make it well drained. The gravel assists the roots of the vines to go deeper into the soil and reach the micronutrients embedded deeper in the rich soil. The world Cultivated area is around 56% of the total land area. Nashik is situated 2,000 feet above sea level in the Western Ghats of India. Located in northern Maharashtra approximately 200 km from Mumbai and Pune-it is an important industrial and agricultural area. The climate of the area is mild throughout the year, ranging from winter lows of 8-10°C to summer highs of 32-35°C. The Nashik region consists of two rainfall zones. The first is the high rainfall (80-100 cm) hilly Konkan area in the west, and the second is the low rainfall fertile plain to the east.

Nashik District is a major agricultural centre known for grapes, onion, flowers, sugar cane, rice and popular vegetables. Grapes, onions and flowers are exported all over.



Sample Preparation

Soil samples were collected in the depth of 0-20cm from 10 sites from Dindori tehsil of Nasik District. Soil samples were completely air dried and passed through 2mm sieve and stored in properly labelled cloth bags as per the standard procedures. Quartering technique was used for the preparation of soil samples. The sieved out particles are then oven dried to a temperature around 110° C in order to completely remove any trace of moisture.

Dielectric Measurements

In the present study, Two Point Method has been used to measure the complex dielectric constant of soils. The wave guide cell method is used to determine dielectric constant of these soil samples. The X-band microwave bench is setup in TE₁₀ mode with Reflex Klystron source operating at frequencies 9.56 GHz is used for this purpose. The dielectric cell shorted with matched load is connected at load end. The reflected wave combined with incidental wave to give standing wave patterns. These standing wave patterns used to determine the values of shift in minima resulted due to before and after inserting the sample. The Dielectric constant (ϵ') is determined.

Fig.2 shows experimental set-up of microwave X-band waveguide transmission line.

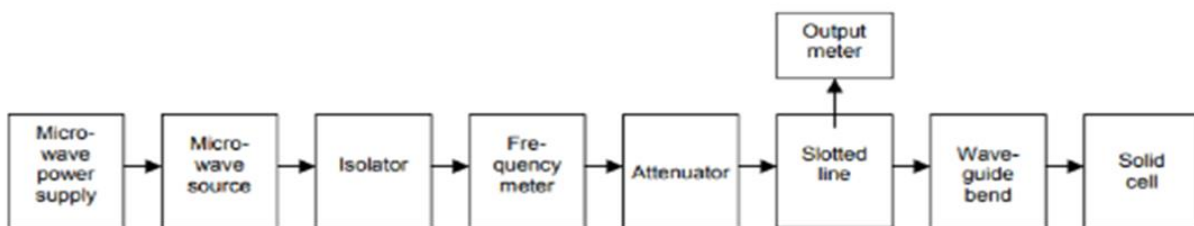


Fig.2: Experimental set-up of microwave X-band waveguide transmission line

The dielectric constant ϵ' of the soils is then determined from the following relation:

$$\epsilon' = \frac{g_E + (\lambda_g / 2a)^2}{1 + (\lambda_g / 2a)^2}$$

and

$$\epsilon'' = -\frac{\beta_E}{1 + (\lambda_g / 2a)^2}$$

Where,

a = Inner width of rectangular waveguide.

λ_g = wavelength in the air-filled guide.

g_E = real part of the admittance

β_E = imaginary part of the admittance

III. RESULTS AND DISCUSSIONS:

Bulk density is most important in converting gravimetric soil moisture to volumetric soil moisture. In the Wang and Schmugge [9] model the bulk density is insignificant. The Dobson et al. [10] model uses the bulk density in its calculations of the conductance properties of the soil water that, in turn, affect the dielectric constant. In remote sensing, early research on soil water-dielectric relationships was hindered by different opinions on exactly which soil water property should be used. Many studies used the gravimetric soil moisture and others related dielectric and emission parameters to moisture-tension characteristics. These approaches have been abandoned in favour of volumetric soil moisture.

Soil texture, density, and structure have important effects that must be accounted for if soil moisture is to be estimated. Recent research has examined the effects of a number of soil characteristics on the relationship between soil moisture and dielectric properties or emissivity. Soil salinity, temperature, and organic matter content are not important at longer wavelengths. Dielectric permittivity of a material is its bulk property which defines the interaction of electromagnetic wave with material.

When a dielectric media are placed in electric field, the number of induced dipoles per unit volume defines the real part of dielectric constant. In presence of oscillating electric field, these dipoles try to align themselves with the field direction. For a given value of the gravimetric moisture content, decrease in the bulk density will decrease the soil dielectric constant. Fig.3 gives variation of dielectric constant with bulk density. Further, dielectric loss decreases with decrease in bulk density. Fig.4 shows variation of dielectric loss with bulk density. The emissivity of soil for normal incidence were calculated using the relation

$$e = 1 - \left[\frac{1 - \varepsilon^{1/2}}{1 + \varepsilon^{1/2}} \right]^2$$

Where ε = dielectric constant of soil

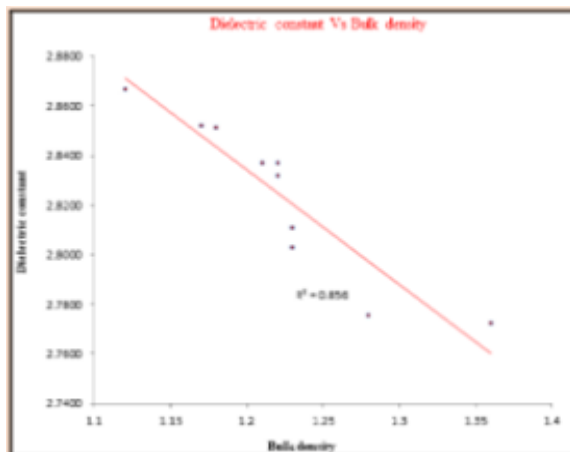


Fig. 3: Variation of dielectric constant with bulk density

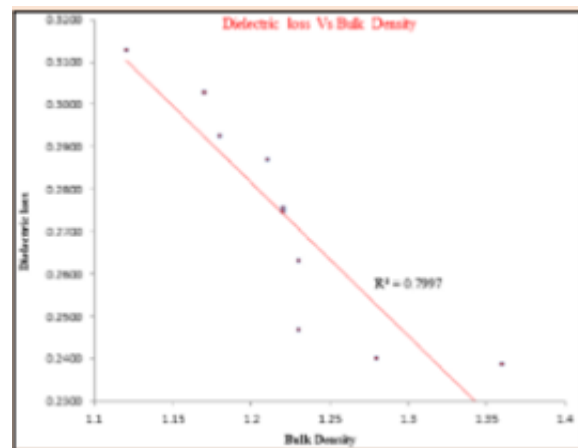


Fig.4: Variation of dielectric loss with bulk density

Emissivity is the important parameter, which provides information about soil. All the natural objects such as soil with °C temperature absolute are capable of emission, absorption and transmission.

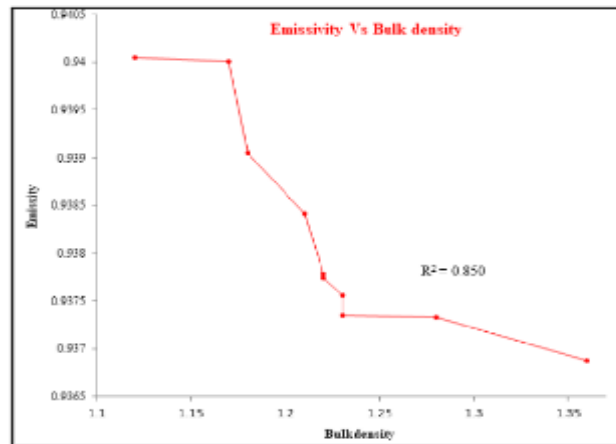


Fig. 5: Variation of Emissivity with Bulk density

The emitted radiation from soil depends upon its dielectric constant, surface roughness, chemical composition, physical temperature, frequency of polarization, and angle of observation. The emissivity of the soil also varies with different moisture contents. Acknowledge of the emissivity of the soil is useful for the efficient use of soil [11]. Fig.5 gives relation between bulk density and emissivity.

IV. CONCLUSION:

Colour of soil of Dindori tehsil is black. Soil texture has remarkable effect on the dielectric properties. Study of physical properties, chemical properties, dielectric properties of soils with varied organic and inorganic matter is utilizable in agriculture to prognosticate quality and fertility of soil. Additionally it is subsidiary for the researchers working in the field of microwave remote sensing. The results from such studies are paramount to understand the fundamental nature of the replication of particular soil to high frequency electromagnetic field.

The soil of east Dindori tehsil region has pH range 6.93-7.64, Electrical conductivity has range 0.33-0.43mm, Phosphate has range 0.056-0.061%, Potash has range 0.39-0.4 %, Sand is between 36-44 %, Silt is between 24-46 % and Clay is between 9-22 %. The dielectric constant 2.71 to 2.72 may be suitable for onion and bajra, 2.773 for grapes. Soil of east Dindori region is good for great production of grapes. Soil pH, organic carbon, electric conductivity, calcium carbonate, water holding capacity and Bulk density of soil directly affects the dielectric constant and dielectric loss ('and ϵ'').

Hence, the different physical properties of soil such as soil structure, soil water content, soil porosity which depends on bulk density of soil affects the dielectric characteristics of soil. Also, emissivity decreases with bulk density.

These results are very useful for the scientists working in the field of microwave remote sensing for soils and also for agriculture scientists.

V. REFERENCES

- [1]. Irrigation Development In The Nasik District, Maharashtra,1970 To 2005 from: <https://www.researchgate.net/publication/292989192>
- [2]. Nwachokor MA, Uzu FO and Molindo WA, Variations in Physicochemical Properties and Productivity Implications for Four Soils in the Derived Savannah of Southern Nigeria, American-Eurasian Journal of Agronomy, 2009,2 (3), 124-129
- [3]. Joffe JS, 1949. Pedology: PedologyPubl., New Brunswick, N. J.
- [4]. Narkhede SR, BhirudSR,Patil NS and Choudhary RR, Physico-Chemical Analysis Of Soil Collected From Chorwad, Tehsil – Bhusawal, Dist. Jalgaon (M.S.) - Int. J. Chem. Sci., 2011, 9(4), 1973-1978.
- [5]. Pujar KG, HiremathSC, PujarAS, Pujeri US and Yadawe M S, Analysis of Physico-Chemical and Heavy Metal Concentration in Soil of Bijapur Taluka, Karnataka Sci. Revs. Chem. Commun. 2012, 2(1), 76-79.
- [6]. Sumithra S, Ankalaiah C, Rao D and Yamuna RT, A case study on physico – chemical characteristics of soil around industrial and agricultural area of yerraguntla, kadapa district, A. P, india. Int. J. Geo. Earth and Environ. Sci. 2013,3(2), 28-34.
- [7]. Rai M M, Principal of soil science. Macmillan India Publication. 2002,38-91.
- [8]. Ashraf M, Bhat GA, Dar ID, Ali M, Physico-Chemical Characteristics of the Grassland Soils of Yusmarg Hill Resort, Eco.Balkanica, 2012,4(1),31-38.
- [9]. J. R. Wang and T. J. Schmugge. An Empirical Model for the Complex Dielectric Permittivity of Soil as a Function of Water Content. IEEE Transactions on Geoscience and Remote Sensing, Vol. GE-18, 1980, pp. 288-295
- [10]. M. C. Dobson, F. T. Ulaby, M. T. Hallikainen, and M. A. ElRaves. Microwave Dielectric Behavior of Wet Soil, Part II: Dielectric Mixing Models. IEEE Transactions on Geoscience and Remote Sensing, Vol. GE-23, 1985, pp. 35-46.
- [11]. O.P.N Calla &R.K.Singh. Indian Journal of Radio & Space Physics, Vol.31, June 2002, Emission characteristics of dry and wet loamy sand soil layered packed at microwave frequency, pp 285-292
- [12]. Ahire DV, Chaudhari PR, Ahire VD and Patil AA, Correlations of Electrical Conductivity and Dielectric Constant with Physico-Chemical Properties of Black Soils, Inte. J. Scientific and Res. Publications, 2013, 3(2), 1-16.
- [13]. Jha AK and Singh JS, Soil characteristics and vegetation development of an age series of mine spoil in a dry tropical environment. Vegetatio ,1991,97, 63 – 76.
- [14]. Hartemink E, Land use change in the tropics and its effect on soil fertility,2010, 19th World Congress of Soil Science, Soil Solutions for a Changing World 1 – 6 August 2010, Brisbane, Australia.Published on DVD.
- [15]. Paudel S and Sah JP, Physiochemical characteristics of soil in tropical sal (Shorea robusta Gaertn.) forests in eastern Nepal. Himala. J. Sci. 2003, 1(2),107-110.
- [16]. N. R. Peplinski, F. T. Ulaby, & M. C. Dobson, “Dielectric properties of soils in the 0.3–1.3-GHz range,” IEEE Trans. Geosci. & Remote Sensing, vol. 33, no. 3, pp. 803–807, 1995.

Chemically Deposited Copper Sulfide Thin Film for Photo Voltaics Performance

R. V. Suryawanshi¹, M. A. Barote¹, R. M. Mahindrakar², G.D. Tingare¹

¹Department of Physics & Electronics, Azad Mahavidyalaya Ausa, Ta. Ausa, Dist. Latur- 413520, Maharashtra, India

²Department of Physics, Arts, Science and Commerce College Naldurga, Ta. Tuljapur, Dist. Osmanabad – 413620, Maharashtra, India

ABSTRACT

Thin films of CuS with 285-310 nm thickness were deposited by chemical bath deposition technique at temperature range from 50 °C to 70 °C. Deposited samples are characterized by XRD, SEM, ultraviolet–visible spectrophotometers (UV-Vis). Uniform films of CuS hexagonal structure with bandgap variation from 2.25 to 2.45 eV and exhibiting n-type conductivity (highest $2.19 \times 10^{-2} (\Omega \cdot \text{cm})^{-1}$). The PEC performance and IV characteristics shows that cell is sensitive to deposition temperature. The observed I_{sc} and V_{oc} are of the order of $213.7 \mu\text{A}/\text{cm}^2$ and 260 mV respectively. An electrochemical PV-conversion efficiency (η) of the deposited sample is 1.12%. Fill factor of the as deposited sample is calculated

Keywords: Thin films, PEC performance, PV-conversion efficiency, Fill factor.

I. INTRODUCTION

Recent research on solar cells has been aimed at lowering the fabrication cost to decrease the price of the energy obtained. In this framework, suitable materials should be easily preparable, inexpensive, and must show stable behavior over a long period of operation. The photo electrochemical (PEC) cells deliver chemical route for trapping solar energy. It represents a promising semiconductor material used in a variety of technologies such as nanoscale electronic devices, cathode material of lithium ion batteries, chemical sensors, and specially photovoltaic cells because of its excellent optical and electronic structures [1-7]. It is used in a multiplicity of applications, namely, as gas sensor [7] and optoelectronic devices as reported by Nair et al. [6, 8]. Numerous techniques have been used to yield copper sulphide thin films such as spray pyrolysis [9, 10], successive ionic layer absorption and reaction techniques [11], photochemical deposition [12], electrodeposition [13], and chemical bath deposition [13–16]. Among them the chemical bath deposition (CBD) method is gorgeous since the technique has a number of advantages over conformist thin film deposition methods. CBD technique is used for making a thin film of copper sulphide, and the outcome of temperature on deposition is also studied. In the present study, an endeavor was made to deposit polycrystalline CuS thin film of copper sulphide on glass substrates by chemical bath deposition method. Structural, morphological, electrical, and optical properties of copper sulphide thin films were examined as a

role of substrate temperature. Such a comprehensive study on the influence of substrate temperature on the assets of copper sulphide thin films regarding photovoltaic performance is still poor.

II. 2. EXPERIMENTAL DETAILS

In the chemical bath deposition method, it is important to control the preparation conditions such as the concentration of solutions, pH of the solutions time for deposition and the temperature. Virtuous quality thin films of CuS were prepared by using aqueous solutions of copper sulfate (CuSO_4) and Thiourea (H_2NCSNH_2) as a basis of Cu and S separately. The experiment was passed out for temperature 50 °C, 55 °C, 60 °C, 65 °C and 70 °C. Microscope glass substrates have been handed through the cleaning stage before deposition in the dilute sulfuric acid. Later it was then washed with acetone and made ready for deposition by fleeting through pure water. Prepared glass slides were deep vertically in an aqueous solution having copper sulfate, thiourea (0.5molarity and 10ml of each), triethanolamine, sodium hydroxide and ammonia were used as a complexing agent. All the solutions were equipped in double distilled water. The pH of the solution was sustained to 10. After (45mini.) the completion of deposition, films were eroded with distilled water [17-19].

III. 3. RESULTS AND DISCUSSION

The fundamental understanding of the semiconductor/electrolyte interfaces have been gained from both electrochemistry and solid state physics and have become mile stones for various processing steps for solar energy conversion device fabrication. For CuS based PV- cell, interface studies with different electrolyte systems have been reported. The open circuit voltage (V_{oc}) and short circuit current (I_{sc}) were noted under 20 mW/cm² incident illumination. It is observed that I_{sc} and V_{oc} are maximum at 1M polysulphide indicating better electrolyte match with CuS electrode and its concentration (1M) was selected for further evaluation of the interfaces [20, 21]. The I_{sc} and V_{oc} for a cell configuration was therefore measured and are shown in Fig.1. It is seen that both I_{sc} and V_{oc} found to be enhanced with electrode temperature at $t = 65$ °C. Characteristic of the PV-device showing a relationship between the open circuit voltage (V_{oc}) and short circuit current (I_{sc}) and decides the extent of maximum power that can be extracted as the output. The device performance parameters such as series and shunt resistances (R_s & R_{sh}), conversion efficiency (η %), fill factor (ff %) etc. were therefore calculated from these characteristics and are cited in Table 1. It appears from the Table 1 that the device performance is significantly improved for the electrode at 65 °C temperature. It is observed that CuS electrode exhibits n – type conduction, similar results are obtained in DC electrical conductivity measurements [18]. The observed enhancement in the electrochemical performance can be attributed to the below modified properties of the electrode material. It is seen that electrode absorption is more in the visible region and is highest of all at $t = 65$ °C showing larger I_{sc} and V_{oc} . The second reason for boosting I_{sc} and V_{oc} is the observed material band gap (2.25-2.45 eV) and improved electrode morphology shown in figure 3 [21]. The band gap and electrode surface morphology contribution understood to enhancement in I_{sc} and V_{oc} [21].

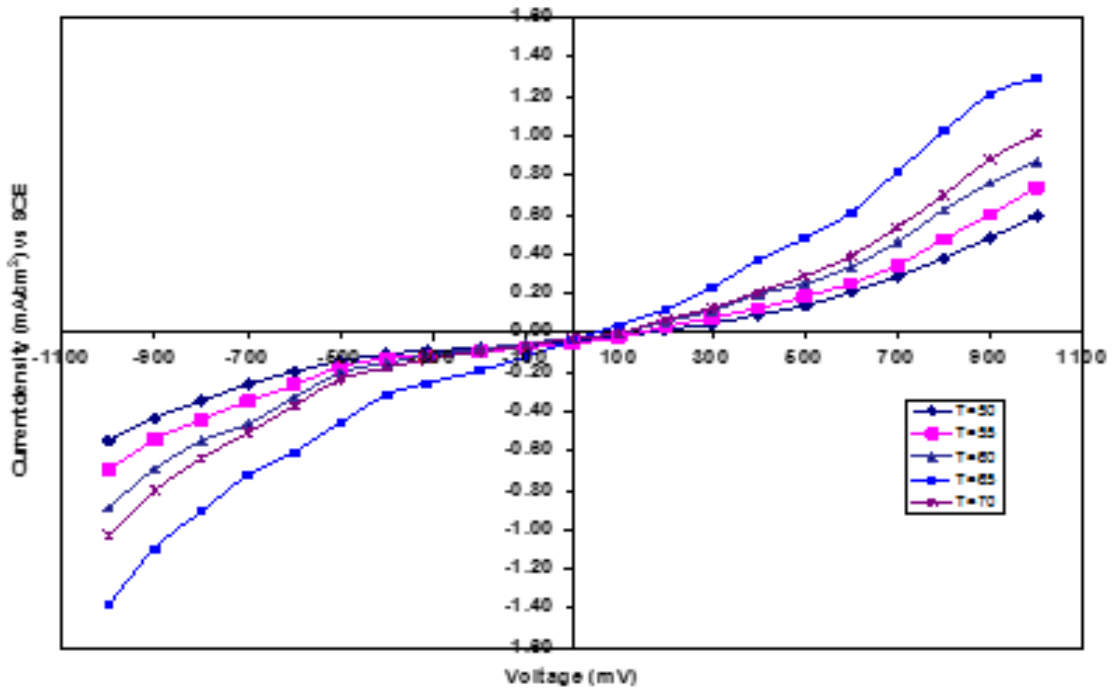


Fig.1. Variation of I_{sc} and V_{oc} as a function of the electrode temperature.

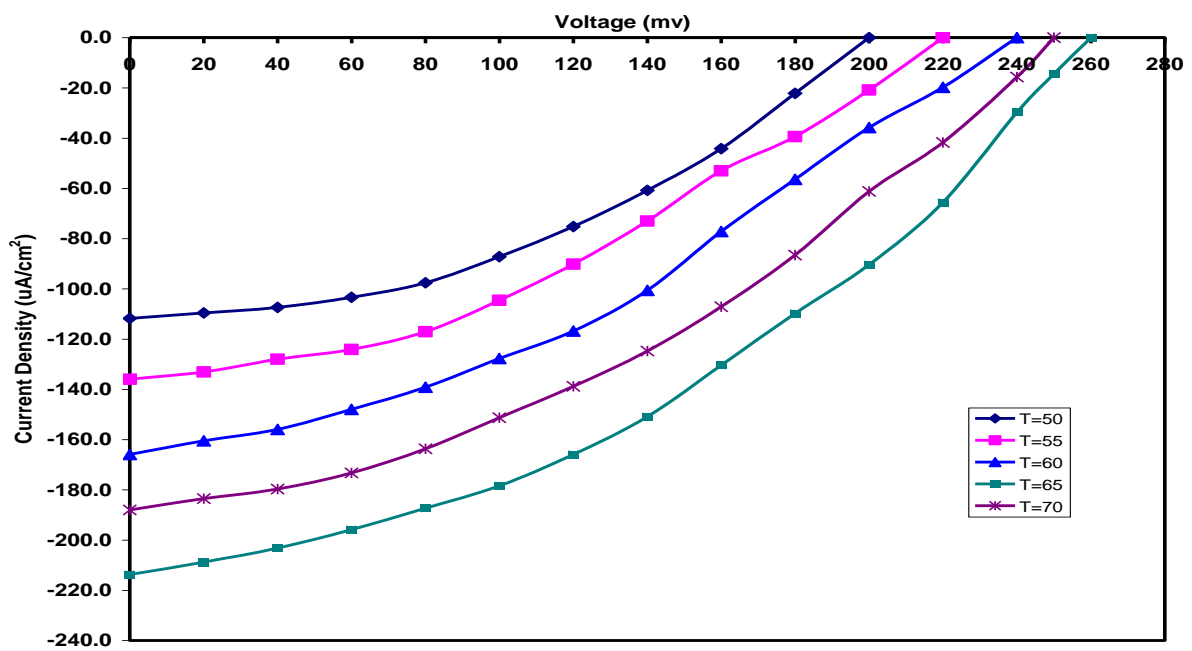


Fig. 2. Power output characteristics of the various PV- devices.

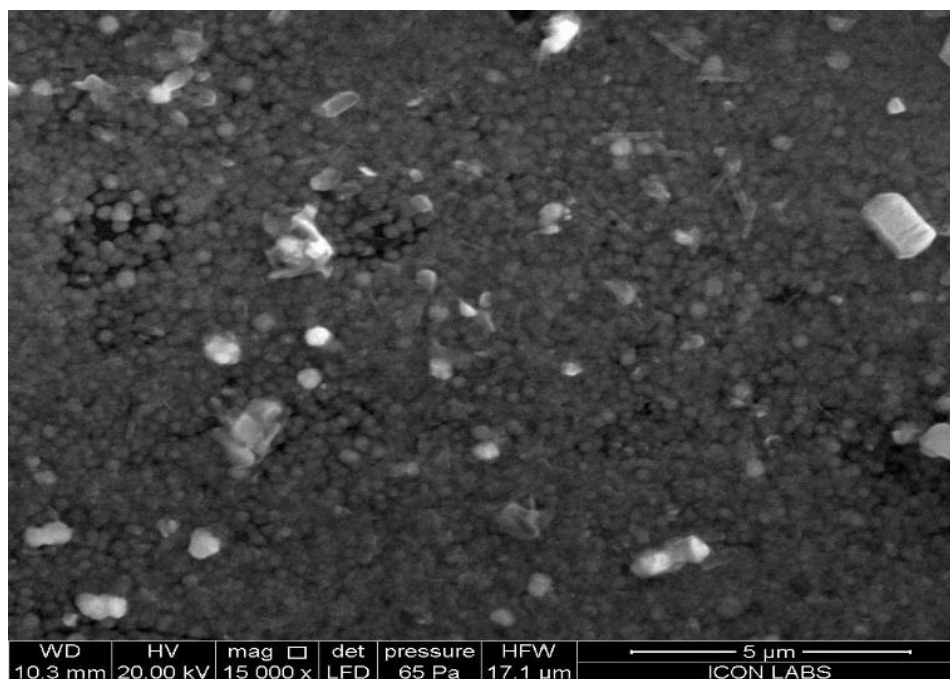


Fig. 3 SEM of CuS thin film at $t = 65\text{ }^{\circ}\text{C}$.

Table 1 Some characteristic performance parameters of the CuS thin films

Temp. $^{\circ}\text{C}$	I_{sc} ($\mu\text{A}/\text{cm}^2$)	V_{oc} (mV)	R_s (Ω)	R_{sh} ($\text{k}\Omega$)	ff	η
50	111.8	200	901	8.32	32.1	0.36
55	136.0	220	826	5.81	32.8	0.52
60	165.9	240	781	3.34	34.8	0.78
65	213.7	260	538	2.85	39.2	1.12
70	188.0	250	637	3.45	34.4	0.81

There is a good grain growth decreasing the intercrystalline resistance, that enhances the electrical conductivity which is clearly reflected in decreased series resistance of a PV – cell that funds to the enhance I_{sc} and V_{oc} . The higher values of I_{sc} and V_{oc} can also be attributed to the crystalline nature of the sample with improved and larger sized crystallites. The capacitance-voltage measurements, to determine the flat band potential (V_{fb}), were also carried out (fig.4) on these electrochemical devices. The Mott-Schottky plots were constructed to determine the flat band potentials and various V_{fb} values are shown in the Table 1. A highest value of V_{fb} , of -850 mV , has been observed for the device with the electrode at 65°C .

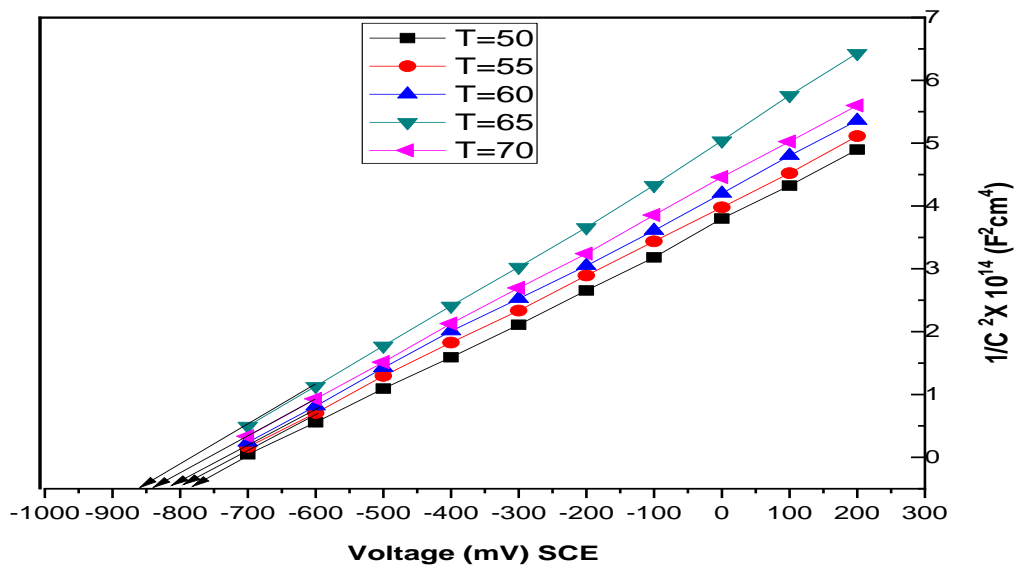


Fig. 4.Determination of the flat band potential for various PV- devices (Mott Schottky plots).

The sensitivity of the different PV- devices to Vis-NIR spectra was also tested. The photocurrent was measured as a function of the input wavelengths from 400 nm to 900 nm and is as shown in Fig.5. The input light was filtered to cut all wavelengths below 400 nm and above 900 nm. Tails in the low wavelength region have often been observed for thin film solar cells and can in general, be ascribed to the poor crystallinity of the semiconductor material that results in a large gap state within the band edges. Envisaging other sources of intraband states, these gap states are responsible for interband transitions which measure the lower optical band gap values.

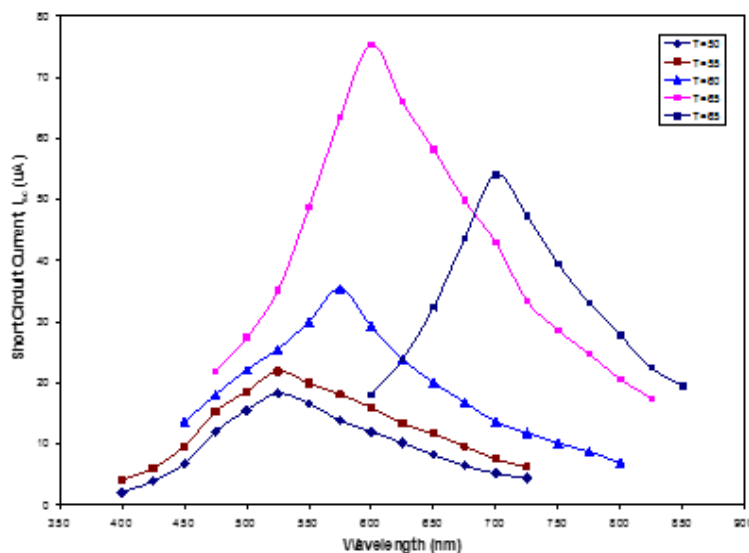


Fig. 5. Action spectra of various PV- devices.

IV. CONCLUSIONS

An effort is made to deposit CuS thin films chemically with a varied temperature to apply them in electrochemical PV- devices. The electrochemical PV- devices were made feasible with these electrodes and polysulphide as an electrolyte system. Upon illumination, these PV devices generated short circuit photo current (I_{sc}) and open circuit photopotential (V_{oc}) which are found to be boosted for the electrode temperature. The maximum conversion efficiency and fill factor are 1.12% and 39.2 respectively. In general temperature of thin film significantly enhances the electrochemical PV performance of the CuS based devices.

V. ACKNOWLEDGMENT

The author, Dr. R.V. Suryawanshi wish to thank the Dept. of Science and Technology, Swami Ramanand Teerth Marathwada University, Nanded for the financial support under minor research project (APDS/Uni.MRP/Sci. &Tech-Electronics/2020-21/2969 Dt. 19.03.2021). The author is grateful to Azad Mahavidyalaya Ausa for this research work.

VI. REFERENCES

- [1]. V. V. Killedar, C. D. Lokhande, and C. H. Bhosale, "(Photo) electrochemical studies on spray deposited Bi₂S₃ thin films from non-aqueous media," Indian Journal of Pure and Applied Physics, vol. 36, no. 11, pp. 643–647, 1998.
- [2]. P. M. Sirimanne, E. V. A. Premalal, P. K. D. D. P. Pitigala, and K. Tennakone, "Utilization of MEH-PPV as a sensitizer in titanabased photovoltaic cells," Solar Energy Materials and Solar Cells, vol. 90, no. 11, pp. 1673–1679, 2006.
- [3]. A. Baheti, P. Tyagi, K. R. J. Thomas, Y. C. Hsu, and J. T. Lin, "Simple triarylamine-based dyes containing fluorene and biphenyl linkers for efficient dye-sensitized solar cells," Journal of Physical Chemistry C, vol. 113, no. 20, pp. 8541–8547, 2009.
- [4]. B. O Regan and M. Gratzel, "A low-cost, high-efficiency solar cell based on dye-sensitized colloidal TiO₂ films," Nature, vol. 353, pp. 737–740, 1991.
- [5]. G. R. R. A. Kumara, A. Konno, G. K. R. Senadeera, P. V. V. Jayaweera, D. B. R. A. de Silva, and K. Tennakone, "Dyesensitized solar cell with the hole collector p-CuSCN deposited from a solution in n-propyl sulphide," Solar Energy Materials and Solar Cells, vol. 69, no. 2, pp. 195–199, 2001.
- [6]. P.K. Nair and M. T. S. Nair, "Chemically deposited SnS-Cu_xS thinfilms with high solar absorptance: new approach to all-glass tubular solar collectors," Journal of Physics, vol. 24, no. 1, p. 83, 1991.
- [7]. A. A. Sagade and R. Sharma, "Copper sulphide (Cu_xS) as an ammonia gas sensor working at room temperature," Sensors and Actuators B, vol. 133, no. 1, pp. 135–143, 2008.
- [8]. P. K. Nair, V. M. Garcia, A. M. Fernandez, H. S. Ruiz, and M. T. S. Nair, "Optimization of chemically

- deposited Cu_xS solar control coatings,” *Journal of Physics D*, vol. 24, no. 3, pp. 441–449, 1991.
- [9]. L. A. Isac, A. Duta, A. Kriza, M. Nanu, and J. Schoonman, “Crystal order in Cu_2S thin films obtained by spray pyrolysis,” *Journal of Optoelectronics and Advanced Materials*, vol. 9, no. 5, pp. 1265–1268, 2007.
- [10]. P. V. Nho, P. H. Ngan, N. Q. Tien, and H. D. Viet, “Preparation and characterization of low resistivity CuS films using spray pyrolysis,” *Chalcogenide Letters*, vol. 9, no. 10, pp. 397–402, 2012.
- [11]. B. Guzeldir, M. Saglam, and A. Ates, “Deposition and characterization of CdS , CuS and ZnS thin films deposited by SILAR method,” *Acta Physica Polonica A*, vol. 121, no. 1, pp. 33–35, 2012.
- [12]. J. Podder, R. Kobayashi, and M. Ichimura, “Photochemical deposition of Cu_xS thin films from aqueous solutions,” *Thin Solid Films*, vol. 472, no. 1-2, pp. 71–75, 2005.
- [13]. C. Wu, J. B. Shi, C. J. Chen et al., “Synthesis and optical properties of CuS nanowires fabricated by electrodeposition with anodic alumina membrane,” *Materials Letters*, vol. 62, no. 6-7, pp. 1074–1077, 2008.
- [14]. E. Guneri and A. Kariper, “Optical properties of amorphous CuS thin films deposited chemically at different pH values,” *Journal of Alloys and Compounds*, vol. 516, pp. 20–26, 2012.
- [15]. S. U. Offiah, P. E. Ugwoke, A. B. C. Ekwealor, S. C. Ezugwu, R. U. Osuji, and F. I. Ezema, “Structural and spectral analysis of chemical bath deposited copper sulfide thin films for solar energy conversions,” *Digest Journal of Nanomaterials and Biostructures*, vol. 7, no. 1, pp. 165–173, 2012.
- [16]. A. K. Singh, S. Mehra, and G. S. Thool, “Synthesis of copper sulphide (CuS) thin film by chemical bath deposition method and its characterization,” *European Chemical Bulletin*, vol. 2, no. 8, p. 518, 2013.
- [17]. Tuba Çayır Taşdemirci, *Study of the physical properties of CuS thin films grown by SILAR method Optical and Quantum Electronics*. Springer Science+Business Media, LLC, part of Springer Nature 2019, 51:245 (2019).
- [18]. R. V. Suryawanshi, R. M. Mahindrakar M. A. Barote, G. D. Tingare B. D. Ingale, A. A. Yadav and E. U. Masumdar *Studies of Copper Sulphide Thin Films Deposited by CBD technique*, *Advances in Engineering science and Technology*, Volume I ISBN: 978-93-91738-89-8.
- [19]. L.P. Deshmukh, R.V. Suryawanshi, E.U. Masumdar and M. Sharon, *$Cu_{1-x}In_xSe_2$ thin films: Deposition by spray pyrolysis and characteristics*. *Solar Energy* 86, 1910 (2012).
- [20]. H. Goslowsky, S. Fiechter, R. Koenekamp, H. J. Lewerenz, *Chemical vapour transport of $CuInS_2$: correlation of growth induced defect structure and photoactivity*, *Sol. Energy Mater.* 13 (1986) 221.
- [21]. Luminita Isaca*, Ionut Popovicia, Alexandru Enesca, Anca Dutaa * *Copper Sulfide (Cu_xS) Thin Films as Possible p-Type Absorbers in 3D Solar Cells* E-MRS Spring meeting 2009, Symposium B Energy Procedia 2 (2010) 71–78.

Analysis of Structural Properties of Nanocrystalline Ni, Zn, Ce, Ferrites

S. L. Gaikwad¹, A.G. Gacche², A. B. Mugutkar³, S. S. Jadhav^{4*}

¹Department of Physics, Pansare Mahavidyalaya, Arjapur, Dist. Nanded 431711, Maharashtra, India

²Department of Physics, Vasantrao Naik Mahavidyalaya, Nanded 431603, Maharashtra, India

³Department of Physics, Bahirji Smarak Mahavidyalaya, Basmath431512, Maharashtra, India

⁴Department of Physics, D. S. M's Arts, Commerce and Science College, Jintur, 431509, Maharashtra, India

ABSTRACT

The nanocrystalline spinel ferrite system, $\text{Ni}_{0.7}\text{Zn}_{0.3}\text{Ce}_x\text{Fe}_{2-x}\text{O}_4$ ($x=0.025, 0.05, 0.075, 0.1$) is synthesized by sol gel auto combustion method. The structural properties of the ferrites restudied by means of powder X-ray diffraction (XRD) and Fourier Transform Infra-Red spectroscopy (FTIR). The spinel phase along with the secondary phase of CeO was revealed from the analysis of XRD of the ferrites. The parameters obtained from the XRD includes lattice parameter, bond lengths, tetra and octahedral edges of the ferrite crystals. The variations of parameters are influenced by the amount of Ce composition within the ferrites.

Keywords: Ni-Zn Ferrites; XRD; FTIR; Bond lengths; Tetrahedral and octahedral edges

I. INTRODUCTION

The nano crystalline particles of spinel ferrites have a great potential in the field of nano science and technology due to their interesting properties such as nanoprticle size with high surface area to volume ratio, high saturation magnetization, increased coercivity and retentivity and improved dielectric properties. A new class of nano materials formed in this way is found to be suitable for the applications such as high density magnetic storage, catalysis, magnetic drug delivery, gas sensors, magneto caloric effect [1], etc.

The Nickel-Zinc (Ni-Zn) ferrites are the soft ferries with low coercivity but high electrical resistivity. Due to their magnetic and electrical properties they have potential applications as the cores of power transformers used in high frequency (MHz) range [2]. Low power loss at all operating frequencies is the unique feature of the Ni-Zn ferrite, which makes it a vital material in the applications like SMPS, microwaves, R/W heads [3]. Specifically for microwave applications, the ferrites with a tangent loss, $\tan\delta \leq 1000$ are suitable and hence the Ni-Zn ferrites are the most suitable material for the microwave applications like isolators, circulators and phase shifters [4].

The substitution of rare earth ions in Ni-Zn ferrite crystal is proved to be an effective way to modify the magnetic and electrical properties of the ferrite [5]. The larger radius and the stable +3 valence have an important role in modifying the properties of the ferrite. The Yittrium ion substitution in Ni-Zn ferrite was reported to modify the properties like coercivity (H_c), susceptibility, Remanent magnetization and Curie

temperature (T_c), where H_c and T_c are increased with the increasing concentration of Y ions [6]. Rare earth (Nd, Ce, La and Pr) substituted Ni-Zn ferrites are proved to be a promising candidate for high frequency applications [7]. A large increase in electrical resistivity with the reduced relative loss factor was reported in case of Y, Eu and Gd substituted Ni-Zn ferrites [8]. The doping of Pr^{3+} ions in Ni-Zn ferrite has reduced the dielectric loss at radio frequency, while there is a great increase in the value of permeability at 36MHz, proving the material as a promising one for high frequency applications [9].

A report on microwave properties of Lithium ferrite shows that the microwave absorbing ability of the lithium ferrite was increased with the proper level of Ce^{3+} doping [10]. The Ce^{3+} substituted Co-Cr ferrites with moderate saturation magnetization and coercivity, $H_c > 600$ Oe, were reported to be the suitable material for magnetic recording media, switching and high frequency applications [11]. Improvement in dielectric properties of Lithium ferrite due to optimum substitution was reported elsewhere [12]. A remarkable influence of Ce^{4+} ions on magnto-structural properties of $NiFe_2O_4$ was reported in previous report [13], where the saturation magnetization was increased and coercivity decreased with the increasing concentration of Ce^{4+} ions.

The research survey suggests that, there is an improvement of properties of the ferrites due to substitution of Cerium ions and it gives rise to the ferrites with more application potential. With this and by considering the technological importance of Ni-Zn ferrites, we decided to study the synthesis, and structural properties of Cerium substituted nanocrystalline Ni-Zn ferrites.

II. SYNTHESIS AND METHODS OF MEASUREMENTS

The Cerium (Ce^{3+}) substituted Ni-Zn ferrites (NZC) with chemical formula, $Ni_{0.7}Zn_{0.3}Ce_xFe_{2-x}O_4$ ($x=0, 0.025, 0.05, 0.075$ and 1) were synthesized by sol gel auto combustion method [14]. The starting chemicals used were of analytical reagent grade (99.99% pure) nitrates, $Ni(NO_3)_2 \cdot 6H_2O$, $Zn(NO_3)_2 \cdot 6H_2O$, $Fe(NO_3)_3 \cdot 9H_2O$, $Ce(NO_3)_3 \cdot 6H_2O$ and citric acid $C_6H_8O_7 \cdot H_2O$. All chemicals were supplied by Lobachemie except cerium nitrate, which was supplied by Acros, India. The clear solutions of nitrates and citric acid were prepared in the minimum amount of double distilled water, by keeping nitrate to citrate ratio equal to 1:3. The aqueous solutions of nitrates and citric acid are mixed together while maintaining the $pH \approx 7$ by addition of an appropriate amount of ammonia solution. This solution was kept on hot plate ($100^\circ C$) with a constant magnetic stirring. The continuous evaporation of water molecules give rise to a viscous gel, which is dark brown in colour. The role of citric acid as a chelating agent begins with removal of all water molecules as an auto ignition of the gel which continues up to few tens of minutes. The blackish brown coloured ashes called precursors were formed, which were powdered to give fine homogeneous ferrite powder. This powder was then sintered in a constant temperature furnace for 3Hrs at $600^\circ C$. The annealed powder is used for characterization and measurement of the properties.

The NZC ferrites annealed at $600^\circ C$ were used to obtain X-ray diffractograms at room temperature by means of Philips: PW1830 with a scanning rate of 10° per minute, within 10° to 80° of 2θ range.

III. RESULT AND DISCUSSION

The Fig. 1 shows X-ray diffractograms of NZC ferrites indexed to reveal FCC structure. The spinel phase with a secondary phase of CeO was revealed from the indexing of XRD of the ferrites. The lattice parameter, X-ray density, bulk density, porosity and specific surface area, particle size are the parameters calculated from the analysis of XRD data by using the reported formulae [15]. The values of the parameters are listed in Table 1, where it is clear that the lattice parameter increases with increasing Ce concentration x . This can be explained on the basis of Vegard's law. The replacement of smaller ions of Fe^{3+} (0.64\AA) by relatively larger ions of Ce^{3+} (1.034\AA) causes swelling of the lattice cell, thereby increasing the lattice parameter [16]. The particle size calculated using Debye-Scherrer formula [15] is listed in Table 1. The particle size shows random variation with Ce content x , which may be due to the variation of the reaction condition favouring the formation of new nuclei during sol-gel synthesis [17].

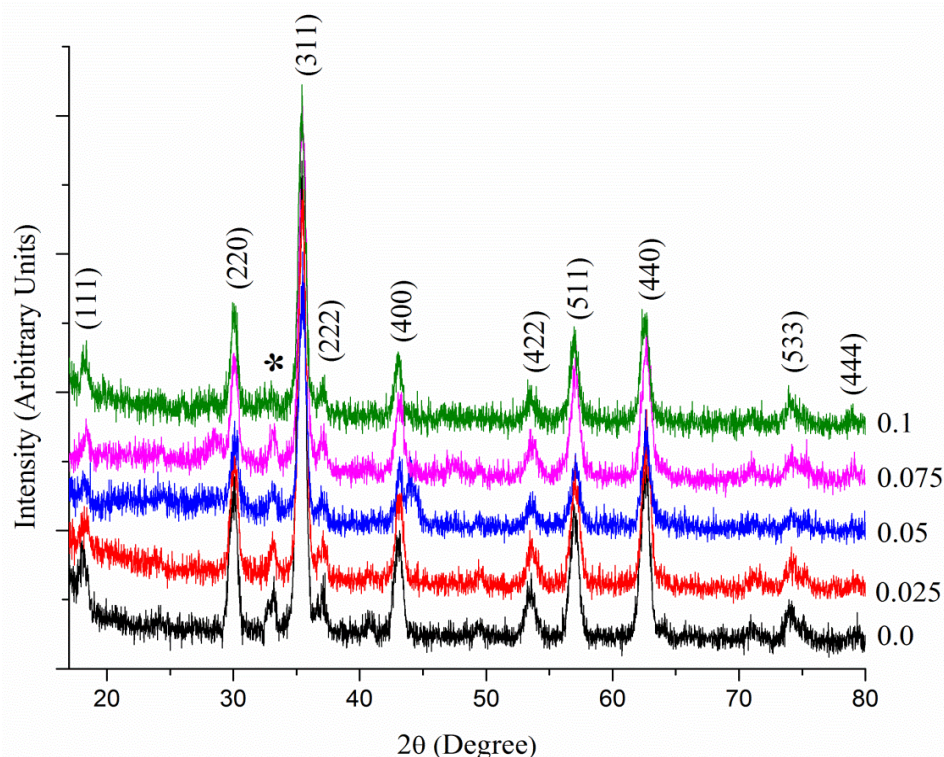


Fig. 1 X-ray diffractograms of NZF ferrites with (hkl) Miller indices of the peaks.* The peak showing phase of CeO.

The X-ray density d_x decreased with increasing Ce content x . This is attributed to the decrease in values of lattice parameter with increasing Ce content x . Similar results were reported earlier [18]. The enlisted values of bulk density d and porosity P show exactly opposite trends. The bulk density decreases and porosity increases with the increasing Ce content x . The identical results were reported earlier for Ce substituted Ni ferrites [13]. The values of specific area S vary from 76.41 to $105.33\text{m}^2/\text{gm}$. On average, specific surface area increases with decreasing particle size. Similar result is reported by George *et. al.* [19].

Table 1: Lattice constant (a), particle size (t), x-ray density (d_x), bulk density (d), porosity (P) and surface area (S) of NZF ferrites

x	a(Å)	t(nm)	d_x (g/cm ³)	d(g/cm ³)	P(%)	S(m ² /g)
0	8.372	24	5.545	3.187	42.53	78.44
0.025	8.375	25	5.491	2.868	47.77	83.69
0.05	8.384	21	5.379	2.712	49.57	105.33
0.075	8.394	21	5.311	2.946	44.54	96.99
0.1	8.414	28	5.367	2.804	47.75	76.41

The values of tetrahedral and octahedral bond lengths (d_{AX} , d_{BX}) and shared and unshared edges (d_{AXE} , d_{BXE}) as well as magnetic hopping lengths L_A and L_B were calculated by using formulae reported earlier [15]. These values are listed in Table 2. It is clear that values of d_{AX} , d_{BX} , d_{AXE} , d_{BXE} and hopping lengths L_A , L_B increase with increasing Ce content x. This increase in values is due to increasing values of lattice parameter.

Table 2: Tetra and octa bonds (d_{AX} , d_{BX}), Tetra (d_{AXE}) and octa (d_{BXE} shared and unshared), magnetic hopping lengths (L_A and L_B) of the NZF ferrites.

'x'	a (Å)	d_{AX}	d_{BX}	d_{AXE}	d_{BXE}		L_A	L_B
					shared	unshared		
0	8.372	1.899	2.046	3.101	2.817	2.967	3.625	2.959
0.025	8.375	1.900	2.046	3.102	2.818	2.968	3.626	2.960
0.05	8.384	1.902	2.049	3.106	2.821	2.971	3.630	2.964
0.075	8.394	1.904	2.051	3.109	2.824	2.975	3.634	2.967
0.1	8.414	1.909	2.056	3.117	2.831	2.982	3.643	2.974

IV. CONCLUSIONS

The nanocrystalline particles of Ce³⁺ substituted Ni-Zn ferrites having formula Ni_{0.7}Zn_{0.3}Ce_xFe_{2-x}O₄ (x=0.025, 0.05, 0.075, 0.1) were successfully synthesised by sol-gel auto combustion method. The spinel phase along with the secondary phase of CeO was observed in the ferrite crystals. The remarkable impact of Ce³⁺ ion doping on lattice parameter was observed. The bond lengths, tetra and octa edges and magnetic hopping lengths increase with increasing Ce³⁺ doping.

V. REFERENCES

- [1]. S. Burianova, J. Poltiero-vepravova, P. Holec, J. Plocek, "Magnetocaloric phenomena in Mg-ferrite Nanoparticles", International Conference on Magnetism (ICM 2009) Journal of Physics: Conference Series, 2010, 200, 072015(1-4).
- [2]. A. Goldman, Modern Ferrite Technology (Van Nostrand Reinhold, New York,), 1990, 145.
- [3]. M. Siva Ram Prasad, BBVSV Prasad, B. Rajesh, K.H. Rao, K. V. Ramesh, "Magnetic properties and DC

- electrical resistivity studies on cadmium substituted Nickel-zinc ferrite system”, *J MagnMagn Mater*, 2011, 323, 2115-2121.
- [4]. A. Verma, D. C. Dube, “Processing of Nickel–Zinc Ferrites Via the Citrate Precursor Route for High-Frequency Applications”, *J. Am. Ceram. Soc.*, 2005, 88 (3), 519–523.
- [5]. N.Rezlescu, E.Rezlescu, C. Pasnicu, M. L.Craus, “Effects of the rare-earth ions on some properties of a nickel-zinc ferrite”, *J. Phys.: Condens. Matter*, 1994, 6, 5707-5716.
- [6]. V. Jancarik, E. Usak, M. Soka, M. Usakova, “Magnetic properties of Yttrium substituted NiZn ferrites”, *ActaPhysica Polonica A*, 2014, 126, 90-91.
- [7]. R. Kesavamoorthi, C. R. Raja, “Substitution Effects on Rare-Earth Ions-Doped Nickel-Zinc Ferrite Nanoparticles”, *J Supercond Nov Magn*, 2017, 30, 1207-1212.
- [8]. G. L. Sun, J. B. Li, J. J. Sun, X. Z. Yang, “The influences of Zn²⁺ and rare-earth ions on the magnetic properties of nickel-zinc ferrites”, *J Mag Magn Mater*, 2004, 281, 173-177.
- [9]. Z. Peng, X. Fu, H. Ge, Z. Fu, C. Wang, L. Qi, H. Miao, “Effect of Pr³⁺ doping on Ni-Zn ferrites by one-step synthesis”, *J MagnMagn Mater*, 2011, 323, 2513-2518.
- [10]. C. Sun, K. Sun, “Preparation and microwave absorption properties of Ce-substituted lithium ferrite”, *Solid Stat Commn.*, 2007, 141, 258-261.
- [11]. G. Mustafa, M. U. Islam, W. Zhang, Y. Jamil, A. W. Anwar, M. Hussain, M. Ahmad, “Investigation of structural and magnetic properties of Ce³⁺ substituted Nanosized Co-Cr ferrites for variety of applications”, *J Alloy Comp*, 2015, 618,, 428–436.
- [12]. V. Verma, R. K. Kotnala, V. Pandey, P. C. Kothari, “The effect on dielectric losses in lithium ferrite by cerium substitution”, *J Alloy Comp*, 2008, 466, 404–407.
- [13]. S. E. Shirsath, S. S. Jadhav, B. G. Toksha, S. M. Patange, K. M. Jadhav, “Influence of Ce⁴⁺ ions on structural and magnetic properties of NiFe₂O₄”, *J. Appl. Phys.*, 2011, 110, 013914 (1-5).
- [14]. S. E. Shirsath. S. S. Jadhav, M. L. Mane, S. Li, “Ferrites obtained by Sol-Gel method”, *Handbook of sol-gel science and technology*, Springer Int. Pub., 2017, 4-6.
- [15]. S. S. Jadhav, S. E. Shirsath, B. G. Toksha, S. M. Patange, S. J. Shukla, K. M. Jadhav, “Structural properties and cation distribution of Co-Zn nano ferrites” *Int. J. Mod. Phys. B*, 2009, 23, 5629-5638.
- [16]. S. K. Gore, U. B. Tumberphale, S. S. Jadhav, R. S. Kawale, Mu. Naushad, R. S. Mane, “Microwave assisted synthesis and magneto-electrical properties of Mg-Zn ferromagnetic oxide nanostructures”, *Physica B*, 2018 530 (2018) 177–182.
- [17]. B. Vishwanathan, V. R. K. Murthy, *Ferrite Material Science and Technology*, Narosa Publ. House, New Delhi, 1990.
- [18]. K. S. Lohar, S. M. Patange, S. E. Shirsath, S. S. Jadhav, “Structural and frequency dependent dielectric properties of magnesium doped nickel ferrites”, *International Conference on Nanoscience, Technology and Societal Implications NSTSI11*, IEEE Conference Series, 2011, 1-2, DOI 10.1109/NSTSI.2011.6111774.
- [19]. M. George, S. S. Nair, A. M. John, P. A. Roy, M. R. Ananthraman, “Structural, magnetic and electrical properties of the sol-gel prepared Li_{0.5}Fe_{2.5}O₄ fine particles” *J. Phys. D: Appl. Phys.*, 2006, 39, 900-910.

Dielectric Relaxation Study of DPG Using a TDR at 20°C

Pankaj A. Chalikwar¹, Abdulrahman W. Pathan², K. R. Borude¹, G. R. Mahajan^{3*}

¹KKM college Manwath, Dist. Parbhani 431505, Maharashtra, India

²ASC college Badnapur, Dist. Jalna 431202, Maharashtra, India

³Shri Datta Arts, Commerce and Science College, Hadgaon, Dist. Nanded, 431712, Maharashtra, India

ABSTRACT

Study of Dipropylene Glycol (DPG)-water mixture have been studied by time domain Reflectometry technique in the frequency range of 10MHz to 30GHz. The measurements have been done at temperature 20°C at different volume fractions. The dielectric parameters such as static dielectric constant and relaxation time for mixture have been reported here. The molecular interaction between Dipropylene Glycol and water is discussed using Kirkwood correlation factor (g^{eff}) and dielectric constant for mixtures. The dielectric relaxation behavior of binary mixtures of Dipropylene glycol-water has been fitted with Cole-Davidson model having an asymmetric distribution of relaxation time. These parameters have been fitted to the Bruggeman mixture formula in the non-linear case.

Key words: Dielectric relaxation, Time Domain Reflectometry, Glycol, Kirkwood correlation factor

I. INTRODUCTION

Over the past several years, the aqueous mixtures of glycols and alcohols have been extensively investigated by means of the dielectric relaxation as a function of -OH group to understand the significance of hydrogen bond interaction. [1-2] Dipropylene glycol (DPG) reveals a strong tendency to form H bonds. Terminal hydroxyl groups of DPG may participate in two types of hydrogen bonds: end-to-end and end-to-ether (C-O-C) groups [3] both can lead to inter and intra molecular structures.

The dielectric relaxation study is very helpful for the understanding of intermolecular interaction and the hydrogen bonding interaction in aqueous mixture due to dipole-dipole interaction. The main interest of the study is to understand the structural and dynamical behavior of aqueous DPG using Time Domain Reflectometry (TDR) Technique. Previously different techniques were used for characterization such as light scattering [4-6], optical Kerr-effect [7] as well as photo thermal. Moreover some physical properties of aqueous mono, di and tri propylene glycol have been reported. [8] The dielectric spectra of propylene glycol and tri-propylene glycol have been studied earlier [9-10] using TDR technique.

The objectives of the present work are to investigate temperature dependent dielectric relaxation properties of DPG-water systems using TDR technique in the frequency range of 10 MHz to 30 GHz. The static dielectric constant, relaxation time, Bruggeman factor, Kirkwood correlation factors, excess dielectric permittivity and thermodynamic parameters have been reported for DPG-water mixtures.

II. EXPERIMENTAL DETAILS

Materials and sample preparation

DPG (100% pure) was purchased from Merck India Limited and used without further purification. The HPLC grade double distilled water was used in preparation of aqueous DPG mixtures. 11 different Samples of total volume 5ml each were prepared such that; a volume fraction 0.1 indicates 0.5ml of DPG added to 4.5ml of water, a volume fraction of 0.2 indicates 1.0ml of DPG added to 4.0ml of water and vice versa. For the measurement samples were placed in an electronically temperature-controlled bath within accuracy of ± 0.1 °C.

The step pulses recorded without sample $R_1(t)$ and with sample $R_x(t)$ and are subtracted and added to get

$$p(t) = [R_1(t) - R_x(t)] \quad 1$$

$$q(t) = [R_1(t) + R_x(t)] \quad 2$$

The complex reflection coefficient $\rho^*(\omega)$ over a frequency range of 10 MHz to 30 GHz were determined as follows.

$$\rho^*(\omega) = \frac{c p(\omega)}{j\omega d q(\omega)} \quad 3$$

Where $p(\omega)$ and $q(\omega)$ are Fourier transforms of $p(t)$ and $q(t)$ obtained using summation and Samulon methods [10] respectively, c is the velocity of light, ω is angular frequency and d is effective pin length (0.16 mm). The complex permittivity spectra $\varepsilon^*(\omega)$ was obtained from reflection coefficient spectra $\rho^*(\omega)$ by applying the bilinear calibration method suggested by Cole [11]. Figure 1 shows frequency dependent complex permittivity spectra $\varepsilon^*(\omega)$ for DPG–water mixtures at 20 °C.

III. RESULTS AND DISCUSSIONS

Dielectric Constant and Relaxation time

Dielectric relaxation for aqueous DPG is described by the Havriliak–Negami equation [12]

$$\varepsilon^*(\omega) = \varepsilon_\infty + \frac{\varepsilon_0 - \varepsilon_\infty}{[1 + (j\omega\tau)^{1-\alpha}]^\beta} \quad 4$$

Where ε_0 is the static permittivity, ε_∞ is the permittivity at high frequency, τ is the relaxation time, α and β are the empirical parameters for the distribution of relaxation times with values between 0 and 1. Temperature dependent dielectric relaxation parameters for aqueous solutions of DPG are listed in Table 1. The errors in the least significant digit are also reported.

The Relaxation time increases systematically in aqueous solutions of DPG as shown in table 1 suggests that water structure is modified due to hydrogen bond by the DPG so as to produce an increase in relaxation time in the mixture. In DPG rich regions relaxation time increases rapidly this may due to higher viscosity of DPG as relaxation time and viscosity has linear relationship. [13]

Table 1. Dielectric Relaxation Parameters for aqueous solution of DPG at 20°C

Of DPG	Vol. Fract.		τ (ps)	β
	ϵ_∞	ϵ_0		
0.0	3.92(3)	79.10(7)	8.82(1)	1.0000(1)
0.1	2.000(1)	72.16(10)	13.16(03)	0.9723(1)
0.2	2.000(1)	63.35(22)	11.57(04)	1.0000(1)
0.3	2.000(1)	58.98(08)	10.47(02)	1.0000(1)
0.4	2.237(2)	52.32(08)	36.00(01)	0.8451(1)
0.5	2.425(2)	48.48(08)	48.28(02)	0.8245(0)
0.6	3.750(3)	42.00(14)	82.42(07)	0.7929(3)
0.7	4.522(2)	37.91(15)	138.56(01)	0.7636(3)
0.8	5.073(2)	35.17(18)	209.30(03)	0.7701(4)
0.9	4.880(2)	28.47(16)	320.07(06)	0.7966(5)
1.0	3.867(1)	20.16(13)	771.20(17)	0.7679(5)

Note: Numbers given in parentheses denote uncertainties in the least significant digits obtained by the least square fit method, e.g. 20.59(14) means 20.59 ± 0.14 and 0.7564(7) means 0.7564 ± 0.007 .

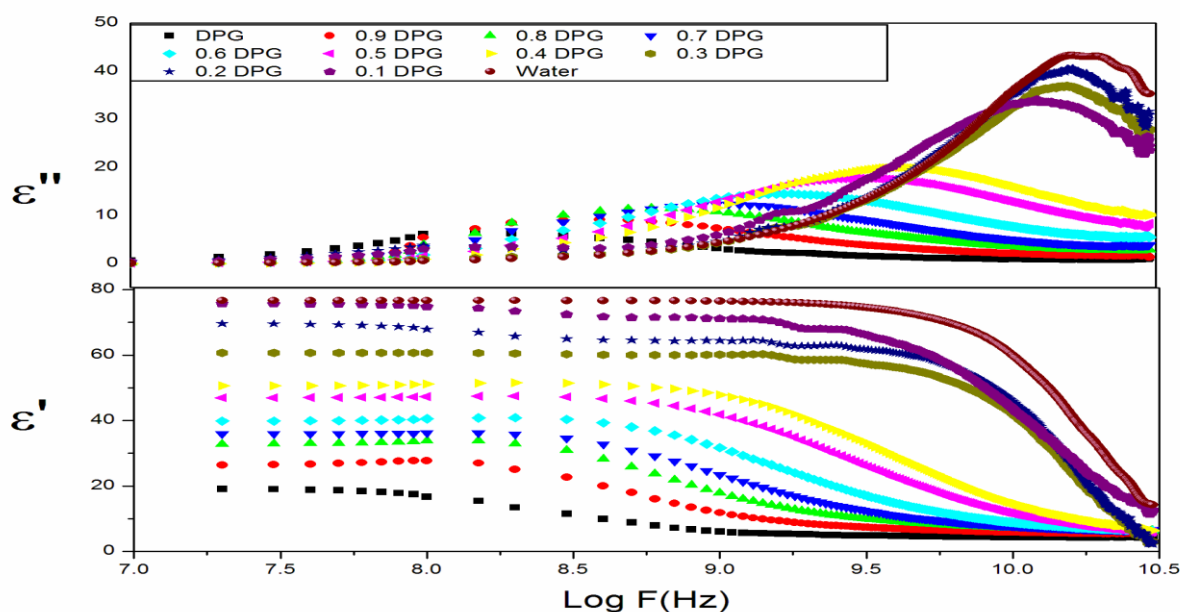


Figure 1 Complex permittivity spectra for DPG-water mixtures at 20°C

Kirkwood correlation factor

Static dielectric constant for the mixture can be explained using the Kirkwood-Frohlich equation as follows [14-15],

$$\frac{4\pi N\rho}{9kTM} g\mu^2 = \frac{(\epsilon_0 - \epsilon_\infty)(2\epsilon_0 + \epsilon_\infty)}{\epsilon_0(\epsilon_\infty + 2)^2} \quad 5$$

Where μ , ρ and M correspond to the dipole moment in gas phase, density and molecular weight respectively, k is the Boltzmann constant, T is the temperature and N is the Avogadro's number.

The Kirkwood correlation factor “ g ” determined from the dielectric constant gives information on the collective orientation correlation between molecules.

$$\frac{4\pi N}{9kT} \left[\frac{\mu_w^2 \rho_w}{M_w} V_a + \frac{\mu_A^2 \rho_A}{M_A} (1 - V_a) \right] g^{eff} = \frac{(\epsilon_{0m} - \epsilon_{\infty m})(2\epsilon_{0m} + \epsilon_{\infty m})}{\epsilon_{0m}(\epsilon_{\infty m} + 2)^2} \quad 6$$

With V_a and $1 - V_a$ as volume fractions of liquids a (water) and b (DPG), respectively. In the mixtures the values of g^{eff} show (Table 2) decreasing trend with the increasing concentration of DPG molecules in the mixtures. This indicates the decrease in interaction between the molecules of the system with increase in volume fraction of DPG in the solution. The values of g^{eff} are greater than unity for all the concentration and all three temperatures suggesting parallel orientation of electric dipoles.

Table 2. Kirkwood correlation factor for DPG Water Mixture at 200C.

Volume Fraction of Solute

0.0	2.79(16)	0.1	2.74(16)
0.2	2.62(15)	0.3	2.68(16)
0.4	2.65(16)	0.5	2.79(16)
0.6	2.82(17)	0.7	3.07(18)
0.8	3.63(22)	0.9	4.09(24)
1.0	4.88(29)		

Note: Numbers given in parentheses denote uncertainties in the least significant digits, e.g. 2.79(16) means 2.79 ± 0.16

Bruggeman factor

The Bruggeman equation [16] is another parameter which may be used as an indicator of solute solvent interaction. The Bruggeman factor (f_B) is given by,

$$f_B = \left[\frac{(\epsilon_{0m} - \epsilon_{02})}{(\epsilon_{01} - \epsilon_{02})} \right] \left(\frac{\epsilon_{01}}{\epsilon_{0m}} \right)^{\frac{1}{3}} = 1 - V \quad 7$$

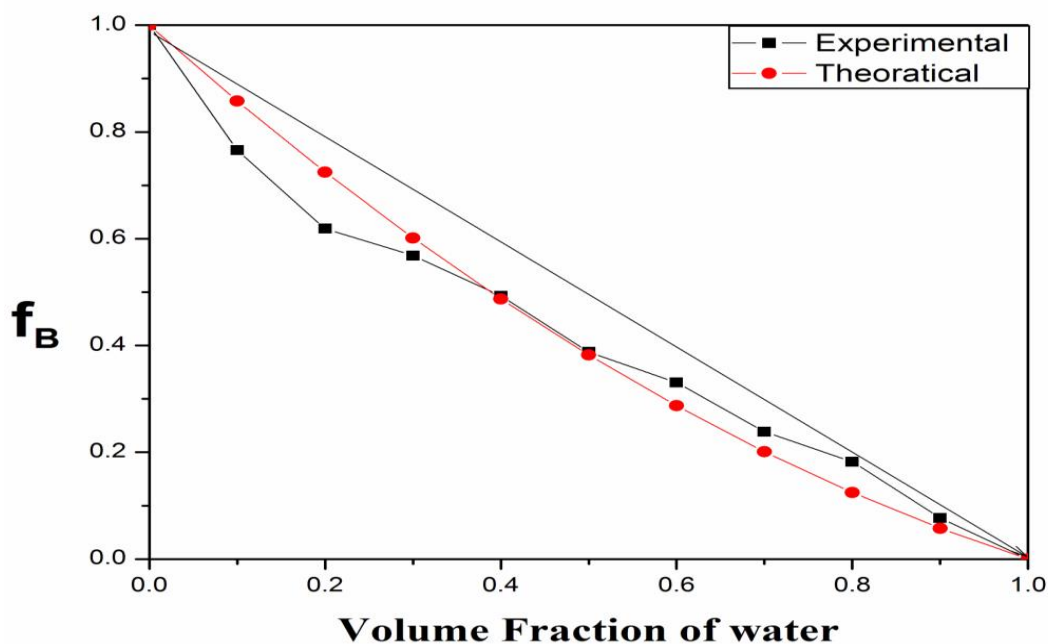


Figure2 Plot of Bruggeman factor (f_B) as function of Volume fraction of water at 20°C

Where ϵ_{0m} , ϵ_{01} and ϵ_{02} are the static dielectric constant corresponding to mixture, solute and solvent respectively; V - is the volume fraction of solvent (water). From above equation, the linear relation is expected from a plot f_B Vs Volume fraction of water. But in binary liquids, there is non-linear relationship.

$$f_B = \left[\frac{(\epsilon_{0m} - \epsilon_{02})}{(\epsilon_{01} - \epsilon_{02})} \right] \left(\frac{\epsilon_{01}}{\epsilon_{0m}} \right)^{\frac{1}{3}} = 1 - [a - (a-1)V]V \quad 8$$

In this equation, volume fraction (V) is changed by a factor ' $a - (a-1)V$ ' of the mixture.

Figure 2 shows variation of Bruggeman factor at 20°C with volume fraction of water. The value of ' a ' equal to 1 corresponds to ideal mixture with no additional interaction between two liquids and reduces to Bruggeman's equation. The value of ' a ', determined by least square fit method is found to be 1.47; its deviation from unity indicates the molecular interaction in the mixture.

IV. CONCLUSION

The values of static dielectric constant, relaxation time, Kirkwood correlation factor and Bruggeman factor for DPG–water mixtures are also investigated. It suggests the formation of strong –H bonds between DPG and Water. The Kirkwood correlation factor value of pure Dipropylene is greater than unity, reveals the hydrogen bond interaction and presence of parallel associated molecules. Using Bruggemann factor the nonlinear relationship between DPG and water molecules has been also studied.

Acknowledgments:

The author P A Chalikwar is thankful to University Grants Commission (UGC) WRO Pune, (File NO. 47-718/13(WRO)).

V. REFERENCES

- [1]. K. Grzybowska, A. Grzybowski, S. Pawlus, S. Hensel-Bielowka, and M. Paluch. Dielectric relaxation processes in water mixtures of tripropylene glycol. *The J of Chem. Phy.* 2005;123:204506.
- [2]. Bo Jakobsen,a_ Kristine Niss,b_ and Niels Boye Olsenc. Dielectric and shear mechanical alpha and beta relaxations in seven glass-forming liquids. *The J of Chem. Phy.* 2005;123:234511.
- [3]. Y. B. Mel'nichenko, J. Schüller, R. Richert, B. Ewen, and C.-K. Loong. Dynamics of hydrogen-bonded liquids confined to mesopores: A dielectric and neutron spectroscopy study. *J Chem. Phys.*
- [4]. A. Yoshihara, H. Sato, S. Kojima. Brillouin Scattering Study of Glass-Forming Propylene Glycol. *Jpn. J Appl. Phys.* 1996;35: 2925.
- [5]. J.-H. Ko, S. Kojima, Brillouin scattering study on the polypropylene glycol by using a nonscanning Fabry-Perot interferometer. *Phys. Lett. A.* 2004;321:141-146.
- [6]. R. Bergman, L. Börjesson, L.M. Torell, A. Fontana. Dynamics around the liquid-glass transition in poly(propylene-glycol) investigated by wide-frequency-range light-scattering techniques. *Phys. Rev. B.*
- [7]. M.S. Beevers, D.A. Elliott, G. Williams. Dynamic Kerr-effect and dielectric relaxation studies of a poly(methylphenyl siloxane). *Polymer.* 1980;21:279-282.
- [8]. Tongfan Sun and Aryn S. Teja. Density, Viscosity and Thermal Conductivity of Aqueous Solutions of Propylene Glycol, Dipropylene Glycol, and Tripropylene Glycol between 290 K and 460 K. *J Chem. Eng. Data.* 2004;49:1311-1317
- [9]. Ganesh V. Mashalkar, Pankaj A. Chalikwar & Ashok C. Kumbharkhane. Temperature-dependent dielectric relaxation study of polyhydric alcohols (propane-1, 3 and 1,2-diol) using a TDR technique, *Phy. and Chem. of Liquids.* 2014;53,3:307-317.
- [10]. Pankaj A. Chalikwar, Avdhut R Deshmukh and Ashok C. Kumbharkhane. Dielectric relaxation of Tripropylene glycol–water mixture using time domain Reflectometry, *Phy. and Chem. of Liquids.*
- [11]. Havriliak S, Negami S. A complex plane analysis of α -dispersions in some polymer systems. *J Polym Sci C.* 1966; 14: 99-117.
- [12]. Hill NE, *Theoretical Treatment of Permittivity and Loss.* Van Nostrand Reinhold Co, London. 1969; Chapter 1: p 1.
- [13]. Frohlich H. *Theory of Dielectrics.* Oxford University Press; London. 1949.
- [14]. Fattepur RH, Hosamani MT, Deshpande DK, Mehrotra SC. Dielectric relaxation and structural study of aniline–methanol mixture using picosecond time domain reflectometry. *J Chem Phys.* 1994; 101:9956.
- [15]. Kumbharkhane AC, Puranik SM, Mehrotra SC. Structural study of amide-water mixtures using dielectric relaxation technique. *J Mol Liq.* 1992; 51: 261.
- [16]. Bruggeman DAG. *Ann Phys (Leipzig).* 1935; 5: 636-679.

Dielectric Dispersion Study of Binary Mixtures of Polysorbate-40 with Aqueous Solutions

G T Jinklor, V S Pabjoj, H N Lakhmawad, K S Kanse*, Y S Joshi, D N Rander

Department of Physics and Electronics, Lal Bahadur Shastri Mahavidyalaya, Dharmabad 431809,
Maharashtra, India

ABSTRACT

The complex relative dielectric properties of polysorbate-40 with water at various concentrations have been measured using Precision LCR meter in the frequency range of 20Hz to 2 MHz at 25°C. The electrical and dielectric properties of the binary mixtures are represented in terms of complex dielectric function $\epsilon^*(\omega)$, electrical modulus $M^*(\omega)$, electrical conductivity $\sigma^*(\omega)$. All these parameters are used to explain the various processes associated with the electric and dielectric properties of the binary mixtures of polymer in aqueous solutions.

Keywords: Precision LCR meter, complex permittivity, electric modulus.

I. INTRODUCTION

The investigation of dielectric parameters of the material in the spectral range from 20 Hz to 2 MHz provide the useful information about the intra and inter molecular dynamics, the degree of intermolecular H-bond interaction, cooperative nature between like and unlike molecules. The information regarding ionic and electrode polarization processes related to the molecular structures also can be studied [1-3]. Polysorbate-40 (P-40) is polymer having molecular formula $C_{62}H_{122}O_{26}$. P-40 is also known as polyoxymethylene sorbitan monopalmitate consists of sorbitol, palmitic acid and ethylene oxide. P-40 is the yellow or orange viscous liquid at room temperature. It has wide range application in cosmetic preparation, cleaning compound, pharmaceuticals, personal care product, emulsifier or surfactant to help mix oil and water.

P-40 is miscible with water in a wide concentration range. As oxygen atoms and $-OH$ groups are present, respectively in the molecular chain and at the ends of the chain, due to which these molecules have several hydrogen bonding sites. They can enter into intra- and intermolecular hydrogen bonding giving rise to several conformations in water mixtures. Extensive experimental attempts have been made to study the dielectric behaviour of polymer molecules and their oligomers at radio waves and microwaves [4-9]. In the present study, dielectric measurement of P-40 in aqueous solutions have been carried out in the frequency range of 20Hz to 2MHz using precision LCR meter and various processes associated with these parameters were discussed.

II. EXPERIMENTAL DETAIL

Materials

P-40 was obtained from RLCC with purity 99% and water with HPLC grade made by Fisher Scientific India Pvt Ltd. They were used without further purification. The solutions were prepared at different mole fraction of water in polysorbate-40.

Measurement:

The complex dielectric function $\varepsilon^*(\omega)$ of liquid sample were determined by Agilent Technologies, E4980 using precision LCR meter. A four terminal liquid dielectric test fixtures (Agilent16452 A) were used for capacitance and parallel resistance measurement in the frequency range 20 Hz to 2 MHz the capacitance and parallel resistance of the liquid dielectric test fixture without and with samples were measured to compensate for short. The test fixture correction coefficient was also considered to cancel the effect of stray capacitance during the evaluation of the value of the complex dielectric function. The complex dielectric function $\varepsilon^*(\omega)$ of the material is determined using Eq. (1).

$$\varepsilon^*(\omega) = \varepsilon'(\omega) - j\varepsilon''(\omega) = \alpha \left[\frac{C_p}{C_0} - j \frac{1}{\omega C_0 R_p} \right] \quad (1)$$

Where $\omega=2\pi f$ is the angular frequency and α is the correction coefficient of the cell. All measurements were made at 25°C.

III. RESULT AND DISCUSSIONS:

Dielectric Spectra:

The frequency dependent spectra of the real part of dielectric permittivity for P-40 and its binary solutions with water are shown in Fig.1. In present study, the static dielectric permittivity values of corresponding liquids samples are recorded at 2 MHz. From the plot it can be observed that, the dielectric permittivity (ε') values for pure P-40 and its binary solutions with water are very high at lower frequency and these values lowers with increase in frequency. The higher values of ε' at lower frequencies are due to the domination of electrode polarization effect which can be explained with the help of $\tan\delta$ plot (Fig. 2).

In the real part of dielectric permittivity spectra (Fig. 1), ε' values for P-40 becomes steady around 1 KHz while that for the binary mixtures with water becomes frequency independent from few KHz to 0.3 MHz. Frequency dependent dielectric loss tangent ($\tan\delta = \varepsilon''/\varepsilon'$) is plotted in Fig. 2. The electric density layer capacitance formation taken place due to the free charge built up at the interface between the dielectric material and electrode surface. This gives rise to the electrode polarization (EP). The electrode polarization frequency corresponds to the peak in $\tan\delta$ spectra (Fig. 2). The EP phenomenon can be separated from the bulk material by using the EP relaxation frequency. The loss peak of $\tan\delta$ is corresponding to the EP relaxation frequency f_{EP} , which can be used to evaluate the EP relaxation time, $\tau_{EP} = (2\pi f_{EP})^{-1}$ which is associated with the overall dynamics of the absorbed ions on the electrode surfaces in the alternating electric

field. On addition of water in P-40, the loss peaks are shifting towards the higher frequency side up to mole fraction of water (X_W) =0.993. Above this concentration again the dielectric loss peak shifts toward the higher frequency.

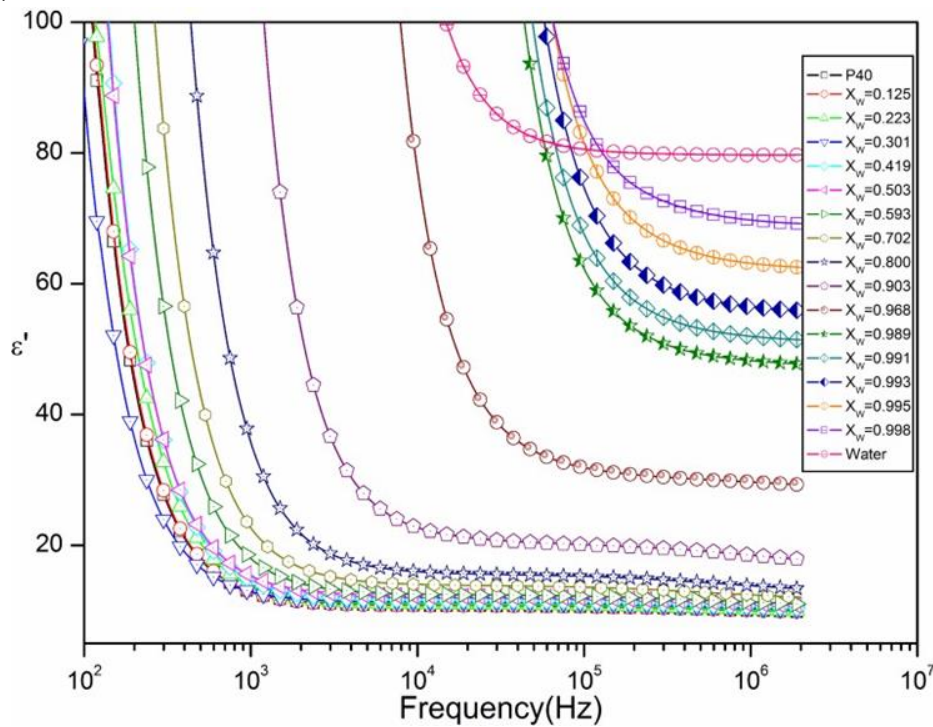


Fig. 1 : Dielectric permittivity spectra (ϵ') for binary mixtures of P-40 with water at 25°C.

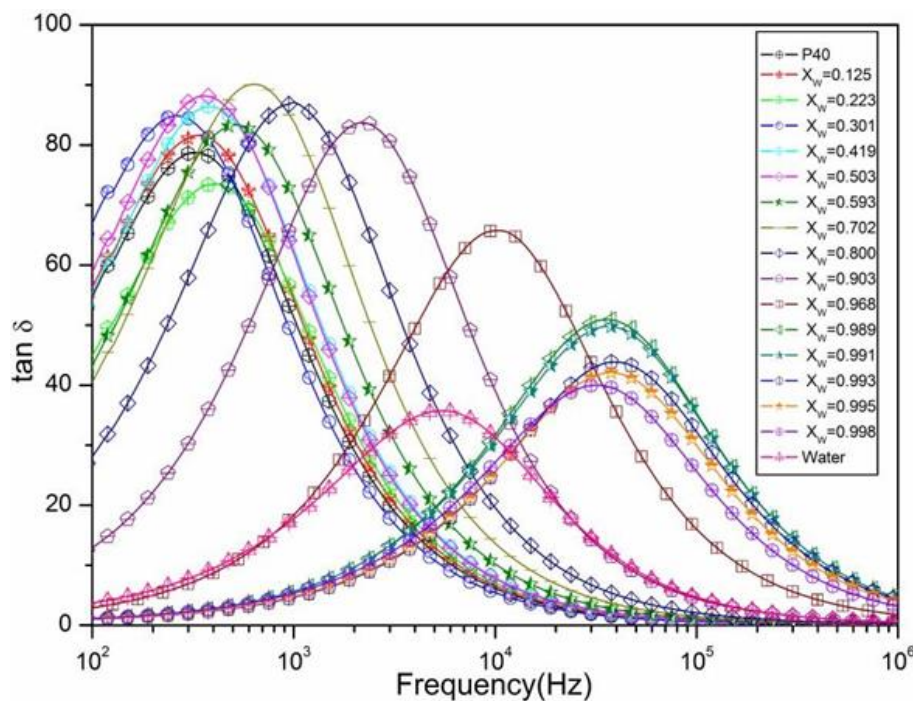


Fig 2: Dielectric loss ($\tan \delta$) for binary mixtures of P-40 with water at 25°C.

The static dielectric permittivity (ϵ_s) values of pure P-40, water and their binary solutions are obtained from the permittivity spectra is plotted and shown in Fig.3. The non linear nature of this plot indicates certain interaction among the unlike molecules. In the polymer rich region ($0 \leq XW \leq 0.8$), the values of ϵ_s are increasing very slowly. It can be attributed as P-40 structure is dominant in the binary solutions whereas for the concentrations $XW > 0.8$, the values of ϵ_s increasing rapidly. It may possible due to water molecules try to form hydrogen bonding with the P-40 molecules. The structure of pure P-40 starts to break and may form complexes of heteromolecules in this region.

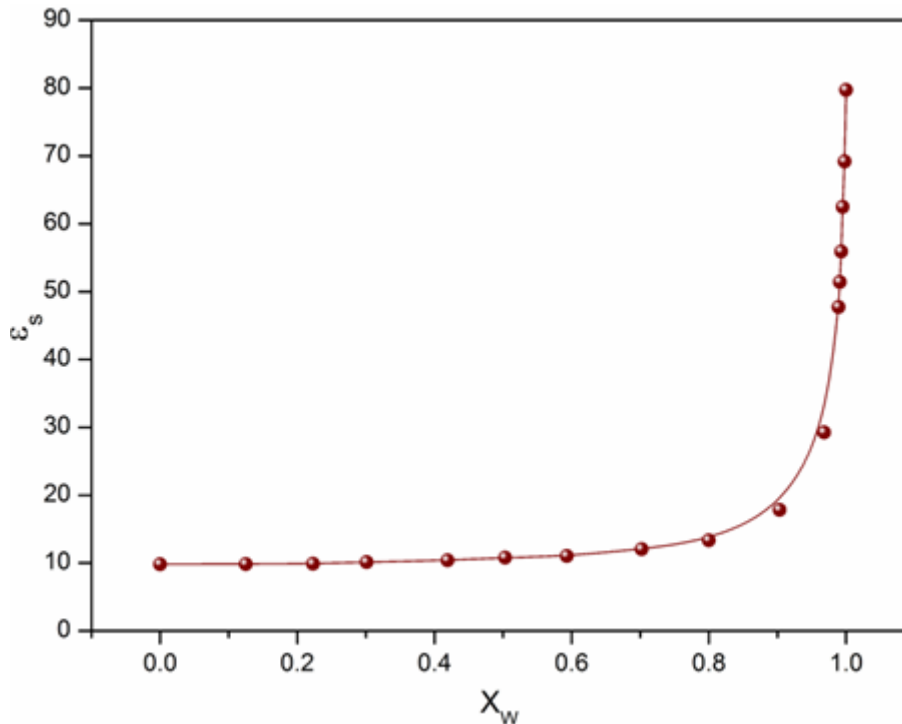


Fig. 3: Static dielectric permittivity (ϵ_s) Vs. Mole fraction of water (XW)

Electric Modulus [$M^*(\omega)$]

The frequency dependent values of $M^*(\omega)$ is obtained using Eq. (2) [10-12]

$$M^*(\omega) = \frac{1}{\epsilon^*(\omega)} = M' + jM'' = \frac{\epsilon'}{\epsilon'^2 + \epsilon''^2} + j \frac{\epsilon''}{\epsilon'^2 + \epsilon''^2} \quad (2)$$

The plots for real and imaginary parts of electric modulus vs. frequency are shown in Fig. 4 and Fig.5. It can be observed in Fig. 4 that M' approaches to zero at lower frequencies. This nature confirms the existence of electrode polarization at lower frequencies. The $M'(\omega)$ increases with increase in the frequency nonlinearly. From the Fig. 5, frequency corresponds to the M'' peak value has gradually shifted towards higher frequency with decrease in the P- 40 concentration in water. Value of the M'' peak frequency $f\sigma$ can be used to evaluate the ionic conductivity relaxation time $\tau\sigma$ ($= 1/2\pi f\sigma$) [13].

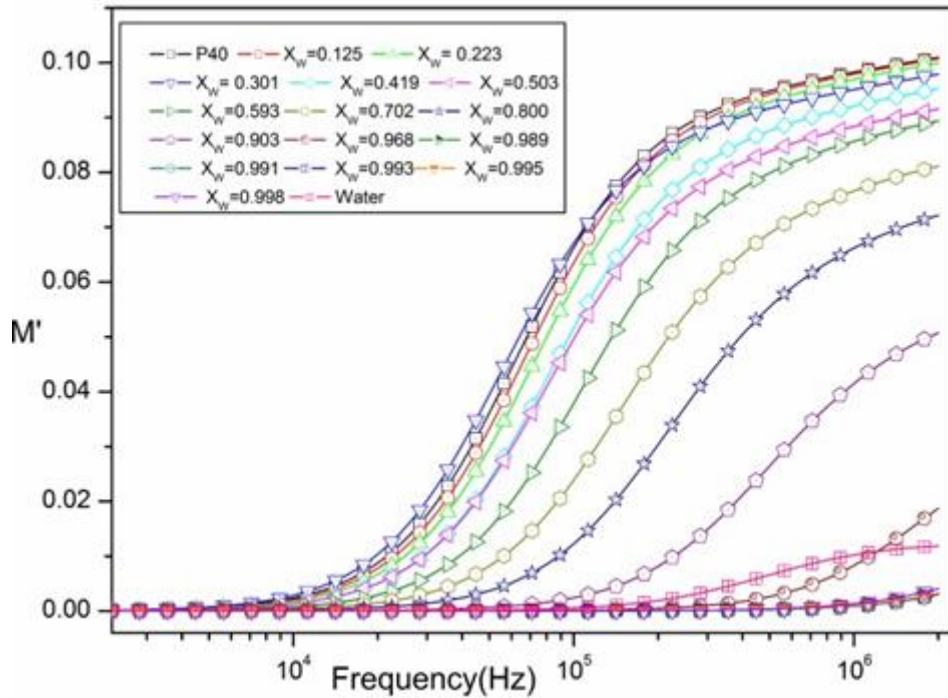


Fig 4. Real Part of electric modulus (M') vs. Frequency.

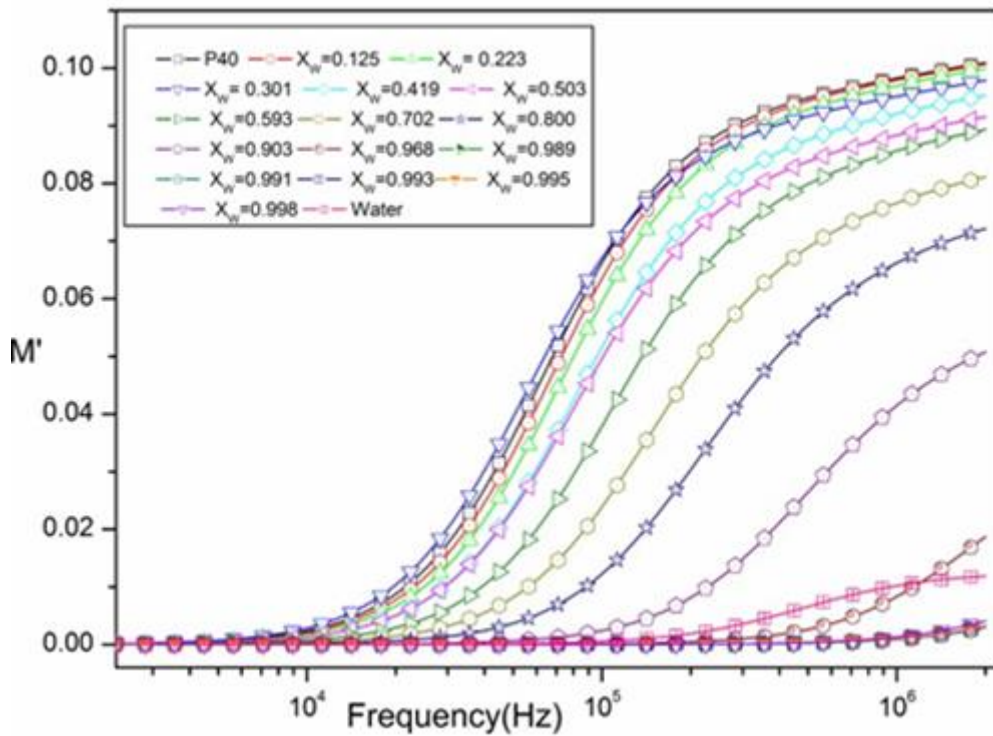


Fig. 5. Imaginary part of electric modulus (M'') vs. Frequency

Complex Electrical Conductivity (σ_{ac})

The alternating current (ac) complex conductivity $\sigma^*(\omega)$ which is the resultant of real part σ' and the imaginary part σ'' of the liquid samples obtained from the following Eq.(3)

$$\sigma^*(\omega) = \sigma' + j\sigma'' = \omega\varepsilon_0\varepsilon'' + j\omega\varepsilon_0\varepsilon' \quad (3)$$

Here ε_0 is free space dielectric permittivity. Fig.6 shows the $\sigma_{ac}(\omega)$ spectra for polysorbate- 40 at different concentrations with water. It can be observed that the value of ac conductivity values are almost frequency independent in this frequency range for the pure P-40 and its binary concentrations of water around $XW = 0.903$. After this, for the concentration $0.968 \leq XW \leq 0.998$ the values of ac conductivity are increasing rapidly upto few KHz and then it becomes independent of frequency. For pure water, very small variation in the values of σ_{ac} at lower frequencies is observed and remains almost steady above 100Hz.

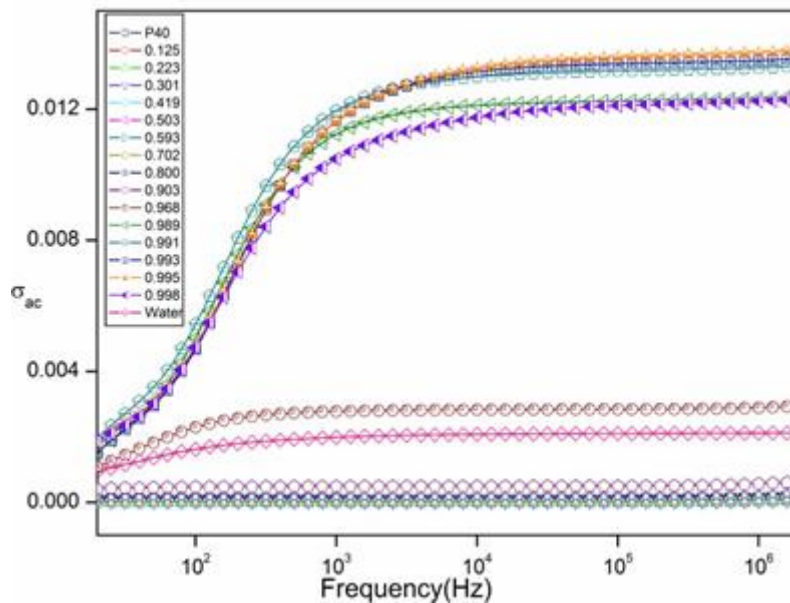


Fig. 6. σ_{ac} for various concentration of P-40 with Water vs. Frequency

IV. CONCLUSION

The dielectric measurement of P-40 with Water mixtures at temperature 25°C have been done in the frequency range of 20 Hz to 2 MHz using precision LCR meter. The electrical and dielectric properties of binary mixtures are plotted in terms of dielectric permittivity $\varepsilon^*(\omega)$, electrical modulus $M^*(\omega)$, electrical conductivity $\sigma^*(\omega)$. All these parameters are used to explain the various processes associated with the electric and dielectric properties of the binary mixtures of polymer in aqueous solutions.

V. REFERENCES

- [1]. Kremer F, J. of Non Cryst. Solids 305 (2002) 1-9.
- [2]. Kremer F, Schonhals A, "Broadband dielectric spectroscopy", Springer, Berlin (2002).

- [3]. Shinyashiki N, Sengwa R J, Tsubotani S, Nakamura H, Sudo S, Yagihara S, J. of phys. Chem. 110 (2006) 4953.
- [4]. Stockmayer W H, Pure Appl. Chem. 15 (1967) 539.
- [5]. Mashimo, Satoru, Macromolecules 9 (1976) 91.
- [6]. Mashimo S, Nakamura H, Chiba A, J. Chem. Phys. 76 (1982) 6342.
- [7]. Mashimo S, Yagihara S, Chiba H, Macromolecules 17 (1984) 630.
- [8]. Matuo K, Kahlman K F, Yong W H M, Geny F, Stockmayer W H, Jones A A, J. Polym. Sci. Polym. Phys. 15 (1977) 1347.
- [9]. Kaatze U, Gottmann O, Podblelski R, Pottel R, Terveer U, J. Phys. Chem. 82 (1978) 112.
- [10]. Pradhan D K, Choudhary R N P, Samantaray B K, EXPRESS Polym. Lett. 2 (2008) 630.
- [11]. Chanmal C V, Jog J P, EXPRESS Polym. Lett. 2(4) (2008) 294.
- [12]. Joshi Y S, Kanse K S, Kumbhatkhane A C, Rana V A, SRTMU'S research Journal of Science 3 (2014) 10.
- [13]. Rana V A, Shah K N, Vankar H P, Trivedi C M, J. Mol. Liqs. 271 (2018) 686.

Dielectric Relaxation Studies of Aqueous Polyvinyl Pyrrolidone

Komal Kabara, Ravi Karale, Suad Alwaleedy, Savita Kamble, Ashok Kumbharkhane, Arvind Sarode*

School of Physical Sciences, Swami Ramanand Teerth Marathwada University Nanded -431606. Maharashtra, India

ABSTRACT

Structural and dynamical properties of Polyvinyl-pyrrolidone (PVP K-30)[C_6H_9NO]_n in the solution state with water has been studied in the frequency region of 10 MHz to 30 GHz over the temperature range of 298.15 K-283.15 K using Time domain Reflectometry(TDR). Dielectric parameters such as static dielectric constant (ϵ_j), relaxation time (τ_j), dipole moment ($\hat{\mu}$), correlation factor (g_j), has been calculated and expressed in terms of molecular interaction and hydrogen bonding. The dielectric permittivity spectra and relaxation behavior of PVP in different concentrations were analyzed using Cole-Cole model.

Keywords: Polyvinylpyrrolidone, Time Domain Reflectometry, Dipole moment.

I. INTRODUCTION

The chemical and physical properties of polymer solutions are determined by the dynamics of solvent molecules and the micro-Brownian motion of polymer chains. Furthermore, the dynamics of polymer solutions can be efficiently considered as a basic model system with molecular motions directly related to biopolymer functionalities [1].PVP is an amorphous polymer. It contains an asymmetric electrical charge distribution in its monomer units, with distinct atoms (N, O, C, and H) close one other. PVP may form complexes with a wide range of substances by forming hydrogen bonds with the hydroxyl groups of solvents such as water, alcohols, ethylene glycol oligomers, and glycerol, among others and its carbonyl group[2].PVP, a flexible and randomly coiled polymer that is easily soluble in water, was used to study the water structure surrounding the coiled polymer. Dielectric measurements are simple to do for such a non-electrolytic solution [3].

II. EXPERIMENTAL

MATERIALS

PVP K-30, a polyvinylpyrrolidone with an average molecular weight of 40,000 g mol⁻¹, was acquired from Sigma Aldrich and utilized without purification.

Dielectric Measurements

The dielectric permittivity(ϵ') and dielectric loss(ϵ'') of pure liquid PVP solution were measured using time domain reflectometry at temperatures ranging from 298.15 K to 283.15 K, using the methodology and procedures reported elsewhere.

III. RESULTS AND DISCUSSION

Dielectric experiments on PVP-Water mixtures were carried out at temperatures ranging from 298.15 K to 283.15 K, with PVP average molecular weights of around 40,000 g mol⁻¹. As demonstrated in Fig. 1, the real (ϵ') and imaginary (ϵ'') components of the dielectric functions of PVP-Water mixture are frequency dependent.

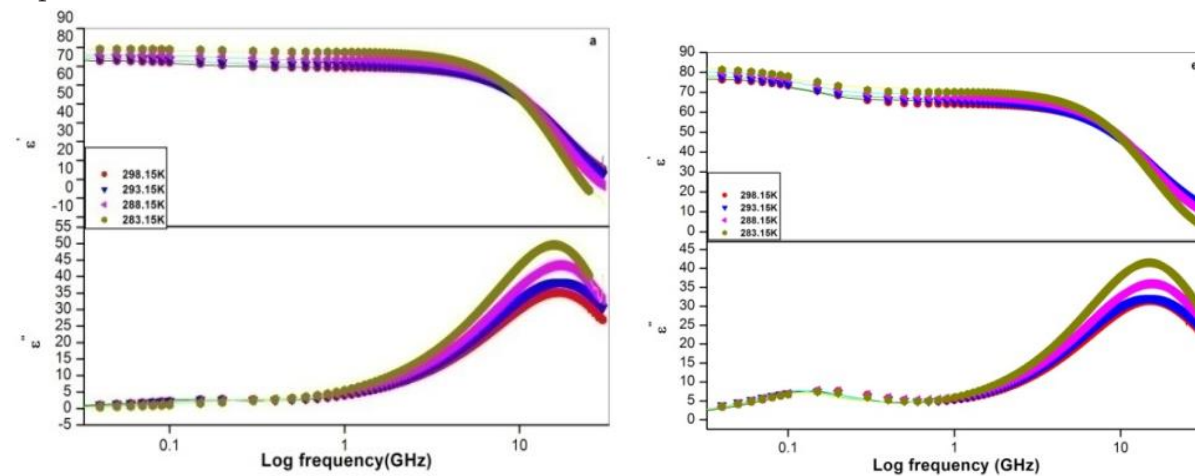


Figure 1. Variation of Complex Permittivity Spectra of Polyvinylpyrrolidone K-30 solution with frequency at different temperatures. Dielectric permittivity (ϵ') and dielectric loss (ϵ'') as a function of frequency (GHz)(Static Permittivity Spectra fig(a): $1.67 \cdot 10^{-04}$ C(M) fig(e): $8.34 \cdot 10^{-04}$ C(M))

As illustrated in Fig. 1, the PVP-water mixture has two relaxation peaks. The primary relaxation process, which corresponds to the rotation of free water molecules, and the secondary relaxation process, which corresponds to the rotational motion of PVP molecules in the aqueous medium.

A sum of n Havriliak-Negami(HN) equations or its variants, the Dabye (D), the Cole-Cole (CC), and the Cole-Davidson (CD), is used to study different types of relaxation process [4].

$$\epsilon^*(\nu) = \sum_{j=1}^n \frac{\Delta\epsilon_j}{[1+(i2\pi\nu\tau_j)^{\beta_j}]^{\alpha_j}} + \epsilon_{\infty} \quad (1)$$

The 2-D model derived from eqn.(1) for the two relaxation processes is

$$\epsilon^*(\nu) = \frac{\Delta\epsilon_1}{1+i2\pi\nu\tau_1} + \frac{\Delta\epsilon_2}{1+i2\pi\nu\tau_2} + \epsilon_{\infty} \quad (2)$$

Static Dielectric constant(ϵ) :

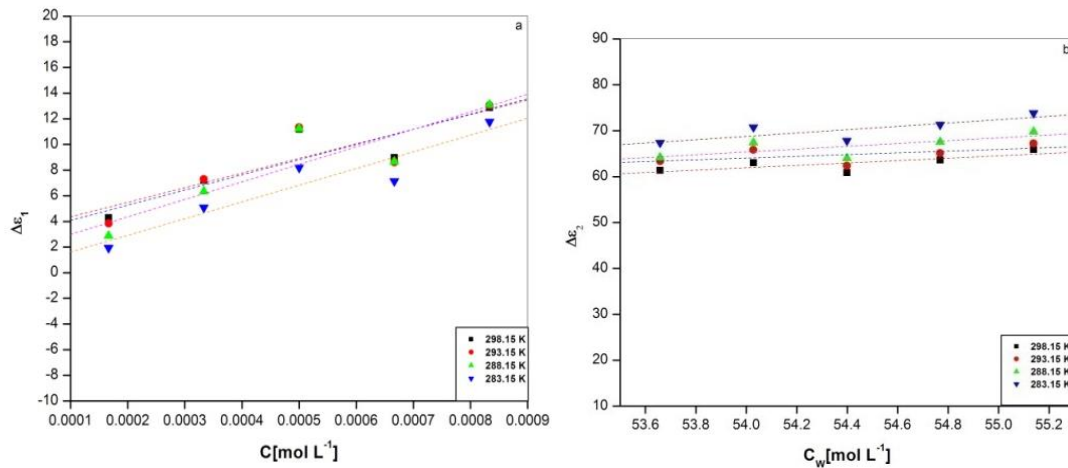


Figure 2. Dielectric relaxation strength of low frequency and high frequency processes.

Low frequency dielectric relaxation strength $\Delta\epsilon_1(c)$ increases with increasing PVP concentration, indicating that the relaxation process in the low frequency region is mostly due to an increase in effective dipole-dipole antiparallel alignment of PVP molecules. Every PVP molecule is entirely surrounded by water molecules at low concentrations, shielding the interaction between PVP molecules; this can be seen in the correlation factor g_1 which drops as concentration increases, indicating strong evidence of antiparallel dipole alignment. The value of $\Delta\epsilon_1(T)$ drops as the temperature decreases.

At all measured temperatures, the concentration dependence of the high frequency relaxation strength $\Delta\epsilon_2(c)$ decreases linearly, indicating that it is related with the cooperative relaxation of bulk-like water occurring in the same frequency range as pure water. This indicates the presence of water associated with PVP molecules and can be linked to the relaxation time (τ_2) of high frequency processes at higher solute concentrations. This could also be due to strong water-water interaction and the dominating high frequency dispersion that is clearly attributed to the rotation of 'bulk-like' water molecules [4,5].

Relaxation time:

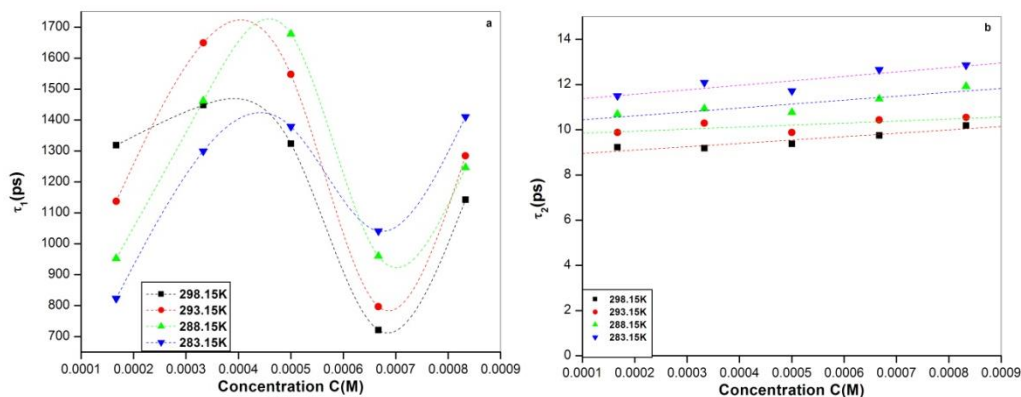


Figure 3. Dielectric Relaxation times τ_1 (ps) and τ_2 (ps) Vs Concentration C_{PVP}

Figure 3 shows that the value of low frequency relaxation time (τ_1) grows steadily with increasing solute concentration up to 0.000333 molar concentration, however there is a monotonous change in τ_1 value above this concentration. The high value of τ_1 for pure water is due to the reorientational motion of hydrogen bonded linear polymeric structure.

With decrease in temperature, the dielectric relaxation time (τ_2) for the high frequency relaxation process increases. The difference in relaxation time between pure water and all concentrations of the system recorded at room temperature (~ 9 ps) could be attributed to molecular interaction between water and PVP in the system, which could enhance steric hindrance for the reorientation of water molecules.

We will use the Cavell equation for multimer system, which is an extension of the Onsagar equation, to learn more about the solute-solute interaction in terms of dipole-dipole correlation [4].

$$\Delta\epsilon_j = \frac{\epsilon_s}{3(\epsilon_s + (1 - \epsilon_s)A_j)} \frac{N_A}{k_B T \epsilon_0} \frac{\mu_{eff,j}^2}{(1 - \alpha_j f_j)^2} C_j \quad (3)$$

Where ϵ_s is the static permittivity, N_A is Avogadro's number. k_B is Boltzmann constant and ϵ_0 vacuum permittivity. A_j the shape parameter of reaction field and accounts for the shape of relaxing particle. f_j is so called cavity field factor and α_j is the molecular polarizability and T is temperature. $\mu_{eff,j}$ (the effective dipole moment of j^{th} species) is connected to the gas phase dipole moment $\mu_{0,j}$ i.e.

$$\mu_{eff,j}^2 = g_j \mu_{0,j}^2 \quad (4)$$

Where g_j is an empirical factor which accounts for correlation between dipoles. $g_j = 1$ indicates no orientational correlation between dipoles, $g_j < 1$ implies a tendency towards anti-parallel alignment and $g_j > 1$ a tendency towards parallel alignment of dipoles.

For the low frequency process, it is assumed that the polarizability (α_L) and the reaction field factor (f_L) are independent of concentration c, so we can define

$$\hat{\mu} = \frac{\mu_{eff,l}}{(1 - \alpha_l f_l)} = \frac{g_l^{1/2} \mu_{0,l}}{(1 - \alpha_l f_l)} \quad (5)$$

The correlation factor g_j takes into account possible orientational correlation between the dipoles. Formula for calculating A_j and f_j are given in the literatures [5,6,7]. In our calculations, a spherical water molecule ($A_j = 1/3$) with radius $r = 0.1425$ nm was assumed and values of μ_{eff} were calculated using equation (3).

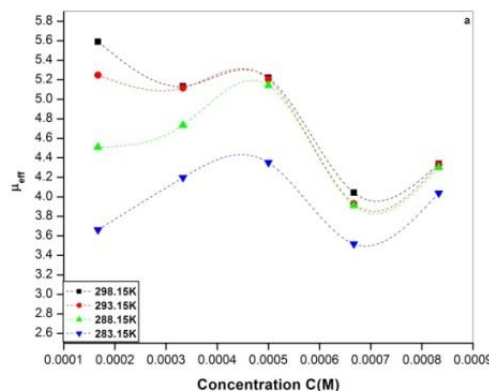


Fig.4. Dipole moment μ_{eff} using cavells equation

The measured values of effective dipole moment calculated using Cavell eqn. appear to be in good agreement with the previously obtained value [8]. Up to 0.0005 molar concentration of solute, the values of μ_{eff} determined by eqn.(3) increases. Above this concentration, the values of μ_{eff} vary. The formation of anti-parallel dipole-dipole interactions between the PVP molecules at greater concentrations is attributed to the decrease in μ_{eff} values. The fact that $\mu_{eff}(T)$ over all measured concentrations is increasing as temperature rises could be attributable to an increase in the induced solute-solute interaction through the hydration layer. At higher concentrations, values of $\mu_{eff}(T)$ are more deviated, which could indicate enhanced solute-solute (PVP-PVP) interaction via the hydration layer.

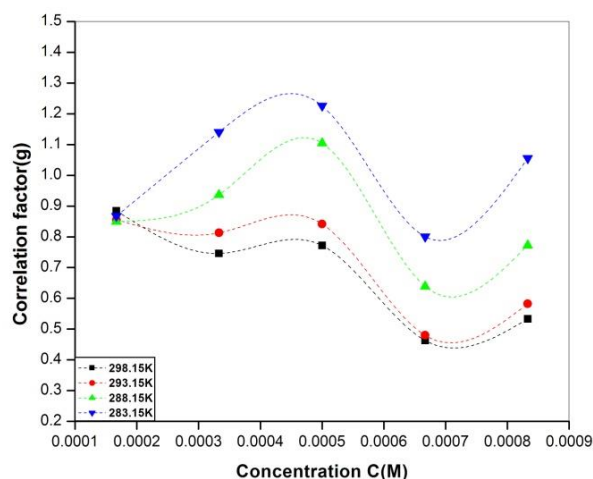


Figure 5. Correlation factor (g_1) as a function of concentration at different temperatures.

In addition to dipole moment, we have estimated the values of correlation factor (g_1) in order to have insights into the magnitude of these anti-parallel alignment by using eqn.

$$\frac{\hat{\mu}(C_{MAX})}{\hat{\mu}(C \rightarrow 0)} \approx \frac{g_1^{1/2}(C_{MAX})}{g_1^{1/2}(C \rightarrow 0)} = g_1^{1/2}(6)$$

Where $g_1(c \rightarrow 0) = 1$, because for infinite dilution, there is no correlation between the PVP molecules. C_{max} is the highest concentration used for PVP. Values of correlation factor (g_1) have been calculated at highest concentration. For the low frequency process, values of correlation factor (g_1) was found to be less than 1 for all concentrations and temperatures except at 298.15 K. The values of g_1 lower than 1 suggests that there is reduced correlation between solute molecules.

IV. ACKNOWLEDGEMENTS

Author KBK is thankful to School of Physical Sciences, S.R.T.M. University Nanded for providing instrumentation facility. The author is also gratefully acknowledged to Dept. of Science and Technology (DST), New Delhi for providing (TDR) facility through project sanctioned to Dr. A.V.Sarode (SERB/F/4632/2013-2015) and Dr. A.C.Kumbharkhane (SB/S2/LOP-032/2013).

V. REFERENCES

- [1]. N.Shinyashiki, D.Imoto, and S.Yagihara, Broadband dielectric study of dynamics of polymer and solvent in poly (vinyl pyrrolidone)/normal alcohol mixtures. *The journal of physical chemistry B*, 111(9)(2007)2181-2187.
- [2]. R.J.Sengwa and S. Sankhla. Dielectric dispersion study of poly (vinyl pyrrolidone)–polar solvent solutions in the frequency range 20 Hz–1 MHz. *Journal of Macromolecular Science, Part B: Physics*, 46(4) (2007) 717-747.
- [3]. N.Shinyashiki, Y. Matsumura, N. Miura, S. Yagihara, and S.Mashimo. Dielectric study of water structure in polymer solution. *The Journal of Physical Chemistry*, 98(51) (1994) 13612-13615.
- [4]. I. Rodríguez-Arteche, S.Cervený, Á. Alegría, and J. Colmenero. Dielectric spectroscopy in the GHz region on fully hydrated zwitterionic amino acids. *Physical Chemistry Chemical Physics*, 14(32) (2012) 11352-11362.
- [5]. T.Sato, R. Buchner, Š. Fernandez, A. Chiba, and W. Kunz, Dielectric relaxation spectroscopy of aqueous amino acid solutions: dynamics and interactions in aqueous glycine. *Journal of molecular liquids*, 117(1-3) (2005) 93-98.
- [6]. R. Buchner, S.G Capewell, G Hefter and P.M. May. Ion-pair and solvent relaxation processes in aqueous Na₂SO₄ solutions. *The Journal of Physical Chemistry B*, 103(7) (1999) 1185-1192.
- [7]. R. Buchner, G.T.Hefter, and P.M. May. Dielectric relaxation of aqueous NaCl solutions. *The Journal of Physical Chemistry A*, 103(1) (1999) 1-9.
- [8]. A.V. Sarode, A.C. Kumbharkhane, and S.C. Mehrotra. Dynamics and interactions in aqueous polyvinylpyrrolidone (PVP K-30): an approach using dielectric relaxation spectroscopy, 56(04) (2018) 335-340

Dielectric Relaxation Studies of Potentised Homeopathic Medicines

Mahajan G. R.¹, Parimal Patwe², Pathan A.W.³, Chalikwar P.A.^{4*}

¹Department of Physics, Shri Datta Arts, Commerce and Science College Hadgaon, Dist.: Nanded, Maharashtra, India

²Radiation Oncology Department, National Cancer Institute, Nagpur, Maharashtra, India

³Department of Physics, ASC college, Badnapur, Dist.: Jalna, Dist. Nanded, Maharashtra, India

^{4*}K.K.M. College, Manvat, Dist.: Parbhani, Maharashtra, India

ABSTRACT

Complex dielectric permittivity measurements in the frequency range 10MHz-30GHz has been carried out for homeopathic medicine Cuprum Metallicum using a time domain reflectometry (TDR) method at different temperatures. The static dielectric constants (ϵ_0), relaxation time (τ) were determined by using least square fit method. Also frequency dependent spectra of for Cuprum Metallicum studied at different potencies. These parameters are used to explain the various processes associated with the dielectric properties of Cuprum Metallicum.

Keywords: Dielectric permittivity; Relaxation time; Time domain reflectometry (TDR).

I. INTRODUCTION

Ever since its discovery in the eighteenth century, the homeopathic system of medicine has been open to criticism from the scientific world as well as from the practitioners of the allopathic system. The practice of homeopathy was well accepted by the public from the very inception due to safety of medicine and effectiveness. Homoeopathic medicine has been one of the world's most widely practiced alternative therapies. The popularity of homeopathy spread across the globe even during the life time of its founder. It was considered as one of the refined medical systems till about 1950s [1, 2].

The dielectric dispersion occurring in potentised homeopathic medicines subjected to variable frequency electric field was studied by using an instrumentation method developed by C R Mahata [3]. The experimental results for three potencies of Cuprum Metallicum (Cuprum met) in the frequency range of 100 kHz - 1 MHz was reported [3]. Dielectric dispersion studies were conducted in a broad range in a frequency range of 100 KHz to 50 MHz with potencies below and above the Avogadro limit by taking 6C and 30C potencies of *Graphite's* and *Cuprum Metallicum* in liquid form. Measurements were made with an Anomalous Dielectric Dispersion Detector (A3D) [4]. Anomalous dielectric dispersion in ordered molecular groups also studied. The homoeo-medicines cannot be anything except specifically ordered molecular groups, is theoretically proposed by Mahata [5, 6].

In the present study, the complex relative permittivity spectra of homeopathic medicine *Cuprum Metallicum* with different potencies (6C, 30C, 200C) have been measured using time domain reflectometry technique from 10MHz to 30GHz.

II. EXPERIMENTAL

Homeopathic medicines *Cuprum Metallicum* with different potencies (6C, 30C, 200C) used for experimental purpose are taken from an *SBL PVT LTD*.

The dielectric spectra have been obtained by the time domain reflectometry (TDR) technique. The Tektronix model no. DSA8200 Digital Serial Analyzer sampling mainframe along with the sampling module 80E08 has been used for the measurement. The Fourier transformation of the pulses and data analysis were done earlier to determine complex permittivity spectra $\epsilon^*(\omega)$ using non linear least squares fit method [17, 18].

III. RESULTS AND DISCUSSION

Fig.1 shows frequency dependent complex permittivity spectra for *Cuprum Metallicum*. The complex permittivity spectra measured using TDR is fitted by the non-linear least squares fit method to the Havriliak - Negami expression [9, 10]-

$$\epsilon^*(\omega) = \epsilon_{\infty} + \frac{\epsilon_0 - \epsilon_{\infty}}{[1 + (j\omega\tau)^{1-\alpha}]^{\beta}} \quad (1)$$

where ϵ_0 is the static dielectric constant, ϵ_{∞} is the permittivity at high frequency, τ is relaxation time and α & β is the Cole-Cole and Davidson-Cole distribution parameter, respectively. Equation (1) includes the Debye ($\alpha = 0, \beta = 1$) [11] Cole-Cole ($0 \leq \alpha \leq 1$ and $\beta = 1$) [12] and Davidson - Cole ($\alpha = 0$ and $0 \leq \beta \leq 1$) [13]. Fig.2 & Fig.3 shows the static dielectric constant and relaxation time of *Cuprum Metallicum* at various temperatures.

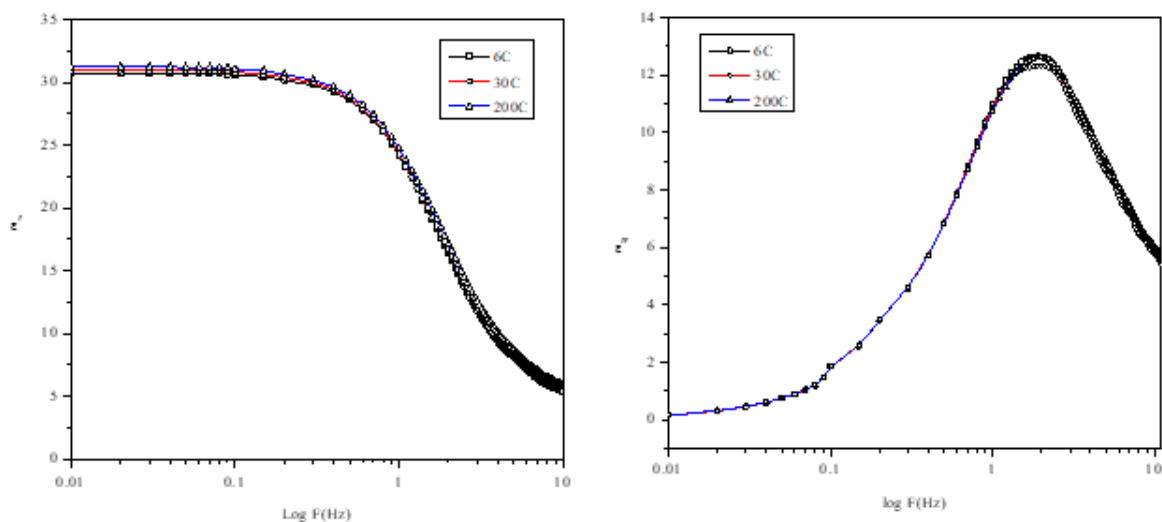


Figure 1. Frequency dependent a) dielectric permittivity (ϵ') and b) dielectric loss (ϵ'') for *Cuprum Metallicum* at different potencies.

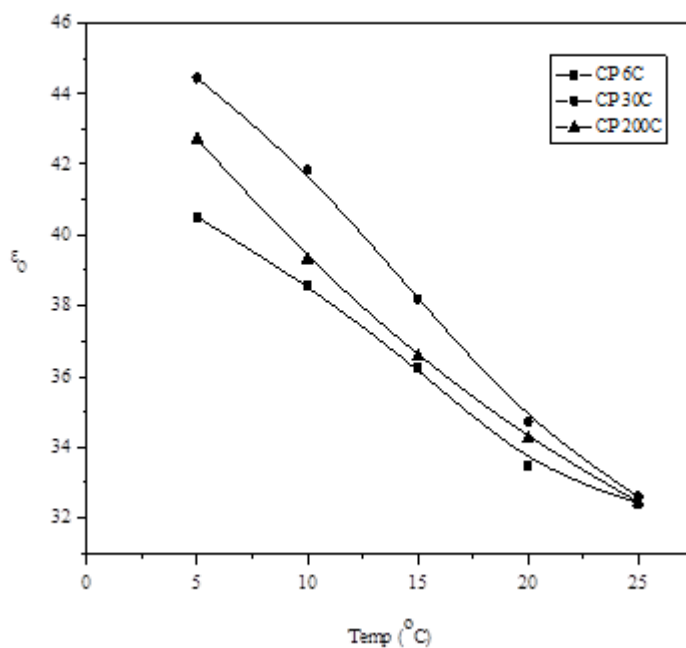


Figure 2. Static dielectric permittivity (ϵ_0) vs. potencies of Cuprum Metallicum at various temperatures.

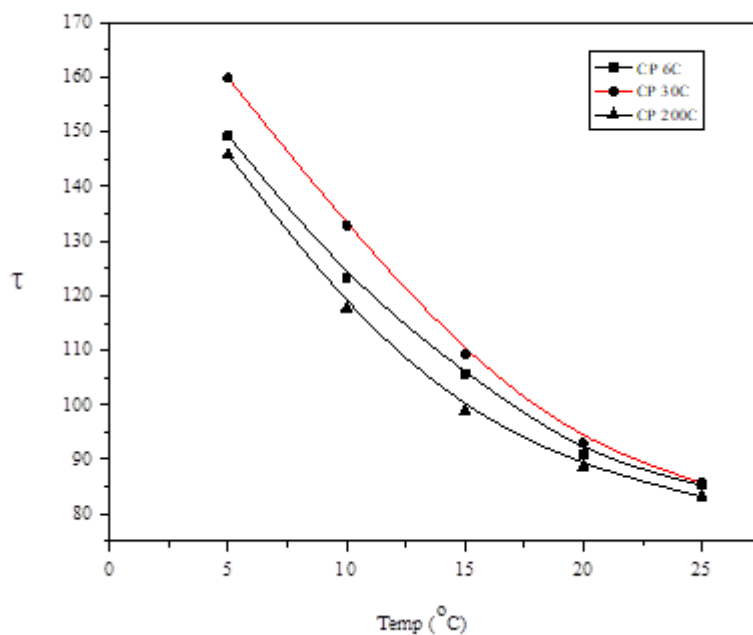


Figure 3. Relaxation times (τ in ps) vs. potencies of Cuprum Metallicum at various temperatures.

Thermodynamic properties

The thermodynamic parameters evaluated using Eyring equation is as follows [14]

$$\tau = (h/KT) \exp (\Delta H/RT) \exp (-\Delta S/R) \quad (2)$$

where ΔS is the entropy of activation, ΔH is the activation energy in kJ/mole. τ is the relaxation time in ps and T is the temperature in K and h is the Planck's constant. Fig.4. shows plot of Thermodynamic energy of Cuprum Metallicum at different potencies. Activation energy (ΔH) for entire concentration is positive.

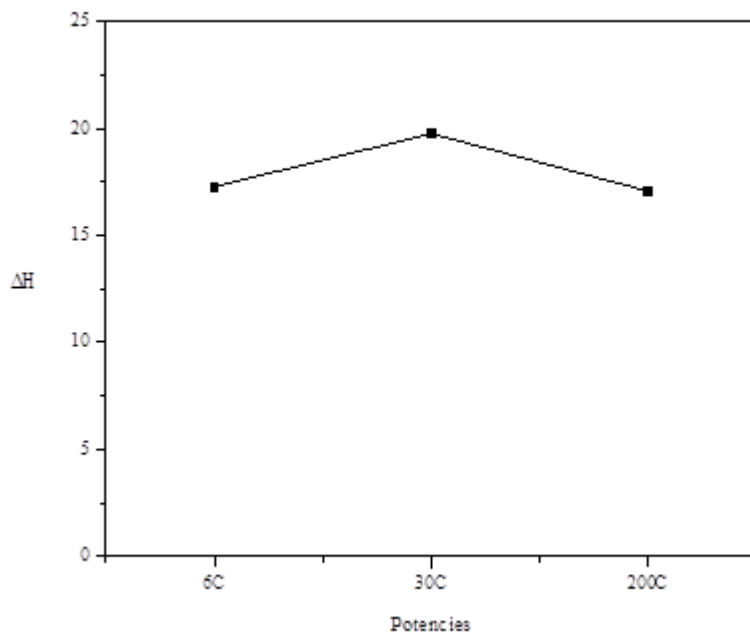


Figure 5. Thermodynamic energy of Cuprum Metallicum at different potencies

IV. CONCLUSION

The complex permittivity spectra of Cuprum Metallicum at different temperature with different potencies have been studied using time domain reflectometry technique in the frequency range 10 MHz to 30 GHz. The experimental dielectric relaxation data contains valuable information.

Acknowledgements:

Financial support provided by Swami Ramanand Teerth Marathwada University, Nanded, Maharashtra [APDS/Uni.MRP/Sci.&Tech./Physics./2019-20/2835] is gratefully acknowledged. Author GRM is also thankful to Swami Ramanand Teerth Marathwada University, Nanded for availing the laboratory facility.

V. REFERENCES

- [1]. A hypothesis on the nature of homeopathic potencies, By Aditya Kumar, Ruplal Jussal, The British Homeopathic Journal, Pages 197-204.
- [2]. Understanding the Principles of Homeopathy on A Research Perspective, Eswara Das, J Complement Med Alt Healthcare J 9(2): JCMAH.MS.ID.555756 (2019).
- [3]. Effect of dielectric dispersion on potentised homeopathic medicines, T Maity¹, D Ghosh and C R Mahata, Homeopathy (2010) 99, 99–103.
- [4]. Dielectric dispersion studies of some potentised homeopathic medicines reveal structured vehicle, C R Mahata, Homeopathy (2013) 102, 262-267.
- [5]. Mahata C. R., Homeopathy explained in the light of recognized science. The homeopathic heritage, Vol. 22, May 1997, pp. 245-252.
- [6]. Mahata C. R., Some studies on physical basis of homeopathic medicines, Journal of Technology, Vol. 29, 1, 1983, pp. 27–34.
- [7]. A. C. Kumbharkhane, S. C. Mehrotra, J. Chin. Chem. Soc. 54, 1457 (2007).
- [8]. A. C. Kumbharkhane, S. M. Puranik, S. C. Mehrotra, J. Chem Soc. Faraday Trans. 87, 1569 (1991).
- [9]. S. Havriliak, S. Negami, A complex plane representation of dielectric and mechanical relaxation processes in some polymers, J. Polym. Sci. C 14 (1966) 99-117.
- [10]. A. V. Sarode, A. C. Kumbharkhane Study of dielectric relaxation and thermodynamic behaviour in poly(propylene glycol) using Time Domain Reflectometry, Journal of Molecular Liquids 160 (2011) 109–113
- [11]. P. Debye, Polar molecules. Chemical Catalog. Co: New York. (1929)
- [12]. K.S. Cole, R.H. Cole, Dispersion and absorption in dielectrics I. Alternating current characteristics, J. Chem. Phys. 9 (1941) 341-351.
- [13]. D.W. Davidson, R.H. Cole, Dielectric relaxation in glycerin [11], J. Chem. Phys. 18 (1950) 1417.
- [14]. N.E. Hill, W.E. Vaughan, A.H. Price, M. Davies, Van Nostrand Reinhold, Co., London, 1969.

Investigation of Solute -Solute interaction and Complex Formation in Binary Mixtures of Iso-Amyl Alcohol and Ethylenediamine at Microwave Frequency

B. S. Narwade

Department of Physics, Degloor College, Degloor Dist: Nanded, Maharashtra, India

ABSTRACT

The values of dielectric constant (ϵ') and loss factor (ϵ'') have been experimentally determined for Iso- amyl alcohol, ethylenediamine and their binary mixture at 9.85 GHz microwave frequency. These values have been used to evaluate molar polarization (P_{12}) and excess values of dielectric constant ($\Delta\epsilon'$) excess dielectric loss ($\Delta\epsilon''$) and used to investigate the complex formation in the mixture Density (ρ), viscosity (η), square of refractive index (n_D^2), activation energy (E_a) also reported for pure liquids of Iso-Amyl Alcohol, Ethylenediamine and their binary mixtures. These values are used to investigate the solute -solute molecular interaction in binary system

Keywords: Dielectric constant, Dielectric loss, Excess parameters

I. INTRODUCTION

Experimental investigation of dielectric properties of organic compound is of great value in understanding the nature of complex formation between the molecules. The knowledge of dielectric properties and thermodynamic properties of organic compounds and their mixture at microwave frequencies helps in their characterization and applications. More investigation may lead to proper understanding of the behaviour of the liquid mixture. When a binary mixture is formed, the dielectric parameters and thermodynamic parameters do not vary linearly¹⁻³. The deviation from linearity of these parameters is called excess parameters. These excess parameters are used to understand the nature of bonding between two constituents of the mixture.

The present paper aims at the estimation of dielectric behaviour of Iso-amyl alcohol (*IAA*) and ethylenediamine (*EDA*) binary mixture by studying the change in the dielectric constant (ϵ') and dielectric loss (ϵ'') of *IAA*, *EDA* and their binary mixture at 25°C temperature.

II. MATERIAL

Iso-amyl alcohol (*IAA*), A.R. grade and ethylenediamine (*EDA*) A.R. grade procured from M/s. S.D. Fine Chemicals and used without further purification. The two liquids according to their proportion by volume were mixed well and kept for six hours to ensure good thermal equilibrium.

III. EXPERIMENTAL METHOD

The density (ρ), viscosity (η) of pure compound and their binary mixtures were measured using Pycknometer and Oswald's viscometer respectively. The refractive indices for sodium D-line were measured by using Abbe's refractometer.

The dielectric constant (ϵ') and dielectric loss (ϵ'') were measured by using Surber's technique⁴ of measuring reflection coefficient from air dielectric boundary of the liquid. Surber's technique is a special system, which permits rapid measurement of VSWR. Since there is a direct relationship between VSWR and reflection coefficient (Γ_r) of a wave guide by measuring the ratio of relative amplitudes of reflected and incident signals, VSWR can be measured.

Dielectric Parameters:

Suber^{4,9} has derived the following relations for dielectric parameters D, ϵ', ϵ'' .

$$D = \tan \left[2 \tan^{-1} \left(\frac{\alpha_d \lambda_d}{2\pi} \right) \right] \quad [1]$$

$$\epsilon' = \left(\frac{\lambda_o}{\lambda_c} \right)^2 + \left(\frac{\lambda_o}{\lambda_d} \right)^2 \left[1 - \tan^2 \left(\frac{1}{2} \tan^{-1} D \right) \right] \quad [2]$$

$$\text{and } \epsilon'' = \frac{1}{\pi} \left(\frac{\lambda_o}{\lambda_d} \right)^2 \alpha_d \lambda_d \quad [3]$$

where λ_o is free space wavelength, λ_c is cut off wavelength for the wave guide, $\alpha_d \lambda_d$ is the attenuation constant per unit length due to dielectric, ' λ_d ' is the wavelength of electromagnetic waves in the wave guide filled with dielectric. Now the parameters to be measured are λ_d and $\alpha_d \lambda_d$. The dissipation factor D for the system may be computed analytically as follows.

Defining a factor M_n such that

$$M_n = \frac{|\Gamma_n|^2}{|\Gamma_\infty|^2} = \frac{I_n}{I_\infty} \quad [4]$$

where $n = 1, 2, 3, \dots$ $|\Gamma_n|$ is the reflection coefficient by the liquid column of length $l = n \left(\frac{\lambda_d}{2} \right)$ and $|\Gamma_\infty|$ is the reflection coefficient for the liquid of infinite length. I_n and I_∞ represent the corresponding current values.

According to Surber^{4,9} attenuation per wavelength is given by

$$\alpha_d \lambda_d = \frac{1}{n} l_n \left[k_1 \left\{ 1 + (1 + k_2)^{1/2} \right\} \right] \quad [5]$$

$$\text{where } k_1 = \frac{(1 - MnY^2)}{Y(Mn - 1)} \quad [6]$$

$$k_2 = \frac{(Mn-1)(1-MnY^4)}{(1-MnY^2)^2} \quad [7]$$

$$\text{and} \quad Y = \frac{\left(1 - \frac{\lambda_d}{\lambda_g}\right)}{\left(1 + \frac{\lambda_d}{\lambda_g}\right)} \quad [8]$$

Thus measuring the values of $\alpha_d \lambda_d$, λ_o , λ_c , and λ_d , the values of dielectric parameters ϵ' , ϵ'' and D may be calculated by using above equations (1 to 8). The values of mole fraction (X) of *EDA*, the wavelength in dielectric (λ_d), output current (I_n) for liquid length $\left(\frac{n\lambda_d}{2}\right)$, the output current (I_∞) for the liquid of infinite length and the attenuation per unit length ($\alpha_d \lambda_d$), obtained experimentally.

The free energy of activation E_a of the viscous flow for the pure liquids and their binary mixtures is obtained by using the following equation ¹⁰

$$\eta = \left(\frac{hN}{V}\right) \exp\left(\frac{E_a}{RT}\right) \quad [9]$$

where η is the viscosity and V is molar volume of the liquid and other symbols have their usual meaning.

The values of molar polarization of the mixtures were obtained by using the formula ⁹

$$P_{12} = \left[\frac{(\epsilon'-1)}{(\epsilon'+2)}\right] \left[\frac{X_1 M_1 + X_2 M_2}{d}\right] \quad [10]$$

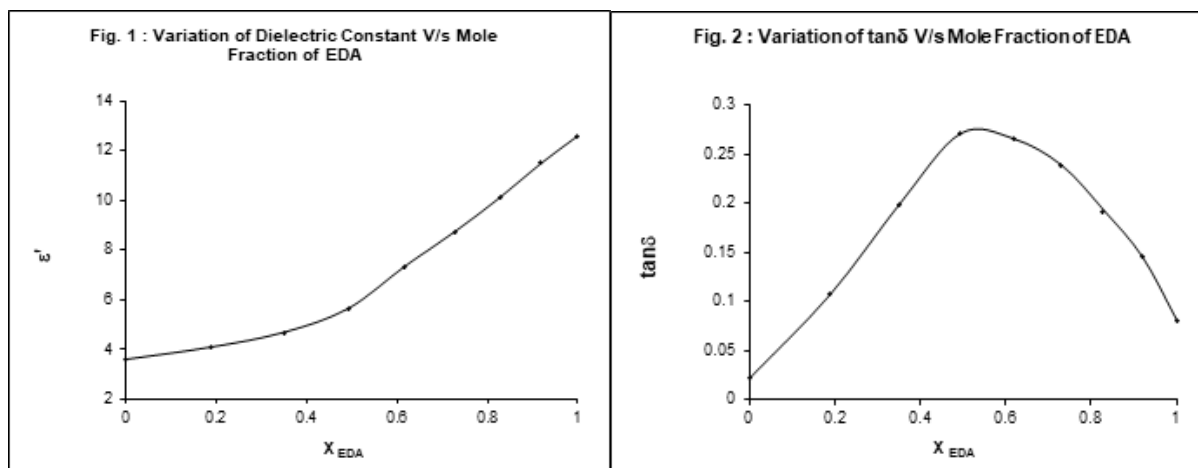
where M_1 and M_2 are the molecular weight, X_1 and X_2 are the mole fraction of the constituents of the mixture. The following Earp and Glasstone ¹¹ and assuming the following formula, the values of P_1 and P_2 are calculated.

$$P_{12} = X_1 P_1 + X_2 P_2 \quad [11]$$

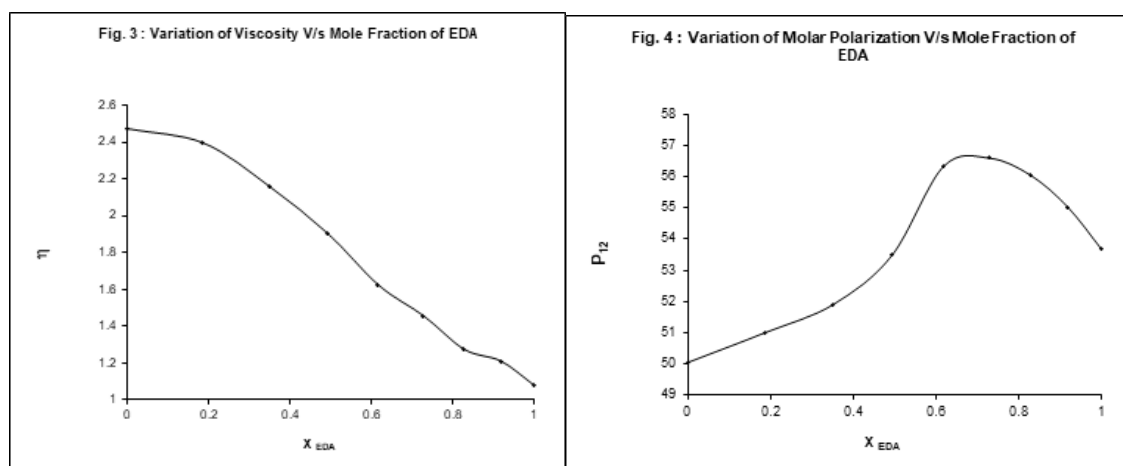
Where P_2 is apparent polarization of each liquid in the mixture if P_1 is the polarization of other component of the mixture in the pure liquid state.

IV. RESULT AND DISCUSSION

The values of dielectric constant (ϵ') with mole fraction of *EDA* is depicted in Fig. (11.1). The non-linear variation of ϵ' with mole fraction is considered to be due to the formation of complex in the mixture ⁶.



The variation of $\tan\delta$ V/S mole fraction of EDA shows that absorption in the mixture is maximum at 0.5 mole fraction of EDA, suggesting the large absorption at this concentration. An interaction causing association between IAA and EDA molecules may be responsible for such type of $\tan\delta$ curve. Earlier Degaonkar et al.,⁷ and Purohit et al.,⁸ observed such marked change in $\tan\delta$ curve. variation of viscosity (η) with mole fraction of EDA. From graph, it is observed that the viscosity of binary mixture lie between viscosity of pure liquids.

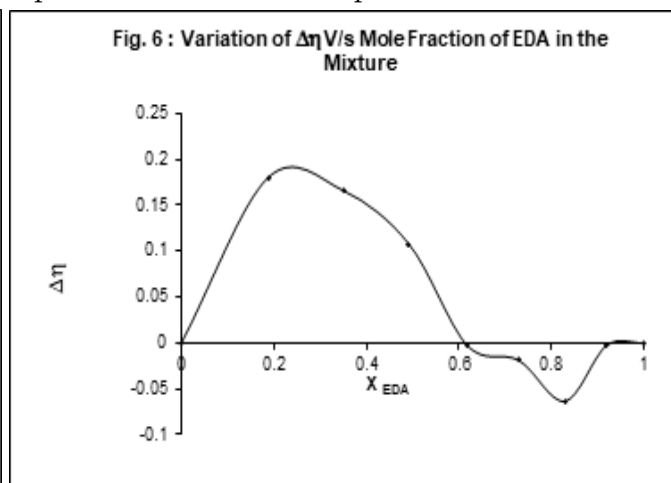
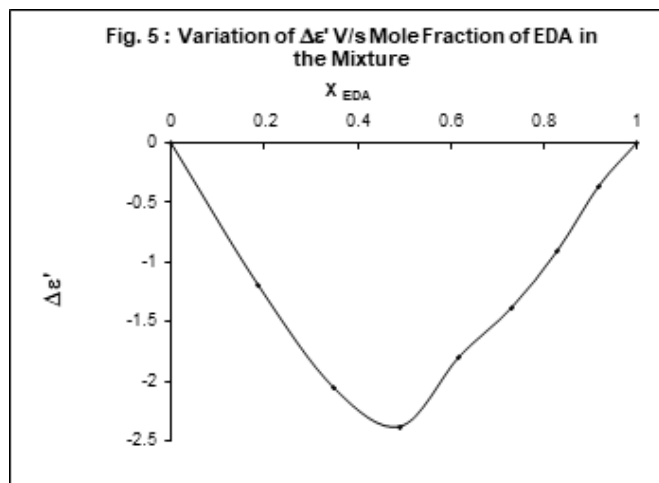


The values of molar polarization (P_{12}) are plotted as a function of mole fraction of EDA for IAA, EDA and their binary mixture (Fig.4) when the molecules are polar, association of permanent molecular dipoles makes a great difference to the value of polarization. This is in fact is a function of number of free dipoles, and association diminishes the number of these free dipoles per unit volume. This explains how the determination of polarization give a quantitative measure of the polar association.

In the present investigation of IAA, EDA and their binary mixture, the amount of complex present is responsible for shape of polarization curve.

The excess parameters for binary liquid system is the measure of deviation from ideal behaviour of the mixture and found to be more sensitive towards molecular interactions in the liquid mixture. The values

of excess permittivity ($\Delta \epsilon'$, $\Delta \epsilon''$), excess viscosity ($\Delta \eta$), excess square refractive index (Δn_D^2) and excess activation energy (ΔE_a) are shown in table The excess dielectric constant ($\Delta \epsilon'$) is found to be negative over entire range of mole fraction of *EDA* in the mixture. The minima in $\Delta \epsilon'$ versus mole fraction of *EDA*, is found to be at 0.5 mole fraction of *EDA*, at which we expect the formation of complex in the mixture.



The excess viscosity ($\Delta \eta$) is found to be positive up to 0.6 mole fraction of *EDA*, with further increase of *EDA* in the mixture, the $\Delta \eta$ values become negative, the negative deviation of $\Delta \eta$ from linearity indicates that dispersive forces are primarily responsible for the interaction¹. These excess parameters suggest interaction between alcohol amine mixture.

V. CONCLUSION

1. Non-linear variation of dielectric constant with mole fraction of *EDA* suggest complex formation in the mixture.
2. $\tan \delta$ curve suggest the absorption in the mixture is more than pure compounds.
3. Excess parameter study indicates solute – solute interactions in the mixture.

VI. REFERENCES

- [1]. Gupta K.K., Bansal A.K., Singh P.J. and Sharma K. Indian J. Phys., 79(2), (2005), 147-152.
- [2]. Das D. and Hazra D.K., Indian J. Phys., 77B(5), (2003), 519-523.
- [3]. Ali Anwar, Kumar A.N., Chand D. and Bhajan Lal, Indian J. Pure and Applied Phys., Vol. 41, (Dec. 2003), 928-935.
- [4]. Surber W.H., J. Appl. Phys., 19, (1948), 514.
- [5]. Sisodia M.L., Raghuwanshi G.S., "Basic Microwave Techniques and Lab Manual," Wiley Eastern Ltd., New Delhi, (1990).
- [6]. Job P. Ann. Chim., 9, (1928), 113.
- [7]. Degaonkar V.S., Adgaonkar C.S. and Jajoo S.N., Indian J. Pure and Applied Phys., 20, (1982), 617-621.

- [8]. Purohit H.D. and Sharma H.S. Indian J. Pure and Applied Phys., 9, (1971), 450.
- [9]. Singh P.J. and Sharma K.S., Pramana J. Phys., 45, (1996), 259-270.
- [10]. Kalamse G.M. and Nimkar M.J. Asian J. Chem., 14, 3-4 (2002), 1487-1493.
- [11]. Hill N.E., Vaughan W.E., Price A.H. and Devies M. (1969)'Dielectric properties and molecular behaviour,' Van Nostrand, London, pp.71 and 253.
- [12]. Gupta K.K., Bansal A.K., Singh P.J., and Sharma K.S.(Jan. 2003), Indian J. of Pure and Applied Phys., Vol.41, 57-63.

Table – 1 Values of mole fraction (X) of EDA, density (ρ), viscosity (η), square of refractive index (n_D^2), dielectric constant (ϵ'), loss factor (ϵ''), loss tangent ($\tan \delta$), activation energy (E_a) and molar polarization (P_{12}) for binary liquid system of (EDA + IAA) at 25°C.

X	ρ	η (cp)	n_D^2	ϵ'	ϵ''	$\tan \delta$	E_a Kcal/mole	P_{12}
0.0000	0.8078	2.478	2.0022	3.571	0.0778	0.0218	3.588	50.06
0.1877	0.8211	2.400	2.0249	4.065	0.4330	0.1065	3.569	51.02
0.3503	0.8330	2.162	2.0420	4.666	0.9260	0.1985	3.507	51.71
0.4925	0.8431	1.908	2.0592	5.627	1.5210	0.2702	3.433	53.48
0.6180	0.8531	1.625	2.0765	7.338	1.9440	0.2649	3.337	56.34
0.7294	0.8621	1.456	2.0909	8.749	2.0831	0.2381	3.272	56.60
0.8291	0.8715	1.274	2.1054	10.132	1.9440	0.1918	3.192	56.05
0.9188	0.8815	1.211	2.1199	11.494	1.6638	0.1448	3.142	55.03
1.0000	0.8894	1.079	2.1316	12.602	1.0070	0.0799	3.126	53.69

Table – 2 Values of excess parameters $\Delta \epsilon'$, $\Delta \epsilon''$, $\Delta \eta$, Δn_D^2 and ΔE_a along with mole fraction (X) of EDA for the binary liquid system of IAA+EDA at 25°C.

X	$\Delta \epsilon'$	$\Delta \epsilon''$	$\Delta \eta$	Δn_D^2	ΔE_a
0.1877	-1.197	0.1887	0.1806	-0.00158	0.0714
0.3503	-2.060	0.5379	0.1663	-0.00550	0.0876
0.4925	-2.381	1.0060	0.1076	-0.00672	0.0817
0.6180	-1.799	1.3185	-0.0026	-0.00569	0.0468
0.7294	-1.392	1.3583	-0.0189	-0.00567	0.0349
0.8291	-0.907	1.1309	-0.0635	-0.00408	0.0037
0.9188	-0.359	0.7712	-0.0028	-0.00158	0.0022

Microwave Frequency Dielectric Dispersion of 1, 2-Ethanediol with Water using TDR

Shamsundar S. Kadam

Department of Physics, N. W. College A. Balapur, Maharashtra, India

ABSTRACT

The Complex dielectric spectra $\varepsilon^*(\omega)=\varepsilon'-j\varepsilon''$ of binary mixture of 1, 2-Ethanediol with water were obtained in the microwave frequency range 10 MHz to 30 GHz using Time Domain Reflectometry (TDR) technique. The static dielectric constant (ε_0) and relaxation time (τ) have been obtained. On the basis of dielectric parameters intermolecular interaction are predicated.

Keywords: Time domain reflectometry, complex dielectric spectra, Relaxation time.

I. INTRODUCTION

Microwave dielectric relaxation studies are useful in understanding the structure of alcohols. Dielectric studies involve measurements of dielectric permittivity and dielectric loss. The measurements can be used to find dielectric relaxation times and distribution parameters. The relaxation time depends upon the molecular size, shape, intramolecular and intermolecular forces, and can be used to investigate molecular and intramolecular motions and their relation to molecular structure.

1, 2-Ethanediol i.e. Ethylene glycol (EG) is organic liquid and has two -OH groups at the ends of their molecular structures. Dielectric relaxation studies on EG have revealed that the microwave frequency region dielectric dispersion is attributed to the reorientation of the molecules as whole and also ends -OH groups [1-3]. Due to the presence of ends -OH groups, the molecules of these liquids can enter into intra and intermolecular hydrogen bonding giving rise to several conformations in water mixture [2-3]. There are two kinds of water structures existing in solutions: "free" and "bound" take a central place among experimental and theoretical studies of different chemical and biological systems, i.e. molecules of water bounded to each other by H bonds from polymolecular clusters or more complex structure (free water). Similarly, molecules of solute can bind to neighboring water molecules also mostly through hydrogen bonding (bound water) [4]. The molecular interactions significantly influences the dielectric relaxation [5]. Further more, the environment of water solvent can be modified by the alcohol molecules because of the strong interactions between the hydroxyl groups of alcohols and water molecule. Zahn *et al* [6] have carried out the dielectric properties of water-ethylene glycol solutions.

In the present paper, dielectric relaxation studies of EG in water solution have been carried out using time domain reflectometry technique in the frequency range of 10 MHz to 30 GHz at 25°C Static dielectric

constant, relaxation time, Kirkwood correlation factors, of aqueous solutions of EG have been evaluated for their molecular conformations.

II. EXPERIMENTAL METHOD AND DATA ANALYSIS

The dielectric spectra were obtained by the time domain reflectometry (TDR) technique. The Tektronix model no. DSA8200 Digital Serial Analyzer sampling mainframe along with the sampling module 80E08 has been used for the time domain reflectometry (TDR). A repetitive fast rising voltage pulse with 18ps incident rise time was fed through coaxial line system of impedance 50 ohm. Sampling oscilloscope monitors changes in step pulse after reflection from the end of line. Reflected pulse without sample $R_1(t)$ and with sample $R_x(t)$ were recorded in time window of 2ns and digitized in 2000 points. The time dependent data were processed to obtain complex reflection coefficient spectra $\rho^*(\omega)$ over the frequency range from 10 MHz to 30 GHz as [2, 3].

$$\rho^*(\omega) = \left(\frac{c}{j\omega d} \right) \left[\frac{p(\omega)}{q(\omega)} \right] \quad (1)$$

where $p(\omega)$ & $q(\omega)$ are Fourier transforms of $[R_1(t) - R_x(t)]$ and $[R_1(t) + R_x(t)]$ respectively, c is the speed of light, ω is the angular frequency, d is the effective pin length and $j = \sqrt{-1}$. The complex permittivity spectra $\epsilon^*(\omega)$ was obtained from reflection coefficient $\rho^*(\omega)$ by applying calibration method as described earlier [4]. The dielectric permittivity ϵ' and dielectric loss ϵ'' of EG with water at 25°C are shown in Figure. It is observed from the dielectric dispersion plot that the value of (ϵ') decreases as the frequency increases, whereas, the dielectric loss (ϵ'') approaches maximum in the frequency range 1GHz to 2GHz.

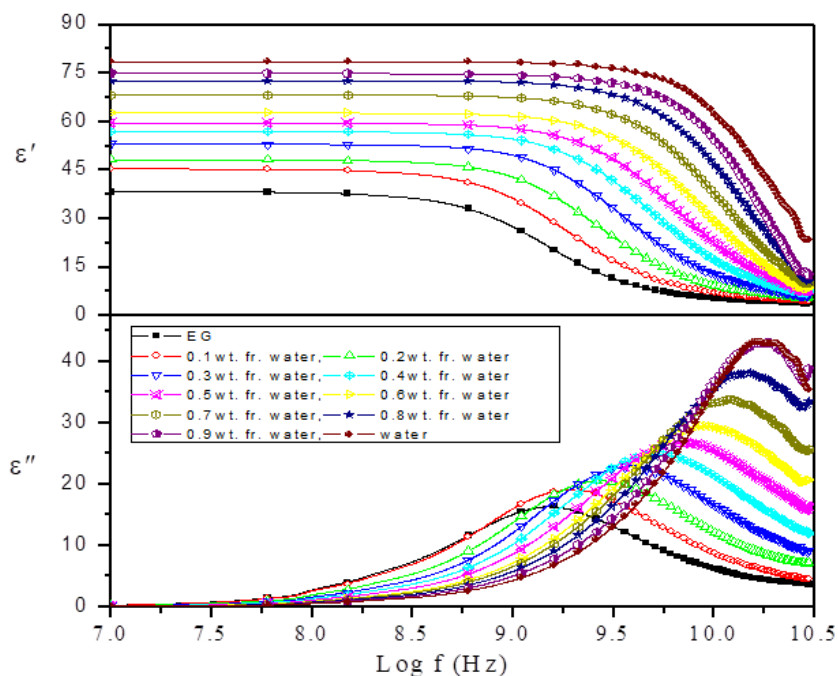


Figure1. Complex permittivity spectra (ϵ') and dielectric loss (ϵ'') for EG-Water at 25°C.

III. RESULT AND DISCUSSION

To calculate static dielectric constant (ϵ_0), molecular reorientation relaxation time (τ) and distribution parameters (α and β), the complex permittivity $\epsilon^*(\omega)$ data were fitted by the non-linear least squares method to the Havriliak-Negami expression [7]

$$\epsilon^*(\omega) = \epsilon_\infty + \frac{(\epsilon_0 - \epsilon_\infty)}{[1 + (j\omega\tau)^{1-\alpha}]^\beta} \quad (2)$$

With $\epsilon_0, \epsilon_\infty, \tau, \alpha$ and β are the fitting parameters. The equation includes the Cole-Cole ($\beta=1$), Davison-Cole ($\alpha=0$) and Debye ($\alpha=0, \beta=1$) relaxation model. The various dielectric parameters obtained from Eq. (2) are reported in table 1. The static permittivity increases with increasing weight fraction of water in the EG-water mixtures. Resultant values agree well with the values of pure EG reported by Sengwa and Kaur [8]. Relaxation time (τ) decreases with water concentration in EGO-water mixture.

Table 1. Dielectric Relaxation parameters for EG-Water mixtures.

Wt.Fra.	25°C			
	ϵ_∞	ϵ_0 of Water	τ (ps)	β
0.0	2.62(1)	41.94(5)	104.42(50)	0.880(2)
0.1	3.06(1)	46.70(3)	78.18(22)	0.930(1)
0.2	2.67(2)	51.43(4)	54.78(23)	0.900(1)
0.3	2.85(1)	55.95(3)	40.77(12)	0.930(1)
0.4	2.43(2)	59.50(4)	30.77(11)	0.940(1)
0.5	1.06(2)	62.21(3)	23.68(8)	0.930(1)
0.6	1.38(2)	65.71(3)	18.61(6)	0.930(1)
0.7	1.91(3)	68.90(4)	14.93(5)	0.980(1)
0.8	2.04(3)	73.06(3)	12.22(4)	0.980(1)
0.9	2.88(4)	75.04(6)	10.27(3)	0.950(1)
1.0	1.98(2)	78.32(2)	8.21(1)	1.000

IV. KIRKWOOD CORRELATION FACTOR:

The Kirkwood correlation factor 'g' is parameter containing information regarding orientation of electric dipoles in polar liquids [9]. The value of 'g' for pure liquid is given by expression

$$g\mu^2 \frac{4\pi N\rho}{9kTM} = \frac{(\epsilon_0 - \epsilon_\infty)(2\epsilon_0 + \epsilon_\infty)}{\epsilon_0(\epsilon_\infty + 2)^2} \quad (3)$$

where ' μ ' dipole moment is in gas phase, ' N ' is Avogadro's number, ' M ' is molecular weight, ' ρ ' is the density of the liquid and ' kT ' has usual meaning. We have taken ϵ_∞ value from refractive index ($\epsilon_\infty = n^2$) data at 25°C.

Table 2: Kirkwood correlation factor for EG water at 25°C.

System	g
Water	2.82
EG	2.62

For binary mixture, the static dielectric permittivity needs to be considered as the dipole orientation correlation factor (g^{eff}). The modified form of Eq. (3) is used to study the orientation of the electric dipoles in the binary mixtures as follows [9, 10].

$$\frac{4\pi N}{9kT} \left[\frac{\mu_W^2 \rho_W X_W}{M_W} + \frac{\mu_{EGO}^2 \rho_{EGO} (1 - X_W)}{M_{EGO}} \right] \times g^{eff} = \frac{(\epsilon_{0m} - \epsilon_{\infty m})(2\epsilon_{0m} + \epsilon_{\infty m})}{\epsilon_{0m}(\epsilon_{\infty m} + 2)^2} \quad (4)$$

where M_W and M_{EG} are molecular weight of water and EG respectively. ρ_W and ρ_{EG} are corresponding densities. X_W is volume fraction of water in EG. ϵ_{0m} and $\epsilon_{\infty m}$ are the static dielectric constant and dielectric constant at high frequency of the mixtures. The observed g^{eff} value is greater than unity in EG-water mixtures leads to the conclusion that the molecules associate to form multimer. The g^{eff} values greater than one indicates average parallel orientation of electric dipoles in a molecule.

V. REFERENCES

- [1]. A C Kumbharkhane, S M Puranik and S C Mehrotra J. Sol. Chem. 21(2), 201 (1992)
- [2]. S Sudo, N Oshiki, N Shinyashiki, S Yagihara, A C Kumbharkhane and S C Mehrotra J. Phys. Chem. A 111(16), 2993 (2007)
- [3]. R J Sengwa, K Kaur and R Chaudhary Polym. Int. 49, 599 (2000)
- [4]. K Grzybowska, A Grzybowski, S Pawlus, S Hensel-Bielowka, and M Paluch J. Chem. Phys. 123, 204506 (2005)
- [5]. R J Sengwa Polym. Int. 45, 43 (1998)
- [6]. M Zahn, Y Ohki, D B Fenneman, R J Gripshover and V H Gehman Proc. IEEE 74, 1182 (1986)
- [7]. S Havriliak and S Negami J. Polym. Sci. 14, 91 (1966)
- [8]. R J Sengwa and K Kaur Indian J. Biochem. Biophys. 36, 325 (1999)
- [9]. A C Kumbharkhane, S M Puranik and S C Mehrotra J. Chem. Phys. 99(4), 2405 (1993)
- [10]. J B Hasted Aqueous dielectric (London: Chapman and Hall) (1973).

Molecular and Dielectric Study of the Binary Liquid Mixture of 2,3-Dichloroaniline and Ethylene Glycol at FDR

Nemmaniwar. G. Bhupesh

Department of Physics, Digamberrao Bindu Arts, Commerce and Science College, Bhokar,
Nanded, Maharashtra, India

ABSTRACT

A binary mixture system of 2,3 Dichloroaniline (2,3-DCA) and Ethylene glycol (EG) including those of pure liquids, over the entire composition range were measured at room temperatures at atmospheric pressure. The physical and chemical properties of viscosity, density and refractive index for the binary mixtures were determined. The temperature dependences of the density, viscosities and refractive index for the system were described. To investigate the internal interactions of the binary mixtures. calculations were employed. The trend of energetic and charge distribution of all ions and molecules involved in interactions between the 2,3-DCA and EG.

Keywords: 2,3-DCA and EG, Molecular Interactions and Physical–chemical properties

I. INTRODUCTION

Recently several workers 1-3 have reported the utility of dielectric measurement while studying the molecular interaction in a binary mixture of liquids. The density and viscosity of binary mixture have studied 4. In this paper our aim is to provide the information regarding the possibilities of complex formation due to molecular association between two polar liquids namely 2,3-DCA and EG at room temperature. In this paper the dielectric properties and molecular behavior of 2,3-DCA with EG and their binary mixture are discussed.

II. EXPERIMENTAL

2,3-Dichloroaniline (GC Grade) from Sigma-Aldrich, Germany and Ethylene glycol (AR Grade) were obtained from Spectrochem PVT. LTD. Mumbai. India. Without further purification the two liquids according to their proportions by volume were mixed well and kept 6 hours in well stoppered bottles to ensure good thermal equilibrium. 2,3-DCA was used as solute and EG as solvent.

III. MEASUREMENTS

The densities, viscosities and refractive index of the pure components and their mixtures were measured by using DMA 35 portable vibrating density meter. Anton paar Autria (Europe) having accuracy of density 0.001

g/cm³, repeatability 0.0005 g/cm³ and resolution 0.0001 g/cm³ 5 and viscosity by LVDL V-pro II Brook field viscometer (USA) 6. Refractive indices for sodium D-line were measured by using Abbe's refractometer, having accuracy up to the third place of decimal 7.

IV. RESULTS AND DISCUSSION

The values of density (ρ), viscosity (η) and refractive index (n) for viscous flow with increasing mole fraction (X) of 2,3-DCA for the binary mixtures of 2,3-DCA+EG are reported in Table 1.

Table 1. Mole fraction (X) of 2,3-DCA and EG density (ρ), viscosity (η) and refractive index (n) for binary liquid mixture at room temperature.

X	ρ g/cm ³	η cp	n
0.0000	0.9966	1.35	1.403
0.09697	1.1370	1.59	1.460
0.17185	1.1834	1.84	1.484
0.27576	1.2024	2.24	1.496
0.38000	1.2436	2.44	1.506
0.42637	1.2680	2.55	1.531
0.56672	1.2950	2.98	1.551
0.72356	1.3631	3.40	1.578
1.0000	1.4084	3.84	1.590

The density of binary mixture of 2,3-DCA+EG are increasing as mole fraction of 2,3-DCA in the binary mixture is increasing. This is expected because density of pure 2, 3-DCA is more than that of pure EG. It can also be seen that viscosity (η), refractive index (n) is increasing with increase in mole fraction of 2, 3-DCA in the binary mixture. This increase in η and n is further supported by the increase in density of the binary mixture with increase in mole fraction of 2, 3-DCA. Increases in viscosity (η) for the acid amine and EG mixture due to the formation of dissociated ions in the mixture. Which is endothermic and depends upon the acidic strength of EG. Since in the present paper the maximum viscosity for 2,3-DCA may be associated with the formation of dissociated ions in the mixture and due to the more acidic character of 2,3-DCA. The spectacular increases in viscosity (η) may also be attributed to the mutual viscosity of the alcohols and amine molecules. Viscosity (η) increases as mole fraction of 2, 3-DCA in the binary mixture increases. Increase in viscosity of binary mixture can be attributed to increase in effect of hydrogen bonding with decrease in mole fraction of EG. This is because pure 2,3-DCA is more viscous than pure EG. It is due to presence of strong hydrogen bonding in 2,3-DCA, more number of carbon atoms and long straight chain compound.

V. CONCLUSION

The density, viscosity and refractive index values of the binary mixtures of 2,3-DCA with EG are reported all binary mixtures are miscible. The density, viscosity and refractive index values increased with the 2,3-DCA mole fraction. In contrast to monotonic increase of density, viscosity and refractive index with the mole fraction of 2,3-DCA and may be attributed to the entropic effects and weakening of hydrogen bonding interaction between ethanol molecules.

VI. REFERENCES

- [1]. Oster G, J Am Chem Soc., 1946, 68(10), 2036-2041;
- [2]. Kamble S, Sudake Y S and Mehrotra S C, J Koren Chem. Soc., 2011, 55(3), 373.
- [3]. Rana V A and Vyas A D, Indian J Pure Appl Phys., 2001, 39(5), 316-320.
- [4]. Das D and Hazra D K, Indian J Phys., 2003,77,519.
- [5]. Nemmaniwar B, Mokle S and Kadam P L, Pak J Chem., 2013, 3(2), 1.
- [6]. Nemmaniwar B G, .Kalyakar N V and Kadam P L, Orbital Elec J Chem., 2013, 5(1), 1-6
- [7]. Nemmaniwar B. G. Science Direct Materials Today: Proceedings 23 (2020) 324–328.

Study of Atmospheric Aerosol Using Optical Remote Sensing: A Review

Govind B. Munde¹, Shafiyoddin B. Sayyad¹, Pradeep D. Gaikwad^{#2}

¹Department of Physics. B. Attal Arts, Science and Commerce College Georai, Beed, Maharashtra, India

²Department of Computer science Milliya Arts, Science and Management Science College, Beed, Maharashtra, India

ABSTRACT

This paper is review of the aerosol optical depth (AOD) of the air pollution, polluted particular matter in the atmosphere, the harmful effect of the air pollution on the human health. The AOD is measured from the retrieval of the data from different platforms, the advancement of the technology in the optical remote sensing and the AOD. The new algorithms are developed to examine and characterizing the AOD the number of satellites are working in space for imagine the aerosol in the atmosphere like Moderate Resolution Imaging Spectroradiometer (MODIS) and the Multiangle Imaging Spectroradiometer (MISR) instruments onboard NASA's Terra satellite in 1999 has provided global measurements of AOD, a measure of light extinction by aerosol in the atmospheric column, during their overpass time of 1030 local time (LT) this paper purpose is the how different kind of algorithms are used for the studying the types of aerosol and their depth by optical remote sensing.

Keywords: Atmospheric Aerosol, Remote sensing, AOD

I. INTRODUCTION

Atmospheric aerosol is the general term for solid and liquid particles suspended in the atmosphere, mainly come from natural sources such as fine ash and dust lifted by the wind, salt particles, volcanic eruption and from human activities the burning of fossil and non-fossil fuels, transportation, and industrial dust. There are two types of atmospheric aerosol, that is Primary aerosol (Soil dust, sea spray, crustal materials, smoke and organic matter) and Secondary aerosol (sulphate, nitrates, ammonia, volatile organic compounds) components [1,2].

Atmospheric aerosol is a most part of Earth's atmosphere system and has most significant role on global climate change and air quality. Aerosol particles are believed to have a net cooling effect on the atmosphere due to light scattering in the visible and ultraviolet ranges. scientific knowledge on the interaction between atmospheric aerosols and solar Emissivity is very low compared to other atmospheric components mainly due to high spatiotemporal variability of atmospheric aerosols [3,4]. Atmospheric aerosols are of great importance in Earth's radiative budget due to their potential Increasing the scattering and absorption of shortwave (solar) radiation [5].

The common objectives of atmospheric aerosol:

- (a) The surface of earth atmospheric aerosol has direct impact on public health.
- (b) Roles in chemical and physical processes in the atmosphere and their potential effects on local and global climate [6].

Remote sensing is, broadly but logically speaking, the collection of information about an object without making physical contact with it. It is a derive information about state and condition of an object by interpreting the information contained in the electromagnetic signal coming from the object [7,8]. The term "Remote sensing" is most commonly used in connection with electromagnetic techniques of information acquisition [9].

In the remote sensing there are two types,

Active sensor

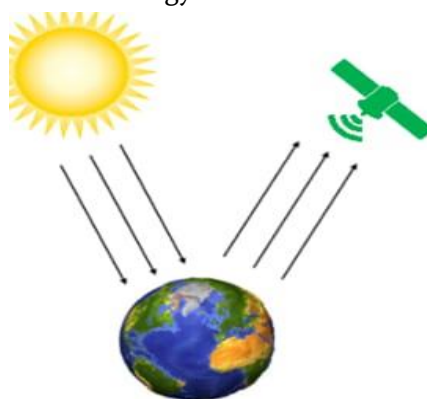
Provides their own electromagnetic energy that is transmitted from the sensors towards the terrain, interacts with the terrain producing a backscatter of energy & is recorded by the remote sensor's receiver.



Active Remote Sensing

Passive sensor

Detects the nature any emitted microwave energy within its field of view.



Passive Remote Sensing

Optical remote sensing makes use of visible near-infrared and short-wave infrared sensors to form images of the earth surface by detecting the solar radiation reflected from targets on the ground different materials

reflect and absorb differently at different wavelengths. Thus, the targets can be differentiated by their spectral reflectance signature in the remotely sensed images. Optical remote sensing systems are classified into the various types depending on the number of spectral bands used in the imaging process.

Needs for the measurement of aerosol-distribution

- (a) Provide a reference climatology for measuring root trends natural and anthropogenic processes;
- (b) Remove aerosol effects from remotely sensed observations of Earth atmospheric system;
- (c) Understand the interaction between the lithosphere, hydrosphere, cryosphere, atmosphere and biosphere resulting from the transport, transformation and deposition of aerosols [10].

Atmospheric Absorption

The atmosphere act as a selective filter at different wavelength, such that certain spectral regions cannot be remotely observed.

The main cause for this absorption are

- 1) Atomic oxygen (O_2), filters out ultraviolet rays less than 0.1 micro meters., as well as small portions in the infrared and microwave bands.
- 2) Ozone (O_3), which removes most of the ultraviolet rays below 0.3 micro meters, some mirror band in the visible spectrum.
- 3) water vapor (H_2O), a strong absorber around 6 micro meter and secondary absorber between 0.6 and 2micro meters.
- 4) carbon dioxide (CO_2), which absorbs in the thermal infrared (15micro meter), has a significant effect in the infrared, between 2.5 and 4.5 micro meters [11].

Atmospheric Scattering

Scattering of electromagnetic radiation occurs due to reflection of incoming solar rays by gases, aerosols and water vapour present in the atmosphere. Aerosol are caused by both natural and human causes. They can be oceanic, due to water moment, or continental, such as dust in suspension or particle emitted by combustion. Origins and characteristics they vary greatly in their size, leading to different types of dispersions, as the process depends on the diameter of the dispersing particles.

There are three types of atmospheric dispersion,

- 1) **Rayleigh scattering**- These scattering affected by smaller wavelength diameter of the particles.
- 2) **Mie scattering**- These scattering affected by particle size and wavelength are same.
- 3) **Non selective scattering**- These scattering affected by particle size is greater than the wavelength [11].

Atmospheric Emission

These emission effects are in the thermal infrared. In order to accurately retrieve the surface temperature from the satellite images, it must be corrected [11].

II. LITERATURE REVIEW

An aerosol is a two-phase colloidal system, consisting of particles (solid or liquid) and gases. In which he has been suspended an individual aerosol particle can be cold or warm depending on its size, refractive index etc. Aerosol optical thickness (AOT) is the most fundamental parameter for determining optical properties of aerosols which is the degree to which aerosols prevent the transmission of light in the atmosphere either through scattering or absorption[12].

Remote sensing data used for road delineation includes ground moving target indicators (GMTI) tracking, smart phone Global Positioning System (GPS) data, Street View images, synthetic aperture radar (SAR) imagery, light detection and ranging (LiDAR) data, high resolution imagery and hyperspectral imagery.Spaceborne high-resolution imaging is still the main technological approach to Earth Observation. Airborne High-resolution images have higher resolution and are less affected by the environment [13].

In fact, all particles for remote sensing applications it is necessary to treat simultaneously without suspending in the environment separation on aerosol and cloud particles. The general function is to receive Chemical composition, concentration and size distribution of particles using various remote sensing technique (e.g. optical observations from satellite). This is due to aerosols and cloud particles (and also atmospheric gases) do not exist in isolation but interact with each other Spatial and time [14].

Remote sensing techniques is ground based remote sensing and the satellite remote sensing, Satellite remote sensing plays an important role in aerosol detection as it can obtain aerosol information (e.g. AOD), but Single Scattering albedo (SSA) is a very difficult to found a aerosol from satellite measurement. Ground-based remote sensing is a very useful approach for detecting columnar aerosols as it provides multi-angle, multi-wavelength and polar measurements of solar and sky radiation [15].

The fine particular matter of diameter less than 2.25PM is very harmful for the human health which causes cancer of lungs pulmonary inflammation and cardiopulmonary mortality the aerosol is valuable for the design of air quality to strategies the forecasting. The estimation of aerosol optical depth(AOD) is important for measurement of harmful particles of matter to study their depth and properties characteristics of that matter. The development and measurement of aerosol optical depth provides unique synopsis of global surface 2.25PM concentration with coupled chemical targets of model on the relationship between aerosol optical depth and 2.25PM [16].

In 1970s researchers starts to use remote sensing data to retrieve the ocean aerosol optical thickness. the new satellite sensors use after 21st century. If the study of atmospheric environment and climate change then then the high temporal resolution of AOD are very important. AOD is a very basic characteristics of Atmospheric aerosol, They impact on climate change and human health. The method of retrieving AOD products using satellite remote sensing provides support of the investigation and monitoring of the climate effects of aerosols and regional air pollution. The proposed an AOD retrieval method based on HJ-1 A/B charge coupled device (CCD) visible light band and found that the AOD retrieved from the HJ-1 A/B CCD data presented the same spatial patterns and trends with the AOD products in Moderate Resolution Imaging Spectroradiometer (MODIS) [17].

Remote sensing provides the capable observation aerosol data the AOD is retrieval by satellitebased data the aerosol are play's important role in the earths balanced by scattering and absorbing solar and terrestrial radiation. the AOD is retrieval by the number of satellite techniques as multispectral thermal imager and ground truth the aerosol retrieval codes are modified and used for MIT single view[18].

A new method to recover AOT from moderate Resolution Imaging Spectroradiometer (MODIS) Satellite images, in which the strategy block partitioning mass communication were adopted, thereby maximizing load balance and reducing overhead time during inter-processor communication. AOT is an indicator of air quality an important geophysical parameter. Application to retrieve passive satellite remote sensing data land aerosol loading depends on prior knowledge of accurate land surface reflectance[19].

III. DISCUSSION

This study explores the estimation of the AOD of the particle present in the atmosphere. The application of the AOD is for to strategies the air quality forecasting and the measurement of the aerosol this paper focus on the different kind of algorithms that are developed for the retrieval of AOD to this algorithms makes to find accuracy in AOD to mitigate the pollution and polluted air in atmosphere. The AOD is important for the study of the air pollution and harmful matter partials present in the atmosphere the negative effect to the human health the aerosol depth in atmosphere. the strategies on the harmful pollution have designed to slow down the negative effects on human health.

IV. CONCLUSION

The AOD is measured by the optical remote sensing to study the properties and characteristics of the optical aerosol for pollution and air quality maintaining. the different kind of algorithms are developed for the AOD. Different kind of strategies are applied for the harmful particle in the atmosphere to mitigate the effect of pollution and harmful particle in the matter. The optical remote sensing is useful for the measuring the optical depth of aerosol.

V. REFERENCES

- [1]. Viana, M. Pey, J. Querol, X. Alastuey, A. Leeuw, F.D. Luekewille, A. Natural sources of atmospheric aerosols influencing air quality across europe. *Sci. Total Environ.* 2014, 472, 825– 833.
- [2]. L. Clarisse, P.F. Coheur, F.Prata, A unified approach to infrared aerosol remote sensing and type specification. *Atmospheric chemistry and Physics*, 13, 2195-2221, 2013.
- [3]. Y.S. Xie, Z.Q. Li, Y.X.Zhang, Estimation of atmospheric aerosol composition from ground-based remote sensing measurements of Sun-Sky radiometer.*Journal of Geophysical Research: Atmospheres.* 2017, 122, 498-518.
- [4]. M. J. Granados-Muñoz, F. Navas-Guzman , J. A. Bravo-Aranda, Hygroscopic growth of atmospheric

- aerosol particles based on active remote sensing and radiosounding measurements: selected cases in southeastern Spain. *Atmos. Meas. Tech.*, 8, 705–718, 2015.
- [5]. J.-F. Leon, P. Chazette, J. Pelon, F. Dulac and H. Randriamiarisoa, Aerosol direct radiative impact over the INDOEX area based on passive and active remote sensing. *JOURNAL OF GEOPHYSICAL RESEARCH*, VOL. 107, NO. D19, 8006, 2002.
- [6]. R. Ravi Krishna, Current atmospheric aerosol research in India. *current science*, vol.102, NO.3, 2012.
- [7]. Thomas M. Lillesand, Ralph W. Kiefer, Jonathan W. Chipman, *Remote Sensing and Image Interpretation*, sixth edition, 2013, ISBN:978-81-265-3223-0.
- [8]. W.G.Rees, *physical principle of remote sensing*, the press syndicate of the university of Cambridge, second Edition 2001, ISBN:0-521-66948-0.
- [9]. Charles Elachi and Jakob van Zyl, *Introduction to the physics and techniques of Remote Sensing*, Wiley publication, Third edition, 2021.
- [10]. P. C. S. DEVARA, Remote sensing of atmospheric aerosols from active and passive optical techniques. *remote sensing*, 1998, vol. 19, no. 17, 3271-3288.
- [11]. Emilio Chuvieco and Alfredo Huete, *Fundamentals of satellite remote sensing*, Taylor and francis group, LLC by 2010, ISBN: 978-0-415-31084-0.
- [12]. Sunita Verma, Divya Prakash, Manish Soni and Kirpa Ram, *Atmospheric Aerosols Monitoring: Ground and Satellite-Based Instruments*. *Atmospheric Aerosols Monitoring: Ground and Satellite-Based Instruments*, DOI: 10.5772/intechopen.80489.
- [13]. JianxinJia ,Haibin Sun, Changhui Jiang , KirsiKarila , Mika Karjalainen, Review on Active and Passive Remote Sensing Techniques for Road Extraction. *Remote Sens.* 2021, 13, 4235.
- [14]. A.A. Kokhanovsky, Remote sensing of atmospheric aerosol using spaceborne optical observations. *Earth-Science Reviews* 116 (2013) 95–108.
- [15]. YisongXie, Zhengqiang Li, Donghui Li, Hau Xu and kaitao, Aerosol optical and microphysical properties of four typical sites of SONET in China based on Remote Sensing Measurements. *Remote sensing.* 2015,7,9928-9953.
- [16]. Aaron van Donkelaar, Randall V. Martin, and Rokjin J. Park, Estimating ground-level PM_{2.5} using aerosol optical depth determined from satellite remote sensing. *JOURNAL OF GEOPHYSICAL RESEARCH*, VOL. 111, D21201.
- [17]. Lijuan Chen, Ying Fei, Ren Wang , Peng Fang, Jiamei Han and Yong Zha, Retrieval of High Temporal Resolution Aerosol Optical Depth Using the GOCI Remote Sensing Data. *Remote Sens.* 2021, 13, 2376.
- [18]. Petr Chylek and Brad Henderson, Satellite based retrieval of aerosol optical thickness: The effect of sun and satellite geometry. *GEOPHYSICAL RESEARCH LETTERS*, VOL. 30, NO. 11, 1553.
- [19]. JianpingGua, Huadong Xiao et al, A new method to retrieve aerosol optical thickness from satellite images on a parallel system. *Particuology* 7 (2009) 392–398.

Annealing Effects on Optical and Electrical Properties of a- (Ge₂₀Se₈₀)₉₀Bi₁₀ Thin Films Deposited by Physical Thermal Evaporation

Akshay Kumar

Government Degree College, Indora Kangra H.P (affiliated to HPU Shimla), Himanchal Pradesh, India

ABSTRACT

In the present study (Bi) doped Ge₂₀Se₈₀ thin films are characterized for their optical and electrical properties. Bulk sample is prepared by melt quenching technique, while thin films are deposited via thermal evaporation. XRD study confirms the amorphous nature of both bulk and thin films samples. Optical parameters like refractive index, band gap and real and imaginary dielectric constant are calculated using transmission spectra in 400 to 1200 nm wavelength range. The dark conductivity (σ_d) measurements of a-(Ge₂₀Se₈₀)₉₀Bi₁₀ thin films have been carried out over temperature range 298-353K. The effect of annealing is studied on optical and electrical properties of thin films.

Keywords: Annealing, Optical properties, Thin Films, Chalcogenide glasses,

I. INTRODUCTION

Chalcogenide bulk glasses and thin films are known for their various applications. They are extensively studied for unique optical and electrical properties. These materials are suitable for infrared detectors and shows reversible phase change electrically and optically which make them useful candidate for memory storage. Chalcogenide glasses based on germanium selenide are promising materials for applications like waveguides and sensors [1, 2]. Chalcogenide glasses having high refractive index, wider band gap, linear and nonlinear properties make them useful for IR sensors, photo detector, holography and other applications [3-7]. The Ge₂₀Se₈₀ glassy alloy has maximum glass forming tendency at $x=20$ for Ge_xSe_{100-x} and Ge₂₀Se₈₀ possess a particular structure with chemical formula GeSe₄ [8]. Addition of third element into the binary alloy results in more stable cross-linked structures. Density of defect states change drastically in case of ternary alloys leading to increase in softening temperature, enhanced mechanical strength and glass forming region expansion [8,9]. Since Bi addition to a Ge-Se system enhance chemical stability, by replacing Se with Bi in a Ge-Se system leads to the modification of optical band gap and other electronic properties. Here Bi act as network modifier in Ge--Se system will lead to the more disordered network which further may led to alter the structural, optical and electrical properties [10]. In the present work, we have measured transmission spectra of a-(Ge₂₀Se₈₀)₉₀Bi₁₀ thin films. From measured experimental data, we have calculated various optical parameters. We also investigated dc conductivity and photoconductivity in these thin films. We have focused

our investigations to see effect of annealing on the optical and electrical properties of such a technically important material.

II. EXPERIMENTAL

Glassy alloy of a-(Ge₂₀Se₈₀)₉₀Bi₁₀ has been prepared by melt quenching technique by taking elements according to their atomic weight percentage. The materials were sealed in quartz ampoules and heated up to 1100 °C in a rocking furnace at a heating rate of 2-3 °C per minute followed by quenching in ice cold water. Thin films were synthesized by thermal evaporation technique on well-degassed Corning 7059 glass substrate under vacuum 2×10⁻⁵ mbar. X-ray diffraction pattern (XRD) was examined at room temperature. The absence any sharp peak in XRD confirms the amorphous nature of thin films. Transmission spectra measured by computer-controlled spectrophotometer [Solar TII, MS 2004]. All the optical constants measurements reported in this paper are performed at room temperature (300 K). The sample is annealed at 130°C for 2 hour under vacuum (10⁻³ mbar).

The dark conductivity (σ_d) measurements of a-(Ge₂₀Se₈₀)₉₀Bi₁₀ thin films have been carried out over the temperature range 298-353K. A vacuum of 10⁻³ mbar were maintained in the sample holder during various measurements. Pre-deposited thick aluminum electrodes on well-degassed Corning 7059 glass substrates have been used for the electrical contacts with planar geometry of the film (length 2.0 cm; electrode gap 2×10⁻² cm) is used for the electrical measurements. The photoconductivity measurements has been studied using metallic sample holder where heat filtered light (200 W tungsten lamp) shone through a transparent quartz window under vacuum of about 10⁻³ mbar. The photocurrent (I_{ph}) is obtained by subtracting the dark current from current in presence of light. Digital Luxmeter (TES-1332) is used for measurement of light intensity.

III. RESULTS AND DISCUSSION

3.1 Structural study

XRD patterns of a-(Ge₂₀Se₈₀)₉₀Bi₁₀ thin films are shown in figure 1. It is clear from this figure that there is no sharp peak in XRD patterns of films suggests that a-(Ge₂₀Se₈₀)₉₀Bi₁₀ films amorphous in nature. The data were collected in a range of $2\theta=20-60^\circ$ at a scanning rate of 10 °C per min at room temperature.

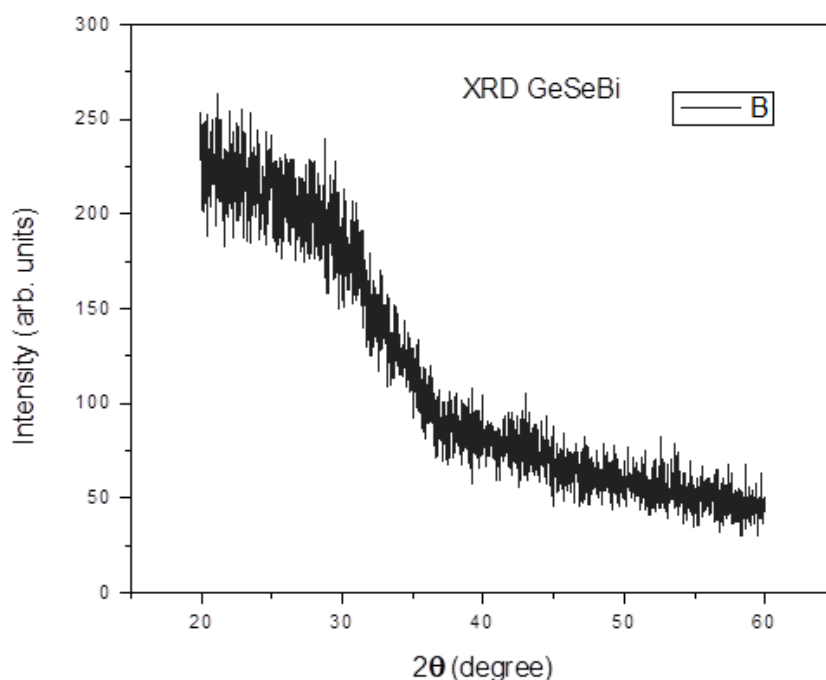


Fig1. X-ray diffraction patterns of a-(Ge₂₀Se₈₀)₉₀Bi₁₀ thin film.

3.2 Optical studies

Figure 2. Shows transmission spectra of thermally evaporated a-(Ge₂₀Se₈₀)₉₀Bi₁₀ thin film. The Swanepoel's envelope method has been employed to calculate the refractive index (n) and extinction coefficient (k) [11, 12]. This model assumes a thin film of uniform thickness deposited on a transparent substrate having a refractive index (s). In the transparent region ($\alpha \approx 0$) the refractive index n , of a thin film is given by

$$n = \left[M + (M^2 - s^2)^{1/2} \right]^{1/2} \quad (1)$$

where s is refractive index of the substrate and M is given by

$$M = \frac{2s}{T_m} - \frac{s^2 + 1}{2}$$

In the weak- and medium-absorption regions where ($\alpha \geq 0$) the refractive index n is found to be given by

$$n = \left[N + (N^2 - s^2)^{1/2} \right]^{1/2} \quad (2)$$

where

$$N = 2s \frac{T_{\max} - T_{\min}}{T_{\max} T_{\min}} + \frac{s^2 + 1}{2}$$

In the strong absorption region absorption coefficient (α) can be calculated by using

$$\alpha = d^{-1} \ln \left(\frac{16n^2 s}{(n+1)^3 (n+s^2) T_0} \right) \quad (3)$$

where d is the thickness of film, $n(\lambda)$ and s are the refractive indices of the film and substrate respectively, and T_0 is the measured transmission. In Amorphous semiconductors absorption is divided namely three regions , higher absorption region ($\alpha \geq 10^4 \text{ cm}^{-1}$), exponential edge region ($1 \leq \alpha \leq 10^4 \text{ cm}^{-1}$) and weak absorption region ($\alpha \leq 1 \text{ cm}^{-1}$)[13].

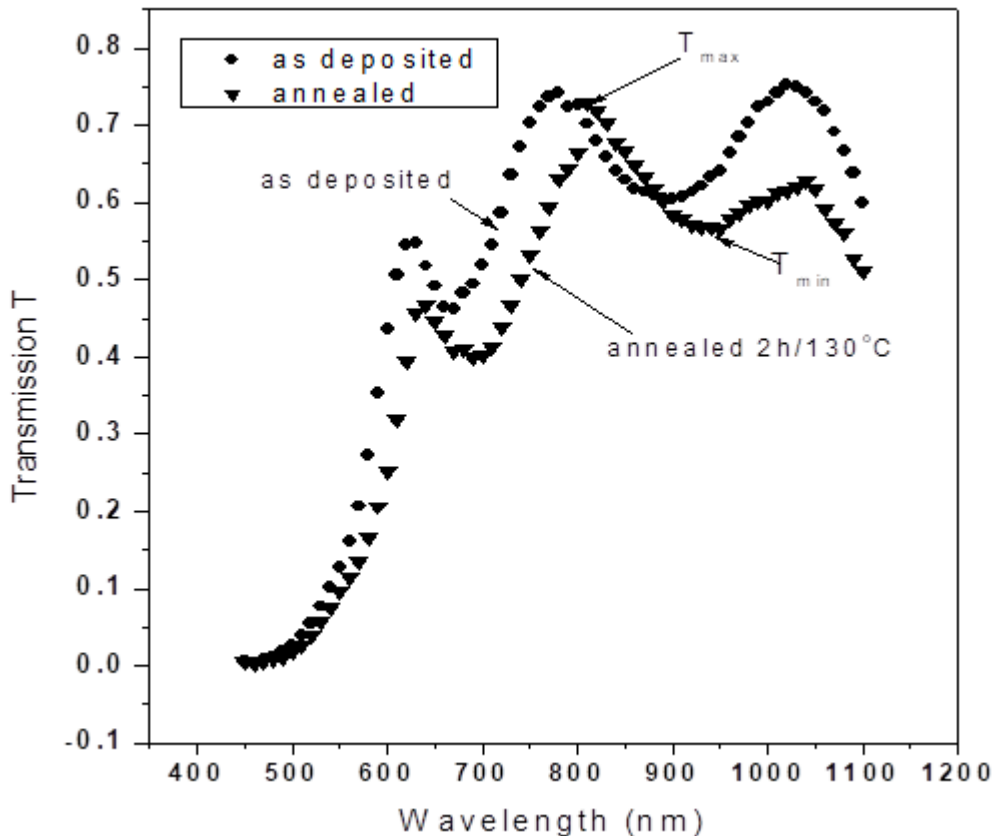


Fig.2. Transmission spectrum vs wavelength of a-(Ge₂₀Se₈₀)₉₀Bi₁₀ thin film.

The calculated value of absorption coefficient and refractive index along with other optical parameters are plotted as function of photon energies in Figure 3. The real (ϵ_1) and imaginary (ϵ_2) parts of the dielectric constant for a-(Ge₂₀Se₈₀)₉₀Bi₁₀ films has been calculated using the relation [14]

$$\epsilon_1 = n^2 - k^2 \quad \text{and} \quad \epsilon_2 = 2nk \quad (4)$$

The values of complex dielectric index (real and imaginary) (ϵ_1 and ϵ_2) plotted in Figure 3. Extinction coefficient k , is obtained from the already known α values, using the basic equation, i.e. $k = \alpha\lambda/4\pi$. The values of extinction coefficient (k) calculated using this equation and are plotted in Fig. 3.

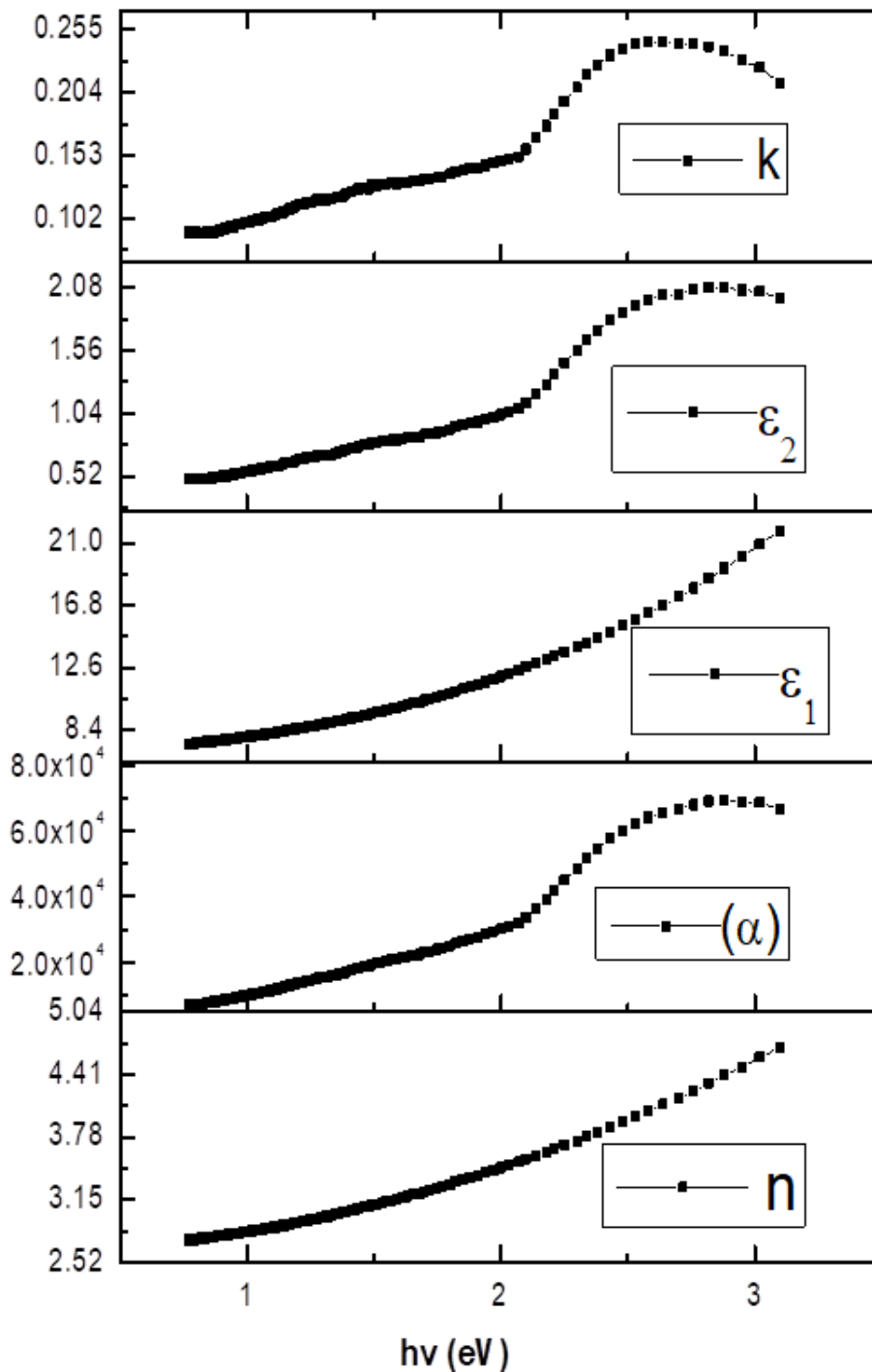


Fig. 3 Refractive index (n), absorption coefficient (α), real dielectric constant (ε₁), Imaginary dielectric constant (ε₂) and extinction coefficient (k) of a-(Ge₂₀Se₈₀)₉₀Bi₁₀ thin film.

Wemple and DiDomenico parameters (E_0 is the oscillator energy and E_d is the so-called dispersion energy) can be determined from experimental data by using the following relation [15, 16].

$$n^2(h\nu) = 1 + \frac{E_d E_0}{E_0^2 - (h\nu)^2} \quad (6)$$

Plot of $(n^2 - 1)^{-1}$ vs. $(h\nu)^2$ (Figure 4) allows us to determine the oscillator parameters, by linear fitting method. The values of E_0 and E_d can directly be determined by the slope $(E_0 E_d)^{-1}$ and intercept on vertical axis (E_0/E_d). The calculated values of E_0 and E_d are shown in the Table 1.

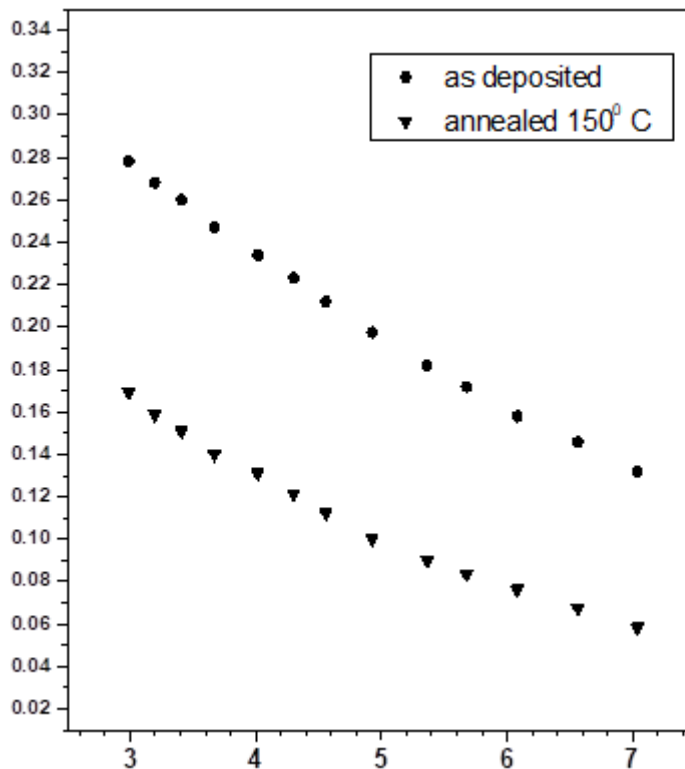


Fig.4 Plot of $(n^2-1)^{-1}$ vs. $(h\nu)^2$ for a-(Ge₂₀Se₈₀)₉₀Bi₁₀ thin film.

The value of static refractive index (n_0) can be obtained using relation as described elsewhere [16]. The value of static refractive index (n_0) is obtained relation (6) by assuming $h\nu$ approaching zero reduce to relation (7).

$$n_0 = \left(1 + \frac{E_d}{E_0} \right)^{1/2} \quad (7)$$

The absorption coefficient (α) is calculated from the relation

$$x = \exp(-\alpha.t) \quad (8)$$

where, x is absorbance as described elsewhere [15, 16]. The absorption coefficient of amorphous semiconductors in the strong-absorption region ($\alpha \geq 10^4 \text{ cm}^{-1}$), the transition between extended states in both valence and conduction bands, is given by [17]

$$\alpha(h\nu) = B(h\nu - E_g^{opt})^n / (h\nu) \quad (9)$$

where E_g^{opt} is the optical band gap. The parameter B is the band tailing parameter and $n = 1/2$ and 2 for direct and indirect band gap materials, respectively. The optical gap (E_g^{opt}) obtained from the intersection of the plot $(\alpha\hbar\nu)^{1/2}$ vs $h\nu$ is (1.49 ± 0.01) eV (Table 1). The degree of disorder and density of defects states decreases by giving heat treatment to chalcogenide thin films, which increases the refractive index and band gap upon annealing. The other associated optical parameter also show changes upon heat treatment of thin films.

Table.1. The refractive index (n), the extinction coefficient (k), real part of dielectric constant (ϵ_1), imaginary part of dielectric constant (ϵ_2), oscillator energy (E_0), oscillator strength (E_d) and optical gap (E_g^{opt}) of as deposited and annealed a-(Ge₂₀Se₈₀)₉₀Bi₁₀ thin films.

Sample (Ge ₂₀ Se ₈₀) ₉₀ Bi ₁₀	n ($\lambda=1000$ nm)	(k)	(ϵ_1)	(ϵ_2)	E_0 (eV)	E_d (eV)	n_0	E_g^{opt} (eV)
As deposited	2.92	0.116	8.52	0.66	2.87	17.58	2.67	1.49
Annealed	2.98	0.118	8.78	0.70	2.91	18.43	2.73	1.54

3.3 Electrical studies

The dark conductivity (σ_d) measurements of a-(Ge₂₀Se₈₀)₉₀Bi₁₀ thin films have been carried out over the temperature range 298-353K. A vacuum of 10^{-3} mbar is maintained in the sample holder during various measurements. The temperature dependence of (σ_d) for thin film a-(Ge₂₀Se₈₀)₉₀Bi₁₀ plotted in Fig. 5(a)-(b). In most of chalcogenide glasses the plot of $\ln\sigma_d$ versus $1000/T$ are straight line indicating that dc conduction is single activation process. Such type of conduction mechanism can be expressed by Arrhenius relation given by

$$\sigma_d = \sigma_0 \exp\left(\frac{-\Delta E}{kT}\right) \quad (10)$$

where σ_0 is pre exponent, ΔE activation energy, k is Boltzmann's constant and T is the absolute temperature respectively.

The calculated values of σ_d , σ_0 , and ΔE_d are given in table 2. It is observed that the value of dc activation energy (ΔE_d) decreases from 0.48 eV to 0.46 eV after annealing at temperature 373K. The value of σ_d decreases from $6.40 \times 10^{-9} \Omega^{-1}\text{cm}^{-1}$ to $6.12 \times 10^{-7} \Omega^{-1}\text{cm}^{-1}$ after annealing at temperature 373K. There is a slight decrease in ΔE_d from 0.48 eV to 0.46 eV post annealing. The variation of steady state photoconductivity (σ_{ph}) shown in Fig 5(c) with temperature at a particular intensity (1035 lux) with accuracy in measurement of I_{ph} is $\pm 1\text{pA}$. A maximum in the photoconductivity (σ_{ph}) is observed in a-(Ge₂₀Se₈₀)₉₀Bi₁₀ thin films. At higher temperature the carrier concentration of thermal carriers exceeds that of photo carriers and σ_{ph} decreases with increase in temperature. The rate of recombination is governed mainly by the dark concentration of the carrier. The decrease in photoconductivity with increasing temperature is called "thermal quenching" [18]. With increasing temperature holes can hop more easily in the localized tail states, resulting in an increase in the recombination rate and hence decrease in photoconductivity.

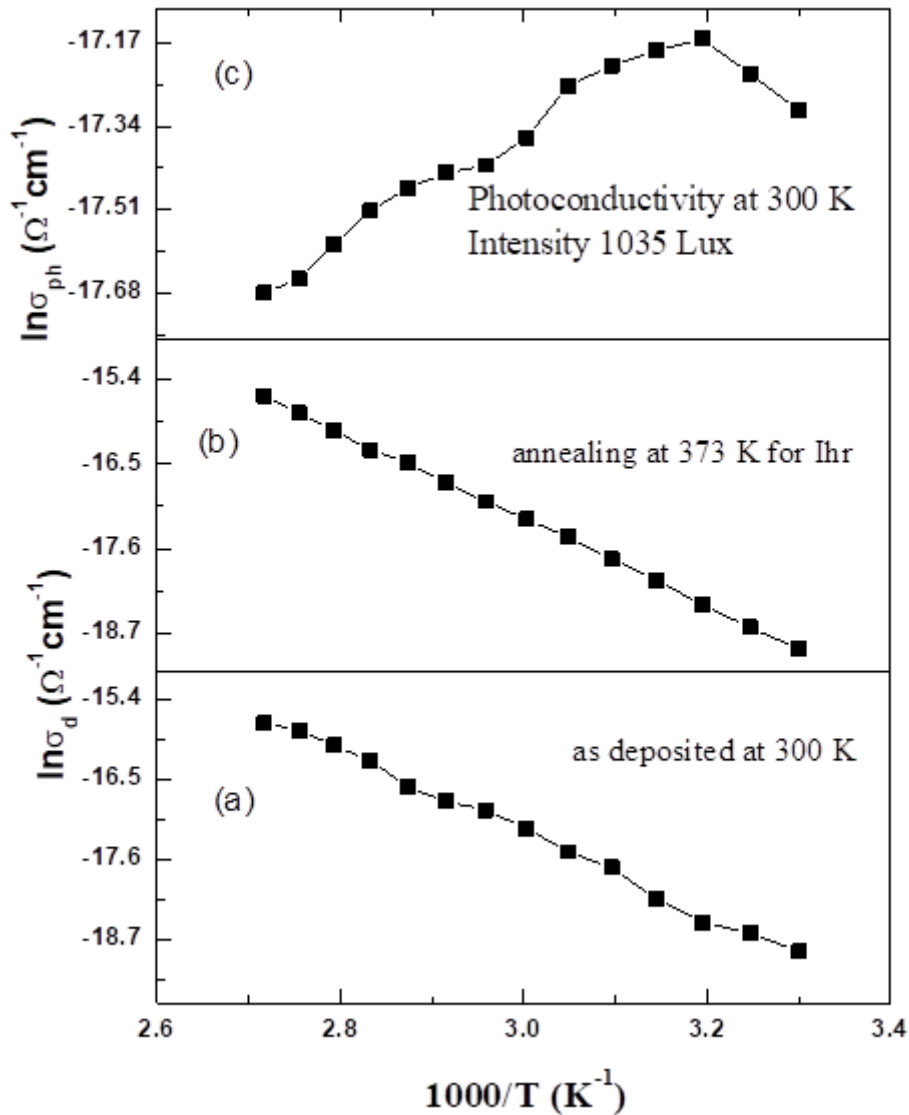


Fig. 5(a)-(c).The temperature dependent (a) dc dark conductivity as deposited 300 K, (b) annealed 373 K and (c) photoconductivity a-(Ge₂₀Se₈₀)₉₀Bi₁₀ thin film.

The occurrence of this maximum in photoconductivity has been discussed in various theories [18, 19]. The value of σ_{ph} and ΔE_{ph} are $3.04 \times 10^{-8} \Omega^{-1} \text{cm}^{-1}$ and 0.12 eV respectively at room temperature (300K). It is clear from the Fig 5(c) that the photoconductivity is an activated process. The activation energy (ΔE_{ph}) for photoconduction is much smaller than dark conduction. The photosensitivity the ratio of light to dark current (σ_{ph}/σ_d) is shown in Table 2. It is observed the photosensitivity increases after annealing from 4.75 to 4.96.

Table.2. The dc conductivity (σ_d), pre-exponential factor (σ_0), dark activation energy (ΔE_d), photoconductivity (σ_{ph}), the activation energy of photoconduction (ΔE_{ph}), photosensitivity (σ_{ph}/σ_d) of a-(Ge₂₀Se₈₀)₉₀Bi₁₀ thin films.

Sample	σ_d ($\Omega^{-1}\text{cm}^{-1}$)		σ_0		ΔE_d (eV)		σ_{ph} ($\Omega^{-1}\text{cm}^{-1}$)	ΔE_{ph}	$\sigma_{ph}/\sigma_d(300\text{K})$	
	as	annealed	as	annealed	as	annealed			as	annealed
(Ge ₂₀ Se ₈₀) ₉₀ Bi ₁₀	6.40 $\times 10^{-9}$	6.12 $\times 10^{-9}$	0.47	0.72	0.48	0.46	3.04 $\times 10^{-8}$	0.12	4.75	4.96

IV. CONCLUSIONS

The effect of annealing on the optical and electrical properties of a-(Ge₂₀Se₈₀)₉₀Bi₁₀ thin film have been studied. It is found that values of the refractive index (n), the extinction coefficient (k), real part of dielectric constant (ϵ_1), imaginary part of dielectric constant (ϵ_2), oscillator energy (E_0), oscillator strength (E_d) and optical gap (E_{g}^{opt}) of a-(Ge₂₀Se₈₀)₉₀Bi₁₀ thin films after annealing which can be attributed due to structural rearrangements and change in the density of defects states. The temperature dependence dark and photoconductivity results indicates changed in the carrier concentration before and after annealing is leading to changes in various electrical parameters. DC activation energy (ΔE_d) decreases from 0.48 eV to 0.46 eV after annealing at temperature while on the other hand photosensitivity increases after annealing.

Acknowledgements

Author is thankful to Dr. S.K Tripathi, Solid state experimental laboratory (SSEL) Department of Physics, PU Chandigarh to providing necessary experimental facility.

V. REFERENCES

- [1]. J.H. Lee, J.H. Choi, J.H. Yi, W.H. Lee, E.S. Lee, Y.G. Choi, Sci. Rep. 8 (2018) 15482.
- [2]. Kadonok, J. Ceram. Soc. Jpn. 115 (5) (2007) 297.
- [3]. J. HoLee, W.Lee J.Yi, B. JePark, Y. Gyu Choi, J. Non-Cryst. Solids 481 (2018) 21–26.
- [4]. A.S. Hassanien, A.A. Akl, J. Non-Cryst. Solids 428 (2015) 112–120.
- [5]. D. Vipin Kumar, K. Dwivedi, Optik 124 (2013) 2345.
- [6]. A.S. Hassanien, A.A. Akl, J. Non-Cryst. Solids 432 (2016) 471–479.
- [7]. A.S. Hassanien, A.A. Akl, Superlattices Microstruct. 89 (2016) 153–169
- [8]. M. Micoulaut and J. C. Phillips, Phys. Rev. B 67, 104204 (2003)
- [9]. G. Abbady, A.M. Abd-Elnaiem, Phase Transitions 92 (7) (2019) 667–682.

- [10]. Pawan Kumar a, S.K. Tripathi, Ishu Sharma, Journal of Alloys and Compounds 775 (2018) 108-113
- [11]. R. Swanepoel, J. Phys. E: Sci. Instrum. 17 (1984) 896-903.
- [12]. R. Swanepoel, J. Phys. E: Sci. Instrum. 16 (1983) 1214-1222.
- [13]. J. Tauc in “Amorphous and Liquid Semiconductors” edited by J, Tauc (Plenum, New York, 1974) p. 159.
- [14]. F. Tepehan, N. Ozer, Solar Energy Mater. Solar Cells 30 (1993) 353-365.
- [15]. S.H. Wemple, M. DiDomenico, Phys. Rev. B 3 (1971) 1338-1351.
- [16]. S.H. Wemple, Phys. Rev. B 7 (1973) 3767-3777.
- [17]. J. Tauc, Amorphous and liquid semiconductors, Plenum, New York, 1974, pp. 171-173.
- [18]. T.S. Ralph. Shiah and Richard H. Bube, Journal of Applied Physics. 47 (1976) 2005
- [19]. J.G. Simmons and G.W. Taylor, J. Phys. C: Solid State Phys. 7 (1974) 3051

Comparison of Radar Backscattering Models IEM, Oh & Dubois for Synthetic Aperture Radar (SAR) Data

Monika S. Khole¹, Dr. Sanjay K. Tupe², Dr. Shafiyoddin Sayyad³

¹Ph.D student, Department of Physics, R.G. Bagdia Arts, S.B. Lakhotia Commerce and R. Bezonji Science College, Jalna 431203, Maharashtra, India

²Department of Physics, Kalikadevi Arts, Commerce and Science College, Shirur Kasar 413249, Maharashtra, India

³Department of Physics, Milliya Arts, Science & Management Science College, Beed 431122, Maharashtra, India

ABSTRACT

Synthetic aperture radar (SAR) observations have been used in numerous studies to estimate soil moisture and surface roughness, because of their important roles in many aspects. The objective of this paper is to compare the most used radar backscattering models: Oh et al., Dubois et al., and the Integral Equation Model (IEM) using a wide dataset of SAR (Synthetic Aperture Radar) data. These forward models reproduce the radar backscattering coefficients (σ°) from soil surface characteristics (dielectric constant, roughness) and SAR sensor parameters (radar wavelength, incidence angle, polarization). This comparison shows that the IEM is the most adequate to estimate soil moisture & roughness from SAR data.

Keywords: Oh Model, Dubois Model, Integral Equation Model (IEM); Synthetic Aperture Radar (SAR), Soilmoisture, Backscattering Coefficients, Surface Roughness.

I. INTRODUCTION

Soil moisture and surface roughness play important roles in various applications such as agronomy, hydrology, agriculture, risk prediction, etc. The radar signal, which depends on several radar parameters (incidence angle, frequency, polarization), is also correlated with soil surface roughness and moisture content. Synthetic Aperture Radar (SAR) data was used widely and successfully used for monitoring the spatial and temporal evolution of soil moisture and roughness. The estimation of soil moisture & roughness is done by inverting the measured SAR backscatter through SAR backscattering models (both empirical and physical).

A number of radar backscattering models have been reported in the literature. The most frequently used empirical models are those developed by Oh et al. [1–4], Dubois et al. [5], and the most popular physical models are the Integral equation model (IEM) [6]. These models are supposed to reproduce the radar backscattering coefficient and allow the estimation of soil surface parameters (moisture content and roughness) from SAR images. Several studies reported important discrepancies between backscattering model simulations and SAR observations [11 – 13].

Most studies have been carried out to evaluate and compare the robustness of the backscattering models such as Oh, Dubois, and IEM. Zribi et al. [13] evaluated the Oh model and IEM using L-, C- and X-band SAR data and in situ measurements. Results show that the IEM provides accurate simulations (RMSE about 2.0 dB) only over smooth surfaces. In addition, for rough surfaces and medium incidence angles, Oh model simulations retrieve backscattering values very close to the measured ones, while showing poor correlation with measured backscattering coefficients over smooth areas. Baghdadi and Zribi evaluated the backscattering models IEM, Oh, and Dubois by using large C-band SAR data and in situ measurements. Results showed that these models frequently tend to over-estimate or under-estimate the radar signal and the errors in model simulation depend on height, surface roughness, rms, soil moisture, mv, and/or incidence angle. This study aims to evaluate the most popular backscattering SAR models (Oh, Dubois, and IEM) by using a wide range of SAR data. Most of the methods for soil moisture mapping are based on backscatter models for soil moisture estimations. The objective of our study is to evaluate the most common backscatter models using a wide dataset of SAR data acquired from numerous agricultural sites. Thus, this study should be of great importance to the scientific community since it helps to understand the backscatter model's performance for a wide range of soil surface conditions, acquired for several study areas throughout the world by numerous SAR sensors.

II. SYNTHETIC APERTURE RADAR (SAR)

Backscattering signals measured using SAR are affected by land surface characteristics i.e. dielectric constant, the soil surface roughness of the soil, and the physical and geometrical properties of vegetation, size, shape, orientation, etc. [15] The main characteristics of the currently operating spaceborne SAR sensors along with some past and future sensors are summarised in Table 1. [16] SAR remote sensing has the following characteristics and advantages [18][15]: (a) estimating SM change using repeat observations, (b) correcting the effects of surface roughness based on a multi-incidence angle (c) a combination of high spatial-spatial resolution observations from active microwave sensors and coarse observations from passive microwave sensors, (d) measuring SM for bare soil quantitatively using dual polarization L-band or three- polarization.

Table 1. Characteristics of major spaceborne SAR systems.

Platform	Sensor	Polarization	Band(s)	Highest Spatial Resolution(m)	Swath Width (km)	Mission
SEASAT	SAR	HH	L	25	100	June-Oct 1978
SIR-A	SAR	HH	L	40	50	Nov 12-15th 1981
SIR-B	SAR	HH	L	25	30	Oct 5-13th 1984
Almaz-1	SAR	HH	S	13	172	Mar 31st 1991 - Oct 17 th 1992

ERS-1	AMI	VV	C	30	100	July 17 th , 1991- Mar 10 th , 2000
JERS-1	SAR	HH	L	18	75	Feb 11 th , 1992- Oct 12 th , 1998
SIR-C/X-SAR	SIR-C X-SAR	VV,HH,HV, VH, HH	L, C, X	30	10-200	April 1994 Oct 1994
ERS-2	AMI	VV	C	30	100	April 21 st 1995-
RADARSAT-1	SAR	HH	C	10	100-170	Nov 28 th , 1995-
SRTM	C-SAR X-SAR	VV, HH HH	C, X	30	50	Feb 11 th – 22 nd 2000
ENVISAT	ASAR	VV,HH,HH/V V	C	30	100-400	Mar 1 st 2002-
ALOS	PALSAR	HV/HH,VH/V V Quad-pol	L	10	70	Jan 24 th 2006-
TerraSAR-X	X-SAR	Quad-pol	X	1	10-100	June 15 th 2007-
RADARSAT-2	SAR	Quad-pol	C	3	10-500	Dec 14 th 2007-
COSMO/ SkyMed Series TecSAR	SAR-2000 SAR	Quad-pol HH, HV, VH, VV	X X	1 1	10-200 40-100	June 8 th & Dec 8 th , 2007- 21 st Jan 2008
SAR-Lupe	SAR	-	X	<1	-	Dec 2006 & Jul 2008-
Kondor-5	SAR	HH,VV	S	1	-	2009
TanDEM-X	SAR	Quad-pol	X	1	10-150	2009
RISAT	SAR	Quad-pol	C	3	30-240	2009
HJ-1C	SAR	HH, VV	S	20	-	2009
ARKON-2	SAR	-	X, L, P	2	-	2011
MapSAR	SAR	Quad-pol	L	3	20-55	2011
KompSAT-5	SAR	HH, HV, VH, VV	X	20	100	2011
SAOCOM-1	SAR	Quad-pol	L	7	50-400	2011
RADARSAT	SAR	Quad-pol	C	3	20-500	2012 – 2014
Constellation Mission SMAP	SAR	HH, HV, VV	L	3km	30-1000	2012
Sentinel-1	SAR	Quad-pol	C	5	400	2013
Sentinel-1A	SAR		C			2014
Sentinel-1B	SAR		C			2016

DESDynl	SAR	Quad-pol	L	25	>340	2015
RADARSAT-Constellation (3 Satellites)	SAR	Quad-pol	C	1-3	350	2018

III. IN-SITU MEASUREMENTS

Most of the techniques have been used for measurements of soil moisture and surface roughness using active microwave-based models.

3.1 Soil Moisture Measurements

The soil moisture is described as the level of saturation in the upper soil layer relative to the soil field capacity and is regulated by the precipitation and potential evaporation and is highly variable in space and time. Most of the studies have compared the estimation of soil moisture using active microwave sensors like (Shoshany et al., 2000; Kelly et al., 2003; Baghdadi et al., 2006; Rahman et al., 2008; Zribi et al., 2011; Das and Paul, 2015). Shoshany et al. (2000) have estimated Gravimetric SM converted into volumetric SM (%).

Gravimetric residual moisture method and volumetric moisture content have been widely used for SM measurements. Gravimetric SM (mg) values were obtained from laboratory analysis and converted into volumetric soil moisture (V_{sm}): [20]

$$V_{sm} = mg * sbd \quad (1)$$

Where, sbd multiplying bulk density.

Further, Mohan et al. (2015) have estimated gravimetric soil moisture (G_{SM}) as:

$$G_{SM} = \frac{M_{water}}{M_{soil}} = \left[\frac{W_{wet} - W_{dry}}{W_{dry}} \right] \quad (2)$$

Using simple formula volumetric soil moisture can be calculated as:

$$\frac{Wet\ weight - Dry\ weight}{height} \quad (3)$$

3.2 Roughness Measurement:

After the soil moisture, the surface roughness is another important factor that affects the backscattering SAR signature, because it determines how the incidence wave interacts with the surface. There are several ways to describe the natural surface roughness, and two frequently used methods are: fractal geometry theory and statistical description [21]. The fractal geometry theory describes the complicated surface roughness structure, especially for irregular and fragmented soil structures [22]. The surface roughness model helps to describe the surface height variations with respect to the ground surface level.

IV. BACKSCATTERING COEFFICIENTS

The backscattering coefficient of soil represents the relationship between soil properties and the scatterometer responses [23]. Some of the factors that are known to govern backscattering behavior are: i) dielectric constant of the vegetation material which is strongly influenced by moisture content; ii) the shape

distribution; iii) orientation distribution. iv) size distribution of the scatterers and roughness and dielectric constant of the underlying soil surface [24]. From the backscattering coefficient, we can directly calculate the soil dielectric constant [25]. It shows a linear relationship with SM as [20].

$$\sigma^{\circ} = A + B.W \quad (4)$$

Where A is the σ° of a completely dry soil surface and B is the sensitivity of σ° to change with the surface SM content.

Description of scattering models:

The most common approaches used to develop models for soil moisture retrieval are developing direct theoretical or physical models by simulating the backscattering coefficients in terms of soil attributes such as the dielectric constant and the surface roughness for an area with known characteristics. The dielectric constant of the soil surface and hence the soil moisture content can be estimated from mathematical inversion of these models.[26]

1.The Semi-Empirical Oh model

Oh, et al. developed from 1992 to 2004 several versions of a semi-empirical backscattering model. Based on theoretical models, scatterometer measurements, and airborne SAR observations, the Oh model is built over a wide variety of bare soil surfaces. The Oh model relates the co-polarized ratio p ($=\sigma_{HH}^{\circ}/\sigma_{VV}^{\circ}$) and the cross-polarized ratio q ($=\sigma_{HV}^{\circ}/\sigma_{VH}^{\circ}$) to incident angle (θ), wave number (k), the standard deviation of surface height (Hrms), correlation length (L), soil moisture (m_v), dielectric constant (ϵ_r), Γ_0 is the Fresnel reflectivity. The initial version of the Oh model is defined as:

$$p = \frac{\sigma_{HH}^{\circ}}{\sigma_{VV}^{\circ}} = \left[1 - \left(\frac{\theta}{90^{\circ}} \right)^{\frac{1}{3\Gamma_0}} e^{-k rms} \right]^2 \quad (5)$$

$$q = \frac{\sigma_{HV}^{\circ}}{\sigma_{VH}^{\circ}} = 0.23\sqrt{\Gamma_0} (1 - e^{-k rms}) \quad (6)$$

Where,

$$\Gamma_0 = \left| \frac{1 - \sqrt{\epsilon_r}}{1 + \sqrt{\epsilon_r}} \right|^2 \quad (7)$$

Oh et al. [14] proposed a new expression for q to incorporate the effect of the incidence angle:

$$q = 0.25\sqrt{\Gamma_0} (0.1 + \sin\theta^{0.9}) (1 - e^{-[1.4 - 1.6\Gamma_0]k rms}) \quad (8)$$

The expressions for p and q were again modified in 2002, and an expression was proposed for the cross-polarized backscatter coefficient (Oh et al. 2002):

$$p = 1 - \left(\frac{\theta}{90^{\circ}} \right)^{0.35 m_v^{-0.65}} e^{-0.4(k rms)^{1.4}} \quad (9)$$

$$q = 0.1 \left(\frac{rms}{L} + \sin 1.3\theta \right)^{1.2} (1 - e^{-0.9(k rms)^{0.8}}) \quad (10)$$

$$\sigma_{HV}^{\circ} = 0.11 m_v^{0.7} \cos^{2.2} \theta (1 - e^{-0.32(k rms)^{1.8}}) \quad (11)$$

Given that the measurement of the correlation length is not exact and that the ratio q is insensitive to the roughness parameters, Oh (2004) proposed a new formulation for q that ignores the correlation length:

$$q = 0.095 (0.13 + \sin 1.5\theta)^{1.4} (1 - e^{-1.3(k rms)^{0.9}}) \quad (12)$$

Oh's models were compared with the experimental database using the ratios p and c. The ratio of c is defined from the semi-empirical formulations of p and q.

2. The semi-empirical Dubois model:

Dubois et al. (1995) suggested a semi-empirical approach for modelling radar backscatter coefficient for co-polarised backscatter only, using scatterometer data collected at six frequencies between 2.5 GHz and 11GHz [25]. The expressions involve the angle of incidence, the dielectric constant, the rms surface height and the wavelength:

$$\sigma_{HH}^\circ = 10^{-2.75} \left(\frac{\cos^{1.5} \theta}{\sin^3 \theta} \right) 10^{0.028 \varepsilon_r \tan \theta} (k \text{ rms } \sin \theta)^{1.4} \lambda^{0.7} \quad (13)$$

$$\sigma_{VV}^\circ = 10^{-2.75} \left(\frac{\cos^3 \theta}{\sin^3 \theta} \right) 10^{0.046 \varepsilon_r \tan \theta} (k \text{ rms } \sin \theta)^{1.1} \lambda^{0.7} \quad (14)$$

3. The Integral Equation Model (IEM):

The IEM is a physically based radioactive transfer backscattering model application to a wide range of roughness values (Fung et al. 1992). The parameters required to compute the backscattering coefficient from the IEM model are correlation length, rms surface height, dielectric constant, polarisation and incidence angle and surface parameters. Over bare soils in agricultural areas, the backscatter coefficients of the surface contribution are expressed as:

$$\begin{aligned} \sigma_{pp}^\circ &= \frac{k^2}{2} |f_{pp}|^2 e^{-4 \text{rms}^2 k^2 \cos^2 \theta} \sum_{n=1}^{+\infty} \frac{(4 \text{rms}^2 k^2 \cos^2 \theta)^n}{n!} W^{(n)}(2k \sin \theta, 0) \\ &+ \frac{k^2}{2} \text{Re} (f_{pp}^* F_{pp}) e^{-3 \text{rms}^2 k^2 \cos^2 \theta} \sum_{n=1}^{+\infty} \frac{(4 \text{rms}^2 k^2 \cos^2 \theta)^n}{n!} W^{(n)}(2k \sin \theta, 0) \\ &+ \frac{k^2}{8} |f_{pp}|^2 e^{-2 \text{rms}^2 k^2 \cos^2 \theta} \sum_{n=1}^{+\infty} \frac{(\text{rms}^2 k^2 \cos^2 \theta)^n}{n!} W^{(n)}(2k \sin \theta, 0) \end{aligned} \quad (15)$$

Where p is H and V polarisation, k is the radar wave number (k=2π/λ), rms is the standard deviation of surface height, θ is the radar angle of incidence, W⁽ⁿ⁾ is the Fourier Transform of the nth power of the surface correlation function, f_{pp} is a function of the incidence angle and the Fresnel reflection coefficient and F_{pp} is a function of the incidence angle, ε_r is the dielectric constant of the soil, μ_r is the relative permittivity.

Where,

$$f_{hh} = \frac{-2R_h}{\cos \theta}$$

$$f_{vv} = \frac{2R_v}{\cos \theta}$$

$$f_{hh} = 2 \frac{\sin^2 \theta}{\cos \theta} \left[4R_h - \left(1 - \frac{1}{\varepsilon_r} \right) (1 + R_h)^2 \right]$$

$$f_{hh} = 2 \frac{\sin^2 \theta}{\cos \theta} \left[\left(1 - \frac{\varepsilon_r \cos^2 \theta}{\mu_r \varepsilon_r - \sin^2 \theta} \right) (1 - R_h)^2 - \left(1 - \frac{1}{\varepsilon_r} \right) (1 + R_v)^2 \right]$$

$$R_h = \frac{\mu_r \cos \theta - \sqrt{\mu_r \varepsilon_r - \sin^2 \theta}}{\mu_r \cos \theta + \sqrt{\mu_r \varepsilon_r - \sin^2 \theta}} \quad : \quad \text{Fresnel reflection coefficient at horizontal polarization}$$

$$R_v = \frac{\varepsilon_r \cos \theta - \sqrt{\mu_r \varepsilon_r - \sin^2 \theta}}{\varepsilon_r \cos \theta + \sqrt{\mu_r \varepsilon_r - \sin^2 \theta}} \quad : \quad \text{Fresnel reflection coefficient at vertical polarization}$$

Wⁿ(a, b) = Fourier transform of the nth power

$$W^n(a, b) = \frac{1}{2\pi} \iint \rho^n(x, y) e^{-i(ax+by)} dx dy \quad (16)$$

The distribution of $\rho(x, y)$ is exponential for low surface roughness values and Gaussian for high surface roughness values. The correlation functions for one-dimensional roughness profiles are defined as follows:

$$\rho(x) = e^{-(x/L)^\tau} \quad (17)$$

where L is the correlation length.

The backscattering IEM has a large validity domain. Baghdadi et al. (2004) and Zribi (1998) showed that, for bare soil in agricultural areas, IEM performs better with a fractal autocorrelation function. This is the function used in the present study. For retrieving surface roughness and soil moisture from SAR data, authors often use the original version of the IEM model.

V. CONCLUSION

The semi-empirical models of Oh and Dubois as well as the IEM physical backscattering model were evaluated using SAR data. The objectives of this paper are to compare the three models Oh, Dubois and IEM models. Comparison between the radar data by the three most commonly used surface radar backscattering models (Oh, Dubois and IEM) concludes that IEM performs better from overview of literatures.

VI. REFERENCES

- [1]. Y. Oh, K. Sarabandi, and F. T. Ulaby, "An empirical model and an inversion technique for radar scattering from bare soil surfaces," *IEEE Trans. Geosci. Remote Sens.*, vol. 30, no. 2, pp. 370–381, Mar. 1992.
- [2]. Y. Oh, K. Sarabandi, and F. T. Ulaby, "An inversion algorithm for retrieving soil moisture and surface roughness from polarimetric radar observation," in *Proc. IGARSS, Pasadena, CA, 1994*, vol. III, pp. 1582–1584, IEEE Catalog Number 94CH3378-7.
- [3]. Y. Oh, K. Sarabandi, and F. T. Ulaby, "Semi-empirical model of the ensemble-averaged differential Mueller matrix for microwave backscattering from bare soil surfaces," *IEEE Trans. Geosci. Remote Sens.*, vol. 40, no. 6, pp. 1348–1355, Jun. 2002.
- [4]. Y. Oh, "Quantitative retrieval of soil moisture content and surface roughness from multipolarized radar observations of bare soil surfaces," *IEEE Trans. Geosci. Remote Sens.*, vol. 42, no. 3, pp. 596–601, Mar. 2004.
- [5]. P. Dubois, J. Van Zyl, and T. Engman, "Measuring soil moisture with imaging radars," *IEEE Trans. Geosci. Remote Sens.*, vol. 33, no. 4, pp. 915–926, Jul. 1995.
- [6]. A. K. Fung, Z. Li, and K. S. Chen, "Backscattering from a randomly rough dielectric surface," *IEEE Trans. Geosci. Remote Sens.*, vol. 30, no. 2, pp. 356–369, Mar. 1992.
- [7]. NICOLAS BAGHDADI and MEHREZ ZRIBI, "Evaluation of radar backscatter models IEM, OH and Dubois using experimental observations." *International journal of Remote Sensing*, Vol.27, No.18, 20 September 2006, 3831-3852.

- [8]. N. Baghdadi, E. Saba, M. Aubert, Mehrez Zribi, Frederic Baup. "Comparison between backscattered TerraSAR signals and simulations from the radar backscattering models IEM, Oh, and Dubois." *IEEE Geoscience and Remote Sensing Letters*, IEEE- Institute of Electrical and Electronic Engineers, 2011, 6(8), p. 1160-1164. [ird-01026279](#).
- [9]. Nicolas Baghdadi, Elie Saba, Maelle Aubert, Mehrez Zribi, and Frederic Baup, "Evaluation of Radar Backscattering Models IEM, Oh, and Dubois for SAR Data in X-Band Over Bare Soils", *IEEE GEOSCIENCE AND REMOTE SENSING LETTERS*, VOL. 8, NO. 6, NOVEMBER 2011
- [10]. Mohammad Choker, Nicolas Baghdadi, Mehrez Zribi, Mohammad El Hajj, Simonetta Paloscia, Niko E. C. Verhoest, Hans Lievens and Francesco Mattia, "Evaluation of the Oh, Dubois and IEM Backscatter Models Using a Large Dataset of SAR Data and Experimental Soil Measurements." *Water* 2017, 9, 38; [doi:10.3390/w9010038](#).
- [11]. Baghdadi, N.; Gherboudj, I.; Zribi, M.; Sahebi, M.; King, C.; Bonn, F. Semi-empirical calibration of the IEM backscattering model using radar images and moisture and roughness field measurements. *Int. J. Remote Sens.* 2004, 25, 3593–3623.
- [12]. Mattia, F.; Le Toan, T.; Souyris, J.-C.; De Carolis, C.; Floury, N.; Posa, F.; Pasquariello, N.G. The effect of surface roughness on multifrequency polarimetric SAR data. *IEEE Trans. Geosci. Remote Sens.* 1997, 35, 954–966.
- [13]. Zribi, M.; Taconet, O.; Le Hégarat-Masclé, S.; Vidal-Madjar, D.; Emblanch, C.; Loumagne, C.; Normand, M. Backscattering behavior and simulation comparison over bare soils using SIR-C/X-SAR and ERASME 1994 data over Orgeval. *Remote Sens. Environ.* 1997, 59, 256–266.
- [14]. Oh, Y.; Sarabandi, K.; Ulaby, F.T. An inversion algorithm for retrieving soil moisture and surface roughness from polarimetric radar observation. In *Proceedings of the IEEE International Geoscience and Remote Sensing Symposium (IGARSS '94)—Surface and Atmospheric Remote Sensing: Technologies, Data Analysis and Interpretation*, Pasadena, CA, USA, 8–12 August 1994; Volume 3, pp. 1582–1584.
- [15]. Du, J., Shi, J. and Sun, R.; The development of HJ SAR soil moisture retrieval algorithm. *Int. J. Remo. Sens.*, 2010, 31(14), 3691-3705.
- [16]. Barrett, Brian W., Edward Dwyer, and Pádraig Whelan. "Soil moisture retrieval from active spaceborne microwave observations: An evaluation of current techniques." *Remote Sensing* 1.3 (2009): 210-242.
- [17]. Thanabalan, P., and R. Vidhya. "Derivation of Soil Moisture using Modified Dubois Model with field assisted surface roughness on RISAT-1 data." *Earth Sciences Research Journal* 22.1 (2018): 13-18.
- [18]. Liu, C. A., Chen, Z. X., Yun, S. H. A. O., Chen, J. S., Hasi, T., & PAN, H.Z. "Research advances of SAR remote sensing for agriculture applications: A review. *Journal of integrative agriculture* (2019), 18(3), 506-525.
- [19]. Sonika Sharma Supervised by Dr. Y.S. Rao Er. Praveen Thakur, "SOIL MOISTURE ESTIMATION USING ACTIVE AND PASSIVE MICROWAVE REMOTE SENSING TECHNIQUES" Indian Institute of Remote Sensing National Remote Sensing Agency (NRSA), Department of Space, Dehradun-248001 March 2006.

- [20]. Vijay S. Bhagat, "Space-borne Active Microwave Remote Sensing of Soil Moisture: A Review" *Remote Sensing of Land* (2017), 1(1), 53-86.
- [21]. Wang, Hongquan. "Soil moisture retrieval from microwave remote sensing observations." *Soil Moisture. IntechOpen*, 29-54, 2018.
- [22]. Mandelbrot BB. *The Fractal Geometry of Nature*. San Francisco, CA: Freeman; 1982
- [23]. Schmugge, T., "Remote Sensing of Soil Moisture." Goddard Space Flight Center, Greenbelt, Maryland; 1976
- [24]. Bindlish, Rajat, and Ana P. Barros. "Including vegetation scattering effects in a radar based soil moisture estimation model." *IAHS PUBLICATION* (2001): 354-361.
- [25]. Song, K., Zhou, X. and Fan, Y. "Empirically Adopted IEM for Retrieval of Soil Moisture From Radar Backscattering Coefficient." *IEEE Transactions on Geoscience and Remote Sensing* (2009), 47(6), 1662-1672.
- [26]. Barrett, Brian W., Edward Dwyer, and Pádraig Whelan. "Soil moisture retrieval from active spaceborne microwave observations: An evaluation of current techniques." *Remote Sensing* 1.3 (2009): 210-242.

Molecular Interaction between Carbohydrates and Amino Acid Using Dielectric Spectroscopy

Savita Kamble, Ravikant Karale, Komal B. Kabara, Suad Alwaleedy, Saeed Mohemmed, Ashok C.
Kumbharkhane, Arvind V. Sarode*

1School of Physical Sciences, Swami Ramanand Teerth Marathwada University, Nanded-431 606,
Maharashtra, India

ABSTRACT

The present work aims at the inter molecular interaction of aqueous D-Glucose with L-Leucine ternary system using time domain reflectometry technique (TDR) within the frequency range 0.01GHz to 30GHz in the temperature region from 278.15K to 298.15K. The frequency dependent dielectric permittivity has been calculated by using Havriliak-Negami equation. For aqueous D-Glucose and L-Leucine ternary system the concentration range covers in molar concentration $0.514 \leq c/M \leq 2.710$ and $0.004 \leq c/M \leq 0.020$ respectively. Cole-Davidson model is used for the well description of complex dielectric permittivity spectra $\epsilon^*(\nu)$. Dielectric parameters such as relaxation time τ_0 , static dielectric constant ϵ_0 , high frequency limiting dielectric constant ϵ_∞ and the orientation correlation between neighbouring molecules due to hydrogen bonding interaction determined by Kirkwood correlation factor g were calculated.

Keywords: D-Glucose, L-Leucine, Dielectric parameters, Time domain reflectometry.

I. INTRODUCTION

Dielectric relaxation spectroscopy (DRS) is a very useful technique for studying molecular interactions and understanding the dynamical behavior of nearly all organic, polymeric and biological macromolecules. (Since with the advent of modern technologies scientists are using electromagnetic waves for getting information through interaction with matter). Dielectric spectroscopy is a tool in which a pulse of high frequency electromagnetic radiation incident upon a sample is reflected back and gives information in the form of electrical signals, which on further analysis gives structural information about the sample under study through dielectric parameters such as complex permittivity, static dielectric constant, relaxation amplitude or strength, relaxation time, dipole moment and so on [1].

Carbohydrates are bio-molecules formed by aldehyde or ketone compounds with multiple hydroxyl groups that account for the majority of organic matter on Earth due to their important role in all forms of life. TDR was used to investigate the temperature dependent complex permittivity spectra of monosaccharides (D-fructose and D-xylose) and disaccharides (D-maltose monohydrate) in aqueous solution. Within the frequency range of 10 MHz to 50 GHz we demonstrated how dielectric parameters such as dielectric constant

(ϵ_0), relaxation time (τ_0) are sensitive to variations in mixture constituents of aqueous sugar solutions. This information could be useful in the pharmaceutical and food processing industries for formulation [2].

Amino acids are biologically important organic compounds composed of amine ($-\text{NH}_2$) and carboxylic acid ($-\text{COOH}$) functional groups, as well as a nitrogen atom. Each amino acid has its own side chain. The essential components of an amino acid are carbon, hydrogen, oxygen, and nitrogen [3].

The amino acids, which are the building blocks of proteins, have sparked widespread interest in multidisciplinary research-leucine (Leu) and L-isoleucine (I-Leu) are amino acids that are required for life in relation to humans. They participate in vital biological processes such as haemoglobin formation and maple syrup detection in new born screening programmes, urine disease is detected among the Characterization of Leucine and L-isoleucine is a popular area of research in Metabolomics and peptide sequencing spectrometry (mass spectrometry) [4].

The interactions of some L—amino acids with D-glucose in dilute aqueous solutions were studied using titration calorimetry and UV absorption spectroscopy. The findings revealed that L—amino acids get the ability to form intermolecular bonds.

Moreover no one studied intermolecular interaction of L-Leucine in aqueous solution of D-Glucose by using dielectric relaxation spectroscopy.

In this work we have studied dielectric relaxation and thermodynamics properties of L-leucine in aqueous solutions of D-glucose with different molar concentration over frequency range 10MHz to 30GHz within temperature range 278.15K to 298.15K.

II. EXPERIMENTAL

2.1. MATERIALS

D-Glucose was purchased from Fisher Scientific chemical company and L-leucine was purchased from sigma Aldrich. Double distilled and deionized water was used for making the solution. The chemicals were weighed in an electronic digital balance (Mettler Toledo ME- 204) with a least count of 0.0001 gm.

III. RESULTS AND DISCUSSION

The Havriliak-Negami equation provides the overall form of the relaxation model.

$$\epsilon^*(\omega) = \epsilon_\alpha + \left[\frac{(\epsilon_0 - \epsilon_\alpha)}{[1 + (j\omega\tau_0)^{1-\alpha}]^\beta} \right] \quad (1)$$

Where the static permittivity ϵ_0 , ϵ_α is the high frequency permittivity, τ_0 is the relaxation time, and α and β are the empirical parameters for the relaxation distribution times with values ranging from 0 to 1.

As the concentrations of L-Leucine in aqueous D-Glucose increase, the dielectric constant values decrease while the relaxation time increases. The decrease in the static dielectric constant with increasing concentration in aqueous solution is due to the formation of hydration layer, which causes water molecules to be influenced by D-Glucose and L-Leucine molecules. As a result, the decrease in static dielectric constant indicates that a large amount of L-Leucine and D-Glucose in solution has been completely associated.

Relaxation time has increased in water solution may be due to L-Leucine and D-Glucose molecules forming a structure around the water molecule, making rotation of the water molecules. The variation in relaxation time reveals information about the hydrophilic nature of the solute particle. The dielectric constant, as well as the relaxation time increases as the temperature drops. This is to be expected because density increases as temperature decreases [5].

Static dielectric constant:

The static dielectric constants of aqueous D-Glucose solutions at different concentrations of L-Leucine and temperatures has been studied. The dielectric dispersion and absorption curves span a wider frequency range[6].

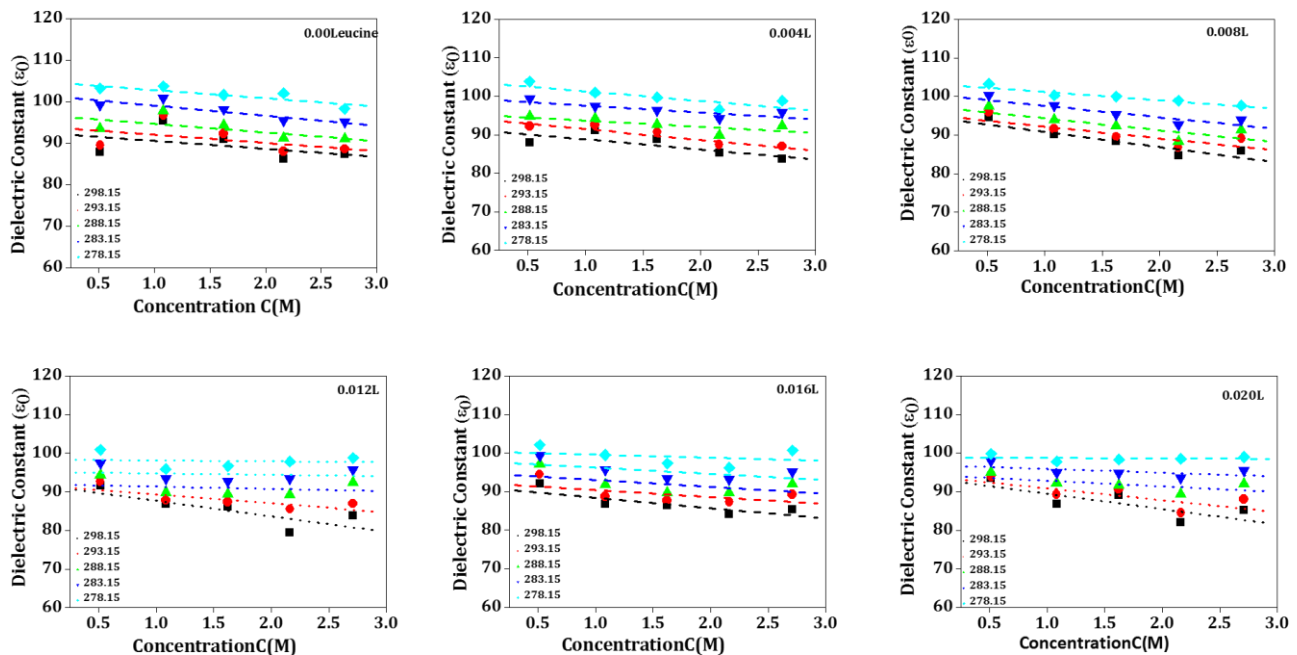


Figure 1: dielectric constant for aqueous D-glucose in presence of L-Leucine

As shown in Fig.1 the dielectric constant increases with decrease in temperature. This may be due to the formation of dipole-dipole antiparallel alignment for all concentrations of L-Leucine. This observation could be explained by the fact that the net decrease in the number of free water molecules with concentration is larger at higher concentrations than for lower molar concentrations [7].

Relaxation time:

The relaxation time is proportional to molecular size and is highly dependent on the nature of the functional group. Furthermore, changing its values provides information about the solute's hydrophilic character. Particles, as well as the apparent the reorientation of a dipole. TDR experiments show that relaxation time increases linearly with decreasing temperature as shown in fig.2.and the addition of L-Leucine in aqueous D-Glucose shows slight interaction.

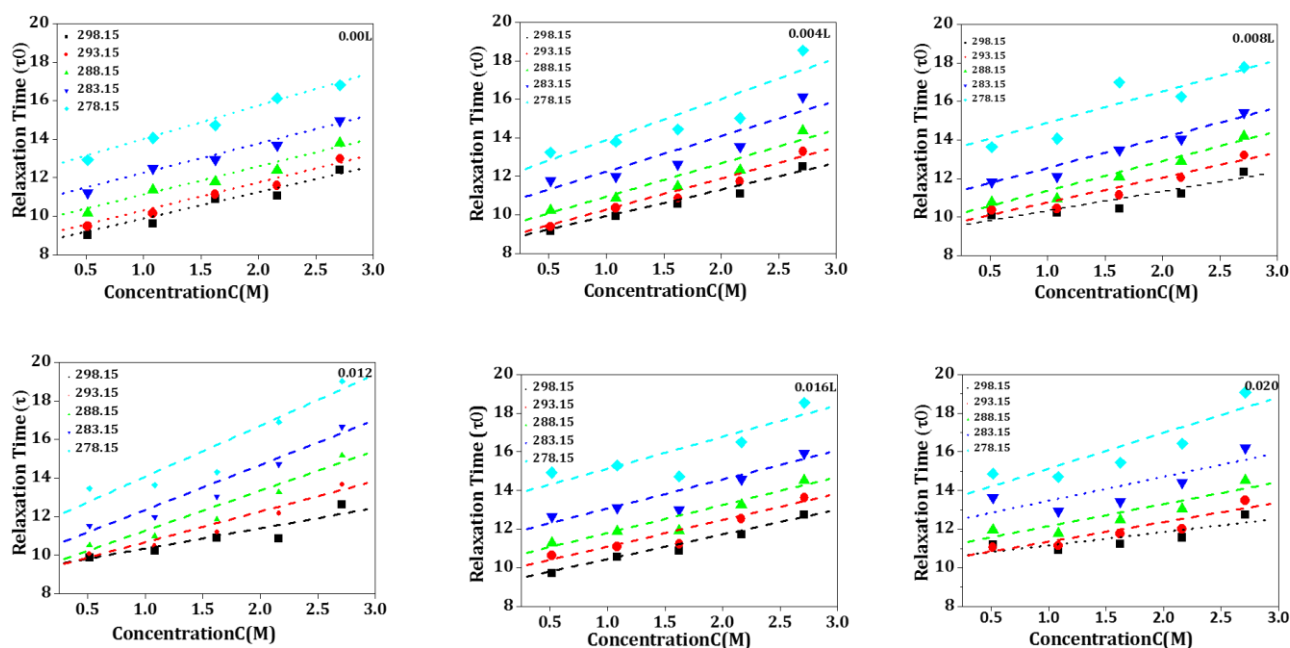


Figure 2:dielectric relaxation time for aqueous D-glucose in presence of L-Leucine

The linear increase in relaxation time with concentration demonstrates molecular interaction [8]. The relaxation time for different concentrations of L-Leucine in aqueous D-Glucose do not deviate significantly from ideal behaviour, suggesting stronger molecular interaction than the others, indicating that molecules have a non-cooperative domain [9].

$$g\mu^2 = \frac{9K_B T M}{4\pi N \rho} \left[\frac{(\epsilon_s - \epsilon_\infty)(2\epsilon_s + \epsilon_\infty)}{\epsilon_s(\epsilon_\infty + 2)^2} \right] \quad (2)$$

The Kirkwood-Frohlich equation provides useful information about the orientation of an electric dipole. The Kirkwood correlation factor 'g' is calculated from the dielectric constant and provides information on the collective orientation correlation of molecules. The extent of hydrogen bonding is measured by the deviation of 'g' from unity [10].

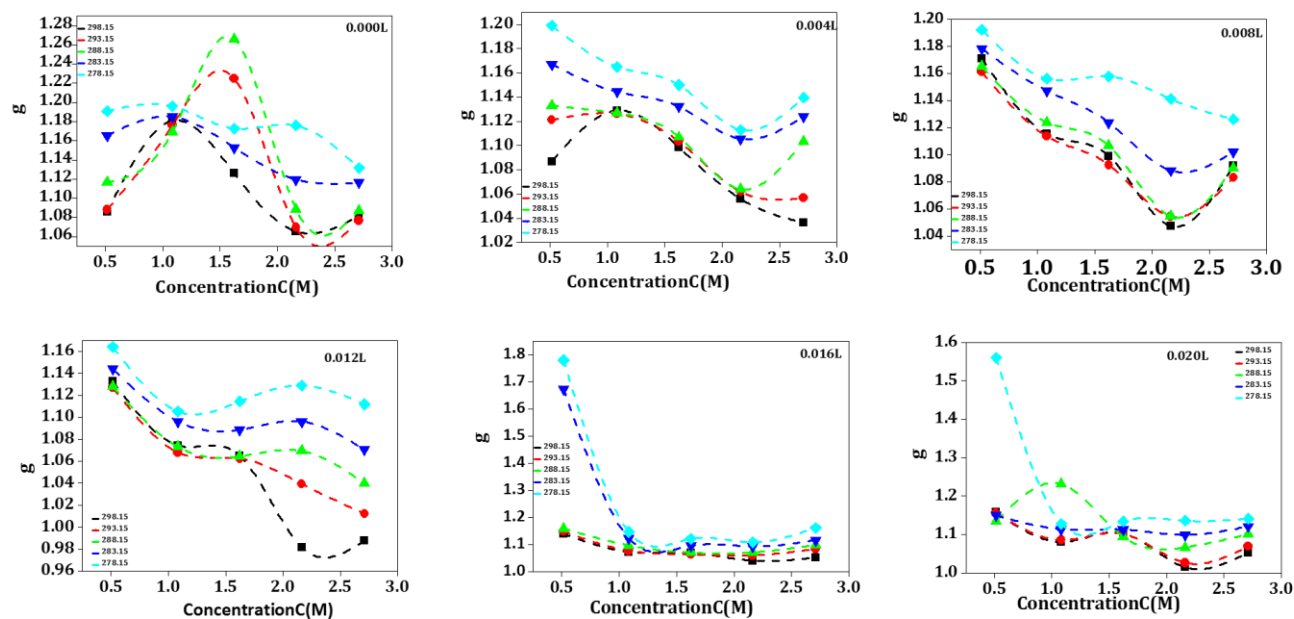


Figure 3: variation in correlation factor 'g' for aqueous D-glucose in presence of L-Leucine.

The molecular interaction of L-Leucine with aqueous D-Glucose mixture can be described by the Kirkwood correlation factor (g), which can be calculated using the modified Kirkwood equation. To calculate 'g' we used values of dipole moment ($\mu=2.34$ D) of aqueous D-Glucose and L-Leucine. Fig.3. shows the plot of g at various concentration of L-Leucine in aqueous D-Glucose. Observed values of g at lower L-Leucine concentrations is more than one suggest that there is a strong possibility of parallel alignment of dipoles. As the concentration of solute increases, molecules become close to each other as a result possibility of antiparallel alignment of dipoles emerges [11].

IV. CONCLUSION

From the overall study of dielectric parameters we may conclude that, the dielectric constant and relaxation time of aqueous D-Glucose at various concentrations of L-Leucine decreases with increasing temperature. This may be due to increase in dipole-dipole antiparallel alignment. Obtained values of relaxation time confirm that environment is not cooperative. Kirkwood correlation factor gives information about the orientation electric dipoles in molecules.

V. ACKNOWLEDGEMENTS

Author Savita Kamble is thankful to School of Physical Sciences, S.R.T.M. University Nanded for providing instrumentation facility, the TDR and other infrastructural facilities related to this work. The author is also gratefully acknowledged to Dept. of Science and Technology (DST), New Delhi for providing (TDR) facility

through project sanctioned to Dr. A.V.Sarode (SERB/F/4632/2013-2015) and Dr.A.C.Kumbharkhane (SB/S2/LOP-032/2013). I am thankful to Dr.T.M.Kalyankar, School of pharmacy ,Swami Ramanand Teerth Marathwada University Nanded for their valuable support. I am also highly thankful to my research colleagues specially Mr. Garda Nitin for timely support during my work.

VI. REFERENCES

- [1]. A.V. Sarode, A.C. Kumbharkhane and S.C. Mehrotra. Dynamics and interactions in aqueous polyvinylpyrrolidone (PVP K-30): an approach using dielectric relaxation spectroscopy (2018).
- [2]. D.G. Rathod, D.N. Rander, K.S. Kanse, Y.S. Joshi and A.C. Kumbharkhane. Dielectric relaxation and molecular interactions study of saccharides in aqueous solutions. *Carbohydrate Research*, 507 (2021) 108375.
- [3]. D. French and J.T. Edsall. The reactions of formaldehyde with amino acids and proteins. In *Advances in protein chemistry* Vol. 2 (1945) 277-335. Academic Press.
- [4]. C.Jiang, C.J. Arthur and P.J. Gates. A computational and experimental study of the fragmentation of l-leucine, l-isoleucine and l-allo-isoleucine under collision-induced dissociation tandem mass spectrometry. *Analyst*, 145(20) (2020) 6632-6638.
- [5]. W. Su, K. Zhao, J. Wei and T. Ngai. Dielectric relaxations of poly (N-isopropylacrylamide) microgels near the volume phase transition temperature: impact of cross-linking density distribution on the volume phase transition. *Soft Matter*, 10(43) (2014) 8711-8723.
- [6]. S.S. Sagiri, B. Behera, R.R. Rafanan C. Bhattacharya, K. Pal, I. Banerjee and D. Rousseau. Organogels as matrices for controlled drug delivery: a review on the current state. *Soft Materials*, 12(1) (2014) 47-72.
- [7]. D.E.Gragson, B.M. McCarty and G.L. Richmond. Ordering of interfacial water molecules at the charged air/water interface observed by vibrational sum frequency generation. *Journal of the American Chemical Society*, 119(26) (1997) 6144-6152.
- [8]. T.R. Nelson and S.M. Tung. Temperature dependence of proton relaxation times in vitro. *Magnetic resonance imaging*, 5(3) (1987) 189-199.
- [9]. J.L. Alonso, and J.C. López. Microwave spectroscopy of biomolecular building blocks. *Gas-Phase IR Spectroscopy and Structure of Biological Molecules*, (2014) 335-401.
- [10]. J.C. Martínez García. Dynamics in orientationally disordered solids. *Universitat Politècnica de Catalunya*. (2011)
- [11]. L.R. Pratt and A. Pohorille. Hydrophobic effects and modeling of biophysical aqueous solution interfaces. *Chemical Reviews*, 102(8) (2002) 2671-2692.

Study of Molecular Interaction in Aqueous Valine-Aceclofenac Mixture Using Dielectric Relaxation Spectroscopy (DRS)

Arvind V. Sarode*, Suad Alwaleedy, Saeed Mohemmed, Ravikant Karale, Komal B. Kabara, Ashok C. Kumbharkhane

School of Physical Sciences, Swami Ramanand Teerth Marathwada University, Nanded-431 606, Maharashtra, India

ABSTRACT

The present work reports structural and dynamical properties of aqueous amino acid Valine [C₅H₁₁NO₂] in the presence of Non steroidal anti-inflammatory drug (NSAID) Aceclofenac (ACF) [C₁₆H₁₃Cl₂NO₄] using time domain reflectometry (TDR) in the frequency region of 0.01 GHz to 30 GHz over the temperature range of 298.15 K-278.15 K. For aqueous Valine and ACF induced aqueous Valine the concentration range covers in molar concentrations are $0.00 \leq c/M \leq 0.10$ and $0.00 \leq c/M \leq 0.01$ respectively. Cole-Davidson model is used for the well description of the complex dielectric permittivity spectra $\epsilon^*(\nu)$. Dielectric parameters such as the static dielectric constant ϵ_0 , the high frequency limiting dielectric constant ϵ_∞ , relaxation time τ_0 , dipole moment μ , Kirkwood correlation factor g were obtained and expressed in terms of molecular interaction and hydrogen bonding.

Keywords: Time Domain Reflectometry, Dielectric Relaxation, Valine, Aceclofenac, Dipole moment.

I. INTRODUCTION

Dielectric relaxation spectroscopy (DRS) is a very useful technique for studying molecular interactions and understanding the dynamical behavior of nearly all organic, polymeric and biological macromolecules. (since with the advent of modern technologies scientists are using electromagnetic waves for getting information through interaction with matter). Dielectric spectroscopy gives structural information about the sample under study through dielectric parameters such as complex permittivity, static dielectric constant, relaxation amplitude or strength, relaxation time, dipole moment and so on. The method has a wide frequency range (from 10^{-5} to 10^{11} Hz) and can therefore be used to study a wide range of processes, from slow and hindered macromolecular vibrations to constrained charge transfer processes (like proton conductivity in nearly dry systems) to relatively quick reorientations of small molecules or side chain groups [1].

Water is remarkable liquid in many aspects. Because of its unusual physical and chemical characteristics, including the latent heat of vaporization, high specific heat and maximum density at 4°C, extensive work is being done to determine its precise structure. The ability of the water molecules to participate in any number of hydrogen bonds by employing their two hydrogen atoms and the two lone pairs on their oxygen is what determines the structural characteristics of liquid water. The local polarization's spontaneous fluctuation,

which results from partial charge separation during cluster formation, may be the cause of the high value of the dielectric constant [2].

Amino acids play various essential roles in living systems. In aqueous solutions, the interactions between the solvent and the various constituent groups of a protein, such as the amino acid side chains and the backbone peptide group, play an important role in the structure and function of proteins. Amino acids are extremely small biomolecules that serve as the primary building blocks of proteins and enzymes [3].

Aceclofenac is a non-steroidal anti-inflammatory drug (NSAID) indicated for various painful indications and proved as effective as other NSAIDs and chemically known as 2-[2-[2-[(2,6-dichlorophenyl)amino]phenyl]acetyl]oxyacetic acid [4]. Other applications includes treatment of osteo arthritis, rheumatoid arthritis, tendinitis, ankylosing spondylitis and joint inflammation and reduces pain intensity and duration of morning stiffness and other inflammatory conditions [5,6]. Aceclofenac is such a carboxylic acid derivative and one of the important non-steroidal anti-inflammatory drug (NSAID) molecules, which also possess analgesic properties [7]. It has free carboxylic acid in its structure, which is found in many pharmaceutical compounds and plays an important role in drug design. Because of the simultaneous presence of carbonyl (C=O) and hydroxyl (O-H) groups, carboxylic acids can act as both hydrogen bond acceptor and donor. As a result, carboxylic acids, which are quite polar in nature [8], can form dimers that correspond to the well-known homo-synthons in supramolecular chemistry [9]. Aceclofenac exhibits very slight solubility in water, and as a consequence, it exhibits low bioavailability after oral administration [10-12]. As, amino acid is a basic building block of protein and amongst 20 different amino acids Valine is a branched chain, hydrophobic, an essential amino acid and usually found in interior of proteins.

After careful literature survey, it was found that no work on the interaction of concentration dependence of aceclofenac with aqueous valine using time domain reflectometry in the GHz frequency, and at 298.15 K, 288.15 K, and 278.15 K temperatures has been reported so far. Amino acids are important biomolecules that interact with drugs inside the body. In biological systems, solvent-mediated interactions are the primary determinants for regulating the structure, dynamics, and thermodynamics of biomolecules, ultimately dictating their biological function and that of the cell. Because biomolecules are embedded in a highly polar medium, electrostatics is a critical component of molecular solvation effects. Although pure aceclofenac has a low water solubility (0.015mg/ml) [13].

The aim of this work is to study the dielectric relaxation of Valine-ACF-Water solution using the time domain reflectometry technique. The solutions were prepared at room temperature for different molar concentrations of valine viz. 0, 0.02, 0.04, 0.06, 0.08, 0.1 and aceclofenac viz. 0, 0.002, 0.004, 0.006, 0.008 and 0.01. We have measured the dielectric relaxation spectra for these solutions at 298.15 K, 288.15 K and 278.15 K using time domain reflectometry in the frequency range of 0.01 GHz-30 GHz. The purpose of the present research work is to investigate the impact of temperature and concentration on the structure and dynamics of water molecules in presence of valine and ACF macromolecules as well as the intermolecular interactions between aqueous Valine and ACF molecules, in terms of various dielectric and thermodynamic parameters. We interpreted the obtained dielectric data by comparing with those of earlier dielectric studies.

II. EXPERIMENTAL

2.1 materials

Valine was purchased from sigma Aldrich and Aceclofenac was purchased from Hi Media Laboratories Pvt. Ltd. Mumbai, India and used without purification. Double distilled and deionized water was used for making the solution. The chemicals were weighed in an electronic digital balance (Mettler Toledo ME- 204) with a least count of 0.0001 gm. The solutions of 15 ml were prepared at room temperature for different concentrations of Valine and ACF and the dielectric measurement were carried out by using TDR.

2.2 Dielectric Measurements

The Tektronix Digital Serial Analyzer model no. DSA8300 sampling mainframe along with the sampling module 80E10B has been used for TDR. A sampling module provides 12 ps incident and 15 ps reflected rise time pulse was fed through a coaxial line system having 50Ω impedance. Sampling oscilloscope monitors show change in step pulse after reflection from the end of line. The reflected pulse without sample $R_1(t)$ and with sample $R_s(t)$ were recorded in the time window of 5 ns and digitized in 2000 points. The Fourier transform of the pulse and data analysis was performed to determine complex permittivity spectra $\epsilon^*(\omega)$ using least square fit method [14-16]. A temperature controller system was used to maintain the constant temperature. The sample cell is surrounded by a heat insulating container and the temperature at the cell is checked by using electronic thermometer. The temperature of sample cell was maintained at desired value within the accuracy of ± 1 °C.

III. RESULTS AND DISCUSSION

Dielectric dispersion and absorption curves obtained for the aqueous Valine at 0.00, 0.02, 0.04, 0.06, 0.08 and 0.1 M concentration in presence of poor water soluble aceclofenac (ACF) with the concentrations 0.002, 0.004, 0.006, 0.008 and 0.01 M used at temperatures 298.15 K, 288.15 K and 278.15 K is shown in fig. 1 where only spectra at low and high concentrations and at all temperatures along with the spectra for water were depicted. The spectra show that there is a gradual decrease in dielectric permittivity for all the used concentrations and temperature and the loss peaks shift towards lower frequency side. This suggests molecular association between solute and solvent molecules.

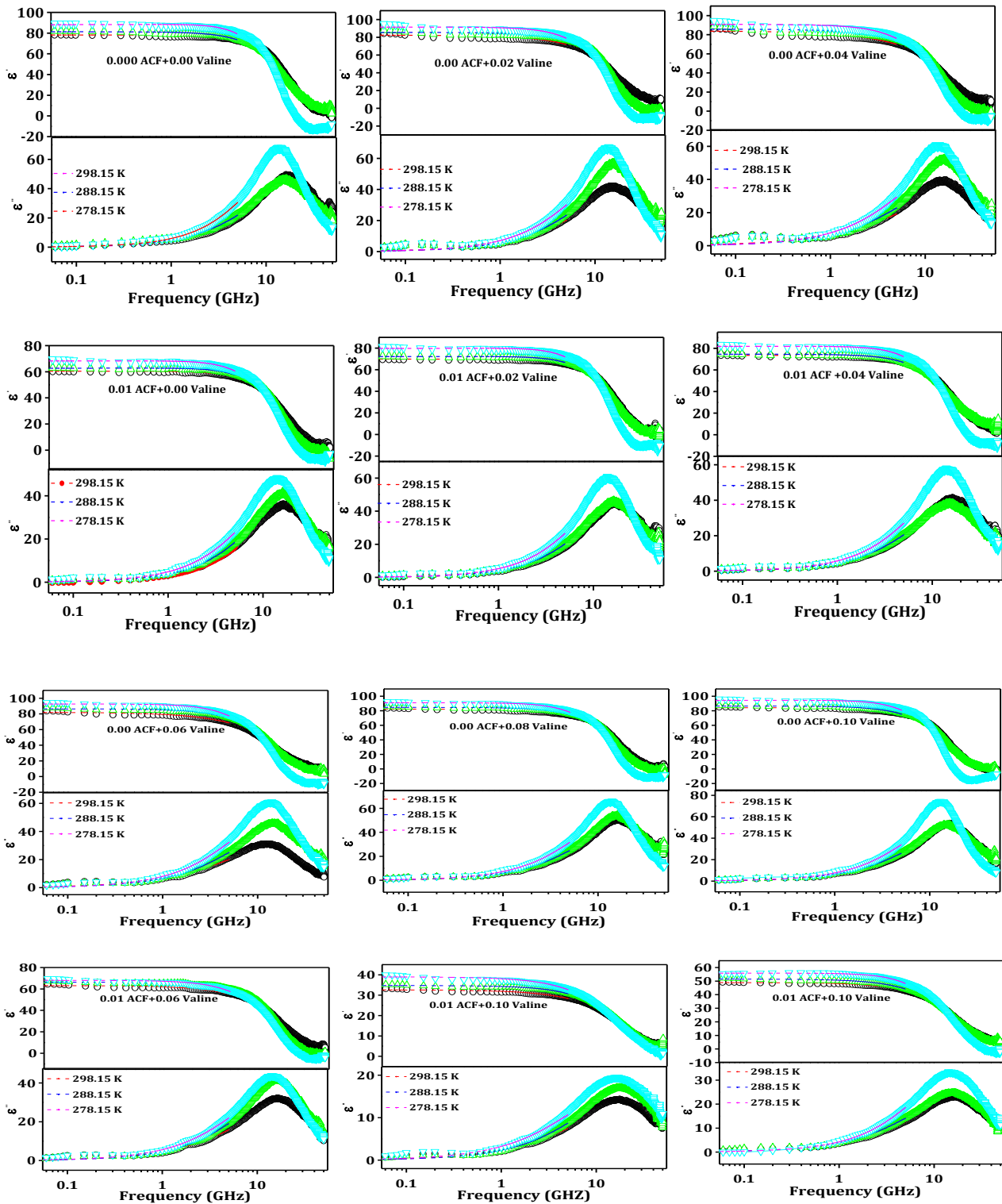


Figure 1: Permittivity spectra contains dielectric permittivity (ϵ') and loss (ϵ'') as a function of frequency for water and aqueous Valine in presence of ACF at different concentration and temperature. (Symbols-Observed data and Dotted lines-Fitted data)

Temperature and Concentration dependent dielectric parameter of Valine was established by studying the variation of dielectric constant, dielectric loss, relaxation time, Kirkwood correlation factor and dipole moment as well as thermodynamic parameters such as free energy of activation, entropy of activation and enthalpy of activation [17].

Dielectric permittivity (ϵ') and loss (ϵ'') for Valine-ACF-Water system obtained for various concentrations in the temperature range of 298.15 K - 278.15 K as a function of frequency is shown in fig. 1. The values of complex permittivity $\epsilon^* = \epsilon' - j\epsilon''$ as a function of frequency for the Valine-ACF-Water system have been analyzed and used for the evaluation of dielectric parameters at various temperatures and concentrations [18]. The process can be described by S. Havriliak -Negami [19] equation using least square fit method.

$$\epsilon^*(\omega) = \epsilon_\infty + \left[\frac{(\epsilon_0 - \epsilon_\infty)}{[1 + (j\omega\tau_0)^{1-\alpha}]^\beta} \right] \quad (1)$$

Where ϵ_0 is the static permittivity, ϵ_∞ the high frequency limiting static permittivity, τ_0 is the average relaxation time, ω is the angular frequency α and β are the distribution parameters. α ($0 < \alpha < 1$) indicates the broadness of the symmetric relaxation curve when the dielectric data are described by the Cole-Cole equation. The relaxation curve with ($0 < \beta < 1$), $\alpha = 1$ corresponds to Debye-type of relaxation and a smaller value of α gives the broader symmetric relaxation curve, whereas the relaxation curve with $\beta = 1$ corresponds to a non-Debye type of relaxation in which the asymmetric relaxation ($0 < \beta < 1$), $\alpha = 0$ is associated with the cooperative mechanics of dielectric relaxation. It has been found that the dielectric data for the studied systems obey the Cole-Davidson dispersion model. As the frequency range of dielectric study in present work is from 1 GHz to 30 GHz, the value of ϵ_∞ is just a fitting parameter. In the fitting procedure, ϵ_∞ is not fitted and assumed to be 3.0. This is done because the data are not sensitive to ϵ_∞ in the high frequency range.

The data collected reveals that the static dielectric constant for aqueous PVP was found more than that of pure water and it increases with increase in concentration of valine except at higher concentrations of ACF. This suggests that increasing valine concentrations decreases the number of water molecules per valine molecule that form hydrogen bonding at hydroxyl and methyl side group and thus form hydration layer around valine molecule. This association between water and valine increases the value of static dielectric constant only at lower ACF concentration but for further increase in concentration of ACF cause decrease the value of static dielectric constant. As higher values of dielectric constant has more significance for drugs stability in pharmacy which is directly related to solubility and stability of the products [20]. The addition of ACF to aqueous valine gives surprising results that decreases the values of static dielectric constant towards higher PVP concentration. The trend and magnitude of the values of static dielectric constants towards higher concentration of ACF show little variations in the values of dielectric constant over the measured concentration range. This suggests that the presence of ACF with higher concentration in aqueous valine make the system less stable. This may be due to formation of hydration layer around valine and the interaction between valine and ACF gets reduced or may be due to the formation of complexes as a result static dielectric constant decreases.

The increase in the values of static dielectric constant for aqueous valine in absence or at lowest ACF concentration clearly indicates that dipole-dipole parallel alignment must present between ACF and water molecules. As valine concentration increases, the values of the quantities $g\mu^2$ [table] which signify the

variation in dipole moment and Kirkwood correlation factor g that describes orientational correlation between solute and solvent molecules decreases. This suggests reduced parallel correlation between the dipoles of aqueous valine and ACF molecules as every ACF molecule is entirely surrounded by a water molecule. At lower ACF concentrations, interactions between valine molecules and ACF molecules gets screened, which lowers the values of the static dielectric constant. The formation of a hydration shell around valine may be the cause of this decrease in the dielectric constant and also suggests the loss of free water molecules. Valine will have an impact on the hydrogen bonding network throughout this procedure [21]. Also, such formation of shielding or hydration layer around valine molecules that reduces the interaction between valine and ACF molecules and so reduces the correlation.

To see the effect of temperature on the structural behavior of aqueous valine the study has been extended towards lower temperature. From the observed data, it has been noticed that by lowering the temperature from 298.15 K to 278.15 K static dielectric constant seems to be increasing for all the used concentrations. This rise in the values of static dielectric constant towards lower temperature over all the valine concentrations may be due to the formation of induced dipoles via hydration layer with the neighbouring or surrounding molecules as the molecules gained lower thermal energy and therefore amplitude of the random thermal motion is restricted [22]. This gives perfect alignment (parallel or antiparallel) with the applied field so that dipoles are more closely aligned with each other; as a result the orientation polarization gets increased and so the static dielectric constant.

This suggests that the system is more stable towards lower temperature and lower valine concentrations and will be more suitable for drug design and other pharmaceutical applications.

The alignment of dipoles can be well explained using dipole moment and correlation factor g calculated and discussed in the next section.

The variation in static dielectric constant for aqueous valine in the presence of varying concentrations of aceclofenac (ACF) is shown in the fig 2. It has been observed that the overall trend for the static dielectric constant measured at 0.002, 0.004, 0.006, 0.008 and 0.01 M concentrations of aceclofenac at different temperatures was found to be decreasing with increasing aceclofenac concentrations. The presence of aceclofenac in aqueous valine resulted in further decrease in the values of static dielectric constant and the variation was observed to be larger at 0.01 (M) concentration of aceclofenac. This variation in the values of static dielectric constant may be due to the molecular interaction between the methyl group (CH_3) of the screened valine by the water molecules and the H from the O-H group of ACF through weak dipole-dipole interaction as a result hydrogen bonding network affected due to the presence of aceclofenac which resulted in lowering the values of static dielectric constant with increasing ACF concentration. But for the highest used concentration of ACF there found very rapid decrease in the values of static dielectric constant because at highest concentration all the possible hydrogen bonding sites are saturated and no site is available for bonding to be taking place; as a result there is no further change in the structural conformation which decrease the static dielectric constant over the used concentrations and temperature [23].

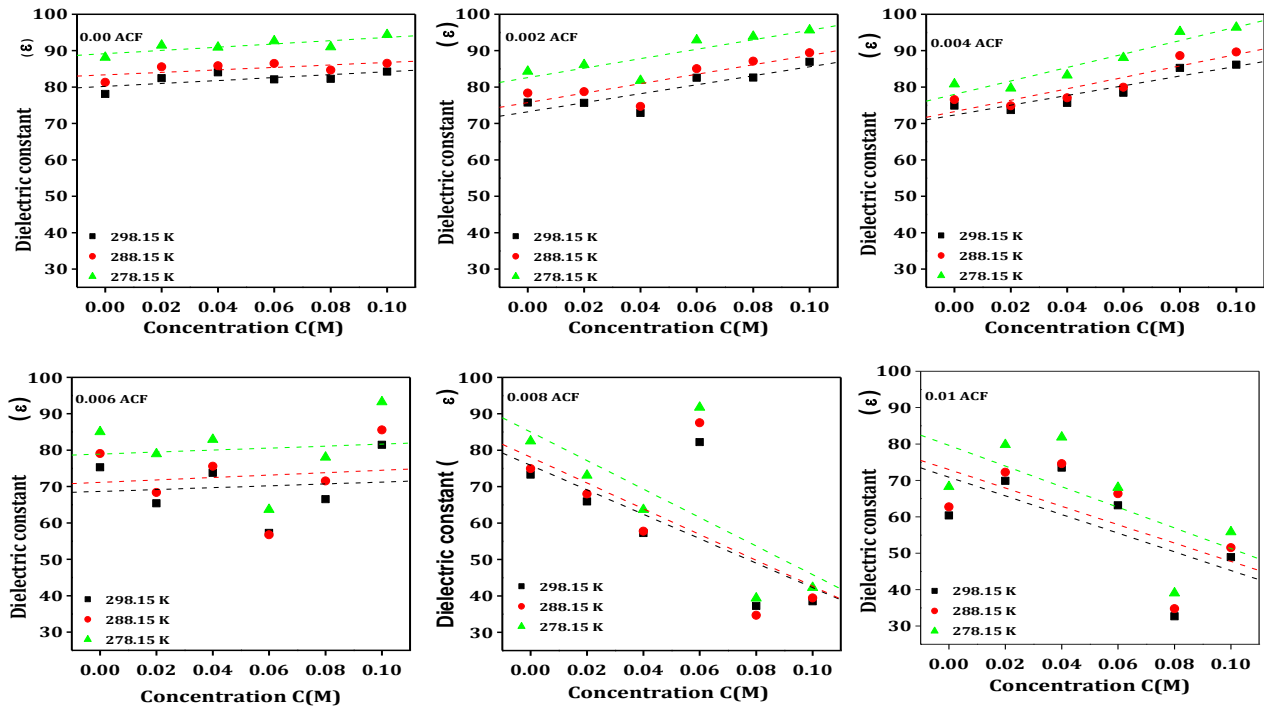


Figure 2: Temperature and concentration dependent static dielectric constant of aqueous valine in presence of different concentrations of aceclofenac.

Variation in static dielectric constant with different molar concentrations of ACF 0.002, 0.004, 0.006, 0.008 and 0.01 M in aqueous valine at different temperatures is shown in the fig 2. It has been observed that for all the used concentrations of aqueous valine the values of static dielectric constant increases for all the measured temperatures with increasing ACF except at higher ACF concentration while it was increasing towards lower temperatures over all the used concentrations of ACFs.

Increase in the values of static dielectric constant by lowering the temperature from 298.15 K to 278.15 K, may be due to increased dipole-dipole interaction (parallel or antiparallel) between valine-aceclofenac molecules via hydration shell and is associated with the cooperative relaxation of bulk-like water.

The relaxation dynamics for the rotational motion of water molecules in the solute environment are given by dielectric relaxation time measured for aqueous valine (fig. 3) and in the presence of aceclofenac. The relaxation time for aqueous valine increased linearly with valine concentration over all the measured temperatures, indicating a more heterogeneous / non-cooperative environment for water molecules that offers a large steric hindrance to the rotational motion of water molecules in the solvent rich (valine) and in the low temperature region.

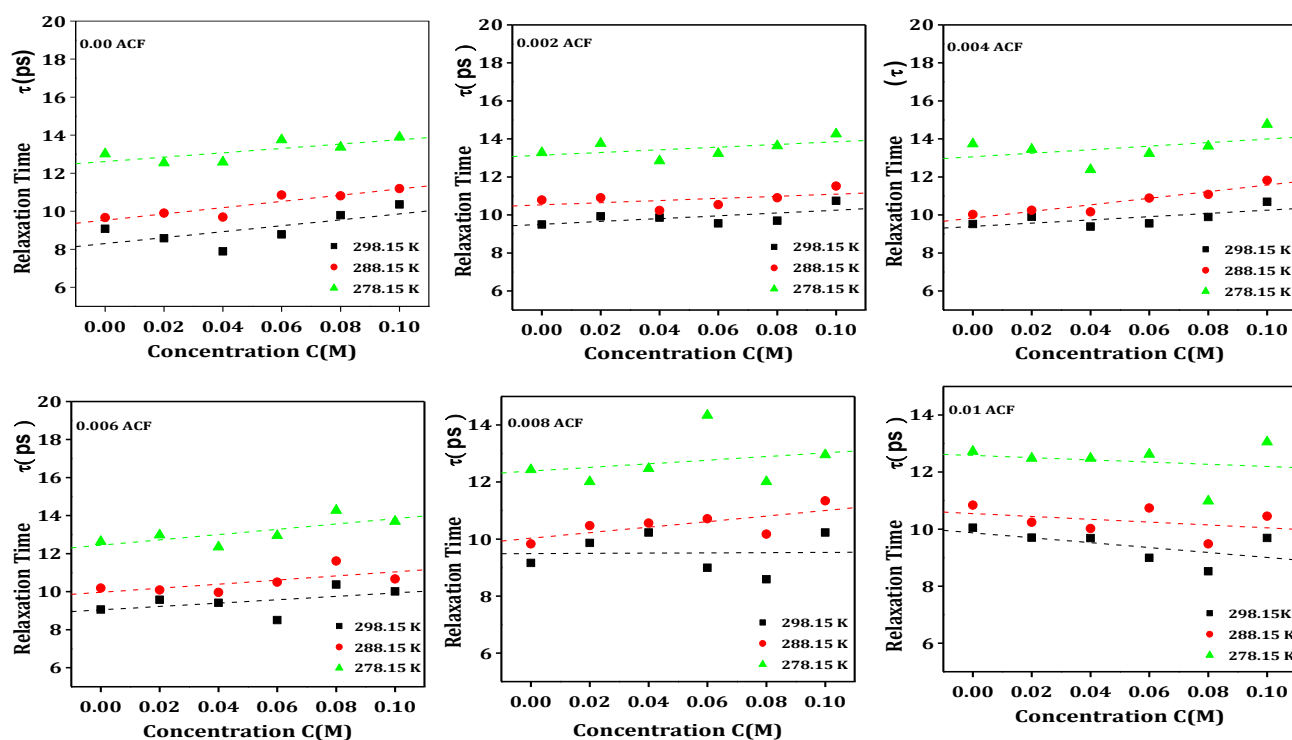


Figure 3: Dielectric relaxation time measured for aqueous PVP in the presence of Ibuprofen at different concentration and temperature.

Relaxation time for the aqueous valine in presence of aceclofenac (ACF) at various valine concentrations is shown in the fig 3. For all the used ACF concentrations, it has been observed that relaxation time increases towards low temperature and with valine concentration except at higher concentrations of ACF. This could be due to the formation of a hydration shell surrounding valine, which interacts with ACF via the hydration shell, or to a dipole-dipole induced interaction between valine and ACF via water molecules. As a result, rotational motion of water molecules gets restricted that results in increasing the values of relaxation time [24]. Towards lower temperature dipole-dipole parallel alignments in the valine-ACF-water system gets increased that affected rotational motion of water molecules due to the increased molecular hindrance and so the relaxation time increases towards low temperature.

The information regarding orientation of electric dipoles in polar liquid is described by Kirkwood correlation factor ' g '. The degree of intermolecular hydrogen bonding is measured by the deviation of the values of ' g ' from unity. If ' g ' is greater than 1 it means that molecules tend to direct themselves with parallel dipole moments; when g is smaller than 1 then molecules prefer an ordering with antiparallel dipole moments. ' g ' =1 may be due to the cancellation of the effects of both kinds of parallel and anti-parallel multimers for associating molecules [25-27]. Due to insufficient data available for the dipole moment at the measured temperature we used dipole moment for water $\mu=2.37$ D as calculated previously [28] to calculate the correlation factor ' g ' from the measured $g\mu^2$ calculated using Kirkwood-Frohlich equation [29-31].

$$g\mu^2 = \frac{9K_B T M}{4\pi N \rho} \left[\frac{(\epsilon_s - \epsilon_\infty)(2\epsilon_s + \epsilon_\infty)}{\epsilon_s(\epsilon_\infty + 2)^2} \right] \quad (2)$$

Where K_B is the Boltzmann constant, T is absolute temperature, M is the molecular weight, N is Avogadro's number and ρ is the density.

Since ' g ' is a measure of orientational correlation between a molecule and its nearest neighbors, the departure of ' g ' from unity could be an indication of molecular association due to short-range ordering interactions. In our case of aqueous valine and ACF induced valine, correlation factors are increases towards higher PVP concentrations (due to the parallel orientation of the dipoles) [32] suggesting increased correlation between solute dipole via hydration shell. The variation in the values of ' g ' with increasing ACF concentration in valine at different temperatures is shown in fig 4. From the observed data, it has been concluded that the correlation (Parallel orientation) between water and the surrounding molecules decreases by the presence of aceclofenac at higher concentrations of ACF. This could be due to the reduced parallel correlation between solutes and solvent. This may also be due to the fact that with increasing concentrations of both valine and ACF; number of water molecules attached to both the solutes under different conformations will be reduced [33]. These results suggest that as the concentration of ACF molecules is increased, parallel orientation of molecular dipole reduces, thereby reducing effective dipole moment. The ' g ' values are found to be lower at higher concentration of ACF. In addition, it was also observed that temperature also plays important role in changing the effective dipole moment. The ' g ' value was found to be increasing towards lower temperature which confirms the increased parallel dipole-dipole interaction due to the increased interaction between ACF, valine and water through hydration shell.

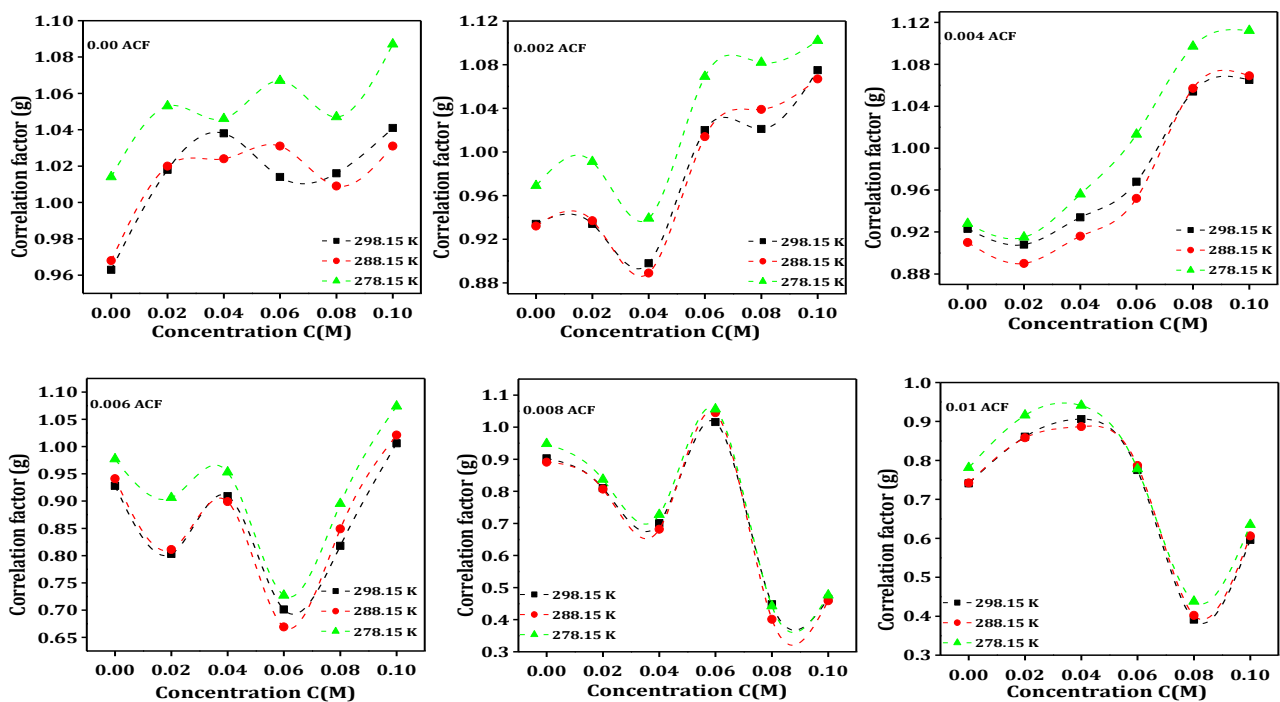


Figure 4: variation in correlation factor ' g ' for aqueous valine and ACF induced valine.

The variation ' g ' for the aqueous valine and ACF induced valine at different concentration and temperature is shown in fig 4 and the values of ' $g\mu^2$ ' and ' g ' are reported in table 1.

Table 1. The values of ' $g\mu^2$ ' and ' g ' for the solution of Valine+ACF+water.

Valine(M)/T(K)	298.15	288.15	278.15	298.15	288.15	278.15
	$g\mu^2$			g		
ACF 0.00 (M)						
0	5.414	5.44	5.697	0.963	0.968	1.014
0.02	5.722	5.731	5.917	1.018	1.02	1.053
0.04	5.834	5.752	5.879	1.038	1.024	1.046
0.06	5.699	5.794	5.994	1.014	1.031	1.067
0.08	5.709	5.671	5.885	1.016	1.009	1.047
0.1	5.851	5.796	6.107	1.041	1.031	1.087
ACF 0.002 (M)						
0	5.247	5.238	5.445	0.934	0.932	0.969
0.02	5.243	5.265	5.563	0.934	0.937	0.991
0.04	5.045	4.989	5.279	0.898	0.889	0.939
0.06	5.73	5.698	6.009	1.02	1.014	1.069
0.08	5.734	5.838	6.078	1.021	1.039	1.082
0.1	6.04	5.994	6.19	1.075	1.067	1.102
ACF 0.004 (M)						
0	5.189	5.115	5.213	0.923	0.91	0.928
0.02	5.101	5.001	5.14	0.908	0.89	0.915
0.04	5.242	5.149	5.375	0.934	0.916	0.956
0.06	5.439	5.348	5.691	0.968	0.952	1.013
0.08	5.922	5.941	6.163	1.054	1.057	1.097
0.1	5.982	6.009	6.241	1.065	1.069	1.112
ACF 0.006 (M)						
0	5.213	5.288	5.492	0.928	0.941	0.977
0.02	4.514	4.558	5.091	0.803	0.811	0.906
0.04	5.108	5.051	5.353	0.909	0.899	0.953
0.06	3.938	3.763	4.086	0.701	0.669	0.727
0.08	4.596	4.774	5.031	0.818	0.849	0.895
0.1	5.653	5.732	6.034	1.006	1.021	1.074
ACF 0.008 (M)						
0	5.074	5.007	5.326	0.903	0.891	0.948
0.02	4.553	4.533	4.705	0.81	0.807	0.837
0.04	3.938	3.834	4.084	0.701	0.682	0.727

0.06	5.707	5.866	5.935	1.016	1.045	1.056
0.08	2.52	2.254	2.484	0.448	0.401	0.442
0.1	2.61	2.581	2.676	0.465	0.459	0.476
ACF 0.01 (M)						
0	4.16	4.172	4.387	0.741	0.742	0.781
0.02	4.833	4.821	5.149	0.861	0.858	0.916
0.04	5.089	4.983	5.285	0.906	0.887	0.941
0.06	4.357	4.421	4.375	0.775	0.787	0.778
0.08	2.194	2.262	2.461	0.391	0.402	0.438
0.1	3.348	3.408	3.57	0.596	0.606	0.635

IV. CONCLUSIONS

From the overall study we may conclude that the static dielectric constant for aqueous valine increases with increasing valine concentration may be due to the formation of hydration shell around valine at all concentrations of ACF except at higher concentrations. During this process hydrogen bonding network will be affected by the presence of valine. Due to formation of hydration shell relaxation time for aqueous valine was found to be increasing with valine concentration over all the measured temperature that indicate more heterogeneous /non-cooperative environment for water molecules or we may say large steric hindrance to the rotational motion of water molecules in the solvent rich and low temperature region. From 298.15 K to 278.15 K static dielectric constant seems to be increasing for all the used concentrations may be due to the formation of induced dipoles via hydration layer with the neighbouring or surrounding molecules as the molecules gained lower thermal energy and therefore amplitude of the random thermal motion is restricted. This gives perfect alignment (parallel or antiparallel) with the applied field so that dipoles are more closely aligned with each other; as a result the orientation polarization gets increased and so the static dielectric constant.

The presence of aceclofenac in aqueous valine resulted in further decrease in the values of static dielectric constant and the variation was observed to be larger at higher ACF concentration. It is because of the molecular interaction between the methyl group (CH_3) of the screened valine by the water molecules and the H from the O-H group of ACF through weak dipole-dipole interaction as a result hydrogen bonding network affected due to the presence of aceclofenac which resulted in lowering the values of static dielectric constant. At highest concentration all the possible hydrogen bonding sites are saturated and no site is available for bonding to be taking place; as a result there is no further change in the structural conformation which decrease the static dielectric constant over the used concentrations and temperature.

Increasing values of dielectric relaxation time with increasing valine concentration reveals non cooperative environment for the molecular or rotational motion for water molecules. This may be due to association

between water molecules that form hydration shell around valine that interacts with ACF through hydration shell or dipole-dipole induced interaction between valine and ACF through water. As a result rotational motion of water molecules gets restricted and observes only increased values of relaxation time.

For aqueous valine and ACF induced valine, correlation factors are lower than 1 (due to the anti-parallel orientation of the dipoles) and increases further towards higher valine concentrations suggesting increased correlation between solute dipole via hydration shell except at higher concentrations of ACF. This may also be due to the fact that with increasing concentrations of both valine and aceclofenac; number of water molecules attached to both the solutes under different conformations will be reduced. At higher ACF the g values are very much less than unity is the clear indication of highly aligned antiparallel conformation. The g value was found to be increasing towards lower temperature which confirms the formation of weak interaction between ACF, valine and water through hydration shell.

V. ACKNOWLEDGEMENTS

Author AVS is thankful to School of Physical Sciences, S.R.T.M.University Nanded for providing instrumentation facility, the TDR and other infrastructural facilities related to this work. The author is also gratefully acknowledged to Dept. of Science and Technology (DST), New Delhi for providing (TDR) facility through project sanctioned to Dr. A.V.Sarode (SERB/F/4632/2013-2015) and Dr.A.C.Kumbharkhane (SB/S2/LOP-032/2013). I am thankful to Dr.T.M.Kalyankar, School of pharmacy ,Swami Ramanand Teerth Marathwada University Nanded for their valuable support. I am also highly thankful to my research colleagues Mrs. Komal B. Kabara, Mr.Ravikant R.Karale, Miss. Kamble Savita and Mrs.Suad Alwaleedy for timely support during my work.

VI. REFERENCES

- [1]. A.V. Sarode, A.C. Kumbharkhane and S.C. Mehrotra. Dynamics and interactions in aqueous polyvinylpyrrolidone (PVP K-30): an approach using dielectric relaxation spectroscopy (2018).
- [2]. A. Chaudhari, A.G. Shankarwar, B.R. Arbad and S.C. Mehrotra. Dielectric relaxation in glycine–water and glycine–ethanol–water solutions using time domain reflectometry. *Journal of solution chemistry*, 33(3) (2004) 313-322.
- [3]. H.C. Chaudhari, A. Chaudhari, and S.C. Mehrotra. Dielectric study of aqueous solutions of alanine and phenylalanine. *Journal of the Chinese Chemical Society*, 52(1) (2005) 5-10.
- [4]. Sunil Kumar Pradhan, Smruti Prava Das, Ashok Kumar Sahoo, Monalisa Das and Ajaya Kumar Patnaik. Molecular interaction of non-steroid anti-inflammatory drug aceclophenac with leucine in dmsol medium: an ultrasonic study. *Int. J. Adv. Res.* 5(6), 1534-1545.
- [5]. S.F. Koly, S.P. Kundu, S. Kabir, M.S. Amran and M. Sultan. Analysis of aceclofenac and bovine serum albumin interaction using fluorescence quenching method for predictive, preventive, and personalized medicine. *EPMA Journal*, 6(1) (2015)1-6.

- [6]. R. Sathish, J. Anbu, A. ANJANA, K.N. AHAMED and G.S. RAO. Pharmacokinetic and pharmacodynamic interaction between aceclofenac and rosiglitazone in rats. *metabolism*, 13 (2012) 14.
- [7]. C. Jelsch, R.N. Devi, B.C. Noll, B. Guillot, I. Samuel and E. Aubert. Aceclofenac and interactions analysis in the crystal and COX protein active site. *Journal of Molecular Structure*, 1205(2020) 127600.
- [8]. R.W. Gora, S.J. Grabowski and J. Leszczynski. Dimers of formic acid, acetic acid, formamide and pyrrole-2-carboxylic acid: an ab initio study. *The Journal of Physical Chemistry A*, 109(29) (2005) 6397-6405.
- [9]. G.R. Desiraju. Supramolecular synthons in crystal engineering—a new organic synthesis. *Angewandte Chemie International Edition in English*, 34(21) (1995) 2311-2327.
- [10]. S. Suresh, S. Gunasekaran and S. Srinivasan. Studies of the molecular geometry, vibrational spectra, Frontier molecular orbital, nonlinear optical and thermodynamics properties of Aceclofenac by quantum chemical calculations. *Spectrochimica Acta Part A: Molecular and Biomolecular Spectroscopy*, 125 (2014) 239-251.
- [11]. B. Lee, and H. Jung. Enhanced bioavailability of poorly water-soluble aceclofenac using PEG-based solid dispersion in rats, beagle dogs and human subjects. In *AAPS Annual Meeting, New Orleans, LA, USA. Pharm Sci Supplement (Vol. 1, No. 4 (1999) S614-614)*.
- [12]. T. Kim, J. Shin and B. Lee. Enhanced dissolution and bioavailability of poorly water-soluble aceclofenac using solid dispersion system. Denver, Colorado, USA: *AAPS. In Annual Meeting (2001) 21-25*.
- [13]. H.B. Samal, J. Debata, N.N. Kumar, S. Sneha, and P.K. Patra. 41. Solubility and Dissolution Improvement of Aceclofenac using-Cyclodextrin. *International Journal of Drug Development and Research*, 4(4) (2012) 0-0.
- [14]. A.C. Kumbharkhane, S.M. Puranik, and S.C. Mehrotra. Dielectric relaxation of tert-butyl alcohol–water mixtures using a time-domain technique. *Journal of the Chemical Society, Faraday Transactions*, 87(10) (1991) 1569-1573.
- [15]. M.T. Hosamani, N.H. Ayachit and D.K. Deshpande. Dielectric studies on some substituted indoles. *Physics and Chemistry of Liquids*, 46(3) (2008) 307-311.
- [16]. R.H. Cole, J.G. Berberian, S. Mashimo, G. Chryssikos, A. Burns and E. Tombari. Time domain reflection methods for dielectric measurements to 10 GHz. *Journal of applied physics*, 66(2) (1989) 793-802.
- [17]. E.P.H.R.A.I.M. Katchalski and I.Z. Steinberg. Proteins and synthetic polypeptides. *Annual Review of Physical Chemistry*, 12(1) (1961) 433-464.
- [18]. A.V. Sarode, and A.C. Kumbharkhane. Dielectric relaxation and thermodynamic properties of polyvinylpyrrolidone using time domain reflectometry. *Polymer international*, 61(4) (2012) 609-615.
- [19]. S. Havriliak and S. Negami. A complex plane representation of dielectric and mechanical relaxation processes in some polymers. *Polymer*, 8 (1967) 161-210.
- [20]. J. Knapik, Z. Wojnarowska, K. Grzybowska, L. Tajber, H. Mesallati, K.J. Paluch and M. Paluch. Molecular dynamics and physical stability of amorphous nimesulide drug and its binary drug–polymer systems. *Molecular Pharmaceutics*, 13(6) (2016) 1937-1946.
- [21]. N.K. Li, F.G. Quiroz, C.K. Hall, A. Chilkoti and Y.G. Yingling. Molecular description of the LCST behavior of an elastin-like polypeptide. *Biomacromolecules*, 15(10) (2014) 3522-3530.

- [22]. M. Maurer and C. Oostenbrink. Water in protein hydration and ligand recognition. *Journal of Molecular Recognition*, 32(12) (2019) 2810.
- [23]. P. Bhavya, R. Melavanki, R. Kusanur, K. Sharma, V.T. Muttannavar and L.R. Naik. Effect of viscosity and dielectric constant variation on fractional fluorescence quenching analysis of coumarin dye in binary solvent mixtures. *Luminescence*, 33(5) (2018) 933-940.
- [24]. D. Ekka. Thermophysical studies on ionic liquids and amino acids in some liquid systems (Doctoral dissertation, University of North Bengal) 2014.
- [25]. T. Thenappan and A.P. Devaraj. Dielectric studies on binary polar mixtures of propanoic acid with esters. *Journal of molecular liquids*, 123(2-3) (2006) 72-79.
- [26]. T.M. Mohan, S.S. Sastry and V.R.K. Murthy. Thermodynamic, dielectric and conformational studies on hydrogen bonded binary mixtures of propan-1-ol with methyl benzoate and ethyl benzoate. *Journal of solution chemistry*, 40(1) (2011) 131-146.
- [27]. H.A. Chaube, V.A. Rana, P. Hudge and A.C. Kumbharkhane. Dielectric relaxation studies of binary mixture of diethylene glycol mono phenyl ether and methanol by Time Domain Reflectometry. *Journal of Molecular Liquids*, 211 (2015) 346-352.
- [28]. A. Luzar and J. Stefan. Dielectric behaviour of DMSO+water mixtures. A hydrogen-bonding model. *Journal of molecular liquids*, 46 (1990) 221-238.
- [29]. R.J. Sengwa. Microwave dielectric relaxation and molecular dynamics in binary mixtures of poly (vinyl pyrrolidone)-poly (ethylene glycol) s in non-polar solvent. *Polymer international*, 52(9) (2003) 1462-1467.
- [30]. V.V. Navarkhele. Static dielectric constant and excess properties of amino acids. *Journal of Chemical and Pharmaceutical Research*, 8(7) (2016) 930-935.
- [31]. M. Buback and W.D. Harder. The Static Dielectric Constant of Ammonia to High Pressures and Temperatures: II. Representation of Experimental Data via Kirkwood-Fröhlich's Equation. *Berichte der Bunsengesellschaft für physikalische Chemie*, 81(6) (1977) 609-614.
- [32]. Rodríguez-Arteche, I. Cerveny, S. Alegría, Á. and J. Colmenero. Dielectric spectroscopy in the GHz region on fully hydrated zwitterionic amino acids. *Physical Chemistry Chemical Physics*, 14(32) (2012) 11352-11362.
- [33]. D. Ekka, and M.N. Roy. Molecular interactions of α -amino acids insight into aqueous β -cyclodextrin systems. *Amino Acids*, 45(4) (2013) 755-777.

Synthesis, Characterisation of Ni-beta Zeolite

A.N.Kalyankar*¹, S.S.Jadhav², A.L.Choudhari³

*¹Department of Physics, Bahirji Smarak Mahavidyalaya, Basmath, Maharashtra, India

²Department of Physics, D.S.M.College, Jintur, Maharashtra, India

³Ex.Prof. School of Physical Sciences, S.R.T.M.University, Nanded, Maharashtra, India

ABSTRACT

The coal fly ash is produced on large scale in India by the thermal power stations. In this paper, the modified zeolite beta synthesized using fly ash is used for studying the dielectric properties. The zeolite is modified by ion exchange process so as to form Ni-beta type zeolite. The samples were tested for dielectric constant (ϵ'), dielectric loss (ϵ''), electrical conductivity (σ_{ac}). The dielectric properties depend upon the percentage of loading metal cations. This zeolite beta reported in this work helps to work as a material for dielectric applications.

Keywords: Coal fly ash, Zeolite beta, dielectric properties

I. INTRODUCTION

Zeolites are crystalline aluminosilicates and they have many applications in industry which are well known. Synthesis of zeolites using coal burnt fly ash is a nice alternative to use this solid waste. As coal fly ash contains a large amount of silica and alumina, which is helpful in zeolite synthesis. Zeolites are synthesized by hydrothermal treatment in an alkaline solution [1]. Fly ash is a fine grained powder, which is mainly composed of spherical glassy particles, produced during the combustion of pulverized coal. Many researchers have been synthesized zeolite beta from solid waste [2]. Nowadays, a novel application of zeolite in electronics is necessary [3]. This paper reports the dielectric properties of zeolite Ni-beta synthesized from coal fly ash.

1. Materials & Methods:

The starting material fly ash was obtained from Parali thermal power station, Maharashtra (India). The fly ash zeolite beta synthesized using fly ash based on previous study [4] is used. The zeolite beta thus formed is ion exchanged with 1 M solution of NH_4NO_3 at 80°C for 12 h. This process was repeated thrice so as to get proper ion exchange. The product was filtered, air dried at 60°C for 24 hr and then calcined at 450°C so that the NH_4 -beta is decomposed into H-beta i.e. protonic form then the zeolite which when ion exchanged with 0.1M, 0.2M and 0.3M solution of nickel nitrate $[\text{Ni}(\text{NO}_3)_2 \cdot n\text{H}_2\text{O}]$, so as to obtain the $\text{Na}_{(1-x)}\text{Ni}_x$ beta zeolite where $x = 0.1, 0.2, 0.3\text{M}$.

1.1.Characterisation:

The physical properties of coal fly ash and synthesized products were measured as follows. The chemical composition fly ash was determined by using a X-ray Fluorescence Spectroscopy. The chemical composition was analyzed using X-ray fluorescence analysis equipment (Phillips PW - 2404).The sample phases were characterized by X-ray diffraction (XRD) using a (Philips PW 3710) diffractometer with Cu- K α radiation (1.5496Å).

2.2. Dielectric Measurement:

The samples of Na-beta and Ni- beta zeolite were compressed to form pellet of 10 mm diameter and 1 mm thickness. The pellets were heated to 300⁰C to obtain a hard solid sintered material. The pellets were polished with silver paste for good electrical contact. The electrical conductivity was measured in the frequency range 20Hz–1MHz at room temperature 25⁰C using LCR-meter (HP-4284A).

2. Results and discussion:

2.1.XRF

Table1. Chemical composition of fly ash

Oxides	% wt	Mol/100 g of fly ash
SiO ₂	70.23%	1.169
Al ₂ O ₃	23.27%	0.228
Fe ₂ O ₃	4.38%	0.027
MgO	1.26%	0.031
Na ₂ O	0.42	0.0067
LOI	0.44%	-

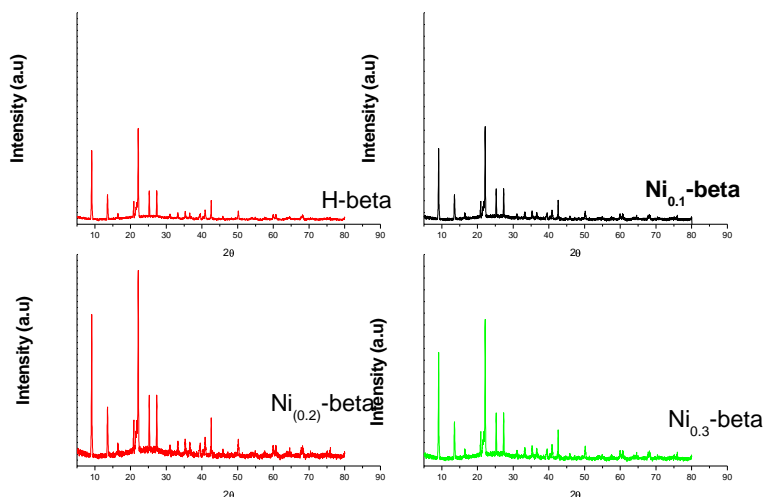
The elemental composition analysis by XRF in Table 1 indicated that coal fly ash contained large quantities of silica and alumina which are the two main components in zeolite. The chemical analysis of the fly ash used as the starting material in this work showed it to be a high-silica ash with the mole ratio of SiO₂: Al₂O₃ = 5.127: 1.

2.2. XRD

The X-ray diffraction pattern of fly ash based zeolite H- beta and its exchanged form Ni-beta is shown in fig.1. The d values are compared with the standard [5] . The powder X-ray diffraction(PXRD) pattern showed characteristic peaks of beta-type zeolite (Figure 1), indicating formation of microporous zeolite beta crystals.. The peaks at 2 θ = 43.23^o is representative peak of a NiO [6]. As can be seen in Figure 1,

the intensity of peaks corresponding to H-beta zeolite decreased, whereas, the intensity of peaks corresponding to nickel increased on increasing the nickel doping on H-beta zeolite.

Figure 1. X-ray diffraction patterns of H-beta/Ni-beta zeolite.



The XRD for Ni-beta were found to be similar to that of original H-beta sample, indicating that there is no structural changes occur after ion exchange with nickel nitrate [7].

2.3. Dielectric Measurement:

The variation of dielectric constant (ϵ'), dielectric loss (ϵ''), ac conductivity (σ) with $\log f$ for H -beta and Ni-beta zeolites are shown in figure 2, 3, and 4. In Figure 2, the permittivity (ϵ') of zeolite H-beta was found to decrease with an increase in frequency. This characteristic gives the increase of the permittivity at low frequency. The low dielectric constant of zeolites (ϵ') suggests, however, that such processes in the zeolite channels should involve concerted action rather than strong charge separation.

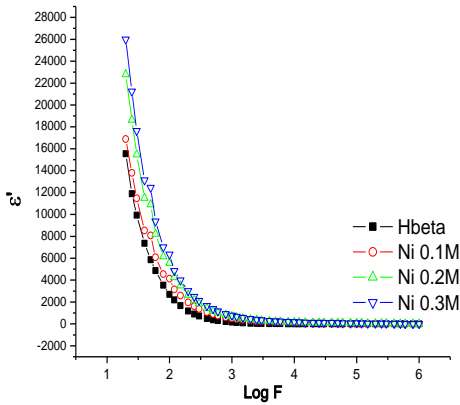


Figure 2. Variation of dielectric constant (ϵ') with $\log f$

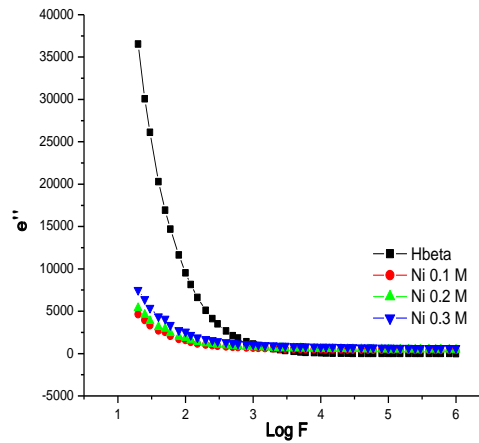


Fig.3 Variation of dielectric loss (ϵ'') with $\log F$

In fig.3 the variation of dielectric loss (ϵ'') with frequency at room temperature is shown. This dielectric loss is frequency dependent and also influenced by water content of the zeolite [8]. The loss is in lowest frequency region and has been frequently observed in zeolites is supposed to be due to a dc ionic conductivity loss and grain boundary effect [9-10].

In fig. 4 the variation of ac conductivity (σ) with frequency at room temperature is shown. The conductivity increases with increase in frequency. The conductivity of zeolite H-beta is less than Ni -beta, as the conductivity depends on the cation size and the channels within the zeolites structure.

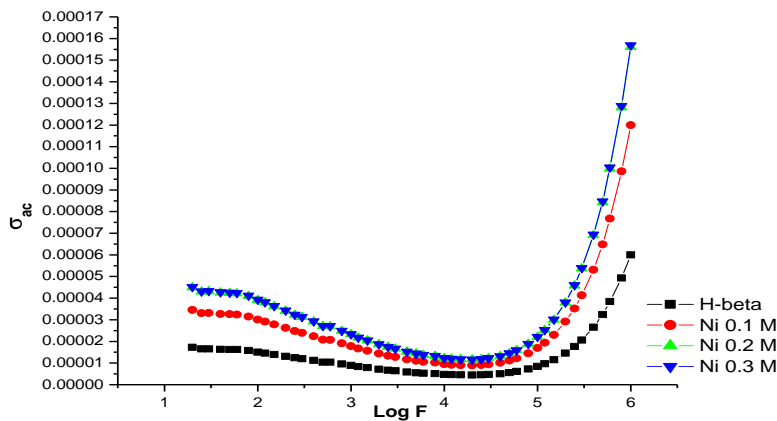


Fig.4 Variation of ac conductivity (σ_{ac}) with $\log F$

3. Conclusion:

Zeolite beta is successfully synthesized from solid waste material fly ash and it shows no structural change after modification with cobalt. The zeolite beta and Ni-beta shows good response for dielectric applications.

References

- [1] Huiyong Chen, James Wydra, Xueyi Zhang, Pyung-Soo Lee, Zhuopeng Wang, Wei Fan, and Michael Tsapatsis, *J. Am. Chem.Soc.* (2011); **133**:12390-12393
- [2] Maria Harja, Sorin Mihai Cimpeanu, Marcel Dirja , Daniel Bucur. (2016). *Zeolites - Useful Minerals* ISBN 978-953-51-2577-8, DOI: 10.5772/64126
- [3] Normann Herron, *Journal of inclusion phenomena and molecular recognition in chemistry*,(1995), 21, 283-298.
- [4] Kalyankar Anil N, *J. Biol. Chem. Chron.* 2019, 5(3)172-173
- [5] Baerlocher, Ch.; McCusker, L. B.; Olson, D. H.*Atlas of Zeolite Framework Types* , 6th ed.; Elsevier: Amsterdam, 2007.
- [6] James T. Richardson , Robert Scates , Martyn V. Twigg, *Applied Catalysis A: General* 246 (2003) 137–150
- [7] Yuelun Wang, Yuan Jiang, Jun Huang, Hui Wang, Zhuo Li ,Jinhu Wu, *RSC Adv.*, 2016,6, 107498-107506.
- [8] Tatsuo Ohgushi, Kazushi Ishimaru, *Chem. Commun.*(2002) 1714.
- [9] R.M.Barrer, P.J.Coen, *Nature*, 199, (1963) 587
- [10] V. Krylov (1970) “Catalysis by Non-Metals”Academic Press, New York

To Analyze Intermolecular Interactions among Hydrogen Bonded Liquids by using TDR and FTIR Spectroscopy

Neware S G^a, Pathan A W^b, Kumbharkhane A C^c, Chalikwar P A^d, Mahajan G R^e., Shaikh Y H^f

^aMaulana Azad College of Arts, Science and Commerce, Aurangabad, MS 431001, India;

^bDept. of Physics ASC College, Badnapur, Jalna, MS 431202, India;

^cSchool of Physical Sciences, SRTM University Nanded, MS 431604, India;

^fDepartment of Physics and Electronics, Shivaji Arts, Science and Commerce College, Kannad, Aurangabad

^dDept. of Physics KKM College, Manwath Dist. Nanded (MS).

^eSri Datta Arts, Commerce and Science college Hadgaon dist Nanded (MS).

ABSTRACT

In the present investigation dielectric measurements have been carried out by making the use of TDR technique in the frequency span of 10 MHz-50 GHz at temperatures 0^oC, 5^oC, 10^oC, 15^oC, 20^oC and 25^oC respectively at 11 volume fractions of 1-PENT in ETOH. Excess properties like excess permittivity and excess inverse relaxation time have been explored using the calculated values of dielectric constant and relaxation time which have been reported in our earlier study, "Dielectric relaxation study of 1-Pentanol-Ethanol binary mixtures at 10 MHZ-50 GHz frequency range using TDR technique". The values of Bruggemann factor (F_B) are calculated at all different aforesaid temperatures and compositions by making the use of least square fit method. Apart from all of these measurements FTIR measurements also been performed to scrutinize the intermolecular interactions in the binary mixture of liquids utilized for the present study.

Keywords: Time Domain Reflectometry (TDR); 1-Pentanol; Ethanol; Excess properties; Functional groups; FTIR.

*Corresponding author

Email address: shaikhyh@gmail.com.(Y.H.Shaikh)

I. INTRODUCTION

TDR is the authentic and dynamic approach for the study of structure of intermolecular interactions both in pure form and binary mixture of liquids, which allows the researchers in just one quantification for the broadband of frequencies [1, 2]. Dielectric measurements is a crucial tool for estimating intermolecular interactions which are due to dipole-dipole interactions which leads to succeeding molecular structural reposition in a binary mixture, and due to the existence of hydrogen bonds in the binary mixture the dielectric properties of the participating constituent liquids alters significantly [3-4]. Alcohols have allured much attentiveness amongst most of the researchers for the dielectric study due to its polarity, as

this polarity character individualize it from other non polar organic compounds this rationality polar character leads to association of alcohol molecules through the rather attraction of positive charge of hydrogen atom of one hydroxyl group with a correspondingly negative charge of oxygen atom of another hydroxyl group. Alcohols can be utilized in many ways, in chemical industries as solvents for oils, resins and antifreeze for explosive and in this way alcohol's participation is noteworthy in chemistry and biology, not only that it can also be employed to realize the associative behavior with multitude of internal structures that relies on carbon chain length and position of O-H group [5, 6]

An extensive analysis have been done to study dielectric properties of 1-alkanols with acrylate group [7]. Recently our research group have given the qualitative data regarding the study of dielectric properties by making the use of medicinal compounds [8-9]. The workers studied the dielectric properties extensively [10]. The study revealed the increase in dipole moments and formation of dimers in the binary mixture [11]. The study has been carried out to study the dielectric properties of amines [12]. The study yields an info in to the structural changes [13].

Fourier transform infrared spectroscopy (FTIR) is the dominant approach for the characterization of samples which are in solid, liquid and gas phase [14]. It is only the IR active molecules which absorbs the IR light if there is change in dipole moment during the course of vibrations [15], and ethanol and 1-pentanol are polar and IR active as both of them possess permanent dipole moment and hence yields absorbance spectra. Sivgurunathan et.al

have studied the comparison between FTIR spectra of O-H and C=O regions between 1-alkanols and alkyl methacrylate [16]. Conduction of study affirmed the ontic of NH₂, CH and C=O stretches in formamide, and dimethyl amino ethanol, both in pure form and in binary mixture [17].

The literature survey have shown that there is not too much work have been done yet for the dielectric study of 1-PENT-ETOH binary system and there is no FTIR study have been performed for the aforesaid system, so the main goal of present investigation is to study intermolecular interactions via excess permittivity (ϵ^E), Bruggemann factor and dipolar rotations through excess inverse relaxation time and also with the aid of FTIR spectroscopy to study the existence of intermolecular hydrogen bonding in polar groups both in pure form and binary mixture of participating liquids.

2. Experimental details

2.1 Chemicals:- The chemicals utilized for the present investigation was obtained from EMD Millipore Corporation Germany grade having 99% purity so was used without further purification.

2.2 Methodology-

Dielectric study

Samples were prepared by mixing the volume fractions of 1-Pentanol in ethanol in the range of 0% to 100%, and measurements were taken by placing the sample in electronically temperature controlled bath with an accuracy of $\pm 0.1^\circ\text{C}$ at temperatures 0°C - 25°C . The Tektronix DSA8300 sampling main frame oscilloscope sampling with the dual-channel sampling module 80E10B has been used for time domain reflectometry. The sampling module is well equipped with 12 ps incident and 15 ps reflected rise time pulse. The coaxial cable which has been utilized to feed pulse has 50 ohm impedance, inner diameter

of 0.28 mm and outer diameter of 1.19 mm. Sampling oscilloscope monitor changes in pulse after reflection from the end of line. Reflected pulse without sample $R_1(t)$ and with sample $R_x(t)$ was recorded in time window of 5 ns and digitized in 2000 points. The addition [$q(t) = R_1(t) + R_x(t)$] and subtraction [$p(t) = R_1(t) - R_x(t)$] of these pulses is done in oscilloscope memory. These subtracted and added pulses are transferred to PC for further analysis. The Fourier transformations of the pulse and data analysis were done to determine complex permittivity spectra $\epsilon^*(\omega)$ using non-linear least square fit method which have been reported in our earlier study [18].

2.3 FTIR measurements:-

To study the FTIR spectra for 1-PENT and ETOH both in pure form and the binary mixture of the same bruker spectrometer have been utilized in the frequency span of 500-4000 cm^{-1} at room temperature.

3 Results and discussion

Excess permittivity

The values of excess permittivity has been figured out using the equation [19]

$$(\epsilon_0)^E = (\epsilon_0)_m - [(\epsilon_0)_E X_E + (\epsilon_0)_A (1 - X_E)] \quad (1)$$

Where X_E represents the volume fraction of an ethanol. Subscripts m, E and A represents Mixture, ethanol and solute 1-pentanol respectively.

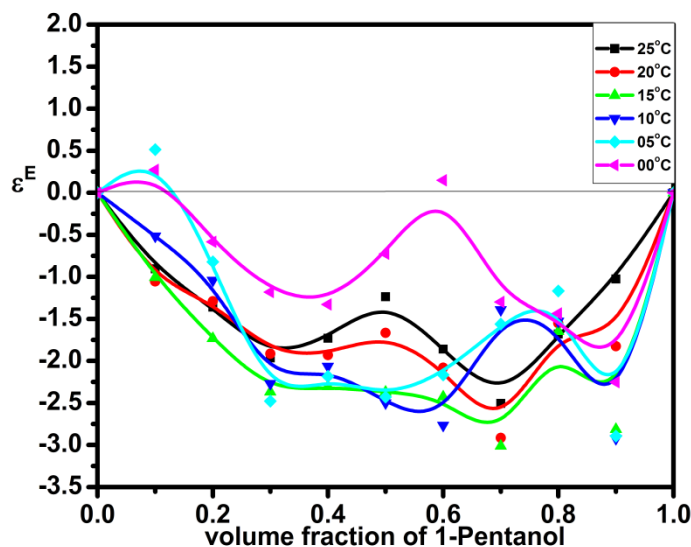


Figure 1. Excess permittivity (ϵ^E) vs. volume fraction of Ethanol at various temperatures

The crucial data regarding the interactions amide the polar-polar binary liquid mixtures can be figured out by utilizing excess permittivity (ϵ^E) [20], which can be summarized as follows.

- (i) $(\epsilon)^E=0$ means no interactions among participating liquids
- (ii) $(\epsilon)^E<0$ designates interaction in such way as to lead reduction in effective dipole moments.
- (iii) $(\epsilon)^E>0$ interactions contributes to increase in dipole moments.

An alterations in the values of Excess properties are as shown in fig (1). the positive values of excess dielectric constant corroborates the formation of monomers contrarily the negative values formation of multimers designating the interaction of molecules in such a way that the effective dipoles gets reduced. The figure reflects all the values of excess permittivity negative at all temperatures and for all concentrations of 1-PENT in ETOH ,this can be attributed to the breaking of hydrogen bonds among solute and solvent molecules with subsequent emergence of multimeric structures ,which stipulates reduction in dipole moments due to alignment of adjacent dipoles in opposite directions.

These results are in conformity with those obtained. by researchers [21] except at 0.70 mole fraction

Excess inverse relaxation time:-

The excess inverse relaxation time was found out using the relation

$$\left(\frac{1}{\tau}\right)^E = \left(\frac{1}{\tau}\right)_m - \left[\left(\frac{1}{\tau}\right)_A X_A + \left(\frac{1}{\tau}\right)_B X_B\right] \quad (2)$$

Where $\left(\frac{1}{\tau}\right)^E$ is the excess inverse relaxation time which represents the average broadening of dielectric spectra [22].

The significant data regarding the rotation of dipoles by using this property is as follows [23]

- (i) $(1/\tau)^E=0$ designates no solute-solvent interaction
- (ii) $(1/\tau)^E<0$ solute-solvent interactions in such way that dipoles rotates slowly under the effect of field of hindrance.
- (iii) $(1/\tau)^E>0$ gives speedy rotation of dipole.

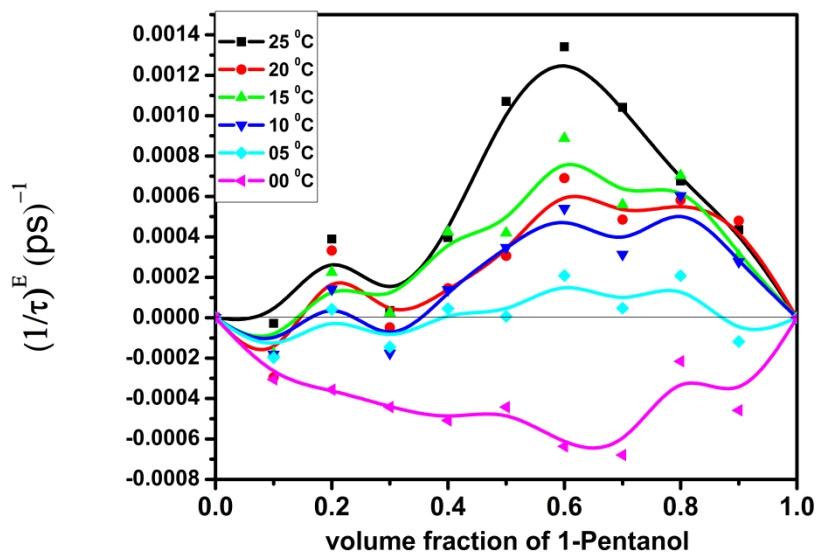


Figure 2. Excess inverse Relaxation time $(1/\tau)^E$ vs volume fraction of 1-Pentanol at various temperatures

The fig. (2) depicts the calculated values of excess inverse relaxation time for all the concentrations of 1-PENT in ETOH at temperatures 0 °C- 25°C. The fig reflects all the values positive at temperatures 5°C-

-25°C for all concentrations with conspicuous maxima at 60% of $\left(\frac{1}{\tau}\right)^E$ 1-PENT at 25°C, these positive values stipulates the solute –solvent interactions via hydrogen bonding in such a manner which leads to faster rotation of dipoles. The fig also shows the negative trend for $\left(\frac{1}{\tau}\right)^E$ values at temperature 0 °C which can be attributed to creation of field of hindrance which leads to slow rotation of dipole moments. These results are different from the results obtained for the same system [24].

Bruggeman factor (F_B)

The Bruggeman factor (F_B) is an additional parameter which gives an informative approach towards intermolecular interactions and which is dependent on dielectric permittivities of solute, solvent, and their binary mixture can be expressed as [25]

$$f_B = \left[\frac{(\epsilon_{0m} - \epsilon_{02})}{(\epsilon_{01} - \epsilon_{02})} \right] \left(\frac{\epsilon_{01}}{\epsilon_{0m}} \right)^{\frac{1}{3}} = 1 - v \quad (3)$$

Where $\epsilon_{0m}, \epsilon_{01}, \epsilon_{02}$ are the static dielectric constants corresponding to mixture solute and solvent respectively. V is the volume fraction of solvent (ethanol). From above equation linear relation is expected from plot F_B versus volume fraction of ethanol, But in binary liquids, there is a nonlinear relationship. The nonlinearity of Bruggeman factor vs. volume fraction of solvent can be expressed by [26].

$$f_B = \left[\frac{(\epsilon_{0m} - \epsilon_{02})}{(\epsilon_{01} - \epsilon_{02})} \right] \left(\frac{\epsilon_{01}}{\epsilon_{0m}} \right)^{\frac{1}{3}} = 1 - [a - (a - 1)V]V \quad (4)$$

In this equation volume fraction (V) is changed by a factor ' $a - (a - 1)V$ ' of the mixture which can be ascribed to the solutes molecular structural readjustment within the mixture [27] and molecular ideal behavior can be resolved by random constant ' a ' where $a=1$ points out Ideal mixture with no additional interaction between two liquids and reduces to Bruggeman equation. ' a ' has been found out by least square fit method.

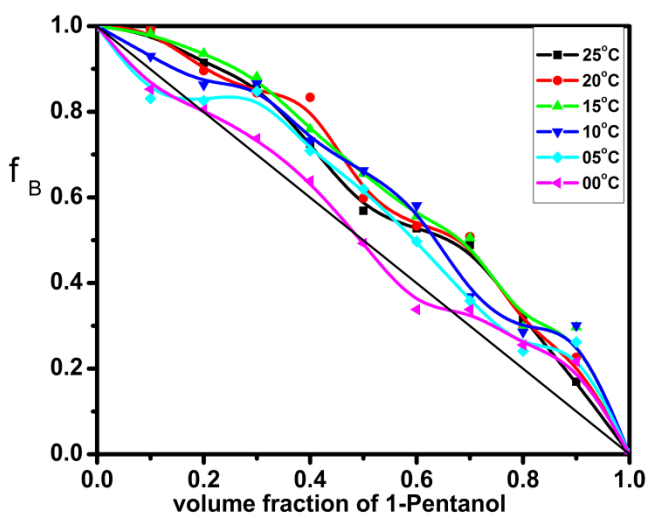


Figure 3. Nonlinearity of Bruggemann factor at various temperatures

The experimental values of 'a' are found to be 0.45,0.28,0.22,0.37,0.57,and 0.92,at temperatures 25 °C , 20 °C, 15 °C, 10 °C, 5 °C,and 0 °C respectively. The nonlinearity of plot F_B vs. volume fraction of 1-pentanol provides an evidence of intermolecular interactions through the hydrogen bonding among the hydroxyl groups of both the liquids and all obtained values of 'a' are less than unity designates reduction in effective volume of solvent than its actual volume [28].

FTIR analysis:-

FTIR is the significant approach which yields a precise data regarding the identification of functional groups at precise frequency and intermolecular Hydrogen bonding. The FTIR measurements were made for pure alcohols and their binary mixtures, and it is observed that the FTIR spectra shown in figure 4(a) and 4(b) for 1-Pentanol and ethanol in pure form is in conformity with spectra reported in literature for the same [29].

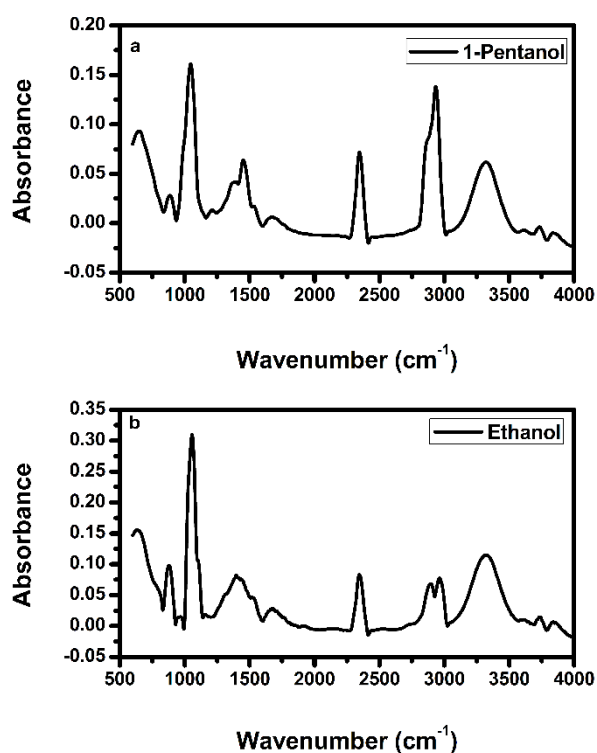


Figure 4. FTIR Spectra in pure form (a)1-Pentanol (b) Ethanol

The absorbance bands at particular frequencies appeared for 1-PENT and ETOH and their binaries can be attributed to OH, C-H and, C-O bands which are in well agreement with literature values for the pure form of liquids. [30-31].

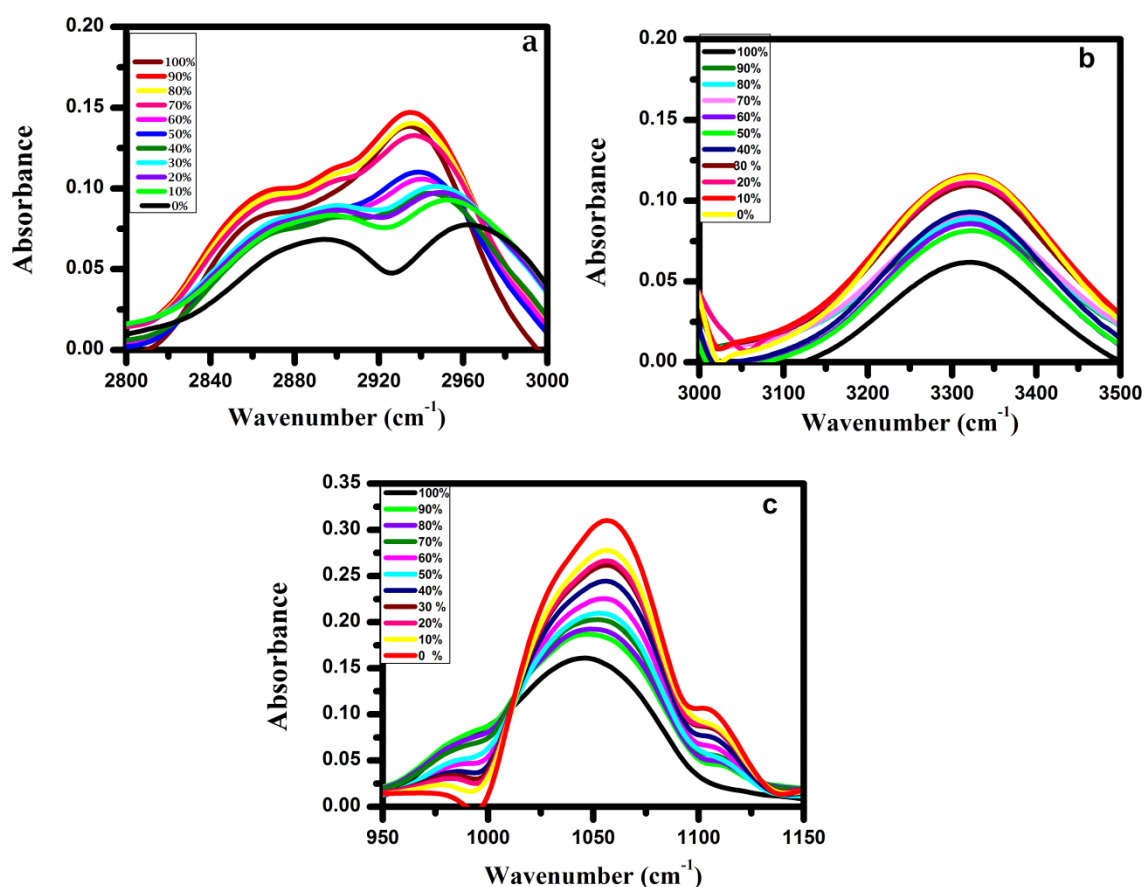


Figure 5-FTIR absorbance peaks for the identification of functional groups [a]CH [b] OH [c] CO

The fig.5 (a) shows sharp bands for asymmetric stretch at 2928.59 and 2972 cm⁻¹ and that for symmetric stretch at 2865.25, and 2881.58 cm⁻¹ respectively for 1-PENT and ETOH, the upsurge in band frequencies can be ascribed to weak intermolecular interactions in the binaries [32]. The bands for 1-PENT are more intense than ETOH as it consist of more C-H groups in comparison with ETOH. Fig. 5(b) exhibits broad bands at 3322.48 and 3325.58 cm⁻¹ for 1-PENT and ETOH and there is a shifting of band frequencies for all concentrations of 1-PENT in ETOH which stipulates the self associative character of 1-PENT [33]. The electro negativity difference between C and O assigns a polarity character to C-O bonds which in turn assign the large dipole moment, and due to change in dipole moment during

bond vibrations the peaks are more intense for primary alcohols and their mixture. The C-O stretch for 1-PENT and ETOH which is shown in fig. 5(c) is at 1049 and 1044 and 1044 cm⁻¹ and there is a decline in C-O stretch frequency from 40% of 1-Pentanol to ethanol in pure form. This shift in frequency is the

sign of disruption of dipole-dipole interactions among the similar species followed by dipole-dipole interactions among unlike species. The table (1) reflects all the wave numbers assigned to the functional groups of liquids utilized before mixing and after mixing.

Table 1-FTIR data for functional group wave numbers.

Volume fraction of 1-Pentanol	Functional groups wave numbers (cm ⁻¹)		
	CH	OH	C-O
0.0	2928.59	3325.58	1044.00
0.1	2970.22	3323.44	1045.73
0.2	2971.02	3322.29	1046.38
0.3	2970.29	3325.35	1046.69
0.4	2964.50	3325.65	1047.25
0.5	2959.90	3327.31	1047.83
0.6	2959.91	3324.83	1048.10
0.7	2957.98	3325.79	1049.95
0.8	2957.52	3324.91	1051.09
0.9	2957.19	3325.74	1052.02
1.0	2972	3322.48	1049.00

4. Conclusion:

The positive value of excess permittivity indicates the formation of monomers while the negative value points out the formation of multimeric structures in the binary mixture.

The trend of positive excess inverse relaxation time values suggest the slow rotation of dipoles on one hand, negative trend of this values leads to the slow rotation of the same. nonlinear plot of (F_B) versus volume fraction of solute in solvent reflects the existence of intermolecular interactions in the mixture and the values of 'a' are found out at all the temperatures, all are found to deviate from the ideality $a=1$. The wave number shifting for Absorbance peaks of functional groups CH, OH, and C-O have been studied for the binary mixture of 1-pentanol in ethanol for all concentrations at room temperature which stipulates there is weak molecular interactions according to the shifting of peaks wave numbers to higher side, and the spectra's and the wave numbers of peaks reported for the systems in pure form are in well conformity with that reported in literature.

Acknowledgement:-

The financial support from the department of Science and technology (DST), New Delhi is thankfully acknowledged (project no. DST PROJECT-SB/S2/LOP-032/2013) The authors are significantly grateful towards School of Physical Sciences, SRTM for providing the facility of TDR. The authors are also thankful towards respected Dr. M. D. Shirsat Dept of Physics Dr. BAMU Aurangabad M.S. to sanction for FTIR purpose

Reference:

- [1]. S A Ingole, A R Deshmukh, R V Shinde, A C Kumbharkhane. Dielectric relaxation study of aqueous tetraethylene glycol using time domain reflectometry technique in the frequency range 10MHz-50GHz. *J. Mol. Liq.* 272(2018) 450-455.
- [2]. Y S Joshi, P G Hudage, A C Kumbharkhane. Dielectric relaxation study of aqueous 2-ethoxyethanol using time domain reflectometry technique. *Ind. J. Phy.* Vol. 85 (2011) 1603-1614
- [3]. T. Vishwam, K Parvateesam, S. Babu, S.S. Sastry, V. R. K. Murthy *Ind. J. P. App. Phy* Study of excess dielectric and thermodynamic parameters of hydrogen bonded system :isobutanol and ethyl benzoate. Vol. 54 (2016) 597-611.
- [4]. T. V. Krishna, S. S Sastry, S. T. Ha, V R K Murthy Dielectric, Thermodynamic, and computational studies of hydrogen bonded binary mixtures of N-methylaniline with propan-1-ol and isopropyl alcohol *J. Che* (2013) 1-10.
- [5]. G. Ravi, P.B. Undre, K. Ramachandran, K. Samuvel. Dielectric relaxation study of amides with alcohol mixtures by time domain reflectometry. *Sou. Afri. J. Che. Engg.* 24 (2017) 71-81
- [6]. S. Begum, A. Vardhan, A. Chaudhary, R. Subramanian Disruption of self-molecular association of Pentanol in binary mixtures with Alkylbenzoates: A dielectric relaxation spectroscopy study *J. Ryl. Soc. Che* (2016) 1260-1267.
- [7]. K. Dharmalingam, K. Ramchandran, P. Sivgurunathan, P. B. Undre, P. W. Khirade, S. C. Mehrotra Dielectric relaxation of binary mixtures of alcohols with ethyl methacrylate. *Tkg. J. Sci. Eng.* 2009;12:123-128.
- [8]. Abdul Jaleel A. H, A. R. Khan, F. B. Quadri, U. H. Shaikh. Dielectric properties of medicinal compound using microwave. *Int. J. Uni. Prt.* 2018;4:138-143.
- [9]. Abdul Jaleel A.H, A. R Khan, Shaikh Ifrah Fatima, Shaikh Y. H, Dielectric spectroscopy of lactose in DMSO at broad frequency range from 10MHz to 50GHz. *Conf. on Recent Advances in Sciences, OUR HERITAGE Vol-68 Issue-38 February 2020* 315-323.
- [10]. S. A. Ingole, A. C. Kumbharkhane. Temperature dependent Broadband dielectric relaxation study of aqueous polyvinyl pyrrolidone (PVP K-15, K-30 & K-90) using a TDR *Int. Phy. Che. Liq.* (2020).
- [11]. V. L. Jadhavpatil, P. B. Undre, S. N. Helambe. Dielectric relaxation study of mixtures of methanol and dimethylaminoethanol using time domain reflectometry *Int. J. Pha. Bio. Sci.* (2013) 761-769.

- [12].A. R. Deshmukh, S. A. Ingole, R V Shinde, M .P. Lokhande, A C Kumbharkhane. Dielectric relaxation properties of aqueous dimethylamine, trimethylamine and ethylamine using time domain reflectometry technique Ind.J. P.App.Phy.Vol. 57. (2019) 406-410.
- [13].S. Tabassum, V. P .Pawar,G. N. Shinde, Study of structural properties of polar liquids in binary mixture using microwave technique Int.J.Inno.Reas.Sci.Eng.Tech.Vol.6(2017) 19017-19022
- [14].Asep Bayu Dani Nandiyanto,Rosi Oktiani,Risti Ragadhita How to read and interpret FTIR spectroscopy of organic material.Indo.J. Sci. Tech.(2019) 97-118.
- [15].Catherine Berthomieu,Rainer Hienerwadel Photosynth Fourier transform infrared (FTIR) spectroscopyRes (2009) 157-170.
- [16].P.Sivgurunathan, K.Dharmalingam,K.Ramchandran. FTIR study of hydrogen bonding between acrylic esters and alcohols. J.Sol.Che. 35 (2006) 1467- 1475.
- [17].V M Khandelwal,P B Undre,F A Saif,A S Alameen,S A Yaseen, S S Patil,P Khirade Investigation of intermolecular interactions between formamide-dimethyl amino ethanol binary mixtures through dielectric relaxation and FTIR study.Pro.Int.Conf.Phy.Mat.Nano. 2244 (2019) 050011-1-050011-4.
- [18].S. G. Neware, A. W. Pathan, A. C. Kumbharkhane, A. R. Deshmukh, Abdul Jaleel A. H. Ansari, Y. H. Shaikh Dielectric relaxation study of 1-pentanol-ethanol binary mixtures at 10 MHz-50GHz frequency range using TDR technique Int.J.Phy.Che.Liq. (2021) 1-6.
- [19].A. W. Pathan, A. C. Kumbharkhane. Temperature dependent dielectric relaxation study of 2-butanol – water mixtures from 10MHz-30 GHz. Ind.J.P.App.Phy.Vol.57 (2019) 447-452.
- [20].V. V. Navarkhele dielectric relaxation study of binary mixtures at different temperatures Int.J.Phay.Phal.Sci.Vol.8,(2016).
- [21].B. G. Lone, Ph. d thesis Dr. Babasaheb Ambedkar Marathwada University Aurangabad, MS, India (2006).
- [22].S. D. Deshmukh, P. B. Undre, K. L. Pattebahadur, A. G. Mohod, S. S. Patil, P. W. Khirade Investigation of intermolecular interactions between amide-amine binary mixtures through dielectric relaxation study J.Ferr Vol. 519, (2017) , 23-32.
- [23].R. V. Shinde, A. R. Deshmukh, S. A .Ingole, A. C. Kumbharkhane. Dielectric spectroscopy and hydrogen bonding studies of 1-chloropropane–ethanol mixture using TDR techniqueJ.Adv.Die.Vol.9 (2019) .
- [24].B. G. Lone, P. W. Khirade, S. C. Mehrotra.Molecular interaction of 1-pentanol in ethanol, Bio. Fro. Vol.8(3) (2015).
- [25].D. A. G. Brugmann, Ann. Phy. (Leipzig) 416(7) , (1935) 636.

- [26].S. M. Puranik, A. C. Kumbharkhane, S. C. Mehrotra ,The static permittivity of binary mixtures using an improved bruggeman model *J.Mol.Liq.*Vol.59 (1994) 173-177.
- [27].P. Jeevanandham, S. Kumar,P. Periyasamy, A. C. Kumbharkhane Dielectric relaxation studies of 2-Butoxyethanol with aniline and substituted anilines using time domain reflectometry *Adv. Phy .Che.* (2014) 1-9.
- [28].V. V. Navarkhele Dielectric and excess properties of glycols with formamide binary mixtures at different temperatures.*Rus.J.Phy.Che.A* Vol.92 (2018) 1417–1422.
- [29].Irina Doroshenko, Valeriy Pogorelov, Valdas Sablinskas, Infrared absorption spectra of monohydric alcohols *Dat.Pap. Che* (2013)1-6.
- [30].S. Karlapudi, C. Prasad,L. O. Olasunkanmi, S. Singh,I. Bahadur,,K.S.Kumar,
- [31].E E. Ebenso. Hydrogen bonding interactions of m-Chlorotoluene with 1-alkanol analyzed by thermodynamic, fourier transform infrared spectroscopy,density functional theory, and natural bond orbital*Ame.Che.Soc.* (2018),4679-4687.
- [32].Ahmed M. Khalique , Ali Sheikh , Wojcik Ewa. The C-O Stretching Infrared Band as a Probe of Hydrogen Bonding in Ethanol–Water and Methanol-Water Mixtures *Int.J.Rap.comm.*Vol.45,(2012),420-423.
- [33].S. D. Deshmukh, K. L. Pattebahadur, A. G. Mohod, P. B. Undre, S. S. Patil, P. W. Khirade. Dielectric and spectroscopic study of binary mixture of acrylonitrile with chlorobenzene *2nd Int Conf Cond. Matt. App. Phy.* (2017) 050039-1-050039-4.
- [34].P. Bhanuprakash, N.V.V. Jyothi, C. Narasimharao, M. Raveendra,K. Sivakumar Elucidation of molecular interactions in the mixtures of benzylalcohol with (C2–C4) alkylacetates through volumetric,ultrasonic, theoretical and ATR-FTIR spectroscopic studies atT=(298.15, 303.15, 308.15 and 313.15) K *J.Mol.Liq.*(2017)



Incorporation of Zeolites Na-A and Na-X from Condensed and Calcite Coal Fly Ash

Dr. Kapure G.P.

Department of Physics, S.G.B. College, Purna (Jn) –431 511.

Email:gpk_2010@rediffmail.com

ABSTRACT

The major components of CFA are silicon dioxide (SiO_2) and Aluminium trioxide (Al_2O_3), which are the essential reagents in the synthesis of zeolites. Synthetic zeolites obtained by reprocessing of CFA have huge potential as a cost-effective, environmentally-friendly solution that can improve the efficiency of these materials as efficient heterogeneous catalysts, mainly as solid acids, as adsorbents, as molecular sieves in gas separation and purification and in purification of contaminated waste water. The low price and the additional ecological benefit of the production of zeolites from wastes increased their popularity and inspired growing interest among zeolite.

This paper presents zeolite synthesis from Coal fly ash (CFA). The Coal fly ash was activated by using NaOH solution prior to fusing process with a weight ratio of 1:2,1:3 and mixing with distilled water at a weight ratio of 1:5. Thereafter, the addition of alumina with a concentration of 0.75 %, 1.82 %, 2.19 %, and 3.2 % was performed. The effects of heating and ultrasound radiation on the characteristic of zeolite products were investigated. SEM images demonstrated that the presence of ultrasound wave resulted in crystals structure morphology as also supported by XRD characterization.

Keywords : CFA, Ultrasonic treatment, IR,SEM, XRD, Na-A and Na-X Zelites

I. INTRODUCTION

Coal fly ash (CFA) is the major residue from coal and biomass combustion and is mainly composed of fine-grained particles of SiO_2 and Al_2O_3 . In 2015, more than 1 billion tons of CFA was produced worldwide¹. The amount of CFA produced grows continuously, making the disposal and handling of CFA an important issue that strongly impacts various aspects of our daily life, especially the environment. Therefore, it is important to develop techniques for the utilization of CFA and several have been proposed in this category. CFA has been used for soil remediation^{2,3} embankments or building as adsorbent for waste and contaminant handling, gas separation and capture and mineral recovery as catalyst or catalyst support etc. Furthermore, it is of more

economic significance to develop eco-friendly techniques that convert CFA to value-added products. CFA utilization as raw material for production of cement and glass has also been reported.

Most of zeolites are periodic framework compounds of aluminium silicates formed by interconnected SiO_4 and AlO_4 tetrahedrons. CFA is mainly composed of particles of SiO_2 and Al_2O_3 at micrometer dimension with a weight percentage up to 85 and can principally be used as the precursor of Si and Al for zeolite synthesis. However, SiO_2 and Al_2O_3 are in the form of their most stable minerals in CFA, such as mullite and quartz. They must be chemically converted to reactive precursors by reactions with concentrated NaOH solution or calcination with solid NaOH or KOH at high temperature and the process is not energy efficient^{4,5}. Following the first synthesis of zeolite with CFA by Holler & Wrisching, the reported procedures for zeolite synthesis are all through hydrothermal crystallization using raw or NaOH or KOH calcinated CFA. Alternative energy sources, such as ultrasonic and microwave radiation, are proposed for the hydrothermal synthesis to lower the cost for zeolite synthesis with CFA^{6,7,8}, though they are less meaningful for industrial mass production. Apart from these, it would be more interesting to replace the expensive NaOH and KOH used for the calcination and activation with low-cost alkalis, such as Na_2CO_3 . However, due to the low alkalinity of Na_2CO_3 and the sluggish reactions at interface, higher calcination temperature will be required unless the process is intensified with other procedures⁹⁻¹². As the size of Al_2O_3 and SiO_2 particles is of micrometer dimension, their reactions will, in principle, be greatly promoted by close contacts with Na_2CO_3 or NaOH. In this work, we used tablet compression to intensify the calcination of CFA with Na_2CO_3 . We also showed phase-pure Na-A can be synthesized with calcinated CFA in low alkalinity solution under low temperature, while phase-pure Na-X can be synthesized in the same way but with the introduction of silica sol^{13,14}. The effects of varying $\text{Na}_2\text{CO}_3/\text{CFA}$ ratio and reaction temperature were also investigated and the optimum conditions for the synthesis of Na-A and Na-X were determined

2. Experimental

2.1. Material and methods

CFA was obtained from Hydrothermal Power Station Chandrapur Maharashtra. Chemical composition of the CFA sample was analysed with X-ray fluorescence (XRF) and the results are summarized in table 1. The X-ray diffraction (XRD) was used to determine the crystalline phase in CFA and the morphology was determined with a scanning electron microscope (SEM). As shown in figure 1, CFA sample is mainly composed of microspheres of quartz and mullite. The measured Si/Al molar ratio of 1.67 in the sample is suitable for the synthesis of Na-A zeolite. As the synthesis of Na-X zeolite requires higher Si/Al molar ratio, silica sol was introduced as additional Si source and sodium hydroxide was also added.

2.2. Synthesis of zeolite Na-A and zeolite Na-X

Synthesis of Na-A zeolite was done by a two-step process. First, a tablet compression machine was used to treat the mechanically mixed CFA and Na_2CO_3 . The resulting mixture was calcinated at 800°C for 3 h and then cooled to room temperature. According to the XRD patterns of the CFA sample before and after calcination (figure 1), the mullite and quartz phases in CFA disappear and are converted into sodium

aluminum silicate (NaAlSiO_4) and sodium silicate (Na_2SiO_3) after calcination at 800°C . It is hard to get phase-pure zeolite Na-A through the hydrothermal process if the mixture of CFA and

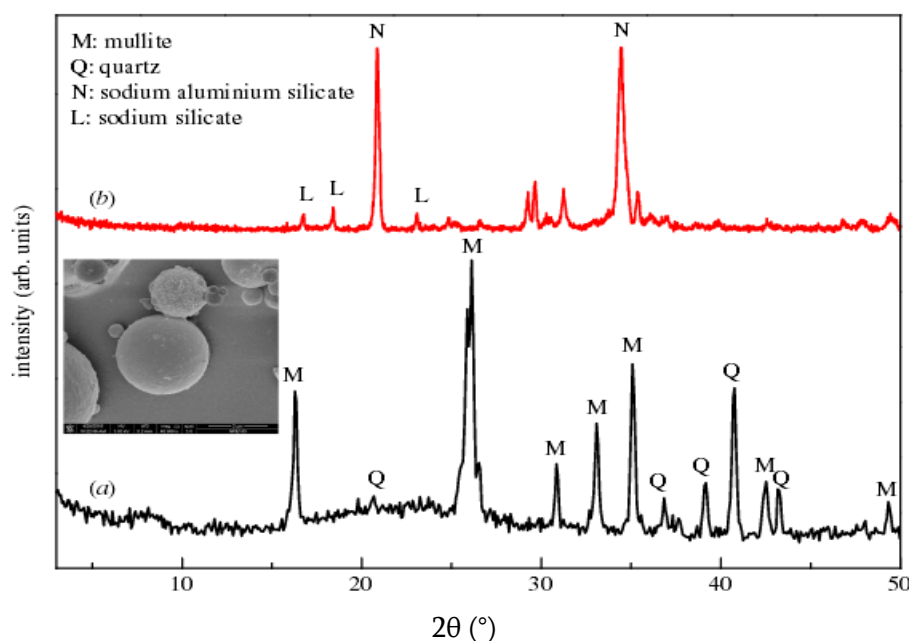


Figure 1. (a) XRD patterns of the raw CFA sample (b). The SEM image of raw CFA

Table 1. The chemical composition of coal fly ash.

component	Al_2O_3	Fe_2O_3	SiO_2	CaO	TiO_2	P_2O_5	SO_3	ZrO_2	SrO	MgO
content(%)	45.48	44.86	2.73	2.69	2.19	0.45	0.35	0.30	0.25	0.22

Na_2CO_3 has not been tablet-compressed. The calcinated mixture was mixed with different quantity of deionizer water at room temperature for 1 h under magnetic stirring, and then further heated to different temperatures and subjected to hydrothermal crystallization for a period of time. After that, the reaction mixtures were annealed to room temperature, filtered, washed with demonized water and then the solid residues were dried at 90°C for 20 h before further measurement and characterization. The addition of silica sol and sodium hydroxide to the mixture before stirring is needed to get phase-pure zeolite Na-X.

3. Hydrothermal synthesis of zeolite Na-A from coal fly ash

The impacts of Na_2CO_3 /CFA mass ratio and crystallization temperature on the crystallinity of the resulting zeolite synthesized from calcinated CFA powder were investigated. Controlled experiments were carried out, with Na_2CO_3 /CFA mass ratio of 0.5, 0.7, 0.9, 1.2, 1.5, calcinated at 800°C for 2 h and hydrothermally treated

at 100°C for 6 h, to investigate the influence of alkalinity on the formation of zeolite. Figure 2 shows the XRD patterns of products obtained at different Na₂CO₃/CFA mass ratios. According to the XRD pattern of calcinated Na₂CO₃/CFA mixture (figure 1), the product is mainly unconverted NaAlSiO₄ formed during calcination with the lowest Na₂CO₃/CFA mass ratio of 0.8. The XRD patterns of the samples obtained after crystallization at different temperatures for 8 h are shown in figure-3. The characteristic XRD peaks of Na-A zeolite appear even after crystallization at

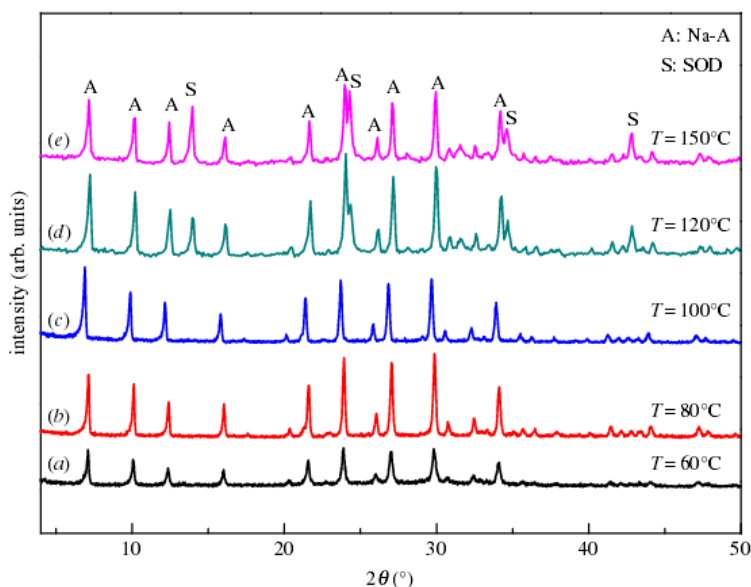


Figure 3. The crystallization temperature on the structure of the products (Na-A)

60°C. However, these peaks are broad and short, showing the low crystalline and purity of the product (figure 3a). The XRD peaks are narrowed and sharp from 60°C to 100°C (figure 3a–c), showing that in this temperature range, rising temperature would promote the crystallization of Na-A and there is a positive correlation between the crystalline of the zeolite product and the crystallization temperature. According to the XRD pattern, phase-pure Na-A can be obtained from 60°C to 100°C. As zeolite Na-A is thermodynamically less stable than sodalite (SOD) in the current reaction mixture, we noted the SOD phase from 120°C to 150°C (figure 3c–e). This is because higher temperature will promote the conversion of metastable zeolite into a more thermodynamically stable phase [30]. Thus, to obtain pure-phase Na-A zeolite from CFA and to lower the energy consumption for the synthesis, the crystallization temperature should be controlled in the range 80–100°C.

3.1. Hydrothermal synthesis of zeolite Na-X from coal fly ash

As aforementioned, the Si/Al ratio in the CFA sample used eventually satisfied the requirement for the synthesis of Na-A zeolite. It would be more interesting if other zeolites of industrial significance can be synthesized by altering the Si/Al ratio. We then investigated the potential synthesis of Na-X from the same CFA sample by changing the composition of calcinated Na₂CO₃/CFA mixture with silica sol and using NaOH to keep the Na/Si ratio to satisfy the requirements for Na-X crystallization. In the controlled experiments,

silica sol and NaOH were added to the calcinated $\text{Na}_2\text{CO}_3/\text{CFA}$ mixture to keep the $\text{Na}_2\text{O}/\text{SiO}_2$ and $\text{H}_2\text{O}/\text{Na}_2\text{O}$ constant as 2.2 and 40, respectively.

The characteristic XRD peaks of zeolite Na-A disappear and new peaks associated with zeolite Na-X appear when the $\text{SiO}_2/\text{Al}_2\text{O}_3$ molar ratio reaches 3 (figure 4b). With the increase of $\text{SiO}_2/\text{Al}_2\text{O}_3$ molar ratio, the peaks of Na-X get intensified and sharpened and those of Na-A disappear completely (figure 4c–e). This is in excellent agreement with previous reports [30]. These findings prove that the $\text{SiO}_2/\text{Al}_2\text{O}_3$ molar ratio is a key parameter to obtain phase-pure zeolite Na-X.

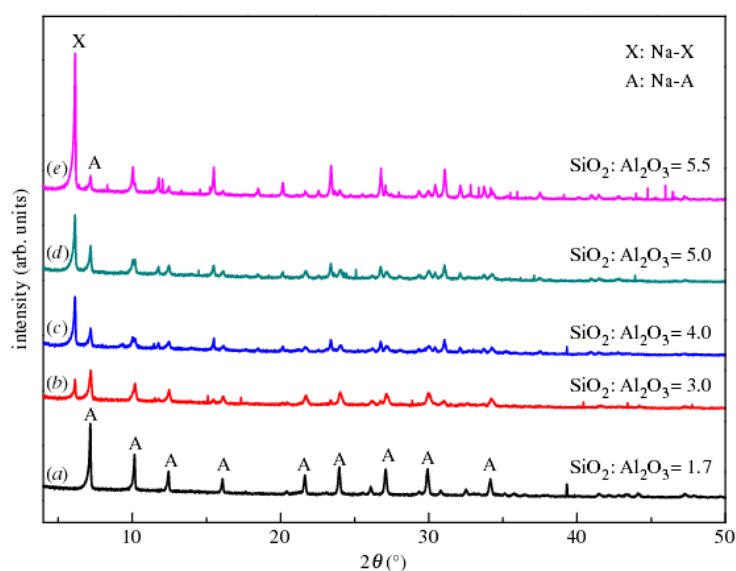


Figure 4. The impact of $\text{SiO}_2/\text{Al}_2\text{O}_3$ molar ratio on the structure of the hydrothermal reaction products at 100°C for 8 h

In controlled experiments, the $\text{Na}_2\text{O}/\text{SiO}_2$ and $\text{H}_2\text{O}/\text{Na}_2\text{O}$ were kept constant as 2.2 and 40, respectively. The crystallization temperature was 100°C and the duration for crystallization was 8 h. The XRD patterns of the products after hydrothermal crystallization are shown in figure 5. When only tablet-compressed calcinated CFA was used as reactant (fig 5a), there are only quartz and mullite in the product, showing that Na_2CO_3 is required to convert quartz and mullite into precursors for zeolites. When the $\text{Na}_2\text{CO}_3/\text{CFA}$ ratio is increased to 1, phase-pure Na-X zeolite was obtained, as indicated by the sharp characteristic XRD peaks of Na-X in figure 5b. When the $\text{Na}_2\text{CO}_3/\text{CFA}$ ratio is increased further, the characteristic peaks of Na-A appear on the XRD patterns of the products (figure 5c,d). This shows that a mixture of Na-A and Na-X will be obtained at $\text{Na}_2\text{CO}_3/\text{CFA}$ ratio larger than 1. According to the chemical composition of the CFA (table 1) and the mentioned experiments, we concluded that phase-pure zeolite Na-A can be synthesized with CFA at reactant molar ratio, hydrothermal reaction temperature and reaction time of $1.3\text{Na}_2\text{O}: 0.6\text{Al}_2\text{O}_3: 1\text{SiO}_2: 38\text{H}_2\text{O}$ at 80°C for 6 h, respectively, while phase-pure zeolite Na-X can be synthesized at $2.2\text{Na}_2\text{O}: 0.2\text{Al}_2\text{O}_3: 1\text{SiO}_2: 88\text{H}_2\text{O}$ at 100°C for 8 h, respectively. With these set-ups, the yields of Na-A and Na-X are approximately 68% and approximately 62%, respectively. The relatively low yield of Na-X is due to the introduction of silica sol to get phase-pure Na-X.

3.2. Characterization of zeolite Na-A and Na-X

We then characterized the chemical composition of synthesized Na-A and Na-X samples with XRF. The result of XRF on Na-A sample indicates that it contains 44.64% SiO₂, 37.29% Al₂O₃, 18.22% Na₂O, 3.80% CaO, 3.36% Fe₂O₃, 3.06% TiO₂, 0.55% MgO and 0.41% K₂O and the corresponding Si/Al molar ratio is

1.48 and is typical for commercial Na-A, while that for the Na-X sample is 5.12. The high Si/Al molar ratio of Na-X is due to the introduction of silica sol to get phase-pure Na-X. FT-IR spectroscopy was used to confirm the structure of synthesized Na-A and Na-X samples.

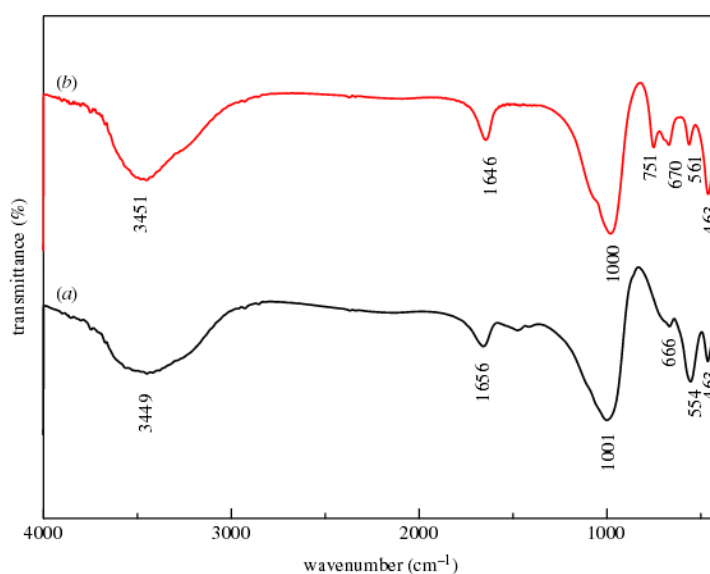


Figure 6. FT-IR spectra of Na-A (a) and Na-X (b) zeolites synthesized from calcinated CFA.

The band at 463 cm⁻¹ was ascribed to the internal vibration of T-O bending. Moreover, the bands observed at 1656 and 3449 cm⁻¹ correspond to the presence of H₂O and hydroxyls, respectively. The observed FT-IR bands of Na-A samples are in good agreement with those reported in previous works, which further proves the successful synthesis of Na-A from CFA [30,31]. We also examined the FT-IR spectrum of the synthesized zeolite Na-X sample. As shown in figure 6b, Na-X zeolite has FT-IR bands at wave numbers of 459, 561, 669, 747, 982, 1646 and 3451 cm⁻¹. A broad band at 3451 cm⁻¹ and the sharp peak at 1646 cm⁻¹ can be assigned to the structural hydroxyl groups and bending mode of physically adsorbed water, respectively. The peak at 561 cm⁻¹ can be attributed to the vibration of distorted double five-member ring in the high silica framework.

4. Conclusion

We showed that tablet compression can enhance the contact with Na₂CO₃ for the activation of CFA through calcination for the synthesis of zeolites Na-A and Na-X under mild conditions. We optimized the control variables for zeolite synthesis and showed that phase-pure zeolite Na-A can be synthesized with CTA at

reactant molar ratio, hydrothermal reaction temperature and reaction time of $1.3\text{Na}_2\text{O}: 0.6\text{Al}_2\text{O}_3: 1\text{SiO}_2: 38\text{H}_2\text{O}$ at 80°C for 6 h, respectively, while phase-pure zeolite Na-X can be synthesized at $2.2\text{Na}_2\text{O}: 0.2\text{Al}_2\text{O}_3: 1\text{SiO}_2: 88\text{H}_2\text{O}$ at 100°C for 8 h, respectively.

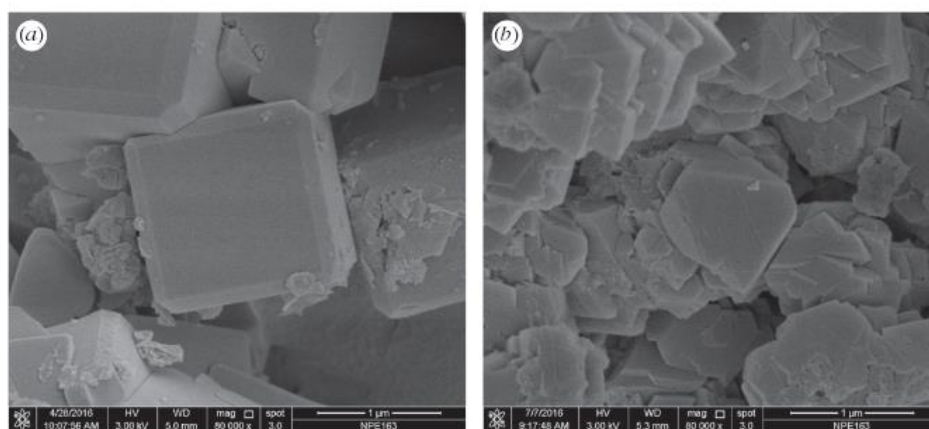


Figure 8. SEM images of synthesized Na-A (a) and Na-X(b) zeolites obtained from calcinated CFA.

Further SEM, BET, FT-IR characterization confirmed that the Na-A and Na-X synthesized under optimized conditions would exhibit properties the same as phase-pure Na-A and Na-X. In this sense, the zeolites synthesized can principally be used as adsorbents for gas separation, wastewater treatment and soil remediation, as heterogeneous Lewis/Bronsted acid catalysts for the conversion of chemicals, as support materials for stabilization and dispersion of catalytic reaction centers, as cation-exchange materials for resource recovery and in other industrial applications where Na-A and Na-X play a role. Furthermore, the developed protocols for the synthesis of Na-A and Na-X from CFA are simple and cost- and energy effective, so they can be adapted for mass production of zeolites in chemical plants. Related works are now being carried out in our laboratory.

References

1. Yao ZT, Ji XS, Sarker PK, Tang JH, Ge LQ, Xia MS, XiYQ. 2015 A comprehensive review on the applications of coal fly ash. *Earth Sci. Rev.* 141, 105121. (doi:10.1016/j.earscirev.2014.11.016)
2. Izquierdo M, Querol X. 2012 Leaching behaviour of elements from coal combustion fly ash: an overview. *Int. J. Coal Geol.* 94, 54–66. (doi:10.1016/j.coal.2011.10.006)
3. Jankowski J, Ward CR, French D, Groves S. 2006 Mobility of trace elements from selected Australian fly ashes and its potential impact on aquatic ecosystems. *Fuel* 85, 243–256. (doi:10.1016/j.fuel.2005.05.028)
4. Pandey VC, Singh N. 2010 Impact of fly ash incorporation in soil systems. *Agric. Eco syst. Environ.* 136, 16–27. (doi:10.1016/j.agee.2009.11.013)

5. Bukhari SS, Behin J, Kazemian H, Rohani S. 2015 Conversion of coal fly ash to zeolite utilizing microwave and ultrasound energies: a review. *Fuel* 140, 250–266. (doi:10.1016/j.fuel.2014.09.077)
6. Dermatas D, Meng XG. 2003 Utilization of fly ash for stabilization/solidification of heavy metal contaminated soils. *Eng. Geol.* 70, 377–394. (doi:10.1016/s0013-7952(03)00105-4)
7. Iyer RS, Scott JA. 2001 Power station fly ash—a review of value-added utilization outside of the construction industry. *Resour. Conserv. Recycl.* 31, 217–228. (doi:10.1016/s0921-3449(00)00084-7)
8. Vassilev SV, Baxter D, Andersen LK, Vassileva CG. 2013 An overview of the composition and application of biomass ash. Part 1. Phase-mineral land chemical composition and classification. *Fuel* 105, 40–76. (doi:10.1016/j.fuel.2012.09.041)
9. Wang SB. 2008 Application of solid ash based catalysts in heterogeneous catalysis. *Environ. Sci. Technol.* 42, 7055–7063. (doi:10.1021/es801312m)
10. Ram LC, Mastro RE. 2014 Fly ash for soil amelioration :a review on the influence of ash blending with inorganic and organic amendments. *Earth Sci. Rev.* 128, 52–74. (doi:10.1016/j.earscirev.2013.10.003)
11. Ukwattage NL, Ranjith PG, Bouazza M. 2013 The use of coal combustion fly ash as a soil amendment in agricultural lands (with comments on its potential to improve food security and sequester carbon). *Fuel* 109, 400–408. (doi:10.1016/j.fuel.2013.02.016)
12. Usmani Z, Kumar V, Mritunjay SK. 2017 Vermicomposting of coal fly ash using epigeic and epi-endogeic earthworm species: nutrient dynamics and metal remediation. *RSC Adv.* 7, 4876–4890. (doi:10.1039/c6ra27329g)
13. Zhang YW, Huang T, Huang X, Faheem M, Yu L, Jiao BQ, Yin GZ, Shiao Y, Li DW. 2017 Study on electrokinetic remediation of heavy metals in municipal solid waste incineration fly ash with a three-dimensional electrode. *RSC Adv.* 7, 27 846–27 852. (doi:10.1039/c7ra01327b)
14. Joseph B, Mathew G. 2012 Influence of aggregate content on the behavior of fly ash based geo polymer concrete. *Sci. Iran.* 19, 1188–1194. (doi:10.1016/j.scient.2012.07.006)

Synthesis, Characterization and Biological Activity of Novel Thiazole Derivatives : A Mini Review

Vishnu A. Gore¹, Sunil U. Tekale¹ and Rajendra P. Pawar^{1*}

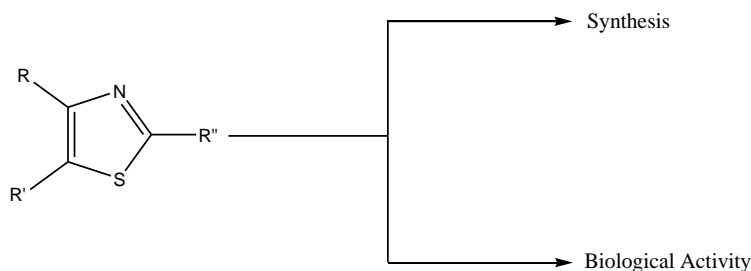
¹Department of Chemistry, Deogiri College, Aurangabad-431005, MS, India.

²Department of Chemistry, Shivchhatrapati College, Aurangabad-431005, MS, India.

*Corresponding email: rppawar@yahoo.com

ABSTRACT

Thiazoles constitute an important heterocyclic compound possessing numerous biological activities, such as antibacterial, antifungal, anti-inflammatory, antitumor, anti-tubercular, antidiabetic, antiviral, and antioxidant potential. Substituents on the specific site of thiazole ring affect the biological activities; consequently, investigators have synthesized compounds having thiazole ring with flexible substituents as target structures, and appraised their biological activities. The present review discusses synthesis and biological importance of newly developed thiazole derivatives.



Keywords : Biological activity synthesis thiazole

I. INTRODUCTION

Antimicrobial activity of thiazole derivatives has been comprehensively studied by numerous researchers.^[1-2]

Thiazole containing heterocyclic compounds possess a diverse range of biological activities including anti-inflammatory activity.^[3-4] The thiazole nucleus is a part of the vitamin B (thiamine). Thiazoles are used to obtain free carbene particles and complexed with transition metals, while their salts are used as catalysts in the reaction of Stetter and benzoin condensation.^[5,6] Thiazoles occupy potent biological applications, described by Hantzsch and Weber for the first time in 1887.^[7] It showed similar chemical and physical properties to pyridine and pyrimidine, although some of their derivatives behave similarly to the thiophene and furan. The molecular electrostatic potential points out that nitrogen is the most negative atom as compared to carbon and sulfur, which are neutral.^[8] Thiazole and related

heterocycles are one of the supreme significant potential things in the mainly increasing chemical world of compounds having thiazoles showing notable pharmacological actions. Current review highlights the preparation and biological activities of materials having thiazole moiety.^[9]

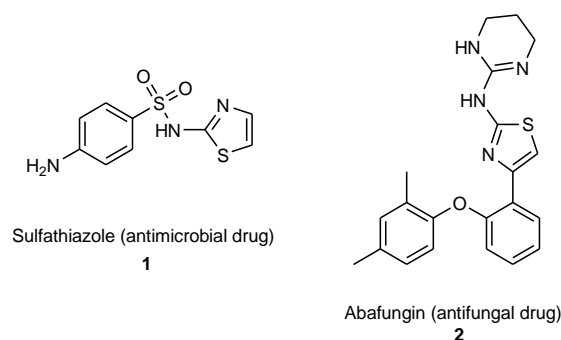
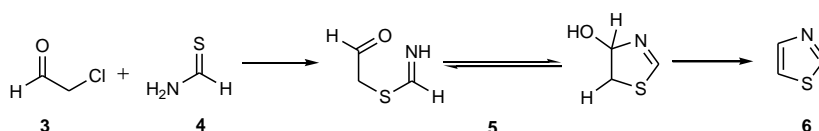


Figure 1: Several bioactive thiazoles 1-2

Cancer is one of the major causes of death worldwide. Several materials have been prepared for cancer therapy. Thiazoles are an adaptable heterocycle present in several drugs in the treatment of cancer.^[10]

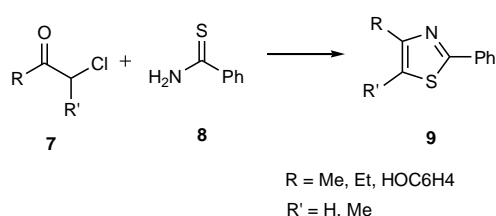
Synthesis of thiazoles:

Thiazole (6) itself can be obtained by condensing α -chloroacetaldehyde (3) and thioformamide (4) in excellent yield (Scheme 1).^[11, 12]



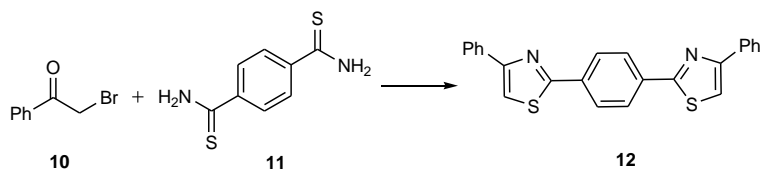
Scheme 1: Condensation of α - chloroacetaldehyde 3 with thioformamide 4.

The reaction of a thioamide 8 with α -halocarbonyl 7 compounds has been used extensively, and several thiazoles 9 with alkyl, aryl, arylalkyl or heteroaryl functional groups at 2-, 4- or 5-positions have been reported (Scheme 2).^[11, 12]



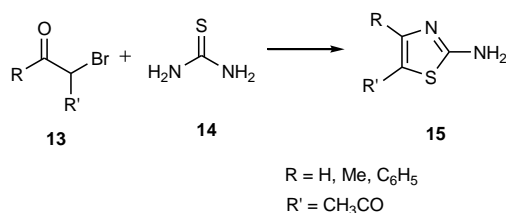
Scheme 2: Reaction of a thioamide **8** with α -halo carbonyl compounds **7**.

The cyclization of 2-bromo-1-phenylethan-1-one **10** with benzene-1,4-bis(carbothioamide) **11** gives rise to 1,4-bis(4-phenylthiazol-2-yl)benzene **12** in excellent yield (**Scheme 3**).^[13]



Scheme 3: Synthesis of bithiazole **12**.

The most efficient method for the synthesis of thiazoles involves the condensation of equimolar parts of thiourea **14** and α -haloketones or α -haloaldehydes **13** to yield the corresponding 2-aminothiazoles **15** with no by-products (**Scheme 4**).^[14]



Scheme 4: Synthesis of 2-aminothiazole **15**.

Biological activities

Many organic compounds with biological activity contain thiazole fragments as a part of their structure. Thiazoles are found in numerous natural products such as the secondary metabolites in marine organisms. The biological activities of these compounds have been evaluated and studied as leading structures to manufacture new drugs. Thiazoles are of great importance in pharmacology for their presence in most therapeutic agents. The biological activity of compounds containing thiazole is very popular in terms of antineoplastic 16, antibiotic 17, anti-inflammatory agents 18, antiulcer 19, antimicrobial 20, antifungal drugs 21 and many more.^[15,16,17]

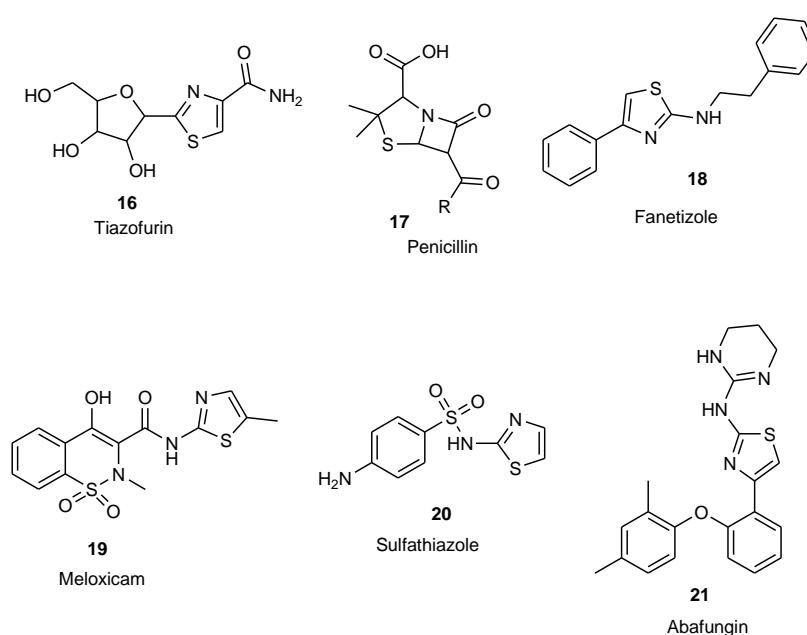
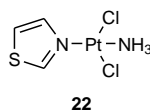


Figure 2: Several bioactive thiazoles 16-21

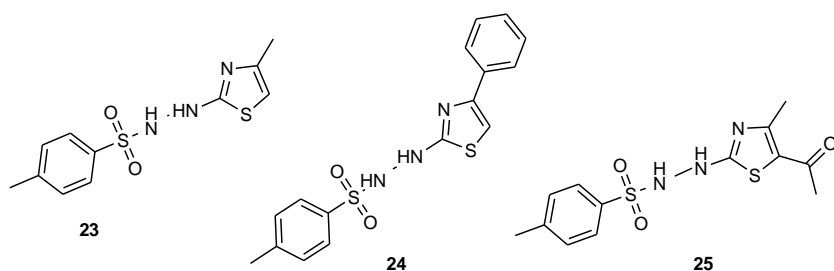
Most biologically active thiazole-containing compounds have substitutions at positions 2 and 4 or one of them. It was found that these substituents give rise to the compounds of different biological properties depending upon nature of substituents present on them.^[17]

1) Antitumor activity

Marini et al. studied the effect of thiazoles implication on inactive compounds such as transplatin²².^[18]

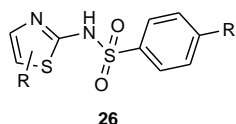


Zaharia et al. synthesized several bis-thiazoles derivatives and studied their biological activity against the most common types of cancers, prostate and liver cancer (hepatocellular carcinoma). It was found that compounds 23-25 exhibited remarkable activity against previously mentioned types of cancers.^[19]



2) Antibacterial activity

Compound **26**, which contain a benzenesulfonamide fragment, was prepared for biological purposes and tested against Gram-positive/negative bacteria. This compound was found to have potent properties against Gram-positive bacteria such as *Staphylococci*, *Streptococci*, and *Bacillus*. The hybrid compounds of two molecules known for their biological activity.^[17]



CONCLUSION

In conclusion, the present review indicates the synthetic and biodynamic potential of thiazoles as attractive entities in medicinal chemistry. The widespread biological activities of these heterocyclics have intrigued them in terms of antimicrobial, anticancer, antitubercular etc. activities.

REFERENCES

- [1] C.A. Gandolfi, G. Long, G. De Cillis, L. Gallico, WO 9311134, 1993.
- [2] H. Tripathy, D.G. Pradhan, Agric. Biol. Chem. 37 (1973) 1375.
- [3] P.K. Sharma, S.N. Sownhney, A. Gupta, G.B. Singh, S. Bani, Indian J.Chem., Sect. B 37 (1998) 371.
- [4] B.S. Holla, K.V. Malini, B.S. Rao, B.K. Sarojini, Eur. J. Med. Chem. 38 (2003) 313

- [5] Sayed, A. R.; Wiggins, J. S. *Polymer* 2008, *49*, 2253–2259. DOI: 10.1016/j.polymer.2008.02.038. Siddiqui, N. S.; Arya, K.; Ahsanb, W.; Azad, B. *IJDDR* 2011, *3*, 55–67.
- [6] Hantzsch, A.; Weber, J. *Ber. Dtsch. Chem. Ges.* 1887, *20*, 3118–3132. DOI: 10.1002/cber.188702002200. Moradi, A.; Peyghan, A.; Hashemian, S.; Baei, M. *Bull. Korean Chem. Soc.* 2012, *33*, 3285–3292. DOI: 10.5012/bkcs.2012.33.10.3285. Nosrat, O. M.; Fateme, G. P. *Phosphorus Sulf. Silicon.* 2016, *191*, 811–843. Xie, X.-X.; Li, H.; Wang, J.; Mao, S.; Xin, M.-H.; Lu, S.-M.; Mei, Q.-B.; Zhang, S.-Q. *Bioorg. Med. Chem.* 2015, *23*, 6477–6485. DOI: 10.1016/j.bmc.2015.08.013.
- [7] Omar, A. M.; Bajorath, J.; Ihmaid, S.; Mohamed, H. M.; El-Agrody, A. M.; Mora, A.; El-Araby, M. E.; Ahmed, H. E. A. *Bioorg. Chem.* 2020, *101*, 103992 DOI: 10.1016/j.bioorg.2020.103992. Zou, X.-Z.; Feng, A.-S.; Liao, Y.-Z.; Xu, X.-Y.; Wen, H.-Y.; You, A.; Mei, M.; Li, Y. *Inorg. Chem. Commu.* 2020, *118*, 108030. DOI: 10.1016/j.inoche.2020.108030. Safaa, I. E.; Mansour, E.; Nassar, I. F.; Mekawey, A. A. I. *Russ. J. Bioorg. Chem.* 2020, *46*, 382–392. DOI: 10.1134/S1068162020030061.
- [8] Mohareb, R. M.; Wardakhan, W. W.; Abbas, N. S. *Anticancer. Agents Med. Chem.* 2019, *19*, 1737–1753. DOI: 10.2174/1871520619666190402153429.
- [9] Willstatter, R.; Wirth, T. *Berichte* 1909, *42*, 1908–1922. Process for the production of thiazoles, OtteHrematka, Darmstadt, Germany, assignor to Merk & Co, Inc., Rahway, N. J., Corporation of new Jersey, Application September 23, 1937, serial No. 165413. In September 26, 1936, U.S. Patent No. 2160867; *Chem. Abstr.* **1939**, *33*, 7320
- [10] Mulvaney, J. E.; Marvel, C. S. *J. Org. Chem.* 1961, *26*, 95-97.
- [11] Bonzom, A.; Metzger, J. *Bull. Soc. Chim. France* 1963, *11*, 2582. *Chem. Abstr.* 1964, *60*, 5474. Young, T. E.; Amstutz, E. D. *J. Am. Chem. Soc.* 1951, *73*, 4773–4775. DOI: 10.1021/ja01154a088.
- [12] Emanuel, W.; Stamford, conn., assignor to American Cyanamid Company, New York, N.Y. A Corporation of Maine, No Drawing. Application July 2, 1949, Serial No. 102, 926, U.S. Patent No. 1951, 2 547 677; *Chem. Abstr.* **1951**, *45*, 6351.
- [13] Watt, G. W. *J. Org. Chem.* 1939, *4*, 436–441. DOI: 10.1021/jo01216a010.
- [14] Ahangar, N.; Ayati, A.; Alipour, E.; Pashapour, A.; Foroumadi, A.; Emami, S. *Chem. Biol. Drug Des.* 2011, *78*, 844–852. DOI: 10.1111/j.1747-0285.2011.01211.x.
- [15] Siddiqui, N.; Ahsan, W. *Eur. J. Med. Chem.* 2010, *45*, 1536–1543. DOI: 10.1016/j.ejmech.2009.12.062.
- [16] Marchesini, G. *Gazz. Chim. Ital.* 1894, *24*, 65.
- [17] Abdelhamid, A. O.; Sayed, A. R. *Phosph. Sulf. Silicon Rel. Elem.* 2007, *182*, 1767–1777. DOI: 10.1080/10426500701313938.

Structural and Electrical Properties of Nickel Ferrite Nanoparticles: Influence of Mixed Fuel Approach

V.K. Mande¹, A.R. Bansode¹, S.R. Daruwale¹, S.P. Gadekar¹, R.B. Borade²,

¹Department of Physics, Shivchhatrapati College, Aurangabad, (M.S), India

²Department of Electronics Shivchhatrapati College, Aurangabad, (M.S), India

²Department of Physics Ankushrao Tope College Jalna (M.S), India

Corresponding address: drmandevishwanath@gmail.com

ABSTRACT

Nickel ferrite nanoparticles were synthesized by sol-gel auto combustion method using mixed fuel approach (citric acid and ethylene glycol) as a fuel. The metal nitrate to fuel ratio was taken as (1:3). The as synthesized powder of nickel ferrite nanoparticles is annealed at 650 °C for 6 h and prepared sample was used for characterization and investigations of structural and electrical properties. The structural characterization of nickel ferrite nanoparticles were done by X-ray diffraction technique. The average crystallite size obtained by Scherrer's formula is of the order of 18 nm. The lattice constant determined from XRD data is in the reported range 8.3783 Å. The porosity estimated from X-ray density and bulk density shows large value of the order of 48%. The DC electrical resistivity was investigated from room temperature to 850 K using two probe techniques. DC electrical resistivity behaviour of nickel ferrite nanoparticles suggests that the sample is semiconducting in nature.

Keywords: Nickel ferrites, Sol-gel auto-combustion, XRD, Citric acid and ethylene glycol

I. INTRODUCTION

Ferrites are ferrimagnetic oxides of interest to the scientist and technologist as they exhibit several applications viz. high density storage, telecommunications, magnetic fluid, drug delivery, sensors, catalytic. On the basis of crystal structure ferrites are grouped into three classes namely garnet, spinel and hexagonal ferrite. The spinel ferrites are widely studied because of their superior properties such as structural, magnetic, electrical and catalytic properties, all of which are different from those of their bulk counterparts and applications point of view in various and new fields like magnetic drug delivery, catalyst, sensors, biological, biomedical and medical science [1-4]. The spinel ferrite has the general formula of $M-Fe_2O_4$ where M is a divalent metal ion (Mn, Co, Ni, and Zn etc). Among spinel ferrites, nickel ferrite ($NiFe_2O_4$) has an inverse spinel structure and promising magnetic material for high-density recording applications because of their high magneto crystalline anisotropy, high coercivity, moderate saturation magnetization and high chemical and structural stability at higher temperatures, which make it a good candidate for the electronic components used in computers, recording devices, and magnetic cards [5- 9]. The properties of nanoparticles

mostly depend on synthesis method therefore nowadays different synthesis methods are being used for synthesis nanomaterials. Nickel ferrite nanoparticles have been synthesized using various methods, such as co-precipitation method, hydrothermal method, micro emulsion method, sol-gel method, sonochemical reaction method, ball milling, laser ablation and aerosol method [10-14]. Among synthesis methods, sol-gel auto combustion method has been used for synthesis of nickel ferrite nanoparticles. Auto-combustion synthesis process is based upon the thermo-chemical concept used in the field of propellants and explosives, its extrapolation to the combustion synthesis of nano-oxides. A various fuels have been used in the combustion synthesis of ferrite nonmaterial, like glycine, urea, oxalyl-hydrazine, citric acid, and sucrose. All these fuels serve two purposes :(i) they are the source of C and H, the reducing elements, which from CO₂ and H₂O on combustion and liberates heat (ii) they form complexes with the metal ions facilitating homogeneous mixing of the cations in solution. The exothermicity of the redox reaction ranges from 1200 K to 1800 K. The nature of combustion differs from flaming to non-flaming depending upon which fuel used for preparation of nano-material. In the present work new approach has been used to prepare nickel ferrite nanoparticles using mixed fuel (citric acid and ethylene glycol). To date very less work have been reported using mixture of citric acid and ethylene glycol. The present research reports deals with the synthesize nickel ferrite nanoparticles by sol-gel auto combustion method using mixture of citric acid and ethylene glycol as fuel and to investigate the structural and magnetic properties of nickel ferrite nanoparticles. In the literature, structural and magnetic properties of nickel ferrite nanoparticles are reported, but no systematic investigation of their electrical behaviour is reported. The electrical properties of spinel ferrite nanoparticles are important from the point of view of its use in transformer cores, humidity and gas sensor devices.

2. Experimental Detail

The NiFe₂O₄ nanoparticles were synthesized by sol-gel auto-combustion method using citric acid + ethylene glycol as a fuel. The metal nitrates to fuel ratio was taken as 1: (1:3) or (metal nitrate: (citric acid: ethylene glycol). All the reagents used for the synthesis of nickel ferrite nanoparticles were analytical grade and used as received without further purification. The stoichiometric proportion of nickel nitrate Ni(NO₃)₂ 6H₂O, ferric nitrate Fe(NO₃)₃ 9H₂O, citric acid C₆H₈O₇.H₂O and ethylene glycol C₂H₆O₁₂ were separately dissolved in minimum complete dissolution of metal nitrates in distilled water amount of distilled water using magnetic stirrer. After complete dissolution of metal nitrates in distilled water then nickel nitrate and ferric nitrate solution were mixed and stirred sometime with constant heating at 90 °C. After some stirring mixed citric acid + ethylene glycol solution was added to the nitrates solution. The all solution was again stirred for about 6 h at 90° C on a hot plate with continuous stirring until it becomes viscous and finally formed a very viscous gel. The temperature is further raised up to 120°C so that the ignition of the gel suddenly starts. The dried gel was subsequently swelling into foam like and undergoes a strong self-propagating combustion reaction to give a lose nickel ferrite nano-powder. Finally the as prepared lose nickel ferrite powder was grinded for 30 min and annealed at 650 °C temperature for 6 h in muffle furnace to improve the ordering and for further characterization. The crystalline phase of the prepared nickel ferrite sample was identified by X-ray diffraction technique using XPERT-PRO system. X-ray powder diffractions were performed at room temperature using monochromatic Cu-K α radiation with $\lambda=1.54060$ Å operated at

40 kV and 35 mA with 2θ ranging from 20° to 80° at a step size 0.02° per second. DC electrical resistivity was measured by two probe method. A small constant voltage was applied across the sample and the current through the sample was measured with respect to temperature. Temperature of the sample in the form of pellet was measured with chromel- alumel thermocouple.

3. Results and discussion

Structural Properties

Fig. 1 shows the XRD pattern of the annealed nickel ferrite nanoparticles. The diffraction peaks observed at 30.32° , 35.65° , 43.33° , 53.67° , 57.24° , 62.80° corresponding to the (220), (311), (400), (422), (511) and (440) planes, respectively. In this XRD pattern other oxides or impurity phases are not detected therefore XRD patterns confirm the formation of cubic spinel type lattice of NiFe_2O_4 , which matches well with the standard XRD pattern (JCPDS No: 22-1087). The lattice constant (a) of nickel ferrite samples was obtained from the following equation.

$$a = d\sqrt{h^2 + k^2 + l^2} \quad (1)$$

where, (h k l) are the Miller Indices, d is inter planner spacing. Thus, lattice constant was computed using the d value and the (h k l) parameters.

The crystallite size (t) has been calculated from FWHM (full width at half maximum) of most intense peak (311) data using Debye-Scherrer's equation [15].

$$t = \frac{k\lambda}{\beta \cos \theta} \quad (2)$$

where, t is the crystallite size, λ is the wavelength of Cu-K α (1.5405 Å), β is the full width at half maxima of the most intense diffraction peaks and θ is the Bragg's angle. The reflection from (311) plane was used for determination of average crystallite size.

The volume (V) of the unit cell calculated by using the following equation;

$$V = a^3 \quad (3)$$

where, V is the volume of unit cell, 'a' is the lattice constant. The X-ray density (ρ_b) of the sample was calculated using the relation given by Smit and Wijn following formula [16].

$$d_x = \frac{8M}{N_A a^3} \quad (4)$$

Where, M is the molecular weight and N_A is the Avogadro's number and 'a' is the lattice parameter. As there are 8 molecules in the unit cell, so 8 is included in the formula.

The bulk density (ρ_m) of nickel ferrite sample was determined using standard formula.

$$d_B = \frac{M}{\pi r^2 t} \quad (5)$$

Where m is mass of pellets, r is the radius of pellets and t is thickness of pellet. Porosity (P %) of the NiFe_2O_4 sample was calculated from X-ray density and bulk density.

$$P = (1 - \rho_m/\rho_b) \times 100 \% \quad (6)$$

Where, ρ_x is the X-ray density and ρ_m is the bulk density. The structural parameters such as lattice constant, unit cell volume, X-ray density, bulk density, porosity and specific surface area of nickel ferrite nanoparticles are given in Table 1. From table 1, it was understood that the calculated values of lattice constant of nickel ferrite nanoparticles is 8.378 Å which agree with the reported values [17]. The crystallite size of the nickel ferrite nanoparticles is 16 nm. Small crystallite size is due to using mixed. The X-ray density is found to be of the order of 5.301 gm/cm³. The bulk density of nickel ferrite nanoparticles was measured from the standard formula [18].

Table 1. Lattice constant, volume of unit cell, X-ray density, bulk density, porosity and crystallite size from XRD data.

Structural Parameters	Values
Lattice constant (a)	8.377 Å
Volume of unit cell (V)	588.0 Å ³
X-Ray density (ρ_x)	5.301 g/cm ³
Bulk density (ρ_b)	2.750 g/cm ³
Porosity (p)	48.14 %
Crystallite Size (t)	18.00 nm

The value of bulk density is of the order of 2.749 gm/cm³. It was observed that X-ray density of sample is greater than its bulk density. This was due to the pores present in the prepared materials. The percentage porosity (% P) was calculated from X-ray density and bulk density values. The porosity of nickel ferrite nanoparticles is of the order of 48.14%, which is quite greater than that of bulk NiFe₂O₄. The increase in porosity is due to preparation condition [19]. All the structural data of prepared nickel ferrite nanoparticles is in the reported range.

Electrical Properties

The electrical behaviour of nickel ferrite nano particles was studied by measuring dc resistivity as a function of temperature using two probe techniques. Temperature variation of dc resistivity is shown in Fig. 2 It is evident from Fig. 2 that the plot of $\log \rho$ versus $1000/T$ exhibit the similar nature to that of bulk nickel ferrite. It can be further observed from Fig. 2 that resistivity decreases with increases in temperature indicating the semiconducting nature of the samples and obeys the Arrhenius relation;

$$\rho = \rho_0 \exp(\Delta E/KT) \quad (8)$$

where, ρ_0 is resistivity at room temperature, k is the Boltzmann constant, ΔE is the activation

energy and T is the absolute temperature

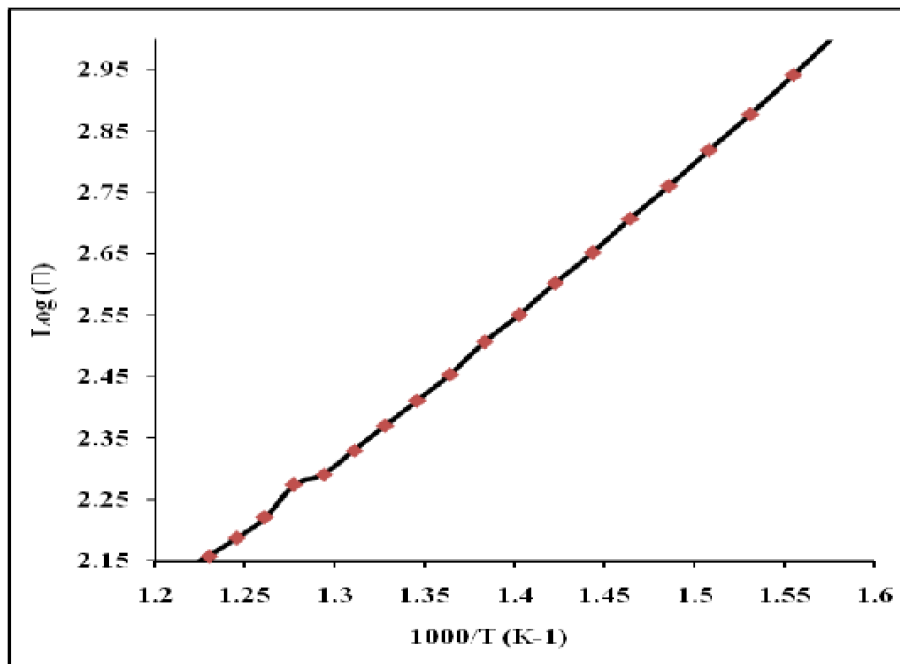


Fig.2. Temperature dependence of d c resistivity of nickelferrite nanoparticles

The resistivity plot shows two regions high temperature region (ferrimagnetic) and low temperature region (paramagnetic) separated at a particular temperature which may correspond to Curie temperature of nickel ferrite. A change in slope is contributed to change in conduction mechanism or phase transition from ferrimagnetic to paramagnetic. The conduction mechanism can be explained on the basis of Verwey model [20].

According to Verwey, the conduction mechanism in ferrite occurs mainly due to hopping of Fe^{2+} and Fe^{3+} ions in the octahedral [B] sites. It is well known that hopping probability depends upon the separation between ions and the activation energy. The activation energy can be determined from slope of the linear plots of dc electrical resistivity (Fig. 2) and the Arrhenius relation [Eq.8]. The calculated value of activation energy is of the order of 0.398 eV. The activation energy of material is associated with mobility of charge carrier. The charge carriers are located with ions or vacant site and conduction takes place through hopping process.

4. Conclusion

Nickel ferrite nanoparticles of nano size have been synthesized successfully by sol-gel auto combustion method using mixed fuel. X-ray diffraction pattern confirms the formation of cubic spinel structure in single phase without any impurity peak. The average crystallite size is obtained was of the order 18 nm. The lattice constant and other structural parameter are in the reported range. The D.C. electrical resistivity decreases with increase in temperature obeying Arrhenius plot. The activation energy calculated from D.C electrical resistivity versus temperature is of the order of 0.398 eV.

References

- [1] V. J. Sawant, S. R. Bamane, *Int. J. Pharm. Sci. Rev. Res.* 20(2013) 159.
- [2] M. Kooti, M. Afshari, *Scientia Iranica.* 19 (2012) 1991.
- [3] J. A. Paulsen, A. P. Ring, and C. C. H. L., *J. of Applied Physics* 97 (2005) 044502
- [4] O. Caltun, G.S.N. Rao, K.H. Rao. *J. of Magn. and Magnetic Materials* 00 (2006)
- [5] S. Amiri, S. shokrollahi. *Material Science and Engineering C33(1)* (2013)1.
- [6] M. H. Sousa, F. A. Tourinho, J. Depeyrot, G. J. da Silva, and M. C. F. L. Lara, *J. Physical Chem. B.* 105 (2001) 1168.
- [7] Z. Chen and L. Gao, *Mater. Sci. and Eng: B.*141 (2007) 82.
- [8] A. P. Alivisatos, *Science.* 271 (1996) 933.
- [9] M. Sugimoto, *J. of the Amer. Ceramic Society.* 82 (1999)269.
- [10] Yue Zhang, Zhi Yang, Di Yin, Yong Liu, *J. Magn. and Magnetic Materials* 322 (2010) 3470
- [11] A. Cabañas and M. Poliakoff, *J. Mater. Chem.*, 11 (2001)1408.
- [12] Y. Ahn, E. J. Choi, S. Kim, and H. N. Ok. *Mater Letters*50 (2001) 47.
- [13] J.-G. Lee, J. Y. Park, and C. S. Kim, *J. Mater. Science* 33(1998) 3965.
- [14] K. V. P. M. Shafi, A. Gedanken, R. Prozorov and J. Balogh, *Chem. of Materials* , 10 (1998) 103445
- [15] B.D. Cullity, *Elements of X-Ray Diffraction*, Second ed., Addison-Wesley. (1967).284.
- [16] J. Smit, H.P.J. Wijn, *Ferrites*, John Wiley, New York (1959)233.
- [17] M. George, S.S. Nair, A.M. John, P. A. Joy, *J. Phys. D:Appl. Phys.* 39 (2006) 900.
- [18] S. P. Yadav, S. S. Shinde, A. A. Kadam, and K. Y. Rajpure. *Journal of Semiconductors.* 34 (2013) 093002
- [19] Sagar E. Shirsath, B.G. Toksha and K.M. Jadhav. *Mat. Chem. Phys.* 117 (2009) 163. [20] R. D Waldron, *Physical review.* 99 (1955) 1727.

A Comprehensive Review on Biological Activity of Flavonoids

Sindhu A. Bhosale,^a Sandip S. Dhotre,^a Vidya S. Dofe,^b Rajendra P. Pawar^{a*}

^a Department of Chemistry, Shivchhatrapati College, Aurangabad, Maharashtra, 431 003 India

^b Department of Chemistry, Deogiri College, Aurangabad, Maharashtra, 431 005 India

*Corresponding author. e-mail: bhosalesindhu64@gmail.com

ABSTRACT

Plants and herbs consumed by humans are rich sources of phytonutrients compounds synthesized in plants itself. Such bioactive ingredients are responsible for the plant's antioxidant and medicinal values. Flavonoid might recover cancer and cardiovascular diseases. Flavonoids are considered as disease preventing and health promoting dietary supplements. Flavonoids are an important group of naturally occurring polyphenolic compounds, and its flavone nucleus characterizes it. The main purpose of this present review is to deliberate the current trends of research and development on flavonoids, functions, prediction of flavonoids and applications of flavonoids, as potential drugs in inhibiting several chronic diseases and future research guidelines. Flavonoids have the capacity to control the accumulation of reactive oxygen species (ROS) via scavenger ROS when they are designed. Thus, these antioxidant compounds have a significant role in plant stress tolerance and a high significance in human health, mainly due to their anti-inflammatory and antimicrobial properties.

I. INTRODUCTION

The pigments which is responsible for the color of most fruits, flowers, as well as seeds are flavonoids. Flavonoids are phenolic compounds extensively disseminated in the human diet. The intake of flavonoids has been related through a decreased risk of different diseases like cancer, immune dysfunction and coronary heart disease. Flavonoids has six subgroups that can be considered as major. Chalcones, flavones, flavonols, flavandiols, anthocyanins, and proantho-cyanidins or condensed tannins Flavonoids are a crucial collection of naturally occurring polyphenolic compounds, it is one of the most collective types of compounds accessible in vegetables, fruits, and plant-derived beverages. Moreover, they subsidize to the nutritional merits of vegetables as well as fruits (**Table 1**). Flavonoids are considered as health stimulating and disease avoiding nutritional supplements. It is now measured as an essential component in a variety of pharmaceutical, cosmetic, nutraceutical, medicinal, and further uses. Molecular weight of the flavonoids is low. Many functions and biological utilities are implemented by Flavonoids like comprising protecting from the ultraviolet (UV) radiation and phytopathogens, signaling during nodulation, male fertility, auxin transport, cell growth regulations, appealing pollinator insects, and protection against biotic and abiotic stresses.

Flavonoids are also accountable for the display of fall color in many plants (**Table 2**), which might defend leaf cells by harming from photooxidative, improving the effectiveness of nutrient repossession through senescence. In humans, these compounds are connected with a great collection of health benefits rising from their bioactive properties, such as anti-inflammatory, anticancer, anti-aging, cardio-protective, neuroprotective, immunomodulatory, antidiabetic, antibacterial, antiparasitic, and anti-viral properties. However, the industrial use of these antioxidants implies extraction processes with high purity and quality. Therefore, several measures for the extraction of flavonoids have been discovered, and in recent years further environmentally approachable extraction methods and strategies that accomplish great yields have been established [1]. Flavonoids are extensively dispersed subordinate metabolites with different metabolic functions in plants. Converse connection can be observed among chronic diseases and dietary flavonoids, which exhibited the significance of reviewing flavonoids. At present have come to the conclusion that the flavonoid might recover cardiovascular diseases and cancer as well.

TABLE 1 : FLAVONOIDS SUBCLASSES AND THEIR OCCURRENCE IN FOODS

Sr. No.	Subclass of Flavonoid	Examples of Compounds	Food source	References
1	Flavonol	Kaempferol, quercetin, Myricetin and tamarixetin	olive oil, red wine, kale, broccoli apples, Onion, cherries, berries, and grapefruit and tea	1
2	Flavones	Chrysin, apigenin Rutin, luteolin, and Glucosidestangeretin	Fruit skins, red wine, buckwheat, red pepper, tomato skin, Parsley, Thyme	2-5
3	Flavonones	Naringin, naringenin, taxifolin, and hesperidin	Citrus fruits, grapefruits, lemons, and oranges	6-7
4	Flavanol	Catechin, epicatechin, epigallocatechin, glausan-3-epicatechin, proanthocyanidins	Apple, tea	1
5	Anthocyanidins	Apigenidin, cyaniding, delphinidin, pelargonidin, malvidin	Cherries, easberry, strawberry, and Grapes	1,5
6	Isoflavones	Genistein, daidzein	Soya beans, Legumes	8, 9

TABLE 2: FEW COMMON MEDICINAL PLANTS RICH IN FLAVONOIDS

Plant	Flavonoids	References
Aloe Vera	Luteolin	10
Bacopa Moneirra	Luteolin	10
Acalypha Indica	Kaempferol	10
Azadirachta indica	Quercetin	11
Betula pendula	Quercetin	12
Butea monospermea	Genistein	13
Oroxylum indicum	Chrysin	16
Cannabis sativa	Quercetin	11
Mimosa pudica	Isoquercetin	16
Clitoria ternatea	Kaempferol-3-neohesperidoside	15
Brysonima crassa	Catechin (+)-	14
Pongamia pinnata	Pongaflavonol	17

Plant Sources of Flavonoids:

Flavonoids can be found in numerous beverages and foods, like beer, wine, and tea, but vegetables, fruits, flowers, and seeds are the sources with the maximum quantities of natural flavonoids [19]. Flavonols that comprise, for example, quercetin, kaempferol, isorhamnetin, fisetin, and myricetin are abundant in green fruits, leaves, and grains [20,21]. Flavones are among the most important flavonoids and are represented by luteolin, isosinensetin, apigenin, sinensetin, nobiletin, galangin, tangeretin, and chrysin [20]. These compounds can be mainly found in leaves, flowers, and fruits as glucosides of luteolin, apigenin, and diosmetin [21]. Flavanones, also known as dihydroflavones, are an important class of flavonoids usually found in citrus fruits. Anthocyanins are the flavonoids responsible for the red, blue, purple, and orange color of several leaves, flowers, and fruits.

This class of compounds is usually present as glycosides of anthocyanidins, such as cyanidin, pelargonidin, delphinidin, peonidin, petunidin, and malvidin [18,22]. Natural flavonoids can be taken out and used in the food industry instead of synthetic compounds to increase food quality. In recent years, the limitation imposed on the use of some synthetic antioxidants, such as the case of butylated hydroxyanisole (BHA), butylated hydroxytoluene (BHT), and propyl gallate, improved the interest in natural flavonoids commonly due to their capacity to check oxidative degradation of lipids, increase the quality and nutritional value of food, and diminish toxicity [23]

Biological Activities of Flavonoids:

1. Antioxidant Activity:

Flavonoids have many biochemical properties, but the best described property of nearly every group of flavonoids is their capacity to act as antioxidants. It is depending upon the arrangement of functional groups in the nuclear structure. The benefit of antioxidant activity assay was to simulate cellular biological processes which include uptake, distribution, and metabolism. Antioxidant Activity assay was focused to quantify the capacity of the analyte to prevent the formation of DCF by AAPH-induced peroxy free radical in HepG2 cells. Other techniques commonly used for measuring chemical antioxidant activity, this assay has been developed a more biologically representative protocol. Antioxidants can act at the cell membrane to break peroxy radical chain reactions at the cell surface or can be up taken by the cell and react with ROS intracellularly [24]. The efficiencies of membrane binding and cell uptake are two major factors influencing the antioxidant activity of the tested chemical. It is significant that although the antioxidant Activity assay signifies a reliable and cost-effective approach to estimate the potential biological activity of dietary flavonoids on cellular level and conveys significant reference value to the functional food development.

Flavonoids are one of the best phytochemicals that act as antioxidants and thus inhibit the factors of disease-causing. Antioxidant activity depends on the arrangement of functional groups in the flavone nucleus. Flavonoids are also protecting the cell membranes which are damaged due to lipid peroxidation. Thus, the flavonoids contribute as antioxidants, in the prevention of many diseases caused due to oxidative stress. The antioxidant mechanisms of flavonoids can be by the direct scavenging of ROS, spontaneity of ROS development through the chelation of trace elements (e.g., quercetin has iron-chelating and iron-stabilizing properties).

2. Anti-Inflammatory Activity:

Inflammation is a composite biological response of body tissues to harmful stimuli, such as tissue injury, damaged cells, pathogen infection and chemical irritation. It is a defensive response including blood vessels, immune cells, and molecular mediators. Inflammation happens in response to several causes, such as a chemical exposure, tissue physical injury or trauma, and microbial infection. Usually, the inflammation is rapid process and self-limiting, but in some cases, prolonged inflammation periods contribute to the progress of several chronic or degenerative disorders like cardiovascular, cancer, diabetes and neurodegenerative diseases, and obesity [25]. Flavonoids also prevent phosphodiesterases present in cell activation.

3. Antiviral Activity:

Since the 1940s and numerous information specify that naturally occurring flavonoids show a significant anti-viral activity. They are useful in the inhibition of several enzymes related with the lifecycle of viruses. Flavon-3-ol was found to be more effective than flavones and flavonones in selective inhibition of HIV-1 & HIV-2 and similar immune deficiency virus triggering infections. The different study shows the quercetin, hesperetin, and naringin also possess anti-dengue activity virus causing infections. The study shows that quercetin, hesperetin, and naringin also have anti-dengue activity.

4. Anticancer Activity:

Because of the anti-inflammatory properties, flavonoids also have a significant influence on cancer expansion. Flavonoids have been reported for their probable applications in the anti-cancer therapies. They have been testified to interfere in the beginning, raise, and development of cancer by modulating different enzymes and receptors in signal transduction pathways related to cellular proliferation, differentiation, apoptosis, Inflammation, Flavonoids significantly impact the cascade of immunological proceedings related with the growth and development of cancer. These compounds utilize their activity by inactivating carcinogen, inducing apoptosis, triggering cell cycle arrest, and inhibiting angiogenesis [27].

5. Antibacterial Action:

Flavonoids may exert numerous mechanisms of accomplishment against bacteria. They can obstruct with lipid bilayers by inducing bacterial membrane disruption and inhibit some progressions such as, synthesis of cell envelope, biofilm formation, synthesis of nucleic acid, electron transport chain, and synthesis of ATP. The diverse study indicates that the flavonoid-rich plant extracts from diverse plants possess antibacterial activity.

The approach of antimicrobial action may be associated to their capability to cell envelope, enzymes, and microbial adhesins transport proteins.

6. Antifungal Action:

There are numerous antifungal mechanisms employed by flavonoids, such as plasma membrane disruption, cell division, induction of several mitochondrial dysfunctions, and inhibition of cell wall formation, and RNA and protein synthesis [30]. Some isoflavones, such as glabridin, can inhibit the production of the main components of fungi cell walls, β -glucans, and chitin [31]. Apigenin interferes with the cell cycle, while naringenin, myricetin, quercetin, luteolin, kaempferol and genistein inhibit DNA, RNA, and protein synthesis [32].

Conclusion:

Fruits and Vegetables are natural sources of flavonoids. Flavonoids are such phytochemicals exhibit many biological activities such as Antifungal, antiviral, antibacterial, anticancer, antioxidant and anti-inflammatory which are beneficial for human health. Taking into consideration the biological importance of flavones, it was thought worthwhile to synthesize novel flavonoids. Thus, the main purpose of this present review is to deliberate the current trends of research and development on flavonoids, functions, prediction of flavonoids and applications of flavonoids, as potential drugs in inhibiting several chronic diseases and future research guidelines.

References:

1. Stewart AJ, Bozonnet S, Mullen W, Jenkins GI, Lean ME and Crozier A: Occurrence of flavonols in tomatoes and tomato-based products. *Journal of Agricultural and Food Chemistry* 2000; 48(7): 2663-2669.
2. Middleton EJ: Effect of plant flavonoids on immune and inflammatory cell function. *Advances in Experimental Medicine and Biology* 1998; 439: 175-182.
3. Lopez M, Martinez F, Del Valle C, Orte C and Miro M: Analysis of phenolic constituents of biological interest in red wines by high-performance liquid chromatography. *Journal of Chromatography A* 2001; 922(1-2): 359-63.

4. Hara Y, Luo SJ, Wickremasinghe RL and Yamanishi T: Special issue on tea. *Food Reviews Inter* 1995; 11: 371-42.
5. Kreft S, Knapp M and Kreft I: Extraction of rutin from buck wheat (*Fagopyrum esculentum* Moench) seeds and determination by capillary electrophoresis. *Journal of Agricultural and Food Chemistry* 1999; 47(11): 4649-52.
6. Miyake Y, Shimoi K, Kumazawa S, Yamamoto K, Kinae N and Osawa T: Identification and antioxidant activity of flavonoid metabolites in plasma and urine of eriocitrin-treated rats. *Journal of Agricultural and Food Chemistry* 2000; 48(8): 3217-3224.
7. Rousseff RL, Martin SF and Youtsey CO: Quantitative survey of narirutin, naringin, hesperidin, and neohesperidin in citrus. *Journal of Agricultural and Food Chemistry* 1987.
8. Kaufman PB, Duke JA, Briellmann H, Boik J and Hoyt JE: A comparative survey of leguminous plants as sources of the isoflavones, genistein and daidzein: implications for human nutrition and health. *J Altern Complement Med* 1997; 3(1): 7-12.
9. Reinli K and Block G: Phytoestrogen content of foods: a compendium of literature values. *Nutrition and Cancer* 1996.
10. Lázaro ML: Distribution and biological activities of the flavonoid luteolin. *Mini-Reviews in Medicinal Chemistry* 2009.
11. Tripoli E, Guardia ML, Giammanco S, Majo DD and Giammanco M: Citrus flavonoids: molecular structure, biological activity and nutritional properties: a review. *Food Chemistry* 2007; 104(2): 466-479.
12. Gupta KK, Taneja SC, Dhar KL and Atal CK: Flavonoids of *Andrographis paniculata*. *Phytochemistry* 1983; 22(1):314-315.
13. Murlidhar A, Babu KS, Sankar TR, Redenna P, Reddy GV and Latha J: Anti-inflammatory activity of flavonoid fraction isolated from stem bark of *Butea monosperma* (Lam): a mechanism based study. *International Journal of Phytopharmacology* 2010; 1: 124-132.
14. Aderogba MA, Ogundaini AO and Eloff JN: Isolation of two flavonoids from *Bauhinia monandra* leaves and their antioxidative effects. *The African Journal of Traditional, Complementary and Alternative Medicines* 2006; 3(4): 59-65.
15. Sankaranarayanan S, Bama P and Ramachandran J: Ethnobotanical study of medicinal plants used by traditional users in Villupuram district of Tamil Nadu, India. *Journal of Medicinal Plant Research* 2010; 4(12): 1089-1101.
16. Sannomiya M, Fonseca VB and Silva MAD: Flavonoids and antiulcerogenic activity from *Byrsonima crassa* leaves extracts. *Journal of Ethnopharmacology* 2005; 97(1): 1-6.
17. Agarwal M and Kamal: Studies on flavonoid production using in-vitro cultures of *Momordica charantia*. *Indian Journal of Biotechnology* 2007; 6(2): 277-79.
18. Khoo HE, Azlan A, Tang ST, Lim SM: Anthocyanidins and anthocyanins: Colored pigments as food, pharmaceutical ingredients, and the potential health benefits. *Food Nutr. Res.* 2017, 61, 1361779.
19. Rodríguez-García C, Sánchez-Quesada C, Gaforio JJ: Dietary flavonoids as cancer chemopreventive agents: An updated Review of human studies. *Antioxidants* 2019, 8, 137.

20. Kozłowska A, Szostak-Węgierek D: Flavonoids—Food sources, health benefits, 2014, 65, 79-85.
21. Terahara, N: Flavonoids in foods: A Review. *Nat. Prod. Com.* 2015, 10, 521–528.
22. Agrawal AD: Pharmacological activity of flavonoids: A Review. *Int. J. Pharmaceut. Sci. Nano* 2011, 4, 1394–1398.
23. Ruiz-Cruz S, Chaparro-Hernández S, Hernández-Ruiz KL, Cira-Chávez LA, Estrada-Alvarado MI, Ortega LEG, Ornelas-Paz LL, Mata MAL: Flavonoids: Important Biocompounds in Food. In *Flavonoids—From Biosynthesis to Human Health*; Justino, G.C., Ed.; IntechOpen: London, UK, 2017.
24. Rice-Evans CA, Miller NJ, and Paganga G: Structure antioxidant activity relationships of flavonoids and phenolic acids. *Free Radical Biology & Medicine*, 933–956, 1996.
25. Maleki, SJ.; Crespo, JF.; Cabanillas, B. Anti-inflammatory effects of flavonoids. *Food Chem.* 2019, 299, 125124.
26. Mishra A, Kumar S and Pandey AK: Scientific validation of the medicinal efficacy of *Tinospora cordifolia*. *The Scientific World Journal* 2013; Article ID 292934.
27. Mishra A, Sharma AK, Kumar S, Saxena AK and Pandey AK: *Bauhinia variegata* leaf extracts exhibit considerable antibacterial, antioxidant and anticancer activities. *BioMed Research International* 2013; Article ID 915436: 10.
28. Mishra A, Kumar S, Bhargava A, Sharma B and Pandey AK: Studies on in-vitro antioxidant and antistaphylococcal activities of some important medicinal plants. *Cellular and Molecular Biology* 2011; 57(1): 16-25.
29. Pandey AK, Mishra AK, Mishra A, Kumar S and Chandra A: Therapeutic potential of *C. zeylanicum* extracts: an antifungal and antioxidant perspective. *International Journal of Biological and Medical Research* 2010; 1: 228-233.
30. Al Aboody MS, Mickymaray S: Anti-fungal efficacy and mechanisms of flavonoids. *Antibiotics* 2020, 9, 45.
31. Lagrouh F, Dakka N, Bakri Y: The antifungal activity of Moroccan plants and the mechanism of action of secondary metabolite from plants. *J. Med. Mycol.* 2017, 27, 303–311.
32. Cassetta A, Stojan J, Krastanova I, Kristan K, Brunskole Sveglj M, Lamba D, Lanisnik Rizner T: Structural basis for inhibition of 17β hydroxysteroid dehydrogenases by phytoestrogens: The case of fungal 17β -HSDcl. *J. Steroid Biochem. Mol. Biol.* 2017, 171, 80–93.

Structural and Compositional Study of Al³⁺ doped Cobalt Zinc Nanoferrite Synthesized by Sol-Gel Auto Combustion Method

Anil G. Gacche^(a), Arati Chandragupta Mehre^(b), Satish V. Gaikwad^(b), Sopan M. Rathod^{*}

Email- smragc@rediffmail.com*

Advance Materials and Nanotechnology Research Laboratory, Department of Physics, MES
Abasaheb Garware College, Pune - 411004, Maharashtra, India

ABSTRACT

Nanoparticles of Al³⁺ doped Cobalt Zinc ferrites having general formula Co_xZn_(1-x)Al_yFe_(2-y)O₄, y=0, 0.1, 0.2, 0.4 was synthesized by sol-gel auto combustion method. The structural and optical properties of the samples were studied by taking X-ray diffraction and FTIR pattern. XRD analysis was done to confirm the single phase cubic spinel structure of the prepared samples of Al³⁺ doped Cobalt Zinc ferrites. The crystallite size of the samples was decreases from 21 to 17 nm by increasing amount of Al³⁺. Also, lattice parameter was decreases from 8.40 to 8.37 Å⁰ systematically by increasing amount of Al³⁺ content, because of difference in the ionic radius of Al³⁺ and other material cations. FTIR spectra confirmed the formation of spinel Al-Co-Zn ferrite having two main absorption band at tetrahedral and octahedral site of metal oxide.

Keywords-sol-gel auto combustion, XRD, FTIR

I. INTRODUCTION

Nanotechnology is nothing but manipulation of materials in between size 1 to 100 nm and creation of materials of which have at least one of the dimension of that material is within this range. The properties like optical, structural, magnetic, electrical etc. are change due to change material from bulk to nano-form. By improving efficiency, cost, power, durability etc. Ferrite is combination of different iron oxide includes Hematite or magnetite and oxides of other metals, are one of the electrically non-conducting compounds of ceramic ferromagnetic material, having general formula MFe₂O₄, where M is divalent metal ion (Mn, Fe, Co, Ni, Cu and Zn transition metals) (1). The properties of ferrites, structural, magnetic, electrical, optical etc. are depends on the crystallite and grain size, doping of different cations and distribution in interstitial sites, sintering temperature and duration, method of preparation etc (2).

Among ferrites, spinel structure shows interesting properties, depend on magnetic interaction and distribution of cation at the two sub lattices i.e. (A) tetrahedral and (B) octahedral sites, having general formula, AB_2O_4 , where, A is divalent ion of metal and B is ferric ion (3). Normal spinel structure consists of A cations located in tetrahedral sites and B cations are located in octahedral site. But in an inverse spinel structure, half of B cations and all these A cations are randomly distributed in an octahedral sites (4).

Samarium doped Nickel Cobalt ferrite ($Ni_{0.5}Co_{0.5}Sm_xFe_{2-x}O_4$) with $x=0, 0.025, 0.05, 0.075, 0.10, 0.125$ was prepared using sol-gel autocombution method by M.K.Kokare et.al. (5). Lattice constant decreased from 8.342 to 8.321 Å and also increased upto 8.370 Å. Crystallite size varies non linearly between 33 to 25 nm, with adding Sm^{3+} in Ni-Co nanoferrite. Amgnetic properties are reduced when Sm^{3+} is doped that indicates a soft ferromagnetic behavior useful for recording and storage devices.

Detailed study was performed by G.R.Kumar and coworkers (6) on Copper substituted Nickel ferrite synthesized by sol-gel method and sintered at high temperature. In this work the particle size is found to be beyond the nanoscale range due to high temperature of sintering. The magnetization findings indicates a non-collinear structure of ferromagnetic. It was noted that with an increasing doping amount of copper content and lattice parameter was increased from $X=0$ to 0.5.

M. Penchal Reddy et.al. wassynthesized polycrystalline NiCuZn soft spinel ferrite by microwave sintering method, with the stoichiometric method, sintered at 950 °C for 30 min. The lattice content was found to be increase by increasing amount of zinc. The obtained sample was posseses properties which are suitable for core material in the multilayer chip inductors.XRD patterns confirm the formation of single phase cubic spinel structure. (7)

S. R. Gibin and colleagues (8) performed experiments for the synthesis of $Ni_{1-x}Co_xFe_2O_4$ nano particles by co-precipitation method using citrate as chelating agent ($x = 0.3, 0.5, 0.7$). The obtained samples were sintered at 400, 600 and 800 °C for 3 hrs. XRD confirms that $Ni_{1-x}Co_xFe_2O_4$ nano particles belong to spinel type lattice of space group $Fd3m$. The surface morphology of $Ni_{1-x}Co_xFe_2O_4$ studied through FESEM and FETEM indicate that the particles are found crystalline and are in cubic shape. EDAX analysis revealed the presence of Ni, Co, Fe and O. Capacitance value 865 Fg⁻¹ was observed for the scanning rate of 2 mV s⁻¹ from the CV study and used as supercapacitor.

There are many methods are developed by scientist for the synthesis of nanoferrites like, Hydrothermal method (9), Solvothermal method (10), Chemical method (11), ball milling method(12), sol-gel method

(13) etc. Among all the methods, sol-gel method is one of the simplest, small time consuming, non-toxic and cost effective method for preparation of nanoferrites (14).

Many previous research shows that work had done on Cobalt-Zinc ferrite nanoparticles by different method. But very few work exist on Aluminium doped Cobalt-Zinc nanoferrites. Present work shows novelty that effect of Aluminium on Cobalt-Zinc ferrite

Aim of present work consists of synthesis of $\text{Co}_x\text{Zn}_{(1-x)}\text{Al}_y\text{Fe}_{(2-y)}\text{O}_4$ ($y=0$ to 0.4) by simplest and cost effective sol-gel auto-combustion method and investigate the simultaneous influence of Aluminium and Zinc on the Cobalt ferrite on structural and optical properties. Particle size of the samples was decreases from 21 to 17 nm and also, lattice constant decreases from 8.40 to 8.37 Å systematically by increasing amount of Al^{3+} content.

1. Materials and Experimental details-

Nanoferrite $\text{Co}_x\text{Zn}_{(1-x)}\text{Al}_y\text{Fe}_{(2-y)}\text{O}_4$ ($y=0, 0.1, 0.2, 0.4$) are synthesized by cost effective sol-gel auto combustion method by AR grade Marck materials having 99 % pure and used without further purification. Cobalt Nitrate ($\text{Co}(\text{NO}_3)_2 \cdot 6\text{H}_2\text{O}$), Zinc Nitrate ($\text{Zn}(\text{NO}_3)_2 \cdot 6\text{H}_2\text{O}$), Aluminium Nitrate ($\text{Al}(\text{NO}_3)_3 \cdot 9\text{H}_2\text{O}$), Ferric Nitrate ($\text{Fe}(\text{NO}_3)_3 \cdot 9\text{H}_2\text{O}$) are used as precursors and Citric acid ($\text{C}_6\text{H}_8\text{O}_7$) used as burning agent, are dissolved in desired amount in 100 ml double distilled water. Metal nitrates and citric acid was mixed with each other during the process of synthesis in the molar ratio of 1:3. Whole solution was kept on hot plat magnetic stirrer with continuous stirring for 600 rpm at 100°C . After completely dissolution of all the chemicals suitable amount of Ammonia solution was added drop wise as precipitating agent for arranging PH of the solution around 7. Further, the growth solution was kept on magnetic stirrer around 3 hrs. at 100°C . After particular time, solution becomes gel form and proceed with burning process. The final powder of the samples was grind and sintered at 500°C for 5 hrs, proceed to use further characterization and applications.

2. Characterization techniques and Results-

2.1.X-ray Diffraction:

The structural analysis of the samples were analyzed by X-ray diffraction recorded by $\text{Cu-K}\alpha$ radiation having $\lambda=1.54056 \text{ \AA}$. Figure 1 is the XRD pattern of the samples of $\text{Co}_x\text{Zn}_{(1-x)}\text{Al}_y\text{Fe}_{(2-y)}\text{O}_4$ ($y=0, 0.1, 0.2, 0.4$) synthesized by sol-gel auto combustion method, shows cubic spinel structure, due to presence of (111), (220), (311), (222), (400), (511) and (440), having maximum diffraction intensity at (311) plane (15). Bragg law used for observations of XRD patterns to index all the reflection peaks. The obtained peaks in XRD pattern are matched with standard JCPDS data of card number 742081 (16) and 791744

(17) for NiFe₂O₄ and CoFe₂O₄ respectively. All samples shows intense and sharp peaks and shows no extra impurities in the prepared samples. Average crystallite size of the samples was calculated using Scherrer method using relation (18),

$$D = \frac{0.9\lambda}{\beta \cos\theta} \dots \dots \dots (1)$$

Where, λ is wavelength of X-rays used (0.15406)

B is FWHM of peaks

Θ is Bragg angle

D is Crystallite size

The results of the above calculations are tabulated in figure 1.

Crystallite size was varies from 21 to 17 nm from x=0 to x=0.4 systematically. The crystallite size goes decreasing due to the difference in ionic radii of the contents.

Al³⁺ have small ionic radius (0.50 Å⁰) as compared to Zn²⁺ (0.87 Å⁰). Al³⁺ ions gets shift towards tetrahedral site and fit to an ion of Zn²⁺. Due to this crystallite size gets decreasing systematically as amount of dopant Al³⁺ gets increasing.

The lattice parameter of the samples was calculated using relation (19),

$$a = d_{hkl} * \sqrt{h^2 + k^2 + l^2} \dots \dots \dots (2)$$

Where,

a is lattice constant

d is interplaner spacing

h,k,l are millar indices of planes

The lattice parameter of the samples were decreasing from 8.40 to 8.37 Å⁰ by increasing value of x from 0 to 0.4. The systematic decreasing of the lattice constant is due to less ionic radius of Al³⁺ substitution with large ionic radius of Zn²⁺ at tetrahedral site, corresponding to theory and calculation of crystallite size from Scherrer formula, detailed in table (1).

2.2. Fourier Transform Infrared Spectroscopy (FTIR):

FTIR spectra of the Co_xZn_(1-x)Al_yFe_(2-y)O₄ (y=0, 0.1, 0.2, 0.4) samples was recorded over 500 to 4000 cm⁻¹ shown in figure 2.

Two strong absorption bands nearly, 600 cm⁻¹ and 400 cm⁻¹, confirmed that formation of Co_xZn_(1-x)Al_yFe_(2-y)O₄ (y=0, 0.1, 0.2, 0.4) was observed from Infra-red spectroscopy is nothing but common characteristic of spinel ferrite, due to the vibrations of bands between the metal ions and oxygen ions

along with the lattice sites. The two main bands assigned to the tetrahedral (A) and octahedral (B) stretching of metal, observed at ranges of 600-500 cm⁻¹ at higher frequency ν_1 and 450-380 cm⁻¹ at lower frequency band ν_2 , shows the typical spinel structure bands (20). Small shifting of absorption frequency bands is observed due to the shifting of tetrahedral site of Fe³⁺ ions towards an oxygen ions that decreases with the Fe³⁺-O²⁻ distance. The spectra of FTIR for all the above samples shows two main bands of absorptions, which corresponds to vibrations of the metal-oxides modes. No other new group of peaks are observed, means synthesized material is free from organic compound.

3. Conclusions-

Aluminium substituted Cobalt Zinc nanoferrites have been synthesized by sol-gel auto combustion method using citric acid as burning agent successfully. The obtained samples were sintered at 500 °C for 5 hrs. The crystallite size and the lattice parameter was decreases from 21 to 17 nm and 8.40 to 8.37 Å⁰ respectively as amount of Al³⁺ increases, with linear variations, due to the smaller ionic radius of Al³⁺ as compared to other metal ionic radii and ionic radii differences. The prepared samples shows the cubic spinel structure, by comparing standard JCPDS data.

References-

- 1) AjitanshuVedrtnam, KishorKalauni, Sunil Dubey and Aman Kumar, A comprehensive study on structure, properties, synthesis and characterization of ferrites (2020) AIMS Materials Science, 7(6): 800–835
- 2) Khalid Hussain, Nasir Amin, Muhammad Imran Arshad, Evaluation of structural, optical, dielectric, electrical, and magnetic properties of Ce³⁺ doped Cu_{0.5}Cd_{0.25}Co_{0.25}Fe_{2-x}O₄ spinel nano-ferrites (2020) Ceramics International, 47 (3)
- 3) Sanchez-Lievanos, Karla and Stair, James and Knowles, Kathryn, Cation Distribution in Spinel Ferrite Nanocrystals: Characterization, Impact on their Physical Properties, and Opportunities for Synthetic Control (2021) Inorganic Chemistry, 60 (7)
- 4) D. Carta, M. F. Casula, A. Falqui, D. Loche, G. Mountjoy, C. Sangregorio and A. Corrias, A Structural and Magnetic Investigation of the Inversion Degree in Ferrite Nanocrystals MFe₂O₄ (M) Mn, Co, Ni) (2009) J. Phys. Chem. C 113, 8606–8615
- 5) Kokare M.K, Jadhav N. A., Rathod S.M, Effect of Nd³⁺ doping on structural and magnetic properties of Ni_{0.5}Co_{0.5}Fe₂O₄nanocrystalline ferrites synthesized by sol-gel auto combustion method (2018)Journal of Alloy and compound, 748, 1053-1061

- 6) Kumar G.R, Kumar K.V, Synthesis, structural and magnetic properties of copper substituted Nickel Ferrites by sol-gel method (2012) material sciences and applications, 87-91
- 7) Reddy, M. &Gugamsetty, Balakrishnaiah&Wuppulluri, Madhuri&Mudinepalli, Venkata& Reddy, N. Sivakumar, Kota and Murthy, Vemuriand Ramakrishna reddy, Rajuru, Structural, magnetic and electrical properties of NiCuZn ferrites prepared by microwave sintering method suitable for MLCI applications (2010) Journal of Physics and Chemistry of Solids. 71. 1373-1380
- 8) S. R. Gibin, P. Sivagurunathan, Synthesis and characterization of nickel cobalt ferrite ($\text{Ni}_{12x}\text{Co}_x\text{Fe}_2\text{O}_4$) nano particles by co-precipitation method with citrate as chelating agent (2016) J Mater Sci: Mater Electron
- 9) Nejati, K, Zabihi, R. Preparation and magnetic properties of nano size nickel ferrite particles using hydrothermal method (2012) Chemistry Central Journal 6, 23
- 10) Abbasian, A.R., Lorfasaeei, Z., Shayesteh, M. et al. Synthesis of cobalt ferrite colloidal nanoparticle clusters by ultrasonic-assisted solvothermal process (2020) J Aust Ceram Soc 56, 1119–1126
- 11) RamjiLal and P. Ramakrishnan, Preparation of Ferrite Powders by Chemical Methods—A Review (1979) Transactions of the Indian Ceramic Society, 38:5, 166-180
- 12) Ding Chen, Yingzhe Zhang, Biyu Chen and Zhitao Kang, Coupling Effect of Microwave and Mechanical Forces during the Synthesis of Ferrite Nanoparticles by Microwave-Assisted Ball Milling (2013) Ind. Eng. Chem. Res. 52, 39, 14179–14184
- 13) Saragi T, Nurjannah S, Novia R, Syakir N, Simanjuntak E, Safriani L, Synthesis of Cobalt Ferrite Particles by Utilized Sol-Gel Method (2015) Material Science Forum, 827, 219–22.
- 14) Thomas Dippong, Erika Andrea Levei and OanaCadaru, Recent Advances in Synthesis and Applications of MFe_2O_4 (M = Co, Cu, Mn, Ni, Zn) Nanoparticles (2021) Nanomaterials 11, 1560
- 15) SagarMitra, Pavan S. Veluri, AntaraChakraborty, and Ramesh K. Petla, Electrochemical Properties of Spinel Cobalt Ferrite Nanoparticles with Sodium Alginate as Interactive Binder (2014) ChemElectroChem, 1, 1068 – 1074
- 16) JCPDS card number 742081
- 17) JCPDS card number 791744
- 18) Monsh Ahmad, Foroughi Mohammad Reza and Monshi Mohammad, Modified Scherrer Equation to Estimate More Accurately Nano-Crystallite Size Using XRD (2012) World Journal of Nano Science and Engineering. 2. 154-160.

19) Seok-Jae Lee, Young-Kook Lee, Quantitative analyses of ferrite lattice parameter and solute Nb content in low carbon microalloyed steels (2005) *Scripta Materialia*, 52, 10, 973-976

20) Hazen Robert and Yang Hexiong, Effects of cation substitution and order-disorder on P-V-T equations of state of cubic spinels (1999) *American Mineralogist*, 84, 1956-1960

List of figures:

1. XRD of $\text{Co}_x\text{Zn}_{(1-x)}\text{Al}_y\text{Fe}_{(2-y)}\text{O}_4$ ($y=0, 0.1, 0.2, 0.4$)
2. FTIR of $\text{Co}_x\text{Zn}_{(1-x)}\text{Al}_y\text{Fe}_{(2-y)}\text{O}_4$ ($y=0, 0.1, 0.2, 0.4$)

List of Tables:

1. Table of crystallite size and lattice constant of $\text{Co}_x\text{Zn}_{(1-x)}\text{Al}_y\text{Fe}_{(2-y)}\text{O}_4$ ($y=0, 0.1, 0.2, 0.4$)

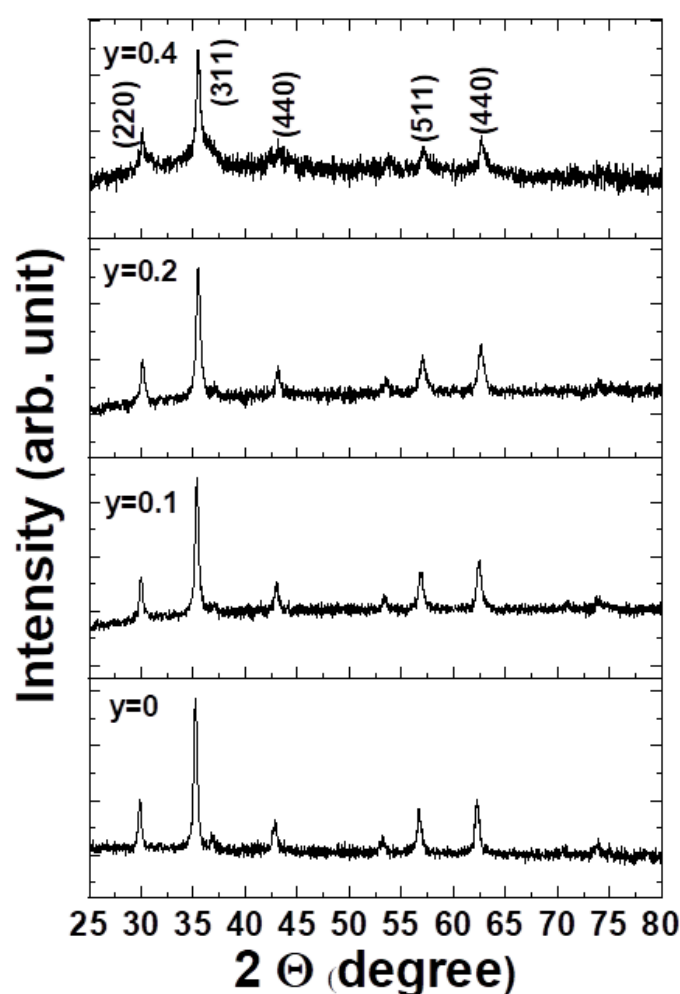


Figure 1. XRD of $\text{Co}_x\text{Zn}_{(1-x)}\text{Al}_y\text{Fe}_{(2-y)}\text{O}_4$ ($y=0, 0.1, 0.2, 0.4$)

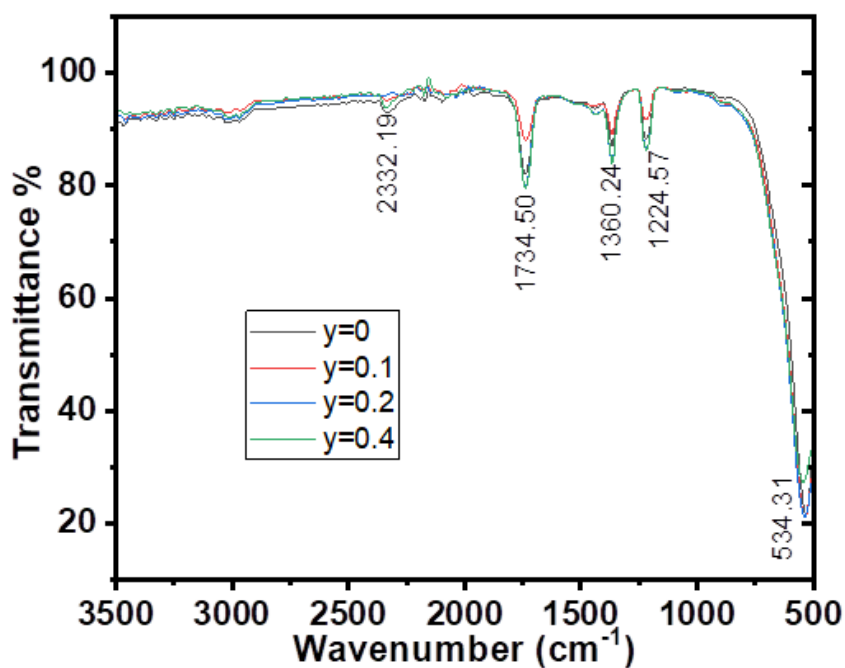


Figure 2. FTIR of $\text{Co}_x\text{Zn}_{(1-x)}\text{Al}_y\text{Fe}_{(2-y)}\text{O}_4$ ($y=0, 0.1, 0.2, 0.4$)

Composition (y)	Diffraction angle (θ)	FWHM	Crystallite size (nm)	Lattice constant (\AA)
0	17.63	0.00758	21	8.40
0.1	17.74	0.00959	20	8.48
0.2	17.74	0.00960	19	8.39
0.4	17.78	0.00785	17	8.37

Table 1. Variation of crystallite size and lattice constant with y value, $\text{Co}_x\text{Zn}_{(1-x)}\text{Al}_y\text{Fe}_{(2-y)}\text{O}_4$ ($y=0, 0.1, 0.2, 0.4$)

Introductory Optical and Microwave Remote Sensing : A Review

Rajeshwari C. Pangarkar¹, Dheeraj B. Raut², Archana D. Kusale¹,

Satyawan N. Arsul¹, Nitin B. Gaikwad¹, Pradnya R. Maheshmalkar¹, Sayyad Shafiyoddin²

¹Department of physics, Mrs. K.S.K. College, Beed (MH), India.

²Department of physics, Milliya College, Beed (MH), India.

Corresponding author E-mail : raje.pangarkar17@gmail.com

ABSTRACT

Remote sensing technology is widely used in many fields which collects a wide range of observations in a timely manner and use less restricted data collection methods. In recent years, there have been great progresses in remote sensing developments, especially in the microwave remote sensing over the optical remote sensing. Due to the advantages of independency on weather conditions as well as day/night detection of target of interest the microwave remote sensing becoming the main focus of researchers. It is used for collecting information about object of interest on the earth surface and also used for monitoring many environment related disciplines, glacial dynamics, crop classification, forest cover, flood mapping, coastal vegetation and many more. This paper concludes that microwave remote sensing has great potential than optical remote sensing and will play more significant role in the various fields of interest.

Keywords : Remote sensing, Active and Passive, Optical, Microwave

I. INTRODUCTION

Remote sensing is the greatest achievement for acquiring information from objects on earth or other planetary bodies. It performs the detection, collection and interpretation of target of interest. Getting information about an object, area or phenomenon without being in contact with it called as remote sensing. By measuring the amount and the nature of the reflection of visible light energy from our external source(such as the sun or light bulb, tube), we can gather information around us, as it reflects away from the objects in the field of our approach. In simple words we can say that, with the help of our eyes we can collect information about surroundings without touching it. i.e., our eyes are excellent example of remote sensing device.

The principle of remote sensing is based on measurement made by the satellite sensor in different wavelength or frequency regions of electromagnetic spectrum. The electromagnetic radiation have an

enormous range of wavelengths and frequencies, the range is called as electromagnetic spectrum. Fig.1, shows the different regions of the electromagnetic spectrum.

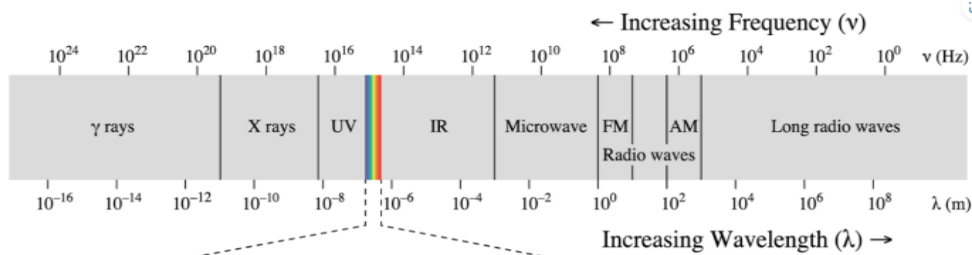


Fig.1. Electromagnetic Spectrum

According to frequency used of electromagnetic spectrum, there are different types of remote sensing [1-2].

I. Optical Remote Sensing :

It is operate in the Visible (0.38-0.72nm), Near Infrared (0.72-1.30nm), middle infrared (1.30-3.00nm), short wave infrared (7.00-15.0nm) portion of electromagnetic spectrum. Optical remote sensing is a passive technique for earth observation which relies on solar illumination. Below we have discussed the passive remote sensing.

Passive Remote Sensing :

Such remote sensing requires an external energy source (such as the Sun). It detects natural radiations. This kind of remote sensing collects data from the Earth's atmosphere and not from the Earth's surface hence, passive remote sensing mostly perform from satellites. Fig.2. give the idea about passive remote sensing. Mainly this remote sensing is used in the applications in optical, infrared, and thermal electromagnetic radiation. The drawback of this technique is, it's applicable only during daytime with full of sun radiations without interfering clouds or smoke or rainfall, etc. another drawback is that the noise is very much comparable to the desired signal. Hence, the resolution of each cell degrades the quality of the images.

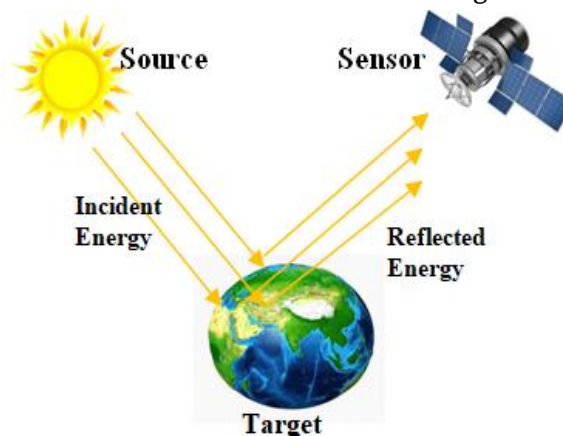


Fig.2. Passive Remote Sensing

The earliest application was aerial photography for surveying and military use. Multiple spectral Earth observation systems were introduced in the mid-1960s that captured spectra in the form of images, also

known as imaging spectroscopy (IS) [3]. However, when cloud cover, rain, haze persists over an area of interest in that case, such remote sensing fails to retrieve data.

II. Microwave Remote Sensing :

It is operate in the microwave region of EM spectrum. Wavelength of this region is 1mm – 1m and frequency of this region is 40,000Hz – 300Hz. It has along wavelength thus it penetrate through clouds or any other weather conditions without any restrictions (except during periods of heavy rain). It provide unique information like sea, wind and wave direction which are derived from frequency characteristics, Doppler Effect, polarization, backscattering etc. it overcomes the disadvantages of optical remote sensing. Microwave wavelength region is used in remote sensing to provide useful information about the earth's surface (atmosphere, land and ocean).The microwave remote sensing basically carried out using active remote sensing.

Active Remote Sensing :

Such remote sensing has its own energy source for illuminations. Thus they can send their own signals for acquiring data. Major advantage of active remote sensing is, data can available both time day or night and also capable of measuring electromagnetic signals in all weather conditions. Fig.3. give the idea about active remote sensing. The most common examples of this remote sensing are LiDAR (Light Detection and Ranging) **is used to examine the surface of the earth and** RADAR (Radio Amplitude Detection And Ranging).

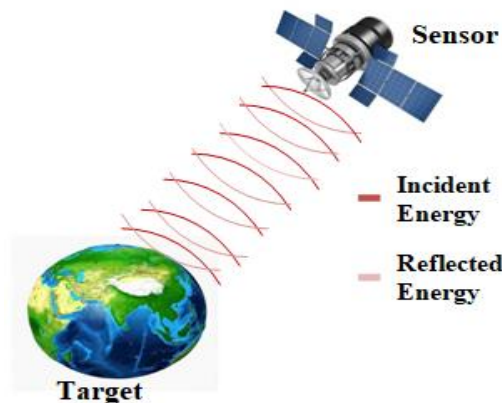


Fig.3. Active Remote Sensing

It transmits and receives its own radio wave pulses towards the object. The active microwave radar system can be classified in two types as following.

1) Non – Imaging Radar :

It first contains an altimeter that is used to measure sea surface height as well as wind speed. It can be used in aircraft and spacecraft [4]. The other is a scatterometer that is used to measure the direction and speed of the ocean wind. Applications of scatterometer play an essential role in regulating the global climate [5-8].

2) Imaging Radar :

It includes side looking airborne radar (SLAR), real aperture radar (RAR) and synthetic aperture radar (SAR). All the types of imaging radar produce images of the area on the earth. SAR is the modified version of imaging radar which provides very high resolution imagery of the earth as well as planetary bodies [9].

Literature Review

Natural environment is essential for human survival and development as it provides water resources, land resources, biological resources and climate resources etc. The development trends and future directions are forwarded to direct the research application of environmental monitoring and protection in the new era. Global and regional environmental monitoring relies heavily on remote sensing satellites and sensors that are able to quickly collect local and spectral data of large-scale components on the Earth's surface. With the rapid development of space technology, remote sensing data is becoming increasingly abundant [10].

Remote sensing provides an ideal platform for gathering empirical data, such as mapping of global climate change, to help decision makers and support policies that ensure the right balance between land development and environmental protection[11]. The main advantage of remote sensing is gaining information without any direct human or machine contact, achieved by sending electromagnetic radiations. i.e., gaining information about large sections of earth in a very less time and again and again of the same patch to observe the changes in a given list of parameters.

India is not behind the leading countries in the developed world in taking big steps forward in remote sensing. ISRO, the Indian Space Research Organization, has launched numerous satellites since 1975, the latest being the PSL V-C14 (Earth Satellite Launch Vehicle) on September 23, 2009 and the Prithvi-II satellite in October 2009. Due to all this, modernization, broad casting networks also provided very valuable information [12].

The field of remote sensing can be divided into two general categories: Analog remote sensing and digital remote sensing. Analog remote sensing uses film to record the electromagnetic energy. Digital remote sensing uses some type of sensor to convert the electromagnetic energy into numbers that can be recorded as bits and bytes on a

Computer and then displayed on a monitor [13].

Remote sensing works on electromagnetic radiation. Electromagnetic radiation consists of the electrical and magnetic field. An electromagnetic radiation is a type of energy which travels at universal speed of light through free space or through a material medium in the form electromagnetic waves.

Remote sensing system that measures naturally available energy is called a passive sensor. We categorize each spectral region based on its frequency (ν) or wavelength. There are two types of imagery for passive sensors, Multispectral imagery and Hyperspectral imagery.

The main difference between multispectral and hyperspectral is the number of bands and how narrow the bands are. Hyperspectral images have hundreds of narrow bands, multispectral images consist of 3-10 wider bands. Both imagery give the power to see like humans (red, green, and blue), goldfish (infrared), and bumblebees (ultraviolet). Actually, we can see even more than this as reflected EM radiation to the sensor [14].

Optical imaging is the widely used passive remote sensing where the range is from $0.4\mu\text{m}$ to 1mm . In it electromagnetic energy of the sun is reflected by the earth is received and measured. It cannot penetrate through clouds; therefore, image is acquired only in clear weather [15].

Optical remote sensing is the oldest method of remote sensing which is started with the invention of photography. As the optical remote sensing has started much earlier than the advance imaging techniques

like SAR therefore temporal studies are well supported by the optical images. In optical remote sensing many types of error are shown including skew distortion, panoramic distortion, haze, error due to varying solar illumination conditions and error due to unstable platform [16]. It is affected by the shadow that leads to the misclassification of pixel into low reflectance objects like water [17]. Over the time, resolution of the images has improved. Now a day's several images have the centimeter level of accuracy. Hence microwave remote sensing is used for data detection and collection.

Microwave remote sensing can be passive as well as active. The process involves transmitting the pulses of microwave in the direction of interest and record the reflection which contains strength and position of the object. Its electromagnetic spectrum range is from 1mm to 1m. Microwave can penetrate through clouds; therefore, image is acquired in any weathers [15,17].

SAR is the type of microwave remote sensing which can provide a quantitative estimation of ground changes and can be used in all weathers. It also has the some errors like speckle, layover and foreshortening but these are less than optical remote sensing [16].

Remote sensing plays an important role in various applications such as Agriculture, Vegetation, Wetland Mapping, River Mapping, Glacier Mapping, Urbanization, Analysis of Landslide-Earthquake ,Forestry, Geology, Hydrology, Ocean and Coastal Monitoring, Surface Topography and many more [17-22].

Optical remote sensing gives the biophysical and biochemical data through the study of leaf pigmentation and structure is performed [20]. Under the optical remote sensing, pest infection and disease can be identified as it appears in the form of change in spectral reflectance. Also change in photosynthetic processes can be determined through the near-infrared band and Crop growth monitoring and yield estimation can be performed. Abandoned agricultural land also can be identified [21].

Microwave remote sensing can give the information about the moisture content and structure of the canopy. It can penetrate the vegetation canopy and can study the surface water or flood extent. It detects water content of the plant and the soil characteristics which can support the crop disease detection and also helps in crop growth monitoring [20-22].

Currently available satellite imagery has been applied to numerous applications in disaster prediction, investigation and or management at global, regional and local scales. Data have been mostly used for more detailed assessments of an earth's aftermath and reconstruction as well as in post disaster scientific research [23].

Discussion :

A systematic review of remote sensing is discussed in this paper. In this paper, we have discussed Active and passive remote sensing and also discussed about the microwave remote sensing and optical remote sensing with positive and negative points of the given remote sensing.

Conclusion :

This study is to investigate the capability of remote sensing for various applications. It has numerous applications related to our environment. Microwave remote sensing gives clarity about images and shows high-resolution images thus nowadays microwave remote sensing is a growing technique for acquiring data.

its advantages which overcome the disadvantages of optical remote sensing. Satellite imagery is a great data source for quickly responding to different emergency events. In the field of agriculture (crop monitoring, crop mapping), forestry, geology, hydrology, marine ice conditions, glacier exploration, ocean and coastal monitoring, remote sensing are of great benefits.

References

1. Lillesand, Kiefer, Chipman. "Remote sensing & image interpretation", 2012. (6thed.). Wiley India Edition.
2. Jensen R. J. "Remote sensing of the environment an earth resource perspective", 2014. (2nd ed.) Pearson.
3. Rene Booyesen, Richard Gloaguen, et.al. "Geological Remote Sensing", Encyclopedia of Geology (second edition) 2021, pages 301-314.
4. Basics of Altimeter. Retrieved from <http://www.radartutorial.eu/02.basics/Altimeter.en.html>
5. Calla, OPN. "Microwave Remote Sensing", 2009. Director, DESIDOC, Metcalfe House: Delhi.
6. About Scatterometer. NASA, JPL. Retrieved from <https://winds.jpl.nasa.gov/aboutscatterometry/history>
7. NASA/JPL's Imaging Radar Program, 1996. Retrieved from <https://southport.jpl.nasa.gov/desc/>.
8. NASA Earth Observatory, 2017. from https://earthobservatory.nasa.gov/Features/RemoteSensing/remote_08.php.
9. Didier, Massonnet & Souyris, Jean-Claude. "Imaging with Synthetic Aperture Radar", 2008, (1st ed.), EPFL Press.
10. Jun Li, Yanqui pei, et.al., "A review of remote sensing for Environmental Monitoring in China", Remote Sensing (2020), 12(7), 1130.
11. George Joseph, Jeganathan Chockalingam, "Fundamentals of Remote Sensing", Nov 2017, 3rd edition, , ISBN: 9789386235466.
12. The Remote sensing (2020). Retrieved from <https://civilengineeringnotes.com>
13. Russell G. Congalton (2010) Remote Sensing: An Overview, GIScience & Remote Sensing, 47:4, 443-459.
14. About remote sensing from <https://gisgeography.com/>
15. S. Agrawal, G. B. Khairnar, "A Comparative Assessment Of Remote Sensing Imaging Techniques: Optical, Sar And Lidar", 2019. The International Archives of the Photogrammetry, Remote Sensing and Spatial Information Sciences, Volume XLII-5/W3.
16. Devapal, D., Hashna, N., Aparna, V.P., Bhavyasree, C., Mathai, J., Soman, K.S., "Object Detection from SAR Images based on Curvelet Despeckling", 2019. Materials Today: Proceedings 11, 1102-1116.
17. Lin, Y., Zhang, H., Li, G., Wang, T., Wan, L., Lin, H., "Improving Impervious Surface Extraction With Shadow-Based Sparse Representation From Optical, SAR, and LiDAR Data", 2019. IEEE Journal of Selected Topics in Applied Earth Observations and Remote Sensing 12, 2417-2428.
18. Tiwari, A., Narayan, A.B., Dwivedi, R., Dikshit, O., Nagarajan, B. "Monitoring of landslide activity at the Sirobagarh landslide, Uttarakhand, India, using LiDAR, SAR interferometry and geodetic surveys", 2018. Geocarto International, 1- 24.

19. Zhang, J., Huang, Y., Pu, R., Gonzalez-Moreno, P., Yuan, L., Wu, K., Huang, W. "Monitoring plant diseases and pests through remote sensing technology: A review", 2019. *Computers and Electronics in Agriculture* 165, 104943.
20. Li, Z., Guo, X., "Remote sensing of terrestrial nonphotosynthetic vegetation using hyperspectral, multispectral, SAR, and LiDAR data" 2016. *Progress in Physical Geography: Earth and Environment* 40, 276–304.
21. Kumar, V., Agrawal, S., 2019. Agricultural land use change analysis using remote sensing and GIS: A case study of Allahabad, India, in: ISPRS-GEOGLAM-ISRS Joint Int. Workshop on "Earth Observations for Agricultural Monitoring." *The International Archives of the Photogrammetry, Remote Sensing and Spatial Information Sciences*, New Delhi, India, pp. 397–402.
22. Montgomery, J., Brisco, B., Chasmer, L., Devito, K., Cobbaert, D., Hopkinson, C., "SAR and Lidar Temporal Data Fusion Approaches to Boreal Wetland Ecosystem Monitoring" 2019. *Remote Sensing* 11, 161.
23. P.R.Maheshmalkar, S.B. Sayyad et.al. "SAR remote sensing for environmental monitoring", 2021. *International Journal of Scientific Research in Science, Engineering and technology*. ISSN 2395-1990, 9(5), 46-51.



Online National Conference on Recent Advances in Chemical and Physical Sciences

[**RACPS-2022**]

Date : 14th December 2022

Organized By

B. S. V Education Society Wapti's

Bahirji Smarak Mahavidyalaya, Basmath Dist. Hingoli, Maharashtra, India

[NAAC Reaccredited B+ Grade]

Affiliated to S, R. T. M University, Nanded

Best College Award of 2020, S, R. T. M University, Nanded

In Collaboration with

Shiv Chatrapati College, N3, CIDCO, Aurangabad



Publisher

Technoscience Academy



Website : www.technoscienceacademy.com

Email : editor@ijsrst.com Website : <http://ijsrst.com>